lontay.beata_285_24

MTA doktori értekezés

A miozin foszfatáz szerepe és szabályozása fiziológiás és patológiás sejtfolyamatokban



Dr. Lontay Beáta

DEBRECENI EGYETEM

Általános Orvostudományi Kar

Orvosi Vegytani Intézet

Debrecen, 2025.

TARTALOMJEGYZÉK

TARTALOMJEGYZÉK **2**
RÖVIDÍTÉSEK JEGYZÉKE **5**
1. BEVEZETÉS **8**
2. IRODALMI ÁTTEKINTÉS **9**
2.1. Poszttranszlációs módosítások funkcionális diverzitása 9
2.2. A fehérjék reverzibilis foszforilációja 10
2.3. A protein foszfatázok osztályozása 11
2.4. A protein foszfatáz 1 holoenzimek szerkezete 13
2.4.1. A protein foszfatáz 1 katalitikus alegysége 13
2.4.2. A protein foszfatáz 1 szabályozó alegységei 15
2.5. A miozin foszfatáz 16
2.5.1. A miozin foszfatáz szerkezete 16
2.5.2.A miozin foszfatáz szubsztrátjai és élettani szerepe 18
2.5.3. A miozin foszfatáz szabályozása 20
2.6. A smoothelin fehérjék és az SMTNL1 23
3. CÉLKITŰZÉSEK **27**
4. ANYAGOK ÉS MÓDSZEREK **28**
4.1. Anyagok 28
4.2. Sejtvonalak 28
4.2.1. A kísérletben használt sejtvonalak 28
4.2.2. Sejtkultúra modellek 28
4.2.3. Sejttenyésztés és a sejtek lizálása 29
4.3. Egér törzsek fenntartása és élettani vizsgálata 29
4.3.1. Az egérkolóniák fenntartása 29
4.3.2. A reproduktív fitnessz vizsgálata 30
4.3.3. Átfogó Laboratóriumi Állatfigyelő Rendszer (Comprehensive Laboratory Animal Monitoring System (CLAMS) 30
4.3.4. Sebgyógyulás tanulmányozása egérbőrön 30
4.4 Szövetminták kinyerése és feldolgozása 31
4.4.1. Humán minták 31

4.4.2. Humán szöveti minták lízise 31
4.4.3. Agyszeletek preparálása, kezelése és szinaptoszóma preparálás 31
4.4. Biokémiai mérések 32
4.4.1. Protein foszfatáz aktivitásmérés 32
4.4.2. In vitro protein kináz esszé 32
4.4.3. Proteome Profiler humán foszfo-kináz és foszfo-MAPK array 32
4.4.4. Protein foszforilációs és defoszforilációs vizsgálat 33
4.4.5. Kaszpáz esszé 33
4.4.6. In vitro protein arginin metiltranszferáz kísérlet 33
4.5. Fehérje vizsgáló módszerek 34
4.5.1. Western blot analízis 34
4.5.2. Fehérje kölcsönhatások kimutatása immunprecipitációval 34
4.5.3. Fehérje kölcsönhatások kimutatása pull-down kísérlettel 34
4.5.4. Felületi plazmon rezonancia (SPR) vizsgálatok 35
4.5.5. Immunfluoreszcenciás vizsgálatok 35
4.5.6. Trikróm festés és immunhisztokémia 35
4.5.7. Duolink PLA fehérje-fehérje kölcsönhatási vizsgálat 36
4.5.8. Szöveti array elemzése 36
4.6. Nukleinsav alapú technikák 36
4.6.1. Myoblast sejtek tranziens transzfekciója 36
4.6.2. Géncsendesítés siRNS segítségével keratinocita sejtekben és ex vivo humán bőrszövetben 37
4.6.3. RNS izolálás és szemi-kvantitatív RT-PCR 37
4.6.4. Microarray analízis 38
4.6.5. Irányított mutagenezis 38
4.6.6. Rekombináns fehérjék termeltetése és tisztítása 38
4.6.7. Emlős két hibrid vizsgálatok 38
4.7. Sejtbiológiai kísérletek 39
4.7.1. Sejtéletképességi vizsgálat MTT festékkel 39
4.7.2. Sejtéletképességi vizsgálat SRB festékkel 39
4.7.3. Karcolási (scratch) vizsgálat 40
4.7.4. Valós idejű sejtvizsgálat JuLI™ készülékkel 40
4.7.5. Elektromos cellaszubsztrát impedancia érzékelés (ECIS) 40
4.7.6. Exocitózis esszé 40

4.7.7. Sejtanyagcsere vizsgálat SeaHorse készülékkel 41
4.7.8. Glükóz felvétel vizsgálata 42
4.7.9. Intraperitoneális glükóztolerancia teszt 42
4.7.10. Kolonizációs vizsgálat 42
4.8. Bioinformatikai analízis 42
4.8.1. Proteomikai elemzés 42
4.8.2. Statisztikai analízis 43
5. EREDMÉNYEK ÉS MEGBESZÉLÉSÜK 44
5.1. A miozin foszfatáz szerepe a neurotranszmitter-kibocsátás szabályozásban 44
5.2. A miozin foszfatáz szerepe a génexpresszió szabályozásban 50
5.3. A protein foszfatázok szerepe a bőrszövet homeosztázisának fenntartásában és a patofiziológiai folyamatok molekuláris 61
5.4. Az SMTNL1 kettős hatásmechanizmusa: citoszkeletális regulátor és transzkripciós kofaktor 69
5.4.1. A vázizom felépítése és plaszticitása 69
5.4.2. Az SMTNL1 a progeszteron receptor koregulátora szteroidhormon függő szövetekben 72
5. 4. 3. Az SMTNL1 a terhesség során izotípusváltozást indukál a vázizomzatban 74
5.5. Az SMTNL1 inzulinérzékenyítő hatása 79
5.5.1. Az inzulin jelátviteli pálya és az inzulin rezisztencia 79
5.5.2. Az SMTNL1 szerepe a vázizom inzulinérzékenyítésében 82
5.5.3. Az SMTNL1 szerepe a reproduktív tulajdonságok kialakításában 88
5.6. Az SMTNL1 szerepe a pajzsmirigyhormon által indukált fiziológiás és pathológiás folyamatokban izomban 92
5.6.1. A SMTNL1 fehérje szerepe a hyperthyreosisos vázizom anyagcseréjének szabályozásában 92
5.6.2. A SMTNL1 és a T3 szelektíven szabályozzák a MYPT1 és MYPT2 izoformákat a miotubulusokban 97
6. KITEKINTÉS 103
7. AZ ÚJ TUDOMÁNYOS EREDMÉNYEK ÖSSZEFOGLALÁSA 105
8. KÖSZÖNETNYILVÁNÍTÁS 107
9. A TÉZISEK ALAPJÁUL SZOLGÁLÓ KÖZLEMÉNYEK 109
10. FÜGGELÉK 111
11. IRODALOMJEGYZÉK 115

RÖVIDÍTÉSEK JEGYZÉKE

2-DG	2-deoxi-D-glükóz
8BrcAMP	8-bromoadenozin-3’-5’-ciklikus monofoszfát
AP	alkalikus foszfatáz
ATP	adenozin-5’-trifoszfát
ATP-γS	adenozin-5’-O-(γ-tio)-trifoszfát
BCA	bikinkoniniksav
BCIP	5-bromo-4-kloro-3-indoil-foszfát
BSA	borjú szérum albumin
CaM	Ca^{2+}-kalmodulin
CaMK-II	kalmodulin-függő kináz-II
cAMP	ciklikus adenozin-3’,5’-monofoszfát
cGMP	ciklikus guanozin-3’,5’-monofoszfát
CK-2	kazein kináz-2
CPI-17	17 kDa PKC által aktivált inhibitor
DARPP-32	32 kDa dopamin és cAMP által szabályzott foszfoprotein
D-MEM	Dulbecco minimális esszenciális tápfolyadék
ECAR	extracelluláris savasodási ráta
ERK1/2	extracelluláris szignál által regulált kináz 1/2
ECL	nagy érzékenységű kemilumineszcencián alapuló reagens
EDTA	etiléndiamin-tetraacetát
EGTA	etilénglikol-bisz-(2-aminometiléter)-tetraacetát
ERM	ezrin radixin moezin
FBS	marhaszérum
FITC	fluoreszcein-izotiocianát
FT-SMTNL1	Flag jelölőt tartalmazó rekombináns SMTNL1
G_L	a PP1c glikogénhez is kötődő regulátor alegysége májban
G_M	a PP1c glikogénhez is kötődő regulátor alegysége vázizomban
GLUT4	glükóz transzporter 4

GST-MYPT	glutation-S-traszferáz-MYPT fúziós fehérje
GTP-γS	guanozin-5'-O-(γ-tio)trifoszfát
HCS	high content screening
HK II	hexokináz II
HepG2	humán hepatokarcinóma
HGF	hepatocita növekedési faktor
HRP	torma peroxidáz
I-1	inhibitor-1
I-2	inhibitor-2
ILK	integrinekhez kapcsolódó kináz
InR	inzulinrezisztencia
IR	inzulin receptor
IRS1	inzulin receptor szubszrát 1
IP	immunoprecipitáció
KEPI	kináz által aktivált PP1 inhibitor
M20	a miozin foszfatáz 20 kDa regulátor alegysége
MEM	minimális esszenciális tápfolyadék
MLC20	a miozin 20 kDa könnyűlánca
MLCK	miozin könnyűlánc kináz
MP	miozin foszfatáz
MYPT	miozin foszfatáz regulátor alegység
OCR	oxigénfogyasztási ráta
PAS	protein A sepharose
NBT	nitroblue-tetrazolium klorid
NIPP-1	nukleáris protein foszfatáz inhibitor-1
NKA	Na^+/K^+ ATPáz
OA	okadainsav
PAGE	poliakrilamid-gélelektroforézis
PAK	p21-aktivált protein kináz
PBS	foszfáttal pufferelt sóoldat

PBST	Tween 20-at tartalmazó foszfáttal pufferelt sóoldat
PI3K	foszfatidilinozitol-3-kináz
PFA	paraformaldehid
PGF2α	prosztaglandin F2α
PHI-1	foszfatáz holoenzim inhibitor-1
PJ	propídium-jodid
PKA	cAMP-függő protein kináz
PKC	protein kináz C
PKGIα	cGMP-függő protein kináz Iα
PLK1	poló-szerű kináz 1
PP1	protein foszfatáz-1
PP1c	protein foszfatáz-1 katalitikus alegység
PP2A	protein foszfatáz-2A
PP2B	protein foszfatáz 2B
PP2C	protein foszfatáz 2C
PPM	fémion-függő foszfatázok
PR	progeszteron receptor
PTM	poszttranszlációs módosítás
Rb	retinoblasztóma fehérje
RIPA	radioimmunprecipitációs esszé puffer
RhoA	Ras fehérjével homológiát mutató onkoprotein
ROK	RhoA-aktivált protein kináz
SAPK/JNK	stressz-aktivált protein kináz/Jun amino terminális kináz
SDS	nátrium-dodecilszulfát
SMTNL1	smoothelin-szerű fehérje 1
T3	trijód tironin
TBS	Tris pufferelt sóoldat
TBST	Tween 20-at tartalmazó Tris pufferelt sóoldat
ZIPK	leucin cipzár motívummal kölcsönható protein kináz

1. BEVEZETÉS

A poszttranszlációs módosítások, például a fehérjék foszfát- és metilcsoporttal, lipidekkel illetve ubikvitinnel történő konjugációja, jelentősen befolyásolják a fehérjék biológiai működését. Emiatt a módosításokat katalizáló enzimek gátlása és aktiválása, és az azok expresszióját szabályozó egyéb faktorok szelektív terápiás célpontok lehetnek számos betegség kezelése során. Munkánkban a reproduktív betegségek, az inzulinrezisztencia, a hipertireózis és a tumorképződés folyamatiban kórosan eltolódott poszttranszlációs módosítási mintázatokat és az azok által kiváltott patobiokémiai folyamatokat vizsgálom biokémiai, molekuláris biológiai és proteomikai módszerekkel. Ismeretes, hogy a fehérjék reverzibils foszforilációja különösen fontos szerepet játszik a jelátviteli folyamatokban, és már több, a foszforilációt végző kinázokat gátló gyógyszer került az orvostudomány fegyvertárába. Ezzel szemben a fehérjék defoszforilációját katalizáló foszfatázokat célbavevő terápiák száma ma még korlátozott, annak ellenére, hogy ezen enzimek sokfélesége és számos szabályozó alegysége lehetőséget kínál a nagy specifitású beavatkozásra. Ezért munkák során elsősorban a miozin foszfatáz (MP) holoenzim szerepét vizsgáltuk, illetve annak egyik szabályozó fehérjéjét, a smoothelin-szerű 1 fehérjét (SMTNL1) helyeztük érdeklődésünk középpontjába. Az utóbbi évtizedekben született új eredmények jelentősen kiszélesítették a MP-zal kapcsolatos ismereteinket. Fény derült arra, hogy ez az enzim nemcsak a simaizomban expresszálódik, hanem a szervezet megannyi szövetében is megtalálható. Változatos szubcelluláris lokalizációja lehetővé teszi, hogy az izomösszehúzódáson kívül számos eddig még kevésbé ismert sejtélettani folyamatban vegyen részt. Munkcsoportunk vizsgálatai alapján megállapítható, hogy a MP és SMTNL1 fehérjék egymással együttműködve szerteágazó biológiai folyamatban játszanak meghatározó szerepet. Értekezésemben ezeket a jelátviteli folyamatokat szeretném bemutatni az alapvető molekuláris mechanizmusoktól az orvosi szempontból fontos patofiziológiai elváltozásokig.

2. IRODALMI ÁTTEKINTÉS

2.1. Poszttranszlációs módosítások funkcionális diverzitása

Az elmúlt néhány évtized kutatásai alapján világossá vált, hogy az emberi proteom komplexitása túlmutat a human genomén. Míg a becslések szerint az emberi genom 20 000-25 000 fehérjét kódoló gént tartalmaz, addig az emberi proteomban található fehérjék száma a poszttranszlációs módosítások figyelembevételével ennek akár hússzorosa is lehet [8]. A genomi rekombináció, az alternatív promótereken történő transzkripció, a transzkripció eltérő terminációja és a transzkriptum alternatív szerkesztésén kívül a komplexitást a genom szintjétől a proteom szintjéig a fehérjék poszttranszlációs módosításai (PTM) még tovább növelik [9]. A PTM-ek olyan kémiai módosítások, amelyek kulcsszerepet játszanak a funkcionális proteomikában, mivel szabályozzák az aktivitást, a lokalizációt és a kölcsönhatást más biomolekulákkal, például fehérjékkel, nukleinsavakkal, lipidekkel és kofaktorokkal.

Az emberi proteom dinamikus, számos ingerre reagálva folyamatosan változik. Az eukarióta élőlények a poszttranszlációs módosításokat nagyon gyakran alkalmazzák a sejtaktivitás szabályozására. A PTM-ek különböző aminosav-oldalláncokon vagy a peptidkötéseken következnek be, és leggyakrabban enzimatikus reakciók közvetíti őket. Becslések szerint a proteom 5%-a olyan enzimeket tartalmaz, amelyek több mint 200 féle poszttranszlációs módosítást végeznek [10]. Sok fehérje képes önmagát is módosítani autokatalitikus domének, például autokináz és autoprotolitikus domének segítségével [11].

A fehérje PTM-ek a módosítás jellegétől függően megfordíthatók is lehetnek, így például a protein kinázok a fehérjéket specifikus aminosav-oldalláncokon foszforilálják, ami a katalitikus aktiválás vagy inaktiválás gyakori fiziológiás mechanizmusa. Ezzel szemben a protein foszfatázok hidrolizálják a foszfátcsoportot, és visszafordítják a biológiai változást [12]. Ezzel ellentétben például a peptidkötések proteolítikus hasítása termodinamikailag kedvező, irreverzibilis reakció [13]. Következésképpen a fehérjék poszttranszlációs módosulásainak elemzése különösen fontos a fiziológiai folyamatok és a kóros elváltozások mint a szívbetegségek [14], a rák [15], a neurodegeneratív betegségek [16] és a cukorbetegség [17] megértése szempontjából. Bár a PTM-ek jellemzése nagy kihívást jelent, elvitathatatlanul fontos betekintést nyújt az etiológiai folyamatok hátterében álló sejtfunkciókba.

2.2. A fehérjék reverzibilis foszforilációja

Az eukarióta szervezetek legelterjedtebb szabályozási mechanizmusa a fehérjék foszforilációja és defoszforilációja. A foszforilációt a protein kinázok katalizálják, úgy hogy a nukleozid-trifoszfátok (leggyakrabban ATP) terminális foszfátcsoportját kovalens kötéssel hozzákapcsolják a fehérjék szerin (Ser), treonin (Thr) vagy tirozin (Tyr) oldallánhoz. A foszforiláció megfordíthatóságát a protein foszfatázok (PP) biztosítják a fehérjékben észterkötéssel kapcsolódó foszfátcsoportok hidrolízisével. A fehérjékhez kötött foszfátcsoport negatív töltése különféle szerkezeti változásokat indukálhat, amelyek befolyásolhatják a fehérje-fehérje vagy a fehérje-ligandum kölcsönhatások erősségét, a fehérje vízoldékonyságát és membrán-permeabilitását, illetve a fehérje stabilitását és biológiai aktiválását. Egy adott célfehérje foszforiláltságát a kinázok és a foszfatázok együttesen határozzák meg és ily módon közösen szabályozzák egyes jelátviteli útvonalak aktiválódását vagy deaktiválódását.

A protein kinázok szabályozó szerepének első leírása Edmond Fisher és Edward Krebs nevéhez köthető, akik 1955-ben felfedezték, hogy a glikogén lebontása során az inaktív foszforiláz *b* enzimet aktív *a* formába konvertáló enzim nem más, mint a foszforiláz kináz. Később az 1960-70-es években azonosították a cAMP és Ca^{2+} másodlagos hírvivőket, amelyek hatását a protein kinázok aktivitásának változásával hozták összefüggésbe. A glikogén szintézis és lebontás, a lipid- és piruvát anyagcsere, valamint koleszterin bioszintézis szabályozásáért egyértelműen a fehérjék foszforilációs változásait tették felelőssé [18]. Azonban egészen az 1970 évek végéig a folyamatok reverzibilitásáért felelős protein foszfatázokat csak „háztartási" segédenzimeknek tekintették. Az áttörés az 1980-as évek elején történt, amikor a 35 kDa méretű protein foszfatáz katalitikus alegységeket tisztításával lehetővé vált a foszfatázok biokémiai és molekuláris szintű jellemzése. Ezzel megkezdődött a foszfatáz-kutatás "aranykora", amikor is számos humán, gomba és növényi foszfatáz enzimet írtak le [12; 19; 20].

Az eukarióta sejtekben fellehető, kovalensen fehérjékhez kapcsolódó foszfátcsoportok több mint 99%-a szerin (Ser) vagy treonin (Thr) aminosav oldalláncon található [21]. Ez a mennyiségi túlsúly azonban nem jelenti azt, hogy a Tyr oldallánc foszforilációja nem jelentős, ugyanis a Tyr kinázok alapvető szerepet játszanak a jelátvitel elindításában [22]. Míg az emberi szervezetben található hozzávetőlegesen 450 protein kináz katalitikus alegység egyetlen közös ősre vezethető vissza, a protein foszfatázok nagyon sokfélék, minden bizonnyal konvergens evolúció révén alakultak ki. A humán protein foszfatáz katalitikus alegységet kb.150 gén kódolja;

ezek között mintegy 40 Ser/Thr specifikus protein foszfatáz található [23]. A protein foszfatáz katalitikus alegységek viszonylag kis számát a katalitikus alegyégekkel holoenzimet alkotó szabályozó alegységek kompenzálják. Az foszfatázok kombinatórikus természete nagyszámú holoenzim kialakulását eredményezi [24]. A szabályozó alegységek a holoenzim szubsztrát-specificitását, valamint katalitikus aktivitását határozzák meg, a katalitikus alegységhez illetve az enzimeket különböző szubcelluláris kompartmentekhez irányítják.

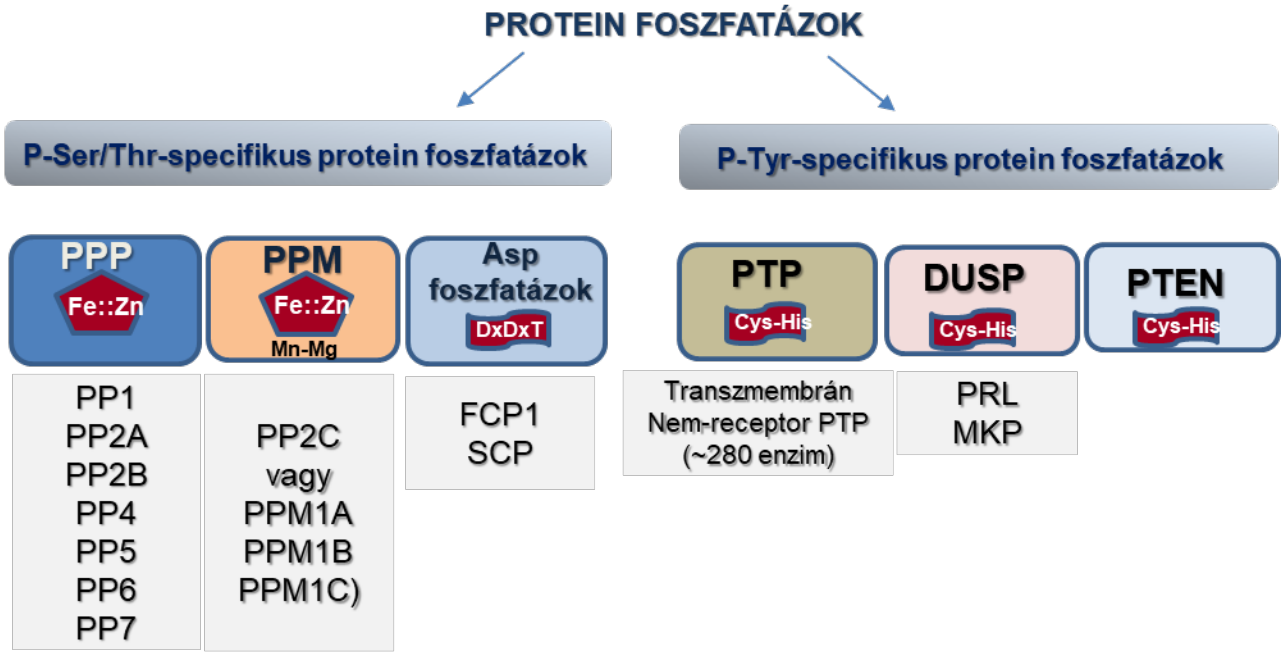
2.3. A protein foszfatázok osztályozása

A hőskorszakban, a 1980-as évek elején az eukarióta Ser/Thr protein foszfatázokat a tisztított katalitikus alegységek enzimológiai sajátságai alapján két csoportba, 1-es és 2-es típusba osztották. Ezek szerint az 1-típusba tartozó PP1 foszfatáz a foszforiláz kináz β alegységét defoszforilálja, míg a 2-es típusú protein foszfatázok (PP2A, PP2B, PP2C) elsősorban az α alegységet preferálják [20]. További osztályozását tett lehetővé a kis molekulatömegű hőstabil inhibitorok iránti érzékenységük: míg az inhibitor-1 (I-1) és inhibitor-2 (I-2) fehérjék, valamint a heparin gátolják a PP1 enzimcsalád tagjait, addig ezek az anyagok a 2-es típusú protein foszfatázokra nem fejtenek ki jelentős gátló hatást [25; 26]. Fémion igényük szerint a 2-es típusú foszfatázokat további három alcsoportba sorolták: míg a PP2A aktivitásához nem igényel fémiont, addig a PP2B – vagy más néven a kalcineurin (CN) – Ca^{2+}/kalmodulin-függő enzim, míg a PP2C aktivitásához Mg^{2+}-ion szükséges [20; 27]. A 2-es típusú foszfatázok az okadánsavval szemben mutatott érzékenységük alapján is elhatárolhatóak: ez a toxin a PP2A enzimcsalád tagjait nanomoláris koncentrációban gátolja, míg szinte hatástalan a PP2B enzimcsalád tagjainak aktivitására [28; 29]. Ez a kezdetleges osztályozás még nem vehette figyelembe a katalitikus alegységek szerkezetét és evolúcióját. A katalitikus alegységek klónozása és aminosav sorrendjük meghatározása után kiderült, hogy a PP2A és a PP2B filogenetikailag sokkal közelebb állnak a PP1-hez, mint a PP2C enzimekhez [25] (*1. ábra)*.

Továbbá a fentiekben leírt szempontrendszerek szerint nem besorolható tulajdonságú újabb Ser/Thr specifikus protein foszfatáz enzimek felfedezése is szükségessé tette az eredeti osztályozás felülvizsgálatát [12]. Az első ilyen „új típusú” protein foszfatáz a PPX volt, amely a nevezéktanba, PP4 néven került be. A PPX 45%-ban hasonló a PP1-hez és 65%-ban a PP2A-hoz, tehát filogenetikailag az utóbbihoz áll közelebb [30]. A későbbiekben a PP5 [31], a PP6 [25] és a PP7 [32] enzimcsaládokat is azonosították és jellemezték [12]. A Ser/Thr specifikus protein

foszfatázokat tehát filogenetikai szempontból két nagy csoportba sorolhatjuk, melyek két különböző géncsalád tagjai [33].

Az újabb Ser/Thr specifikus enzimek, illetve a Tyr-specifikus foszfatázok felfedezése után azt mondhatjuk, hogy a protein foszfatázok 6 fő családra bonthatók [18] (*1. ábra)*.



1. ábra. A protein foszfatázok csoportosítása.

A foszfoprotein foszfatázok (PPP) családjának tagjai aktív centrumokban Fe^{2+}-Zn^{+} ionokat tartalmaznak, akárcsak a fémion-függő foszfatázok (PPM) családtagjai. Az utóbbiak azonban ezen kívül Mn^{2+} vagy Mg^{2+} fémionokkal igényelnek az aktivitásukhoz. Az aszpartát foszfatázok aktív centrumában egy DxDxT motívum található [34]. A PPP családba sorolják a protein foszfatáz 1 (PP1), protein foszfatáz 2A (PP2A), kalcineurin (CN vagy PP2B), PP4, PP5, PP6 és PP7 enzimeket, valamint a molekuláris biológiai módszerekkel felismert „új típusú" foszfatázok különleges képviselőit [34] [35]. Ezek közül kiemelkedően fontosak a PP1 és PP2A enzimek, amelyek a sejtekben viszonylag nagy koncentrációban fordulnak elő és számos esszenciális biológiai folyamatot szabályoznak. A Tyr-specifikus foszfatázok (PTP) családjának tagjai aktív centrumukban Cys aminosavat tartalmaznak. A Tyr-specifikus foszfatázok közé tartoznak a protein tirozin foszfatázok (PTP), a Ser, Thr és Tyr oldalláncokat is defoszforiláló úgynevezett kettős specificitású foszfatázok (Dual Specificity Protein Phosphatase, DUSP), illetve a protein

foszfatázokkal távoli filogenetikai rokonságban álló lipid foszfatázok (mint a PIP foszfatázok és Phosphatase and Tensin homolog; PTEN) [36].

A PPM foszfatázokat ma PPM1 névvel jelöljük, és izoformáit nagybetűvel különböztetjük meg (A, B, C, D stb.). Az emlősökben a PPM-foszfatázoknak 20 izoformája van, pl. PPM1A, PPM1B, stb. A toxinok, (például OA, MC és CLA) gátlásával szembeni teljes rezisztencia és a PPM1A kristályszerkezete megerősítette, hogy ezek a foszfatázok a PPP családtól eltérő külön fehérje szupercsaládot alkotnak [37]. A PPM-család tagjai konzervált katalitikus régióval rendelkeznek, amely a a PPP enzimekhez hasonló felépítésű [38]. A különböző izoformák specifikus régiói részt vehetnek a szubsztrát felismerésben és/vagy a foszfatázok funkcionális szabályozásában. Számos kis molekulatömegű inhibitorukat jellemezték már, de izoforma szelektivitást mutató inhibitort eddig nem találtak. Ezek az inhibitorok az általuk okozott káros mellékhatások miatt nem kerültek terápiás használatba. Legismertebb közülük a Sanguinarine (SNG), ami a PPM1A és PPM1B potenciális gátlószere [39].

2.4. A protein foszfatáz 1 holoenzimek szerkezete

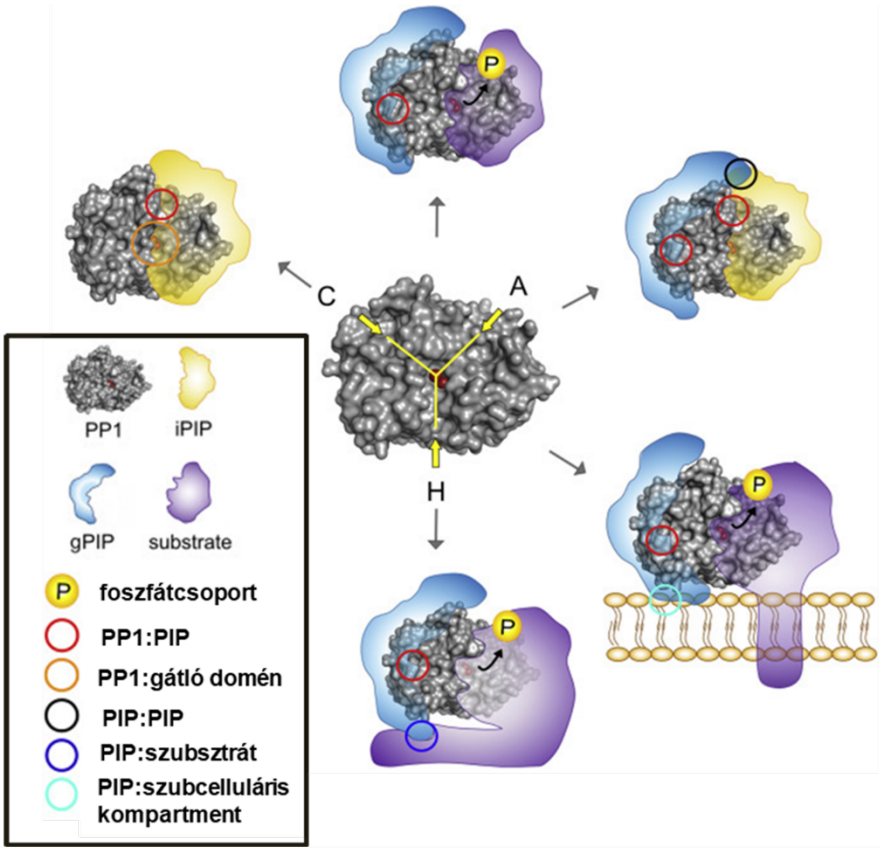
2.4.1. A protein foszfatáz 1 katalitikus alegysége

A protein foszfatáz 1 (PP1) holoenzimek katalitikus alegységből (PP1c) és egy vagy több szabályozó alegységből állnak. A PP1c (35-38 kDa) az egyik legkonzerváltabb eukarióta fehérje. A PP1 a foszfohidrolázok olyan nagy szupercsaládjának a tagja, amely mindhárom nagy filogenetikai csoportban (eubaktériumok, archeák és eukarióták) jelen van [40]. Az emlősökben három PP1 katalitikus alegységet kódoló gén van: PP1cα, PP1cγ és PP1cβ/δ [41]. A PP1cγ izoformának két alternatív splicing-gal képződő variánsa ismeretes: a PP1cγ$_1$ és a PP1cγ$_2$ [19; 42; 43]. A PP1cα–nak szintén két splice variánsa van, a PP1cα$_1$ és PP1cα$_2$ [44]. A variánsok létezését a humán transzkripom szekvencia elemzése is alátámasztotta (Ensembl, ENSP0000176139). A PP1cγ$_2$ csak a tesztiszben és agyban expresszálódik, a többi izoforma minden szövetekben általánosan előfordul, de eltérő sejten belüli lokalizációt mutat [45].

A PP1c szerkezetét a foszfát analóg wolframáttal [46], a mikrocisztin inhibitorral [47], a glikogén-kötő alegység rövid peptidszakaszával [48] és a MYPT szabályozó alegység N-terminális peptidjével [7] együtt kristályosítva Rtg diffrakcióval határozták meg. A fehérje N- és C-terminális szubdoménokra tagolható. Az N-szubdomén kompakt szerkezetű, Y-alakú katalitikus

árka magába foglalja az aktív centrumot annak két esszenciális fémionjával együtt. A katalitikus árok három ága, a C-terminális, a hidrofób-, illetve a savas-árok közül az utóbbi kettőnek van jelentősége a szubsztrátok kötésében. A PP1c izoformák aminosav szekvenciájának hasonlósága közel 90 %-os. A PP1 holoenzimek változatos szubsztrátspecifitása arra utal, hogy elsősorban a szabályozó alegységek azok, amelyek meghatározzák a PP1 funkcióinak tág spektrumát (*2. ábra*).

A PP1c katalitikus aktivitását a hozzá kötődő inhibitor fehérjék mellett mikroorganizmusok és rovarok által termelt sejtpermeábilis toxinok is gátolhatják. Ilyen például a mikrocisztin LR, egy ciklikus hexapeptid, ami részben a két fémion által kötött vízmolekulával lép kapcsolatba, valamint a hidrofób árokban kötődve lefedi a katalitikus centrumot is, és így gátolja a foszfoszubsztrát kötődését és hidrolízisét [49]. A mikrocisztin okozta gátlás irreverzibilis, ugyanis a mikrocisztin kovalens kapcsolatot is létesít a katalitikus alegységgel, bár ez a kötés a gátlásnak nem előfeltétele. A poliéter okadánsav (OA) a hidrofób árokhoz kötődik, és hidrogén-kötést alakít ki a Tyr-272-vel, amely a katalitikus centrum része [50]. A PPP foszfatázokat gátló toxinok között említhetők még a tautomicin (TM) [51], tautomicetin (TMC) [52], fostreicin, kalikulin A (CLA) [53] és egyéb lipidoldékony inhibitor molekulák, így a ciklosporin A (CsA) vagy FK506) [54], amelyek szintén a sejtmembránon átdiffundálva különböző specificitással gátolják az endogén defoszforilációs folyamatokat [55]. Az OA csak nagy koncentrációban gátolja a CN-t, viszont hatékony, de eltérő gátló hatást fejt ki a PP2A-ra (IC50 ~ 0,2-0,3 nM) és a PP1-re (IC50~ 10- 100 nM) *in vitro*. A CN specifikus gátlószerei a CsA és az FK506. A foszfatázgátló toxinok bizonyos koncentráció tartományban sejtkultúrákban is alkalmasak lehetnek specifikus gátlás létrehozására. Így pl. a sejtek 50 nM CLA vagy 1 μM TM kezelése a PP2A vagy a PP1 specifikus gátlását okozza, tehát ezzel a két foszfatáz által befolyásolt defoszforilációs folyamatok intracelluláris szinten is elkülöníthetők [56].



2. ábra A PP1 holoenzimek szerkezete. *A PP1 katalitikus doménjének felületi ábrázolása (középen). A PP1 aktív centruma két fémiont (piros gömbök) tartalmaz, amely három szubsztrátkötő árok Y alakú metszéspontjában helyezkedik el: a savas árok (A), a C-terminális árok (C) és a hidrofób árok (H). Az r PP1-inhibitor fehérjék (PIP) (iPIP) sárgával, a célra irányító PIP fehérék (gPIP) kékkel, a szubsztrátok pedig lilával vannak ábrázolva. A terápiás célok szempontjából fontos kölcsönhatási helyeket színes körök ábrázolják. A hajlított fekete nyilak a szubsztrát defoszforilációját jelzik. A PP1 felszíni struktúrája PyMOL (www.pymol.com) segítségével készült. A PIP-ek és a szubsztrátok sematikusan helyezkednek el a PP1-en. PP1, protein-foszfatáz 1; PIP, PP1-el interakcióban lévő fehérje. Módosított Ferreira és mtsai [3]*

2.4.2. A protein foszfatáz 1 szabályozó alegységei

A PP1c túltermeltetése citotoxikus hatású ezért a szabad katalitikus alegység a sejtben legfeljebb rövid ideig átmenetileg létezhet, sokkal inkább különböző szabályozó alegységekhez kapcsolódva holoenzim formában fordul elő. Eddig közel 200 szabályozó alegységet írtak le, de a humán genom szekvencia elemzése alapján még számos további potenciális PP1-kötő fehérje prediktálható [40].

A protein kinázokkal összehaonlítva a Ser/Thr protein foszfatázok katalitikus doménjei viszonylag alacsony specifitásúak, így a protein kinázokkal ellentétben csak kismértékben képesek arra, hogy konzenzus aminosavszekvenciák alapján kössék meg a szubsztrátokat. A PP1c katakitikus alegység működését a szabályozó elegységek célfehérjékkel való kölcsönhatása

szabályozza [24]. Ezek a szabályozó alegységek az PP1c-vel kialakított kölcsönhatásuk révén képesek a holoenzimet a sejt különböző régióiba lokalizálni és módosítani annak szubsztrátspecificitását [57]. Továbbá a PP1-specifikus gátló fehérjék, mint például az Inhibitor-2 (I-2), kinase-enhanced protein phosphatase type 1 inhibitor (KEPI) [58] és a dopamine- and cAMP-regulated neuronal phosphoprotein (DARPP-32), blokkolják a PP1 aktív centrumát [59; 60]. A legtöbb PP1 szabályozó fehérje és néhány PP1 szubsztrát egy elsődleges PP1-kötő motívumon, az RVxF motívumon keresztül lép kölcsönhatásba a PP1c-vel, amely általában megfelel a [K/R][K/R][V/I][x][F/W] konszenzus szekvenciának, ahol x a Phe, Ile, Met, Tyr, Asp vagy Pro kivételével bármely más aminosavmaradék lehet [61; 62]. Bár az RVxF kölcsönhatás szükséges a szabályozó fehérje kötődéséhez, közvetlenül nem befolyásolja a PP1c enzimatikus aktivitását, mivel 20 Å távolságra van az aktív centrumtól. Újabban további szabályozó alegység dokkolóhelyeket is azonosítottak, mint például a SILK és MyPhoNE motívumok, amelyek szintén hozzájárulnak a PP1 aktivitásának és szubsztrátspecificitásának szabályozásához [62].

A PP1 fiziológiai szubsztrátjai a katalitikus alegységhez való kötődésük alapján két csoportba sorolhatók [24]. Egyes szubsztrátok (pl. a tumorszuppresszor BRCA1) nagy affinitású PP1-dokkolóhelyekkel rendelkeznek, és stabil heterodimer komplexeket alkotnak a foszfatázzal, akár defoszforilált állapotban is. Ezzel szemben más szubsztrátok (pl. glikogén-foszforiláz) csak gyenge kölcsönhatást alakítanak ki a katalitikus alegységgel [63]. A szubsztrátok hatékony *in vivo* defoszforilációjához olyan PP1-kölcsönható fehérjékre (PIP) van szükség, amelyek további szubsztrát-dokkolóhelyeket biztosítanak, vagy növelik a helyi szubsztrátkoncentrációt a foszfatáz adott kompartmenthez való kötésével. Ezek alapján a PP1 enzimek szubsztrátspecificitása egyértelműen a foszfatázt dokkoló motívumoktól és az ezekhez kapcsolódó célzó alegységektől függ [64].

2.5. A miozin foszfatáz

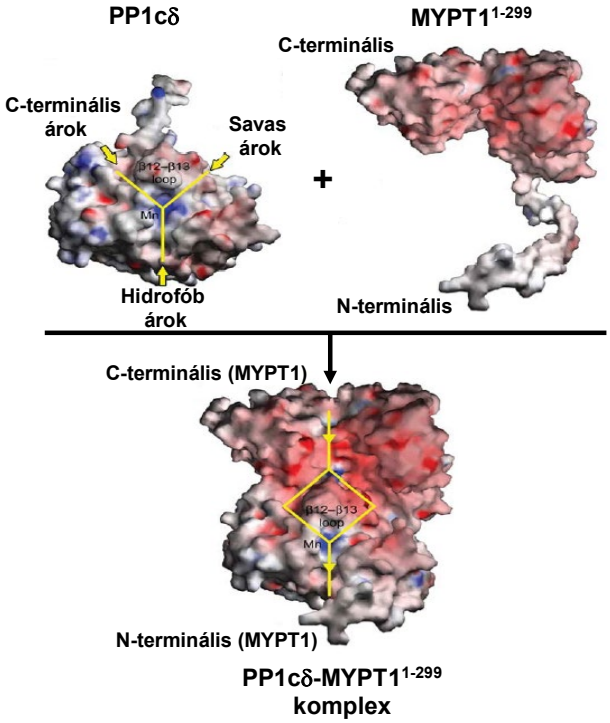
2.5.1. A miozin foszfatáz szerkezete

A miozin foszfatáz (MP) holoenzim egy foszfo-Ser/Thr-specifikus foszfatáz, amely a protein foszfatáz-1 (PP1) enzimcsalád tagja. Heterotrimer szerkezetű: a defoszforilációt katalizáló PP1c β/δ katalitikus alegységből, egy 130/133 kDa molekulatömegű miozin foszfatáz célra irányító alegységből (myosin phosphatase targeting subunit, MYPT1) és egy jelenleg még ismeretlen funkciójú 20 kDa molekulatömegű alegységből épül fel [65]. A miozin foszfatázt

először Dario Alessi és munkatársai izolálták csirkezúzából, és igazolták, hogy defoszforilálja a 20 kDa miozin könnyű láncát (MLC20), ami a simaizom relaxációját segíti elő [66]. Néhány évvel később a miozin foszfatázt sikerült tisztítani emlős szövetekből; sertés húgyhólyagból [67] és patkány aortából is [68], továbbá kimutatták egy hosszabb (133 Da) és rövidebb (110-130 kDa) MYPT1 izoforma létezését is. A miozin foszfatáz nevezéktana a szakirodalomban nem egységes, így különböző rövidítéseit ismerjük, például MP, MLCP vagy PP1M. Emellett az enzimet korábban M110-nek, myosin binding subunit-nak (MBS) és M130/M133-nak is nevezték [2]. Az értekezésben a MP-t rövidítést használom, valamint a Humán Genom Projekt nevezéktana szerint a PP1cβ/δ (PPP1CB) és a MYPT1 (PPP1R12A) rövidítéseket alkalmazom a katalitikus alegység és a 130-133 kDa fő szabályozó alegység elnevezésére .Megállapítást nyert, hogy a három fő PP1c izoforma (α, β/δ, γ1) közül az emlős sejtekben a MYPT1 kizárólag a PP1cβ/δ izoformával lép kölcsönhatásba [69]. Azt is tudjuk, hogy a M20/21 alegység a MYPT1 C-terminális régiójához kötődik, és nem befolyásolja a foszfatáz aktivitását [70]. A MYPT1 regulátor alegység a MYPT fehérjecsaládba tartozik, melynek további tagjai a MYPT2, a MYPT3, a 85 kDa molekulatömegű miozin kötő alegység (MBS85), illetve a TGFβ által gátolt membránasszociált fehérje (TIMAP). Közös jellemzőjük, hogy N-terminális régiójukban mindegyikük tartalmazza a PP1c-kötő RVxF motívumot, majd ezt egy ankirin-ismétlődéskeből álló régió követi. A MYPT1, MYPT2 és az MBS85 C-terminális végén egy leucin cipzárt is hordoz, ami a dimerizációban és a fehérje-fehérje kölcsönhatások kialakításában játszik szerepet [71].

Mivel a miozin foszfatáz felépítésében a MYPT1 vesz részt, ezért ennek a fehérjének a szerkezetét és funkcióját ismertetem részletesebben (*3. ábra*). A MYPT1 N-terminális régiójában tartalmaz egy konszenzusos RVxF PP1c-kötő motívumot (K35VKF38), amely úgy tűnik, hogy elengedhetetlen a MYPT1-PP1c kölcsönhatás kialakításában [72]. Emellett további fehérje kötő helyeket írtak le (*lásd 4. ábra*); ezek az N-terminális régióban a MYPT1$^{10–17}$ miozin foszfatáz N-terminális elemnek vagy MyPhoNE-nak nevezett motívum; az ankirin ismétlődő régió 1, 5, 6 és 7 eleme [7]; valamint a 301 és 511 aminosav maradékok közötti savas régió(k) [73].

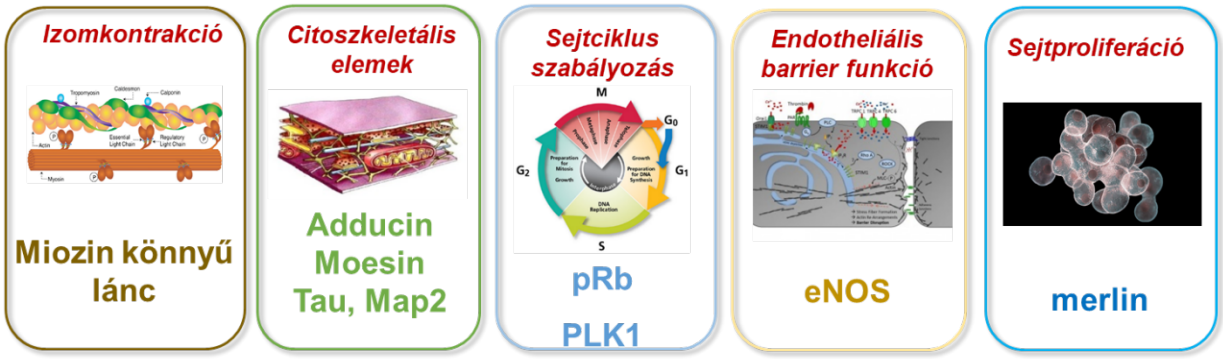
A MYPT1 regulátor alegység kötődése módosítja a PP1cδ szubsztrát-specificitását és aktivitását. A MP holoenzim mintegy 10-15-ször nagyobb aktivitással defoszforilálja a foszforilált miozint, mint a szabad katalitikus alegység [74].



3. ábra. A PP1cδ–MYPT$^{1-299}$ komplex elektrosztatikus felszín megjelenítése. *Módosítva [7]*

2.5.2.A miozin foszfatáz szubsztrátjai és élettani szerepe

A miozin foszfatáz elsőként azonosított szubsztrátja a 20 kDa molekulatömegű miozin könnyű lánc (MLC20), amelynek foszforilációját követően a miozin II kötődik az aktinhoz, és így az aktomiozin komplex kontrakcióját indukálja. Ezt ellensúlyozza a MP által katalizált defoszforiláció, ami elernyedéshez vezet [65]. Az MLC20 foszforiláltsági szintjét a Ca^{2+}/kalmodulin-függő miozin könnyű lánc kináz (MLCK) és a MP aktivitások közötti viszony határozza meg (4. *ábra*). A MP további citoszkeletális szubsztrátjai az ERM (ezrin, radixin, moezin), szerkezetileg rokon citoszkeletális fehérjecsalád tagjai [75; 76], amelyek összekötőként működnek a transzmembrán fehérjék és a citoszkeleton között, és számos sejtfunkciót töltenek be a sejtadhézióban, a migrációban vagy a proliferációban. Az inaktív ERM fehérjék zárt konformációban a citoszolban találhatóak, de konzervált treonin oldalláncukon történő foszforilációjuk (amit a Rho A-aktivált kináz (ROK) vagy PKC katalizál) indukálja a nyitott és



4. ábra. Az MP szubsztrátjai és élettani szerepük. *Polo-like kinase 1 (PLK1); Retinoblasztoma fehérje (pRb), endotheliális nitrogén monoxid szintáz (eNOS)*

aktív konformáció kialakulását, amely lehetővé teszi számukra, hogy kötődjenek a célmolekulákhoz [77]. A mikrotubulusokhoz kapcsolódó fehérjék, a Tau és a MAP2 szintén kölcsönhatásba lépnek a ROK-zal és a MYPT1-gyel. Kimutatták, hogy a MP defoszforilálja a ROK-foszforilált Tau fehérjét *in vitro*, ami azt sugallja, hogy az MP is szabályozhatja a mikrotubulus dinamikát [78] (*5. ábra*). Az is bizonyítást nyert, hogy a MP által defoszforilált szubsztrátok foszforilációjáért az esetek többségében a ROK a felelős. A miozin és ERM foszforiláció/defoszforiláció számos simaizomhoz kötött folyamatot szabályoz, így a vaszkuláris tónust, a gasztrointesztinális motilitást, hörgőasztmát és a méhösszehúzódást is. Ezáltal szerepe van a vaszkuláris simaizom hiperkontraktilitásban, ami magas vérnyomásban, koronáriás görcsben és kisagyi érgörcsben fejeződik ki [40; 79]. Az MP azonban nemcsak a simaizmokban, hanem a szervezet számos más szövetében is expresszálódik, változatos szubcelluláris lokalizációt mutat és ezzel társulva a sejtélettani folyamatok széles körét szabályozza.

A MP egyik újonnan leírt szubsztrátja az endotheliális nitrogén-monoxid-szintáz (eNOS). Az eNOS és a MYPT1 kölcsönhatásba lép az endotélsejtekben és ezáltal az eNOS a MP szubsztrátja. A MP az eNOS Thr497 oldalláncát képes defoszforilálni. A MP gátlása csökkentette mind az endothélsejtek NO-termelését, mind a transzendotheliális rezisztenciát [80].

A klasszikus citoszkeletális szubsztrátok mellett számos más szubsztrátját is azonosították, így a sejtciklus és a proliferáció szabályozását meghatározó retinoblasztóma fehérje (pRb), polo-szerű kináz 1 (PLK1) és merlin fehérjéket is (*5. ábra*). A MYPT1 egyik figyelemreméltó sejtciklus-függő partnere a pRb, egy tumorszuppresszor. Az alulfoszforilált pRb úgy szabályozza a sejtciklust és a proliferációt, hogy az E2F transzkripciós faktort megköti és az E2F-függő gének transzkripcióját visszaszorítja. A ciklin-függő kinázok hiperfoszforilálják az pRb-t ami elősegíti a sejtciklusok progresszióját. Ismeretes, hogy a PP1 és/vagy PP2A foszfatázok felelősek a pRb

defoszforilációjáért és reaktiválásáért [81]. Leukémiás sejtekben a MYPT1-et a foszforilált pRb-re ható PP1-et célra irányító alegységként azonosították [82]. Egy másik tanulmányban a MYPT1 overexpressziója a pRb foszforilációjának csökkenését eredményezte a Ser807/811 oldalláncokon, ami arra utal, hogy az MP más szabályozó helyen is modulálhatja a pRb aktivitását [83].

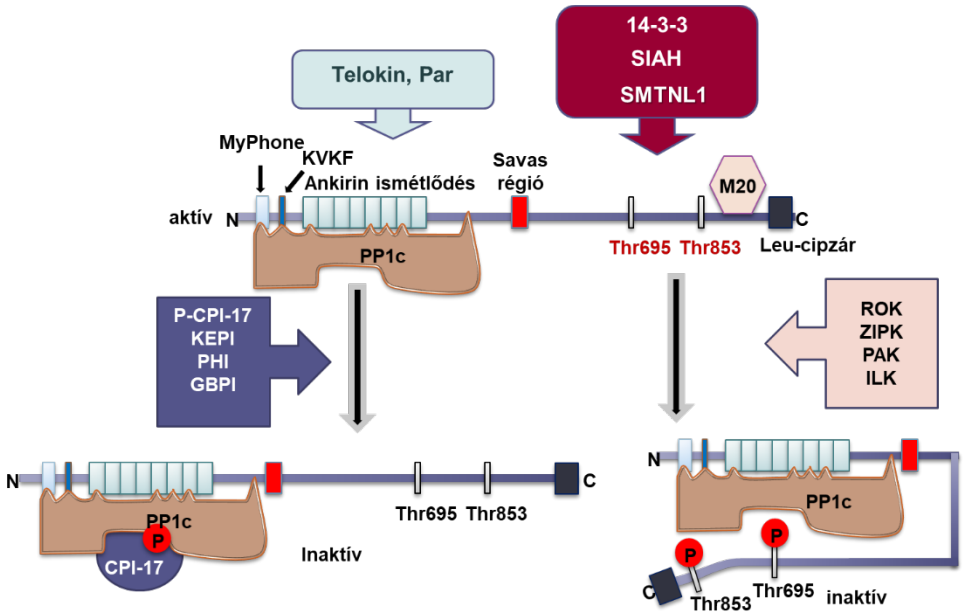
Az MP a polo-szerű kináz 1 (PLK1) defoszforilálásával a mitozis folyamatát is szabályozza. A PLK1 egy Ser/Thr kináz, amely számos mitotikus eseményt irányít, beleértve a G2/M átmenetet, a centroszómák érését, a mitotikus orsó-összeszerelést, a kromatidák szegregációját, a mitózisból történő kilépést és a citokinézist [84]. A mitozis során a foszfo-MYPT1 és a PLK1 a centromereken és a kinetokorokon lépnek egymással kölcsönhatásba [84]. Kimutatták, hogy a MYPT1 alegység a PLK1 térbeli és időbeli koordinációjával hozzájárul a mitotikus progresszió szabályozásához [85].

Az NF2 tumorszuppressor géntermék, a merlin is a MP szubsztrátja. A merlinnek az ERM-család fehérjéihez hasonló a szerkeszete, de szabályozása azokkal ellentétes: a foszforilált merlin inaktív, míg a defoszforilált forma aktív [86]. Több mechanizmuson keresztül is gátolja a sejtproliferációt, anti-mitogén jelátvitelt indít el és gátolja az onkogén génexpressziót. Az MP a merlin zárt konformációját a Ser518 oldallánc defoszforilációval aktiválja [87]. Kimutatták, hogy a MP a merlin defoszforilációját és aktiválódását közvetítő oxidatív stressz hatására aktiválódik, és ezáltal modulálja a Hippo jelátviteli útvonalat a kardiomiocitákban [88].

2.5.3. A miozin foszfatáz szabályozása

A miozin foszfatáz szabályozásának egyik lehetséges módja a MYPT1 alegységének Ser és/vagy Thr oldalláncokon történő foszforilációja. Számos foszforilációs helyet azonosítottak eddig a MYPT1 szekvenciáján belül, de a foszfatáz aktivás változást szemponjából a Thr696 és Thr853 oldalláncok foszforilációja a legjelenetősebb (5. *ábra*).

A Thr696 és Thr853 oldalláncok RhoA aktivált protein kináz által katalizált foszforilációja a holoenzim gátlását eredményezi [89]. A ROK mellett számos más kináz gátolja a miozin foszfatázt a MYPT1 Thr696 oldalláncának foszforilációjával, így a leucin cipzár motívummal kölcsönható protein kináz (ZIPK), integrinhez kötött kináz (ILK)[65], miotónusos disztrófia protein kináz, Raf-1 [90] és a p21-aktivált protein kináz enzimek [71]. A MYPT1 Thr696Ala és Thr853Ala mutánsait felhasználva azt is megállapították, hogy a Thr696 vagy Thr853



5. ábra. Az MP szerkezete és szabályozása. *Az ábra felső része a MYPT1 főbb szerkezeti régióit és a PP1c-vel valamint az M20/21alegységgel való kölcsönhatását ábrázolja. Az alsó rész az MP gátlását mutatja a MYPT1 szabályozó alegységének Thr696 és Thr853 oldalláncokon történő foszforilációjával -(jobbra). Alul a foszforilált CPI-17 okozta gátlás sémája is látható (balra). Az MP-aktivitás foszforilációtól függő szabályozásának további részleteit lásd a szövegben.[2]*

foszforilációja okozza a PP1c gátlását [91]. A jelenleg elfogadott hipotézis szerint ezeknek a helyeknek a foszforilációja olyan szerkezeti elmozdulást idéz elő a MYPT1-ben, amely lehetővé teszi, hogy a MYPT1-ben található gátló foszforilációs peptid kölcsönhatásba lépjen a PP1c szubsztrátkötő árkával és katalitikus centumával (5. *ábra*). Ezeket a konformációs változásokat elősegítheti a MYPT1 C-terminális régióinak feltételezett, részben rendezetlen szerkezete.

A cdc2 kináz foszforilálja a MYPT1 Thr435 és/vagy Ser432 oldalláncát, ami megnöveli a MP miozin iránti affinitását [2]. Ezzel szemben a MYPT1 Ser445, Ser472 és Ser910 oldalláncokon a foszfatáz gátlását, a miozin emelkedett foszforilációját és a sejtek tapadásának gyengülését eredményezi. A már ismertetett Thr696 és Thr853 gátló foszforilációs helyek előtt található a Ser695 és a Ser852 oldalláncok is foszforilálhatók a cAMP- és cGMP-függő protein kinázokkal (PKA és PKG). A PKA vagy PKG-függő Ser695 foszforiláció gátolja a Thr696 foszforilációját ROK, vagy más MYPT1 kináz által, megakadályozva ezzel a MP gátlását [92]. Fontos kérdés az MP szabályozásával kapcsolatban annak reverzibilitása. Így pl. a gátlás "visszafordításában" MYPT1 foszfatázoknak van szerepe, és számos közlemény bizonyította, hogy az izolált PP1c, PP2A katalitikus alegység (PP2Ac), a PP2A holoenzimek és a PP2B is részt vehet a foszfo-Thr696 és -Thr853 defoszforilációjában [80; 93] (*5. ábra)*.

A MP holoenzim szabályozása kölcsönható fehérjékkel kialakított kapcsolaton keresztül is megvalósulhat. Az inhibitor-1 (I-1) és inhibitor-2 (I-2) kisméretű, PP1-et gátló hőstabil fehérjék, amelyek a szabad PP1 katalitikus alegységhez kötődve csökkentik annak aktivitását, de a holoenzimeket csak kisebb mértékben gátolják. Ezzel szemben a 17 kDa (CPI-17) C-kináz-függő foszfatáz inhibitora (CPI-17) fehérje nagy hatékonysággal gátolhatja mind a PP1c, mind az MP (PP1c-MYPT1 komplex) aktivitását, és bár nem tartalmaz kanonikus PP1c-kötő motívumot, a PP1c-vel és a MYPT1-gyel is szoros interakciót hoz létre [94]. A CPI-17 család másik tagja, a C kináz által aktivált PP1 inhibitor (KEPI), hasonló gátló hatással bír. A KEPI egyaránt gátolja A PP1c- és a MP-t [56], és foszforilációját, valamint gátló hatását az MP-re THP-1 sejtekben is leírták [93]. Egyéb CPI-17 családtagok: a foszfatáz holoenzim inhibitor-1 és -2 (PHI-1 és -2) és a gyomor-bél-és agy-specifikus PP1 inhibitor (GBPI), amelyek PP1c-kötő RVxF motívumot tartalmaznak, és gátló foszforilációs szekvenciájuk nagymértékű hasonlóságot mutat a CPI-17-hez [27]. A 14-3-3β citoszkeletális átrendeződést elősegítő fehérje, a MYPT1-hez kapcsolódva csökkenti annak miozinhoz való kötődését és a MP miozinról történő disszociációját eredményezi, ami a miozin könnyű lánc fokozott foszforilációjához vezet. A telokin MYPT1 kölcsönható fehérje aktiválja az MP-t anélkül, hogy megváltoztatná a MYPT1 Thr696 vagy Thr853 oldalláncok foszforilációját [95]. A telokin egy 17 kDa fehérje, amely a miozin könnyűlánc-kináz C-terminális doménjét tartalmazza [96], és a fázisos simaizmokban nagymértékben expresszálódik [97]. A telokinnak nincs kináz aktivitása, és a MP-t aktiváló mechanizmusa még nem ismert. A tumorszuppresszor prosztata apoptózisválasz (Par-4) fehérjéről szintén kiderült, hogy fokozza a MP aktivitását. Érrendszeri simaizomsejtekben a Par-4 kolokalizálódik az aktin filamentumokkal [98], és közvetlenül kötődik a MYPT1-hez. A Par-4 fehérjével kialakított kapcsolat gátolja a ZIPK hozzáférését a MYPT1 gátló foszforilációs helyeihez, így aktív állapotban tartja a MP holoenzimet [99] (*5. ábra*).

A közelmúltban azonosítottuk a MP egy új gátló fehérjét, a smoothelin-szerű 1 fehérjét (SMTNL1), amely a simaizom összehúzódásában játszik szerepet (*6. ábra*). Az SMTNL1 az izomfehérjék smoothelin családjának tagja, és egy C-terminális kalponin homológia (CH) domént tartalmaz [100]. Az SMTNL1 közvetíti a sima- és vázizomzat nemtől függő, edzés által kiváltott adaptációit [101] és gátolja a miozin-foszfatáz aktivitást [102]. Az SMTNL1 fehérje jellemzőit és a MYPT1-re és MP-re kifejtett hatását később részletezem (ld. a “Smoothelin-like 1 protein (SMTNL1)” fejezetet).

Az MP szabályozásában mindezek mellett a MYPT1 alegység foszforilációtól eltérő poszttranszlációs változásai is szerepet játszhatnak. Így például a MYPT1 alegységet az aszparaginil hidroxiláz gátló hypoxia-indukált faktor hidroxilálja az ankirin ismétlődések régiójában. A módosítás fiziológiai jelentősége még nem teljesen jellemzett, de a kíséreti eredmények az sugallják, hogy szabályozhatja a HIF/hypoxia modulált jelátviteli pályát [103]. Emellett a MYPT1 alegységet a hiszton lizil metiltranszferáz (SETD7) metilálja a Lys442 oldalláncán, és a folyamat reverzibilitását a hiszton demetiláz LSD1 biztosítja. Daganatos sejtekben a fokozott demetiláció miatt a MYPT1 stabailitása csökken, ami a MYPT1 ubiquitin-proteaszómális útvonalon történő lebomlását eredményezi. Ennek következtében a retinolasztóma fehérje foszforilációja megnő, ami a sejtciklus beindulását okozza [83]. A MYPT1 proteoszómális degradációját a Seven in absentia homolog 2 (SIAH2) E3-ligáz is elősegíti [104]. Végül a kaszpáz-3 a MYPT1 C-terminális régióját hasítja (Asp884), ezáltal fokozza a Thr696 és Thr853 gátló foszforilációját [105] (*5. ábra)*.

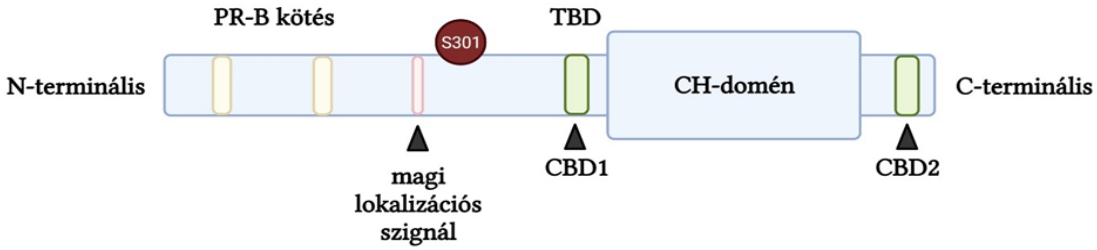
2.6. A smoothelin fehérjék és az SMTNL1

A miozin foszfatáz egyik lehetséges szabályozó fehérjéje a smoothelin-szerű 1 fehérje (SMTNL1), a simaizomra jellemző smoothelin (SMNT) fehérjecsalád tagja. Ebbe a családba tartozik még a smoothelin A (SMTN-A) és smoothelin B (SMTN-B), valamint egy smoothelin-szerű 2, ismeretlen funkciójú fehérje. Az SMTN-A egy 59 kDa molekulatömegű rövid izoforma, mely a viszcerális simaizmokban expesszálódik, míg a 100 kDa nagyságú hosszú izoforma, az SMTN-B az erek simaizomzatára jellemző. Az SMTN fehérjecsalád tagjai nagyfokú szekvencia homológiát mutatnak főként a C-terminális végükön, ahol egy 2-es típusú kalponin homológ (CH) domén (342-459 aminosavmaradék) található. Az SMTN-A és -B fehérjékkel ellentétben az SMTNL1 nem képes az aktin megkötésére. Ennek oka feltehetően az aktin-kötő domén/ek hiánya, melyből az SMTN-B fehérjén kettő, míg az SMTN-A fehérjén egy található. Továbbá az utóbbiak tartalmaznak még egy-egy tropomiozin-kötő motívumot is. Az SMTNL1 szintén képes kötődni a tropomiozinhoz, ami elősegíti a vékony filamentumokhoz való asszociációját a CH-doménen és a rendezetlen N-terminális végen keresztül (*6. ábra*).

Az SMTNL1 CH-doménjének N-terminális végén található IQ motívum (apo-CaM-kötő domén, CBD2) a fehérje Ca^{2+}-mentes kalmodulinnal (CaM) való kölcsönhatását teszi lehetővé, míg a Ca^{2+}-kötött kalmodulinhoz elsősorban az ún. Ca^{2+}-CaM-kötő doménen keresztül (CBD1)

kapcsolódik. Az SMTNL1 N-terminális szakasza erősen rendezetlen, ami felveti a más fehérjékkel történő kapcsolódás és szabályozás lehetőségét.

Az SMTNL1 fehérjét foszfoproteomikai elemzésekkel a PKG szubsztrátjaként írták le nyúl



6. ábra. A SMTNL1 fehérje szerkezete. *A SMTNL1 fehérje C-terminálisán (342-459) CH doménnel rendelkezik, míg N-terminális vége (1-341) rendezetlen szerkezetű. A CH domén a kalmodulinhoz, illetve a tropomiozinhoz való kötődéshez szükséges, azonban F-aktinhoz nem kapcsolódik. A fehérje intracelluláris lokalizációját a CH domén közelében található Ser301-es oldallánc foszforilációs állapota szabja meg, amely a ciklikus nukleotid függő kinázok célpontja a sima- és vázizomban. A foszforiláció feltehetően olyan konformációváltozást idéz elő, amely a foszforilációs helytől N-terminálisan elhelyezkedő magi lokalizációs szignált exponálja. Az ábra a biorender.com felületén készült. PR-B: progeszteron receptor-B; TBD: tropomiozin kötő domén; CBD: kalmodulin kötő domének*

ileumban (akkori elnevezése szerint CHASM; calponin homology-associated smooth muscle) [100]. Jelenlegi ismereteink szerint az SMTNL1 Ser301 oldallánca az egyetlen hely, amit a PKA és a PKG protein kinázok foszforilálnak [100], és kulcs szerepet játszik a SMTNL1 funkciójában. Érdekes módon az SMTN család többi tagjából hiányzik [100]. Az SMTNL1 gátló hatással van az simaizom MP aktivitásra és a rekombináns SMTNL1 fehérje permeabilizált, simaizomba történő bejuttatása a kontraktilis erő jelentős változását okozta. Míg a CH-domén elengedhetetlen volt a maximális relaxációhoz, önmagában nem okozott jelentős erőváltozást. Míg a teljes hosszúságú SMTNL1 képes volt elnyomni az MP aktivitását *in vitro*, az SMTNL1 CH-domént nélkülöző variánsa hatástalan volt, ami arra utal, hogy a CH-domén fontos szerepet játszik az SMTNL1 simaizom-összehúzódásra gyakorolt hatásainak közvetítésében [106].

Az SMTNL1 fehérje funkcionális vizsgálataihoz posztdoktori éveim során a Duke Egyetemen létrehoztuk az *smtnl1 -/-,* KO egértörzseket (B6 és 129 alapon) úgy, hogy a fehérje 3-8 exonjait (a 230-421 aminosavakat kódoló szakaszt, mely tartalmazza a Ser301 foszforilációs helyet és a CH domént) célzott géndelécióval eltávolítottuk. Az egerek embrionális fejlődése, az utódok mérete és alapaktivitása kezdetben normálisnak bizonyult [101], azonban több ezer szaporulatot követően három jól jellemezhető fenotípusbeli elváltozást találtunk.

Az első fenotípus jellemzője, hogy az *smtnl1* KO állatok WT alomtársaikhoz képest edzéshez adaptálódott fenotípust mutattak, ami mind a sima-, mind a vázizomban leírt hatásokban megmutatkozott. *Smtnl1*-/- egerekből származó aorták fokozott vazorelaxációt mutattak. Kontroll egerekben az adrenerg agonisták hatására az SMTNL1 Ser301 oldalláncon emelkedett foszforilációt detektáltunk [101], amelyet az agonistákra adott kontraktilis válaszok jelentős csökkenése kísért [101]. Vázizomban az SMTNL1 2a típusú izomrostra specifikus expresszióját írtuk le. Az SMTNL1 deléció hatására a 2a típusú rostok és az miozin nehézlánc 2a típusának (MHC2A) expressziója növekedett, addig a 2b típusú rostok és az MHC2b expressziója pedig csökken míg más, ismert edzés-indukálta fehérjék expressziója nem változott [101]. Az SMTNL1 KO egerekkel végzett vizsgálatok azt sugallják, hogy a fehérje fiziológiai szerepe a testmozgásra adott adaptív válaszok elősegítése a sima- és vázizomban. A *m. soleus* izomból készített metszetek elektronmikroszkópos vizsgálata nem mutatott változást az izom ultraszerkezetében a SMTNL1 kiütésének hatására. Azonban a SMTNL1 KO egerek 5 hetes állóképességi edzése és az azt követő terheléses vizsgálatok rávilágítottak arra, hogy a hím KO egerek szignifikánsan később fáradnak el, többet futnak és a munkavégzésük is nagyobb a vad típusú (WT) társaikhoz képest, míg a nőstény KO egerek teljesítménye nem különbözik jelentősen a WT nőstényekétől. A vázizom rosttipizálásából kiderült, hogy a SMTNL1 deléciója a vázizom rostösszetételének átalakítását indukálja: a mozgásszegény KO egerek *m. plantaris*-a alapállapotban több 2a és kevesebb 2b rostot tartalmaz a WT egerekhez képest, hasonlóan az 5 hetes edzésen átesett WT egerekhez, de a SMTNL1 delécióját az 1 és 2x típusú rostokra nincs hatással. A KO egereken végzett további vizsgálatok feltárták, hogy az egerek testsúlya, izomtömege, vérnyomása, glükóztoleranciája, szérumértékei nem változtak jelentősen, minden érték a normál tartományba esett [101].

Kimutattuk, hogy az SMTNL1 a MYPT1 expresszióját szabályozza az egyedfejlődésben és meghatározó szabályozó eleme a simaizom kontraktilitásának. Az izom adaptációs változásai közben mind az egyedfejlődés mind a terhesség során, a MYPT1 és SMTNL1 expressziója is változott. Így például a MYPT1 expressziójának és a miozin foszfatáz aktivitásának megkétszereződését mutattuk ki a születést követő 6-12. napokon. Az SMTNL1 hiánya, illetve a Ser301 oldalláncon történő foszforilációjának hatására kialakult magasabb miozin foszfatáz aktivitás következtében egy relaxáltabb izom fenotípus jelent meg, mely a foszforilálatlan SMTNL1 MP-t gátló hatásával állhat összefüggésben. Ezzel öszhangban bizonyítottuk a MYPT1 és a SMTNL1 kölcsönhatását is és igazoltuk, hogy az SMTNL1 gátolja a MP holoenzim

aktivitását. A SMTNL1 Ser301 oldallánc PKA/PKG általi foszforilációjának hatására az SMTNL1 transzlokációját mutattuk ki a sejtmagba, ami lehetővé teszi, hogy a *mypt1* gén expresszióját szabályozza [102]. Feltérképeztük az SMTNL1 expresszióját, és leírtuk, hogy az nem korlátozódik a vázizomra, hanem megtalálható még simaizomban és szteroidhormonokra érzékeny szövetekben is, így jelentős expressziós szintet mutat a petefészekben, herében, az emlőállományban, de a mellékvesében is. Eredményeink szerint a terhesség során a MP szerepet játszik az anya vérnyomásának és a méhizomzat kontraktilitásának szabályozásában. A MYPT1 magasabb expresszióját és a MP fokozott aktivitását mutattuk ki a méh és a vaszkuláris simaizomban a terhesség során egér és humán mintákon. A MYPT1 expressziója nemcsak terhesség hatására, hanem a SMTNL1 fehérje hiányában is emelkedett, illetve a terhesség és a SMTNL1 hiányának együttes hatására a MYPT1 húszszorosan megnövekedett expresszióját tapasztaltuk. A terhesség koordináltan megváltoztatta mind az érrendszeri, mind a méh simaizomzatának összehúzódási tulajdonságait, csökkentve a szisztémás vérnyomást és fenntartva a méh relaxációját. A terhesség okozta adaptációk hátterében álló pontos molekuláris mechanizmusokat még nem sikerült teljes mértékben meghatározni, de valószínűleg a miozin foszforilációját szabályozó fehérjék expressziójának változásaihoz kapcsolódnak. Az SMTNL1 elsődleges célgénje ezekben az izmokban a MYPT1. Az SMTNL1 deléciója 30-40-szeresére növeli a MYPT1 expresszióját újszülöttekben, és a fejlődés során mind az SMTNL1, mind a MYPT1 expressziója több mint 20-szorosára nő. A terhesség szintén szabályozza az SMTNL1 és a MYPT1 expresszióját, és az SMTNL1 deléciója nagymértékben fokozta a MYPT1 expresszióját a vaszkuláris simaizomban, ami a fenilefrinre adott válaszként az erőfejlődés jelentős csökkenését eredményezi, valamint az izmot acetilkolinra érzékennyé teszi. Eredményeink alapján a szexuális fejlődés és a terhesség az SMTNL1 és a MYPT1 révén közvetíti a sima és harántcsíkolt izmok adaptációját [102].

Mivel a változások szteroidhormon-függő, izomspecifikus szabályozásáról szóló ismereteink továbbra is hiányosak voltak, és a MP aktivitásának szabályozása ezen folyamatokban még ismeretlenek maradtak, disszertációmban új eredményként bemutatom a folyamatok hátterében álló molekuláris mechanizmusok felderítésére irányuló újabb kutatásainkat. Ugyancsak a disszertáció Eredmények fejezetében tárgyalom az *smtnl1* KO állatok reproduktív és metabolikus fenotípusánk felismerését és jellemzését.

3. CÉLKITŰZÉSEK

A MP a citoszkeletális folyamatokban és az izom összehúzódásban betöltött szerepét elsősorban a miozin II 20 kDa könnyű láncának defoszforilációján keresztül fejti ki, és így szabályozza a kontraktilitást, a sejtmozgásokat és a migrációt izom és nem-izom sejtekben. A MP széleskörű fiziológás szerepére utal, hogy a miozin II mellett számos egyéb szubsztrátját azonosították illetve, hogy a MP szabályozó alegysége, a MYPT1 változatos sejten belüli lokalizációt mutat különböző sejttípusokban. Munkacsoportunk kimutatta és jellemezte a MP egyik új szabályozó elemét, a MYPT1 alegységgel kölcsönható SMTNL1 fehérjét. Ezek alapján szerettük volna feltárni a MP diverz sejtélettani funkcióit és bonyolult szabályozási lehetőségeit fiziológiás és patológiás folyamatokban. Főbb célkitűzéseink a következők voltak:

- A MP agyszövetbeli lokalizációja, de ismeretlen neuronális funkciója miatt célul tűztük ki a neurotranszmitter kibocsátásban betöltött szerepének leírását, különös tekintettel az exocitózist kiváltó SNARE komplex elemeivel való kölcsönhatására neuroblasztóma, szinaptoszóma és agykérgi modelleken.
- A MP sejtmagban betöltött szerepének tanulmányozása a MYPT1 sejtmagon belüli pontos lokalizációjának és kölcsönható partnereinek meghatározásával humán hepatokarcinóma sejtekben, valamint a génexpresszió szabályozásában betöltött szerepének feltárása.
- A protein foszfatáz-1 enzimek, és ezen belül a MP szerepének vizsgálata a bőr homeosztázisának fenntartásában és a sebzáródás hatására indukálódó molekuláris mechanizmusokban szabályozásában.
- A MYPT1 alegység SMTNL1 általi szabályozásának jellemzése vázizom szövetben az terhesség során.
- Az SMTNL1 mint transzkripciós kofaktor terhességben betöltött szerepének vizsgálata a vázizomzat adaptációs folyamataiban.
- Az SMTNL1 KO állatok reproduktív fenotípusának hátterében álló molekuláris mechanizusok felderítése az endometriumban.
- Az SMTNL1 KO állatok inzulinrezisztens fenotípusának hátterében álló molekuláris mechanizmusok megismerése.
- A SMTNL1 fehérje szerepének meghatározása hyperthyreosisos betegek vázizomzatában.

4. ANYAGOK ÉS MÓDSZEREK

4.1. Anyagok

A felhasznált anyagok, antitestek és vegyszerek a Sigma-Aldrich (St. Louis, MO, USA) cégtől származtak, az ettől való eltérést minden esetben külön jelöltem. A Mikrocisztin-LR előállítása és tisztítása korábban leírt módon történt [107].

4.2. Sejtvonalak

4.2.1. A kísérletben használt sejtvonalak

Humán keratinocita (HaCaT), a B50 neuroblasztóma, HeLa, hepG2 hepatocelluláris carcinoma, C2C12 myoblast, tsA201 és normál humán epidermális keratinocita (NHEK) sejteket használtunk.

4.2.2. Sejtkultúra modellek

C2C12 sejtek differenciációja: A normál felnőtt nőstény C3H egerek combizmából létrehozott, immortalizált C2C12 egér mioblaszt (ECACC 91031101; C2C12) sejteket 1000 mg/L glükózt, 2 mM L-glutamint (Lonza; Basel, Switzerland), 10% (V/V) foetális borjú szérumot (FBS) tartalmazó DMEM-ben, 5% CO_2 szint mellett, 37 °C-on tenyésztettük. A C2C12 sejtek differenciációjához 1000 mg/L glükózt, 2 mM L-glutamint és 2% (V/V) lószérumot tartalmazó, fenolvörös nélküli DMEM-et (differenciáltató médium) alkalmaztunk 6 napon keresztül.

A *hipertireózis modellben* a differenciáció 1. napjának vagy 4. napjának kezdetétől a differenciáltató médiumot 1 M HCl:EtOH 1:4 arányú oldatában oldott, 10 nM-os végkoncentrációjú 3,3′,5-trijód-tironinnal (T3) is kiegészítettük. A kontroll minden esetben 1 nM T3-at tartalmazott. A sejtek állapotát, valamint a differenciáció következtében végbemenő morfológiai változásokat fénymikroszkóp alatt követtük nyomon.

Az inzulinrezisztencia modellben a 3 napos differenciáltatás elteltével még 3 napig kezeltük a sejteket az inzulinrezisztencia kialakításához. Az indukált inzulinrezisztenciához (HG – 25 mM glükóz) fenolvörös mentes DMEM-et használtunk 2% (V/V) lószérummal, 2 mM L-glutaminnal, valamint 100 nM inzulinnal kiegészítve. A nem inzulinrezisztenciás sejteket normál cukortartalmú (LG – 5,5 mM glükóz) fenolvörös mentes 2% (V/V) lószérummal 2 mM L-glutaminnal, valamint 50 pM inzulinnal kiegészített médiummal kezeltük. Ezt a két kezelést egészítettük ki 10 nM medroxiprogeszteron-17-acetát (MPA) hozzáadásával vagy anélkül. Minden kezelési formát az

üres plazmiddal transzfektált sejteken és a N-terminális Flag-jelölővel ellátott SMTNL1 pcDNA-3.1 expressziós plazmiddal (FT-SMTNL1) transzfektált sejteken is végrehajtottuk.

4.2.3. Sejttenyésztés és a sejtek lizálása

A humán keratinocita (HaCaT), a B50 neuroblasztóma, HeLa, hepG2 hepatocelluláris carcinoma, és a tsA201 sejteket 10% (V/V) borjú szérumot (FBS), illetve 2 mM L-glutamint tartalmazó Dulbecco által módosított Eagle médiumban (DMEM) tenyésztettük 37 °C hőmérsékleten és 5%-os szén-dioxid szint mellett. A normál humán epidermális keratinocita (NHEK) sejteket EpiLife médiumban tenyésztettük, mely humán keratinocita növekedési faktorokat is tartalmazott (Gibco, Life Technologies).

A sejtlízishez RIPA puffert használtunk, melynek összetétele: 25 mM Tris-HCl, pH 7,6, 150 mM NaCl, 0,25% (m/V) nátrium-dezoxikolát, 1% (m/V) NP-40, 0,1% (m/V) nátrium-dodecil-szulfát (SDS). HaCaT sejtek lizálásához Tris-Triton puffert használtunk: 10 mM Tris-HCl, pH 7,4, 100 mM NaCl, 1 mM etilén-diamin-tetraecetsav (EDTA), 1 mM etilén-glikol-tetraecetsav (EGTA), 1% (V/V) Triton X-100, 10% (V/V) glicerin, 0,1% (m/V) SDS, 0,5% (m/V) nátrium-dezoxikolát. A pufferekhez használat előtt, frissen 1x proteáz inhibitor mixet (Roche, Bázel, Svájc) és 1x protein foszfatáz inhibitor koktélt (1 mM NaF, 1 mM $Na_4P_2O_7$, 1 mM β-glicerofoszfát, 1 mM Na_3VO_4) adtunk. A fehérje koncentrációkat Pierce BCA Protein Assay Kittel (Thermo Scientific, Waltham, MA, USA) határoztuk meg.

4.3. Egér törzsek fenntartása és élettani vizsgálata

4.3.1. Az egérkolóniák fenntartása

A sebgyógyulás tanulmányozására 6-7 hetes hím Balb/c egereket használtunk fel. Az egereket 35-75% relatív páratartalmú, 19-25 °C hőmérsékletű környezetben tartottuk *ad libitum* etetéssel. Az állatkísérletek a Debreceni Egyetem Munkahelyi Állatkísérleti Bizottság (DEMÁB) (9/2008/DEMÁB, 7/2010/DEMÁB, 6/2011/DEMÁB, 5/2015/DEMÁB) vagy a Duke University Animal Care and Use Committee engedélyével történtek és megfeleltek az állatokon végzett kísérletekre vonatkozó hazai, európai uniós és USA etikai szabályoknak és a Debreceni Egyetem Etikai Kódexnek. A kongenikus 129 SvEv *smtnl1-/-* egértörzset a Charles River Laboratories közreműködésével készült [101]. A vemhességi vizsgálatokhoz 6-8 hetes ivarérett nőstény egereket a lavarge módszerrel [108] választotuk ki. Az ivarzó nőstényeket egy éjszakán át felnőtt hímekkel párosítottuk. A hüvelydugó meglétét a vemhesség 0. napjának tekintettük. Az

álvemhességi vizsgálatokhoz a Taconic cégtől beszerzett vazektomizált hímekkel 1:2 arányban vegyítettük a nőstényeket.

4.3.2. A reproduktív fitnessz vizsgálata

Az *smtnl1-/-* kolóniák szaporodási adatait másfél év alatt gyűjtöttem össze az *smtnl1+/+* x *smtnl1+/+* és *smtnl1-/-*x *smtnl1-/-* egerek (n=1651) között létrehozott, életkorban illeszkedő keresztezésekből. Az embrionális letalitás, a vemhességig eltelt idő és a vemhesség közötti intervallum, mint a reproduktív fenotípus jellemzői és a vemhesség gyakorisága tekintetében adatok gyűjtésére *smtnl1*+/+ x *smtnl1*+/+ és *smtnl1-/-*x *smtnl1-/-* kísérleti tenyész párokat (egyenként n=40) használtunk. A már bizonyítottan termékeny hímek és szűz nőstények 6-8 hetesek voltak. Az alom mérete az egyes alomban megszámlált utódok száma volt. Az embrionális letalitást úgy mértük, hogy a vemhesség 7., 13., 17. napján vagy a születéskor a méh felboncolásakor megkerestük az elhalt embriókat, és az elhalt embriók átlagos számaként adjuk meg. A hímek aránya a hím utódok százalékos aránya volt az egyes alomban. A vemhességig eltelt idő a tenyész pár felállítása és a megtermékenyítést jelző hüvelyi dugó első megfigyelése közötti napok száma volt. A vemhességek közötti időintervallum az első vemhességben a hüvelyi dugó első megfigyelése és a második vemhességben a dugó első megfigyelése közötti napok száma volt.

4.3.3. Átfogó Laboratóriumi Állatfigyelő Rendszer (Comprehensive Laboratory Animal Monitoring System (CLAMS)

Normál tápon tartott egereket anyagcsere paramétereinek vizsgálatára CLAMS-be helyeztünk és 48 óra étetés/24 óra koplalás/24 óra táplálási periódusokkal monitoroztuk 4 napon keresztül. Az oxigénfogyasztás, a termelt szén-dioxid térfogata és a légzéscsere arány, a hő, a felhalmozott tápanyag- és folyadékmennyiség és az állatok mozgása 20 percenként került mérésre.

4.3.4. Sebgyógyulás tanulmányozása egérbőrön

A sebzés előtt az egerek hátáról eltávolítottuk a szőrt, majd izoflurránnal altattuk őket (Abbott Animal Health, Abbott Park, IL, USA). A dorzális bőrfelületen három 4 mm átmérőjű, kör alakú, teljes vastagságú sebet ejtettünk [109]. A sebeket 1 μM végkoncentrációjú szelektív protein foszfatáz-1 (PP1) inhibitor tautomycinnel (TM), illetve 10 μM végkoncentrációban H1152 ROK inhibitorral kezeltük, a gátlószereket hidrofil anionos krémben alkalmaztuk, és napi kétszer 12 órás időközönként (n=6) kentük a sebekre 7 napon keresztül. A sebekről minden nap Olympus kamerával (Olympus, Tokió, Japán) felvételeket készítettünk méretarány mellett ugyanazon

beállításokkal, területüket pedig ImageJ (National Institutes of Health, Bethesda, MD, USA) programmal határoztuk meg. A relatív sebfelszíneket a 0. napi területekhez viszonyítottuk százalékos értékekben (átlag ±SEM). A sebeket hisztológiai és Western blot analízissel vizsgáltuk.

4.4 Szövetminták kinyerése és feldolgozása

4.4.1. Humán minták

A MYPT1 fehérje expresszióját humán *ex vivo* bőrszöveti biopsziákban is vizsgáltuk. A sebészi úton eltávolított felnőtt donorokból származó biopsziák tartalmazták a bőrszövetben előforduló összes sejttípust, és érett *stratum corneum*mal rendelkeztek. A mintákat a Genoskin (Toulouse, Franciaország) cégtől rendeltük.

A 73 eu- és hyperthyreosisos donor *m. sternohyoideus* izmából vett biopsziákon végzett kísérleteket a Debreceni Egyetem Regionális és Kutatásetikai Bizottsága (DEOEC RKEB/IKEB 3517-2011) hagyta jóvá, és azok megegyeznek az Európai Unió Tanácsa által előírt etikai szabályoknak. A donorok írásos beleegyező nyilatkozatot írtak alá a jelen értekezésben foglalt tanulmányban való részvételre. A donorokat elsősorban nemük és betegségük alapján választottuk ki. Minden biopszia *struma nodosá*ban (euthyreosisos), illetve Graves-kórban vagy *struma nodosa colloides*-ben (hyperthyreosisos) szenvedő nőbetegtől származik. Törekedtünk rá, hogy minden feltárásra kerülő minta 60 év alatti pácienstől származzon. Az humán vázizom biopsziákat érintő eljárásokat az East Carolina University and Medical Center intézményi felülvizsgálati bizottsága hagyta jóvá. Human cervicalis carcinoma biopsziákat RIPA pufferben szolubilizálva rendeltük (Protein Biotechnologies (Ramona, CA, USA)).

4.4.2. Humán szöveti minták lízise

A minták homogenizálását módosított RIPA pufferben [25 mM Tris (pH 7,6), 150 mM NaCl, 0,1% SDS, 1% Triton X-100, 1 mM etilén-diamin-tetraecetsav (EDTA), 1 mM ditiotreitol (DTT), 1 mM PMSF, 10x PIC, 50x PPIC, 1 μM MC-LR] jégen, üvegből készült Potter-Elvehjem szövethomogenizáló eszköz segítségével végeztük el. A homogenizátumokat 10 percig centrifugáltuk (16 000 x *g*-n, 4 °C-on), majd a felülúszót használtuk további vizsgálatokra.

4.4.3. Agyszeletek preparálása, kezelése és szinaptoszóma preparálás

C3H egerekből perparált agykéregből Microm HM 650 V vibratómmal 200 μm vastagságú szeleteket metszettünk, melyeket mesterséges cerebrospinális folyadékba helyeztük. Az

agyszeletekhez inhibitorokkal inkubáltuk majd 8 mM KCl-ot adtunk hozzá. Az inzerteket egy órára enyhe túlnyomásos karbogén gázt tartalmazó kamrába helyeztük. C3H egereket CO_2-dal eutanizáltunk és agypreparátumot készítettünk. Az agykérget homogenizáltuk, a felülúszót Percoll-gradiens (23-15-10-3%) tetejére mértük, és ultracentrifugával centrifugáltuk 32500 *g*-vel 5 percig 4 °C-on. A 10/15%-os, illetve a 15/23%-os fázisok határán lévő frakciókat centrifugáltuk és a pelletet Krebs-pufferben reszuszpendáltuk.

4.4. Biokémiai mérések

4.4.1. Protein foszfatáz aktivitásmérés

Protein foszfatáz aktivitásméréssel vizsgáltuk az inhibitorok és a csendesítés hatását a sejtek protein foszfatáz aktivitására. A lizátumok felülúszóit 0,1% β-merkaptoetanolt tartalmazó 20 mM koncentrációjú Tris-HCl (pH 7,4) pufferben a hígítottuk, és 1 µM ^{32}P-jelölt pulykazúza miozin 20 kDa könnyű láncának (^{32}P-MLC20) vagy 1 µM ^{32}P-jelölt pulykazúza teljes miozin (^{32}P-miozin) szubsztráttal 30 °C-on inkubáltuk. Az előbbi teljes PP1 enzimaktivitást, míg a második csak a miozin foszfatáz aktivitásméréséhez használtuk. A reakcióidő 20-60 másodperc volt, a reakciót, amelyet 200 µl 10% (V/V) triklórecetsav (TCA) és 200 µl 6 mg/ml BSA hozzáadásával állítottuk le. A reakció során felszabadult radioaktívan jelölt foszfátot ($^{32}P_i$) folyadék szcintillációs számlálóval (Perkin Elmer) határoztuk meg. A foszfatáz aktivitást a minták fehérjetartalmához normalizáltuk, a kezelt minták aktivitását pedig a kontroll érték %-ában adtuk meg.

4.4.2. In vitro protein kináz esszé

5 µM Flag-SNAP-25[110], Flag-PRMT5 [111] vagy GST-MYPT1 [112] fehérjét 120 percig 30 °C-os vízfürdőben inkubáltunk 20 ng/µl ROK enzimmel, 1 mM γ-[^{32}P]ATP-vel és 1 µM mikrocisztin-LR protein foszfatáz inhibitorral. A reakciót forró 5x SDS-PAGE mintapuffer hozzáadásával állítottuk le. Poliakrilamid gélelektroforézist követően a beépült foszfátot autoradiográfiával detektáltuk.

4.4.3. Proteome Profiler humán foszfo-kináz és foszfo-MAPK array

A humán foszfo-kináz (ARY003B) és foszfo-MAPK (ARY002B) array kiteket (R&D Systems; Minneapolis, MN, USA) a gyártó utasításait követkve alkalmaztuk humán vázizom és kezelt C2C12 sejlizátumokon. A mintákat az Array Buffer 1-ben hígítottuk és a membránokkal együtt inkubáltuk 4 °C-on, majd a membránokat detektálás céljából biotinilált antitest koktélban inkubáltuk. Végül a membránokat hígított Streptavidin-HRP-ben inkubáltuk szobahőn, majd a

sávokat kemilumineszcenciásan, a kitben lévő Chemi Reagent Mix segítségével, röntgenfilmen tettük láthatóvá.

4.4.4. Protein foszforilációs és defoszforilációs vizsgálat

Anti-Flag gyöngyökhöz rögzített Flag-SNAP-25 vagy Flag-PRMT5^{wt} és -PRMT5^{T80A} fehérjéket foszforiláltunk nem-radioaktív módon 0,5 mM ATP, 5mM $MgCl_2$ és ROK (0.4 U/ml) jelenlétében. A kináz reakciót követően a foszforilált PRMT5 fehérjék defoszforilálására Flag-MYPT1 vagy rPP1cδ oldatot, illetve ezek kombinációjával létrehozott holoenzimet (PP1c és MYPT1) alkalmaztunk.

A PPM1B defoszforiláviós vizsgálatához GST illetve a GST-MYPT1 ROK-kal történő foszforilációját követően a gyöngyöket 1xTBS-el mostuk, majd PPM1B-t tartalmazó vagy anélküli inkubáció következett PPM1B esszé pufferben (20 mM Tris pH 7.4, 150 mM NaCl, 5 mM $MgCl_2$, 5 mM $MnCl_2$, 1 mM DTT, 1 mg/ml BSA, 0.1% Tween és proteáz gátlók) 45 percig, 30°C-on. Az inkubációt követően a mintákat 1xTBS-el mostuk, és a gyöngyöket SDS minta pufferrel inkubáltuk100°C-on, 5 percig.

4.4.5. Kaszpáz esszé

A kaszpáz-3 aktivitásmérése során az enzim az Ac-DEVD-AMC szubsztrát (Calbiochem, San Diego, CA, USA) hasításával fluoreszcens AMC-t szabadít fel, melynek intenzitását fluoriméterrel mérjük. A kezelést vagy csendesítést követően a sejteket lízis pufferrel (10 mM HEPES, pH 7,25, 2 mM EDTA, 0,1% (V/V) CHAPS, 1 mM PMSF, 5 mM DTT, 1x proteáz inhibitor mix) felvettük, centrifugáltuk, majd a felülúszókat 200 µl 2x reakció pufferrel (200 mM HEPES, pH 7,25, 20% (m/V) szacharóz, 0,1% (V/V) CHAPS, 5 mM DTT) mértük 37 °C-os vízfürdőben 60 percig történő inkubálást követően. Az AMC fluoreszcenciáját 360 nm gerjesztési, és 460 nm emissziós hullámhosszon mértük Fluoroskan FL készülékkel (Thermo Scientific, Waltham, MA, USA).

4.4.6. In vitro protein arginin metiltranszferáz kísérlet

A ROK által foszforilált, anti-Flag gyöngyökhöz kikötött Flag-PRMT5^{wt} fehérjék felhasználásával metiltranszferáz kísérleteket végeztünk. S-adenozil-L-metionint és hiszton fehérjékből álló keveréket adtunk a reakcióelegyhez. A metiltranszferáz reakció rPP1cδ, Flag-MYPT1 vagy ezek keverékének jelenlétében vagy hiányában ment végbe.

4.5. Fehérje vizsgáló módszerek

4.5.1. Western blot analízis

A sejtlizátumokat és szöveti homogenizátumokat 5x SDS-poliakrilamid gélelektroforézis (SDS-PAGE) mintapufferrel (50% (V/V) glicerin, 10% (m/V) SDS, 100 mM DTT, 0,01% (m/V) brómfenolkék, 0,31 M Tris, pH 6,8) inkubáltuk 100 °C hőmérsékleten, 5 percig, majd SDS PAGE-t követően nitrocellulóz membránra (Bio-Rad, Hercules, CA, USA) transzferáltuk. A membránt 5%-os (m/V) marhaszérum-albumin (BSA) oldatban inkubáltuk Tris pufferben (TBS: 125 mM NaCl, 2,7 mM KCl, 25 mM Tris-HCl, pH 7,4). Az elsődleges antitestekkel 0,5% (m/V) BSA/0,1% Tween-20-at tartalmazó TBS (TBST) oldatban hígítottuk. A membránokat mosás után a megfelelő másodlagos antitestekkel inkubáltuk, majd a mosás után a detektáláshoz SuperSignal West Pico Chemiluminescent Substrate Kitet (Thermo Scientific, Waltham, MA, USA) használtunk és a jeleket FluorChem FC2 Imager (Alpha Innotech, San Leandro, CA, USA) vagy ChemiDoc Touch Imaging System (Bio-Rad, Hercules, CA, USA) készülékkel vizualizáltunk.

4.5.2. Fehérje kölcsönhatások kimutatása immunprecipitációval

A Protein A Sepharoset (PAS) előzetesen duzzasztottunk (GE Healthcare, Chicago, IL, USA; #17-0780-01), melyhez hozzáadtuk a kötőpufferben [50 mM Tris, pH 7,0] 1:60 arányban hígított, az immunprecipitálni kívánt fehérjét kötő antitestet és 2 órán keresztül, folyamatos kevertetés mellett 4 °C-on inkubáltuk. Miután az antitestekhez bekötődtek a megfelelő fehérjék, a felülúszót eltávolítottuk, a gyantát pedig átmostuk 1x immunprecipitációs pufferrel, illetve PBS-sel. A gyantát 100 °C-on 5 percig főztük 1x SDS-PAGE mintapufferrel, és a mintákból Western blotot végeztünk. Az immunoprecipitációt Anti-Flag M2 Affinity Gel gyöngyökkel is végeztünk hasonló módon. Itt az elúció vagy 1x SDS mintapufferrel való 5 perces főzéssel történt vagy a tisztított Flag peptiddel történő kompetícióval szorítottuk le a Flag-jelölt rekombináns fehérjét.

4.5.3. Fehérje kölcsönhatások kimutatása pull-down kísérlettel

A MYPT1-gyel kölcsönható sejtmagi fehérjék meghatározásához Flag-MYPT1 fehérjét kötöttünk anti-Flag M2 affinitás gélhez és HepG2 sejtmagi frakciót és szinaptoszóma lizátumot adtunk hozzá. A Flag-MYPT1-et a hozzá kötődött fehérjékkel Flag-peptid segítségével eluáltuk, majd SDS-gélelektroforézist követően MS kompatibilis ezüst-festéssel tettük láthatóvá a fehérjesávokat és a fehérjéket tömegspekrometriás analízissel azonosítottuk.

GST-t (Glutathione-S-transzferázt) vagy GST-MYPT1-et expresszáló *E.coli* lizátumokat

Glutathion Sepharose 4B gyöngyökkel (P1743-1VL, Merck) kötő pufferben (50 mM Tris, 150 mM NaCl, 1 mM EDTA, 1% (V/V) Triton X-100, pH: 7,4) kiegészítve 1x PIC-el) inkubáltunk, majd 1x-esTBS-sel mostuk, majd üres vektor által transzfektált MOCK, vagy FT-PPM1B által transzfektált tsA201 lizátumokkal inkubáltuk, 120 percig, 4°C-on. A gyöngyöket mostuk 1xTBS oldattal, majd 2x-es SDS minta pufferrel 5 percig, 100 °C inkubáltuk.

4.5.4. Felületi plazmon rezonancia (SPR) vizsgálatok

A PRMT5 és a SNAP25 fehérjék MYPT1-gyel való kölcsönhatását SPR alapuló kötődési kísérletekkel tanulmányoztuk Biacore 3000 készülékkel. CM5 szenzor chip felszínére GST-MYPT1$^{1\text{-}1004}$, GST-MYPT1$^{667\text{-}1004}$ és His-MYPT1$^{1\text{-}633}$ fehérjéket kötöttünk ki. PRMT5 vagy SNAP25 fehérjéket injektáltunk a felszínre különböző koncentrációban, a szenzorgrammokat a BIAevaluation 3.1 szoftver segítségével elemezve meghatároztuk az asszociációs állandókat (K_a).

4.5.5. Immunfluoreszcenciás vizsgálatok

A sejteket 4% paraformaldehid/PBS oldattal (HaCaT, hepG2, HeLa) vagy felszálló etanol sorral (B50) fixáltuk, majd Triton X-100/PBS oldattal permeabilizáltuk, és 1% lószérum vagy BSA/PBS oldatával blokkoltuk. Az elsődleges antitesteket 1:250, a másodlagos antitesteket és a Texas Red-X phalloidint pedig 1:2000 higításban alkalmaztuk éjszakán át. A sejtmagokat DAPI-val festettük meg, és ProLong Gold Antifade médiummal fixáltuk. Az immunjeleket Leica konfokális mikroszkóppal vagy Opera Phoenix High Content Analysis műszerrel (PerkinElmer, Waltham, MA, USA) vizualizáltuk, és a beépített Harmony szoftverrel (4.8 verzió) elemeztük.

4.5.6. Trikróm festés és immunhisztokémia

A kivágott sebeket 10%-os formalinnal fixáltuk, paraffinba ágyaztuk, majd 4 μm vastagságú szeleteket metszettünk ki belőlük. A metszeteket rögzítettük, xilénnel deparaffinizáltuk, és etanollal dehidratáltuk, majd Masson-Goldner-féle trikróm festéssel megfestettük őket. A metszeteket pikrinsavval pácoltuk, majd a sejtmagokat timsós hematoxilinnal festettük. A metszeteket mostuk, majd narancs G és savanyúfukszin-Ponceau oldattal (0,05 g savanyúfukszin, 0,05 g Ponceau S, 2 ml tömény ecetsav, 100 ml desztillált víz) festettük, ezután 2 percig 5 g/dl foszforvolfrámsav oldattal, végül 10 percig anilinkék oldattal (0,5 g anilinkék, 2 ml tömény ecetsav, 100 ml desztillált víz) inkubáltuk. Humán bőrszöveti mintákban a metszeteket 4 °C-on inkubáltuk az elsődleges antitestekkel, majd mosást követően két órán át a torma peroxidázzal konjugált második antitestekkel. Az immunjeleket 3,3’-diamino-benzidin kromogén

szubsztráttal hívtuk elő. A metszeteket xilénnel megtisztítottuk, beágyaztuk és tárgylemezre ragasztottuk, végül Leica S40 mikroszkóppal vizualizáltuk.

4.5.7. Duolink PLA fehérje-fehérje kölcsönhatási vizsgálat

A Duolink PLA fehérje-fehérje interakciós esszét (DUO92007, Sigma-Aldrich, St. Louis, MO, USA) a gyártó utasításai alapján végeztük el, HeLa sejtkultúrán. A HeLa sejteketCell Carrier Ultra üveg aljú lemezre szélesztettük (PerkinElmer, Waltham, MA, USA, 4%(v/v) PFA/TBS oldatban fixáltuk, majd 0,2% Triton-X-100/TBS oldatban permeabilizáltuk. A mintákat elsődleges antitestekkel inkubáltuk, pozitív kontrollként az MP holoenzimet reprezentáló módon MYPT1 és PPc1β ellen termeltetett elsődleges antitesteket illetve a MYPT1 ismert szubsztrárját, a pRb fehérjét alkalmaztuk. A negatív kontroll csoportban elsődleges antitestet nem alkalmaztunk. A Duolink PLA próbát az elsődleges antitestekhez ligáltunk, majd az így kifejlődő fluoeszcens jeleket Opera Phoenix™ HCS mikroszkóp segítségével vizualizáltuk. A sejtek területének meghatározására a citoplazmát Alexa 688-as Falloidin-nal (Invitrogen™, Waltham, Massachusetts, USA, Katalógusszám: A22284**)**, a sejtmagot DAPI-val festettük. A sikeres fehérje-fehérje kölcsönhatást jelző fluoreszcens jelek mértékét a mikroszkóp beépített szoftvere analizálta (Harmony software, version 4,8). A fluoreszcens szignál értékét a sejtszámra normalizáltuk. A negatív kontroll csoport értékének átlagát 100%-nak vettük, minden más csoport eredményét erre a számra normalizáltuk, eredményeinket oszlopdiagrammon ábrázoltuk.

4.5.8. Szöveti array elemzése

25 klinikai esetből származó humán májtumor és normál szövetmintát, valamint 15 tumoros sejtlizátumot triplikátumban tartalmazó SomaPlex fehérje microarray slide-okat elemeztünk 3% anti-foszfo-PRMT5^{T80}, -foszfo-MYPT1^{T850} és -hiszton H2A, anti-PRMT5, -MYPT1$^{1-296}$ és H2AR3me2s antitestek segítségével. A szöveti array lemezeket ECL eljárással detektáltuk.

4.6. Nukleinsav alapú technikák

4.6.1. Myoblast sejtek tranziens transzfekciója

A mioblaszt sejtek transzfekcióját GeneJuice transzfekciós reagenssel végeztük a *pM11-NT-FT-SMTNL1*: M11 vektorba klónozott, N terminálisán Flag jelölőt tartalmazó rekombináns SMTNL1 fehérjét (NM_024230.2; GeneCopoeia Inc.; Rockville, MD, USA) kódoló plazmiddal és *pcDNA3.1.* (V790-20; Thermo Fisher Scientific; Waltham, MA, USA) üres vektorokkal. A

sejteket előre kollagénezett sejttenyésztő lemezen tenyésztettük egy éjszakán át 37 °C-on. Kontrollként minden esetben az üres plazmiddal transzfektált (MOCK) sejteket használtuk. A transzfekció sikerességét a Flag jelölő elleni antitesttel, Western blot analízissel ellenőriztük.

4.6.2. Géncsendesítés siRNS segítségével keratinocita sejtekben és ex vivo humán bőrszövetben

A HaCaT, B50 és hepG2 sejtek MYPT1 expressziójának és a HaCat sejtek PP1c expressziójának downregulációját siRNS-sel kiviteleztük. Lipofectamine 2000 transzfekciós reagenshez (Thermo Fisher Scientific, Waltham, MA, USA) siRNS-t adtunk, melyeket előzetesen OptiMEM-ben (Life Technologies, Carlsbad, CA, USA), hígítottunk. A kontroll sejtekhez non-target siRNS/Lipofectamine mixet adtunk. Az siRNS végkoncentrációja 40 nM volt mind a kontroll (NT siRNS), mind az siMYPT1-transzfektált sejtek esetében. A sejteket 4 órán keresztül szérummentes, majd 44 órán át 10% (V/V) FBS-t tartalmazó DMEM-ben tenyésztettük.

A MYPT1 fehérje expresszióját humán *ex vivo* bőrszöveti biopsziákban is gátoltuk. Humán *ex vivo* bőrszövetben az siRNS-t és a Lipofectamine 2000-t Genoskin médiumban az *ex vivo* humán bőrszövetbe injektáltuk, majd 2 napra inkubátorba helyeztük (37 °C, 5% CO_2). Ezután a bőrszövetekből homogenizáló pufferben (10 mM HEPES, pH 7,9, 1,5 mM MgCl2, 10 mM KCl, 1 mM EDTA, 10% (V/V) glicerin, 1% NP-40) készítettünk kivonatot. A fehérje koncentrációkat ezúttal is BCA esszével határoztuk meg.

4.6.3. RNS izolálás és szemi-kvantitatív RT-PCR

A human vázizom biopsziákból a gyártó előírásai alapján teljes RNS-t izoláltunk az RNeasy Fibrous Tissue kit (Qiagen; Hilden, Germany) segítségével. A minták homogenizálásához TissueRuptor-t (Qiagen; Hilden, Germany) használtunk, majd a mintákat proteináz K-val kezeltük 55 °C-on, 10 percig. Az RNS koncentrációt NanoDrop ND-1000 spektrofotométerrel (Thermo Fisher Scientific; Waltham, MA, USA) határoztuk meg.

Ischikawa sejtek RT-PCR elemzéséhez a reverz transzkripciót cDNS-szintézis készlettel (Thermo Fisher Scientific, Waltham, Massachusetts, USA) végeztük. A cDNS-t PCR-amplifikációhoz 2x Xceed qPCR SyberGreen Master mix (Institute of Applied Biotechnologies, Prága - Strašnice, Cseh Köztársaság) használtuk. A PCR-t LightCycler 480 (Roche Applied Science, Penzberg, Németország) géppel végeztük. Az egyes minták Cp-értékeit a belső háztartási gének, köztük a GAPDH és a Cyclophilin A átlagára normalizáltuk.

4.6.4. Microarray analízis

Az euthyreosisos és hyperthyreosisos vázizom minták, az UV kezelt HaCat sejtek, *Smtnl1* WT és KO vemhes és nem vemhes állatok vázizom és méhizom minták, valamint a siMYPT kezelt HepG2 sejtek génexpressziós mintáinak vizsgálatát Affymetrix Human Gene 1.0 ST microarray analízissel hajtottuk végre. Affymetrix Mouse Genome 430 vagy Human Affymetrix Mouse Genome 430 microarray elemzések az GenoMed Medical Genomic Technologies Ltd. és a Duke University Microarray Facilityben készültek. A microarray analízis nyers adatai a Gene Expression Omnibus (GEO) adatbázisban tekinthetők meg (***http://www.ncbi.nlm.nih.gov/geo/GSE178996***).

4.6.5. Irányított mutagenezis

A vad típusú humán teljes hosszúságú PRMT5, SNAP25 és PPM1B-t kódoló pReceiver-M11 expressziós vektort a GeneCopoeia Inc., (USA) cégtől vásároltuk. A PRMT5T80A, a SNAP25T187A és SNAP25T138A pontmutációit, illetve a PPM1B inaktív foszfatáz mutánsát a QuickChange II XL Site-Directed Mutagenesis Kit segítségével végeztük a gyártó utasításai szerint. A mutagenezishez használt primerpárokat a közleménye tartalmazzák [110; 111]. A mutációkat tartalmazó plazmidok szekvenciáját DNS-szekvenálással ellenőriztük, amelyet az UD-GenoMed Medical Genomic Technologies Ltd. végzett. (Debrecen, Magyarország) végezte.

4.6.6. Rekombináns fehérjék termeltetése és tisztítása

Emlős tsA201 sejtekbe polietilénimin (PEI) segítségével Flag-SNAP-25, Flag-MYPT1 vagy Flag-KEPI fehérjét kódoló plazmidot juttattunk be. A sejteket a transzfekció kezdete után 24 órával lizáltuk és a termeltetett fehérjét Anti-Flag M2 affinitási géllel tisztítottuk. A kikötött fehérjéket 300 μg/ml Flag-peptid/TBS-sel eluáltuk.

4.6.7. Emlős két hibrid vizsgálatok

Az emlős két hibrid vizsgálatokat HepG2 sejteken végeztük. A sejteket Fugene 6 reagenssel (Roche) transzfektáltuk 1500 ng 5xGal4-luciferáz riporter plazmiddal, 500 ng VP16 vagy 500 ng nukleáris receptor-VP16 fúziós plazmiddal (PR-A, PR-B (vagy PR-B deléciós/mutáns konstrukciók), ERα, ERβ, AR és GR), 500 ng pM-Gal4DBD vagy pM-Gal4DBD-SMTNL1 plazmidokkal (vagy pM-SMTNL1 deléciós plazmidok), és 200 ng citomegalovírus β-galaktozidáz (β-gal) és 300 ng pBSIIKS plazmidokkal. A 24 órás transzfekciót követően a sejteket vivőanyaggal (etanol) vagy a megfelelő receptor ligandumával kezeltük az alábbiak szerint: 10nM R5020 a PR-

A és B esetében, 100 nM 17ß-ösztradiol az ERα és β esetében, 100 nM Dexametazon a GR esetében, 100nM R1881 az AR esetében, vagy 100 nM RU486 és ZK98299. A 8-Br-cAMP PR-B transzkripciós aktivitásra gyakorolt hatásának elemzéséhez a HeLa sejteket 10 ng SV40-PR-B-vel, 1500 ng MMTV-luciferáz riporter plazmiddal, 200 ng β-gal és 1290 ng pBSIIKS plazmiddal transzfektáltuk, majd hordozó vagy 10 nM R5020-mal 8-Br-cAMP (10 nM-1 mM) jelenlétében inkubáltuk, majd ezt követően a luciferáz és β-gal vizsgálatokhoz lizáltuk. Az SMTNL1 PR-B transzkripciós aktivitásra gyakorolt hatásának elemzéséhez riporterpróbákat végeztünk HeLa sejtekben. A sejteket tranziens módon transzfektáltuk 10 ng SV40-PR-B-vel, a pcDNS 3.1-SMTNL1 növekvő koncentrációjával (75, 150 és 300 ng), valamint 1500 ng MMTV-luciferáz riporter plazmiddal és különböző mennyiségű pBSIIKS plazmiddal együtt, majd inkubáltuk hordozóval vagy 10 nM R5020-mal 100 μM 8-Br-cAMP- dal vagy anélkül. Az adatokat normalizált értékként mutatom be, amely az abszolut luciferáz-aktivitást jelenti, korrigálva a transzfekciós hatékonysággal a β-gal-aktivitással való normalizálással.

4.7. Sejtbiológiai kísérletek

4.7.1. Sejtéletképességi vizsgálat MTT festékkel

A különböző kezeléseknek a sejtek életképességére gyakorolt hatását metil-tiazol-tetrazólium (MTT) esszével tanulmányoztuk. A sejteket konfluens állapotig növesztettük, majd 24 órán át szérummentes DMEM-ben tartottuk. Ezt követően a sejteket kezeltük, a médiumot eltávolítottuk, szérummentes DMEM-et majd 10-10 μl 5 mg/ml koncentrációjú MTT oldatot (3-(4,5-dimetil-tiazol-2-il)-2,5-difenil-tetrazólium-bromid) adtunk hozzá. A kék színű formazán zárványok megjelenését követően a médiumot eltávolítottuk, és a formazán kristályokat 100-100 μl dimetil-szulfoxidban (DMSO) feloldottuk. A színintenzitást LabSystems Multiskan MS spektrofotométerrel határoztuk meg az abszorbancia 540 nm hullámhosszon történő detektálásával.

4.7.2. Sejtéletképességi vizsgálat SRB festékkel

A sejtek proliferációját szulforodamin B (SRB) esszével tanulmányoztuk. A kezelést követően a sejtekhez triklórecetsavat (TCA) adtunk 10% (V/V) végkoncentrációban, 4 °C-on 1 órán át inkubáltuk, majd mosást és szárítást követően a mintákhoz 0,4% (m/V) SRB-t tartalmazó 1%-os ecetsav oldatot pipettáztunk.

4.7.3. Karcolási (scratch) vizsgálat

A sejtek migrációs képességét karcolási vizsgálattal tanulmányoztuk. Tecan Freedom EVO 150 készülékkel (Tecan Group Ltd., Männedorf, Svájc) karcoltot ejtettünk, majd 24 órán át növesztettük a sejteket, kezeltük, majd Leica DM IL LED mikroszkóppal (Leica Camera AG, Wetzlar, Németország) fotókat készítettünk a karcolatokról. A kezelések során a negatív kontrollhoz 0%, a pozitív kontroll sorozathoz 10% FBS/DMEM-et adtunk. A C2C12 sejtek migrációját festést követő High Content Screening vizsgálattal követtük nyomon Opera Phoenix™ HCS készülékkel. A végső karcolatok méretét ImageJ szoftverrel (National Institutes of Health, Bethesda, MD, USA) vagy az Opera beépített szoftverével határoztuk meg. A szabad területek nagyságát minden esetben a kontrollhoz viszonyítottuk, azt 100%-nak véve.

4.7.4. Valós idejű sejtvizsgálat JuLI™ készülékkel

Konfluens sejtkultúrát megkarcoltunk, kezeltünk és 24 órán át 0% FBS/DMEM-ben inkubáltuk, majd a sejteket JuLI™ Br készülékkel (NanoEnTek, Szöul, Dél-Korea) vizsgáltuk, mely 24 órán keresztül óránként készített felvételt a sebzáródás állapotáról. A karcolatok méretét ImageJ-vel (National Institutes of Health, Bethesda, MD, USA) határoztuk meg.

4.7.5. Elektromos cellaszubsztrát impedancia érzékelés (ECIS)

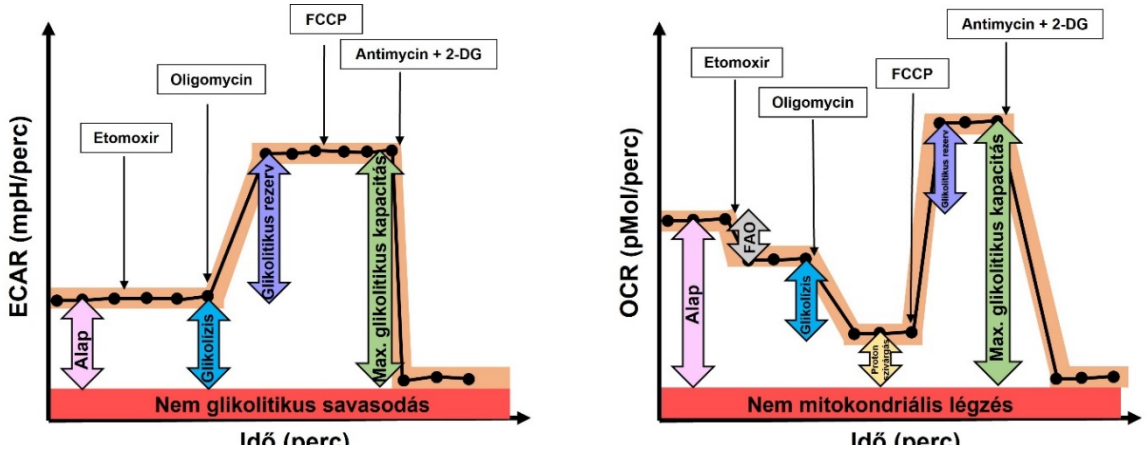
Az élő, adeherens sejtek közötti ellenállás mérésére szolgáló electric cell-substrate impedance sensing (ECIS) (Applied Biophysics) készülék a sejtrétegen sebet égetett (5 mA áramerősségű és 60 kHz frekvenciájú elektromos impulzus), majd a terület benövését és a sejt-sejt kapcsolatok helyreállását az impedancia folyamatos monitorozásával követi nyomon. A sejtréteg integritásának helyreállását az impedancia plató maximális értéke jelentette. Az impedancia mérésével a sejtek barrier funkcióját is tanulmányoztuk az impedancia valós idejű (real-time) nyomon követésével 6 órán keresztül.

4.7.6. Exocitózis esszé

A szinaptoszómák membránjának FM 2-10 festékkel történő feltöltését 30 mM KCl hozzáadásával stimuláltuk. A pelletet Krebs-pufferben reszuszpendáltuk, az exocitózist 30 mM KCl-dal váltottuk ki, a fluoreszcencia intenzitás változásait pedig Fluoroskan FL készülékkel követtük nyomon.

4.7.7. Sejtanyagcsere vizsgálat SeaHorse készülékkel

Kísérleteinkben a laktát termelés és a mitokondriális oxidatív foszforiláció vizsgálatát az extracelluláris savasodási ráta (ECAR) illetve az oxigénfogyasztási ráta (OCR) mérésén keresztül, SeaHorse analízissel végeztük el. (*7. ábra*).



7. ábra: Az extracelluláris savasodási ráta (ECAR) és az oxigénfogyasztás (OCR) mérése. *Kísérleteinkben a laktát termelést és a mitokondriális oxidatív foszforilációt az extracelluláris savasodási ráta (ECAR) illetve az oxigénfogyasztási ráta (OCR) mérésével, SeaHorse készülék határoztuk meg. Méréseink során a következő inhibitorokat használtunk. (1) Az etomoxir egy kismolekulájú inhibitor, mely irreverzibilisen gátolja a zsírsavak β-oxidációját. (2) Az oligomycin a mETC V-ös komplex protoncsatornájának gátlásán keresztül fejti ki hatását. (3) Az FCCP egy szétkapcsoló ágens, mely átjárhatóvá teszi a mitokondrium belső membránját a protonokra, ami az oxidatív foszforiláció fokozódásával jár. (4) Az antimycin A a mETC III-as komplexét gátolja, míg a 2-deoxi-D-glükóz egy olyan glükóz analóg, melynek jelenléte az ATP szintézis kompetitív gátlásához vezet.*

A kísérlet kivitelezése során a mioblaszt sejteket XF96 sejttenyésztő lemezen (Agilent Technologies; Santa Clara, CA, USA) növesztettük, majd 1000 mg/L glükózt tartalmazó XF Assay médium (Agilent Technologies; Santa Clara, CA, USA) jelenlétében inkubáltuk. Az XX ábrán részletezett inhibitorokat szenzor kazettára töltöttük fel (50 µM etomoxir; 2 µM oligomycin; 4 µM FCCP; 10 µM antimycin + 100 mM 2-deoxi-D-glükóz). Ezt követően a szenzor cartridge-ot oxigénezett inkubátorba tettük 1 órára 37 °C-ra, majd az injektálást, inkubációt és mérést követően 1 N NaOH-ban oldottuk fel a sejteket és BCA esszé kittel fehérjekoncentrációt mértünk. Az adatok kiértékeléséhez használt műveleteket a *1. táblázat* foglalja össze.

ECAR
anaerob glikolízis = alap – antimycin+2-DG
maximális glikolízis = oligomycin – antimycin+2-DG
glikolitikus rezerv = oligomycin – alap

OCR
aerob glikolízis = etomoxir – oligomycin
maximális légzés = FCCP – antimycin+2-DG
FAO= alap – etomoxir
glikolitikus rezerv = maximális légzés – FAO – aerob glikolízis

1. táblázat: A SeaHorse analízis kiértékelése során alkalmazott eljárások

4.7.8. Glükóz felvétel vizsgálata

2-NBDG (2-(N-(7-Nitrobenz-2-oxa-1,3-diazol-4-il) Amino)-2-Deoxiglükóz) felvételi mérésekhez C2C12 sejteket tenyésztettük és kezeltük. A sejteket 100 nM inzulinnal kezeltük 30 percig, majd glükóz mentes médium került a sejtekre, mely 2 µM 2-NBDG (Sigma-Aldrich) tartalmazott. Az inkubálást 120 percig végeztük 37°C-on. A fluoreszenciát 485 nm-es exitáció és 535 nm-es emissziós beállítással mértük egy Tecan Spark Multimode mikroplate olvasóval (Tecan Treading AG, Mannedorf, Germany). A fluoreszcens adatokat pmol-ban kaptuk, mely 1 mg fehérjére vonatkoztattunk.

4.7.9. Intraperitoneális glükóztolerancia teszt

Smtnl1 WT és KO vemhes és nem vemhes állatokat 12 órás éheztetést követően 2 mg/testsúly kg intraperitoneális injekcióval kezeltük majd a vércukorszintet 120 percen keresztül követtük nyomon Ascensia Breeze Blood Glucose Monitoring System készülékkel.

4.7.10. Kolonizációs vizsgálat

A HeLa sejteket transzfektáltuk, az üres vektorral kezelt mock szolgált kontrollként. A sejteket 12 napig tenyésztettük, majd a kultúrákat 1X PBS-szel mostuk, és 30 percig RT-n szárítottuk. A sejteket 0,27 m/m% Coomassie Brilliant Blue R250 festékkel (B0149) festettük, vizualizáltuk és a telepeket ImageJ szoftverrel számoltuk. A kolóniák számát a kiindulási sejtek számához normalizáltuk. A MOCK transzfektált csoportok átlagos kolóniaszámát 100%-nak vettük, az összes többi csoportot arányként fejeztük ki.

4.8. Bioinformatikai analízis

4.8.1. Proteomikai elemzés

A proteomikai elemzéshez a WT és SMTNL null egerek Plantaris-mintáit a vemhesség 0. és 14. napján homogenizáltuk. A mintákat párhuzamosan többdimenziós proteomikai elemzésnek

vetettük alá mikro-anioncserélő elválasztás, 1D SDS PAGE és LC-MALDI TOF-TOF MS/MS elemzés segítségével. A fehérjéket ezüstfestéssel tettük láthatóvá, majd kivágtuk MALDI-TOF TOF tömegspektrometriás azonosítás céljából. Az egyes fehérjék változását denzitometria és iTRAQ kombinációjával határoztuk meg [113]. A MYPT1 interakcióban lévő fehérjék azonosításához a peptid keverékeket közvetlenül "triple play" LC-MS/MS-sel elemeztük 3D-ioncsapdás tömegspektrométerrel (LCQ-Fleet, Thermo Fisher Scientific). Az MS/MS-adatokból a Mascot Distiller szoftver (v2.2.1.0) által generált csúcslistákat a Mascot rendszer segítségével az NCBI adatbázis humán alcsoportjában azonosítottuk.

4.8.2. Statisztikai analízis

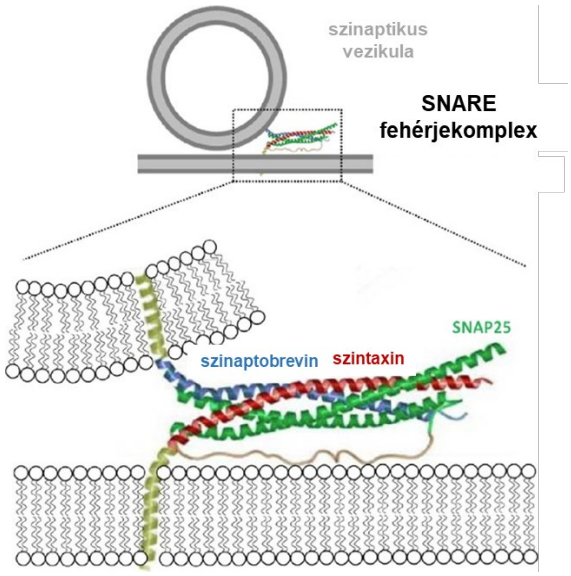
Az immunoblottok és fehérje array-k eredményeinek denzitometrálását ImageJ szoftverrel végeztük. Az oszlopdiagrammok elkészítéséhez, valamint a statisztikai analízisekhez GraphPad Prism 8 szoftvert használtunk. A foszforilált fehérjéket a nem foszforilált fehérjékre, a nem foszforilált fehérjéket pedig a belső kontrollra normalizáltuk. A normalizált adatok statisztikai kiértékelését parametrikus összehasonlításban két csoport esetén t-teszt, 2-nél több csoport esetén egyutas ANOVA vagy általános lineáris modell alkalmazásával végeztük. Varianciaanalízis során Tukey-tesztet alkalmaztunk. Két csoport összehasonlítására párosítatlan kétmintás *t*-próbát, 4 vagy több csoport összehasonlítására egy- vagy kétutas ANOVA-t használtunk, kiegészítve a *post hoc* teszttel. Az adatok átlag +/- SEM értékét mutatják, ahol „*n*” az egymástól független kísérletek számát jelzi. A kiugró értékeket Thompson-Tau teszttel és Grubbs’s teszttel szűrtük ki. A különbségeket statisztikailag szignifikánsnak értékeltük, amennyiben $p < 0.05$ (*). Az egérkolónia elemzése esetén a normalizált adatokat t-tesztekkel (két csoport esetén) vagy általános lineáris modellekkel (GLM,>2 csoport esetén) elemeztük. Ha bármely kovariáns vagy tényező szignifikáns volt a GLM-ekben, a Tukey-féle eljárást alkalmaztuk a csoportátlagok páronkénti különbségeinek tesztelésére. A teszteket az R statisztikai környezet (R Development Core Team 2008) vagy az SPSS 17.0 for Windows segítségével végeztük.

5. EREDMÉNYEK ÉS MEGBESZÉLÉSÜK

5.1. A miozin foszfatáz szerepe a neurotranszmitter-kibocsátás szabályozásban

A miozin foszfatáz (MP) fiziológiai szerepének vizsgálata eddig nagyrészt a simaizom kontrakcióra irányult, amely folyamatban a miozin II 20 kDa könnyűláncának defoszforilációjával annak foszforilációs szintjét szabályozza. Azonban a MP a simaizom mellett számos más szövettípusban is előforul, így többek között az idegszövetben. Emiatt feltételeztük, hogy élettani szerepe túlmutat klasszikus citoszkeletális szubsztrátjainak szabályozásán. A MP és a MYPT1 valamennyi agyrégióban kimutatható, de magasabb expressziós szintje egyes magcsoportokban az idegsejtekre specifikus fiziológiai funkciókat sejtet. Magas expressziós szintet a mutatott a MYPT1 a látópályában (*tractus opticus*) és a boltozatban (*fornix)*, a paraventrikuláris magok parvocelluláris részében és a periventrikuláris magokban, a középagyban, a harmadik agyidegmag központjában (*nucleus oculimotorius*), a vörösmagban (*nucleus ruber*), az emlőmagokban (*nucleus mammillaris*), valamint a kocsányközti magokban (*nucleus interpeduncularis*) [114]. Mukacsoportunk a MP-t már előzetesen kimutatta az agykéregből izolált szinaptoszómák preszinaptikus frakciójában, és igazolta kölcsönhatását a szinaptofizin fehérjével, a ROK-kal és a PP1cδ izoformával [114]. Ezek alapján feltételeztük, hogy a MP szerepet játszhat a szinapszisok vezikuláris transzportjában és a neurotranszmitterek kibocsátásában.

A neurotranszmitter-kibocsátást elsődlegesen a beáramló kalciumion váltja ki, de a folyamat végbemenetelét a neuronális fehérjék foszforilációja és defoszforilációja is szabályozza. Az ingerületátvitel első lépéseként a vezikulumok aktív transzport révén feltöltődnek neurotranszmitterekkel. Ezután a vezikulumok az aktív zóna közelébe vándorolnak, ahol megtörténik a dokkolódás, amely során a vezikulumok a preszinaptikus membránhoz horgonyzódnak. Ezután további molekuláris átrendeződés zajlik le, mely a vezikulumok sejtmembránnal való fúziójára, a „priming”-ra irányulnak. Végül a beáramló Ca^{2+} a fúziós pórus megnyílásával kiváltja a vezikulumok exocitózisát [115]. A vezikulák dokkolódásában és fúziójában az ún. SNARE (szolubilis N-etilmaleimid szenzitív faktort kötő fehérje receptor) komplex játszik kulcsszerepet (*8. ábra*).



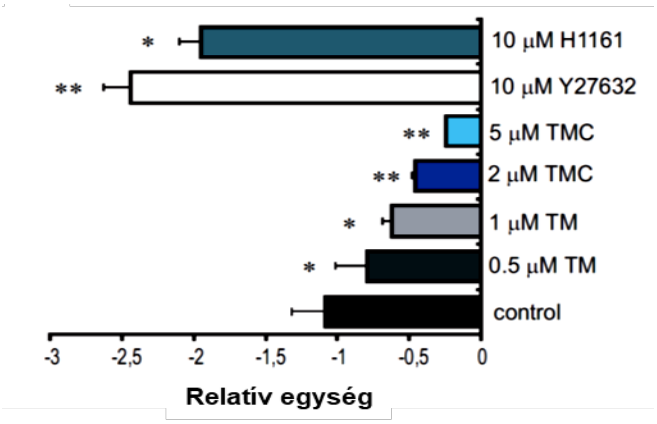
8. ábra. A SNARE komplex szerkezete. *Módosítva [6] alapján*

A komplexet három fehérje alkotja: a vezikulumok membránjához kihorgonyzott szinaptobrevin, illetve a sejtmembránhoz kapcsolódó SNAP-25 és szintaxin. A SNARE komplexben részt vevő fehérjék mindegyike hordozza a 60-70 aminosav hosszúságú, evolúciósan konzervált SNARE motívumot, melyeken keresztül összekapcsolódnak [116]. A három fehérje komplex képződése N-terminálisuktól kiindulva a C-terminálisuk irányába halad, és az eközben fellépő mechanikai erőhatások a két membránfelületet egymás irányába nyomják és fúzionáltatják. A folyamat eredményeként pórus képződik, melyen keresztül a neurotranszmitterek a szinaptikus résbe jutnak. A folyamat exergonikus, a fehérjék összeépülése spontán módon történik; energia csak a SNARE komplex felbontásához szükséges [117].

A SNAP-25 két legfontosabb foszforilációs helye a Thr138 és a Ser187, melyeket a protein kináz A (PKA) és C (PKC) is foszforilálhatja [118]. A Thr138-nak a priming folyamatában lehet szerepe, mivel PKA általi foszforilációja együtt jár az exocitózisra kész („primed") állapotban lévő vezikula pool-ok méretének növekedésével. A SNAP-25 Thr138 oldalláncon történő foszforilációja befolyásolja a SNAP-25 és a szintaxin közötti kölcsönhatás erősségét és a SNARE-komplex összeépülést, továbbá a sejtek noradrenalin szekrécióját is. A Ser187 aminosavmaradék foszforilációja a SNARE-komplex összekapcsolódását, a vezikulumok plazmamebránhoz történő vándorlását, vagy éppen a feszültség kapuzott kalcium-csatornák SNAP-25 általi gátlását is szabályozhatja. Míg a foszforilációt katalizáló protein kinázok ismertek, a reverzibilitást biztosító preotin foszfatázokról hiányosak ismereteink. Előzetes eredményeink alapján a MP az

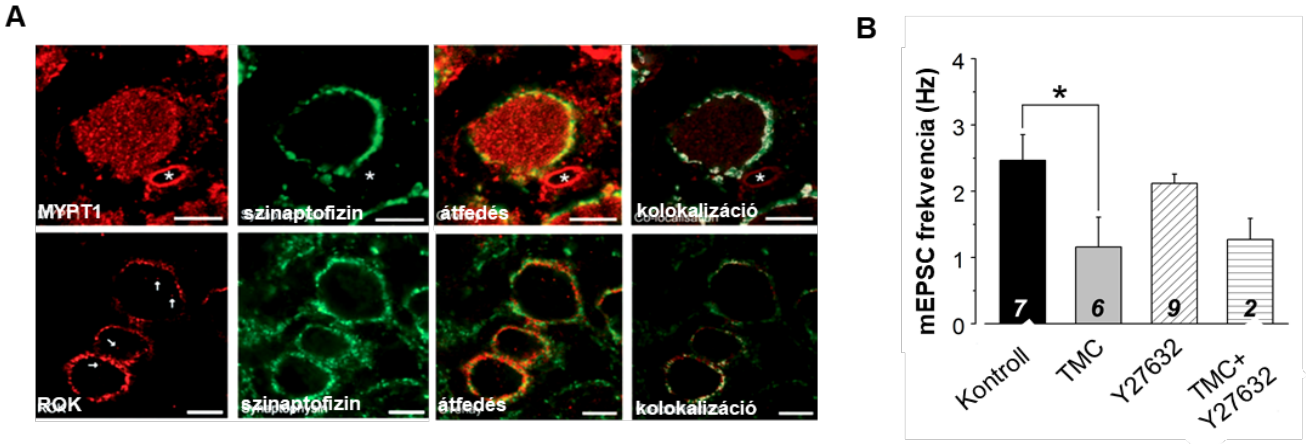
idegrendszerben is expresszálódik, és számos idegi fehérjével mutat kölcsönhatást, ennek ellenére az enzim idegrendszerben betöltött szerepe kevéssé ismert [119].

Munkánk során igazoltuk a MYPT1 és a ROK jelenlétét a patkány agykérgi szinaptoszómákban és a ventrális cochleáris magban elektron-, illetve konfokális mikroszkópia segítségével. A MYPT1 mind a preszinaptikus terminálisokban, mind a posztszinaptikus sejttestekben megjelent, míg a ROK a preszinaptikus terminálisokban dominált [120]. A PP1 specifikus inhibitora, a tautomicetin (TMC) koncentráció-függő módon gátolta a szinaptoszómák depolarizáció által kiváltott exocitózisát és csökkentette a neurotranszmitter felszabadulást *(9. ábra)*.



9. ábra. PP1 és ROK inhibitorok hatása a KCl-indukált, Ca^{2+}-függő exocitózisra az agykérgi szinaptoszómákban*. 10 μM Y27632 és 5 μM TMC önmagában vagy együttes alkalmazásuk hatása a Ca^{2+}-függő exocitózisra a kortikális szinaptoszómákból Az exocitózis sebességét az FM 2-10 fluoreszcencia relatív változásaként fejeztük ki.. n = 3-5. ** p < 0,01, * p < 0,05.*

A MYPT és a ROK a glutamaterg óriásszinapszisban az akusztikus rostok végterminálisai és a "bushy-sejtek" sejttestjei között helyezkednek el *(10. ábra*). A MP-gátló TMC és a ROK-gátló Y27632 és H1161 inhibitorok ellentétes irányú hatást fejtettek ki mind a szinaptoszómákban, mind a cochleáris magban, ami a két enzim összehangolt, ugyanazon célfehérjére ható szabályozó szerepére utalt (*10. ábra)*. A patkány hallóidegeken elektrofiziológiás méréseket végeztünk a DE Élettani Intézetével kollaborációban excitatórikus posztszinaptikus áramokat (EPSC) mérve a MP és ROK specifikus inhibitorainak jelenlétében, amiből azok pre- és posztszinaptikus lolizációjára következtettünk, amit az elektromikroszkópiás felvételek is alátámasztottak [5].

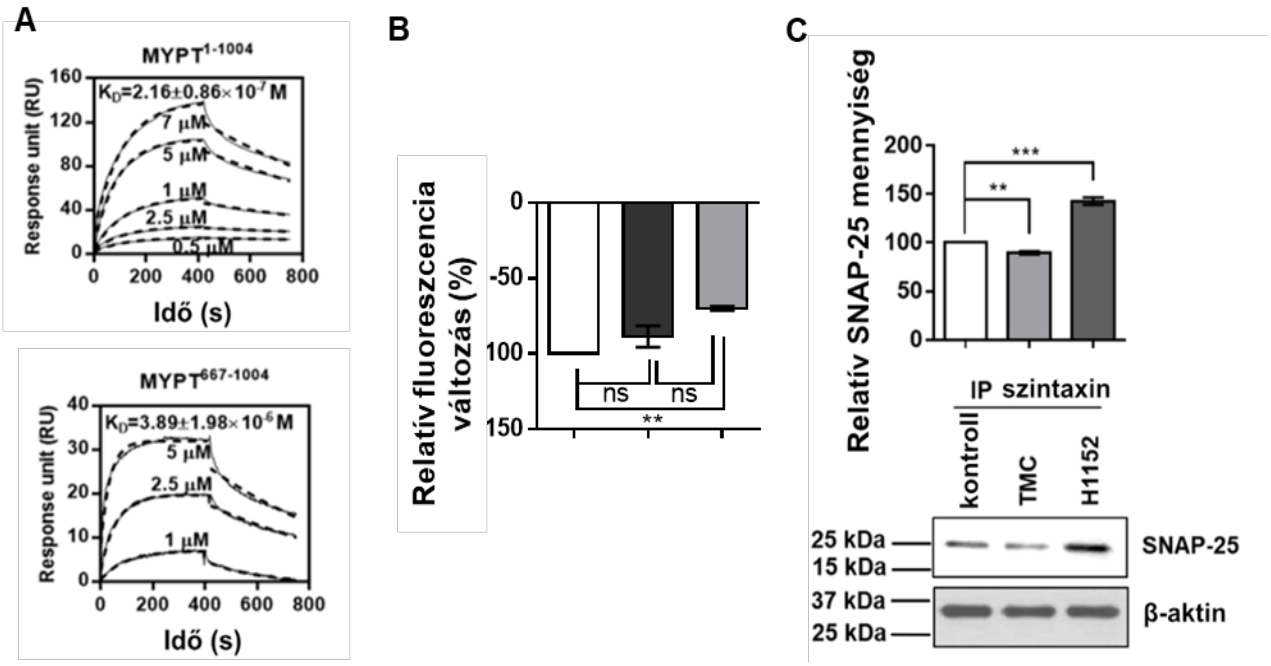


10. ábra A MP és ROK lokalizációja és szerepe az akusztikus ideg- bushy sejt szinapszisokban. *(A) A MYPT1 és ROK (piros)-specifikus immunreakciók jelenlétének és eloszlásának konfokális vizsgálata a hallóidegvégződés bokorsejt szinapszisban. *: egy kapilláris keresztmetszete. Szinaptofizin (zöld) jelöli a preszinaptikus végződést. A MYPT1 és szinaptofizin, illetve ROK és szinaptofizin kolokalizációja a jobb szélen látható. A kolokalizációt mutató pixeleket az ImageJ szoftver "Co-localization highlighter" plug-injének segítségével azonosítottuk. A méretarány: 10 µm. (B) A PP1 inhibitor (TMC) és a ROK inhibitor (Y27632), illetve az inhibitorok kombinált alkalmazásának hatása a hallóideg-bushy sejt között kialakult szinapszisban kiváltott excitatórikus posztszinaptikus áramokra (EPSC) (50 Hz). n = 3-5. * p < 0,05.*

A molekuláris mechanizmus feltérképezésére MYPT1 pull down vizsgálatot követő tömegspektrometriás elemzéssel 18 MYPT1 alegységgel kölcsönható szinaptoszómális fehérjét azonosítottunk, amelyek közül a szinapszin-I, a SNAP-25, a szintaxin-1, a kalcineurin-A alegység és a Ca^{2+}-kalmodulin függő kináz II kölcsönhatását a MYPT1-gyel koimmunoprecipitációs és pull-down kísérletekkel is megerősítettük [120].

A SNAP-25 fehérje és a MYPT1 szabályozó alegység közötti fehérje-fehérje kölcsönhatását felületi plazmonrezonanciás módszerrel is bizonyítottuk. A SNAP-25 fehérje a különböző hosszúságú MYPT1 mutánsokkal keresztkötött felületére való fecskendezését követően mért szenzorgrammok alapján viszonylag erős kölcsönhatást észleltünk a teljes hosszúságú MYPT1-gyel (K_d =2,16 ± 0,86x10^{-7}), (*11. A. ábra* felső panel), azonban a SNAP25 a MYPT1 N- és

C-terminális régióihoz is egyaránt kötődött. A disszociációs állandók alapján azonban egyértelmű preferenciát mutatott a C-terminális régió felé (K_d=4,25 ± 3,13x10^{-7}) (*11. A ábra* alsó panel) .

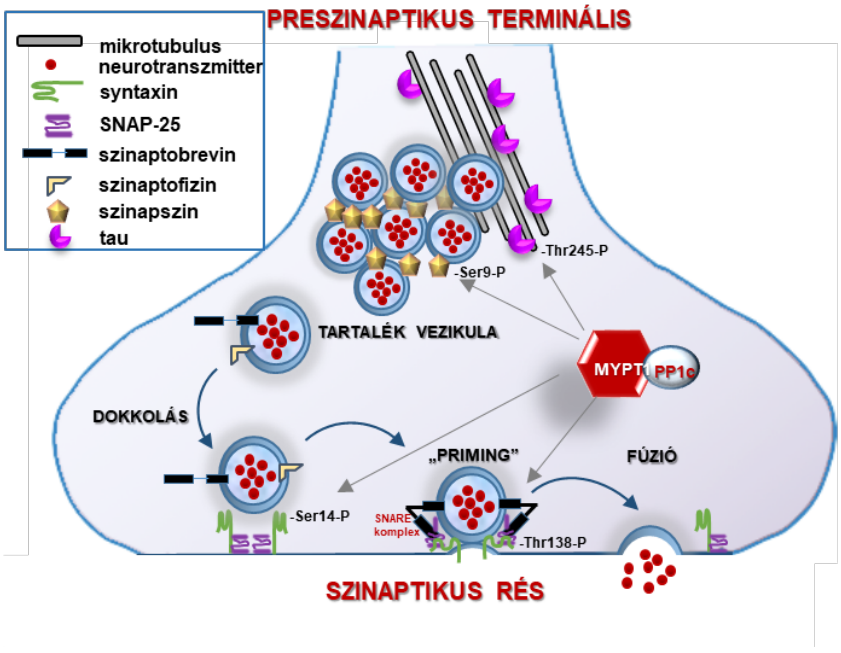


11. ábra. A MP kölcsönhat a SNAP-25 fehérjével, ezáltal elősegíti a neurotranszmitter kibocsátást. *(A) Felületi plazmonrezonanciás vizsgálatok céljából a teljes hosszúságú GST-MYPT1$^{1-1004}$ (A fent) és a C-terminális GST-MYPT1$^{667-1004}$ (A lent) fehérjéket GST elleni ellenanyaggal immobilizáltuk a szenzochipre. (B) A MP inhibitor Flag-KEPI fehérje, hatása a neurotranszmitter-kibocsátásra. Flag-peptidet (fekete oszlop) és Flag-KEPI fehérjét (szürke oszlop) juttattunk be a szinaptoszómákba fehérje transzdukcióval, és Exocitózis esszével vizsgáltuk hatásátukt a neurotranszmitter-kibocsátásra. A szinaptoszómába bejuttatott, membránkötött FM 2-10 festék fluoreszcencia intenzitása az exocitózis mértékével egyenes arányban csökken. (C). A TMC és H1152 hatása szinaptoszóma preparátumokban a SNAP-25 és a szintaxin kölcsönhatására. A szinaptoszómákat inhibitorokkal kezeltük, lizáltuk, majd elvégeztük az immunprecipitációkat szintaxin elleni antitesttel. A kihúzott fehérjék mennyiségét SNAP-25 elleni antitestekkel detektáltuk. ANOVA: p<0,0001. (n=3-5). Átlagok ± SEM (n=5), ANOVA Dunett's post hoc elemzés, *p<0,05; **p<0,01; ***p<0,001; ****p<0,0001.*

Emellett a TMC növelte, míg az Y27632 csökkentette a MYPT1 Thr696, a miozin-II könnyű lánc Ser19, a szinapszin-I Ser9 és a szintaxin-1 Ser14 foszforilációs szintjét intakt szinaptoszómákban, amelyet szemi-kvantitatív Western blot analízissel igazoltunk. Az eredmények arra utalnak, hogy a PP1M és a ROK szabályozza a preszinaptikus fehérjék foszforilációs állapotát, és ezáltal a neurotranszmissziót [120]. A MP szelektív gátlása Flag-KEPI fehérjével egyértelműen a neurotranszmisszió mértékének csökkenéséhez vezetett, amelyet a membránhoz kötött fluoreszcens festék csökkent változásával igazoltunk (*11. ábra B panel*).

Továbbá rekombináns fehérjéket használva *in vitro* foszforilációs/defoszforilációs vizsgálatokkal és tömegspektrometriás elemzéssel igazoltuk, hogy a ROK foszforilálja, míg az MP defoszforilálja a SNAP-25 fehérjét annak Thr138 oldalláncán. A MYPT1 csendesítése a B50 neuroblasztóma sejtekben növelte a SNAP-25 foszforilációját a Thr138 aminosavmaradékon. A PP1 tautomicetinnel (TMC) történő gátlása növelte, míg a ROK H1152-vel történő gátlása csökkentette a SNAP-25 Thr138-foszforilációját a B50 sejtekben, agykérgi szinaptoszómákban és agyszeletekben is [110]. Fehérje transzdukcióval a MP-t szelektíven gátló KEPI fehérjét juttatva a kortikális szinaptoszómába a SNAP-25 foszforiláció növekedését és az exocitózis mértékének csökkenését tapasztaltuk, ami arra utal, hogy a MP a SNAP-25 defoszforilációja révén elősegíti a neurotranszmitter-kibocsátást. A Flag-KEPI transzdukció hatására a SNAP-25 Thr138 foszforiláció megemelkedett a kontrollhoz képest.

A foszforilációs mértéke és a SNARE komplex elemeinek kölcsönhatása közötti összefüggést is tanulmányoztuk kortikális szinaptoszómában (*11.ábra C panel*). Ezek alapján a ROK kináz gátlása fokozta , míg a MP foszfatáz gátlása csökkentette a SNAP-25 és a szintaxin közötti kölcsönhatást.Eredményeink alapján a MP a SNAP-25 fehérje Thr-138 oldalláncának defoszforilációja által elősegíti az ingerületátvivő anyagok idegsejtekből történő felszabadulását.



12. ábra A MP neurotranszmitter kibocsátásban betöltött szerepe. *Az MP defoszforilálja a szintaxin Ser14 és a SNAP-25 Thr138 oldalláncait, ami fokozza a szinaptikus vezikulák befűződését. A szinapszin Ser9 oldalláncának foszforilációs szintje befolyásolja a szinaptikus tartalék vezikulákhoz való affinitását, szabályozva azok transzportját az aktív zónába. A Tau Thr245 foszforilációja-defoszforilációja szabályozza a mikrotubulusok összeszerelődését és a vezikulák mozgását.*

Vizsgálatainkat egér agyszeleteken is elvégeztük, és azt tapasztaltuk, hogy a KCl indukált depolarizáció a SNAP-25 Thr138 foszforilációs szint csökkenését eredményezte, amelyet a MP inhibitor szignifikánsan növelt. A fenti eredmények alapján a ROK/MP enzimpár a szinaptikus vezikulumok szállításában, fúziójában és a neurotranszmitter kibocsátás folyamatában antagonisztikusan szabályozza a SNAP25 foszforilációját annak Thr138 oldalláncán keresztüli katalízis során *(12. ábra*).

5.2. A miozin foszfatáz szerepe a génexpresszió szabályozásban

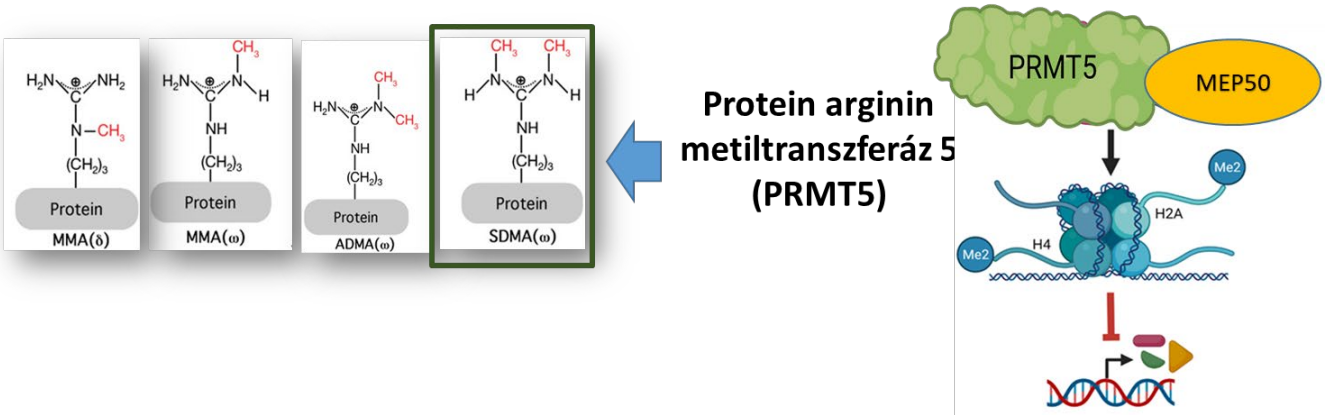
A MP alegységei a citoszkeletonon kívüli sejtfrakciókban, így a HepG2 sejtek sejtmagjában és mikroszomális frakciójában [111], valamint neuronális sejtek sejtmagjában is immunreaktivitást adtak [114]. Az egyik nem-citoszkeletális MP szubsztrát a hiszton-deacetiláz 7 (HDAC7), amely a génexpresszió szabályozásában résztvevő transzkripciós komplex tagja, amely többek között a T-limfociták differenciálódásában szerepet játszó Nur77 represszoraként működik [121]. A HDAC7 enzimet a protein kináz D is foszforilálja, ami ezt követően transzlokálódik a citoplazmába, ahol a 14-3-3 fehérjékkel társul. A HDAC7 a citoplazmában a MP holoenzimhez kötődik, amely defoszforilálja a HDAC7 foszfo-Ser oldalláncát és elősegíti a visszatérését a sejtmagba [2].

Az MP másik génexpresszió szabályozó hatása az Nkx2.5 transzkripciós faktor szubcelluláris transzlokalizációján keresztül érvényesül. Az Nkx2.5 a kardiomiogén differenciálódás egyik legkorábbi markere, ami szükséges a szívizomsejtek differenciálódásához. A MP és a Nkx2.5 közöti kölcsönhatását kísérletesen igazolták. A Wnt3a-jelátviteli pálya aktiválja a ROK-t, amely foszforilálja a MYPT1-et a Thr853 gátló foszforilációs helyen, ami a MP transzlokációját okozza a sejtmagba, ahol komplexet képezhet az Nkx2.5-tel. Egy kromoszómarégió-karbantartó 1 (Crm1) -függő útvonalon keresztül a MP az Nkx2.5 sejtmagból citoplazmába történő kijutását indukálja, és így a Nkx2.5 transzkripciós aktivitásának gátlását eredményezi [122].

Bár a fent említett MP szubsztrátok szerepet játszanak a génexpresszió szabályozásában, de valamennyi folyamatban a MP közvetett, a transzkripciós faktorok transzlokációját szabályozó módon hat. A MP közvetlen sejtmagi szerepének és szabályozásának feltérképezése érdekében azonosítottuk a nukleáris MYPT1 interaktómot pull down vizsgálatot követő tömegspektrometriás analízissel, és számos fehérjét, köztük az RNS helikázt, fémion függő protein foszfatáz 1B-t (PPM1B) és a replikációs protein A-t azonosítottunk humán hepatocelluláris karcinóma sejtekből.

Érdekes módon kimutattuk a MYPT1 kölcsönhatását az metiloszóma komplex valamennyi tagjával, így a protein arginin metil-transzferáz 5 (PRMT5), MEP50 és PCln fehérjékkel is [111].

A PRMT5 az arginin guanidin csoportjának metilációs módosítását végző Protein Arginin Metiltranszferáz (PRMT) enzimcsalád tagja. Ezek közül a PRMT1, -3, -4, -5, -6 és -8 enzimeknek aktivitását már leírták, azonban a PRMT2, -7, -9 enzimek aktivitása még nem bizonyított. A PRMT5 az egyetlen szimmetrikus metiltranszferáz aktivitással rendelkező enzim (*13. ábra)*.



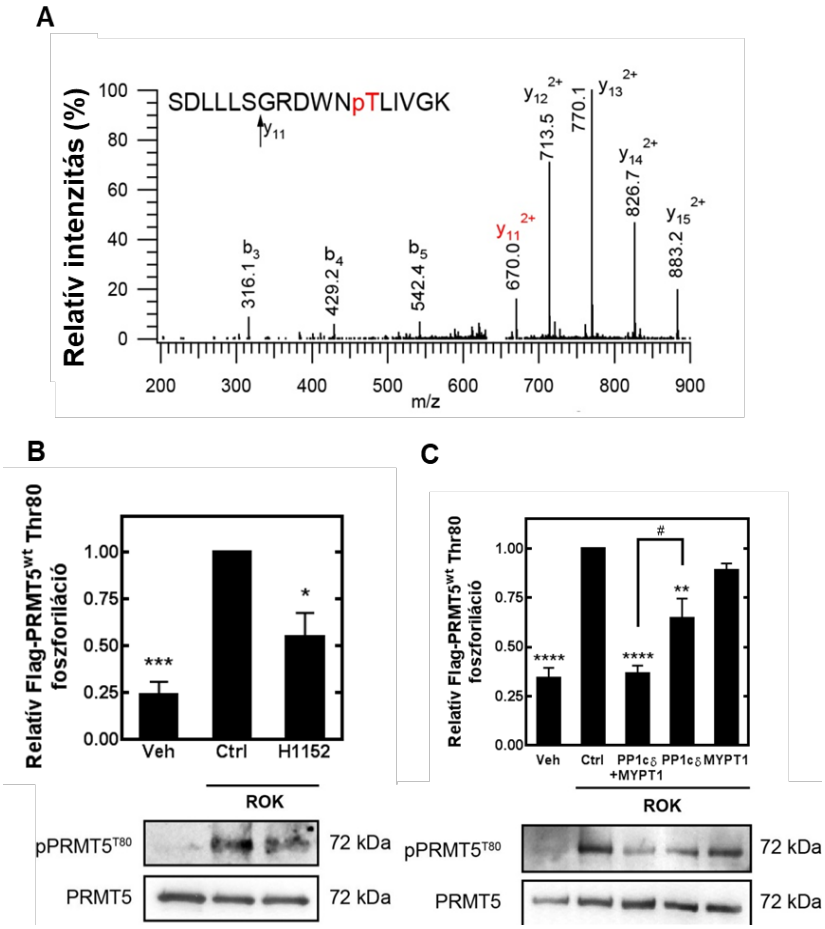
13. ábra. A PRMT5 szimmetrikus dimetilációt katalizál. *A protein arginin metiltranszferáz enzimcsalád (PRMT) tagjai -a PRMT5 kivételével- az arginin különböző N-atomjait monometilálják (MMA δ, ω) vagy aszimmetrikusan dimetilálják (ADMA). SDMA: szimmetrikus arginin dimeiláció. MEP50: methylosome protein 50 vagy más néven WD repeat-containing protein 77.*

A PRMT5-nek számos citoszolikus és sejtmagi kölcsönható partnere van, melyek a génexpresszióban, RNS szállításban, valamint a sejten belüli jelátviteli folyamatokban játszanak szerepet. A metiloszóma komplex többek között az Sm fehérjék metilációja révén snRNP-k (small nuclear ribonucleic proteins) biogenezisében játszik szerepet, de a sejtmagban számos, transzkripciós elongációt szabályozó, valamint a kromatin szerkezetét befolyásoló, átrendező faktorokkal kölcsönhatva transzkripciós koaktivátorként működik. Az enzim főbb szubsztrátjai a kromatint fölépítő hisztonfehérjék. A PRMT5 a hiszton H2A és H4 harmadik argininjét szimmetrikusan dimetilálja, ami jelentős génexpresszió gátlást eredményez. A PRMT5 aktivitását befolyásolja a működéshez szükséges partnerek kötődése, így a metiloszóma tagjai: a methylosome protein 50 vagy más néven WD repeat-containing protein 77(MEP50) és a PLCln fehérjék. Ez utóbbiak enzimatikus aktivitással nem rendelkeznek, de az enzimkomplex aktivitása a PRMT5 egyéni aktivitásához képest nagyobb [123; 124]. A PRMT5 enzim több szeril-, treonil-, és tirozil oldalláncon foszforilálódhat, így lehetőség van a működésének foszforiláció általi szabályozására [125]. A PRMT5 foszforilációját végző protein kináz enzimekről, és a

defoszforilációt végző protein foszfatáz enzimekről azonban nem állt rendelkezésre információ [123].

Konfokális mikroszkópiával HepG2 sejtekben kimutattuk a MYPT1 sejtmagi és citoplazmatikus kolokalizációját a metiloszóma komplex MEP50 és PRMT5 tagjaival, A kölcsönhatást a Pearson-féle kolokalizációs koefficiens meghatározásával számszerűsítettünk Tömegspektroszkópiás kísérletekben a MEP50 és PICln fehérjék 2-2, míg a PRMT5 8 peptidtalálattal lett azonosítva a Flag-MYPT1 interaktómban. Mivel a PRMT5 felelős a metiloszóma komplex katalitikus aktivitásáért, a továbbiakban a MYPT1 PRMT5 enzimmel való kölcsönhatására koncentráltunk. Immunpreciptációs kísérletekkel igazoltuk a két fehérje közötti kapcsolatot, majd SPR kötődési kísérlettel bizonyítottuk, hogy közvetlenül is kötődnek egymáshoz. A PRMT5 egyaránt asszociálódott a teljes hosszúságú GST-MYPT1$^{1\text{-}1004}$ (K_a=(1,62 ± 0,29 x 10^7) M^{-1}) és az N-terminális His-MYPT1$^{1\text{-}633}$ fehérjékhez (K_a=(8,82 ± 0,31 x 10^6) M^{-1}), azonban nem kötődött a C-terminális GST-MYPT1$^{667\text{-}1004}$ fragmentumhoz, ami alapján feltételezhetően a MYPT1 N-terminális szakasza biztosítja a PRMT5 fehérje kötődését.

A MP feltételezett defoszforilációs helyének azonosításához olyan protein kinázokkal végeztünk *in vitro* kináz esszét, amelyek által foszforilált aminosavmaradékokat és környéküket a MP felismerheti. Így rekombináns Flag-PRMT5 fehérjét radioaktív ATP (γ-^{32}P-ATP) szubsztrát jelenlétében PKA és PKC, illetve ROK enzimek jelenlétében foszforiláltunk, de csak az utóbbi esetén tapasztaltunk szignifikáns foszforilációt. A foszforilált PRMT5 tömegspektrometriás analízisével a PRMT5 fehérje Thr^{80} oldalláncát azonosítottuk, mint specifikus ROK foszforilációs helyet *(14. ábra*). Ezután a Thr^{80} oldallánc ROK-általi foszforilációját *in vitro* kináz esszét követően anti-foszfo-PRMT5^{T80} antitest segítségével Western blot analízissel is igazoltuk. Ezt tovább erősítette az, hogy a PRMT5 Thr^{80} oldallánc foszforilációja szelektív ROK inhibitor (H1152) jelenlétében közel 50%-kal csökkent.



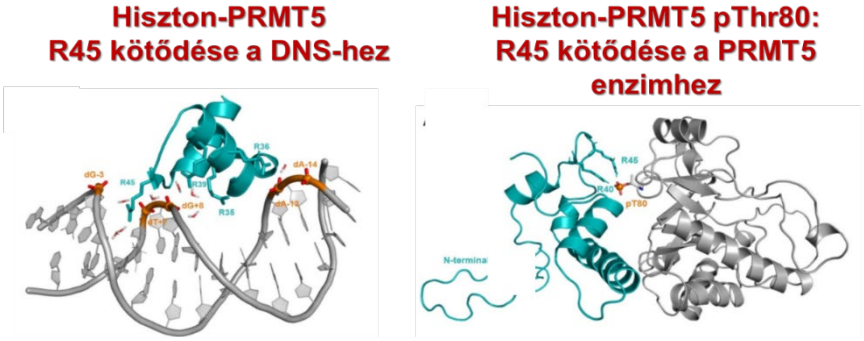
14. ábra. A PRMT5 Thr80 oldalláncát módosítja a ROK/MP enzimpár. *A ROK foszforilálja a PRMT5 Thr80 oldalláncát. (A) A PRMT5 foszfopeptidek ioncsapdás ütközésindukált disszociációs (CID) spektrumai. CID m/z: 656,338 (3+) SDLLLSGRDWNpTLIVGK peptidet azonosított, amely a vad típusú fehérje [69-85 aminosavak] peptidjének felel meg. A módosítási helyként a Thr80-at azonosítottuk (lásd az y11 fragmentumiont (foszforilált)). A peptidfragmentumok jelölése a Biemann-féle nomenklatúra szerint történt [5]. (B) A ROK-inhibitor (10 μM H1152) hatása a PRMT5 ROK általi foszforilációjára. A negatív kontroll mintákat ROK hiányában (Veh), a pozitív kontroll mintákat pedig ROK jelenlétében (Ctrl) készítettük. A Thr80 relatív foszforilációs szintjét anti-pPRMT5^{T80} antitesttel, Western blot segítségével határoztuk meg.A PRMT5 blotok belső kontrollként szolgáltak. (C) 25 nM FT-MYPT1 és 5 nM rPP1cδ vagy ezek kombinációjának hatása a PRMT5 Thr80 foszforilációs szintjére Western blot analízis szerint. Az adatokat a ROK-foszforilált PRMT5-tel hasonlítottuk össze. Az értékek átlagok ± SEM; *p<0,05, **p<0,01, ***p<0,001, ****p<0,0001, #p<0,05, egyirányú ANOVA, majd Tukey-féle többszörös összehasonlító teszt, n=3.*

Továbbá Flag-MYPT1 és rekombináns PP1cδ enzimek együttes alkalmazása esetén ~63%-kal csökkent a foszforilált Flag-PRMT5^{T80} foszforilációs szintje, míg a PP1cδ önmagában csak ~36%-kal csökkentette a Thr^{80} foszforilációt. A PRMT5 Thr^{80} PP1cδ általi fokozott defoszforilációja

MYPT1 jelenlétében a MYPT1 célrairányító és aktiváló szerepére utal a MP által katalizált defoszforiláció során (*14. ábra*).

A Thr^{80} foszforiláció PRMT5 fehérjére gyakorolt hatását az enzim metiltranszferáz aktivitásának mérésével vizsgáltuk *in vitro* kísérletekben. A hiszton H4 és H2A fehérjék Arg3 oldalláncának szimmetrikus dimetilációja csökkent (a H4R3met2 46%-kal és a H2AR3met2 64%-kal) a miozin foszfatáz jelenlétében, míg a PRMT5 fehérjéhez kötődő MEP50 mennyisége nem változott. A PRMT5 aktivitásához szükséges MEP50 kötődését tehát nem befolyásolja a PRMT5 ROK általi foszforilációja.

A PRMT5 foszforilációjának a metiloszóma komplexre kifejtett esetleges hatásait a 4 PRMT5 és 4 MEP50 egységből álló oktamer komplexben kívántuk vizsgálni. Azonban a komplex kristályosítása és szerkezetvizsgálata méretéből adódóan nem volt megoldható. Emiatt kiterjedt molekuladinamikai szimulációkat végeztünk a Pécsi Tudományegyetem Biofizikai Intézetének munkatársai (Hetényi Csaba és Börzsei Rita) segítségével. A nem-foszforilált illetve a Thr80 oldalláncon foszforilált humán PRMT5 és a MEP50 közötti dimer modelljéhez illesztettük a teljes hosszúságú hiszton H4 fehérje modelljét. A teljes hosszúságú hiszton H4-et *in situ* építettük be a humán PRMT5-MEP50 dimerbe, kísérleti H4-fragmentumok felhasználásával, valamint szerkezet- és energiaelemzéseket végeztek a komplexált és az egyedi fehérje partnerekre is. Az eredmények alapján a foszforilált PRMT5 metiltranszferáz aktivitása nagyobb a foszforilálatlan PRMT5 enzimhez képest (*15. ábra*) [126].



15. ábra. A PRMT5 kizárólag a hiszton 4 szabad formáját metilálja.

Ezzel összhangban az találtuk, hogy HepG2 sejtekben MYPT1 csendesítés hatására a PRMT5 Thr^{80} foszforilációja mintegy 46%-kal megemelkedett, és 40%-kal, illetve 45%-kal növekedett a H2AR3 és H4R3 oldalláncok szimmetrikus dimetilációja, míg a hiszton fehérjék mennyisége nem változott. A fenti eredményeket kvantitatív módszerrel is megerősítettük.

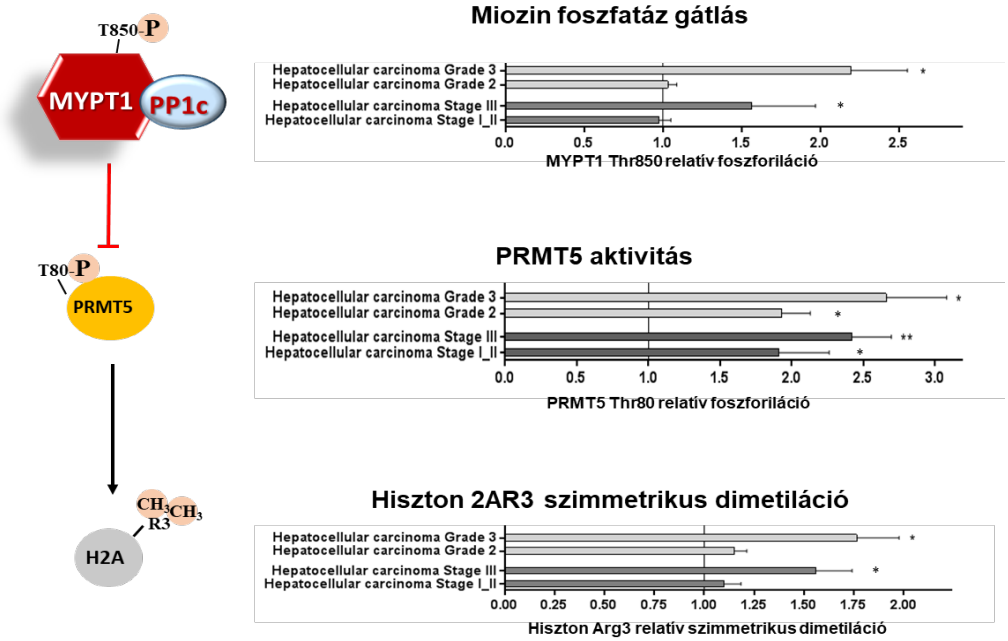
MYPT1 csendesített HepG2 sejtmagi frakciókban a specifikus PRMT5 aktivitás 65%-kal emelkedett a non-target kontroll sejtek magfrakciójához képest. Továbbá, hasonló tendenciát tapasztaltunk MCF7 emlőkarcinóma sejtek magi frakcióiban is az siMYPT1 kezelés hatására. Ezen eredmények arra utaltak, hogy a Thr^{80} oldallánc a PRMT5 működését szabályozó foszforilációs hely, és hogy foszforiláció hatására emelkedik, míg defoszforiláció hatására csökken az enzim metiltranszferáz aktivitása.

A miozin foszfatáz hiszton fehérjék dimetilációjának szabályozásához kapcsolódó funkciójának pontosabb meghatározására microarray analízist végeztünk az Affymetrix Human Gene 1.0 ST Array alkalmazásával. A non-target kontroll és siMYPT1 HepG2 sejtekből származó minták összehasonlítása során 2429 gén mutatott megváltozott expressziós mintázatot a két csoport között. A bioinformatikai analízis eredményét különböző szabályozási útvonalakkal összevetve változást mutatott például az RXR-funkció (PPAR α, γ, IL1R, JUN) az LPS/IL-1 útvonal általi gátlása, a C-vitamin antioxidáns hatása (STAT5, MAPK3 and 9), a sejtciklus szabályozása (Not7, PPP2C, CDK2, E2F3, Rb protein) vagy az IL-4 és IL-8 jelátviteli útvonal génjeinek expressziója (*Függelék Táblázat S1).* A MYPT1 csendesítésének eredményeként azt találtuk, hogy az összes érintett gén 39.5%-a kapcsolódik valamilyen daganatos megbetegedéshez, mint pl. limfohaematopoetikus-, máj- vagy emlőrák és vesesejtes karcinóma képződése. Fertőző betegségekhez és fejlődési zavarokhoz kapcsolódó géneket 10,9% -ban és 6,99% -ban azonosítottunk. Emellett számos tumorszuppresszor és transzkripciós faktor expressziója jelentős mértékben csökkent a MYPT1 csendesítés hatására, mint pl. a retinoblasztóma és *c*-Myc fehérje esetében.

Mivel a microarray-elemzés adatai arra mutattak rá, hogy MP csökkent expressziós szintje daganatképződéssel összefüggésbe hozható gének expressziójának változását eredményezte. Fordított fázisú szöveti array analízist végeztünk húsz hepatocelluláris karcinómában szenvedő beteg mintáján és 15 egyéb daganatos sejtvonal lizátumán az egészséges kontrolljaihoz képest (*16. ábra*). A PRMT5 fehérjeexpressziója a vizsgált daganatos szövetek ~75%-ában növekedést mutatott az egészséges kontrollokhoz képest. A THP-1 monocitikus leukémia és a Raji Burkitt lyphomoma sejtek mutatták a legnagyobb növekedést [111]. A PRMT5 relatív foszforilációja a Thr80-on a daganatos szövetek mindegyikében jelentősen megemelkedett, különösen a leukémiás, tüdő-, vastagbél- és emlőrákos karcinómákban, valamint a HCC szövetekben. A MYPT1 relatív expressziója változatos expressziós mintázatot mutatott, azonban a MP holoenzim aktivitását

meghatározó MYPT1 Thr850 gátlóhelyen történő foszforilációjának emelkedését tapasztaltuk szinte minden esetben, így például akár 10-12-szeres emelkedést is detektáltunk az emlő- és tüdőkarcinómákban (*16. ábra*).

Korábbi vizsgálatok [127] eredményeit alátámasztva a daganatos szövetlizátumokban a hiszton fehérjék emelkedett expresszióját és szimmetrikus dimetilációját igazoltuk így a vizsgált

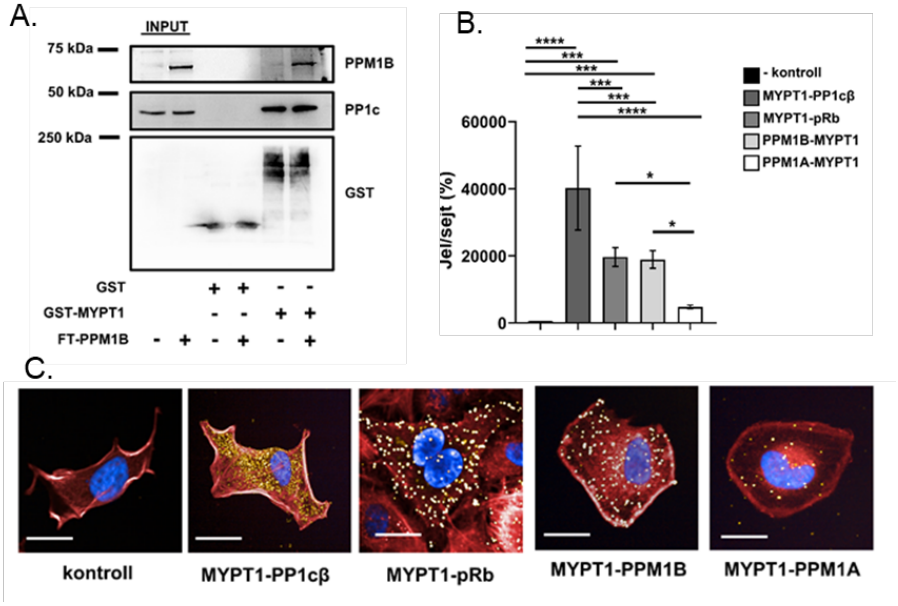


16. ábra. Human hepatocelluláris karcinóma (HCC) biopsziák fehérje expressziós profilja. *Fordított fázisú fehérje microarray analízist végeztünk a PRMT5 (felső), MYPT1 (középső) és hiszton H2A (alsó) fehérjék poszttranszlációs módosításának tanulmányozására normál és daganatos human biopsziákban. A humán HCC-mintákat (n=20) a klinikailag igazolt tumor stádium (világisszürke oszlopok) vagy grádus, fokozat (világosszürke oszlopok) besorolása alapján csoportosítottuk. Az értékek az adott fehérje foszforilációjának vagy szimmetrikus dimetilációjának átlagát jelentik a megfelelő nem daganatos mintákhoz képest expressziójukra normalizálva. Az adatok átlagok ± SEM; *p<0,05, **p<0,01, Student t-próbával.*

ráktípusok 88%-a a génexpresszió gátlását eredményező Arg3 szimmetrikus dimetilációs jel emelkedését mutatta, és a tumorszupresszorok, így a pRb génjexpresszió gátlását eredményezte. Méréseink arra utalnak, hogy az MP csökkent aktivitása kapcsolatban áll a PRMT5 megnövekedett aktivitásával és a hiszton fehérjék szimmetrikus dimetilációjával, különösen a hólyag- és vastagbélrákban, az MCF7 emlőrákban, a THP1 monocitás leukémiában, a vese adenokarcinómában és a hepatocelluláris karcinómában. Elemzéseink alapján a PRMT5 foszforilációja és aktiválása valamint a H4 hiszton arginin-metilációja korrelál a hepatocelluláris karcinóma szövetek grádusával és státuszával (n=20) (*16. ábra*). A fentiek bizonyították, hogy a

tumorszupresszor útvonalak szabályozásában, a MP a PRMT5 onkoprotein negatív szabályozója. Tehát a MP kettős funkcióval rendelkezik a daganatképződésben, mivel nemcsak a sejtmigrációt és metasztázis kialakulását szabályozó citoszkeletális elem, hanem a génexpresszió kulcsfontosságú szabályozójaként is működik, és tumorszuppresszor tulajdonságokkal rendelkezik.

Mivel nukleáris lokalizációt csak a MP és a PRMT5 mutat, de ezen enzimek effektora a ROK nem, , felmerült a kérdés, hogy mi lehet a MP/PRMT5/hiszton jelátviteli útvonal upstream



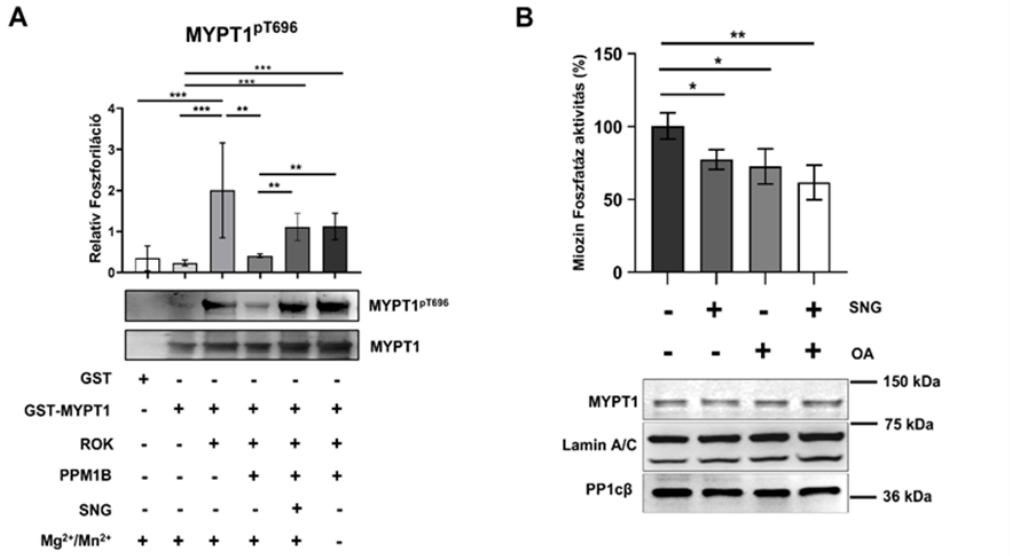
17. ábra: A PPM1B és MYPT1 közötti fehérje-fehérje kölcsönhatás igazolása *(**A**) GST-hez vagy GST-MYPT1-hez kötött Glutathione-Sepharose 4B gyöngyöket inkubáltunk FT-PPM1B transzfektált vagy nem transzfekciólt tsA201 sejtlizátumokkal. A kölcsönhatást Western blot analízissel detektáltuk anti-GST és anti-Flag antitestek alkalmazásával. A PP1cβ szolgált pozitív kontrollként. **(B)** A MYPT1 és PPM1B közötti kölcsönhatások kvantitatív elemzése Duolink PLA fehérje-fehérje interakciós esszé segítségével. A retinoblasztóma fehérjére (pRb), illetve a PP1cβ-ra specifikus antitestekkel jelölt csoportokat pozitív kontrollként használtuk. Az MYPT1 kölcsönhatását PPM1A antitesttel is vizsgáltuk. Az oszlopdiagram mutatja a Duolink PLA esszé során megjelenített fluorescens jelek számát mutatja, sejtszámra normalizálva. A negatív kontroll csoport értékét 100%-nak tekintettük. A csoport átlaga ± SD (n=3-9). A csoportokat egyutas ANOVA segítségével hasonlítottuk össze, ahol (*) p<0,05, (***) p<0,001 és (****) p ≤ 0,0001.(**C**) Az F-aktint Alexa688 Falloidinnal (piros), a sejtmagokat pedig DAPI-val (kék) festettük meg. A fehérje-fehérje kölcsönhatásokat sárga fluoreszcens jel mutatja. Méretarány: 10 µm.*

szabályozója. Korábbi eredményeink alapján a MYPT1 nukleáris interaktomjában a hiszton és a metiloszóma-komplex tagjain kívül több más fehérjét is leírtunk [111]. A MYPT1 kölcsönható fehérjék között egyetlen katalitikus aktivitással rendelkező fehérjét azonosítottunk tömegspektrometriás elemzéssel, ez pedig a $Mg^{2+/}Mn^{2+}$ -függő fehérje-foszfatáz 1 B izoforma

(PPM1B vagy más néven a PP2Cβ izoforma) volt [111]. Ezért célul tűztük ki, hogy megvizsgáljuk a PPM1B szerepét a PRMT5 által szabályozott onkogén jelátvitel szabályozásában.

Modellként a már korábban MP/PRMT5 jelátviteli pálya szabályozó hatására egyértelműen korreláló human cervikális karcinóma sejtvonalat (HeLa), majd human cervikális biopsziákat használtunk. Elsőként immunoprecipitációval[112], pull down kötődési vizsgálattal ((17. A.), és Duo Link fehérje-fehérje kölcsönhatási vizsgálattal (17. B és C.) igazoltuk, hogy a PPM1B kölcsönhatásba lép a MP MYPT1 szabályozó alegységgel. Szintén igazoltuk, hogy a MYPT1 szelektíven a PPM1B izoformával lép interakcióba (*17. ábra*), és nem a hozzá 76%-os szekvenciahomológiát mutató PPM1A izoformával [38].

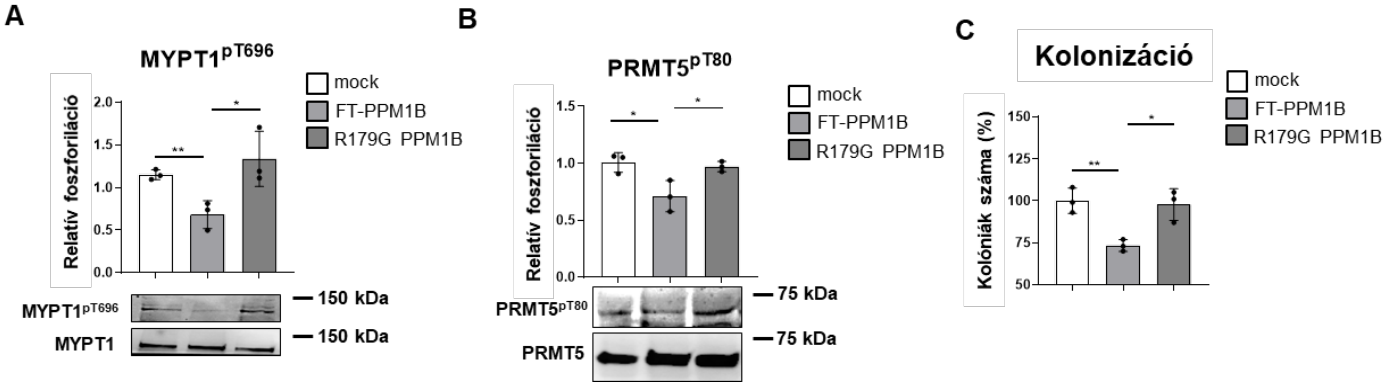
Emellett bizonyítottuk, hogy a MP MYPT1 alegysége a PPM1B szubsztrátja. MP MYPT1 szabályozó alegységének gátló foszfo-Thr696 aminosavmaradékát defoszforilálta a PPM1B *in vitro*, és ez a hatás egyértelműen fémion függést mutatott (*18.A. ábra*)[112]. A PPM1B



18. ábra: A PPM1B aktiválja az MP-t a MYPT1 Thr696 gátló foszfát csoport eltávolításával. *(**A**) GST Sepharose-hoz kapcsolt GST vagy GST-MYPT1- ROK enzimmel foszforiláltunk, majd PPM1B-vel inkubáltuk Mg^{2+} és Mn^{2+} ionok jelenlétében, vagy a nélkül, vagy Mg^{2+} és Mn^{2+} ionok és 1 µM Sanguinarine jelenlétében. A GST-MYPT1 foszforilációjának változását Western blot analízissel vizsgáltuk $MYPT1^{pT696}$ ellen termeltetett antitest alkalmazásával. Két csoportot párosítatlan kétmintás t-próbával, több csoportot egy utas ANOVA-val hasonlítottunk össze, ahol $p < 0,05$ (*), $p < 0,01$ (**) és $p < 0,001$ (***).n=3–11, átlag ± SD. (**B**) A HeLa sejteket 1 µM SNG-vel vagy 50 nM OA-val, avagy ezek kombinációjával kezeltük, kontrollként kezeletlen mintát alkalmaztunk. A miozin-foszfatáz aktivitását 1 µM ^{32}P-miozin szubsztráttal mértük. Az értékeket normalizáltuk az MYPT1 fehérje mennyiségéhez, és a kontroll csoport %-os arányában ábrázoltuk. ± SD; n=3. A csoportokat egyutas ANOVA-val, Tukey post-hoc teszttel követve hasonlítottuk össze, ahol $p < 0,05$ (*) és $p < 0,01$ (**). A sejtlizátumok MYPT1 és PP1c MP holoenzim tartalmának vizsgálata céljából Western blot analízis készült MYPT1 és , PP1cβ elleni antitestek felhasználásával, belső kontrollként lamin A/C szolgált. SNG:sanguinarine, OA:okadánsav.*

szanguinarinnal (SNG) történő gátlása kivédte a MYPT1 defoszforilációját. A HeLa lizátumok miozin foszfatáz aktivitásának mérése teljes ^{32}P-miozinnal is alátámasztotta ezeket az eredményeket (*18. B ábra*). A MP enzimaktivitása a PPM1B SNG általi gátlása következtében 23%-os (p=0,02) csökkenést mutatott a kezeletlen kontroll 100%-nak vett értékéhez képest. Az OA (okadánsav), amely szelektív protein-foszfatáz 1 és 2A inhibitor, 50 nM-os koncentrációban alkalmazva 29%-os aktivitáscsökkenést (p=0,04) eredményezett az MP aktivitásban. Az OA és SNG inhibitorok kombinált alkalmazása additív hatást mutatott, és 40%-os csökkenést eredményezett (p=0,007) a kezeletlen kontrollhoz képest. Mivelaz OA 50 nM-os koncentrációban csak a PP2A-t gátolja, a PP1-et nem [128], és még 1 μM OA alkalmazása sem befolyásolta a PP1 aktivitását a sejtekben [129], ezért eredményeink alapján elmondható, hogy a hogy a MP holoenzim aktivitását nem a PP1c katalitikus alegység közvetlen gátlása módosította, hanem a MYPT1 szabályozó alegység poszttranszlációs módosításán keresztül, közvetetett szabályozó elemek, mint pl.: a PP2A vagy PPM1B gátlása csökkentették.

A PPM1B szerepének további validálása érdekében HeLa sejteket transzfektáltunk (*19. ábra)* a Flag-PPM1B vad típusú (FT-PPM1B) és a foszfatáz-inaktív R179G mutáns formájával (R179G PPM1B) [130]. Egyik overexpressziós körülmény sem befolyásolta a MYPT1 és PRMT5



19. ábra. Az aktív PPM1B és az inaktív R179G mutáns hatása a MYPT1 expressziójára, a MP aktivitására, valamint a HeLa sejtek kolonizációs képességére. *Az üres vektor (mock), a vad típusú Flag-PPM1B (WT PPM1B) és a Flag-R179G inaktív PPM1B mutáns (R179G PPM1B) transzfektált HeLa sejtek fehérjéit anti-MYPT1^{pT696} (A), és anti-PRMT5^{pT80} (B) antitestek segítségével Western blot elemzéssel vizsgáltuk. Az értékek átlag +/- SD, n=3. A csoportokat párosítatlan t-próbával hasonlítottuk össze két csoport összehasonlítása esetén, vagy egyutas ANOVA-val több csoport összehasonlítása esetén, amelyet Tukey post-hoc teszt követett, ahol p < 0,05 (*) és p < 0,01 (**).(C) A kontroll, FT-PPM1B és R179G mutáns PPM1B overexpresszáló HeLa sejteket 12 napig tenyésztettük és a festődő kolóniák számából kiszámítottuk a túlélési tényezőt Az értékek átlaga +/- SD, és n=3. A csoportokat egyirányú ANOVA-val hasonlítottuk össze, majd Tukey többszörös összehasonlító teszttel, ahol p<0,05 (*) és p<0,01 (**).*

expresszióját. A MYPT1 foszforilációja a Thr696 oldalláncon csökkent FT-PPM1B jelenlétében, a R179G PPM1B -t overexpresszáló mintákban mért értékekhez képest (*19A. ábra*). Az MP szubsztrátjának, a PRMT5-nek az aktivitását is befolyásolta az aktív PPM1B jelenléte. A PRMT5 relatív foszforilációja a Thr80 oldalláncon csökkent az FT-PPM1B overexpressziójának hatására, míg az R179G PPM1B mutáns overexpressziója nem volt szignifikáns hatással (*19B. ábra*).

Ezek az eredmények a PPM1B *in vivo* szerepére utalnak a MYPT1 Thr696 gátló foszforilációs helyének szabályozásában és a PRMT5 aktivitására gyakorolt közvetett hatásában. A WT PPM1B és annak foszfatáz-inaktív R179G mutánsának overexpressziója hatásai közötti különbség további igazolására 12 napos kolonizációs vizsgálatot végeztünk. A WT-PPM1B-t overexpresszáló csoport kolonizációs aktivitása 27%-kal csökkent a mock kontrollhoz képest, a mutáns R179G PPM1B overexpressziója pedig gyakorlatilag hatástalan volt, ami az aktív PPM1B gátló szerepét bizonítja a HeLa sejtek kolóniaképződésében (*19C. ábra*).

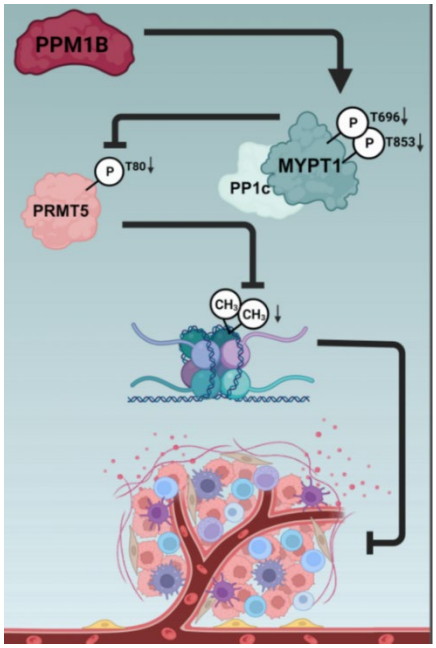
A PPM1B SNG-vel történő gátlása az MP gátlását és a PRMT5 fokozott aktivitását eredményezte, ami a H4 hiszton szimmetrikus dimetilációjának növekedéséhez, és a tumorszuppresszor retinoblasztóma fehérje szintjének csökkenéséhez vezetett HeLa sejtekben. A PPM1B overexpressziója ezekkel ellentétes hatást fejtett ki [112]. Végül a humán méhnyakrák biopsziák az egészséges kontroll mintákhoz képest a PPM1B fehérje teljes eliminációját mutatták. A daganatos biopsziákban megemelkedett a gátló MYPT1^{pT696} és a szabályozó PRMT5^{pT80} aminosavmaradékok foszforilációja, valamint a H4 szimmetrikus dimetilációja, amit a retinoblasztóma fehérje szignifikánsan csökkent expressziója kísért. Ezért a PPM1B/MP tengely tumorszupresszor szerepét a PRMT5 gátlásán keresztül értelmezzük, ami a H4 arginin-dimetilációja révén szabályozva a génexpressziót [112].

Bár a legtöbb korábbi eredmény azt sugallta, hogy az MP a ROK jelátvitel downstream effektora, egyre több eredmény utal a ROK-független hatására a daganatképzés kialakulásának gátlásában. A MYPT1 stabil Thr696 foszforilációja a daganatképződéssel egyértelmű korrelációját igazoltuk több másik munkacsoporttal összhangban, akik a MYPT1 mutációit, valamint megváltozott foszforilációját és expresszióját dokumentálták különböző ráktípusokban [131]. Érdekes módon a MYPT1 csökkent expressziója nem mindig kísérte a tumor kialakulását, de a MYPT gátló foszforilációja igen. Ez a jelenség-legalábbis részben- az MP PPM1B-vel történő szabályozásával magyarázható. Érdekes módon azokban a daganattípusokban, ahol a PPM1B downregulációját mutattuk ki, mint például a hólyag-, a gyomor- és a hepatocelluláris karcinóma,

csak a MYPT1 gátló foszforilációja mutatott korrelációt, a MYPT1 fehérjeexpresszió nem [111], ami magyarázza az MP tumorszupresszor aktivitását anélkül, hogy a fehérjeexpressziójában bármilyen változás történt volna. Bár ez a hipotézis még további kísérleteket igényel, a miRNS általi szabályozás lehetősége sem zárható ki.

Összességében eredményeink szerint a PPM1B-t a MP új foszfatázaként és az MP/PRMT5/hiszton jelátviteli útvonal upstream szabályozójaként azonosítottuk.

Betekintést nyújtottunk abba a molekuláris mechanizmusba, amellyel a PPM1B a miozin foszfatáz aktiválásán keresztül szabályozza a daganatos sejtek kialakulását. A jelátviteli útvonalak szabályozásának részletes megértése új célzott terápia fejlesztésére ad lehetőséget azáltal, hogy a PPM1B enzim új tumorszuppresszorként írtuk le. (*20. ábra*)



20. ábra A PPM1B/MP/PRMT5/hiszton jelátviteli pálya szerepe a daganatképződésben

5.3. A protein foszfatázok szerepe a bőrszövet homeosztázisának fenntartásában és a patofiziológiai folyamatok molekuláris

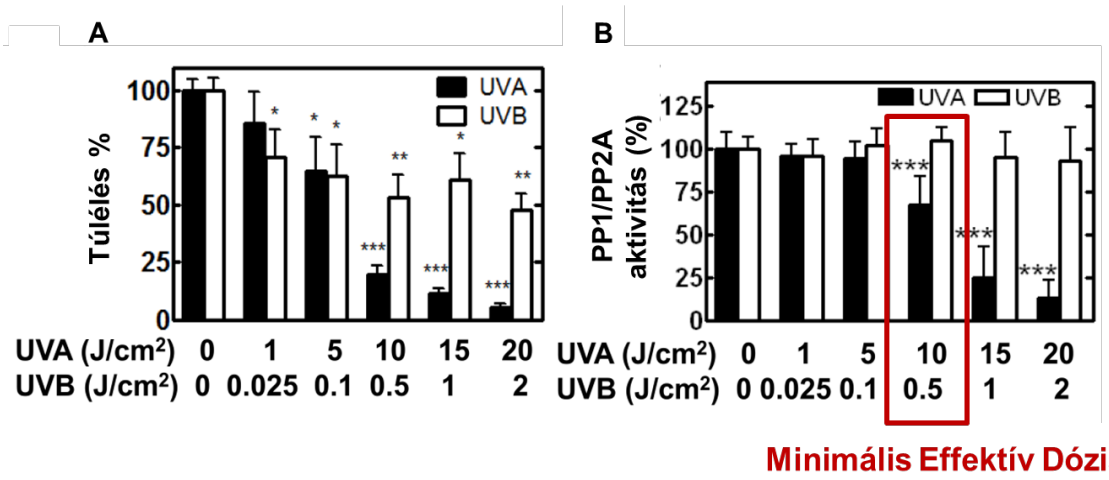
Az emlősök felhámja, a bőr külső rétege létfontosságú határfelületet képez a test és a külvilág között amely a szervezet első védvonala a kórokozók, az UV-fény és a vegyi anyagok, valamint a mechanikai sérülések ellen. A human bőr három jól elkülöníthető rétegből áll, ezek kívülről befelé haladva az epidermisz, a dermisz és a hipodermisz. A rétegek közül az epidermisz a biológiailag leginkább aktív, mivel a bazális réteg (*stratum basale*) sejtjei állandóan osztódva

folyamatosan megújítják azt. Az epitéliális sejtek a tight junction struktúrák által szorosan összekapcsolódva találhatóak az epidermiszben, miközben a bőrfelszín közelében lévő sejtek fokozatosan elszarusodnak és elhalnak [131]. Az epidermisz barrier funkcióját elsősorban ez a terminálisan differenciálódott, sejtmagjukat vesztett keratinocitákból álló elszarusodott réteg (*stratum corneum*) biztosítja [132]. A bazális réteg felett a *stratum spinosum* helyezkedik el, melyet a dezmoszómák kiterjedt hálózata jellemez. A következő réteg a *stratum granulosum*, ahol a sejtek fehérjéket és lipideket magukba záró granulumokat termelnek, melyeket a terminális differenciáció későbbi szakaszában kiürítenek az intercelluláris térbe. A *stratum granulosum* feletti szöveti régióban a sejthalál folyamata felgyorsul, az intracelluláris struktúrák elpusztulnak, és kialakul a teljesen differenciálódott korneocitákból álló *stratum corneum* [133]. Mindegyik kompartment folyamatosan önmegújuláson vagy örökös növekedési cikluson megy keresztül a posztnatális homeosztatikus és regeneratív folyamatok során. A bazális réteg sejtjei főként őssejtek vagy proliferatív progenitorok. Miután leválnak az alapmembránról (bazális membrán; BM), kifelé vándorolnak, és egy szorosan szervezett differenciálódási folyamaton mennek keresztül.

A bőrt gyakran érik különböző külső stresszhatások, így UV sugárzás vagy sebképződés, amelyek szöveti sérülést és barrier károsodást eredményeznek. Ezen patomechanizmusok mögött az egyik legfontosabb szabályozási folyamat a fehérjék reverzibilis foszforilációja. A protein Ser/Thr kinázok szerepét már leírták ezekben a folyamatban, [134], de a reverzibilitásért felelős protein foszfatázok közreműködéséről sokkal kevesebbet tudunk. Ennek felderítésére az UV sugárzás által kiváltott patomechanizmusokat és a sebgyógyulás folyamatát vizsgáltam.

A szélsőségesen magas UV sugárzás káros hatással van a bőrre, mivel bőrpírt, égést, pigmentációt, hiperpláziát, immunszupressziót, bőröregedést és rákot okoz [135]. Az ultraviola (UV) spektrumot három tartományra osztják: UVC (200-290 nm), UVB (290-320 nm) és UVA (320-400 nm). A napfényből a Föld légkörében lévő ózon, oxigén és vízgőz kiszűri az UVC és UVB sugarakat, emiatt az UVA teszi ki a Földet érő ultraibolya sugárzás 95%-át. Az UVA hosszabb hullámhossza miatt a bőrszövet mélyebb rétegeibe hatol, egészen a *dermis*ig, amíg az UVB az *epidermis* rétegében nyelődik el. Az UVA sugárzás reaktív oxigén gyököket (ROS) kelt a sejtekben, amik a lipidek, fehérjék és nukleinsavak sérülést okozzák [135].

Vizsgálatainkban a PP1 és PP2A enzimcsaládok szerepét tanulmányoztuk az UV sugárzásra adott sejtválaszokban. A human epidermist modellező HaCaT keratinocitákon és Balb/c egérbőrön a PP1 szelektív gátlószerének, a tautomycin (TM) jelenlétében mértük a sejtek



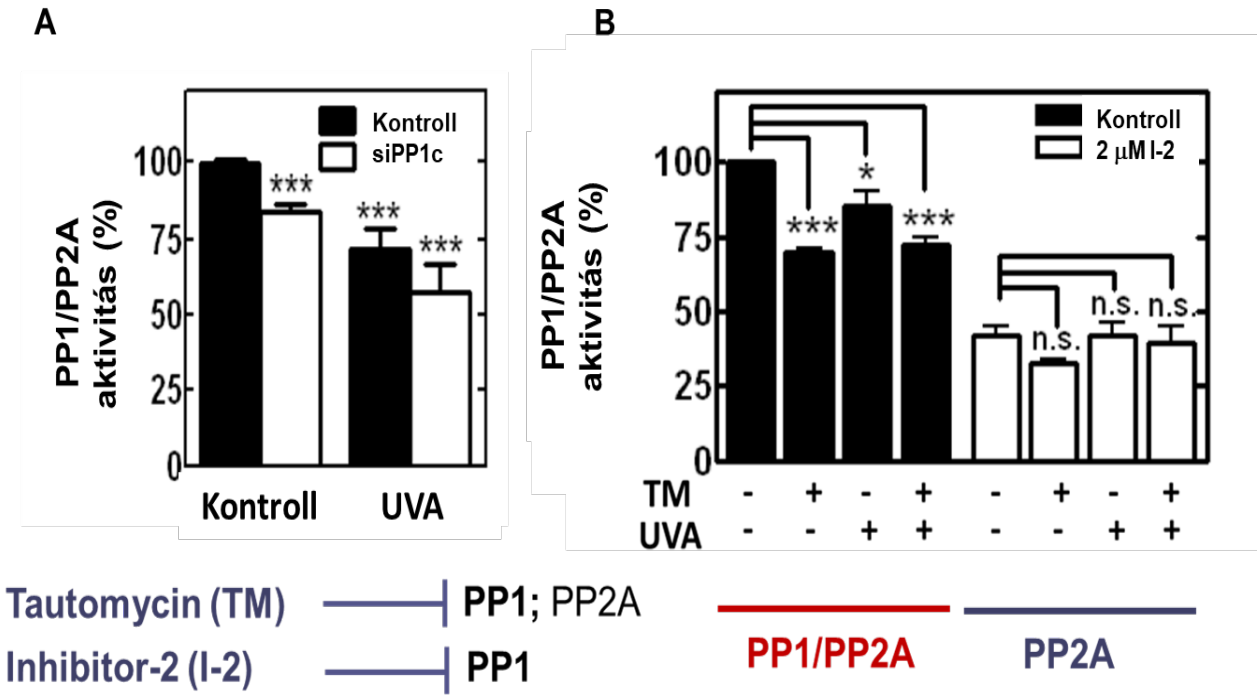
21. ábra. Az UV-sugárzás hatása a HaCaT sejtek életképességére és a protein foszfatázok aktivitására. *(a) A sejteket különböző UVA (1-20 J/cm²) és UVB (0,0025-2 J/cm²) dózisokkal sugároztuk be. MTT-méréseket végeztünk a HaCaT-sejtek sejtéletképességének értékelésére az UVA-sugárzás előtt (kontroll) és után. (b). A HaCaT sejteket a jelzett dózisú UVA- vagy UVB-sugárzásnak tettük ki, majd ^{32}P-MLC20 szubsztráttal vizsgáltuk a PP1 és PP2A foszfatázok együttes specifikus **a**ktivitást. A nem besugárzott sejtek foszfatázaktivitását 100%-nak vettük. n=5 A csoportokat egyirányú ANOVA-val hasonlítottuk össze, majd Tukey többszörös összehasonlító teszttel, ahol p<0,05 (*) és p<0,01 (**).*

túlélését, valamint a lizátumban lévő legfontosabb foszfatáz enzimek a PP1 és PP2A aktivitását (21. *ábra*).

A 10 J/cm^2 UVA-dózis a HaCaT-sejtek halálát idézte elő, és a foszfatáz-aktivitás 30 %-os csökkenését eredményezte, míg az ettől alacsonyabb dózis tartományban az UVA besugárzásnak nem volt hatása. Az UVB sugárzás befolyásolta a foszfatáz aktivitást a vizsgált dózis tartományban. Ezek alapján határoztuk meg a minimális effektív dózist (10 J/cm^2) és így a továbbiakban összesen 531 J/cm^2 dózist alkalmaztuk (21. *ábra*).

HaCaT sejtekben a PP1c-csendesítés csökkentette a foszfatáz aktivitást és gátolta a sejtek életképességét a kontroll és az UVA besugárzásnak kitett sejtekben (*22.A. ábra*). Érdekes módon az UVA sugárzás a Ser/Thr PPP enzimcsalád másik alcsaládjára, a PP2A enzimekre nem volt hatással, de jelentősen gátolta a PP1 enzimek aktivitását a PP1 család szelektív inhibitora (I-2) jelenlétében végzett mérések szerint (*22. B. ábra*). Az UVA PP1 enzimre kifejtett hatásának hátterében a katalitikus központban lévő ciszteinil oldalláncok és a fémion(ok) oxidációja állhat, ami az UVA sugárzás során termelődött reaktív oxigén gyökök keletkezésének tulajdonítható [136].

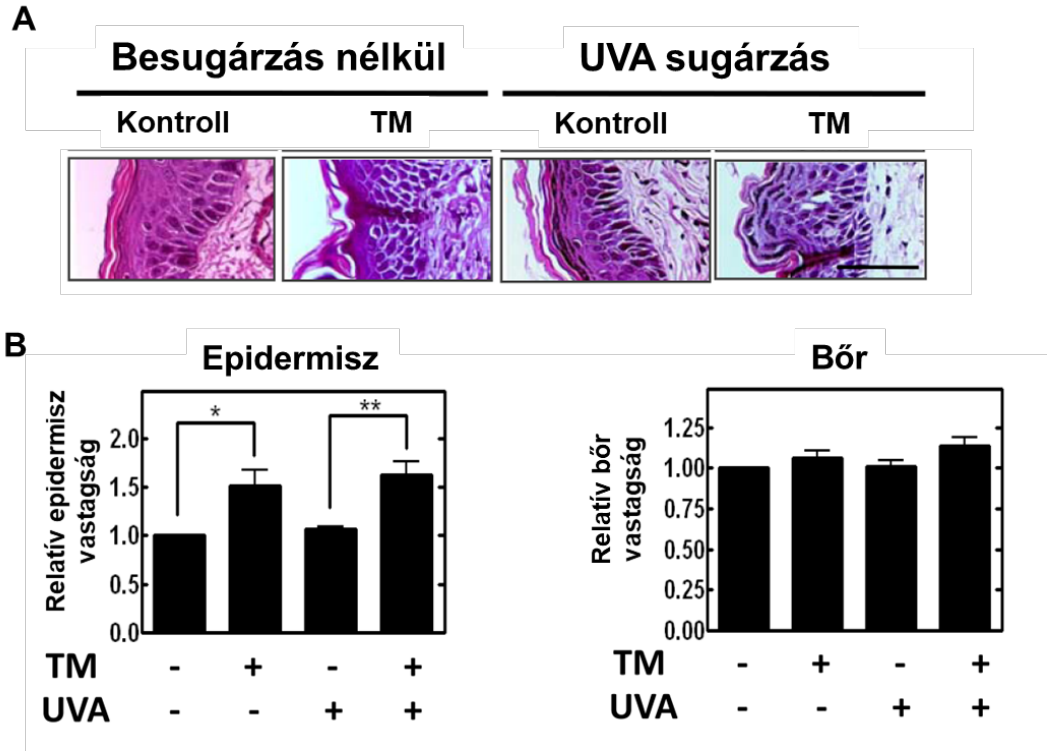
A PP1c-csendesítés és az UVA-sugárzás megváltoztatta a HaCaT sejtek génexpressziós profilját. 19 olyan gént találtunk, amelynek génexpressziója PP1-enzimtől függő módon változott



22. ábra. A PP1 csendesítés és az UVA-sugárzás hatása a HaCaT sejtek életképességére és protein foszfatáz aktivitására. *(A) A HaCaT sejteket "non-target" (kontroll) vagy PP1-specifikus siRNS-sel (siPP1) transzfektáltuk, vagy 10 J/cm^2 UVA-sugárzásnak (UVA) vagy kombinált kezelésnek tettük ki. A lizátumok foszfatáz aktivitását vizsgáltuk. (B) Az 1 μM TM-mel kezelt HaCaT sejtek foszfatáz aktivitását 10 J/cm2 UVA besugárzással vagy anélkül vizsgáltuk. A teljes (PP1+PP2A) és a PP2A aktivitásokat 2 μM inhibitor-2 (I-2) hiányában (fekete sávok) és jelenlétében (fehér sávok) mértük. A csoportokat egyirányú ANOVA-val hasonlítottuk össze, majd Tukey többszörös összehasonlító teszttel, ahol p<0,05 (*), p<0,01 (**) és p<0,01 (***).*

UVA sugárzás hatására keratinocitákban, így a microarray-analízis a keratin1/10-et, az S100A8 kalciumkötő fehérjét, és a hiszton 1b-t kódoló gének megváltozott expressziós szintjét mutatta ki [137]. Az említett gének expressziójának változását NHEK normál humán keratinocita és TM? kezelt egér bőrmintákon is igazoltunk. A PP1-specifikus gátló TM-kezelt Balb/c egerekben a keratin1/ 10 és az S100A8 fehérjék szintjének növekedését, valamint a hiszton H1b fehérjék szintjének csökkenését mutattuk ki microarray és fehérje expressziós módszerekkel az UVA-sugárzást követően. Ebből arra következtethetünk, hogy az UVA hatását legalább részben a PP1 aktivitás csökkenése okozta génexpressziós módosulások mediálják.

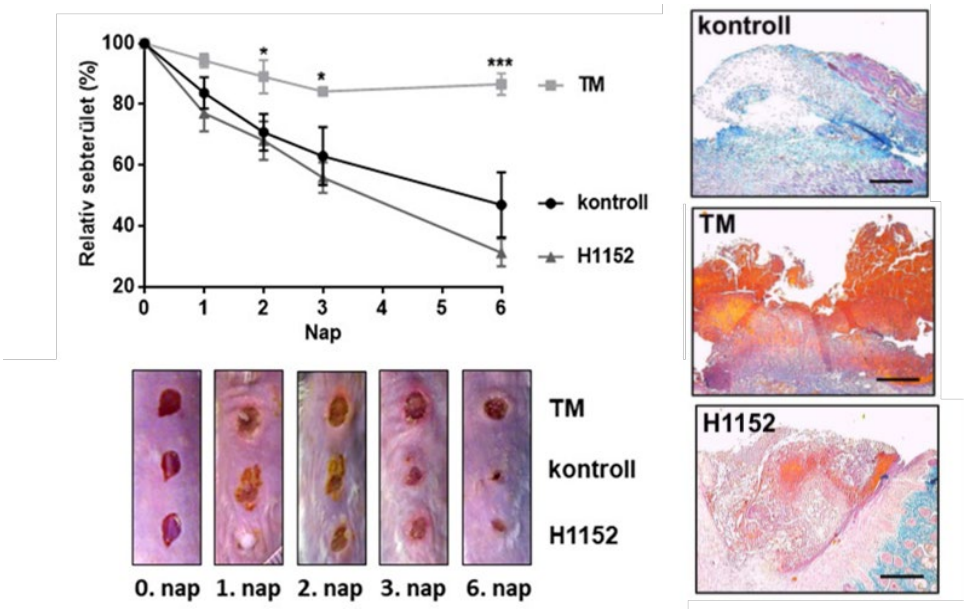
Meglepő módon a PP1 gátlószer önmagában jelentős vastagodást okozott az epidermiszben és UVA kezeléssel kombinálva ez tovább fokozódott, a teljes bőrvastagság szignifikáns változása nélkül (*23. ábra*). Emellett jelentős hegesedést, fokozott pigmentációt és pruritogén hatást tapasztaltunk.



23. ábra A PP1-gátlás és az UVA-sugárzás hatása az egér háti bőr vastagságára. *(A) Nem-besugárzott és UVA-besugárzott egerek háti bőrén kontroll és TM-kezelt felületet jelöltünk meg, majd H&E festés után fénymikroszkóppal dokumentáltuk Méretsáv=20 μm. (B) A képeket Image J program segítségével elemeztük és ábrázoltuk. és (B). Átlagok±SEM párosított t-próba *p<0,05, **p<0,01. n=9…*

A protein foszfatázok bőr homeosztázisának szabályozásában nemcsak az UV sugárzás elleni védekezésben játszanak szerepet, de az epidermis sejtjeinek differenciációjában és az akut, külső környezeti tényezőkre adott válaszokban is. A sebgyógyulás folyamata négy elkülönített fázison át történik: véralvadás, gyulladás, proliferációs fázis és szöveti újrarendeződés (remodelling). Ezek a szakaszok egymás után, de időben átfedő módon, szabályozottan zajlanak le [138]. A seb kialakulása után azonnal megindul a vérzéscsillapítás, a proinflammatorikus citokinek és növekedési faktorok felszabadulása, majd a mikroorganizmusok neutrofil granulociták általi fagocitózisa [139]. A re-epitelizáció folyamata során az epitélsejtek proliferálnak és a seb felszínére vándorolnak, hogy helyreállítsák az epidermisz barrier funkcióját. Az érési fázis során az extracelluláris mátrix újjáépül, szerkezeti felépítése pedig felveszi a normális struktúrát. A sebgyógyulás egyik fontos története a re-epitelizáció, mely a seb környékén található keratinociták proliferációját, migrációját és differenciációját foglalja magában. A proliferáció és a migráció eseményei térben elkülönülnek egymástól: a sebszél közvetlen

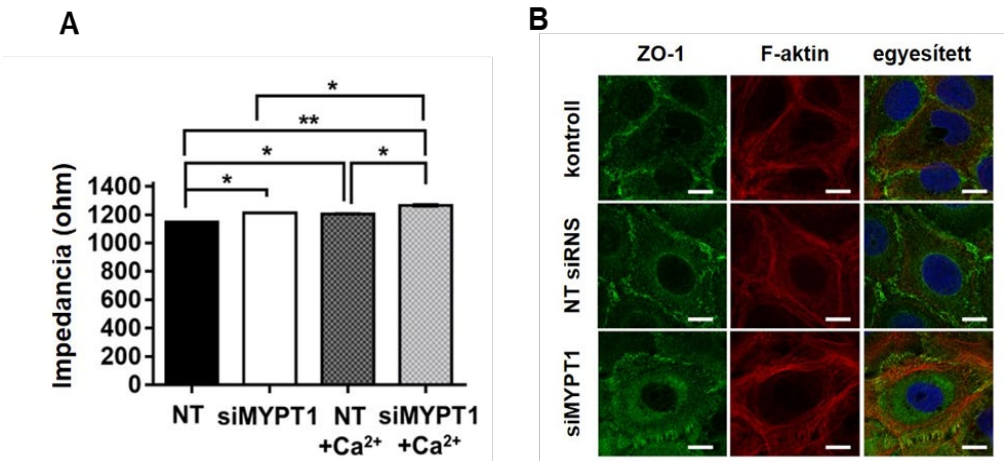
közelében lévő sejtek migrálnak, míg az attól távolabb lévő keratinociták proliferálnak [140]. A re-epitelizáció szabályozásában számos növekedési faktor vesz részt.



24. ábra: A PP1 gátlása megakadályozza az egérbőrön ejtett sebek gyógyulását. *Relatív sebterület mérete az egyes kezelések és a sebzés óta eltelt napok függvényében. n=6, kiértékelés kétutas ANOVA-val és post-hoc Dunnett-teszttel. *p<0,05; ***p<0,001. (bal fent) A sebekről készült fényképek reprezentatív minták. Egérbőrből kimetszett sebminták trikróm festése a re-epitelizáció tanulmányozására a sebzés utáni 6. napon Masson-Goldner eljárással. (jobb oldali panelek) A sejtmagok sötétbarnák, a citoplazma és az izmok téglavörösen festődnek, míg a kötőszövet és a nyálkahártya kék. Méretskála hossza: 300 µm.*

Korábbi munkánk szerint a protein foszfatázok és kinázok is jelentős szerepet játszanak a folyamatban [141]., A foszfatázok szerepének pontos kivizsgálása érdekében HaCaT sejteket okadánsavval és kalikulin-A-val kezeltünk és karcolási eszével vizsgáltuk a sejt migrációt. Azt tapasztaltuk, hogy a PP1 és a PP2A együttes gátlása lassította a migrációt. A PP1 és a ROK sebzáródásban játszott szerepét egerek hátbőrén ejtett sebek TM és H1152 inhibitorokkal történő kezelésével tanulmányoztuk. A TM, a PP1 inhibitora a sebgyógyulás teljes elmaradását eredményezte és a trikróm festés szerint a re-epitelizáció folyamatának teljes leállását eredményezte *(24. ábra*).

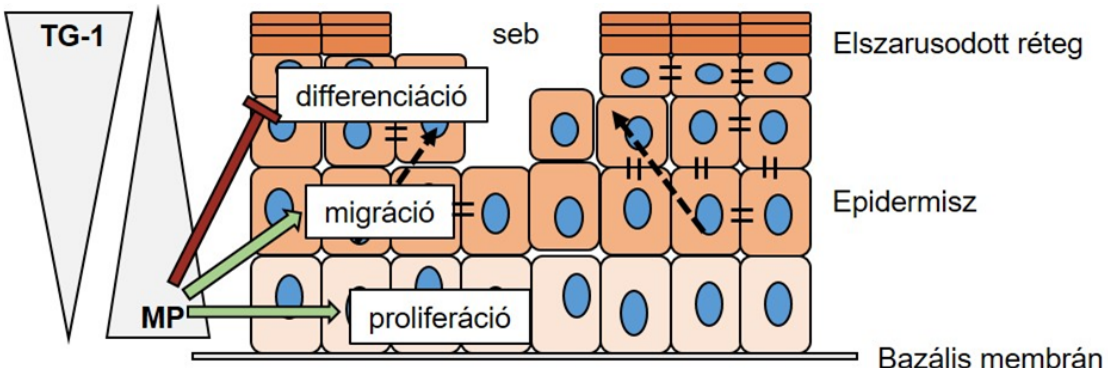
Mivel a PP1 enzimcsaládon belül a MP specifikus hatását kívántuk vizsgálni, ezért nemcsak a PP1 gátlószereit alkalmaztuk, de a MYPT1 szabályozó alegység csendesítését is elvégeztük. Humán keratinocita (HaCaT) sejtek migrációját karcolási esszével tanulmányozva azt tapasztaltuk, hogy a TM, valamint a MYPT1 csendesítése szignifikánsan lassította, míg a ROK inhibitora, a H1152 gyorsította a sebzáródást [1]. A MYPT1 csendesítése és a keratinociták barrier



25. ábra: A MYPT1 csendesítés hatása humán keratinociták közötti sejt-sejtkapcsolatokra. *(A) Differenciálatlan és kalciummal differenciáltatott (+Ca^{2+}) HaCaT sejteket non-target (NT), illetve siMYPT1 plazmidokkal transzfektáltunk, és ECIS készülékkel mértük az impedanciát. A statisztikai elemzést kétutas ANOVA-val és post hoc Tukey-teszttel végeztük. *p<0,05; **p<0,01, ns: nem szignifikáns. (B) HaCaT sejtek immunfluoreszcenciás festése (B) anti-zonula 1 (ZO1) antitesttel (zöld), illetve fluoreszcensen jelölt Texas Red-X phalloidinnel az F-aktin (piros) kimutatására. A sejtamgokat (kék) DAPI-val festettük meg. A sejteket siRNS-sel transzfektáltuk. a méretskála: 10 µm.*

funkciójára is hatással volt (25.A. *ábra*), azáltal, hogy gátolta a sejt-sejt adhéziót, amit az ECIS módszerrel mérhető impedancia növekedése igazolt. A MP alegység csendesítése gyengítette a keratinociták közötti sejt-sejt kapcsolatot. Látható, hogy a két sejt közötti membránszakasz egymástól szakaszosan elvált, a zonula 1 membránmarker festődése szakaszossá és heterogénné vált (*25. ábra B panel zöld*).

Bár a MP csendesítése jelentős fiziológiai hatást váltott ki, de a háttérben álló molekuláris mechanizmus még jellemzésre várt. Mivel a fentiekben részletezett módon már meghatároztuk a PP1 enzimektől függő géneket [137], ezért a keratinociták migrációjával, proliferációjával vagy differenciációjával, illetőleg a sebgyógyulással összefüggésbe hozható géneket vizsgáltuk MYPT csendesítés hatására. Megállapítottuk, hogy az S100A8, low density lipoprotein receptor, vanilloid receptor-1, transzglutamináz-1, továbbá a keratin-1 és a keratin-10 fehérjék közül egyedül a transzglutamináz-1 (TG1) expressziós szintje mutatott szignifikáns eltérést a siMYPT mintákban. Míg a keratin-1 és -10 a korai terminális differenciáció markerei, addig a TG1 a *granulosum* és a *stratum corneum* érett keratinocitáiban expresszálódik, és a késői terminális differenciáció indikátorai [142]. A TG1 enzim egyes fehérjék (pl. involukrin, lorikrin) közötti γ-glutamil-ε-lizin izopeptid kötések kialakítása által elősegíti az úgynevezett elszarusodó sejtboríték, plazmamembrán alatt található fehérjeréteg – létrejöttét a differenciálódó keratinocitákban.



26. ábra A miozin foszfatáz sebzáródásban betöltött szerepe. *A MP serkenti a keratinociták proliferációját és migrációját (zöld nyilak), míg gátolja a differenciációjukat (piros nyíl). Az enzim az alsóbb, osztódó és vándorló sejteket tartalmazó rétegekben aktív, míg a felsőbb rétegekben expressziója gátlódik, ezzel párhuzamosan pedig a TG-1 expresszió fokozódik, ami hozzájárul a hámsejtek terminális differenciációjához. (módosított ábra: [1].)*

Vizsgálataink egyediségét az adja, hogy a normal és HaCat immortalizált keratinociták és egér bőrön végzett kísérletek mellett sebészeti úton eltávolított *ex vivo* human bőrön is elvégeztük a MYPT1 csendesítési kísérletet. Mind HaCaT sejtekben, mind *ex vivo* bőrszövetben a MYPT1-csendesítés fokozta a transzgultamináz-1 (TG1) expressziót. A normál bőrben a MYPT1 inkább az epidermisz mélyebb rétegeiben található meg, míg a TG1 elsősorban a *stratum granulosumban* és *stratum spinosumban*. Sebzés hatására a bazális rétegben még erősebb MYPT1 festődést tapasztaltunk, a TG1 pedig a bazális réteget kivéve az epidermisz valamennyi rétegében expresszálódott. Elképzelésünk szerint a bazális rétegben a MP elősegíti a sejtek proliferációját és migrációját, illetve a TG1 downregulációjával meggátolja a differenciációt (*26. ábra*).

A külső sejtrétegekben (*stratum granulosum*) a MYPT1 expressziója lecsökken, a TG1-é pedig megemelkedik és így járul hozzá a keratinociták differenciációjához és a bőr elszarusodásához. MYPT-csendesített *ex vivo* humán bőrszövetek lizátumait humán foszfo-MAPK array-vel vizsgáltunk, és így a MYPT1-től függő foszforilációs állapotváltozásokról kaphattunk képet. Vizsgálati eredményünk az Akt jelátviteli útvonal és a hsp27 fehérje upstream regulátorainak jelentős változását mutatta. A hsp27 különféle sejtfolyamatokat szabályoz. A felsőbb, granuláris rétegekben foszforiláltabb formában fordul elő [143], és ismert, hogy expressziója és foszforilációja szükséges a keratinociták differenciációjához és a megfelelően rétegzett epidermisz kialakulásához [144] . Ezek alapján lehetséges, hogy az epidermisz felsőbb rétegében a downregulálódó MP-zal párhuzamosan aktiválódó Hsp27 segíti elő a differenciációt (*26. ábra*).

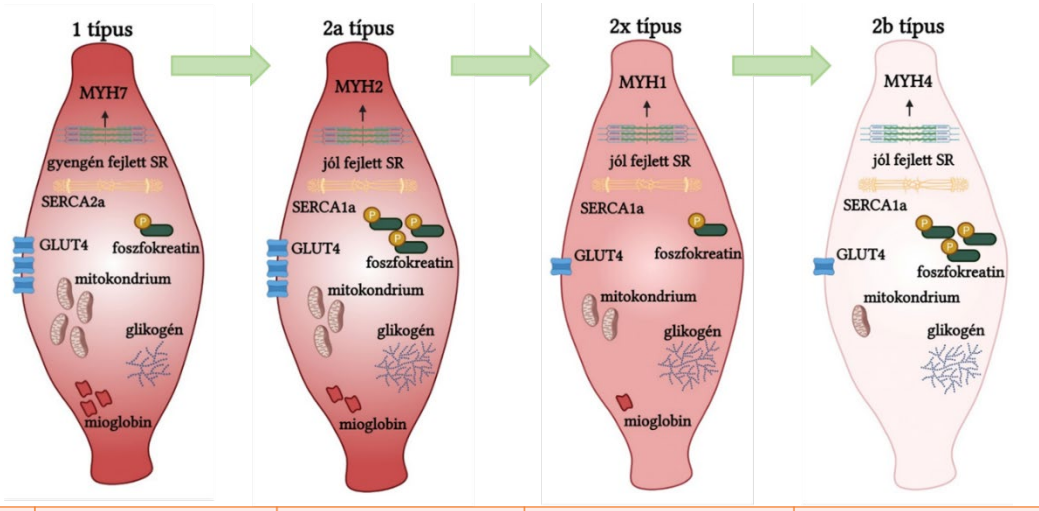
Ezek az adatok arra utalnak, hogy a PP1 enzimcsalád, azon belül is a MP kiemelt jelentőségű az epidermis homeosztázisának fenntartásában nemcsak az UV sugárzás elleni védelemben, de az a keratinociták proliferációjának és migrációjának előmozdítása révén, így ez az enzim potenciális célpontnak tekinthető a sebgyógyulás zavaraival összefüggésben lévő betegségek (fibrózis, szaruhártya betegségek, krónikus fekélyek) kezelésében.

5.4. Az SMTNL1 kettős hatásmechanizmusa: citoszkeletális regulátor és transzkripciós kofaktor

5.4.1. A vázizom felépítése és plaszticitása

A szervezet fiziológiás (például a terhesség vagy edzés) és patológiás változásainak hatására a sima- és vázizomzat jelentős átalakuláson megy keresztül. Minden állapotot a strukturális, kontraktilis és receptorfehérjék egyedi készletének kifejeződése jellemez, amelyek a génexpresszió különböző mintázataival korrelálnak. A vázizom alapvető szerkezeti egysége a többmagvú, harántcsíkolt izomrost. Az emlősök vázizomrostjainak 4 fő típusát a 27. *ábra* szemlélteti. Az 1 típusú lassú, a 2a típusú gyors oxidatív és a 2b típusú gyors glikolitikusabb rostok aránya változik, ami kihatással van az izomzat kontraktilis sajátságai mellett a szervezet anyagcsere folyamataira is. A 2x típusú rostok átmeneti rosttípust jeleznek. Rágcsálók esetében a különböző típusú izomrostokat arab számmal, míg a humán eredetű izomrost típusokat római számmal szokás jelölni, disszertációm megírásakor én is ezt a jelölést követtem.

A kisebb átmérőjű 1-es típusú rostok miozin nehézlánc 1 fehérjét (MyHC 1) és 2a típusú Ca^{2+}-ATPázt (SERCA2a) expresszálnak, lassú összehúzódásúak, nem fáradékonyak, szarkoplazmás retikulumuk gyengén fejlett. Mitokondriumban gazdagok és kiterjedt kapillárishálózattal rendelkeznek. A szarkoplazmában lévő nagy mennyiségű mioglobin adja jellegzetes vörös színüket. Ezen felül magas trigliceridtartalom és a szarkoplazma alacsony glikogéntartalma jellemzi (27. ábra). Döntően aerob anyagcserét folytatnak, melynek üzemanyaga a glikolízisből származó piruvátból a piruvát dehidrogenáz (PDH) enzim aktivitása nyomán előállított, vagy a szabad zsírsavak β-oxidációjából keletkező acetil-CoA, amely a mitokondriális oxidatív foszforilációban hasznosul. A folyamat során 36-38 mol ATP / mol glükóz keletkezik,



Miozin nehézlánc (MyHC)	1	2a	2x	2b
Kontrakció/relaxáció	lassú	gyors	gyorsabb	leggyorsabb
Anyagcsere	aerob	anaerob	anaerob	anaerob
Oxidatív kapacitás	magas	magas	közepes	alacsony
Glikolitikus kapacitás	alacsony	magas	magasabb	legmagasabb
Fáradékonyság	nem fáradékony	kevésbé fáradékony	közepesen fáradékony	nagyon fáradékony

27. ábra: A vázizmot felépítő különböző típusú rostok összehasonlítása.

amely biztosítja a kontrakció teljes ATP igényének hosszútávú fedezését. Ezzel szemben glikolitikus kapacitásuk és foszfokreatin szintjük alacsony [145; 146] (*27. ábra*).

A nagyobb átmérőjű 2-es típusú rostok gyors összehúzódásúak, szarkoplazmás retikulumuk jól fejlett, SERCA1a-t expresszálnak és a rostokat kevésbé dús kapillárishálózat veszi körül az 1-es típusú rostokhoz képest. Energiaszükségletüket anaerob glikolízisből fedezik, amely energetikailag kedvezőtlen, de gyors módja az ATP előállításának (2-3 mol ATP / mol glükóz). Az ehhez szükséges glükóz az extracelluláris térből vagy a szarkoplazmában raktározott glikogénből származik, a folyamat végterméke a laktát. A fehér színű, miozin nehézlánc 2b-t (MyHC 2b) expresszáló 2b típusú rostok igen magas glikogén- és foszfokreatintartalmuknak köszönhetően nagy erőkifejtésre képesek, de ehhez kevés és kisméretű mitokondrium társul, ezért intenzív igénybevétel esetén hamar kifáradnak *(27. ábra*). Ezzel szemben a rózsaszín, miozin nehézlánc 2a-t (MyHC 2a) expresszáló 2a típusú rostok oxidatív és glikolitikus kapacitása egyaránt nagy (a magas mitokondrium-, foszfokreatin- és mioglobin tartalomnak köszönhetően), ennélfogva kevésbé fáradékonyak, de kisebb erőkifejtésre képesek a 2b típusú rostokhoz képest (*27. ábra*). A humán vázizmokban az MyHC 2b nem detektálható, annak ellenére, hogy a fehérjét kódoló gén (Myh4) megtalálható a genomban. A 4 rosttípus közül a legkésőbb fedezték fel a

miozin nehézlánc 2x (MyHC 2x) fehérjét expresszáló 2x típusú rostokat, amelyek tulajdonságaikat tekintve átmenetet képeznek a 2a és 2b típusú rostok között (7. ábra). Érdemes megjegyezni, hogy a patkány és egér 2x típusú rostokkal ellentétben a humán IIx típusú rostok rendelkeznek a legalacsonyabb oxidatív kapacitással [145; 147]. Bár léteznek olyan izmok, melyek szinte kizárólag egyféle rosttípusból épülnek fel, pl. a rágcsálók *m. soleus* izma (1-es típus), a legtöbb emlős vázizomban az 1-es és 2-es típusú rostok változartos kombinációja figyelhető meg, és az expresszált MyHC fehérjék minősége és mennyisége jellemző az adott izomra. Az érett vázizomrost MyHC összetétele és ezáltal a fenotípusa dinamikusan változik, amit a beidegzésük és a szervezet működésében betöltött funkciójuk mellett számos hormonális faktor -különösképpen a pajzsmirigyhormonok- befolyásolhat. Az 1-es típusú rostokra jellemző lassú fenotípus kialakításáért és fenntartásáért nagyrészt a beidegző motorneuronoktól szinte folyamatosan érkező alacsony frekvenciájú stimulusok felelősek, míg a 2-es típusú rostok gyors fenotípusára jellemző tulajdonságok megjelenését a beidegzés kevésbé befolyásolja [148; 149]. A pajzsmirigyhormonok a beidegzéssel ellentétes hatást fejtenek ki, ugyanis a gyors fenotípusra jellemző kontraktilis fehérjék expressziójának transzkripciós szintű szabályozása révén a 2-es típusú rostok kialakulását indukálják. Hormonhatásra az izotípus arány az 1. típusú rostoktól a 2. típusú rostok felé tolódik el (*27. ábra*). A váziziom izotípusa az izomzat testtömeghez viszonyított magas aránya miatt meghatározza nemcsak a kontraktilis sajátságokat, de a teljes szervezet anyagcseréjét is

Az előző fejezetekben ismertetett módon a MP egyik potenciális regulátora az SMTNL1. Azt, hogy a MP aktivitását az SMTNL1 gátlolja, már korábban kimutattuk teljes miozin és az izolált miozin könnyű lánc szubsztrátokkal is *in vitro* [27, 28]. Továbbá, leírtuk azt is, hogy az SMTNL1 a vázizomban specifikusan expresszálódik a 2a típusú adaptív rostokban, és hogy a gén deléciója elősegíti e rostok megnövekedtek. Eredményeink arra utaltak, hogy az SMTNL1 mind a vázizom, mind az érrendszeri plaszticitás közvetítésében szerepet játszik [28]. Az SMTNL1 KO egerekkel végzett vizsgálatok során számos nemhez kapcsolódó különbséget figyeltünk meg [28]. Így például a mozgásszegény és edzett nőstény SMTNL1 KO egerek érrendszeri simaizomzata jelentősebb változásokat mutatott adrenerg agonisták hatására, mint hím alomtársaiké. Az edzés az SMTNL1 expressziójának nagyobb mértékű csökkenését eredményezte a nőstényekben, mint a hímekben. A hím SMTNL1 KO egerek harántcsíkolt izmai nagyobb hajlamot mutattak az oxidatív fenotípusra való átállásra. Ezek az eredmények együttesen azt sugallták, hogy az SMTNL1

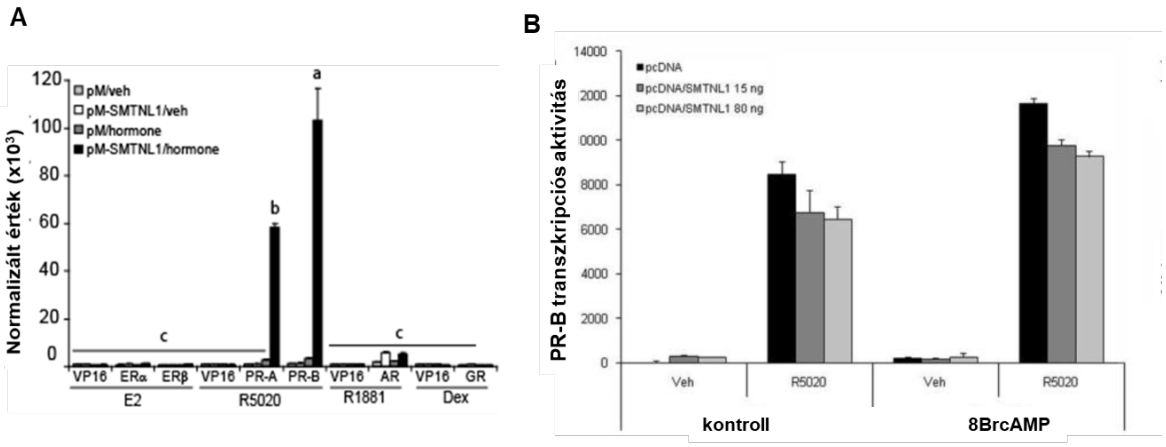
szerepet játszik a nemi hormonok hatásának közvetítésében mind az érrendszeri, mind a vázizomzat plaszticitásában. Disszertációmban az ezzel kapcsolatos újabb vizsgálataink eredményeit ismertetem.

5.4.2. Az SMTNL1 a progeszteron receptor koregulátora szteroidhormon függő szövetekben

A kérdés, miszerint milyen molekuláris mechanizmussal szabályozza az SMTNL1 az izom adaptációs folyamatait a női nemi hormonok hatására, még megválaszolatlan maradt. Ennek felderítésére sejtkultúrában, SMTNL1 KO állatmodellen és humán vázizom mintákon végeztünk vizsgálatokat. Korábbi munkánk alapján már ismert volt, hogy az SMTNL1 fehérjét a PKA és PKB foszforilálja az N-terminálishoz közeli calponin homológ domén közelében található Ser301-es oldalláncon, és β-adrenerg stimulációt követően az SMTNL1 citoplazmából a sejtmagba ifányiló transzlokalizációját mutat [100; 101]. Az SMTNL1 overexpresszáló HeLa sejtekben a defoszforilált SMTNL1 fehérje a citoszolban halmozódik fel, de a PKA aktiválását (8BrcAMP) követően az foszforilációja megnő és a sejtmagba transzlokálódik. A foszforiláció feltehetően olyan változást idéz elő a fehérje konformációjában, amely a foszforilációs helytől N-terminálisan elhelyezkedő, a fehérje defoszforilált állapotában nem hozzáférhető sejtmagi lokalizációs szignált exponálja. A foszforilációs hely szerin aminosavának alaninná mutálása blokkolta a SMTNL1 transzlokációját a sejtmagba [102].

Emlős kéthibrid rendszerben és koimmunprecipitációs kísérletekkel összesen 3 különböző sejtvonalban (HepG2, 293T, T47D) igazoltuk, hogy foszforilációját és a sejtmagba való transzlokációját követően a SMTNL1 szelektíven és ligandfüggő módon, csak a progeszteron receptorhoz (PR) kötődik (*28.ábra A panel*). Ezzel bizonyítottuk, hogy az SMTNL1 a sejtmagban transzkripciós koregukátorként funkcionálva gátolja a PR által szabályozott gének kifejeződését [150].

Az SMTNL1 ligandumfüggő kötődése a PR-hoz az SMTNL1 1-230 amonisavat tartalmazó régiója és a PR 1-722 régiója között alakult ki. A két fehérje közötti fiziológiai kapcsolatot globális génexpressziós és transzkripciós riporter vizsgálatokkal is igazoltuk vad típusú és *smtnl1-/-*



28. ábra. Az SMTNL1 köti és szabályozza a progeszteron receptort. *(A) HepG2 sejteket transzfektáltunk és emlős kéthibrid vizsgálatot végeztünk ösztrogén receptor (ER α és β izoforma), progeszteron receptor A és B (PR-A és B), androgen receptor (AR) illetve glikokortikoid receptorokkal (GR). A sejteket 24 óra elteltével a receptorok megfelelő szintetikus liganumaival kezeltük (E2: ösztrogén, R5020: medroxyprogeszteron, R1881: tesztoszteron, Dex: dexametozon) majd ezt követően luciferáz és β-gal vizsgálatokhoz gyűjtöttük be őket. pM: üres plazmmid; pM-SMTNL1: human SMTNL1 gént tartalmazó plazmid; veh.: vivőanyag (B) Az SMTNL1 koncentráció függését és a cAMP hatását vizsgáltuk a PR-B transzkripciós aktivitására. HeLa sejteket HeLa sejteket PR-B expressziós vektorral transzfektáltuk SMTNL1 expressziós vektor nélkül (0 ng) vagy növekvő koncentrációval (75, 150 és 300 ng) az MMTV-luciferáz riporter plazmiddal együtt. A transzfekciót követően a sejteket 24 órán át inkubáltuk hordozóval vagy 10 nM R5020-mal 8Br-cAMP (10 nM-1mM) jelenlétében, majd a sejteket luciferáz és β-gal aktivitását mértük. n= 3 ± SEM*

vemhes és nem vemhes egereken, valamint kontroll és RNS-interferenciával csendesített progeszteronérzékeny sejtvonalakon. A hormonkötő régió meglétét kiemelt jelentőségűnek találtuk a fehérjék közötti kölcsönhatás kialakulásában (PR 632-687 régió [151]) de az emlős kéthibrid vizsgálatok alapján ez nem volt elégséges a stabil interakció kialakulásához. Az SMTNL1 koncentrációfüggő módon gátolta a PR transzkripciós aktivitását, és ehhez a progeszteronon kívül az SMTNL1 Ser301 foszforilációját kiváltó 8BrcAMP agonista kezelésre is szükség volt (*28. B. ábra*). Ez a terhesség során a Ser301 oldalláncon történő foszforilációt követő SMTNL1 sejtmagi transzlokációjához és az az SMTNL1 kofaktorkénti működéséhez volt szükséges. Microarray vizsgálatok alapján az SMTNL1 kontraktilits elemek, sejmagi receptorok, anyagcsere enzimek és maga a *mypt1* génexpresszióját is modulálta (https://discovery.genome.duke.edu/express/resources/2419). Kísérleteink alapján bizonyítottá vált, hogy az endometriális simaizom kontrakcióval kapcsolatos és progesztinérzékeny gének (oxitocin receptor, connexin 43 és ciklooxigenáz-2) és a prolaktinok génexpressziója csökkent vemhes SMTNL1 KO egerekben. Azt sugalljuk, hogy az SMTNL1 a PR-B jelátvitel

bifunkcionális társszabályozója, és így egy olyan molekuláris mechanizmust biztosít, amelynek révén a PR-B célzottan megváltoztatja a génexpressziós mintázatokat az simaizom sejteken belül, hogy koordináltan elősegítse a simaizom funkció változását a terhesség alatt.

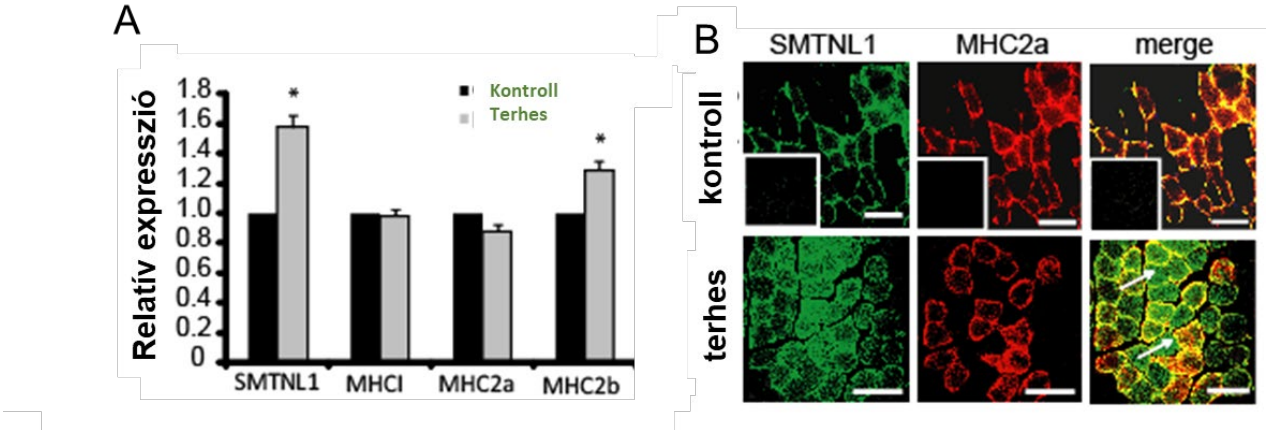
5. 4. 3. Az SMTNL1 a terhesség során izotípusváltozást indukál a vázizomzatban

Az SMTNL1 terhesség során kifejtett hatását, vemhes és nem-vemhes, WT és SMTNL1 KO egerekből származó soleus és plantáris vázizom mintákon vizsgáltuk. Az SMTNL1 expressziója jelentősen megemelkedett vemhesség és álvemhesség hatására a nem-vemhes egyedekhez viszonyítva, és az SMTNL1 Ser^{301} oldalláncának foszforilációja 3,5-szeres emelkedést mutatott vemhesség hatására [152]. Rágcsáló és humán vázizom minták izomrost-tipizálása során a 2b típusú glikolitikusabb izomrostok számában szignifikáns emelkedést, míg a 2a típusú oxidatívabb rostok esetében tendenciális csökkenést tapasztaltunk terhesség SMTNL1 hiányos egerekben (*2. táblázat*).

	Nem-vemhes		Álvemhes		Vemhes	
GENOTÍPUS	***smtnl1* +/+**	***smtnl1* -/-**	***smtnl1* +/+**	***smtnl1* -/-**	***smtnl1* +/+**	***smtnl1* -/-**
2a rosttípus %	34.77±1.9	32.22±2.5	24.84±2.2 *	26.00±2.5 #	25.29±1.8 *	24.45±2.1 **
2b rosttípus %	45.58±2.7	49.22±2.7	58.44±1.9	60.96±3.3 *	61.12±2.4 *	65.32±3.0 **
SMTNL1 pozitív rostok %	36.06±1.6	N/A	39.77±1.9	N/A	42.87±1.9 #	N/A
Relatív glikogén tartalom	1.00±0.0	1.18±0.2	1.25±0.03	1.32±0.1 #	1.26±0.04 #	1.39±0.2 *

2.táblázat. Az SMTNL1 eléciója és a vemhesség glikolitikus fenotípusra való rosttípusváltást indukált *egér vázizomban.* ***Nem-vemhes****, álvemhes és vemhes smtnl1+/+ és smtnl1-/- állatok plantaris izmának kvantitatív rostszámlálása. Középértékek ±SEM (n=14-15/csoport), t-próba, p<0,1#, p<0,05* és ** p<0,001.*

A szövetminták immunhisztokémiás elemzése alapján elmondhatjuk, hogy vad típusú nem-vemhes egerek vázizmában az SMTNL1 expressziója a 2a típusú rostokra korlátozódik, míg vemheség hatására más, a 2a típustól eltérő rostokban is megjelenik az SMTNL1, mint például a 2a-2b átalakulás során az 2x típusú izomrostokban. Vemhesség és álvemhesség hatására 15-20%-kal megemelkedett a 2b típusú glikolitikusabb izomrostok száma, míg nem változott az 1-es típusú oxidatívabb izotípus. A 2a típusú izomrostok indikátoraként ismert MHC2a expressziója csökkent, míg az MHC2b expresszió 20%-os emelkedést mutatott humán vázizom mintákban, ami a vemhesség hatására bekövetkező oxidatívból glikolitikusabb típusba történő átalakulást mutatja (*29. ábra*).

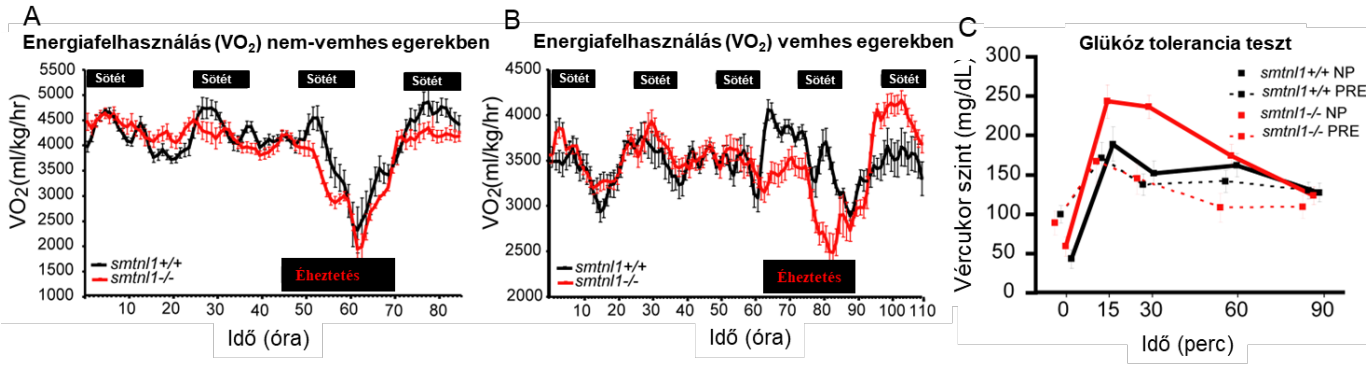


29. ábra. A terhesség a human vázizomban glikolitikus fenotípusra való rosttípusváltást indukált *(A) A plantaris izom rosttipizálásának számsuerűsített adatai (B) A plantaris izom vizsgálata immunfluoreszcenciás konfokális mikroszkópia segítségével. Az SMTNL1 (zöld) a kontroll vázizomban a 2a típusú rostokban (piros) expresszálódik. Az SMTNL1 expressziója a 2a rosttípustól eltérő típusú rostokban is kimutatható (nyilak). A bal alsó inzertek másodlagos antitest kontrollokat mutatnak.*

A 2b típusú rostok számának emelkedése növeli az izomerőt, ezáltal képessé teszi az anyaállatot a fejlődő magzat súlya jelentette teher jobb hordására a vemhesség késői szakaszában. A vázizom fizikai erejének, teherbírásának növelése kiemelten fontos az anyaállat számára. A 2b típusú rostok számának növekedése mellett azonban 21%-kal emelkedett az izomrostok glikogén tartalma a vemhes SMTNL1 KO állatokban (2. táblázat). Ezen adatok tükrében arra következtethetünk, hogy a terhesség során az vázizomzat oxidatívból glikolítikusabb típusba történő fenotípusváltása játszódik le, és hogy az SMTNL1 szabályozó szerepet játszhat ebben a folyamatban

Microaaray analízissel és tömegspektrometriás analízissel azt találtuk, hogy az *smtnl1* gén csendesítésének hatására számos anyagcsere útvonalhoz, illetve szteroidhormon által indukált jelátviteli pályához kapcsolhatót gén expressziója megváltozott, köztük az inzulinrezisztenciára utaló gének is (https://discovery.genome.duke.edu/express/resources/2419). Az mRNS szintű változásokat proteomikai elemzéssel is alátámasztottunk (*http://dx.doi.org/10.6084/m9.figshare.127394*) (*Függelék 2. táblázat*). Az SMTNL1 KO állatok anyagcseréjüket tekintve kevésbé hatékonyak, glükózintoleranciát mutatnak. A Comprehensive Lab Animal Monitoring System (CLAMS) vizsgálatok alapján az SMTNL1 KO állatok a sötétciklusban csökkent aktivitást mutattak. Vemhes és nem-vemhes SMTNL1 KO egerek légzési hányadosának meghatározását is elvégeztük, melynek értékéből következtetni lehetett a szervezet által felhasznált makrotápanyagok egymáshoz viszonyított arányára. Megfigyeléseink alapján a SMTNL1 KO egerek anyagcsere aktivitása jelentősebb kisebb, kifejezetten a vemhes állatokban

(33.2%-os csökkenés) a WT egerekéhez képest (vemhesség hatására ott mindössze 6.2%-os csökkenés), ami a metabolikus hatékonyság csökkenésére utal.



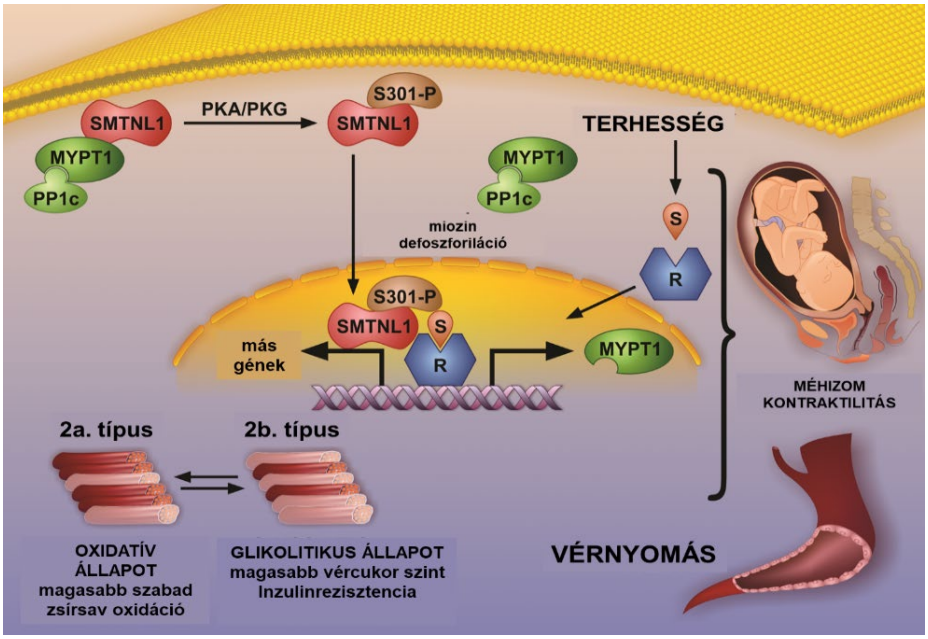
30. ábra. A vemhesség és az SMTNL1 deléció hatása az állatok anyagcseréjére *(A)Nem-vemhes (NP) és (B) vemhes (PRE) egerek energiafelhasználása az elfogyasztott oxigén mennyiségének (ml/kg/h) mérésével történt az idő múlásával. (C) Vércukorszint-változások (átlag ± 1 S.E.) smtnl1+/+ és -/-, vemhes vagy nem-vemhes egereknél az intraperitoneális glükózinjekciót követő időben. n = 6-13 egyed/csoport, az eredményeket átlag ± SEM-ben fejeztük ki.*

Az oxigénfogyasztás (VO_2) vemhes állatok esetén alacsonyabb volt a nem-vemhesekhez képest (*30.A ábra*), míg a vemhes állatok mind a WT és a KO állatok esetén kisebb csökkenést mutattak a VO_2 értékekben éheztetés során (*30.B. ábra*). A légzéscsere arány (VCO_2/VO_2; RER) a vemhes és nem-vemhes KO állatok esetén egyaránt csökkent. A KO állatok jelentősen emelkedett tápanyag eltolódási értéket mutattak a WT kontrolljaikhoz képest, ami arra utal, hogy a zsírsavakról a szénhidrátfelhasználás felé tolódott el az anyagcseréjük. Bár a vemhes KO állatok anyagcsereútvonaluk eltolására hatékonyabban képesek, anyagcseréjük a fokozott szénhidrátfelhasználás miatt mégis sérült, és a vemhesség során fokozottabbá vált.

Az intraperitoneális glükóztolerancia teszt azt mutatta, hogy a SMTNL1 KO egerek csökkent glükóztoleranciával rendelkeznek (*30. C ábra*). A csökkent glükóztolerancia eredményeképpen kialakuló inzulinrezisztencia feltehetően a SMTNL1 kiütése következtében lecsökkenő GLUT4 és IRS1 expresszió következménye [152]. Elmondható tehát, hogy a terhesség és a SMTNL1 delécióját a vázizomzatban glikolitikusabb fenotípust eredményez. Már maga a terhesség is képes volt a vázizomzat fenotípusát oxidatívból a glikolitikusabb irányba tolni. Ezt a folyamatot a SMTNL1 és a progeszteron közötti kölcsönhatása is szabályozza, amely megváltoztatta a kontraktilis, és metabolikus fehérjék expresszióját. Az *smtnl1*$^{-/-}$ KO egerek esetében alacsonyabb metabolikus hatékonyságot, és csökkent glükóz toleranciát figyeltünk meg. A vemhessség esetén fordított hatást figyeltünk meg a SMTNL1 delécióját során, ebben az esetben

nőtt a metabolikus aktivitás és a glükóz tolerancia. Ezen eredmények alapján úgy tűnik, hogy a SMTNL1-nek szerepe van a szteroid hormonok által közvetített rosttípus váltásban a terhesség során [152].

Eredményeinket összegezve elmondható, hogy leírtuk a sima- és vázizom terhesség során hormonális hatásra történő izotípus változását. A terhesség során a glikolitikus fenotípusra való átállás, a vázizom csökkent oxidatív rosttartalma molekuláris alapot szolgáltat a terhes nők fokozott súlygyarapodásának és inzulinrezisztenciájának magyarázatára. Ez a terhességre adott normális válasz evolúciós előnyt jelent az anya számára, ami által lehetővé válik a vércukorszint növelése a megfelelő magzati fejlődés érdekében, valamint a zsír hatékonyabb elraktározása a szoptatás kalóriaigényének kielégítésére. Eredményeink arra is utalnak, hogy a glikolitikus fenotípusra való átállás az anya fizikai erejének növelése révén is előnyt jelent, ui. a 2b típusú izomrostok az erő- és ellenállás-fokozással hozhatók kapcsolatban (mint például a súlyemelés



31. ábra. Az SMTNL1 hatásának molekuláris mechanizmusa. *A citoszolban az SMTNL1 a miozin foszfatáz (PP1c-MYPT1) MYPT1 szabályozó alegységéhez köződve gátolja a holoenzim aktivitását. PKA/PKG enzimek általi foszforiláció hatására a sejtmagba transzlokálódik. A terhesség során a megemelkedett szteroidhormon, a progeszteron (S) szintjére válaszul az SMTNL1 és a progeszteron receptor B (PR-B; R) együttesen segítik elő a vázizomzat adaptációját. Nem-terhes állapotban az SMTNL1 a PR-B aktivitásának gátlására szolgál; terhesség alatt azonban ez a gátlás feloldódik, ami elősegíti a metabolikus és kontraktilis fehérjék expresszióját szabályozó vázizom-specifikus gének aktiválódását. Ez az összehangolt szabályozás alkalmazkodik az anya fiziológiai állapotához.*

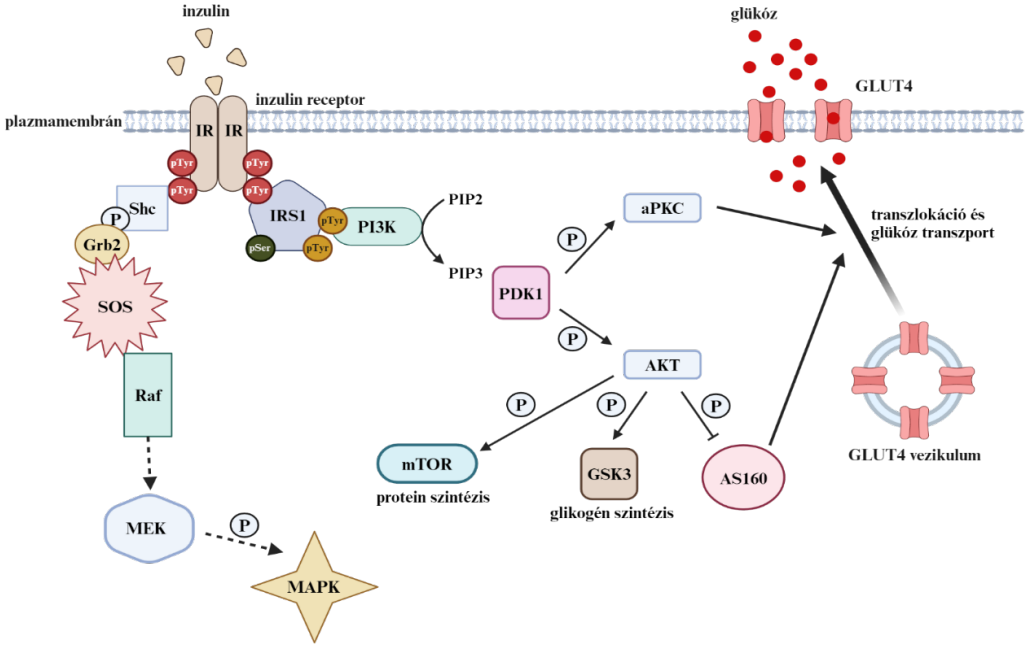
esetében). Az anya fizikai erejének növekedése lehetővé teszi a terhesség utolsó szakaszában a magzat megnövekedett súlyának viselését (31. *ábra*).

Azonban a terhességek ~4%-ában a terhesség okozta inzulinrezisztencia terhességi cukorbetegséggé alakul. Ha tehát a terhesség evolúciós előnyként elősegíti a glikolitikusabb fenotípusra való átállást, akkor ez egyes nőket még fogékonyabbá teheti a terhességi cukorbetegség kialakulására, különösen a magas energiatartalmú nyugati étrend hatására. Így mivel az SMTNL1 hiányában inzulinrezisztens állapot alakult ki, feltételeztük, hogy normális vagy akár emelkedett szintje inzulinérzékenyítést vált ki Az ezzel kapcsolatos további vizsgálataink eredményét a következő fejezetben mutatom be.

5.5. Az SMTNL1 inzulinérzékenyítő hatása

5.5.1. Az inzulin jelátviteli pálya és az inzulin rezisztencia

A vázizomzat fiziológiás körülmények között a bevitt glükóz felvételének fő felhasználója [153]. Míg a máj a véráramban lévő posztprandiális glükóznak körülbelül egyharmadát veszi fel,



32. ábra. A vázizom inzulin mediált glükózfelvétele. *A vázizom inzulin által mediált glükóz felvétele során az inzulin kötődik a szarkolemmában található inzuliin receptor (IR) extracelluláris α alegységéhez, melynek hatására a β alegység meghatározott Tyr oldalláncokon autofoszforilálódik, majd foszforilálja a hozzá kapcsolódó inzulin receptor szubsztrát fehérjét (IRS1). A Tyr oldalláncokon foszforilált IRS1 fehérje dokkoló helyet biztosít a PI3K számára. Az aktiválódott PI3K enzim membránban megjelenő produktumai a protein kináz B/Akt enzim membránhoz való kötődését és aktiválódását idézik elő, amely az intracelluláris vezikulákban tárolt GLUT4 transzporter fehérjék szarkolemmába való transzlokációját indukálja. Az ábra a biorender.com felületén készült.*

a maradékot a perifériás szövetek, elsősorban a vázizom veszi fel inzulinfüggő mechanizmuson keresztül. Az inzulin kötődése az inzulinreceptorhoz (IR) olyan jelátviteli kaszkádot indít el, amely az inzulinérzékeny glükóz transzporter fehérje 4 (GLUT4) transzlokációját eredményezi a plazmamembránba, hogy megkönnyítse a glükóz sejtbe történő szállítását (32. *ábra*).

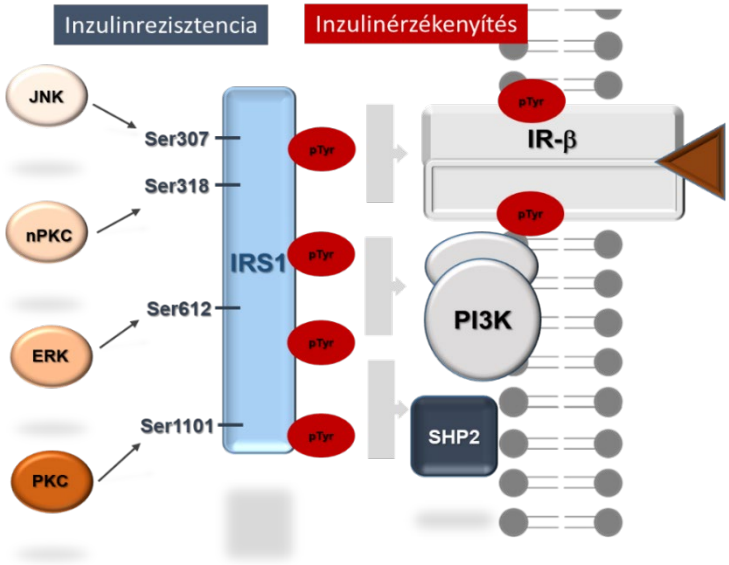
Az IR aktiválódása az inzulin kötődését követően az inzulinreceptor 1-es szubsztrát (IRS1) fehérje foszforilációját eredményezi, amely viszont dokkolja és aktiválja a foszfatidil-inozitol-3-kinázt (PI3K). A PI3K katalitikus doménje konformációs változásokon megy keresztül, ami az

enzim aktiválódását eredményezi. Ezt követi a PI3K által katalizált PIP2 foszforilációja PIP3 -á, amely a PDK1 aktivációjához vezet. Ez az inzulinjel továbbítását eredményezi egy Ser/Thr specifikus protein kináz, az Akt/protein kináz B felé [154], amely foszforiláció hatására aktiválódik. Az Akt kináz doménjében található Thr308 oldalláncon történő foszforiláció aktiválja az enzimet míg a Ser473 oldallánc foszforilációja meghatározza a szubsztrát-szelektivitást és tovább fokozza az aktivitás. Ez utóbbi szabályozásáért a PIP3K mellett az mTORC2 is felelős [155]. Az Akt foszforilálja a 160 kDa molekulatömegű Akt szubsztrát fehérjét (AS160-at). A foszforilált AS160 a 14-3-3 fehérjével kölcsönhatást kialakítva gátolja a Rab fehérjék GTPáz aktivitását, amely következtében a Rab fehérjék GTP-kötött állapotban maradnak. Ez a Glut4 glükóztranszportrer transzlokációját eredményezi a plazmemembránhoz. Így az Akt elősegíti a GLUT4-tartalmú vezikulák transzlokációját a plazmamembránba, hogy közvetítse az inzulin által stimulált glükóztranszportot a vázizomba [156] *(32. ábra).*

Az inzulinrezisztencia (InR) a szövetek normál inzulin koncentrációra adott csökkent válaszadó képességét jelenti. Bár számos genetikai és fiziológiai faktor közrejátszik az InR kialakulásában és súlyosbításában, önkéntes emberek bevonásával készült tanulmányok az IRS fehérjék megváltozott aktivitását jelölik meg, mint az InR hátterében álló közös mechanizmust [157]. Az IRS a Tyr oldalláncok mellett Ser/Thr oldalláncokon is foszforilálódhat, melyek pozíciójuktól függő módon serkentik vagy gátolják az IRS inzulinjel közvetítő hatását (33. *ábra*). Az inzulin hatására aktiválódó PKB/Akt általi Ser foszforiláció például védelmet nyújt a tirozin foszfatázok ellen, pozitív visszacsatolási mechanizmussal aktív állapotban tartva az IRS1-t [158]. Az inzulin azonban áttételesen más Ser/Thr kinázokat is aktivál (ERK, JNK, PKC, mTOR), melyek meghatározott oldalláncok foszforilálódását indukálják és negatív visszacsatolási mechanizmussal gátolják az IRS működését, ami az inzulinhatás megszűnésével jár. Az mTOR és a JNK általi Ser307-es foszforiláció például gátolja az IR és az IRS1 közötti kölcsönhatást, míg a PI3K kötésért felelős Tyr oldalláncok közelében található Ser612-es oldallánc ERK általi foszforilációja a PI3K kötődését akadályozza, míg a zsírsavak által indukált inzulinrezisztenciában

az atípikus PKC enzimcsalád tagjai a Ser1101 oldallánc foszforilációjával az SHP2 tirozin foszfatáz dokkolódását szabályozzák [159; 160; 161] (*33. ábra*).

Kényes egyensúly létezik tehát a pozitív IRS1 tirozin/szerin foszforiláció és a negatív IRS1



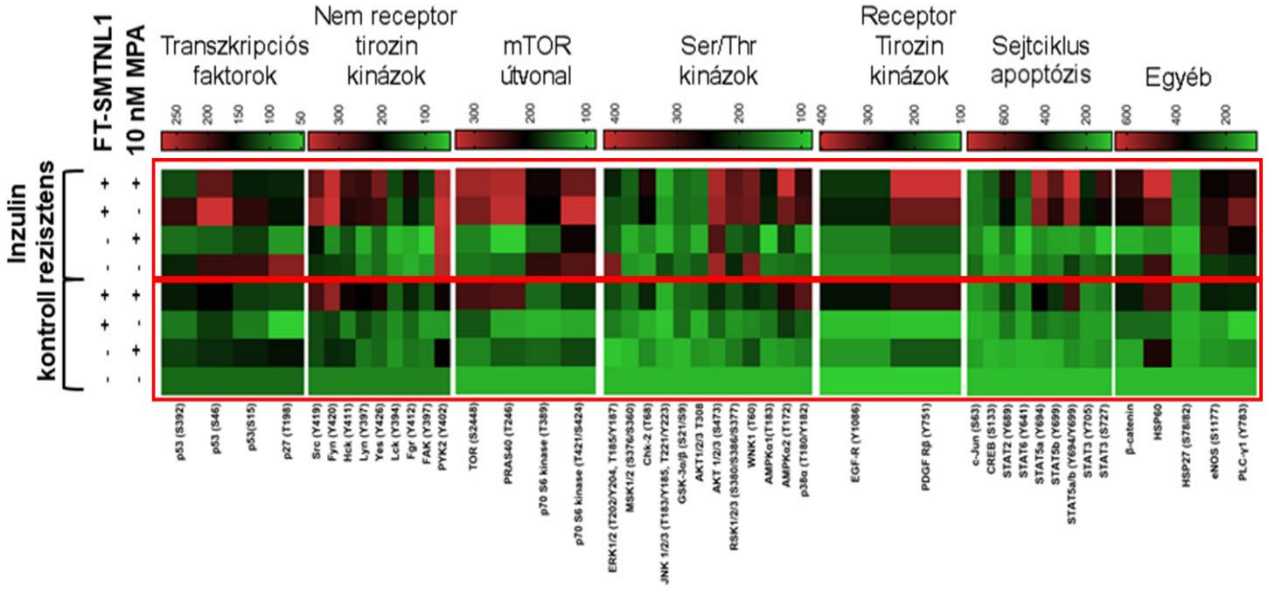
33. ábra. Az IRS1 Ser-aminosavmaradékokon történő foszforilációja szabályozza az IRS1 funkcióit. *Az IRS1 Ser oldalláncokon történő foszforilációja kettős szerepet játszik az inzulinhatás fokozásában (inzulinérzékenyítés) vagy megszüntetésében (inzulinrezisztencia). A PKB/Akt inzulinra adott válaszként történő aktiválása kiváltja az inzulin jelátvitelt és elősegíti az IRS1 Tyr-maradékokon történő foszforilációját (ld. 32. ábra), pozitív visszacsatolási hurkot hozva létre az inzulinhatás számára. Az inzulin aktiválja a JNK-t, az ERK-t, a PKC-t és az mTOR-t is, amelyek az IRS1 foszforilációját specifikus helyeken indukálják és gátolják a funkcióit. Ez része az inzulin által indukált negatív visszacsatolású szabályozási mechanizmusnak, amely megszünteti az inzulin hatását.*

szerin foszforiláció között, amely szabályozhatja az IRS1 működését. A szabad zsírsavak, citokinek, angiotenzin II, endotelin-1, aminosavak, sejtstressz és a hiperinsulinaemia fokozhatják a negatív IRS1 Ser-foszforilációt, ami inzulinrezisztenciához vezethet, amely a Ser/Thr kinázok (JNK, PKC, mTOR, S6K, IKK, ERK) aktiválódását és általuk IRS1 foszforilálcióját eredményezik, ami gátolja az IRS1 funkcióit. Az IRS pozitív Tyr/Ser foszforilációja és negatív Ser foszforilációja közötti egyensúly fontos szerepet játszik az IRS aktivitásának szabályozásában, ezáltal pedig a normál inzulinjelátvitelben. Ez az egyensúly különböző stresszhatások (pl. betegség) és molekulák (pl. hormonok, aminosavak, citokinek, zsírsavak) hatására felborulhat, ami a negatív Ser foszforiláció túlsúlyba kerülését és InR kialakulását eredményezi [162]. Az inzulinrezisztencia-szindróma a 20 évesnél idősebb felnőttek mintegy 24%-át érinti, és számos

rendellenességben nyilvánul meg, beleértve a glükóztolerancia károsodását, a 2-es típusú cukorbetegséget, az elhízást és a reprodukciós zavarokat [159] *(33. ábra*).

5.5.2. Az SMTNL1 szerepe a vázizom inzulinérzékenyítésében

Előzetes eredményeink rávilágítottak az SMTNL1 anyagcsere szabályozásában betöltött szerepére a vázizom fenotípusának modulációján keresztül. A háttérben álló pontos molekuláris mehanizmus, az általa befolyásolt jelátviteli pálya azonban még nem volt ismert. Mivel a microarray analízis és a proteomikai vizsgálatok is arra világítottak rá, hogy az inzulin jelátviteli pálya érintett lehet (ld. előző fejezet), ezért munkánk során az SMTNL1 inzulinjelátviteli pályára kifejett hatását vizsgáltuk, differenciált C2C12 sejtekben és SMTNL1 KO egérmodellben. Vizsgálatainkhoz hiperglikémiás/hiperinzulinémiás differenciáltatott C2C12 miotubulusokat használtunk az SMTNL1 természetes ligandumának, a progeszteronnak jelenlétében és anélkül, és így modelleztük az inzulinrezisztens és terhességi cukorbeteg állapotot a vázizomban.

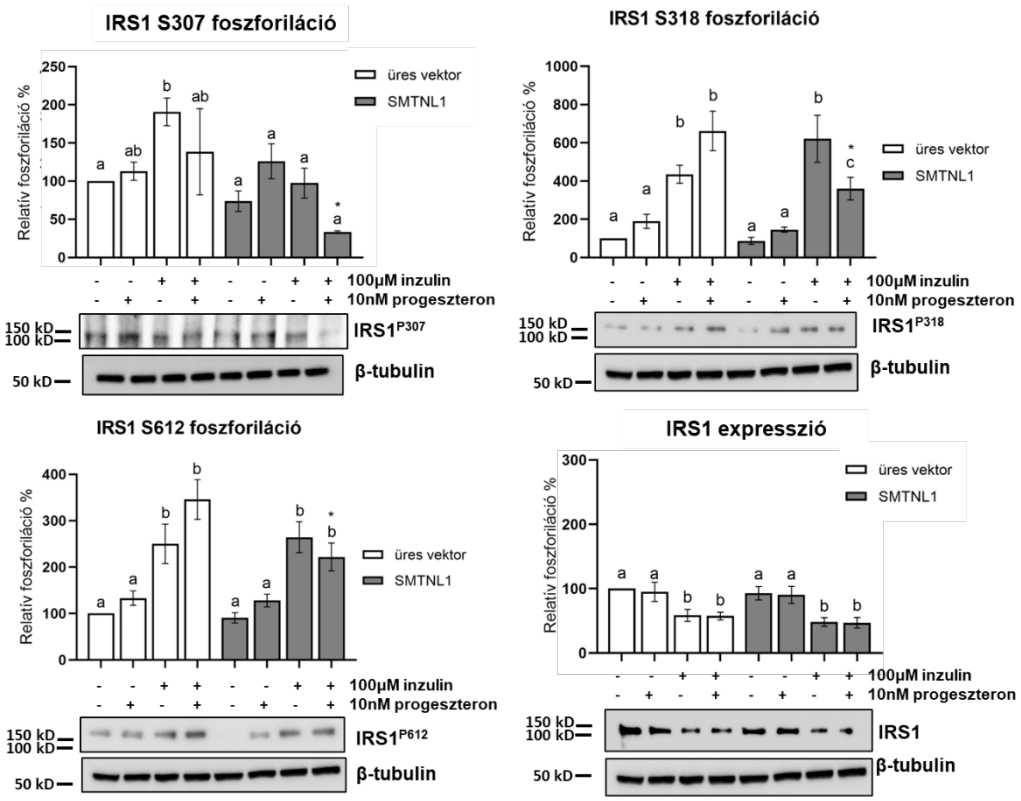


34. ábra. Az SMTNL1 progeszteron-függő hatása inzulinrezisztens vázizomsejtekben. *FT-SMTNL1-transzfektált és merdoxyprogeszteronnal (MPA) kezelt C2C12 sejtlizátumok Proteome Profiler elemzését végeztük. A vizsgált fehérjék foszforilációs állapotát a heatmap alapján osztályoztuk, a kezeletlen kontrollt használva viszonyítási alapként. Színkód: piros jobban foszforilált, zöld: kevésbé foszforilált. Az elemzésekhez 200µg fehérjét használtunk, a folt intenzitásokat ImageJ segítségével értékeltük ki. MPA: medroxyprogeszteron FT: Flag-jelölt SMTNL1.*

Eredményeink alapján az SMTNL1 overexpressziója progeszteron jelenlétében csökkenti az IRS1 gátló Ser-foszforilációját, ami a PI3K/Akt jelátviteli útvonalat indukálja a C2C12 hiperinzulinémiás/hiperglikémiás inzulinrezisztens miotubulusokban *(34. ábra*). Adataink arra utalnak, hogy az SMTNL1 egy új típusú PKC expressziójának szabályozásával fejti ki hatását,

amely közvetlenül a Ser318 oldalláncon, közvetve pedig az ERK1/2 jelátviteli útvonal által a Ser612-en keresztül járul hozzá az IRS1 foszforilációjához. Az SMTNL1 által megváltoztatott jelátviteli útvonalakat Proteom Profiler analízissel vizsgáltuk a C2C12-es miotubulus mintákban. Az SMTNL1-hez kapcsolódó útvonalakként elsősorban az mTOR és a Ser/Thr-kináz jelátviteli pályákat azonosítottuk (*34. ábra*). Ezek az eredmények összhangban vannak az *Smtnl1* KO egerek vázizom mintáin végzett proteomikai és microarray-elemzéseinkkel [152].

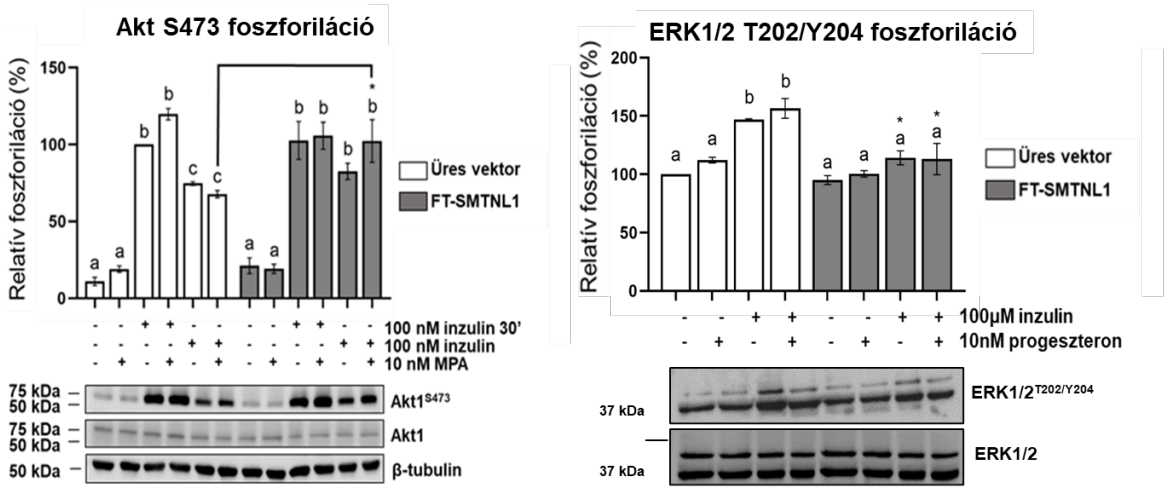
Az előszűrés szemi-kvantitatív Western blottal történő validációjának alapján az IRS1 foszforilációja a Ser307, Ser318 és Ser612 helyeken az inzulinrezisztens modellben jelentősen megemelkedett *(35. ábra)*, és az SMTNL1 overexpressziója csökkentette a foszforilációt ezeken



35. ábra. Az IRS1 expressziójának és foszforilációjának Western blot elemzése C2C12 inzulinrezisztens miotubulusokban. *A differenciálást és az inzulinrezisztencia indukcióját követően a sejteket az IRS1 S307 (bal fent), S318 (jobb fent) és S612 (bal lent)) foszforilációs helyei elleni antitesttel; valamint a fehérje alapexpresszióját IRS1 abtitesttel (jobb lent) viszgáltuk szemi-kvantitatív Western blot módszerrel. A foszforilációs szinteket a nem-foszforilált fehérjéhez viszonyítottuk, amelyet viszont a β-tubulinhoz, mint belső terheléses kontrollhoz normalizáltunk. Az SMTNL1 kódoló vs. az üres vektorral transzfektált sejtek hatásait hasonlítottuk össze (kétutas ANOVA és Sidak's post hoc teszt, átlag ± SEM; n=3; *, p < 0,05). A különböző kezelések hatását is összehasonlítottuk (Kétirányú ANOVA és Tukey-féle post hoc teszt, Átlag ± SEM; n=3; p < 0,05; Különböző betűk jelzik az összehasonlított csoportok közötti szignifikáns különbségeket).*

az aminosavmaradékokon, de csak progeszteron jelenlétében *(35. ábra)*. Az IRS1 Ser307 és Ser318 foszforilációja megbontja az IR/IRS1 komplexet, és lehetővé teszi az inzulinnal szembeni deszenzitizációt [161; 163]. A Ser307 az IRS1-en a JNK foszforiláció fő helye. Eredményeink összhangban vannak más *in vivo* diabéteszes állatokon végzett és *in vitro* sejtkultúrás vizsgálatokkal, amelyek azt mutatták, hogy a JNK aktivitása az InR sejtekben megemelkedett [164]. Az SMTNL1 overexpressziója nem változtatta meg a JNK kinázok expresszióját, de aktivitásuk jelentősen csökkent SMTNL1 overexpresszió hatására az inzulinrezisztens modellben. Az IRS1 Ser318 foszforilációját is jellemeztük, amely az inzulin által indukált PKCζ és ε célpontja [160]. Bár az előbbi PKC izoformának az aktivitása és expresszió nem volt SMTNL1-függő, az SMTNL1 overexpressziója mérsékelte a PKCε szintjét, ami az IRS1 Ser318 foszforilációjának egyidejű csökkenésével járt. Az IRS1 Ser612 maradékának foszforilációjában túlnyomórészt az ERK1/2 és az mTOR útvonalak vesznek részt. Modellünkben az ERK1/2 foszforilálódott krónikus inzulinkezelést követően, és az SMTNL1 overexpressziója gátolta az ERK1/2 foszforilációját és ezáltal aktivitását, különösen progeszteron jelenlétében (36. ábra). Emellett az IRS1 Ser612 foszforilációja csökkent, ami valószínűleg az ERK1/2 aktivitás SMTNL1-függő csökkenésének eredménye. Továbbá feltételezzük, hogy az ERK1/2 nem csak a Ser612 foszforilációján, hanem a GLUT4 szabályozásán keresztül is inzulindeszenzitáló hatást fejt ki a C2C12 miotubulusokban, mivel az ERK1/2 krónikus aktivációja a GLUT4 expressziójának downregulációjához és csökkent inzulin-indukált glükóz transzporthoz vezet [165].

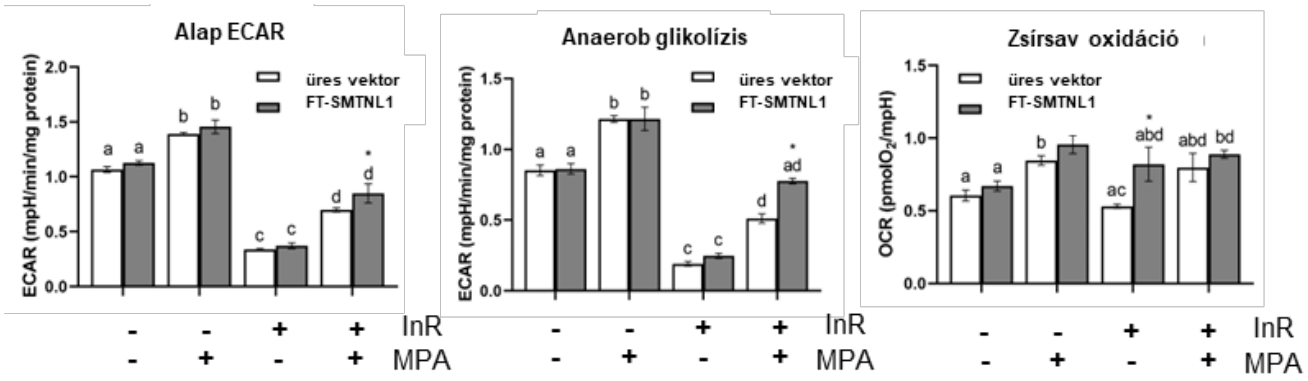
Az ERK1/2 fehérje mennyisége nem változott, de foszforilációja és feltehetően aktivitása csökkent az SMTNL1 overexpressziójának hatására progeszteronnal történő együttes kezelésre, ami arra utal, hogy az SMTNL1 a génexpresszió szintjén szabályozza az upstream Ser/Thr kinázokat és/vagy foszfatázokat *(36. ábra jobb panel*). A vemhes SMTNL1 KO egerek microarray-analízise során egyik MAP-kináz kináz sem változott a WT-hez képest [152]. Ezért megvizsgáltuk az ERK1/2 lehetséges szabályozó elemeit. Míg a protein foszfatáz 2A (PP2A) génexpressziója nem változott ebben a vizsgálatban [166], addig a másik lehetséges szabályozó enzim, az új típusú PKCε expressziója jelentősen csökkent az SMTL1 overexpresszió hatására, elősegítve a miotubulusok inzulinérzékenységét. Ez összhangban van a korábbi eredményeinkkel, amelyek a PKC izoformák változását mutatták ki SMTNL1 KO állatokban microarray analízis segítségével [152].



36. ábra. Az SMTNL1 overexpresszió hatása az Akt és ERK1/2 expressziójára és foszforilációjára Western blot analízissel*. Az Akt1 foszforilációhoz (bal panel) az általános inzulinrezisztencia modellhez minden transzfekcióhoz két további mintát vittünk be. A fiziológiás körülmények között végzett 72 órás differenciálást követően a kezelés utolsó 30 percében 100 nM inzulint adtunk a sejtekhez az inzulinrezisztencia kialakulásának ellenőrzésére. A foszforilált fehérjéket normalizáltuk a nem-foszforilált fehérjék szintjéhez, amelyet viszont a β-aktinhoz, mint belső terheléses kontrollhoz normalizáltunk. Az ERK1/2 expressziót és foszforilációs (job panel) semi-kvantitatív Western blot analízissel vizsgáltuk. Az SMTNL1 vs. az üres vektorral transzfektált sejtek értékeit (kétutas ANOVA és Sidak's post hoc teszt, átlag ± SEM; n=3; *, p < 0,05), valamint a különböző kezelések hatását is összehasonlítottuk (kétutas ANOVA és Tukey's post hoc teszt átlag ± SEM; n=3; p < 0,05; az eltérő betűk a csoportok közötti szignifikáns különbségeket jelzik).*

A PI3K aktivitás, a felszabadult PIP3 koncentrációjával mérve, megnövekedett a C2C12 miotubulusok inzulin stimulációjának hatására, és ez a szint jelentősen alacsonyabb volt az inzulinrezisztens körülmények között. A p85 expressziója csökkent az inzulinrezisztencia esetén, de ezt és a PI3K aktivitását az SMTNL1 overexpressziója helyreállította [161]. A PI3K megváltozása befolyásolja downstream effektorának, az Akt-nak az aktivitását is. Érdekes módon az Akt fehérjeszintje nem változott semmilyen kezelés hatására a differenciált C2C12 sejtekben. Eredményeink alapján azonban az SMTNL1 differenciáltan szabályozta az Akt foszforilációját: az SMTNL1 overexpressziója megemelte a Thr473 foszforilációját, így aktivitását az inzulin-indukált kontroll sejtekben, de az inzulinrezisztens sejtekben a Ser473 foszforilációt csak kis mértékben indukálta a kontrollhoz képest (*36. ábra jobbl panel*).

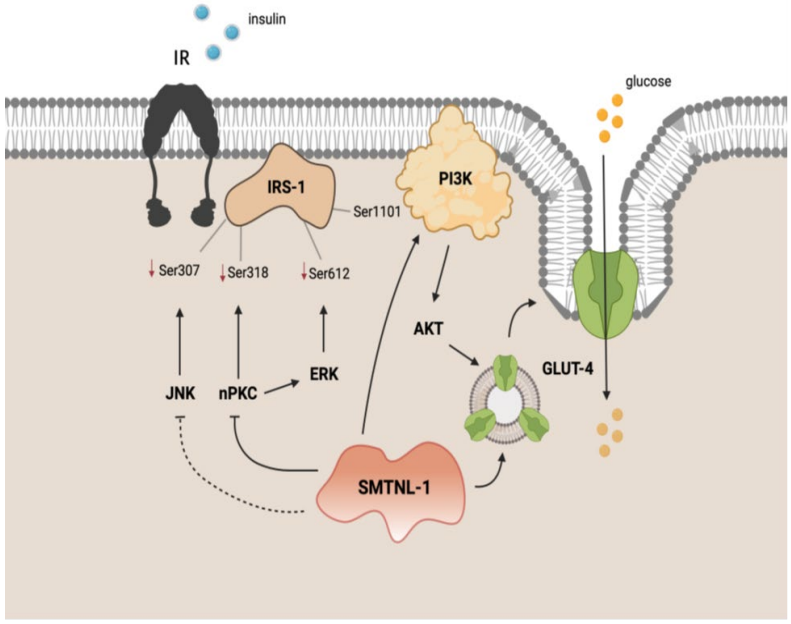
Az inzulin/PI3K jelátvitel downstream célpontja a Glut4 (*32. ábra)*, ami a plazmamembránba transzlokálódva fokozott glükóztranszporthoz vezet [167]. Az SMTNL1 overexpressziója C2C12 miotubulusokban fokozott GLUT4 expresszióval járt az inzulinrezisztens



37. ábra A C2C12 inzulinrezisztens sejtek energetikai paramétereinek változása SMTNL1 vagy üres vektor transzfekcióját követően. *A C2C12 sejteket sejtanyagcsere paramétereit Seahorse XF 96 műszerrel mértük. Mind a glikolitikus (ECAR - Extracelluláris savasodási ráta), mind az oxidatív (OCR - Oxigénfogyasztási ráta) változókat elemeztük. A mérések során az inhibitorok beadása előtt a sejtek ECAR (bal panel) és OCR alapszintjét mértük. A mitokondriális aktivitástól független anaerob glikolízis paramétereket úgy számoltuk ki, hogy az alapértékekből kivontuk az Antimycin A + 2-DG értékeket (középső panel). A zsírsav-oxidációt mérését az etomoxir beadása után mért OCR-értékeket kivonásával végeztük (job panel). Az SMTNL1 vs. az üres vektor-transzfektált sejtek értékeit hasonlítottuk össze (kétutas ANOVA és Sidak's post hoc teszt, átlag ± SEM; n=3; *, p < 0,05), valamint a különböző kezelések hatását (kétutas ANOVA és Tukey's post hoc teszt, átlag ± SEM; n=23; p < 0,05; különböző betűk jelzik a csoportok közötti szignifikáns különbséget. A mérések után az értékeket a fehérjetartalomra normalizáltuk. InR: inzulin rezisztens modell; MPA: medroxiprogeszteron*

modellben [152]. A glikolitikus funkció és a mitokondriális légzés kvatitatív mérése szintén alátámasztotta az SMTNL1 inzulinérzékenyítő hatását az inzulinrezisztens C2C12 sejtekben. Az oxigén fogyasztási ráta (OCAR) és az extracelluláris savasodási ráta (ECAR) valós idejű metabolikus mérései kimutatták, hogy az SMTNL1 javította a glikolízist és elősegítette az alternatív energiaforrások felhasználását (37. ábra). Az inzulinrezisztenciás modellben csökkent az alap ECAR és az anaerob glikolízis. Az SMTNL1 overexpressziója progeszteron jelenlétében azonban enyhítette az ECAR és a glikolízis csökkenését anélkül, hogy befolyásolta volna a maximális glikolízist vagy a glikolitikus tartalékkapacitást. A progeszteron növelte a glikolitikus aktivitást és az ATP-termelődést a vázizomsejtekben, de az inzulinrezisztenciás sejtekben az értékek még mindig a kontrollszint alatt maradtak; csak az SMTNL1 overexpressziója progeszteron jelenlétében tudta visszaállítani a glikolitikus aktivitást és az ATP-termelődést. Az OCAR szintekben a kontroll és az SMTNL1-overexpresszáló sejtek között nem találtunk jelentős eltérést [4]. Ezekkel az eredményekkel összhangban állnak azzal, hogy az *smtnl1* KO egerek metabolikusan kevésbé hatékonyak voltak és glükóz intoleranciát mutattak; és azt, hogy a

terhesség a glükóztoleranciát a WT állatok szintjére emelte [152], ami megerősíti az SMTNL1 inzulin jelátviteli útvonal génexpressziójára gyakorolt szabályozó hatását.



38. ábra. Az SMTNL1 inzulinértzékenyítő hatása inzulinrezisztens C2C12 miotubulusokban. *Az SMTNL1 csökkenti az új típusú PKCε gén expresszióját (nPKC), ami közvetlenül csökkenti a Ser318 fosszforilációt és az ERK1/2 aktivitásának gátlásával csökkenti az IRS1 Ser612 foszforilációját is. A Ser612 foszforiláció szabályozza a PI3K kötődését,és aktiválja a PI3K-Akt-mTOR útvonalat. Emellett az SMTNL1 feltehetően a DUSP7 kettős specificitású protein foszfatáz közreműködésével gátolja a JNK aktivitást, ami az IRS1 Ser307 foszforilációjának csökkenéséhez vezet. Az SMTNL1 elősegíti a glükózfelvételt az Akt és AMPK útvonalak aktiválásával, valamint a GLUT4 expressziójának indukálásával elősegíti a glükózfelvételt.[4].*

Ezek az adatok együttesen arra utalnak, hogy az SMTNL1 több mechanizmuson keresztül indukálja a C2C12 miotubusok inzulinérzékenységét (38. ábra). 1) Az SMTNL1 negatívan szabályozza az inzulinfüggő Ser/Thr-kinázok upstream szabályozóinak expresszióját, amelyeket a hosszan tartó inzulin- és glükóz-expozíció aktivál. A PKCε expressziójának csökkentésével az SMTNL1 gátolja az ERK1/2 aktivitását, ami az IRS1 Ser612 foszforilációjának későbbi csökkenésével a PI3K-Akt-mTOR útvonal aktiválását eredményezi. 2) Az SMTNL1 a heterológ IRS1 kinázokra is hat azáltal, hogy az inzulinrezisztencia kialakulása során az IRS1 Ser307 foszforilációjának szabályozásával gátolja az inzulin hatását, ami viszont az IR/IRS1 kölcsönhatásokat befolyásolja. 3) Az SMTNL1 elősegíti a glükózfelvételt az Akt útvonalak aktiválásával és a GLUT4 expressziójának indukálásával inzulinérzékenyítést okoz (*38. ábra*). Tehát az SMTNL1 az inzulinszignalizáció fontos szabályozójaként szolgál és potenciális terápiás célpont lehet az inzulinrezisztencia javítására vázizomban [4].

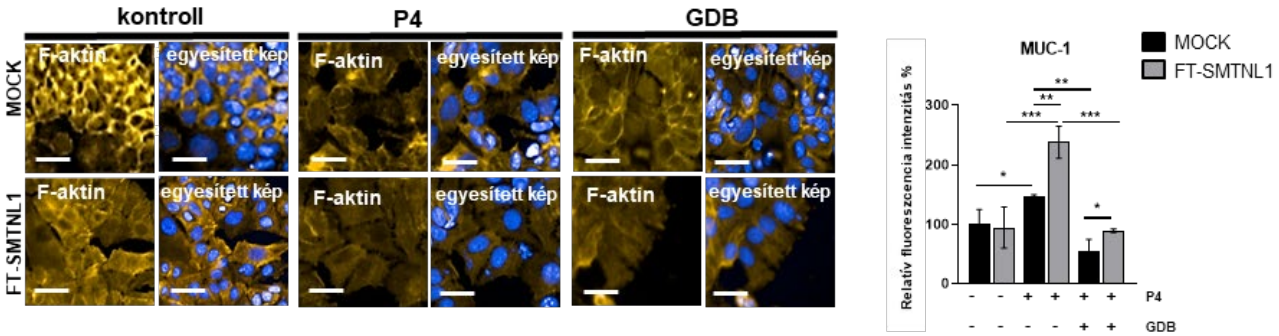
5.5.3. Az SMTNL1 szerepe a reproduktív tulajdonságok kialakításában

Az SMTNL1 KO állatokon végzett kísérletek fényében, az edzéshez adaptálódott és inzulinrezisztens fenotípus mellett csökkent reproduktív képességet is leírtunk. Megfigyeltük, hogy az embrionális letalitás szignifikánsan nagyobb, az utódszám jelentősen kevesebb volt, a vemhesség nehezebben alakul ki, vagyis a vemhesség kialakulásához jelentősen hosszabb időre volt szükség. Emellett az újszülött hím utódok száma meghaladta a nőstények számát, ami összességében egy gyengébb reprodukciós fenotípusra, valamint a populáció reproduktív fitneszének csökkenésére utal [150]. További kíséreteink célja a háttérben álló molekuláris mechanizmusok vizsgálata volt az endometriumban.

Az endometriális sejtek biztosítják a blasztociszták első érintkezési helyét [21]. A blasztocita és az az endometriális epithelsejtek közötti párbeszéd, és az utóbbi megfelelő differenciálódása döntő fontosságú. A méhnyálkahártya szekréciós sejtjei morfológiai változásokon mennek keresztül a női ciklus luteális fázisában. A sejtfelszíni molekulák, mint például a Mucin-1 (MUC-1) kifejeződése a sikeres differenciálódást és a fogékony endometriumot jelzik [168]. Az egyrétegű oszlopos epitheliumban és a szekréciós sejtekben fellépő rendellenességek nem megfelelő trophoblast-endometrium kommunikációt okoznak, ami implantációs elégtelenséghez vezet. Az inzulinrezisztencia és az ebből eredő metabolikus szindróma súlyos anyagcsere eltolódást, differenciálódási rendellenességeket és a méhnyálkahártya integritásának kóros elváltozásait okozhatja [169]. Ezek a hibák különböző meddőségi rendellenességekhez, például policisztás petefészek szindrómához vezethetnek, ami az embrió beágyazódását megakadályozó elváltozások oka lehet, amelyek végső soron meddőséget is okozhatnak [170]. A meddőség a reproduktív korú női lakosság 5–10%-ában fordul elő [171]. Emellett a magas inzulin- és glükózszint, valamint a hámsejtek proliferációját és differenciálását fokozó külső tényezők növelik az endometriózis és az endometriális hiperplázia kockázatát, ami az endometrium daganatos elváltozásához vezet, bár a folyamat pontos molekuláris mechanizmusa még nem ismert [171]. Mivel az SMTNL1 KO állatok egyértelműen fertilitási zavarokkal küzdöttek, további célunk az volt, hogy feltárjuk az SMTNL1 szerepét az endometriális epitheliális sejtek működésében, különös tekintettel a terhesség és a terhességi cukorbetegség körülményeire. Modellrendszerként Ishikawa sejteket, egy humán endometriális adenokarcinóma sejtvonalat használtunk. Ez a sejtvonal funkciójában és szerkezetében különbözik az endometriumban alatta elhelyezkedő endometriális sztrómális sejtektől. Ezek a sejtek luminális epitheliumot alkotnak,

amely a méhüreg felszínén, amely a csöves mirigyeket alkotja, és mélyen eléri az endometriális stromát [172]. Munkánk során az SMTNL1 fehérjét overexpresszáltattuk Ishikawa sejtekben és három különböző környezetben vizsgáltuk a túltermelés hatásait: kontroll, progeszteron-kezelt (P4, a terhességet modellezve), és terhességi cukorbetegség (gesztációs diabétesz; GDB, magas glükóz és inzulin) körülmények között. A sejtek differenciálódását, migrációs képességét, valamint különböző jelátviteli útvonalak aktivitását mértük.

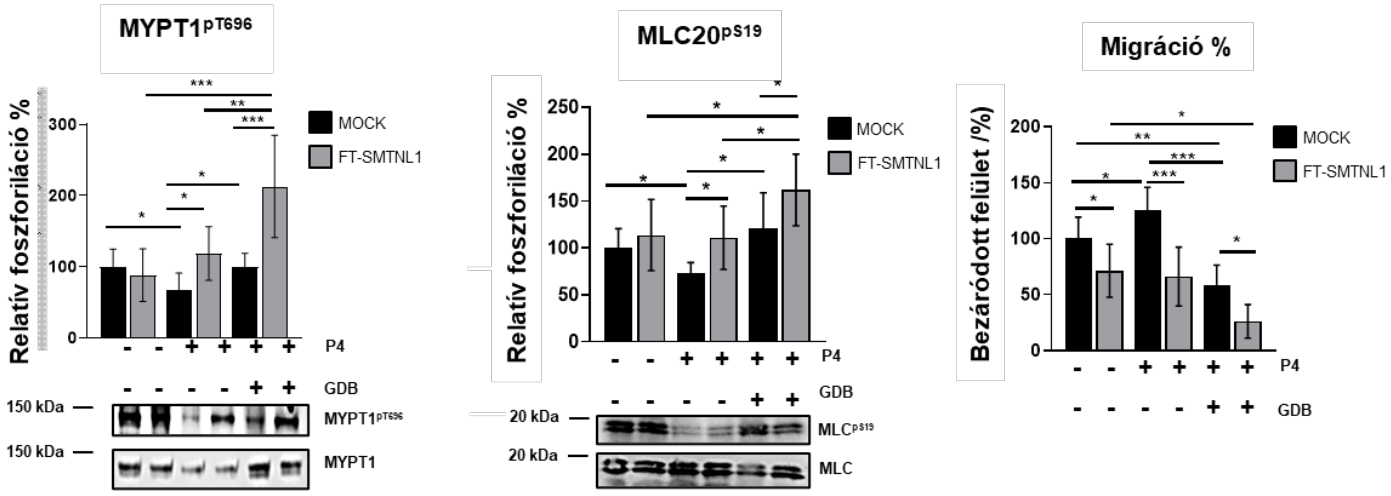
Eredményeink azt mutatták, hogy az SMTNL1 overexpressziója jelentősen fokozta az Ishikawa sejtek differenciálódását, különösen progeszteron jelenlétében (*39. ábra*).



39. ábra. Az SMTNL1 overexpresszió fokozza az Ishikawa sejtek differenciáciálódását. *Kontroll, P4 (terhességi modell) és GDP (terhességi cukorbeteg) sejteket üres plazmiddal (MOCK) és FT-SMTNL1 expressziós vektorral (FT-SMTNL1) transzfektátun. A differenciációt a sejtek aktin citoszkeltonjának Texas-Red falloidinnel (sárga) történő festésével követtük. A sejtmagokat DAPI-val (kék) festettük. Méretsáv: 100 µm. (bal oldali panel). A sejteket MUC-1 differenciációs markerrel is jellemeztük A MUC-1 fehérje fluoreszcencia értékeit HCS vizsgálattal mértük, és a MOCK kontroll értékeihet viszonyítottuk %-os értékben. n=7-8 +/- SD. Két csoportot párosítatlan t-teszttel, a három csoportot kétutas ANOVA teszttel elemeztük p< 0.05 (*), p<0.01 (**) és p<0.0001 (***). P4: terhességi csoport (progeszteron), GDB: inzulin rezisztens és P4 (terhességi cukorbeteg csoportok.*

Ezt a MUC-1 endometriális epitheliális differenciációs marker expressziójának növekedésével igazoltuk. A terhességi cukorbetegséget modellező környezet csökkentette a MUC-1 expressziót, de az SMTNL1 overexpresszálása részben ellensúlyozta ezt a hatást. A kontroll és a MOCK transzfektált Ishikawa sejtek sokszögűek, pleomorf tulajdonságúak, szabálytalan alakú magokkal és kisméretű, magas mag/citoplazmatikus aránnyal jellemezhetőek, de ezek progeszteron hozzáadására differenciálódtak: alacsonyabb sejtszámmal és kis vakuólumokkal és pleomorf magokkal rendelkező sejtekké váltak (*39. ábra*). A progeszteron-hiperglikémiás állapot megakadályozta az Ishikawa-sejtek morfológiai átalakulását, és a köbös szerkezet fennmaradt, ami a differenciálódás elmaradását mutatta. Ezt az SMTNL1 overexpressziója kompenzálni volt képes.

Kimutattuk, hogy az SMTNL1 overexpressziója csökkentette a MP MYPT1 szabályozó alegységének expresszióját és fokozta annak gátló foszforilációját, ami a miozin könnyű lánc (MLC20) foszforilációjának növekedéséhez vezetett (40. ábra).

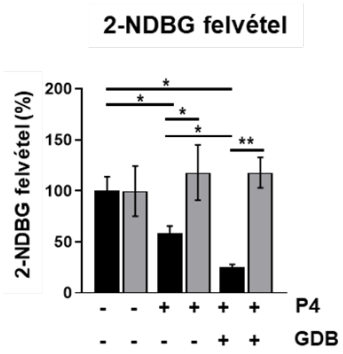


40. ábra. Az SMTNL1 overexpressziója növeli a MYPT1 és a miozin könnyű lánc (MLC20) foszforilációját és csökkenti az endometriális epitélsejtek migrációs képességét *. Ischikawa sejtek kontroll, progeszteronnal kezelt (P4) és tehességi cukorbeteg (GDB) csoportjait üres plazmiddal vagy FT-SMTNL1 expresszáló plazmiddal transzfektáltunk és a sejtek lizátumait Western blot analízissel elemeztük a MYPT1, MYPT1 ^{pT696}, MLC20 és MLC201^{pS19} elleni antitestekkel. DiD fluoreszcens festékkel jelölt, üres vektorral (MOCK) vagy FT-SMTNL1-gyel transzfektált és a kezeletlen kontroll, progeszteron kezelt (P4) vagy terhességi cukorbetegség (GDB) környezetben tartott Ishikawa sejteket scratch esszével vizsgáltuk (jobb panel). Két csoportot t-próbával, négy vagy több csoportot pedig kétutas ANOVA-val hasonlítottunk össze, ahol: p<0,05 (*), p<0,01 (**) és p<0,0001 (***), n=5*

Ezek a foszforilációbeli változások együttesen jelentősen csökkentették az Ishikawa sejtek migrációs képességét mindhárom vizsgált környezetben [173]. A nyálkahártya endometriális szöveteiben [174] végzett vizsgálatok alapján úgy tűnik, hogy a MP-nak fontos szerepe van az endometriális hámsejtekben, és a MYPT1 a fő szabályozó alegység az Ishikawa sejtekben jelen lévő MP-ben [173]. Ezenkívül az SMTNL1 csökkentheti az MP aktivitást mind a simaizomban [102], mind az endometriális hámsejtekben a MYPT1 expressziójának gátlásával is. Összességében eredményeink azt mutatják, hogy az MP elősegíti az Ishikawa-sejtek migrációját, amit az SMTNL1 csökkenteni képes inzulinrezisztens állapotban. Ez a megállapítás azért fontos, mert a szteroidhormonok egyensúlyának felbomlása kórosan módosítja a hám integritását és az endometriumsejtek migrációs képességét, és újabb bizonyítékot szolgáltat a szteroidhormonok hatása és a metabolikus rendellenességek között (*40. ábra*).

Számos bizonyíték szolgál az izolált endometriális sejtkultúrákban az inzulin ligandumok és az inzulinreceptorok aktivitásának hatásáról a sejtek proliferációjára és az endometrium sejtek differenciálódására. Az endometrium hiperglikémiás/hiperinzulinemiás metabolikus változásai a reproduktív diszfunkcióhoz és a szöveti atrófiához kapcsolódnak [175]. Megfigyeltük, hogy az SMTNL1 overexpressziója pozitív hatással volt az inzulin jelátvitelre is. Csökkentette az IRS1 gátló Ser612 oldalláncokon történő foszforilációját és növelte az Akt1 Ser473 foszforilációját terhességi és GDB modellben, ami a vázizomban leírt hatáshoz hasonlóan az inzulin érzékenység növekedésére utal.

Emellett az SMTNL1 overexpressziója növelte a glükóz felvételét (*41. ábra*) és a glikogén raktározást az Ishikawa sejtekben, különösen a terhességi cukorbetegséget modellező körülmények között. Az SMTNL1 progeszteronfüggő módon elősegítette a glükóz felvételét, és növelte a glikogéntartalmat az Ishikawa sejtekben, kompenzálva az inzulinrezisztenciát. Továbbá kimutattuk, hogy az SMTNL1 hatással volt az ERK1/2 MAPK jelátvitelre is, csökkentve annak foszforilációját és aktivációját a PP2A és DUSP9 foszfatázok fokozott expressziójának köszönhetően [173] *(41. ábra*).



41. ábra. Az SMTNL1 fokozza a glükóz felvételt. *Az Ishikawa-sejtek 2-NDBG glükózfelvételét kontroll, progeszteron (P4) és terhességi cukorbetegség (GDB) körülmények között vizsgáltuk SMTNL1 overexpresszióval vagy anélkül. Az értékeket normalizáltuk és a kontroll MOCK csoporthoz viszonyított arányban fejeztük ki, amelyet 100%-nak tekintettünk. (job oldali panel) Két csoportot t-próbával, négy vagy több csoportot pedig kétutas ANOVA-val hasonlítottunk össze, ahol: p<0,05 (*), p<0,01 (**) és p<0,0001 (***), n=5*

Összefoglalva, tanulmányunk betekintést nyújt az endometriális epitheliális sejtek működését szabályozó molekuláris mechanizmusokba terhesség és terhességi cukorbetegség során. Eredményeink kiemelik az SMTNL1 kulcsszerepét a sejt differenciálódás, migráció és metabolikus válaszok koordinálásában. Ezek a megállapítások potenciális jelentőséggel bírnak az endometriális diszfunkcióval összefüggő különböző reproduktív rendellenességek, így az endometriózis és az endometriális tumorok korai szakaszainak megértésében és kezelésében. Az ezen a területen folytatott további kutatások új terápiás stratégiákhoz vezethetnek a metabolikus rendellenességekkel vagy egyéb, az endometrium normál működését befolyásoló állapotokkal küzdő nők reproduktív eredményeinek javítására.

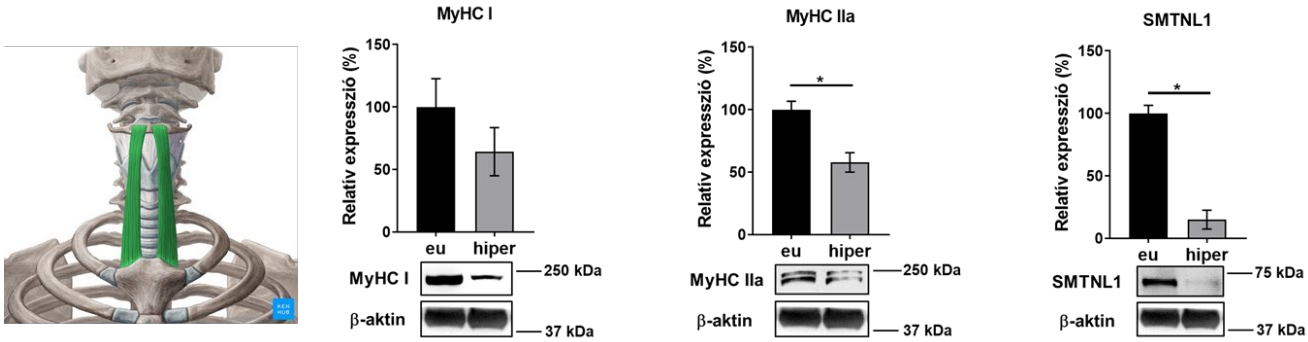
5.6. Az SMTNL1 szerepe a pajzsmirigyhormon által indukált fiziológiás és patológiás folyamatokban izomban

5.6.1. A SMTNL1 fehérje szerepe a hyperthyreosisos vázizom anyagcseréjének szabályozásában

A vizsgálataink középpontjában álló transzkripciós kofaktor, a SMTNL1 fehérje figyelemreméltó abban a tekintetben, hogy képes szabályozni a vázizom különböző stresszhatásokra bekövetkező adaptálódását. A 5.4.1. fejezetben tárgyalt módon a vázizom adaptációja fiziológiás és patológiás folyamatok hatására is bekövetkezik. Patkányokon végzett kísérletekben kimutatták, hogy a pajzsmirigy megváltozott hormontermelése is képes a vázizom rostösszetételét jelentős mértékben átalakítani az MyHC expressziójának transzkripciós szintű szabályozása révén. Hyperthyreosis során a kiindulási rosttípustól függően az MyHC 1-ből 2a, a 2a-ból 2x, a 2x-ből pedig 2b lesz [176]. Ennek molekuláris mechanizmusa ismert, de szabályozó elemei még nem kerültek azonosításra.

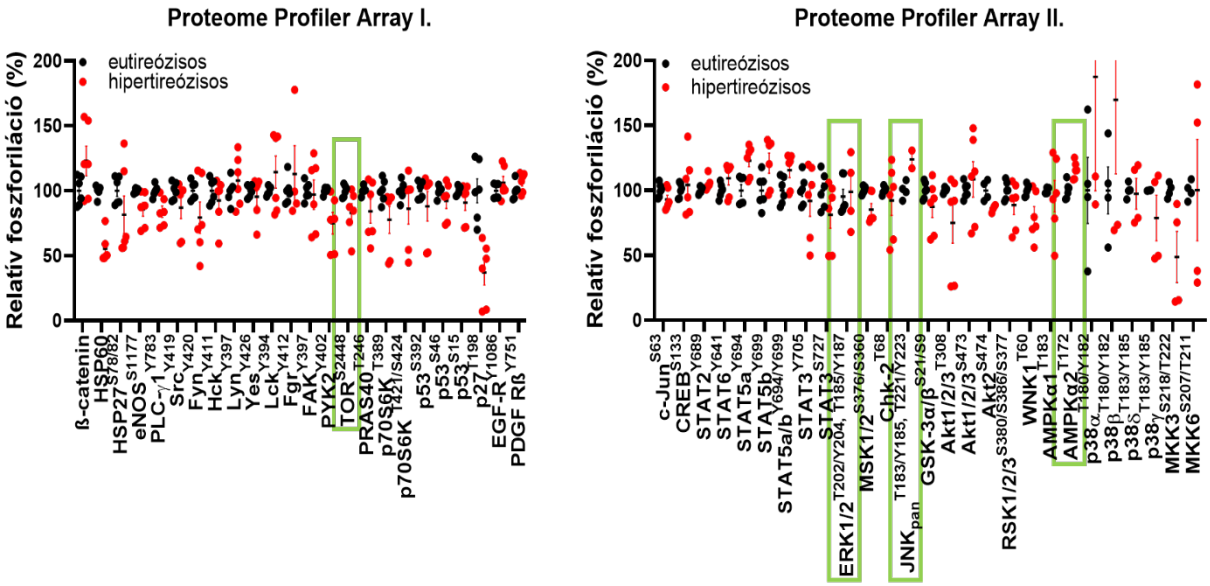
Az a munkahipotézisünk, miszerint az SMTNL1 fehérje szabályozza a pajzsmirigyhormon által kiváltott izotípus változást a következő tényeken alapult: i, az SMTNL1 KO egerek vázizomzatában az 2a típusú rostokban expresszálódó SMTNL1 deléciója a vázizom rostösszetételének 2x vagy b irányú átalakulását indukálta [101]; ii, a vemhes nőstény egerek *m. plantaris* izmában a SMTNL1 deléciója a 2a/2b típusú rostok arányának csökkenését eredményezi, ami egy összességében egy glikolitikusabb fenotípus kialakulását vonja maga után [152]. Vizsgálataink modellrendszereként pajzsmirigyműtéten átesett euthyreosisos és hyperthyreosisos nőbetegektől származó *m. sternohyoideus* biopsziákat, valamint fiziológiás és szuprafiziológiás aktív pajzsmirigyhormon kezelést kapott differenciáltott C2C12 miotubulusokat használtunk. Western blottal a MyHC IIa fehérje expressziójának számottevő csökkenését figyeltük meg a hyperthyreosisos humán vázizomban (42. ábra). Mivel szignifikáns izomtömeg-csökkenést nem írtunk le, ezért feltételezhető, hogy az MyHC I és IIa rostok csökkenése mellett az MyHC IIx rostok száma nőtt, ami az oxidatív(abb) rostok csökkenése miatt egy összességében glikolitikusabb fenotípust eredményezett. Bár az MyHC I fehérje expressziója is csökken, ez a változás statisztikailag nem szignifikáns, ami humán adatok hiányában a patkány *m. sternohyoideus* rostösszetételével magyarázható: fiziológiás körülmények között az 1-es típusú rostok aránya mindössze 9%, míg a 2a típusú rostoké 24,2%, a 2x típusú rostoké pedig 20,8%.

A legmagasabb arányban a 2b típusú rostok vannak jelen (44,2%), azonban ez az izoforma a rágcsálókkal ellentétben a humán vázizmokban nem detektálható [147], így ezt nem vizsgáltuk. Érdekes módon a SMTNL1 expressziója drámaian csökkent a hyperthyreosis során, ami arra enged következtetni, hogy a SMTNL1 szerepet játszhat a hyperthyreosisos vázizom patofiziológiájában (42. *ábra*).



42. ábra. ***MyHC IIa, MyHC I és SMTNL1 expresszió a hyperthyreosisos humán vázizomban.*** *A vázizom biopsziák m. sternohyoideus-ból származtak (baloldali képen zölddel jelölve) és a fehérjéket Western blot analízissel vizsgáltuk. Az MyHC IIa, MyHC I és a SMTNL1 elleni specifikus antitestekkel kapott sávok denzitását elosztottuk a belső kontrollként használt β-aktin denzitásával, majd a hyperthyreosisos értékeket az euthyreosisos értékekre normálizáltuk. Az n=3 kísérletből származó relatív fehérje expressziót oszlopdiagramon ábrázoltuk (átlag ± SEM). A csoportokat kétmintás párosítatlan t-próbával hasonlítottuk össze, ahol p<0,05 (*). A baloldali kép forrása: https://www.kenhub.com/en/library/anatomy/sternohyoid-muscle*

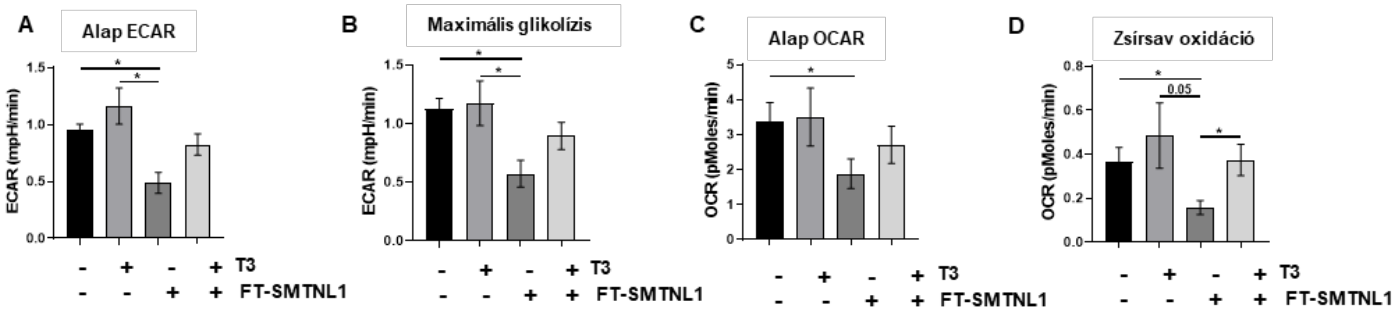
Az euthyreosisos és hyperthyreosisos humán biopsziák globális génexpressziós profiljának összehasonlítása és az adatok génontológiai analízise feltárta, hogy az mTOR, AMPK, PI3K/Akt és a MAPK szignalizációban résztvevő gének expressziója változott a legjelentősebb mértékben a hyperthyreosis hatására. Ezek a jelátviteli útvonalak többek között olyan biológiai folyamatokban játszanak szerepet, mint a sejtszerkezet és szerveződés, a sejt- és szövetfejlődés, a lipid metabolizmus, az anyagcsere és energiatermelés, valamint ezek zavarai. A microarray analízis során azonosított jelátviteli útvonalak hyperthyreosis által indukált fehérjeszintű változásainak tanulmányozására számos kináz relatív foszforilációs szintjét is megvizsgáltuk a hyperthyreosisban szenvedő donorok vázizmában (43. *ábra*). A Proteome Profiler eredményekből kiderül, hogy a Ser/Thr kinázok csoportján belül egyebek mellett az $mTOR^{S2448}$ és az $Akt2^{S474}$ foszforilációja és ezáltal az aktivitása szignifikánsan csökken míg az $ERK1/2^{T202/Y204}$, $AMPK\alpha2^{T172}$ és a $JNK_{pan}{}^{T183/Y185,T221/Y223}$ foszforilációja és aktivitása szignifikánsan nő a hyperthyreosis során *(43. ábra*).



43. ábra. Humán euthyreosisos és hyperthyreosisos vázizom biopsziák foszforilációs mintázatának vizsgálata.. *A minták homogenizálását követően számos fehérje relatív foszforilációs szintjének egyidejű, gyors és érzékeny meghatározását végeztük el a human foszfo-kináz (bal panel) és foszfo-MAPK array segítségével (jobb panel) Az n=3 kísérletből származó eredményeket átlag ± SEM formában ábrázoltuk. A csoportokat kétmintás párosítatlan t-próbával hasonlítottuk össze, a részletes grafikon a függelékben található (1S. ábra), ahol p <0,05 (*), p <0,01 (**), p <0,001 (***)*

A microarray és a Proteome Profiler array-k eredményeiből kitűnik, hogy a hyperthyreosisnak jelentős befolyása van a vázizom fejlődésére és anyagcseréjére az ezen folyamatokban szerepet játszó fehérjék expressziójának vagy aktivitásának módosításán keresztül, és a hyperthyreosis kulcsfontosságú szignalizációs útvonalakat szabályoz a humán vázizomban, ami az irodalom alapján várható, mivel a T3 az anyagcsere regulátora (43. ábra). A differenciáltatott C2C12 sejtekben a TRα/TRβ arány csökkenését és a MyoD1 szignifikáns növekedését detektáltuk a szuprafiziológiás T3 kezelés hatására, míg a SMTNL1 overexpressziója a TRα expresszióját markánsan csökkentette [3].

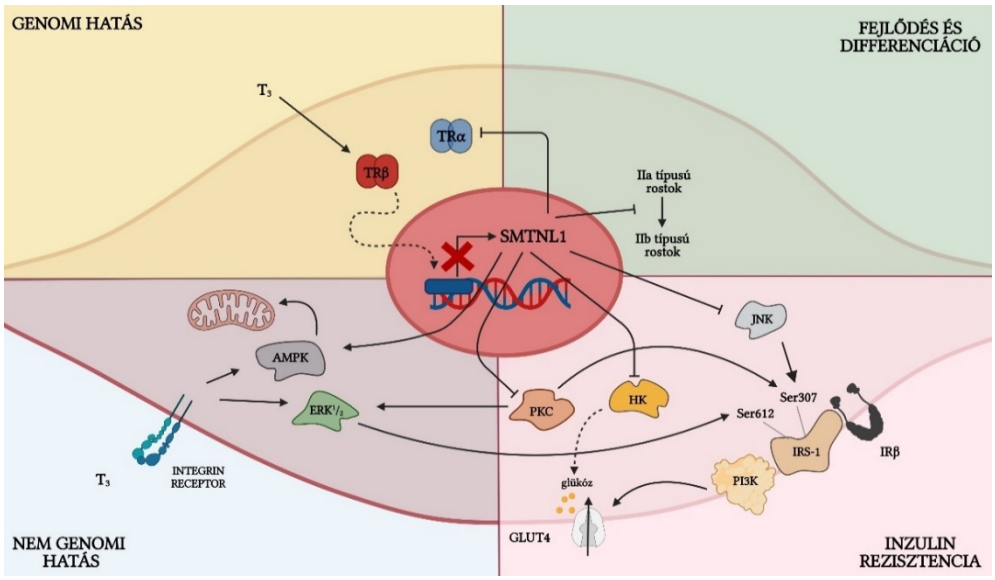
Továbbá a mioblasztok SeaHorse analízise rávilágított arra, hogy a SMTNL1 a glikolízis gátlásán keresztül antagonizálja a T3 hatását a miotubulusokban (*44. ábra*). A T3 kezelésre fokozódik a laktáttermelés, és a SMTNL1 overexpressziója nemcsak, hogy meggátolta a T3-indukált anaerob glikolízis fokozódását, de a mitokondriális oxidatív foszforiláció és a zsírsav oxidáció mértékét is szignifikánsan csökkentette. A kapott adatok fényében elmondható, hogy a feleslegben lévő T3 a laktáttermelés és a zsírsav oxidáció fokozódását indukálja, miközben a SMTNL1 a különböző anyagcserefolyamatok, főként a glikolízis szabályozásán keresztül antagonizálja a T3 hatását. Eredményeink alapján a SMTNL1 fehérje inzulinérzékenyítő és T3



44. ábra. A pajzsmirigyhormon hatás és az SMTNL1 overexpresszió hatása azC2C12 mioblasztok anyagcseréjére. *Az extracelluláris savasodási ráta (ECAR) és az oxigénfogyasztási ráta (OCR) mérése SeaHorse-elemzéssel történt. Az üres vektorral vagy FT-SMTNL1-transzfektált mioblasztok 72 órás T3-kezelése után glükózzal kiegészített Seahorse XF vizsgálati közeget adtunk a sejtekhez. A mioblasztokat etomoxirral (50 µM), oligomycinnel (2 µM), FCCP-vel (4 µM) és antimycinnel (10 µM) + 2-deoxi-D-glükózzal (100 mM) kezeltük. A protonkoncentráció-növekedés (A-B) és az oxigénkoncentráció-csökkenés (C-D) sebességét mértük. Az ábra az alap ECAR (A), alap OCAR (B) értékeket, a maximális glikolízist (C) és a zsírsav oxidáció mértékét (D) mutatja. Az értékek 4 csoportot jelentenek 23 technikai ismétléssel/csoport, n=3, átlag +/- SEM. Az adatokat a fehérjetartalomra normalizáltuk. A csoportokat egyutas ANOVA és Tukey-féle post hoc teszt segítségével hasonlítottuk össze, p <0,05 (*), p <0,01 (**).*

antagonizáló hatása révén képes a hyperthyreosis és az azt kísérő inzulinrezisztencia mérséklésére, melyet többek között az IRS kinázok aktivitásának, valamint a HK enzim expressziójának csökkentésén keresztül ér el (44. *ábra*).

A hyperthyreosis egy felfokozott anyagcserével járó állapot, melyben a sejtek megnövekedett glükózigényét az intracelluláris glikogénraktárak fokozott lebontásából és/vagy az extracelluláris glükóz felvételének serkentéséből próbálja fedezni a sejt, azonban tünetként írták le a csökkent perifériális inzulinérzékenységet és glükóz intoleranciát is hyperhyreosis során [177; 178]. Ennek oka a vázizom inzulin-mediált glükózfelvételét szabályozó jelátviteli útvonal, ezen belül az IRS fehérjék megváltozott aktivitásában keresendő [157]. Eredményeink bizonyítékul szolgálhatnak arra vonatkozóan, hogy a szuprefiziológiás T3 szint zavart okoz az inzulin jelátvitelben egyrészt az IRS1 307-es és 612-es Ser foszforilációjának növelése által [3], ami a fehérje inaktiválódását és a PI3K disszociációját vonja maga után, másrészt a PI3K expressziójának csökkentésén keresztül, ami a serkentő PI3K általi foszforiláció csökkenését eredményezi. Ezek együttesen a negatív Ser foszforiláció túlsúlyba kerüléséhez járulnak hozzá, ami inzulinrezisztencia kialakulását indukálja. Az IRS1 gátló Ser foszforilációjának mérséklése révén a SMTNL1 fehérje azonban képes lehet a glükóz transzport inzulinra adott normál válaszadó képességét visszaállítani.



45. ábra: A SMTNL1 szerepe a hyperthyreosisos vázizom anyagcseréjének szabályozásában. *A SMTNL1 a következő mechanizmusokon keresztül képes a hyperthyreosis által indukált anyagcsereváltozások megelőzésére a vázizomban: 1) ellensúlyozza a szuprafiziológiás T3 által kiváltott glikolitikus irányú eltolódást; 2) inzulinérzékenyítő hatását a JNK gátlásán keresztül fejti ki; 3) gátolja a T3 nem genomi útvonalának eredményeképpen aktiválódó ERK1/2-t a PKCδ expressziójának szabályozásán keresztül; 4) a HK II enzim szabályozásán keresztül a glükóz foszforiláció és a glikolízis szabályozásában is részt vesz és 5) szelektíven gátolja a TRα expresszióját, amely a T3 fő effektora.Módosítva: [3]*

Munkahipotézisünk szerint a megnövekedett IRS1 Ser foszforiláció a szuprafiziológiás T3 kezelés következtében aktiválódott IRS1 kinázok, mint a ERK1/2 és a JNK hatásának eredménye, melyet a hyperthyreosisos humán minták Proteome Profiler elemzése is alátámaszt. A SMTNL1 túltermeltetése következtében csökkenő IRS1 és ERK1/2 foszforiláció a PKCδ expressziójának visszaesésével magyarázható, amely egyrészt a 307-es Ser oldalláncot foszforilálja az IRS1-en[179], másrészt az ERK1/2 aktiválásáért is felelős [180]. A T3 által feltehetően nem genomi útvonalon aktivált ERK1/2 az IRS1 Ser612 foszforiláció fokozódásáért tehető felelőssé. A kapott adatok magyarázatot jelenthetnek a szuprafiziológiás T3 koncentráció által előidézett gátló IRS1 Ser foszforiláció fokozódására, továbbá alátámasztják a SMTNL1 fehérje inzulinérzékenyítő hatását. A T3-mal kezelt sejtekben a PP2Ac expressziójának csökkenése az AMPK foszforiláció tartós megemelkedését vonta maga után, ami a GLUT4 és hexokináz II (HK II) expressziójának indukálásán keresztül fokozta a glikolízist (*45. ábra*) [3].

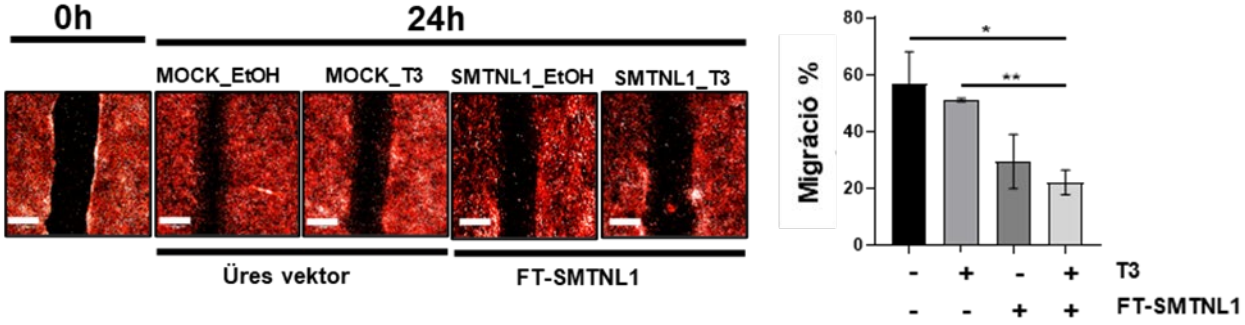
Eredményeinket összefoglalva a SMTNL1 általi szabályozás ígéretes lehet a hyperthyreosis és az azt kísérő inzulinrezisztencia gyógyításában (45. ábra), mivel képes szelektíven képes gátolni a TRα expresszióját. Emellett inzulinérzékenytő hatást fejt ki egy inzulintól független, heterológ útvonalon, a JNK aktivitásának gátlásán keresztül, és gátolja a T3

nem genomi hatásait. Mindemellett szabályozza a glükóz foszforilációt és a glikolízist, és ezen keresztül ellensúlyozza a T3 által indukált glikolitikus fenotípus kialakulását. Mindezen tulajdonságai miatt a SMTNL1 overexpressziója vagy -alternatív megoldásként- egy membránpermeábilis SMTNL1 mimikáló peptid inzulinérzékenyítő hatása révén képes lehet a hyperthyreosis során fellépő kezdődő inzulinrezisztencia ellensúlyozására a vázizomban.

5.6.2. A SMTNL1 és a T3 szelektíven szabályozzák a MYPT1 és MYPT2 izoformákat a miotubulusokban

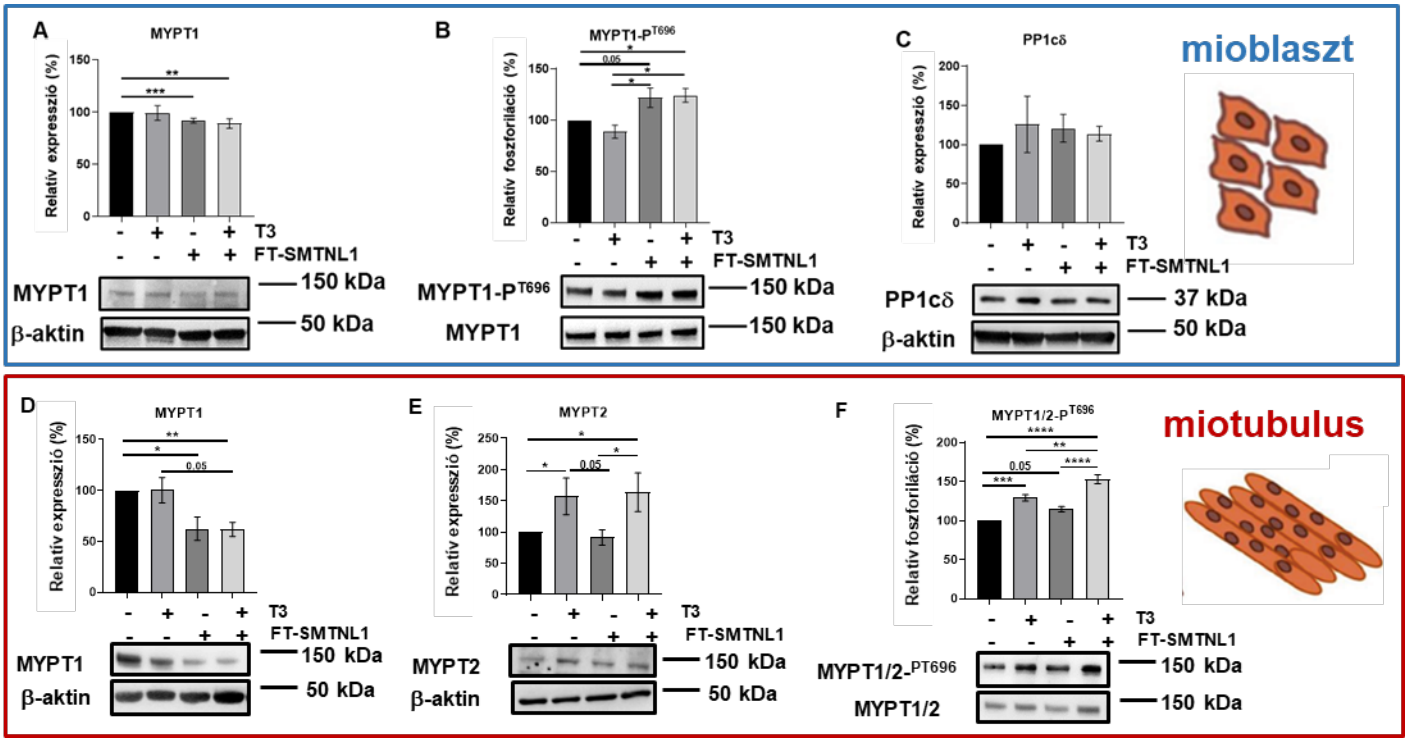
Korábbi tanulmányokból kitűnik, hogy a MP enzim aktivitása nem csak a különböző sejtek migrációs képességét [1; 128; 181], de a vázizom modellezésére használt C2C12 sejtek differenciációját is szabályozhatja [182]. Mivel a migráció és a differenciáció a vázizom fejlődésében is fontos szerepet játszik, ezért a SMTNL1 fehérje és a MP közötti kapcsolatot, valamint ezen fehérjék potenciális szabályozó szerepét is vizsgáltuk az említett folyamatokban és a már differenciálódott sejtek homeosztázisának fenntartásában a hyperthyreosis modellezésére szolgáló kísérleti rendszerben. Emiatt utánajártunk, hogy a SMTNL1 túltermeltetése és a szuprafiziológiás T3 kezelés hogyan befolyásolják a C2C12 mioblasztok migrációját. Megállapítottuk, hogy a SMTNL1 overexpressziója jelentős mértékben visszavetette a sejtek migrációs képességét a T3 jelenlétében (*46. ábra*).

A jelenséget a SMTNL1 MP enzimet gátló hatásával magyaráztuk. Felvetésünk igazolására nem csak a MP-t felépítő alegységek, hanem az enzim szubszrátjának (MLC20)



46. ábra. T3-kezelt és SMTNL1 overexpresszáló mioblasztok karcolásos vizsgálata. *A mioblasztokat üres vektorral vagy FT-SMTNL1-tel transzfektáltuk. 48 órás tenyésztés és 5 órás széruméheztetést követően megkarcoltuk, majd további 24 órán át tiszta oldószer (EtOH) vagy etanolban oldott 10 nM T3 jelenlétében növesztettük. A karcolásos területekről 10x-es objektívvel készítettünk fényképeket a jelzett időpontokban. Méretsávok: 500 µm. (bal panel) A jobb oldali daigramm a 24 óra elteltével lefedett karcolásos területeket mutatja. n=3, átlag +/- SEM. Az adatokat az üres vektor-transzfektált kontrollhoz normalizáltuk. A csoportok átlagai közötti különbségeket kétirányú ANOVA (B) vagy egyirányú ANOVA (C), majd Tukey post hoc teszt követte, p <0,05 (*), p <0,01 (**), p <0,0001 (****).*

expresszióját és foszforilációját is megvizsgáltuk. A C2C12 mioblasztokon végzett kísérleti eredményeink értelmében a SMTNL1 overexpressziója önmagában és a T3 kezeléssel kombinálva a MYPT1 expresszióját szignifikánsan csökkentette, míg a Thr696-os oldallánc foszforilációját szignifikánsan növelte. A MYPT1 gátló foszforilációjának növekedését mindkét esetben az MLC20 Ser19-es oldallánc foszforilációjának szignifikáns emelkedése kísérte *(47. ábra)*). Eredményeinket alátámasztja az a megfigyelés, hogy a SMTNL1 KO egerekben a MYPT1 expressziójának növekedése mellett csökkent MLC20 Ser19 foszforilációt detektáltak az állatok



47. ábra. Az SMTNL1 overexpressziója szabályozza a miozin foszfatáz foszforilációját a mioblasztokban és miotubulusokban. *A C2C12 mioblasztokat (A-C) és miotubulusokat (D-F) üres vektorral vagy FT-SMTNL1 plazmiddal transzfektáltuk, és 10 nM T3-mal kezeltük 24 órán át. A teljes sejt lizátumokat anti-MYPT1 (A, D), anti-MYPT1-^{PT696} (B, E), anti-MYPT2 (E), és anti-PP1cδ (C) antitestekkel Western blot segítségével elemeztük. n=3, átlag +/- SEM. Az adatokat az üres vektorral transzfektált kontrollra normalizáltuk. A csoportok átlagai közötti különbségeket egyutas ANOVA és Tukey-féle post hoc teszt segítségével határoztuk meg, p <0,05 (*), p <0,01 (**), p <0,001 (***).*

simaizmában [102]. A MP enzim MYPT1 alegységének Thr696 foszforiláció általi gátlása a nem-izom miozin foszforilációjának lassabb turnoverét eredményezheti, ezáltal stabilabb adhéziós struktúrák jönnek létre, amik akadályozzák a sejtek citoszkeletonjának átrendeződését és a sejtek migrációját.

A SMTNL1 tranziens overexpressziója során a fehérje expressziója kezdetben nagyon magas, majd a differenciáció progressziójával párhuzamosan csökken. Fiziológiás T3 koncentráció mellett a SMTNL1 overexpressziója a korai és késői differenciációs markerek upregulálódását okozza, ami alapján úgy tűnik, hogy a SMTNL1 segíti a C2C12 mioblasztok miotubulusokká történő differenciációját. A molekuláris szintű változásokon túlmenően a differenciáció során bekövetkező morfológiai változásokat is nyomonkövettük. Megfigyeléseink szerint a SMTNL1 overexpressziója kisebb méretű, de nagyobb számú miotubulus kialakulását indukálja, ami támogatja a SMTNL1 fehérje differenciációt elősegítő hatásáról alkotott hipotézisünket.

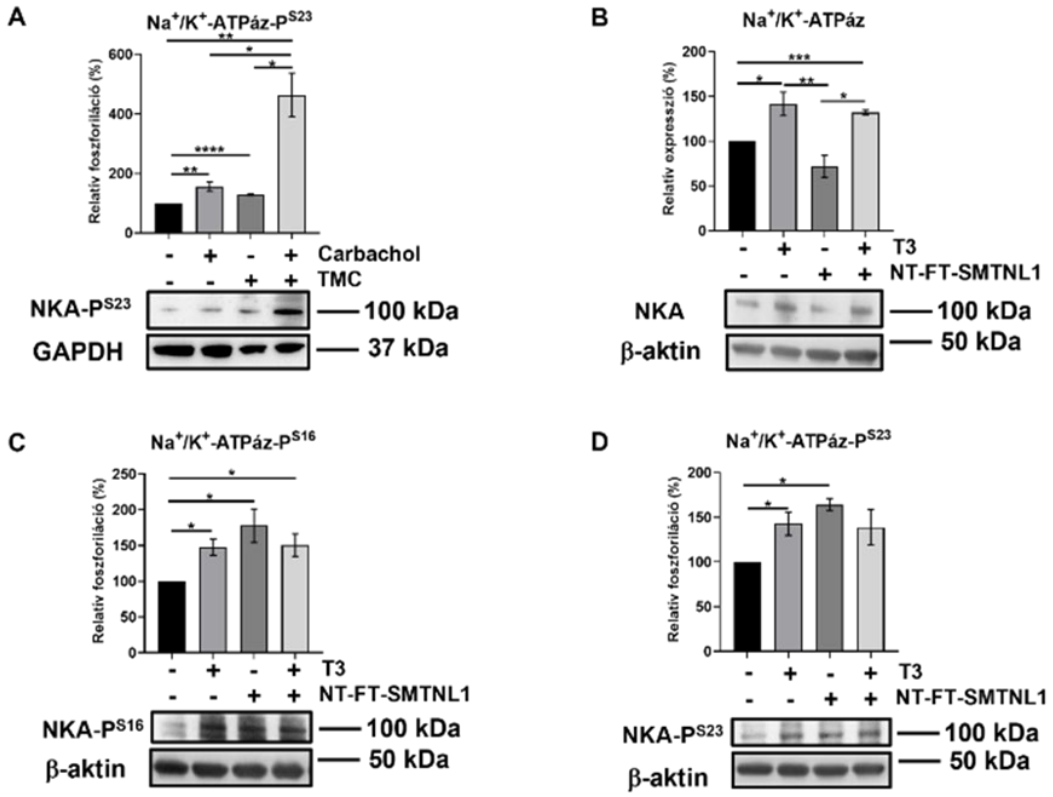
Az eredményekből kitűnik, hogy míg a mioblasztokban a PP1cδ inkább a MYPT1 izoformával alkot komplexet, addig az érett miotubulusokban elsősorban a MYPT2 az, amely a PP1cδ-val közösen vesz részt a MP holoenzim felépítésében (*47. ábra*). Érdekes módon a szuprafiziológiás T3 kezelés a differenciálódó mioblasztokban a MYPT2 expresszióját növelte, míg a PP1cδ és a MYPT1 expressziójára nem volt hatással, ahogy azt a proliferatív fázisban lévő mioblasztok vizsgálatánál is tapasztaltuk (*47. A és C*). A miotubulusok vizsgálatánál is hasonló eredményre jutottunk: a MYPT1 expressziója T3 kezelés hatására nem változott, de a SMTNL1 overexpressziója és a kombinált kezelés szignifikáns visszaesést okozott a fehérje relatív expressziójában (*47.D. ábra*). Ezzel szemben a MYPT2 expressziója drámaian, emelkedett a T3 kezelés, valamint a kombinált kezelés hatására, miközben a SMTNL1 overexpressziója nem volt hatással rá (*47.E. ábra*). A PP1cδ expressziója kis mértékben csökkent a T3 kezelés és/vagy a SMTNL1 overexpressziójának következtében *(47. C ábra*). Ezen eredmények összecsengenek azzal, hogy a SMTNL1 kiütése a MYPT2 expressziós szintjét nem befolyásolja a vázizomban [102]. A mioblasztokon és a miotubulusokon nyert eredményeket összegezve úgy tűnik, hogy a T3 és a SMTNL1 szelektíven szabályozzák a különböző MYPT izoformák kifejeződését mind a differenciálatlan, mind a már differenciálódott sejtekben (*49. ábra*). Az SMTNL1 túltermelés által indukált MYPT1 és MLC20 fokozott foszforilációja arra utal, hogy az SMTNL1 létfontosságú szerepet játszik az MP aktivitás szabályozásában az izomképződés kezdeti szakaszában. A kulcsfontosságú szabályozó fehérjék foszforilációs állapotának modulálásával az SMTNL1 segít összerendezni a mioblasztok differenciálódásának és érett izomrostokká történő fúziójának összetett folyamatát [183].

A C2C12 sejtek differenciálódásával a nem-izom miozinról a vázizom típusú miozin felé történő eltolódás figyelhető meg, és a 6. napon a nem-izom miozin alig volt kimutatható a miotubusokban, míg az vázizom-miozin koncentrációja megnőtt [32]. A MYPT1-PP1cδ simaizom típusú holoenzim alacsony affinitást mutat a foszforilált vázizom-miozinhoz, emellett az vázizom-miozin foszforilációja csökkent, de nem szűnt meg a differenciálódás 6. napján [32], ami arra utal, hogy a miotubulusokban illetve érett vázizomban is jelen lévő MP nincs hatással az izom kontraktilitásának szabályozásával a nem-izom szövetektől eltérően, emiatt a MP alternatív szubsztrátjai léteznek az vázizomban [183].

Az MP egyik lehetséges szubsztrát jelöltje a vázizomban a Na^+/K^+-ATPáz (NKA). Az NKA egy transzmembrán pumpa, amely nélkülözhetetlen a sejtek ion- és vízhomeosztázisához, a membránpotenciálok fenntartásához és a különböző anyagok Na^+ -hoz kapcsolt transzportjához. A vázizomban található az egyik legnagyobb és legdinamikusabb NKA-raktár a szervezetben [184]. Ezért az NKA szabályozása akár szubsztrátjainak koncentrációja, akár az FXYD fehérjékkel való fehérje-fehérje kölcsönhatások, akár kovalens módosítás - elsősorban foszforiláció - révén döntő fontosságú [36]. A NKA számos szabályozó foszforilációs helye közük kiemelendő két foszforilációs hely: a Ser23-as és Ser16-es oldalláncok, amelyek az NKA gátlásáért felelősek [185]. Az NKA-t már azonosítottuk a MYPT1 interaktómban egér szinaptoszóma kivonatból végzett pull-down assay-vel, majd tömegspektrometriás elemzéssel [114]. A C2C12 sejt lizátumból végzett koimmunoprecipitáció szintén kimutatta az NKA és a MYPT közötti kölcsönhatást.

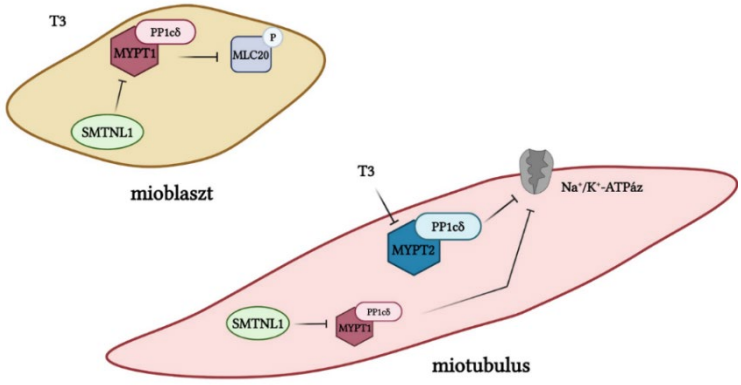
Kísérleteink alapján a NKA expresszióját a szuprafiziológiás T3 kezelés növelte, míg a SMTNL1 overexpressziója kismértékben csökkentette (*48. A. ábra*). Eredményeink összhangban vannak *Riis és mtsai* munkájával, melyben azt találták, hogy az NKA expressziója 89%-ban megemelkedett a hyperthyreosisban szenvedő betegek mintáiban az euthyreosisos donorok mintáival összevetve [186]. A NKA Ser23 és Ser16 foszforilációs helyeinek vizsgálatakor mind a szuprafiziológiás T3 kezelés, mind a SMTNL1 overexpresszió következményeként szignifikánsan emelkedett foszforilációt mutattunk ki *(48. C és D ábra*). Ez vélhetően a MP holoenzim megnövekedett gátló foszforilációjának köszönhető, amely így nem képes a NKA-t defoszforilálni. Ezt a megfigyelést egerek *m. plantaris* izmából készített preparátum PP1 szelektív inhibitorral (TMC) történő kezelése is alátámasztja, melyben fokozott NKAα1 Ser23-as foszforilációt detektáltunk, az NKA aktiváláshoz karbakolt, kolinerg agonistát, alkalmazva (*48. A.*

ábra). Ezen eredmények alapján kijelenthetjük, hogy mind a T3, mind a SMTNL1 a különböző MYPT izoformákat tartalmazó MP holoenzim gátlásán keresztül részt vesz a NKA foszforilációs állapotának és ezáltal aktivitásának szabályozásában *(48. ábra)* [183]



48. ábra: A SMTNL1 overexpresszió és a szuprafiziológiás T3 kezelés hatása a NKA expressziójára és foszforilációjára a miotubulusokban. *Egerek m. plantaris izmából készített preparátumot 10 µM TMC-vel kezeltünk 30 percig, amit egy 10 percig tartó 10 µM-os carbacholos kezelés követett. A mintákat homogenizáltuk, ésa NKA-P^{S23} elleni specifikus antitesttelelemeztük* ***(A)****. A mioblasztokat üres plazmiddal (MOCK) vagy rekombináns SMTNL1 fehérjét expresszáló plazmiddal (NT-FT-SMTNL1) transzfektáltuk, majd differenciáltattuk. A miotubulusokat 10 nM T3-mal kezeltük, majd Western blot analízist végeztünk a NKA* ***(B)****, NKA-P^{S16}* ***(C)*** *és NKA-P^{S23}* ***(D)*** *elleni specifikus antitestekkel. A kapott eredmények n=3 kísérletből származnak, melyek átlag ± SEM értékét ábrázoltuk. Minden esetben a nem kezelt és/vagy üres plazmiddal transzfektált kontrollra normalizáltunk. A csoportok közötti különbségeket Tukey-féle post hoc teszttel kombinált egyutas ANOVA-val elemeztük, ahol p <0,05 (*), p <0,01 (**), p<0,001 (***) és p <0,0001 (****).*

Fontos megjegyezni, hogy a NKA hipo- vagy hiperfunkciója egyaránt hátrányos következményekkel jár az izomfunkcióra nézve: a NKA hiperfunkciója hiperpolarizáló hatású, ami a membránpotenciált még negatívabbá teszi, melyben nehezebb elérni a feszültségfüggő Na^+ csatornák nyitásához és a Ca^{2+} felszabadulásához szükséges küszöböt, ezáltal az izom ingerlékenysége csökken, ami izomgyengeség kialakulásához vezet. A pumpafehérje



49. ábra: A MP enzim különböző módon szabályozódik az eltérő differenciációs állapotú izom sejtekben. *A nem differenciált mioblasztokban a MP felépítésében a PP1cδ mellett a MYPT1 izoforma vesz részt, melynek expresszióját és aktivitását, ezen keresztül pedig a sejtek citoszkeletális átrendeződését és migrációját a SMTNL1 fehérje szabályozza. Ezzel szemben a miotubulusokban a PP1cδ elsősorban a MYPT2 izoformával alkot komplexet, melynek aktivitása T3 által szabályozott, és amely lehetséges szabályozó eleme a NKA-nak, a fehérje foszforilációs állapotának befolyásolásán keresztül. Ezen eredmények hozzájárulhatnak a hyperthyreosis során fellépő izomgyengeség jobb megértéséhez, amely a betegek életminőségének javítását szolgálja.*

hipofunkciója esetén a membránpotenciál pozitívabb, a sejtmembrán deporalizáltabb, emiatt a feszültségfüggő Na^+ csatornák egy része inaktivált állapotba kerül, ezért az akciós potenciál amplitúdója kisebb, kevesebb Ca^{2+} szabadul fel, ami kisebb mértékű összehúzódást, ezáltal pedig izomgyengeséget eredményez [187]. Ezen oknál fogva a rendszer finomhangolása kritikus jelentőséggel bír.

Eredményeink alapján MYPT2 szelektív felülszabályozása a hyperthyroid izomszövetekben egy adaptív válaszra utal, amelynek célja az izom-összehúzódási és elernyedési ciklusok finomhangolása a megemelkedett metabolikus igényekre válaszul. A hyperthyreosis izomgyengeséggel és fáradtsággal jár együtt, ami részben a MP-ok megváltozott szabályozásának tulajdonítható (*49. ábra*). A MYPT2 és a PP1cδ fokozott expressziója egy kompenzációs mechanizmust képviselhet, amely ellensúlyozza a magas T3 szintek által kiváltott fokozott izomkontraktilitást és energiafelhasználást. Az MP-ok aktivitásának modulálásával a pajzsmirigyhormon segít fenntartani az izom-összehúzódás és elernyedés kényes egyensúlyát, biztosítva az optimális izomfunkciót a változó élettani körülmények között. Ezen eredmények integrációja finomhangolt kölcsönhatást tár fel a SMTNL1 és a pajzsmirigyhormon között a MP-k szabályozásában. Míg a SMTNL1 gátló hatást fejt ki a MYPT1-re a korai mioblaszt differenciálódás során, addig a T3 szelektíven felülszabályozza a MYPT2-t a hyperthyroid izomszövetekben. Ez a differenciális szabályozás kiemeli a MP szabályozás összetettségét és a szabályozó fehérjék és hormonális jelek sokoldalú szerepét az izomfunkció modulálásában *(49.*

ábra). Az SMTNL1 és a T3 kölcsönhatásának megértése a MP szabályozás kontextusában értékes betekintést nyújthat a megváltozott izomdifferenciációval és pajzsmirigy-diszfunkcióval összefüggő izombetegségek patogenezisébe [183].

6. KITEKINTÉS

A disszertációmban összefoglalt eredmények rávilágítanak a MP, a simaizomzat kontraktilitását szabályozó enzim sokrétű és rendhagyó funkcióira. Kimutattuk, hogy az MP szabályozó MYPT1 alegysége valamennyi eddig vizsgált sejttípusban expresszálódik és változatos szubcelluláris lokalizációt mutat az eukarióta sejtekben. A citoplazma és a citoszkeleton mellett a MYPT1 és a PP1c egyaránt megtalálható a sejtek nukleáris, mitokondriális és plazmamembrán frakcióiban, és a MYPT1-interaktomokban azonosított fehérjék többsége nem releváns a citoszkeletális szabályozás szempontjából, ami arra utal, hogy az MP sokkal több mint a miozin könnyűlánc defoszforilációjának kizárólagos szabályozója. Továbbá a MYPT1 funkciója is több mint a szubsztrátspecifitás meghatározása a MP holoenzimen belül: ugyanis állványfehérjeként szolgálhat, vagy nukleocitoplazmatikus transzfermechanizmust biztosít a fehérjék számára - még a PP1c-vel való kölcsönhatása nélkül is.

A miozin foszfatázt évtizedek óta a RhoA/ROK jelátvitel downstream célpontjának tekintik, de terápiás potenciálját ezidáig figyelmen kívül hagyták. Számos adat bizonyítja a MP ROK-tól független hatását és szabályozását, ami kiterjeszti a MP jelátvitel hatáskörét és fontosságát. Az MP különböző jelátviteli útvonalakban betöltött szerepére vonatkozó megállapításaink alapján az MP modulálása a miozin foszfatáz holoenzimre specifikus aktivátor(ok) tervezésével lehetőséget biztosíthat a tumorigenezis gátlására vagy az inzulinérzékenység fokozására, miközben a kulcsfontosságú downstream molekulák, mint a pRb, PRMT5 vagy PLK defoszforilációjának fokozása szintén új terápiás megközelítést jelenthet. A genetikai és farmakológiai eszközök kombinációja lehetővé teszi ezen összefüggések feltárását, és hozzájárulhat a defoszforilációs folyamatok által szabályozott molekuláris események teljesebb megértéséhez.

Az SMTNL1 a MP szabályozásával és attól független útvonalakon keresztül szintén szerepet játszhat az inzulinrezisztencia megelőzésében azáltal, hogy az IRS Ser foszforilációjának csökkentésével hozzájárul a progeszteronfüggő inzulinérzékenységhez. Ezért a SMTNL1 fehérjét mimikáló membránpermeábilis peptid reális terápiás eszköz lehet az endometriális hámsejtek progeszteronfüggő gátlására hiperglikémia és inzulinérzékeny endometrium esetén a terhességi

cukorbetegségben vagy más anyagcsere-rendellenességekben. Eredményeink klinikai következményei jelentősek, mivel az SMTNL1 modulálása és a pajzsmirigyhormon-szintek vagy azok downstream célpontjainak modulálása új terápiás stratégiákat kínálhat az izommal kapcsolatos betegségek kezelésében. Például az SMTNL1 expressziós szintjének módosítása az izomregeneráció során elősegítheti a szatellita sejtek differenciálódását és fúzióját, fokozva a sérült izomrostok javítását és regenerációját. Ez különösen releváns lehet az izomdisztrófiák esetében, ahol a károsodott izomregeneráció hozzájárul a progresszív izomgyengeséghez és sorvadáshoz. Hasonlóképpen, a pajzsmirigyhormon jelátvitel modulálása vagy a downstream effektorok, mint például a MYPT2 célzása, enyhítheti az izomtüneteket a hyperthyreosisban szenvedő betegeknél. A hyperthyroid izomszövetekben az MP aktivitás egyensúlyának helyreállítására irányuló farmakológiai beavatkozások javíthatják az izomerőt, az állóképességet és az érintett egyének általános életminőségét.

7. AZ ÚJ TUDOMÁNYOS EREDMÉNYEK ÖSSZEFOGLALÁSA

1. A miozin foszfatáz elősegíti a bőr normal homeosztázisának fenntartását és az epidermális sebgyógyulást. Hatását a proliferáció és migráció aktiválásával és a differenciáció gátlásával valamint a transglutamináz 1 expressziójának szabályozásával az Akt jelátviteli útvonalon keresztül fejti ki.
2. Azonosítottuk a miozin foszfatáz és a Rho A aktivált kináz új neuronális szubsztrátjait, a syntaxin, synapsin és SNAP-25 fehérjéket valamint az ezeket reguláló foszforilációs helyeket. Leírtuk, hogy a miozin foszfatáz a SNAP25 Thr138 defoszforilációjával elősegíti a neurotranszmitter kibocsátást úgy, hogy egyaránt fokozza a SNARE komplex kialakulását és annak stabilitását.
3. A miozin foszfatáz és a Rho A aktivált kináz a protein arginine metiltranszferáz 5 (PRMT5) Thr80 oldalláncának módosítása révén modulálja a hiszton fehéjék génexpresszió-gátló arginin metilációját, ami a tumorszuppresszorok gátlásához vezet. Igazoltuk a miozin foszfatáz tumorgátló szerepét, mivel azt találtuk, hogy gátló foszforilációs helyének megemelkedett foszforilációja korrelált a PRMT5 aktivitásának növekedésével és a kialakult tumorok grádusával valmint státuszával humán hepatocelluláris karcinóma modellben. Igazoltuk, hogy a MP/PRMT5/hiszton onkogén jelpálya upstream regulátora a PPM1B magnézium-ion függő protein foszfatáz, ami az MP MYPT1 szabályozó alegységét defoszforilálva gátolja a tumorigenezist.
4. Kimutattuk hogy az SMTNL egy kettős hatásmechanizmusú fehérje. Egyrészt a citoszolban a miozin foszfatáz MYPT1 alegységéhez kötődve gátolja az MP holoenzim aktivitását. Másrészt PKA/PKG foszforiláció hatására disszociál a MYPT1 alegységről és a sejtmagba transzlokálódva a progeszteron receptor transzkriciós kofaktoraként ligand-függő módon szabályozza egyes sejtmagreceptorok, kontraktilis fehérjék és anyagcsere emzimek valamint a *mypt1* gén expresszióját.
5. Jellemeztük az SMTNL1 fehérje fiziológiás hatásait és új izomadaptációs útvonalakat írtunk le. Az SMTNL1 a vázizomzat terhességhez való adaptációját is szabályozza, ami a vértöbblet és a magzat súlyának hordozására teszi képessé az anyát, azonban patológiás esetekben inzulinrezisztencia kialakulásához is vezethet.

6. Leírtuk az SMTNL1 géncsendesített KO egértörzs reproduktív fenotípusát, amelyet csökkent fertilitás és megnövekedett embrionális halálozás jellemez; illetve felismertünk egy inzulinrezisztens fenotípust, amelyet az izomadaptációs folyamatok eredményeként létrejött glikolitikus izomtípus váltás okoz.
7. Azonosítottuk az SMTNL1 által szabályozott inzulin jelátviteli pálya elemeit, és bizonyítottuk hogy az SMTNL1-nek a Ser/Thr protein kinázok és foszfatázok expressziójának módosításán keresztül inzulinérzékenyítő hatása van a vázizomban.
8. Bizonyítottuk, hogy az SMTNL1 továbbítja az aktív pajzsmirigyhormon által indukált változásokat a vázizomzatban. Az SMTNL1 overexpressziója a MP enzim gátlásán keresztül szignifikánsan lassítja a sejtek migrációját, míg miotubulusokká történő differenciációjukat -a T3 kezeléssel egyetemben- elősegíti. A MP pajzsmirigyhormon és SMTNL1 általi gátlásának köszönhetően az NKA pumpafehérje blokkolását okozzó gátló foszforiláció jelentős mértékben nő, ami hozzájárulhat a hyperthyreosis során tapasztalható izomgyengeség kialakulásához.

8. KÖSZÖNETNYILVÁNÍTÁS

Mindenekelőtt szeretnék köszönetet mondani mentoraimnak, akik pályafutásom kezdete óta a becsületes, szakmai tökéletességre és pontosságra és a tudományos eredmények reális, mértéktartó értelmezésére tanítottak. Elsőként szeretném megköszönni Dr. Erdődi Ferenc egykori PhD témavezetőm azóta is szakadatlan szakmai támogatását és barátságát, disszertációm véleményezését. Szintén köszönöm a Dr. Timothy Haystead (Duke University Cancer Research Institute) posztdoktori munkacsoportvezetőmnél töltött éveket, akinél a változatos módszertani tapasztalatok mellett gondolatébresztő beszélgetésekkel gazdagodhattam, és akivel jelenleg is eredményesen együttműködünk. Dr. William T. Gerthoffer és Dr. Cherie A. Singer (University of Nevada, Reno) segítségét is köszönöm, akiknél egy másfél évig tartó tanulmányutam alkalmával elmélyíthettem molekuláris biológiai tudásom és gyakorlati alkalmazásában is jártasságot szerezhettem. Köszönetet szeretnék mondani Dr. Gergely Pál akadémikus úrnak, aki munkámat mindig támogatta és figyelemmel kísérte pályafutásom során. Köszönöm Dr. Dombrádi Viktor egyetemi oktatóként, majd munkatársként nyújtott segítségét és tanácsaiért, és köszönöm, hogy szamai tanácsaival és észrevételeivel hozzájárult disszertációm elkészüléséhez.

Végtelenül hálás vagyok azért, hogy munkám során nagy szakértelmű együttműködő partnerekkel dolgozhattam, így Dr. Fülöp Péter (DE Belgyógyászati Intézet), Dr Győry Ferenc (DE Sebészeti Intézet), Dr Hetényi Csaba és Dr Börzsei Rita (Pécsi Orvostudományi Egyetem) segítségéért is hálás vagyok.

A jelenlegi disszertáció a PhD hallgatóim lelkiismeretes munkája nélkül nem jöhetett volna létre, ezért köszönöm Dr Sipos Adrienn, Dr. Horváth Dániel, Dr Major Evelin és Dr. Tamás István és munkáját. Köszönöm továbbá Dr Iván Judit munkacsoportomban végzett munkáját és barátságát. Kifejezetten szerencsésnek érzem magam, mert jelen munkacsoportom tagjaival való munka igazán inspiráló, így köszönöm Dr. Keller Ilka, Dr. Makai Attila, Ungvári Ádám, Kinter Richárd PhD hallgatók munkáját. Köszönettel tartozom a TDK munkájukban kiváló teljesítményt nyújtó Dr Tóth Klaudia, Dr. Tari Dóra, Kovács Szonja, Székely Mihály, Reem Khamis, Farkas Emese, Szalmás Fanni, Széles Sára és minden eddigi diplomamunkát és TDK pályamunkát végző hallgatónak.

Szeretnék köszönetet mondani az Orvosi Vegytani Intézet minden dolgozójának, hogy bármikor hozzájuk fordulhattam segítségért. Külön szeretném megköszönni Dr. Kiss Andrea, Dr.

Tar Krisztina, Dr. Jenei Attila, Dr. Kókai Endre és Dr. Bécsi Bálint baratságát és a tőlük munkám során kapott tanácsokat. Köszönöm Kelemenné Szántó Ágota, Docsa Andrea és Dr. Németh Árpádné mindennapos kísérletes munkámban való hibátlan, hatékony segítségét. Köszönöm Dr. Hegedűs Csaba műszeres kísérletekben nyújtott segítségét. Szintén köszönöm Patka Andrea, Gregus Andrea és Kovács Éva segítségét a pályázatokkal valamint a kutató- és oktatómunkával kapcsolatos adminisztratív feladatokban.

Hálás köszönettel tartozom családomnak, aki szeretetükkel végig támogattak munkám során!

Kutató munkámat az alábbi pályázatok támogatták témavezetőként: NKFIH/OTKA 143533, 125043, 104878; University of Debrecen, KutEgy2015; BMC Korea Research Fund 2012; Mecenatúra 7A1YC50007 és résztvevőként: Live Longer, EFOP-3.6.2-16-2017-00006; NKFIH/OTKA 109249, 80709, T043296; TÁMOP-4.2.2. A-11/1/KONV-2012-0025s, OTKA 80709, 2009-2013, ETT266/2006, ETT 206/2003.

9. A TÉZISEK ALAPJÁUL SZOLGÁLÓ KÖZLEMÉNYEK

1. Keller I, Ungvári Á, Major E, Horváth D, Kónya Z, Tóth E, Erdődi F, Kiss A, **Lontay B.** *Magnesium-dependent-Protein Phosphatase 1B Regulates the Protein Arginine Methyltransferase 5 Through the Modulation of Myosin Phosphatase.* J Biol Chem. 2024 Dec 18:108107. doi: 10.1016/j.jbc.2024.108107. (D1 IF=4,1)

2. Keller, I., Ungvári, Á., Kinter, R., Szalmás, F., Kókai, E., **Lontay, B**. *Smoothelin-like protein 1 promotes insulin sensitivity and modulates the contractile properties of endometrial epithelial cells with insulin resistance.* Front Endocrinol (Lausanne). 2024 May 31;15:1375771. doi: 10.3389/fendo.2024.1375771. eCollection 2024. (Q1 IF=5,7)

3. Tamas I, Major E, Horvath D, Keller I, Ungvari A, Haystead TA, MacDonald JA, **Lontay B.** *Mechanisms by which smoothelin-like protein 1 reverses insulin resistance in myotubules and mice.* Mol Cell Endocrinol. 2022 Jul 1;551:111663. doi: 10.1016/j.mce.2022.111663. (Q2 IF=4,1)

4. Major E, Győry F, Horváth D, Keller I, Tamás I, Uray K, Fülöp P, **Lontay B.** Smoothelin-Like Protein 1 *Regulates Development and Metabolic Transformation of Skeletal Muscle in Hyperthyroidism.* Front Endocrinol (Lausanne). 2021 Oct 5;12:751488. doi: 10.3389/fendo.2021.751488. (D1 IF=6,055)

5. Major E, Keller I, Horváth D, Tamás I, Erdődi F, **Lontay B**. *Smoothelin-Like Protein 1 Regulates the Thyroid Hormone-Induced Homeostasis and Remodeling of C2C12 Cells via the Modulation of Myosin Phosphatase.* Int J Mol Sci. 2021 Sep 24;22(19):10293. doi: 10.3390/ijms221910293. (D1 IF=6,208)

6. Horváth D, Sipos A, Major E, Kónya Z, Bátori R, Dedinszki D, Szöllosi A, TamásI, Iván J, Kiss A, Erdodi F, **Lontay B**. *Myosin phosphatase accelerates cutaneous wound healing by regulating migration and differentiation of epidermal keratinocytes via Akt signaling pathway in human and murine skin.* Biochim Biophys Acta Mol Basis Dis. 2018 Oct;1864(10):3268-3280. doi: 10.1016/j.bbadis.2018.07.013. (Q1 IF=4,328)

7. Kiss A, Erdődi F, **Lontay B.** *Myosin phosphatase: Unexpected functions of a long-known enzyme.* Biochim Biophys Acta Mol Cell Res. 2019 Jan;1866(1):2-15. doi: 10.1016/j.bbamcr.2018.07.023. Epub 2018 Aug 2. doi: 10.1016/j.bbamcr.2018.07.023 (D1 IF=4,,05)

8. Sipos A, Iván J, Bécsi B, Darula Z, Tamás I, Horváth D, Medzihradszky KF, Erdődi F, **Lontay B**. *Myosin phosphatase and RhoA-activated kinase modulate arginine methylation by the regulation of protein arginine methyltransferase 5 in hepatocellular carcinoma cells*. Sci Rep. 2017 Jan 11;7:40590. doi: 10.1038/srep40590. (D1 IF=4,122)

9. Horváth D, Tamás I, Sipos A, Darula Z, Bécsi B, Nagy D, Iván J, Erdődi F, **Lontay B** *Myosin Phosphatase and RhoA-activated Kinase Modulate Neurotransmitter Release by Regulating SNAP-25 of SNARE Complex* PLoS One. 2017 May 9;12(5):e0177046. doi: 10.1371/journal.pone.0177046. eCollection 2017. (D1 IF=2,766)

10. **Lontay B**, Bodoor K, Sipos A, Weitzel DH, Loiselle D, Safi R, Zheng D, Devente J, Hickner RC, McDonnell DP, Ribar T, Haystead TA. *Pregnancy and Smoothelin-like Protein 1 (SMTNL1) Deletion Promote the Switching of Skeletal Muscle to a Glycolytic Phenotype in Human and Mice.* J Biol Chem. 2015 Jul 17;290(29):17985-98. doi: 10.1074/jbc.M115.658120. (D1 IF=4,258)

11. **Lontay B**, *Bodoor K, Safi R, Weitzel D, Loiselle D, Wei Z, Lengyel Sz, McDonnell DP, Haystead TA *Smoothelin-Like 1 Protein is a Bifunctional Regulator of the Progesterone Receptor During Pregnancy* J Biol Chem. 285(38):29357-66., 2015 (D1 IF=4,773)

12. Dedinszki D, Sipos A, Kiss A, Bátori R, Kónya Z, Virág L, Erdődi F, **Lontay B** *Protein phosphatase-1 is involved in the maintenance of normal homeostasis and in UVA irradiation-induced pathological alterations in HaCaT cells and in mouse skin.* Biochim Biophys Acta. 2015 Jan;1852(1):22-33. doi: 10.1016/j.bbadis.2014.11.005. (D1 IF=5,158)

13. **Lontay B**, Pál B, Serfőző Z, Kőszeghy A, Szücs G, Rusznák Z, Erdődi F. *Protein phosphatase-1M and Rho-kinase affect exocytosis from cortical synaptosomes and influence neurotransmission at a glutamatergic giant synapse of the rat auditory system.* J Neurochem. 2012 Jul 20. doi: 10.1111/j.1471-4159.2012.07882.x. (Q1 IF=3,973)

* Megosztott első szerzős közlemény

A disszertációban felhasznált saját kötlemények összesített impakt faktora: 59,491.

10. FÜGGELÉK

Táblázat S1. Az siMYPT1 HepG2 sejtekben legalább 1,5-szeres génexpressziós változást mutató gének.

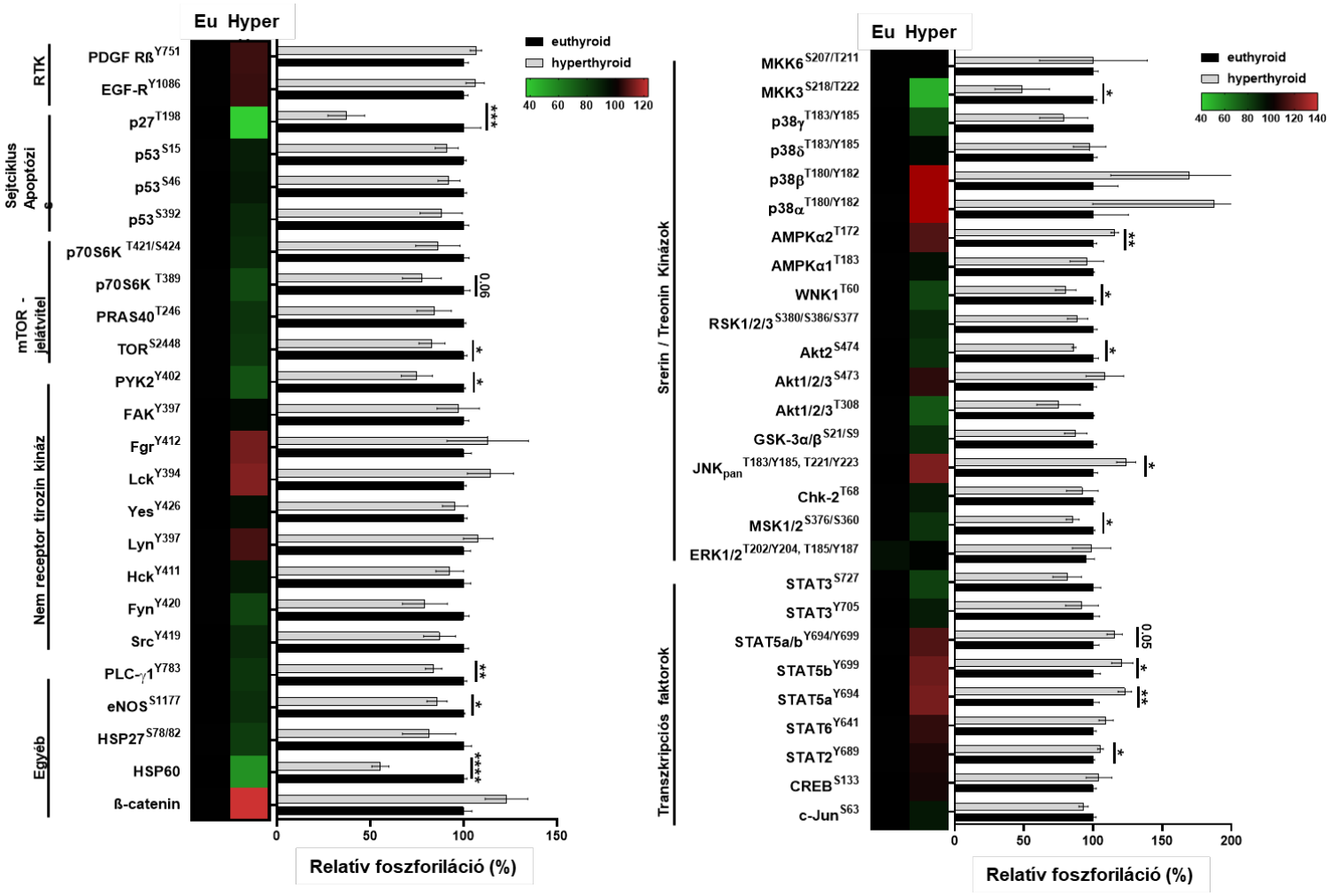
Gén jele	Gén neve	Szabályozás	Változás
PPP1R12A	protein phosphatase 1, regulatory (inhibitor) subunit 12A	down	2.0050275
EPHA2	EPH receptor A2	up	1.5645913
SLC2A1	solute carrier family 2 (facilitated glucose transporter), member 1	up	1.6917205
TGFBR3	transforming growth factor, beta receptor III	up	1.5754458
TMCO1	transmembrane and coiled-coil domains 1	down	1.9577281
KLF6	Kruppel-like factor 6	up	1.6079206
ANKRD1	ankyrin repeat domain 1 (cardiac muscle)	up	2.1838295
HEPACAM|HEPN1	hepatocyte cell adhesion molecule | HEPACAM opposite strand 1	down	1.6288424
OAS1	2',5'-oligoadenylate synthetase 1, 40/46kDa	up	1.6448771
SLC2A1	solute carrier family 2 (facilitated glucose transporter), member 1	up	1.6917205
TGFBR3	transforming growth factor, beta receptor III	up	1.5754458
TMCO1	transmembrane and coiled-coil domains 1	down	1.9577281
KLF6	Kruppel-like factor 6	up	1.6079206
ANKRD1	ankyrin repeat domain 1 (cardiac muscle)	up	2.1838295
HEPACAM|HEPN1	hepatocyte cell adhesion molecule | HEPACAM opposite strand 1	down	1.6288424
OAS1	2',5'-oligoadenylate synthetase 1, 40/46kDa	up	1.6448771
DUSP6	dual specificity phosphatase 6	up	1.5159508
LPAR6	lysophosphatidic acid receptor 6	up	1.5162095
IRF9	interferon regulatory factor 9	up	1.6238389
IFI27	interferon, alpha-inducible protein 27	up	1.6448994
KIAA1199	azonosítatlan fehérje	up	2.1050441

SNORD68|RPL13	small nucleolar RNA, C/D box 68 | ribosomal protein L13	up	1.7279054
MIR21	microRNA 21	up	1.9698615
KRT23	keratin 23 (histone deacetylase inducible)	up	1.5333802
SLC16A6	solute carrier family 16, member 6 (monocarboxylic acid transporter 7)	up	2.1183825
DTNA	dystrobrevin, alpha	up	1.6605202
ICAM1	intercellular adhesion molecule 1	up	1.5522647
GDF15	growth differentiation factor 15	up	1.6862459
MFSD2B	major facilitator superfamily domain containing 2B	down	1.519762
SNX17	sorting nexin 17	down	1.6879824
FETUB	fetuin B	down	1.7819421
KNG1	kininogen 1	down	1.505488
FILIP1L	filamin A interacting protein 1-like	up	1.5426576
SLC7A11	solute carrier family 7, (cationic amino acid transporter, y+ system) member 11	up	1.6259567
ITGA2	integrin, alpha 2 (CD49B, alpha 2 subunit of VLA-2 receptor)	up	1.794632
EGR1	early growth response 1	up	1.6131204
SPRY4	sprouty homolog 4 (Drosophila)	up	1.6954104
GMDS	GDP-mannose 4,6-dehydratase	up	1.5297856
IER3	immediate early response 3	up	2.0160716
SERPINE1	serpin peptidase inhibitor, clade E (nexin, plasminogen activator inhibitor type 1), member 1	up	1.6623654
C8orf4	chromosome 8 open reading frame 4	up	1.5722965

Táblázat S2. ***Az SMTNL1 WT és KO vemhes és nem vemhes egerek vázizom mintáinak MALDI TOF-TOF szekvenciaadatai.*** *A táblázatban csak a többszörös peptidazonosítást (>5) adó fehérjék adatai szerepelnek.*

ENZYME	accession	WTP	KO	KOP	function
malate dehydrogenase (cytosolic)	gi|387129	5	6	3,5	Asp/malate shuttle
aspartate aminotransferase	gi|871422	1	3	2,5	aspartate/malate shuttle
Creatinine kinase	gi|38259206	3	1	2,7	ATP salvage
heat shock protein 1, beta	gi|40556608	4,3	6,6	7,2	chaperone
myomesin 1 isoform 2	gi|145279198	5,5	6,6	6,1	contractile
myosin A1 catalytic light chain fast	gi|91114	3,1	4,5	8,9	contractile
Filamin C	gi|94378467	2,3	5,2	3,2	contractile
myomesin 2	gi|6678996	3,1	6,6	5,8	contractile
novel protein similar to dynein	gi|58864904	1,5	3,4	2,6	contractile
alpha actin 1	gi|4501881	1	3,1	2,5	contractile
myosin A2 catalytic light chain fast	gi|91115	6	5,5	8,2	contractile
Tropomyosin 1 alpha	gi|109081387	2	3,3	2,9	contractile
tropomyosin 2, beta	gi|11875203	2,1	3,1	2,8	contractile
Troponin T fast twitch	gi|2340050	1	3	1	contractile
troponin I, skeletal, fast 2	gi|6678391	2,5	9,2	8,1	contractile
fast skeletal muscle troponin C	gi|6678371	1	3,3	4,1	contractile
calmodulin 2	gi|4502549	1	2,2	2,9	contractile
myosin heavy chain 2B fast	gi|67189167	3,2	4,2	5,1	contractile
calsequestrin 1	gi|112181167	3,1	3	2,9	contractile
Myosin-binding protein C, fast-type	gi|81910387	1,5	9,3	11,3	contractile
TER ATPase	gi|94408011	1,4	3	3,9	endoplasmic reticulum
5-oxoprolinase	gi|23346557	1	1,9	1	gluthione synthesis
glycogen phosphorylase	gi|6755256	8,1	10,6	6,9	glycogen degradation
amylo-1,6-glucosidase	gi|82890909	9,2	1,4	11,2	glycogen degradation
glucose 6 phosphate dehydrogenase	gi|51114	4	1,1	3,5	glycolysis
aldolase	gi|7548322	2	1	5	glycolysis
GAPDH	gi|94396587	4	2,3	4,2	glycolysis
Phosphoglucomutase	gi|33416468	1	5,5	4,6	glycolysis
glyoxylase	gi|21362640	3	3,2	3,1	glycolysis
6-phosphofructokinase	gi|13638207	4,9	2,1	8,9	glycolysis
hexokinase 2	gi|7305143	3,6	8,8	8,1	glycolysis
Transferrin	gi|17046471	2	3,1	2,5	iron transport
isocitrate dehydrogenase	gi|18250284	1	1	2,3	Krebs cycle
oxoglutarate dehydrogenase	gi|56206141	2,2	5,1	4,9	Krebs cycle
mitochondrial ATP synthase beta	gi|89574015	6,9	4,1	4,3	oxidative phosphorylation
ubiquitin-activating enzyme E1	gi|6678483	2,5	3,3	3	protein degradation
elongation factor 1 alpha 2	gi|6681273	1,25	9,6	9,2	protein synthesis

1.S ábra Humán euthyreosisos és hyperthyreosisos vázizom biopsziák foszforilációs mintázatának vizsgálata. *A minták homogenizálását követően számos fehérje relatív foszforilációs szintjének egyidejű, gyors és érzékeny meghatározását végeztük el a human foszfo-kináz (bal panel) és foszfo-MAPK array segítségével (jobb panel) Az n=3 kísérletből származó eredményeket átlag ± SEM formában ábrázoltuk. A csoportokat kétmintás párosítatlan t-próbával hasonlítottuk össze, a részletes grafikon a függelékben található (1S ábra), ahol p <0,05 (*), p <0,01 (**), p <0,001 (***) . RTK: Receptor Tirozin Kináz; Eu: euthyroid; Hyper: hyperthyroid*



11. IRODALOMJEGYZÉK

[1] D. Horvath, A. Sipos, E. Major, Z. Konya, R. Batori, D. Dedinszki, A. Szoll Si, I. Tamas, J. Ivan, A. Kiss, F. Erd di, and B. Lontay, Myosin phosphatase accelerates cutaneous wound healing by regulating migration and differentiation of epidermal keratinocytes via Akt signaling pathway in human and murine skin. Biochim Biophys Acta Mol Basis Dis 1864 (2018) 3268-3280.

[2] A. Kiss, F. Erdodi, and B. Lontay, Myosin phosphatase: Unexpected functions of a long-known enzyme. Biochim Biophys Acta Mol Cell Res 1866 (2019) 2-15.

[3] E. Major, F. Gyory, D. Horvath, I. Keller, I. Tamas, K. Uray, P. Fulop, and B. Lontay, Smoothelin-Like Protein 1 Regulates Development and Metabolic Transformation of Skeletal Muscle in Hyperthyroidism. Front Endocrinol (Lausanne) 12 (2021) 751488.

[4] I. Tamas, E. Major, D. Horvath, I. Keller, A. Ungvari, T.A. Haystead, J.A. MacDonald, and B. Lontay, Mechanisms by which smoothelin-like protein 1 reverses insulin resistance in myotubules and mice. Mol Cell Endocrinol 551 (2022) 111663.

[5] K. Biemann, Appendix 5. Nomenclature for peptide fragment ions (positive ions). Methods Enzymol 193 (1990) 886-7.

[6] H. Witt, F. Savic, S. Verbeek, J. Dietz, G. Tarantola, M. Oelkers, B. Geil, and A. Janshoff, Membrane fusion studied by colloidal probes. Eur Biophys J 50 (2021) 223-237.

[7] M. Terrak, F. Kerff, K. Langsetmo, T. Tao, and R. Dominguez, Structural basis of protein phosphatase 1 regulation. Nature 429 (2004) 780-4.

[8] M. Kokkinidis, N.M. Glykos, and V.E. Fadouloglou, Catalytic activity regulation through post-translational modification: the expanding universe of protein diversity. Adv Protein Chem Struct Biol 122 (2020) 97-125.

[9] S.I. van Kasteren, H.B. Kramer, H.H. Jensen, S.J. Campbell, J. Kirkpatrick, N.J. Oldham, D.C. Anthony, and B.G. Davis, Expanding the diversity of chemical protein modification allows post-translational mimicry. Nature 446 (2007) 1105-9.

[10] S. Ramazi, A. Allahverdi, and J. Zahiri, Evaluation of post-translational modifications in histone proteins: A review on histone modification defects in developmental and neurological disorders. J Biosci 45 (2020).

[11] D.G. Knorre, N.V. Kudryashova, and T.S. Godovikova, Chemical and functional aspects of posttranslational modification of proteins. Acta Naturae 1 (2009) 29-51.

[12] S. Wera, and B.A. Hemmings, Serine/threonine protein phosphatases. Biochem J 311 (Pt 1) (1995) 17-29.

[13] C.T. Walsh, S. Garneau-Tsodikova, and G.J. Gatto, Jr., Protein posttranslational modifications: the chemistry of proteome diversifications. Angew Chem Int Ed Engl 44 (2005) 7342-72.

[14] X. Cheng, K. Wang, Y. Zhao, and K. Wang, Research progress on post-translational modification of proteins and cardiovascular diseases. Cell Death Discov 9 (2023) 275.

[15] S. Pan, and R. Chen, Pathological implication of protein post-translational modifications in cancer. Mol Aspects Med 86 (2022) 101097.

[16] B. Lontay, A. Kiss, L. Virag, and K. Tar, How Do Post-Translational Modifications Influence the Pathomechanistic Landscape of Huntington's Disease? A Comprehensive Review. Int J Mol Sci 21 (2020).

[17] B. Chatterjee, and S.S. Thakur, Investigation of post-translational modifications in type 2 diabetes. Clin Proteomics 15 (2018) 32.

[18] D.L. Brautigan, Protein Ser/Thr phosphatases--the ugly ducklings of cell signalling. FEBS J 280 (2013) 324-45.

[19] V. Dombradi, J.M. Axton, N.D. Brewis, E.F. da Cruz e Silva, L. Alphey, and P.T. Cohen, Drosophila contains three genes that encode distinct isoforms of protein phosphatase 1. Eur J Biochem 194 (1990) 739-45.
[20] T.S. Ingebritsen, and P. Cohen, Protein phosphatases: properties and role in cellular regulation. Science 221 (1983) 331-8.
[21] I.M. Mansuy, and S. Shenolikar, Protein serine/threonine phosphatases in neuronal plasticity and disorders of learning and memory. Trends Neurosci 29 (2006) 679-86.
[22] T. Mustelin, T. Vang, and N. Bottini, Protein tyrosine phosphatases and the immune response. Nat Rev Immunol 5 (2005) 43-57.
[23] E. Pennisi, Human genome project. Genome institute wrestles mightily with its future. Science 298 (2002) 1694-5.
[24] M. Bollen, W. Peti, M.J. Ragusa, and M. Beullens, The extended PP1 toolkit: designed to create specificity. Trends Biochem Sci 35 (2010) 450-8.
[25] P.T. Cohen, N.D. Brewis, V. Hughes, and D.J. Mann, Protein serine/threonine phosphatases; an expanding family. FEBS Lett 268 (1990) 355-9.
[26] P.T. Cohen, Protein phosphatase 1--targeted in many directions. J Cell Sci 115 (2002) 241-56.
[27] T.S. Ingebritsen, and P. Cohen, The protein phosphatases involved in cellular regulation. 1. Classification and substrate specificities. Eur J Biochem 132 (1983) 255-61.
[28] C. Bialojan, and A. Takai, Inhibitory effect of a marine-sponge toxin, okadaic acid, on protein phosphatases. Specificity and kinetics. Biochem J 256 (1988) 283-90.
[29] P. Cohen, S. Klumpp, and D.L. Schelling, An improved procedure for identifying and quantitating protein phosphatases in mammalian tissues. FEBS Lett 250 (1989) 596-600.
[30] O.B. da Cruz e Silva, E.F. da Cruz e Silva, and P.T. Cohen, Identification of a novel protein phosphatase catalytic subunit by cDNA cloning. FEBS Lett 242 (1988) 106-10.
[31] W. Becker, H. Kentrup, S. Klumpp, J.E. Schultz, and H.G. Joost, Molecular cloning of a protein serine/threonine phosphatase containing a putative regulatory tetratricopeptide repeat domain. J Biol Chem 269 (1994) 22586-92.
[32] A.V. Andreeva, D.E. Evans, C.R. Hawes, N. Bennett, and M.A. Kutuzov, PP7, a plant phosphatase representing a novel evolutionary branch of eukaryotic protein Ser/Thr phosphatases. Biochem Mol Biol Int 44 (1998) 703-15.
[33] A.V. Andreeva, and M.A. Kutuzov, Non-classical protein Ser/Thr phosphatases: what are they for? Biochemistry (Mosc) 64 (1999) 228-87.
[34] G.J. Barton, P.T. Cohen, and D. Barford, Conservation analysis and structure prediction of the protein serine/threonine phosphatases. Sequence similarity with diadenosine tetraphosphatase from Escherichia coli suggests homology to the protein phosphatases. Eur J Biochem 220 (1994) 225-37.
[35] P.T. Cohen, Novel protein serine/threonine phosphatases: variety is the spice of life. Trends in biochemical sciences 22 (1997) 245-51.
[36] X.C. Zhang, A. Piccini, M.P. Myers, L. Van Aelst, and N.K. Tonks, Functional analysis of the protein phosphatase activity of PTEN. Biochem J 444 (2012) 457-64.
[37] S. Tamura, K.R. Lynch, J. Larner, J. Fox, A. Yasui, K. Kikuchi, Y. Suzuki, and S. Tsuiki, Molecular cloning of rat type 2C (IA) protein phosphatase mRNA. Proc Natl Acad Sci U S A 86 (1989) 1796-800.
[38] R. Kamada, F. Kudoh, S. Ito, I. Tani, J.I.B. Janairo, J.G. Omichinski, and K. Sakaguchi, Metal-dependent Ser/Thr protein phosphatase PPM family: Evolution, structures, diseases and inhibitors. Pharmacol Ther 215 (2020) 107622.
[39] N. Aburai, M. Yoshida, M. Ohnishi, and K. Kimura, Sanguinarine as a potent and specific inhibitor of protein phosphatase 2C in vitro and induces apoptosis via phosphorylation of p38 in HL60 cells. Biosci Biotechnol Biochem 74 (2010) 548-52.

[40] H. Ceulemans, and M. Bollen, Functional diversity of protein phosphatase-1, a cellular economizer and reset button. Physiol Rev 84 (2004) 1-39.
[41] V. Dombradi, J. Krieglstein, and S. Klumpp, Regulating the regulators. Conference on protein phosphorylation and protein phosphatases. EMBO Rep 3 (2002) 120-4.
[42] K. Sasaki, H. Shima, Y. Kitagawa, S. Irino, T. Sugimura, and M. Nagao, Identification of members of the protein phosphatase 1 gene family in the rat and enhanced expression of protein phosphatase 1 alpha gene in rat hepatocellular carcinomas. Jpn J Cancer Res 81 (1990) 1272-80.
[43] P.T. Cohen, Two isoforms of protein phosphatase 1 may be produced from the same gene. FEBS Lett 232 (1988) 17-23.
[44] T. Durfee, K. Becherer, P.L. Chen, S.H. Yeh, Y. Yang, A.E. Kilburn, W.H. Lee, and S.J. Elledge, The retinoblastoma protein associates with the protein phosphatase type 1 catalytic subunit. Genes Dev 7 (1993) 555-69.
[45] Y.S. Chun, H. Shima, K. Nagasaki, T. Sugimura, and M. Nagao, PP1 gamma 2, a testis-specific protein-serine/threonine-phosphatase type 1 catalytic subunit, is associated with a protein having high sequence homology with the 78-kDa glucose-regulated protein, a member of the 70-kDa heat shock protein family. Proc Natl Acad Sci U S A 91 (1994) 3319-23.
[46] M.P. Egloff, P.T. Cohen, P. Reinemer, and D. Barford, Crystal structure of the catalytic subunit of human protein phosphatase 1 and its complex with tungstate. J Mol Biol 254 (1995) 942-59.
[47] J. Goldberg, H.B. Huang, Y.G. Kwon, P. Greengard, A.C. Nairn, and J. Kuriyan, Three-dimensional structure of the catalytic subunit of protein serine/threonine phosphatase-1. Nature 376 (1995) 745-53.
[48] M.P. Egloff, D.F. Johnson, G. Moorhead, P.T. Cohen, P. Cohen, and D. Barford, Structural basis for the recognition of regulatory subunits by the catalytic subunit of protein phosphatase 1. EMBO J 16 (1997) 1876-87.
[49] M. Campos, P. Fadden, G. Alms, Z. Qian, and T.A. Haystead, Identification of protein phosphatase-1-binding proteins by microcystin-biotin affinity chromatography. J Biol Chem 271 (1996) 28478-84.
[50] S. Shibata, Y. Ishida, H. Kitano, Y. Ohizumi, J. Habon, Y. Tsukitani, and H. Kikuchi, Contractile effects of okadaic acid, a novel ionophore-like substance from black sponge, on isolated smooth muscles under the condition of Ca deficiency. J Pharmacol Exp Ther 223 (1982) 135-43.
[51] X.C. Cheng, T. Kihara, H. Kusakabe, J. Magae, Y. Kobayashi, R.P. Fang, Z.F. Ni, Y.C. Shen, K. Ko, I. Yamaguchi, and et al., A new antibiotic, tautomycin. J Antibiot (Tokyo) 40 (1987) 907-9.
[52] Z.R. Woydziak, A.J. Yucel, and A.R. Chamberlin, Tautomycetin Synthetic Analogues: Selective Inhibitors of Protein Phosphatase I. ChemMedChem 16 (2021) 839-850.
[53] T. Kurisaki, R.G. Taylor, and D.J. Hartshorne, Effects of the protein phosphatase inhibitors, tautomycin and calyculin-A, on protein phosphorylation and cytoskeleton of human platelets. Cell Struct Funct 20 (1995) 331-43.
[54] G.E. Groblewski, A.C. Wagner, and J.A. Williams, Cyclosporin A inhibits Ca2+/calmodulin-dependent protein phosphatase and secretion in pancreatic acinar cells. J Biol Chem 269 (1994) 15111-7.
[55] M. Guo, Z. Li, M. Gu, J. Gu, Q. You, and L. Wang, Targeting phosphatases: From molecule design to clinical trials. Eur J Med Chem 264 (2024) 116031.
[56] D. Dedinszki, A. Kiss, L. Markasz, A. Marton, E. Toth, L. Szekely, and F. Erdodi, Inhibition of protein phosphatase-1 and -2A decreases the chemosensitivity of leukemic cells to chemotherapeutic drugs. Cell Signal 27 (2015) 363-72.
[57] W. Peti, A.C. Nairn, and R. Page, Structural basis for protein phosphatase 1 regulation and specificity. FEBS J 280 (2013) 596-611.
[58] Q.R. Liu, P.W. Zhang, Q. Zhen, D. Walther, X.B. Wang, and G.R. Uhl, KEPI, a PKC-dependent protein phosphatase 1 inhibitor regulated by morphine. J Biol Chem 277 (2002) 13312-20.

[59] M.S. Kelker, R. Page, and W. Peti, Crystal structures of protein phosphatase-1 bound to nodularin-R and tautomycin: a novel scaffold for structure-based drug design of serine/threonine phosphatase inhibitors. J Mol Biol 385 (2009) 11-21.
[60] B. Dancheck, M.J. Ragusa, M. Allaire, A.C. Nairn, R. Page, and W. Peti, Molecular investigations of the structure and function of the protein phosphatase 1-spinophilin-inhibitor 2 heterotrimeric complex. Biochemistry 50 (2011) 1238-46.
[61] J.A. Marsh, B. Dancheck, M.J. Ragusa, M. Allaire, J.D. Forman-Kay, and W. Peti, Structural diversity in free and bound states of intrinsically disordered protein phosphatase 1 regulators. Structure 18 (2010) 1094-103.
[62] A. Hendrickx, M. Beullens, H. Ceulemans, T. Den Abt, A. Van Eynde, E. Nicolaescu, B. Lesage, and M. Bollen, Docking motif-guided mapping of the interactome of protein phosphatase-1. Chem Biol 16 (2009) 365-71.
[63] M.J. Hubbard, and P. Cohen, Regulation of protein phosphatase-1G from rabbit skeletal muscle. 2. Catalytic subunit translocation is a mechanism for reversible inhibition of activity toward glycogen-bound substrates. Eur J Biochem 186 (1989) 711-6.
[64] M. Ferreira, M. Beullens, M. Bollen, and A. Van Eynde, Functions and therapeutic potential of protein phosphatase 1: Insights from mouse genetics. Biochim Biophys Acta Mol Cell Res 1866 (2019) 16-30.
[65] D.J. Hartshorne, M. Ito, and F. Erdodi, Myosin light chain phosphatase: subunit composition, interactions and regulation. J Muscle Res Cell Motil 19 (1998) 325-41.
[66] D. Alessi, L.K. MacDougall, M.M. Sola, M. Ikebe, and P. Cohen, The control of protein phosphatase-1 by targetting subunits. The major myosin phosphatase in avian smooth muscle is a novel form of protein phosphatase-1. Eur J Biochem 210 (1992) 1023-35.
[67] A. Shirazi, K. Iizuka, P. Fadden, C. Mosse, A.P. Somlyo, A.V. Somlyo, and T.A. Haystead, Purification and characterization of the mammalian myosin light chain phosphatase holoenzyme. The differential effects of the holoenzyme and its subunits on smooth muscle. J Biol Chem 269 (1994) 31598-606.
[68] Y.H. Chen, M.X. Chen, D.R. Alessi, D.G. Campbell, C. Shanahan, P. Cohen, and P.T. Cohen, Molecular cloning of cDNA encoding the 110 kDa and 21 kDa regulatory subunits of smooth muscle protein phosphatase 1M. FEBS Lett 356 (1994) 51-5.
[69] E. Scotto-Lavino, M. Garcia-Diaz, G. Du, and M.A. Frohman, Basis for the isoform-specific interaction of myosin phosphatase subunits protein phosphatase 1c beta and myosin phosphatase targeting subunit 1. J Biol Chem 285 (2010) 6419-24.
[70] D. Shichi, T. Arimura, T. Ishikawa, and A. Kimura, Heart-specific small subunit of myosin light chain phosphatase activates rho-associated kinase and regulates phosphorylation of myosin phosphatase target subunit 1. J Biol Chem 285 (2010) 33680-90.
[71] M.E. Grassie, L.D. Moffat, M.P. Walsh, and J.A. MacDonald, The myosin phosphatase targeting protein (MYPT) family: a regulated mechanism for achieving substrate specificity of the catalytic subunit of protein phosphatase type 1delta. Arch Biochem Biophys 510 (2011) 147-59.
[72] A. Toth, E. Kiss, F.W. Herberg, P. Gergely, D.J. Hartshorne, and F. Erdodi, Study of the subunit interactions in myosin phosphatase by surface plasmon resonance. Eur J Biochem 267 (2000) 1687-97.
[73] X. Hu, Z. Li, Y. Ding, Q. Geng, Z. Xiahou, H. Ru, M.Q. Dong, X. Xu, and J. Li, Chk1 modulates the interaction between myosin phosphatase targeting protein 1 (MYPT1) and protein phosphatase 1cbeta (PP1cbeta). Cell Cycle 17 (2018) 421-427.
[74] D. Johnson, P. Cohen, M.X. Chen, Y.H. Chen, and P.T. Cohen, Identification of the regions on the M110 subunit of protein phosphatase 1M that interact with the M21 subunit and with myosin. Eur J Biochem 244 (1997) 931-9.

[75] Y. Fukata, K. Kimura, N. Oshiro, H. Saya, Y. Matsuura, and K. Kaibuchi, Association of the myosin-binding subunit of myosin phosphatase and moesin: dual regulation of moesin phosphorylation by Rho-associated kinase and myosin phosphatase. J Cell Biol 141 (1998) 409-18.
[76] K.M. Kim, C. Csortos, I. Czikora, D. Fulton, N.S. Umapathy, G. Olah, and A.D. Verin, Molecular characterization of myosin phosphatase in endothelium. J Cell Physiol 227 (2012) 1701-8.
[77] M. Amano, T. Kaneko, A. Maeda, M. Nakayama, M. Ito, T. Yamauchi, H. Goto, Y. Fukata, N. Oshiro, A. Shinohara, A. Iwamatsu, and K. Kaibuchi, Identification of Tau and MAP2 as novel substrates of Rho-kinase and myosin phosphatase. J Neurochem 87 (2003) 780-90.
[78] C. Gil, A. Falques, E. Sarro, R. Cubi, J. Blasi, J. Aguilera, and E. Itarte, Protein kinase CK2 associates to lipid rafts and its pharmacological inhibition enhances neurotransmitter release. FEBS Lett 585 (2011) 414-20.
[79] A.P. Somlyo, and A.V. Somlyo, Ca2+ sensitivity of smooth muscle and nonmuscle myosin II: modulated by G proteins, kinases, and myosin phosphatase. Physiol Rev 83 (2003) 1325-58.
[80] R. Batori, B. Becsi, D. Nagy, Z. Konya, C. Hegedus, Z. Bordan, A. Verin, B. Lontay, and F. Erdodi, Interplay of myosin phosphatase and protein phosphatase-2A in the regulation of endothelial nitric-oxide synthase phosphorylation and nitric oxide production. Sci Rep 7 (2017) 44698.
[81] V. Kolupaeva, and V. Janssens, PP1 and PP2A phosphatases--cooperating partners in modulating retinoblastoma protein activation. FEBS J 280 (2013) 627-43.
[82] A. Kiss, B. Lontay, B. Becsi, L. Markasz, E. Olah, P. Gergely, and F. Erdodi, Myosin phosphatase interacts with and dephosphorylates the retinoblastoma protein in THP-1 leukemic cells: its inhibition is involved in the attenuation of daunorubicin-induced cell death by calyculin-A. Cell Signal 20 (2008) 2059-70.
[83] H.S. Cho, T. Suzuki, N. Dohmae, S. Hayami, M. Unoki, M. Yoshimatsu, G. Toyokawa, M. Takawa, T. Chen, J.K. Kurash, H.I. Field, B.A. Ponder, Y. Nakamura, and R. Hamamoto, Demethylation of RB regulator MYPT1 by histone demethylase LSD1 promotes cell cycle progression in cancer cells. Cancer Res 71 (2011) 655-60.
[84] G. Totsukawa, Y. Yamakita, S. Yamashiro, H. Hosoya, D.J. Hartshorne, and F. Matsumura, Activation of myosin phosphatase targeting subunit by mitosis-specific phosphorylation. J Cell Biol 144 (1999) 735-44.
[85] T. Chiyoda, N. Sugiyama, T. Shimizu, H. Naoe, Y. Kobayashi, J. Ishizawa, Y. Arima, H. Tsuda, M. Ito, K. Kaibuchi, D. Aoki, Y. Ishihama, H. Saya, and S. Kuninaka, LATS1/WARTS phosphorylates MYPT1 to counteract PLK1 and regulate mammalian mitotic progression. J Cell Biol 197 (2012) 625-41.
[86] H. Jin, T. Sperka, P. Herrlich, and H. Morrison, Tumorigenic transformation by CPI-17 through inhibition of a merlin phosphatase. Nature 442 (2006) 576-9.
[87] W. Li, J. Cooper, L. Zhou, C. Yang, H. Erdjument-Bromage, D. Zagzag, M. Snuderl, M. Ladanyi, C.O. Hanemann, P. Zhou, M.A. Karajannis, and F.G. Giancotti, Merlin/NF2 loss-driven tumorigenesis linked to CRL4(DCAF1)-mediated inhibition of the hippo pathway kinases Lats1 and 2 in the nucleus. Cancer Cell 26 (2014) 48-60.
[88] T. Matsuda, P. Zhai, S. Sciarretta, Y. Zhang, J.I. Jeong, S. Ikeda, J. Park, C.P. Hsu, B. Tian, D. Pan, J. Sadoshima, and D.P. Del Re, NF2 Activates Hippo Signaling and Promotes Ischemia/Reperfusion Injury in the Heart. Circ Res 119 (2016) 596-606.
[89] D.J. Hartshorne, M. Ito, and F. Erdodi, Role of protein phosphatase type 1 in contractile functions: myosin phosphatase. J Biol Chem 279 (2004) 37211-4.
[90] C.G. Broustas, N. Grammatikakis, M. Eto, P. Dent, D.L. Brautigan, and U. Kasid, Phosphorylation of the myosin-binding subunit of myosin phosphatase by Raf-1 and inhibition of phosphatase activity. J Biol Chem 277 (2002) 3053-9.
[91] S. Mori, R. Iwaoka, M. Eto, and S.Y. Ohki, Solution structure of the inhibitory phosphorylation domain of myosin phosphatase targeting subunit 1. Proteins 77 (2009) 732-5.

[92] A.A. Wooldridge, J.A. MacDonald, F. Erdodi, C. Ma, M.A. Borman, D.J. Hartshorne, and T.A. Haystead, Smooth muscle phosphatase is regulated in vivo by exclusion of phosphorylation of threonine 696 of MYPT1 by phosphorylation of Serine 695 in response to cyclic nucleotides. J Biol Chem 279 (2004) 34496-504.
[93] B. Kolozsvari, E. Bako, B. Becsi, A. Kiss, A. Czikora, A. Toth, G. Vamosi, P. Gergely, and F. Erdodi, Calcineurin regulates endothelial barrier function by interaction with and dephosphorylation of myosin phosphatase. Cardiovasc Res 96 (2012) 494-503.
[94] T.P. Woodsome, M. Eto, A. Everett, D.L. Brautigan, and T. Kitazawa, Expression of CPI-17 and myosin phosphatase correlates with Ca(2+) sensitivity of protein kinase C-induced contraction in rabbit smooth muscle. J Physiol 535 (2001) 553-64.
[95] A.S. Khromov, K. Momotani, L. Jin, M.V. Artamonov, J. Shannon, M. Eto, and A.V. Somlyo, Molecular mechanism of telokin-mediated disinhibition of myosin light chain phosphatase and cAMP/cGMP-induced relaxation of gastrointestinal smooth muscle. J Biol Chem 287 (2012) 20975-85.
[96] P.J. Gallagher, and B.P. Herring, The carboxyl terminus of the smooth muscle myosin light chain kinase is expressed as an independent protein, telokin. J Biol Chem 266 (1991) 23945-52.
[97] N. Choudhury, A.S. Khromov, A.P. Somlyo, and A.V. Somlyo, Telokin mediates Ca2+-desensitization through activation of myosin phosphatase in phasic and tonic smooth muscle. J Muscle Res Cell Motil 25 (2004) 657-65.
[98] S. Vetterkind, and K.G. Morgan, The pro-apoptotic protein Par-4 facilitates vascular contractility by cytoskeletal targeting of ZIPK. J Cell Mol Med 13 (2009) 887-95.
[99] S. Vetterkind, E. Lee, E. Sundberg, R.H. Poythress, T.C. Tao, U. Preuss, and K.G. Morgan, Par-4: a new activator of myosin phosphatase. Mol Biol Cell 21 (2010) 1214-24.
[100] M.A. Borman, J.A. MacDonald, and T.A. Haystead, Modulation of smooth muscle contractility by CHASM, a novel member of the smoothelin family of proteins. FEBS Lett 573 (2004) 207-13.
[101] A.A. Wooldridge, C.N. Fortner, B. Lontay, T. Akimoto, R.L. Neppl, C. Facemire, M.B. Datto, A. Kwon, E. McCook, P. Li, S. Wang, R.J. Thresher, S.E. Miller, J.C. Perriard, T.P. Gavin, R.C. Hickner, T.M. Coffman, A.V. Somlyo, Z. Yan, and T.A. Haystead, Deletion of the protein kinase A/protein kinase G target SMTNL1 promotes an exercise-adapted phenotype in vascular smooth muscle. J Biol Chem 283 (2008) 11850-9.
[102] B. Lontay, K. Bodoor, D.H. Weitzel, D. Loiselle, C. Fortner, S. Lengyel, D. Zheng, J. Devente, R. Hickner, and T.A. Haystead, Smoothelin-like 1 protein regulates myosin phosphatase-targeting subunit 1 expression during sexual development and pregnancy. J Biol Chem 285 (2010) 29357-66.
[103] J.D. Webb, A. Muranyi, C.W. Pugh, P.J. Ratcliffe, and M.L. Coleman, MYPT1, the targeting subunit of smooth-muscle myosin phosphatase, is a substrate for the asparaginyl hydroxylase factor inhibiting hypoxia-inducible factor (FIH). Biochem J 420 (2009) 327-33.
[104] E. Twomey, Y. Li, J. Lei, C. Sodja, M. Ribecco-Lutkiewicz, B. Smith, H. Fang, M. Bani-Yaghoub, I. McKinnell, and M. Sikorska, Regulation of MYPT1 stability by the E3 ubiquitin ligase SIAH2. Exp Cell Res 316 (2010) 68-77.
[105] T. Iwasaki, T. Katayama, K. Kohama, Y. Endo, and T. Sawasaki, Myosin phosphatase is inactivated by caspase-3 cleavage and phosphorylation of myosin phosphatase targeting subunit 1 during apoptosis. Mol Biol Cell 24 (2013) 748-56.
[106] M.A. Borman, T.A. Freed, T.A. Haystead, and J.A. Macdonald, The role of the calponin homology domain of smoothelin-like 1 (SMTNL1) in myosin phosphatase inhibition and smooth muscle contraction. Mol Cell Biochem 327 (2009) 93-100.
[107] C. Mathe, D. Beyer, F. Erdodi, Z. Serfozo, L. Szekvolgyi, G. Vasas, M.H. M, K. Jambrik, S. Gonda, A. Kiss, Z.M. Szigeti, and G. Suranyi, Microcystin-LR induces abnormal root development by altering

microtubule organization in tissue-cultured common reed (Phragmites australis) plantlets. Aquat Toxicol 92 (2009) 122-30.
[108] H. Gruneberg, J.B. Burnett, and G.D. Snell, The Origin of Jerker, a New Gene Mutation of the House Mouse, and Linkage Studies Made with It. Proc Natl Acad Sci U S A 27 (1941) 562-5.
[109] K. Muller-Decker, W. Hirschner, F. Marks, and G. Furstenberger, The effects of cyclooxygenase isozyme inhibition on incisional wound healing in mouse skin. J Invest Dermatol 119 (2002) 1189-95.
[110] D. Horvath, I. Tamas, A. Sipos, Z. Darula, B. Becsi, D. Nagy, J. Ivan, F. Erdodi, and B. Lontay, Myosin phosphatase and RhoA-activated kinase modulate neurotransmitter release by regulating SNAP-25 of SNARE complex. PLoS One 12 (2017) e0177046.
[111] A. Sipos, J. Ivan, B. Becsi, Z. Darula, I. Tamas, D. Horvath, K.F. Medzihradszky, F. Erdodi, and B. Lontay, Myosin phosphatase and RhoA-activated kinase modulate arginine methylation by the regulation of protein arginine methyltransferase 5 in hepatocellular carcinoma cells. Sci Rep 7 (2017) 40590.
[112] I. Keller, A. Ungvari, E. Major, D. Horvath, Z. Konya, E. Toth, F. Erdodi, A. Kiss, and B. Lontay, Magnesium-dependent-Protein Phosphatase 1B Regulates the Protein Arginine Methyltransferase 5 Through the Modulation of Myosin Phosphatase. J Biol Chem (2024) 108107.
[113] C. Schmidt, and H. Urlaub, iTRAQ-labeling of in-gel digested proteins for relative quantification. Methods Mol Biol 564 (2009) 207-26.
[114] B. Lontay, Z. Serfozo, P. Gergely, M. Ito, D.J. Hartshorne, and F. Erdodi, Localization of myosin phosphatase target subunit 1 in rat brain and in primary cultures of neuronal cells. J Comp Neurol 478 (2004) 72-87.
[115] T.C. Sudhof, The synaptic vesicle cycle. Annu Rev Neurosci 27 (2004) 509-47.
[116] J.N. Jovanovic, T.S. Sihra, A.C. Nairn, H.C. Hemmings, Jr., P. Greengard, and A.J. Czernik, Opposing changes in phosphorylation of specific sites in synapsin I during Ca2+-dependent glutamate release in isolated nerve terminals. J Neurosci 21 (2001) 7944-53.
[117] D.A. Snyder, M.L. Kelly, and D.J. Woodbury, SNARE complex regulation by phosphorylation. Cell Biochem Biophys 45 (2006) 111-23.
[118] G. Nagy, U. Matti, R.B. Nehring, T. Binz, J. Rettig, E. Neher, and J.B. Sorensen, Protein kinase C-dependent phosphorylation of synaptosome-associated protein of 25 kDa at Ser187 potentiates vesicle recruitment. J Neurosci 22 (2002) 9278-86.
[119] G. Nagy, K. Reim, U. Matti, N. Brose, T. Binz, J. Rettig, E. Neher, and J.B. Sorensen, Regulation of releasable vesicle pool sizes by protein kinase A-dependent phosphorylation of SNAP-25. Neuron 41 (2004) 417-29.
[120] B. Lontay, B. Pal, Z. Serfozo, A. Koszeghy, G. Szucs, Z. Rusznak, and F. Erdodi, Protein phosphatase-1M and Rho-kinase affect exocytosis from cortical synaptosomes and influence neurotransmission at a glutamatergic giant synapse of the rat auditory system. J Neurochem 123 (2012) 84-99.
[121] C. Compagnucci, S. Barresi, S. Petrini, E. Bertini, and G. Zanni, Rho-kinase signaling controls nucleocytoplasmic shuttling of class IIa histone deacetylase (HDAC7) and transcriptional activation of orphan nuclear receptor NR4A1. Biochem Biophys Res Commun 459 (2015) 179-183.
[122] T. Ryan, M. Shelton, J.P. Lambert, B. Malecova, S. Boisvenue, M. Ruel, D. Figeys, P.L. Puri, and I.S. Skerjanc, Myosin phosphatase modulates the cardiac cell fate by regulating the subcellular localization of Nkx2.5 in a Wnt/Rho-associated protein kinase-dependent pathway. Circ Res 112 (2013) 257-66.
[123] H. Kim, and Z.A. Ronai, PRMT5 function and targeting in cancer. Cell Stress 4 (2020) 199-215.

[124] C.D. Krause, Z.H. Yang, Y.S. Kim, J.H. Lee, J.R. Cook, and S. Pestka, Protein arginine methyltransferases: evolution and assessment of their pharmacological and therapeutic potential. Pharmacol Ther 113 (2007) 50-87.
[125] A. Motolani, M. Martin, M. Sun, and T. Lu, The Structure and Functions of PRMT5 in Human Diseases. Life (Basel) 11 (2021).
[126] R. Borzsei, B. Bayarsaikhan, B.Z. Zsido, B. Lontay, and C. Hetenyi, The Structural Effects of Phosphorylation of Protein Arginine Methyltransferase 5 on Its Binding to Histone H4. Int J Mol Sci 23 (2022).
[127] B. Zhang, S. Dong, Z. Li, L. Lu, S. Zhang, X. Chen, X. Cen, and Y. Wu, Targeting protein arginine methyltransferase 5 inhibits human hepatocellular carcinoma growth via the downregulation of beta-catenin. J Transl Med 13 (2015) 349.
[128] B. Lontay, A. Kiss, P. Gergely, D.J. Hartshorne, and F. Erdodi, Okadaic acid induces phosphorylation and translocation of myosin phosphatase target subunit 1 influencing myosin phosphorylation, stress fiber assembly and cell migration in HepG2 cells. Cell Signal 17 (2005) 1265-75.
[129] B. Favre, P. Turowski, and B.A. Hemmings, Differential inhibition and posttranslational modification of protein phosphatase 1 and 2A in MCF7 cells treated with calyculin-A, okadaic acid, and tautomycin. J Biol Chem 272 (1997) 13856-63.
[130] Y. Zhao, L. Liang, Y. Fan, S. Sun, L. An, Z. Shi, J. Cheng, W. Jia, W. Sun, Y. Mori-Akiyama, H. Zhang, S. Fu, and J. Yang, PPM1B negatively regulates antiviral response via dephosphorylating TBK1. Cell Signal 24 (2012) 2197-204.
[131] R. Wong, S. Geyer, W. Weninger, J.C. Guimberteau, and J.K. Wong, The dynamic anatomy and patterning of skin. Exp Dermatol 25 (2016) 92-8.
[132] T. Wagner, M. Gschwandtner, A. Strajeriu, A. Elbe-Burger, J. Grillari, R. Grillari-Voglauer, G. Greiner, B. Golabi, E. Tschachler, and M. Mildner, Establishment of keratinocyte cell lines from human hair follicles. Sci Rep 8 (2018) 13434.
[133] R.L. Eckert, M.T. Sturniolo, R. Jans, C.A. Kraft, H. Jiang, and E.A. Rorke, TIG3: a regulator of type I transglutaminase activity in epidermis. Amino Acids 36 (2009) 739-46.
[134] L. Koivisto, K. Alavian, L. Hakkinen, S. Pelech, C.A. McCulloch, and H. Larjava, Glycogen synthase kinase-3 regulates formation of long lamellipodia in human keratinocytes. J Cell Sci 116 (2003) 3749-60.
[135] A. Svobodova, D. Walterova, and J. Vostalova, Ultraviolet light induced alteration to the skin. Biomed Pap Med Fac Univ Palacky Olomouc Czech Repub 150 (2006) 25-38.
[136] H.S. Kim, M.C. Song, I.H. Kwak, T.J. Park, and I.K. Lim, Constitutive induction of p-Erk1/2 accompanied by reduced activities of protein phosphatases 1 and 2A and MKP3 due to reactive oxygen species during cellular senescence. J Biol Chem 278 (2003) 37497-510.
[137] D. Dedinszki, A. Sipos, A. Kiss, R. Batori, Z. Konya, L. Virag, F. Erdodi, and B. Lontay, Protein phosphatase-1 is involved in the maintenance of normal homeostasis and in UVA irradiation-induced pathological alterations in HaCaT cells and in mouse skin. Biochim Biophys Acta 1852 (2015) 22-33.
[138] T. Velnar, T. Bailey, and V. Smrkolj, The wound healing process: an overview of the cellular and molecular mechanisms. J Int Med Res 37 (2009) 1528-42.
[139] S. Guo, and L.A. Dipietro, Factors affecting wound healing. J Dent Res 89 (2010) 219-29.
[140] M.C. Robson, D.L. Steed, and M.G. Franz, Wound healing: biologic features and approaches to maximize healing trajectories. Curr Probl Surg 38 (2001) 72-140.
[141] O. Ruzsnavszky, B. Dienes, T. Olah, J. Vincze, T. Gall, E. Balogh, G. Nagy, R. Batori, B. Lontay, F. Erdodi, and L. Csernoch, Differential effects of phosphatase inhibitors on the calcium homeostasis and migration of HaCaT keratinocytes. PLoS One 8 (2013) e61507.

[142] A. Bayer, M. Tohidnezhad, J. Lammel, S. Lippross, P. Behrendt, T. Kluter, T. Pufe, H. Jahr, J. Cremer, F. Rademacher, R. Glaser, and J. Harder, Platelet-Released Growth Factors Induce Differentiation of Primary Keratinocytes. Mediators Inflamm 2017 (2017) 5671615.
[143] M. Bektas, and D.S. Rubenstein, What's in a name?: Heat shock protein 27 and keratinocyte differentiation. J Invest Dermatol 130 (2010) 10-2.
[144] C. Jonak, M. Mildner, G. Klosner, V. Paulitschke, R. Kunstfeld, H. Pehamberger, E. Tschachler, and F. Trautinger, The hsp27kD heat shock protein and p38-MAPK signaling are required for regular epidermal differentiation. J Dermatol Sci 61 (2011) 32-7.
[145] F.F. Bloise, A. Cordeiro, and T.M. Ortiga-Carvalho, Role of thyroid hormone in skeletal muscle physiology. J Endocrinol 236 (2018) R57-R68.
[146] S. Schiaffino, Fibre types in skeletal muscle: a personal account. Acta Physiol (Oxf) 199 (2010) 451-63.
[147] S. Schiaffino, and C. Reggiani, Fiber types in mammalian skeletal muscles. Physiol Rev 91 (2011) 1447-531.
[148] B. Gambke, G.E. Lyons, J. Haselgrove, A.M. Kelly, and N.A. Rubinstein, Thyroidal and neural control of myosin transitions during development of rat fast and slow muscles. FEBS Lett 156 (1983) 335-9.
[149] D. Pette, and R.S. Staron, Mammalian skeletal muscle fiber type transitions. Int Rev Cytol 170 (1997) 143-223.
[150] K. Bodoor, B. Lontay, R. Safi, D.H. Weitzel, D. Loiselle, Z. Wei, S. Lengyel, D.P. McDonnell, and T.A. Haystead, Smoothelin-like 1 protein is a bifunctional regulator of the progesterone receptor during pregnancy. J Biol Chem 286 (2011) 31839-51.
[151] T.A. Manuck, 17-alpha hydroxyprogesterone caproate for preterm birth prevention: Where have we been, how did we get here, and where are we going? Semin Perinatol 41 (2017) 461-467.
[152] B. Lontay, K. Bodoor, A. Sipos, D.H. Weitzel, D. Loiselle, R. Safi, D. Zheng, J. Devente, R.C. Hickner, D.P. McDonnell, T. Ribar, and T.A. Haystead, Pregnancy and Smoothelin-like Protein 1 (SMTNL1) Deletion Promote the Switching of Skeletal Muscle to a Glycolytic Phenotype in Human and Mice. J Biol Chem 290 (2015) 17985-17998.
[153] M.A. Abdul-Ghani, and R.A. DeFronzo, Pathogenesis of insulin resistance in skeletal muscle. J Biomed Biotechnol 2010 (2010) 476279.
[154] J. Boucher, A. Kleinridders, and C.R. Kahn, Insulin receptor signaling in normal and insulin-resistant states. Cold Spring Harb Perspect Biol 6 (2014).
[155] M. Beg, N. Abdullah, F.S. Thowfeik, N.K. Altorki, and T.E. McGraw, Distinct Akt phosphorylation states are required for insulin regulated Glut4 and Glut1-mediated glucose uptake. Elife 6 (2017).
[156] T.A. Kupriyanova, and K.V. Kandror, Akt-2 binds to Glut4-containing vesicles and phosphorylates their component proteins in response to insulin. J Biol Chem 274 (1999) 1458-64.
[157] H.K. Karlsson, and J.R. Zierath, Insulin signaling and glucose transport in insulin resistant human skeletal muscle. Cell Biochem Biophys 48 (2007) 103-13.
[158] K. Paz, Y.F. Liu, H. Shorer, R. Hemi, D. LeRoith, M. Quan, H. Kanety, R. Seger, and Y. Zick, Phosphorylation of insulin receptor substrate-1 (IRS-1) by protein kinase B positively regulates IRS-1 function. J Biol Chem 274 (1999) 28816-22.
[159] J.B. Meigs, Epidemiology of the insulin resistance syndrome. Curr Diab Rep 3 (2003) 73-9.
[160] K. Moeschel, A. Beck, C. Weigert, R. Lammers, H. Kalbacher, W. Voelter, E.D. Schleicher, H.U. Haring, and R. Lehmann, Protein kinase C-zeta-induced phosphorylation of Ser318 in insulin receptor substrate-1 (IRS-1) attenuates the interaction with the insulin receptor and the tyrosine phosphorylation of IRS-1. J Biol Chem 279 (2004) 25157-63.

[161] P. Gual, T. Gremeaux, T. Gonzalez, Y. Le Marchand-Brustel, and J.F. Tanti, MAP kinases and mTOR mediate insulin-induced phosphorylation of insulin receptor substrate-1 on serine residues 307, 612 and 632. Diabetologia 46 (2003) 1532-42.
[162] J.F. Tanti, P. Gual, T. Gremeaux, T. Gonzalez, R. Barres, and Y. Le Marchand-Brustel, Alteration in insulin action: role of IRS-1 serine phosphorylation in the retroregulation of insulin signalling. Ann Endocrinol (Paris) 65 (2004) 43-8.
[163] K.D. Copps, and M.F. White, Regulation of insulin sensitivity by serine/threonine phosphorylation of insulin receptor substrate proteins IRS1 and IRS2. Diabetologia 55 (2012) 2565-2582.
[164] A.M. Manning, and R.J. Davis, Targeting JNK for therapeutic benefit: from junk to gold? Nat Rev Drug Discov 2 (2003) 554-65.
[165] A. Krook, M. Bjornholm, D. Galuska, X.J. Jiang, R. Fahlman, M.G. Myers, Jr., H. Wallberg-Henriksson, and J.R. Zierath, Characterization of signal transduction and glucose transport in skeletal muscle from type 2 diabetic patients. Diabetes 49 (2000) 284-92.
[166] L.G. Yu, L.C. Packman, M. Weldon, J. Hamlett, and J.M. Rhodes, Protein phosphatase 2A, a negative regulator of the ERK signaling pathway, is activated by tyrosine phosphorylation of putative HLA class II-associated protein I (PHAPI)/pp32 in response to the antiproliferative lectin, jacalin. J Biol Chem 279 (2004) 41377-83.
[167] M.P. Czech, and S. Corvera, Signaling mechanisms that regulate glucose transport. J Biol Chem 274 (1999) 1865-8.
[168] F. Wu, D. Mao, Y. Liu, X. Chen, H. Xu, T.C. Li, and C.C. Wang, Localization of Mucin 1 in endometrial luminal epithelium and its expression in women with reproductive failure during implantation window. J Mol Histol 50 (2019) 563-572.
[169] C. Sancakli Usta, G. Turan, M. Hocaoglu, C.B. Bulbul, K. Kilic, A. Usta, and E. Adali, Differential Expressions of Ki-67, Bcl-2, and Apoptosis Index in Endometrial Cells of Women With and Without Type II Diabetes Mellitus and Their Correlation with Clinicopathological Variables. Reprod Sci 28 (2021) 1447-1456.
[170] A. Sharpe, L.C. Morley, T. Tang, R.J. Norman, and A.H. Balen, Metformin for ovulation induction (excluding gonadotrophins) in women with polycystic ovary syndrome. Cochrane Database Syst Rev 12 (2019) CD013505.
[171] M. Dai, X.L. Zhu, F. Liu, Q.Y. Xu, Q.L. Ge, S.H. Jiang, X.M. Yang, J. Li, Y.H. Wang, Q.K. Wu, Z.H. Ai, Y.C. Teng, and Z.G. Zhang, Cholesterol Synthetase DHCR24 Induced by Insulin Aggravates Cancer Invasion and Progesterone Resistance in Endometrial Carcinoma. Sci Rep 7 (2017) 41404.
[172] M. Nishida, The Ishikawa cells from birth to the present. Hum Cell 15 (2002) 104-17.
[173] I. Keller, A. Ungvari, R. Kinter, F. Szalmas, E. Kokai, and B. Lontay, Smoothelin-like protein 1 promotes insulin sensitivity and modulates the contractile properties of endometrial epithelial cells with insulin resistance. Front Endocrinol (Lausanne) 15 (2024) 1375771.
[174] A.N. Tullio, D. Accili, V.J. Ferrans, Z.X. Yu, K. Takeda, A. Grinberg, H. Westphal, Y.A. Preston, and R.S. Adelstein, Nonmuscle myosin II-B is required for normal development of the mouse heart. Proc Natl Acad Sci U S A 94 (1997) 12407-12.
[175] C. Wang, K. Jeong, H. Jiang, W. Guo, C. Gu, Y. Lu, and J. Liang, YAP/TAZ regulates the insulin signaling via IRS1/2 in endometrial cancer. Am J Cancer Res 6 (2016) 996-1010.
[176] S. Izumo, B. Nadal-Ginard, and V. Mahdavi, All members of the MHC multigene family respond to thyroid hormone in a highly tissue-specific manner. Science 231 (1986) 597-600.
[177] G. Dimitriadis, P. Mitrou, V. Lambadiari, E. Boutati, E. Maratou, E. Koukkou, D. Panagiotakos, N. Tountas, T. Economopoulos, and S.A. Raptis, Insulin-stimulated rates of glucose uptake in muscle in hyperthyroidism: the importance of blood flow. J Clin Endocrinol Metab 93 (2008) 2413-5.

[178] P. Mitrou, S.A. Raptis, and G. Dimitriadis, Insulin action in hyperthyroidism: a focus on muscle and adipose tissue. Endocr Rev 31 (2010) 663-79.

[179] M.W. Greene, N. Morrice, R.S. Garofalo, and R.A. Roth, Modulation of human insulin receptor substrate-1 tyrosine phosphorylation by protein kinase Cdelta. Biochem J 378 (2004) 105-16.

[180] Y. Ueda, S. Hirai, S. Osada, A. Suzuki, K. Mizuno, and S. Ohno, Protein kinase C activates the MEK-ERK pathway in a manner independent of Ras and dependent on Raf. J Biol Chem 271 (1996) 23512-9.

[181] D. Xia, J.T. Stull, and K.E. Kamm, Myosin phosphatase targeting subunit 1 affects cell migration by regulating myosin phosphorylation and actin assembly. Exp Cell Res 304 (2005) 506-17.

[182] Y. Wu, F. Erdodi, A. Muranyi, K.D. Nullmeyer, R.M. Lynch, and D.J. Hartshorne, Myosin phosphatase and myosin phosphorylation in differentiating C2C12 cells. J Muscle Res Cell Motil 24 (2003) 499-511.

[183] E. Major, I. Keller, D. Horvath, I. Tamas, F. Erdodi, and B. Lontay, Smoothelin-Like Protein 1 Regulates the Thyroid Hormone-Induced Homeostasis and Remodeling of C2C12 Cells via the Modulation of Myosin Phosphatase. Int J Mol Sci 22 (2021).

[184] L.A. Vasilets, R. Postina, and S.N. Kirichenko, Mutations of Ser-23 of the alpha1 subunit of the rat Na+/K+-ATPase to negatively charged amino acid residues mimic the functional effect of PKC-mediated phosphorylation. FEBS Lett 455 (1999) 8-12.

[185] A.M. Bertorello, A. Aperia, S.I. Walaas, A.C. Nairn, and P. Greengard, Phosphorylation of the catalytic subunit of Na+,K(+)-ATPase inhibits the activity of the enzyme. Proc Natl Acad Sci U S A 88 (1991) 11359-62.

[186] A.L. Riis, J.O. Jorgensen, N. Moller, J. Weeke, and T. Clausen, Hyperthyroidism and cation pumps in human skeletal muscle. Am J Physiol Endocrinol Metab 288 (2005) E1265-9.

[187] W.S. Simonides, and C. van Hardeveld, Thyroid hormone as a determinant of metabolic and contractile phenotype of skeletal muscle. Thyroid 18 (2008) 205-16.

Supplemental Material can be found at:
http://www.jbc.org/content/suppl/2011/07/19/M111.270397.DC1.html

lontay.beata_285_24

THE JOURNAL OF BIOLOGICAL CHEMISTRY VOL. 286, NO. 36, pp. 31839–31851, September 9, 2011
© 2011 by The American Society for Biochemistry and Molecular Biology, Inc. Printed in the U.S.A.

Smoothelin-like 1 Protein Is a Bifunctional Regulator of the Progesterone Receptor during Pregnancy*[S]

Received for publication, June 10, 2011, and in revised form, July 8, 2011 Published, JBC Papers in Press, July 19, 2011, DOI 10.1074/jbc.M111.270397

Khaldon Bodoor[‡1,2], Beata Lontay[‡§2,3], Rachid Safi[‡], Douglas H. Weitzel[‡], David Loiselle[‡], Zhengzheng Wei[¶], Szabolcs Lengyel[‖], Donald P. McDonnell[‡], and Timothy A. Haystead[‡4]

From the [‡]Department of Pharmacology and Cancer Biology and [¶]Institute for Genome Sciences and Policy, Duke University Medical Center, Durham, North Carolina 27710 and the Departments of [§]Medical Chemistry and [‖]Ecology, University of Debrecen, 4032 Debrecen, Hungary

During pregnancy, uterine smooth muscle (USM) coordinately adapts its contractile phenotype in order to accommodate the developing fetus and then prepare for delivery. Herein we show that SMTNL1 plays a major role in pregnancy to promote adaptive responses in USM and that this process is specifically mediated through interactions of SMTNL1 with the steroid hormone receptor PR-B. *In vitro* and *in vivo* SMTNL1 selectively binds PR and not other steroid hormone receptors. The physiological relationship between the two proteins was also established in global gene expression and transcriptional reporter studies in pregnant *smtnl1*$^{-/-}$ mice and by RNA interference in progesterone-sensitive cell lines. We show that the contraction-associated and progestin-sensitive genes (oxytocin receptor, connexin 43, and cyclooxygenase-2) and prolactins are down-regulated in pregnant *smtnl1*$^{-/-}$ mice. We suggest that SMTNL1 is a bifunctional co-regulator of PR-B signaling and thus provides a molecular mechanism whereby PR-B is targeted to alter gene expression patterns within USM cells to coordinately promote alterations in USM function during pregnancy.

Uterine smooth muscle (USM)[5] cells show a high degree of plasticity and are capable of transforming their phenotype in response to a variety of physiological stresses, such as pregnancy. In pregnancy, USM cells go through a number of extensive phenotypic changes characterized by the expression of a distinct set of proteins (1, 2). In early pregnancy, USM cells proliferate rapidly under the influence of endocrine-stimulated growth factors (3). A significant increase in the expression of anti-apoptotic factors is a key feature of this proliferative phase (4). In midpregnancy, USM cells switch into a synthetic phase characterized by cellular hypertrophy, extracellular matrix remodeling, and activation of apoptotic pathways (3). The changes that occur during this phase are under the influence of both mechanical stimuli and endocrine hormones, such as progesterone (2). Toward parturition, the cells adopt a more contractile phenotype, characterized by an up-regulation in the expression of contraction-associated proteins (CAPs) (2). The phenotypic changes in this phase are modulated by mechanical stimuli and sex-related hormones, such as progesterone and estrogen. The molecular mechanisms regulating the transition of the USM through these different stages are limited, and investigation of these mechanisms is of great importance given the fact that preterm labor is still the leading cause of neonatal morbidity and mortality (5, 6).

USM contraction is mainly regulated by phosphorylation of the regulatory light chain of myosin (MLC20) by Ca^{2+}/calmodulin-dependent myosin light chain kinase, whereas relaxation is promoted by dephosphorylation of MLC20 by myosin phosphatase (7, 8). Both myosin light chain kinase and myosin phosphatase are regulated by several accessory proteins, and one such protein is smoothelin-like protein 1 (SMTNL1) (9). Mouse SMTNL1 is divided into two separate domains: a unique N-terminal domain (amino acids 1–346) and a C-terminal single, type-2 calponin homology domain (amino acids 346–459) that is helix-rich and globular in structure essential for binding tropomysin (9, 10). Physiological studies in *smtnl1*$^{-/-}$ mice indicate that the protein plays a key role in modulating the contractile activity of smooth and striated muscle and is involved in adaptation in response to exercise and pregnancy (11, 12). We recently showed that during sexual development and pregnancy, MYPT1 (the myosin-targeting subunit of myosin phosphatase) is a signaling target of SMTNL1. Deletion of SMTNL1 results in a more than 30-fold increase in the expression of MYPT1 in neonates, gradually declining during sexual development. A significant increase in the levels of MYPT1 was also seen in pregnant *smtnl1*$^{-/-}$ mice (11). Our findings suggested that SMTNL1 may function as a transcriptional regulator of MYPT1 expression in smooth and striated muscle, altering their contractile properties. This putative role is supported by nuclear localization of SMTNL1 upon phosphorylation at Ser-301 in response to cAMP/cGMP and by the presence of a number of regulatory transcription factor binding sites in the promoter region of *Smtnl1* (11, 13). SMTNL1 also shows sex-related differences in expression and function, in that male

* This work was supported, in whole or in part, by National Institutes of Health Grant R56DK065954-05 (to T. A. J. H.).

[S] The on-line version of this article (available at http://www.jbc.org) contains supplemental Table I and Figs. 1 and 2.

[1] Supported by a postdoctoral fellowship from the King Hussein Institute for Biotechnology and Cancer, Amman, Jordan. Currently on a sabbatical leave from the Department of Applied Biology-Faculty of Science and Arts at the Jordan University of Science and Technology, Irbid 21110, Jordan.

[2] Both authors contributed equally to this work.

[3] Supported by the J. Bolyai Fellowship.

[4] To whom correspondence should be addressed: Duke University, Research Dr., LSRC, C119, Box 3, Durham, NC 27710. Tel.: 919-613-8606; Fax: 919-668-0977; E-mail: hayst001@mc.duke.edu.

[5] The abbreviations used are: USM, uterine smooth muscle; CAP, contraction-associated protein; PR, progesterone receptor; ER, estrogen receptor; AR, androgen receptor; GR, glucocorticoid receptor; MMTV, murine mammary tumor virus; RMA, robust multichip analysis; IP, immunoprecipitation.

Downloaded from www.jbc.org at Duke University, on September 11, 2011

tomtay : beata_285_24

mice have a 2-fold increase in levels compared with females, and exercise-adapted muscle tissues from *smtnl1*$^{-/-}$ female mice respond differently to adrenergic agonists (11, 12).

Progesterone acting through its receptor PR plays a key role in the establishment and maintenance of pregnancy, coordinating many of the adaptive responses observed in USM (14–16). PR is a member of the steroid hormone family of nuclear receptors and functions as a ligand-activated transcriptional factor to regulate the expression of genes through binding to the corresponding hormone response elements within the promoter regions of target genes (17, 18). PR is expressed in target cells as two distinct isoforms, PR-A and PR-B, generated from a single gene through the use of two alternative promoters (19, 20). In USM, although the precise molecular mechanisms are unknown, PR is thought to promote relaxation by specifically inhibiting expression of the oxytocin receptor and prostaglandin F receptor, targeted by the contractile agonists oxytocin and PGF2α (21–25). In the case of PGF2α, PR is also involved in inhibiting the expression of key enzymes involved in the metabolism of PGF2α, such as cyclooxygense-2 and 15-hydroxy-PG-dehydrogenase (26–29). Additionally, prostaglandins reduces the contractility and excitability of USM cells by inhibiting the expression of key gap junction proteins, such as connexin 43 (Cnx43) (30). Parturition in humans does not involve a drop in progesterone concentrations, and thus "functional progesterone withdrawal" in USM is achieved via an increase in the PR-A/PR-B ratio (31, 32). Concomitantly, this is associated with changes in the expression of both co-activators and repressors of PR transcriptional activity, such as the co-activators SRC-2 and -3 and the co-repressors PSF (polypyrimidine tract-binding protein-associated splicing factor) and p54nrb (non-POU-domain-containing octamer-binding protein) (33–36). Additionally, the miR-200 family and their targets, ZEB1 and ZEB2, are identified as unique progesterone/PR-mediated regulators of USM contractility during pregnancy (37).

In this study, we identify SMTNL1 as a previously unrecognized co-regulator of PR-B, and in this capacity it functions to regulate USM plasticity during pregnancy. We show that SMTNL1 directly and specifically binds PR-B and suppresses its transcriptional activity both *in vivo* and *in vitro*. We suggest that regulation of PR-B by SMTNL1 provides a molecular mechanism whereby PR-B is targeted to alter gene expression patterns within USM cells to coordinately promote alterations in smooth muscle function during pregnancy.

EXPERIMENTAL PROCEDURES

Biochemicals—SV40-hPR-B plasmid was provided by Ligand Pharmaceuticals. FLAG-hPR-B was a gift from S. Nordeen (University of Colorado Health Sciences Center). Pgr 1294 antibody was a kind gift from Dean Edwards (Baylor College of Medicine).

Mouse Colony Maintenance and Pregnancy Studies—The *smtnl1*$^{-/-}$ mouse was created using standard protocols as described (12). The transgenic mice were maintained by backcross breeding over 9 generations to a 129 SvEv background. All mice were fed standard mouse chow (PMI5058 Picolab Mouse Diet 20, LabDiet) and water *ad libitum*. Care of the mice used in the experiments met the standard set forth by the National Institutes of Health guidelines for the care and use experimental animals. All procedures involving mice were approved by the Duke University Animal Care and Use Committee. In order to avoid shifts in the circadian rhythm and hence the estrous cycle, all animals were housed in identical polycarbonate cages and kept in an environmentally controlled room (23 ± 2 °C, 50 ± 10% relative humidity, frequent ventillation, and 12/12-h light/dark cycle). For pregnancy studies, 6–8 weeks mature female mice in estrus were selected by the appearance of their vagina and also with the lavage method of removing by gentle mechanical disruption following vaginal washes, stained with hematoxilin/eosin solution, and analyzed by light microscopy. Female littermates caged together presented synchronized estrus in 98% of cases. Females in estrus were mated with adult males overnight and then examined the following morning(s) for the presence of a vaginal plug. This was designated as day 0 of pregnancy. Mice were euthanized on a selected day of pregnancy (day 7, 13, and 17), the day of giving birth (birth), and the second day of lactation.

Study of Reproductive Fitness—smtnl1$^{-/-}$ colony breeding data were collected over a period of 1.5 years from age-matched crosses generated between *smtnl1*$^{+/+}$ × *smtnl1*$^{+/+}$ and *smtnl1*$^{-/-}$ × *smtnl1*$^{-/-}$ mice (n = 1651) given data on the litter size and the proportion of sexes. To gain data on embryonic lethality, time to pregnancy, and the interval between pregnancy as the hallmarks of reproductive phenotype and the frequency of pregnancy, *smtnl1*$^{+/+}$ × *smtnl1*$^{+/+}$ and *smtnl1*$^{-/-}$ × *smtnl1*$^{-/-}$ experimental breeder pairs (n = 40 each) were used. The already proved fertile males and virgin females were in the age range of 6–8 weeks old. Data are expressed as means ± S.E.

Cell Culture—HeLa, T47D, and 293T cells were maintained in DMEM and HepG2 cells were maintained in minimum Eagle's medium. When cells were treated with hormones, cells were cultured in phenol red-free medium containing 10% charcoal-stripped FBS plus the appropriate hormones for the indicated time periods.

Mammalian Two-hybrid and Luciferase Assays—Mammalian two-hybrid assays were carried out in HepG2 cells. Cells were transfected Fugene 6 reagent (Roche Applied Science) with 1500 ng of 5xGal4-luciferase reporter plasmid, 500 ng of VP16, or 500 ng of nuclear receptor-VP16 fusion constructs (PR-A, PR-B (or PR-B deletion/mutant constructs), estrogen receptors α and β (ERα and ERβ), androgen receptor (AR), and glucocorticoid receptor (GR)), 500 ng of pM-Gal4DBD or pM-Gal4DBD-SMTNL1 construct (or pM-SMTNL1 deletion constructs), 200 ng of cytomegalovirus β-galactosidase (β-gal), and 300 ng of pBSIIKS plasmid for a total of 3 μg of DNA per triplicate. Following a 24-h transfection, cells were treated with vehicle (ethanol) or with the corresponding receptors ligands as follows: 10 nM R5020 for PR-A and -B, 100 nM 17β-estradiol for ERα and -β, 100 nM dexamethasone for GR, 100 nM R1881 for AR, or 100 nM RU486 and ZK98299. After an additional 24 h of incubation, the cells were harvested for luciferase and β-galactosidase assays. For analyzing the effects of 8-Br-cAMP on PR-B transcriptional activity, HeLa cells were transfected with 10 ng of SV40-PR-B, 1500 ng of MMTV-luciferase reporter plasmid, 200 ng of β-gal, and 1290 ng of pBSIIKS plasmid for a total of 3

Downloaded from www.jbc.org at Duke University, on September 11, 2011

μg of DNA per well. After transfection, the cells were incubated with vehicle or 10 nM R5020 in the presence of 8-Br-cAMP (10 nM to 1 mM) for 24 h and subsequently harvested for luciferase and β-gal assays. For analyzing the effects of SMTNL1 on PR-B transcriptional activity, reporter assays were carried out in HeLa cells. Cells were transiently transfected with 10 ng of SV40-PR-B, without (0 ng), or with increasing concentrations (75, 150, and 300 ng) of pcDNA 3.1-SMTNL1 together with 1500 ng of the MMTV-luciferase reporter plasmid and varying amounts of pBSIIKS plasmid for a total of 3 μg of DNA per triplicate. The following day, cells were incubated with vehicle or 10 nM R5020 in the presence or absence of 100 μM 8-Br-cAMP for 24 h and subsequently harvested for luciferase and β-gal assays. Assays for endogenous PR-B transcription activity were carried out in T47D cells. pcDNA3.1-SMTNL1 was transfected into T47D, and the effects of increasing amounts of SMTNL1 (15 and 80 ng) on PR-B transcriptional activity with or without R5020 and 8-Br-cAMP were measured. Data are presented as a normalized response, representing the absolute luciferase activity corrected for transfection efficiency by normalizing against the β-gal activity.

Site-directed Mutagenesis—All SMTNL1 mutants were created with the QuikChange mutagenesis kit (Stratagene) and completely sequenced for confirmation. Primers used in the mutagenesis experiments are listed in supplemental Table I*A*.

SMTNL1 Silencing in T47D Cells—Double-stranded siRNA to knock down endogenous SMTNL1 protein levels and a scrambled sequence were synthesized by Dharmacon Inc. (listed in supplemental Table I*C*). The siRNAs were transfected into T47D cells using Dharmafect 1 transfection reagent (Dharmacon) according to the manufacturer's protocol. After 48 h, the cells were treated with 1 nM R5020 for another 12 h. Subsequently, cells were lysed and analyzed by Western blot analysis using anti-SMTNL1 and anti-PR antibodies.

RNA Isolation and RT-PCR—The RNeasy® lipid tissue mini-kit (Qiagen) was used to isolate total RNA from the uterus (n = 3) of WT and/or *smtnl1*$^{-/-}$ of pregnant and/or non-pregnant mice. RNA (1 μg) was reverse transcribed to cDNA using the iScript cDNA synthesis kit (Bio-Rad). PCR amplification was performed with iQ SYBR Green Supermix (Bio-Rad) with a 0.2 mM concentration of each primer (see supplemental Table I*B* for primer sequences). The 36B4 gene was used for the normalization of amplification.

Microarray—RNA was isolated from the uterus (n = 3) of WT and/or *smtnl1*$^{-/-}$ of pregnant (day 17) and/or non-pregnant mice. For microarray hybridizations, 100 ng of total RNA was amplified and labeled using the MessageAmp Premier Kit (Ambion). Equal amounts of labeled cRNA were hybridized to the Affymetrix Mouse Genome 430 2.0 microarray (Affymetrix) according to the manufacturer's protocol. Partek Genomics Suite 6.4 (Partek Inc., St. Louis, MO) was used to perform data analysis. Robust multichip analysis (RMA) normalization was done on the entire data set. Multiway analysis of variance and -fold change were performed to select target genes that were differentially expressed between the different comparisons. Top differentially expressed genes were selected with a p value of 0.05 based on an analysis of variance test and a -fold change cut-off of ≥2. Gene ontology enrichment analysis was performed with a χ^2 test and limited to functional groups with more than two genes. Hierarchical clustering was performed based on average linkage with Pearson's dissimilarity. GeneGo software was used for obtaining pathway maps and biological networks. All microarray experimental results are available at the Duke Microarray facility Web site.

Immunoprecipitation, Immunoblotting, and Mass Spectrometry—Uterus samples of WT and *smtnl1*$^{-/-}$ mice in day 0 and 14 of pregnancy were homogenized as described previously (9). Samples were processed for immunoprecipitation (IP) and immunoblotting with specific antibodies against SMTNL1, PR, and ERα. For IP experiments with 293T cells, cells were transfected with FLAG-Smtnl1, FLAG-PR-B, SV40-PR-B, and pcDNA-Smtnl1 as indicated. 48 h after transfection, medium was replaced with fresh medium with or without 10 nM R5020 and incubated for 2 h. Subsequently, cells were processed as described previously (67). IPs were boiled for 10 min in SDS sample buffer, and proteins were resolved by 10% SDS-PAGE and visualized with silver staining. For immunoblotting experiments, cells were lysed and processed for Western blotting with the corresponding antibodies as described previously (11). For mass spectrometry experiments, bands of interest from IP studies were in gel-digested with 0.6 μg of trypsin, and the tryptic peptides were subjected to MALDI TOF-TOF mass spectrometry.

Enzyme Immunoassays—Circulating progesterone and estradiol concentrations were determined by using ACE™ competitive enzyme immunoassays (Cayman Chemicals). Hormone concentrations were calculated in pg/ml.

Variables and Statistical Analysis—Litter size was the number of pups counted in each litter. Embryonic lethality was measured by searching uteri for dead embryos at the time of dissection either on day 7, 13, or 17 of pregnancy or at birth and is reported as the mean number of dead embryos. The proportion of males was the percentage of male pups within each litter. Time to pregnancy was the number of days between the set-up of the breeding pair (with female in estrus) and the first observation of the plug (considered as day 0). Interval between pregnancies was the number of days between the first observation of the plug in the first pregnancy and the first observation of the plug in the second pregnancy.

Normalized data were analyzed by t tests (for two groups) or by general linear models (for >2 groups). Parametric statistical tests were used if the assumptions of such tests were met. We also log-transformed data for analyses. In general linear models, we tested all possible interaction terms and report here the final models obtained by excluding non-significant ($p > 0.05$) interactions. When any covariate or factor was significant in general linear models, we applied Tukey's honestly significant difference procedure to test for pairwise differences in group means. Tests were conducted using the R statistical environment (R Development Core Team 2008) or SPSS 17.0 for Windows.

RESULTS

Deletion of SMTNL1 Results in a Poor Reproductive Phenotype—Previous findings suggested an important role for SMTNL1 in the regulation of smooth and striated muscle plasticity during pregnancy. In both vascular and USM cells,

Downloaded from www.jbc.org at Duke University, on September 11, 2011

tomtay : beata_285_24

SMTNL1 expression increased by more than 10-fold by day 13–17 of pregnancy compared with non-pregnant mice and then declines steadily through parturition and the onset of lactation (11). To determine if loss of SMTNL1 function affects normal pregnancy, we examined our *smtnl1*$^{-/-}$ mouse breeding data base. After several thousand breedings, we observed that litter sizes were smaller and embryonic lethality was higher in *smtnl1*$^{-/-}$ mice (Table 1). There was also a statistically significant increase in the proportion of male mice born relative to females (Table 1). An increased proportion of males to females within a population has been shown to be related to a reduction in overall fitness. Additionally, time to pregnancy was longer in *smtnl1*$^{-/-}$ mice and the intervals between pregnancies increased by 3–4 days (Table 1), although the latter difference was not statistically significant. These findings reveal that loss of SMTNL1 results in a phenotype of lower overall reproductive fitness as a physiological effect.

Global Gene Expression Profiles of Uterine Samples from smtnl1$^{-/-}$ *and Wild-type Mice during Pregnancy*—To more fully define the role of SMTNL1 in pregnancy, we performed microarray analysis using the Affymetrix Mouse Genome 430 2.0 Array. Over 39,000 transcripts/single array were examined, essentially encompassing the entire expressed mouse genome. Total uterine RNA was isolated from three different mice for each group: non-pregnant wild type (*WN*), wild type pregnant (*WP*), knock-out non-pregnant (*KN*), and knock-out pregnant (*KP*) (see Fig. 1). Differentially expressed genes between the four comparisons are shown in a Venn diagram in Fig. 1*A*. Comparison 1 consisted of WT mice *versus smtnl1*$^{-/-}$ non-pregnant mice. This comparison identified 31 genes differentially regulated between the two groups. Comparison 2 consisted of WT non-pregnant mice and WT pregnant mice. This comparison identified 3276 that were differentially expressed. Comparison 3 consisted of knock-out non-pregnant mice *versus* knock-out pregnant mice. This comparison identified 3766 genes that were differentially expressed. Finally, comparison 4 consisted of analyzing WT pregnant mice *versus* knock-out pregnant. This comparison identified 128 genes (Tables 2 and 3) that were differentially expressed (Fig. 1*B*). Complete lists of genes for all four comparisons are available at the Duke Microarray facility Web site. Table 2 shows a list of 81 genes that were up-regulated by more than 2–50-fold ($n = 3$) in the WT pregnant mice *versus* the *smtnl1*$^{-/-}$ pregnant ones, and Table 3 shows a list of 47 genes that were down-regulated by more than 2–18-fold ($n = 3$) in the WT pregnant mice when compared with the *smtnl1*$^{-/-}$ pregnant mice. Bioinformatic analysis of genes differentially expressed in this comparison identified the most significant pathways involved, including immune response (*i.e.* oncostatin M signaling via MAPK and histamine H1 receptor signaling), cell adhesion, cytoskeleton remodeling, proteolysis, histidine and proline metabolism, atherosclerosis, cAMP biosynthetic process and activation of pro-

TABLE 1

***Smtnl1* deletion results in a poor reproductive phenotype**

Smtnl1$^{-/-}$ colony breeding data were collected over a period of 1.5 years from age-matched crosses generated between *smtnl1*$^{+/+}$ × *smtnl1*$^{+/+}$ and *smtnl*$^{-/-}$ × *smtnl1*$^{-/-}$ mice ($n = 1651$). Data on embryonic lethality, time to pregnancy, and the interval between pregnancy as the hallmarks of reproductive phenotype and the frequency of pregnancy were collected. Data are expressed as means ± S.E.

	smtnl1$^{+/+}$	*smtnl1*$^{-/-}$	Statistics
Litter size	7.14 ± 1.47	4.23 ± 1.25	$t_{30} = 5.961$, $p < 0.001$
Embryonic lethality	0.05 ± 0.22	0.4 ± 0.68	$t_{23} = 2.185$, $p = 0.039$
Proportion of males	44% ± 19.4%	57% ± 21.8%	$t_{30} = 1.768$, $p = 0.087$
Time to pregnancy	2.8 ± 1.37	4.6 ± 2.23	$t_{38} = 3.156$, $p = 0.003$
Interval between pregnancies	23.6 ± 2.65	27.5 ± 6.22	$t_{16} = 1.827$, $p = 0.086$

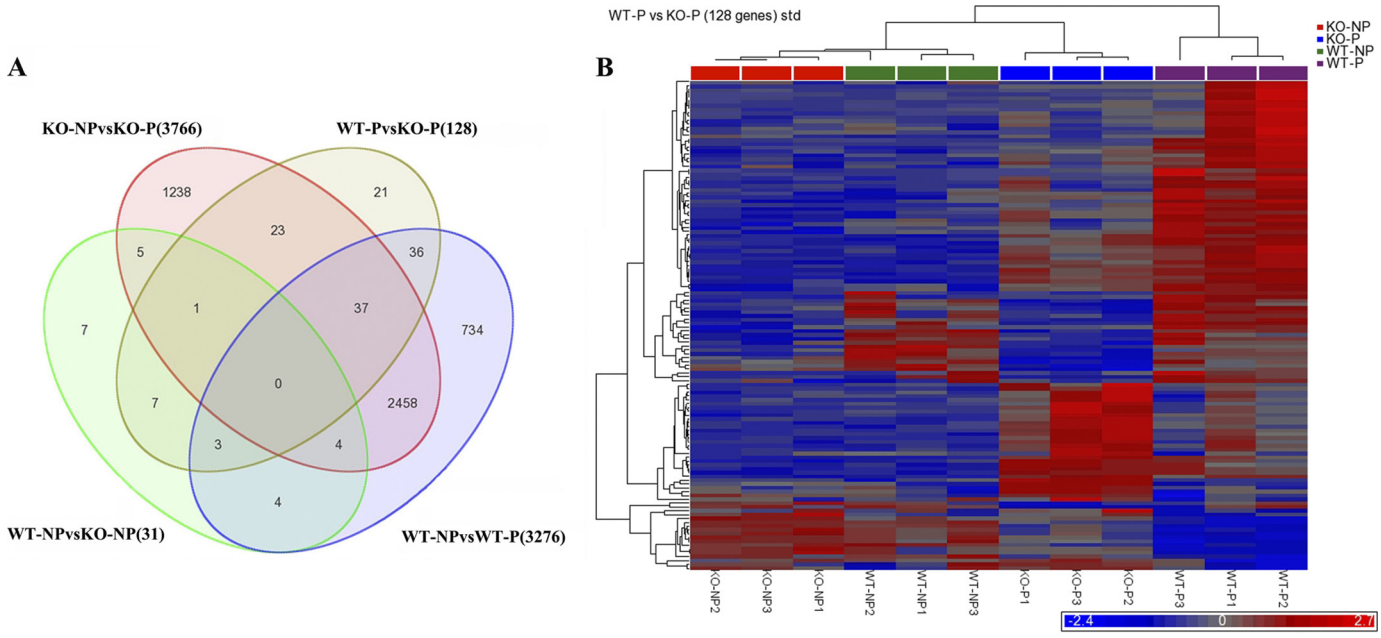


FIGURE 1. **Venn diagram demonstrating the relationship between genes differentially regulated in the different comparisons and hierarchical clustering analysis of the wild type pregnant (*WP*) *versus* knock-out pregnant (*KP*) mice.** *A*, Venn diagram; the *numbers* within the *intersections* of the *circles* indicate the common genes between the different groups. The *numbers outside* the *circles* indicate the number of genes differentially regulated between the two groups, as indicated. *B*, hierarchical clustering analysis of the differentially expressed genes in the wild type pregnant *versus* knock-out pregnant comparison. The *color code* for the signal strength is shown in the *box* at the *bottom*; induced genes are indicated by *red*, and repressed genes are indicated by *blue*. *WN*, non-pregnant wild type; *KN*, knock-out non-pregnant.

Downloaded from www.jbc.org at Duke University, on September 11, 2011

TABLE 2
Genes up-regulated in wild type pregnant *versus* *smtnl1*$^{-/-}$ pregnant mice

Probe set ID	Gene symbol	Change	*p* value
		-fold	
1452426_x_at		50.3404	0.0118484
1415835_at	*Prl3b1*	17.5723	0.000565294
1427760_s_at	*Prl2c2///Prl2c3///Prl2c4*	12.0257	7.87×10^{-5}
1436717_x_at	*Hbb-y*	10.5434	0.0402453
1448532_at	*Prl8a9*	9.53893	0.0063006
1436823_x_at	*Hbb-y*	9.23758	0.0497143
1457446_at	*Opcml*	6.89362	0.00252789
1419430_at	*Cyp26a1*	5.71716	0.0325249
1431379_a_at	*Slc13a1*	5.55238	0.0271946
1435330_at	*Pyhin1*	5.16049	2.88×10^{-6}
1417256_at	*Mmp13*	4.82501	3.77×10^{-5}
1460480_at	*Erv3*	4.79078	0.0198751
1416444_at	*Elovl2*	4.56532	0.0109421
1424959_at	*Anxa13*	4.54885	0.0185272
1422640_at	*Pcdhb9*	4.50123	0.00292992
1429835_at	*2310033E01Rik*	4.46294	0.00207603
1456211_at	*Nlrp10*	4.26845	0.00389898
1449529_s_at	*Prl7a1*	4.24167	4.67×10^{-7}
1419764_at	*Chi3l3*	3.95692	0.00726454
1450621_a_at	*Hbb-y*	3.94281	0.0248618
1449227_at	*Ch25h*	3.91637	0.00256177
1448608_at	*Prl8a2*	3.90766	0.0202838
1419700_a_at	*Prom1*	3.74858	0.0467971
1435212_at	*P2rx2*	3.52183	0.0191051
1453109_at	*Arsk*	3.46635	0.00739499
1422240_s_at	*Sprr2h*	3.34212	0.048739
1460670_at	*Riok3*	3.32078	0.00880283
1455965_at	*Adamts4*	3.30621	0.000183407
1416523_at	*Rnase1*	3.2957	0.0272699
1443109_at		3.20581	0.000563566
1443122_at		3.11984	0.0268743
1444198_at		3.11473	0.000703871
1459183_at		3.01381	0.00259112
1455963_at	*6332401O19Rik*	3.0044	0.00312948
1449211_at	*Bpnt1*	3.00332	9.99E-05
1437667_a_at	*Bach2*	2.99958	0.000357257
1434171_at	*C330011K17Rik*	2.96357	0.0282958
1446130_at		2.94778	6.58×10^{-6}
1435532_at	*LOC100048362*	2.90419	0.0176285
1420282_s_at	*Prss29*	2.88675	0.000879869
1439475_at	*Zfp429*	2.87303	0.00605254
1450364_a_at	*Havcr1*	2.85818	0.0352559
1450802_at	*Prss28*	2.84496	2.72×10^{-5}
1435612_at	*Opcml*	2.76545	0.00503496
1449992_at	*Prss29*	2.7388	0.00216172
1444262_at	*1110017F19Rik*	2.72515	0.0069375
1447096_at		2.70101	0.0150339
1449032_at	*Prl2a1*	2.63682	0.0171069
1448650_a_at	*Pole*	2.59374	0.0247163
1429053_at	*1110012J17Rik*	2.57509	0.00376077
1420566_at		2.48943	0.029121
1429691_at	*Ptprg*	2.48249	0.00238895
1448025_at	*Sirpb1*	2.46555	0.00830697
1456688_at		2.41953	0.00133759
1418945_at	*Mmp3*	2.41295	0.0426652
1429982_at	*4933426K21Rik*	2.4034	0.00943209
1425951_a_at	*Clec4n*	2.38158	0.00402976
1435533_s_at	*4933426K21Rik*	2.37328	0.0255649
1458659_at	*Plac9*	2.37271	0.0287112
1447231_at		2.36516	0.0234413
1425451_s_at	*Chi3l3///Chi3l4*	2.34073	0.0443562
1455208_at	*Pex19*	2.30199	0.00568377
1424502_at	*Oit1*	2.28795	0.0242847
1418429_at	*Kif5b*	2.2702	0.000310519
1424843_a_at	*Gas5*	2.26929	0.0011463
1449475_at	*Atp12a*	2.26072	0.0445511
1418764_a_at	*Bpnt1*	2.25707	0.00255535
1459661_at	*Dcdc2a*	2.24712	0.0225015
1418156_at	*Kcne4*	2.23922	0.001954
1443939_at	*OTTMUSG00000008561*	2.22234	0.0276062
1417280_at	*Slc17a1*	2.21315	0.00660674
1419627_s_at	*Clec4n*	2.16441	0.00979708
1419405_at	*Nmb*	2.16288	0.00802374
1447202_at	*1200009F10Rik*	2.13809	0.000141127
1450291_s_at	*Ms4a4c*	2.12471	0.0362122
1420604_at	*Hesx1*	2.1143	0.000794586
1452590_a_at	*Plac9*	2.10211	0.0306398
1446141_at		2.09829	0.0202272
1449388_at	*Thbs4*	2.09591	0.0033629
1437636_at	*LOC623121*	2.04626	0.000233143
1436222_at	*Gas5*	2.01476	0.00126799

TABLE 3
Genes down-regulated in wild type pregnant *versus* *smtnl1*$^{-/-}$ pregnant mice

Probe set ID	Gene symbol	Change	*p* value
		-fold	
1432216_s_at	*Mpp7*	−2.00481	0.00230603
1428891_at	*9130213B05Rik*	−2.00806	0.02324
1449394_at	*Slco1b2*	−2.01627	0.0272746
1427451_a_at	*BC018473*	−2.07375	0.0153867
1451625_a_at	*C8g*	−2.0821	0.0437489
1427001_s_at	*Hnf4a*	−2.08448	0.0224681
1445824_at	*Zfp458*	−2.11182	0.00204125
1417920_at	*Amn*	−2.11539	0.0438993
1442255_at		−2.11813	0.0241017
1450839_at	*D0H4S114*	−2.15096	0.0101531
1448837_at	*Vil1*	−2.16171	0.0234569
1439109_at	*Ccdc68*	−2.17935	0.0153504
1459733_at		−2.18599	0.000581386
1451610_at	*Cxcl17*	−2.1862	0.0493382
1457435_x_at	*Myom2*	−2.20231	0.0138509
1419670_at	*Ftcd*	−2.23909	0.00127039
1439117_at	*Clmn*	−2.25626	0.0125216
1425749_at	*Stxbp6*	−2.27681	0.0413114
1417600_at	*Slc15a2*	−2.29336	0.0182215
1438699_at	*Srd5a1*	−2.30676	0.0383523
1431101_a_at	*Srd5a1*	−2.32013	0.0246874
1457025_at	*4833413O15Rik*	−2.36177	0.01158
1424072_at	*2010107G23Rik*	−2.38241	0.000154301
1422846_at	*Rbp2*	−2.4153	0.0449952
1433845_x_at	*Dusp9*	−2.47057	0.00662899
1456495_s_at	*Osbpl6*	−2.48547	0.0397768
1456321_at	*Npal1*	−2.52829	0.0261785
1429166_s_at	*Clmn*	−2.52865	0.00630892
1453444_at	*5730437C12Rik*	−2.58443	0.0125215
1416677_at	*Apoh*	−2.65625	0.0337181
1417462_at	*Cap1*	−2.7564	0.0142922
1457483_at		−2.7689	0.00187144
1417461_at	*Cap1*	−2.83218	0.0082928
1452707_at	*Klhl30*	−3.00085	0.027121
1421445_at	*Slc26a3*	−3.29019	0.008087
1416980_at	*Mettl7b*	−3.44204	0.00469039
1449088_at	*Fbp2*	−3.68493	0.0415826
1419063_at	*Ugt8a*	−3.98828	0.0118296
1451788_at	*F11*	−4.324	0.00883293
1428301_at	*LOC671957*	−4.41548	0.00540577
1429467_s_at	*Slc26a3*	−4.41934	0.0103699
1459253_at	*Arrdc3*	−4.77537	0.0106758
1452731_x_at	*B930046C15Rik*	−5.40964	0.00252296
1427798_x_at		−5.44483	0.0171833
1427797_s_at		−7.61701	0.0375428
1439055_at	*OTTMUSG00000001305*	−9.19592	5.53×10^{-5}
1418645_at	*Hal*	−18.0734	7.10×10^{-6}

tein kinase A, transport, plasminogen activation, steroid metabolic process and glucocorticoid receptor signaling, regulation of growth hormone receptor signaling pathway, and negative regulation of protein import into nucleus. Additionally, analysis of networks of transcriptional regulation identified Sp1, c-Myc, NF-κB1, Stat3, Stat5a, Smad-2, -3, and -4, estrogen receptor α, and progesterone receptor as the major transcription factors involved in modulating gene expression in this comparison. Taken together, microarray analysis identified a number of signaling pathways involved in mediating the actions of SMTNL1 and strongly points to a role for the sex-related hormones estrogen and progesterone and their cognate receptors in SMTNL1 functions during pregnancy.

Most notable in this comparison is the deregulation of the prolactin (PRL) family members in the *smtnl1*$^{-/-}$ pregnant mice. All members of this family with an observed expression on the array were found to be significantly down-regulated (3–18-fold) in the *smtnl1*$^{-/-}$ pregnant mice. The deregulation of prolactins in *smtnl1*$^{-/-}$ pregnant mice was confirmed by RT-PCR analysis. Accordingly, the mRNA for Prl3b1, Prl2a1, Prl7a1, and Prl2c2 were all decreased markedly in knock-out (KO-P) pregnant mice when compared with their wild type

Downloaded from www.jbc.org at Duke University, on September 11, 2011

tomtay : beata_285_24

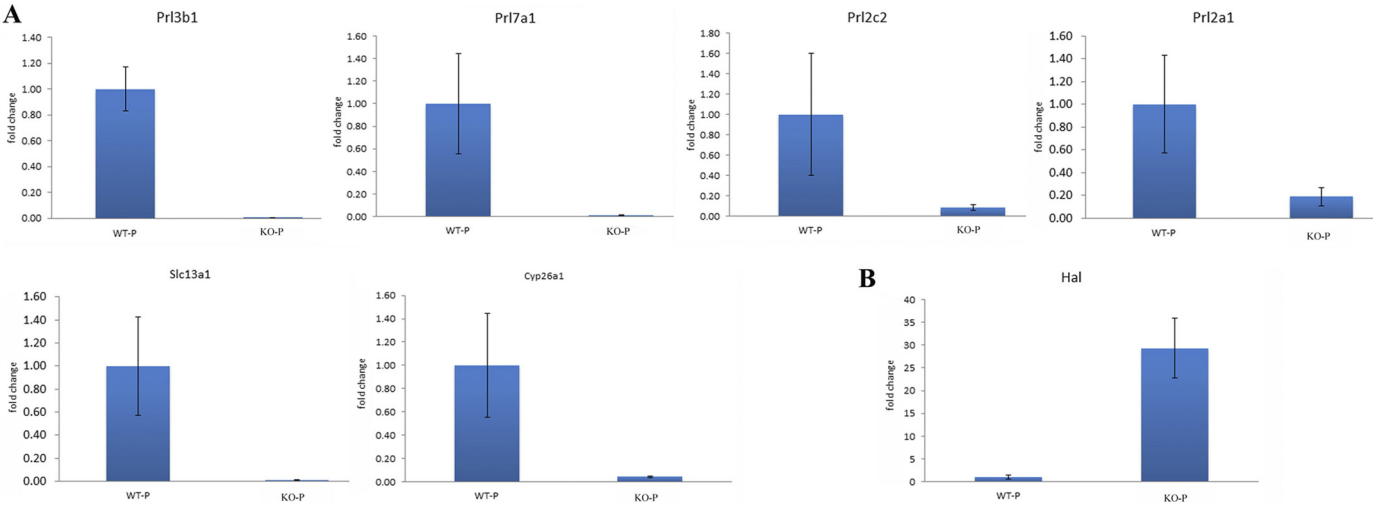


FIGURE 2. **Quantitative RT-PCR validation of microarray data.** Quantitative RT-PCR analysis of Prl3b1, Prl2a1, Prl7a1, Prl2c2, Cyp26a1, and Slc13a1 (*A*) and Hal (*B*) in wild type pregnant (*WT-P*) and *smtnl1*$^{-/-}$ pregnant (*KO-P*) mouse uteri. The results represent the mean ± S.E. (*error bars*), $n = 3$ RNA sets.

counterparts (WT-P) (Fig. 2*A*). The significance of this finding will be elaborated upon below in the context of the function of prolactins as mediators of pregnancy adaptations. Additionally, consistent with microarray results, RT-PCR analysis showed that the mRNAs for *Cyp26a1* and Slc13a1 were down-regulated in the KO-P mice (Fig. 2*A*). Uterine *cyp26a1* down-regulation in KO-P mice is intriguing, given its role in the maintenance of pregnancy during the process of blastocycst implantation and the finding that *cyp26a1* expression in the uterus is induced by steroid hormones (38–40). Additionally, we confirmed that the mRNA of a number of proteases (*i.e.* matrix metallopeptidases 13 and 3, arylsulfatase K, and ADAMTS-4 (a disintegrin and metalloproteinase with thrombospondin-like motifs)) that play an essential role in the ovulation process, through extracellular matrix remodeling, were all found to be down-regulated in the KO-P mice (41, 42). We also confirmed that mRNA of Hal (histidine-ammonia lyase), the histidine-degrading rate-limiting enzyme, is up-regulated in KO-P mice when compared with their WT-P counterparts (Fig. 2*B*). The increase in Hal mRNA in *smtnl1*$^{-/-}$ pregnant mice is intriguing, given the findings that the Hal gene is activated by glucocorticoids and glucagon via the PKA signaling pathway (43).

SMTNL1 Regulates the Expression of ERα and PR-B in the Primary Genital Tissues—Microarray analysis supports a role for SMTNL1 as a key player in USM plasticity mediated through the sex-related hormones. To investigate this hypothesis further, we examined the expression of SMTNL1 in the primary genital tissues selectively targeted by estrogen and progesterone. In non-pregnant uterus, SMTNL1 is expressed within myometrial cells of the uterus as well as in the endometrial layer, and by day 13 of pregnancy, expression is increased >10-fold in both cell types (Fig. 3, *A* and *B*). Non-pregnant mammary gland shows a low level of SMTNL1 expression, with staining being confined to alveolus cells lining the lumens of intralobular duct systems, but by day 13 of pregnancy, the protein is induced 8–14-fold (Fig. 3, *A* and *B*). As observed previously, the deletion of SMTNL1 does not appear to alter the ultrastructure of any tissues, either non-pregnant or pregnant, including uterus and mammary gland (12). Additionally, we observed a low level of SMTNL1 expression in the adrenal gland, but by day 13 of pregnancy, the protein is induced by 3–4-fold (Fig. 3*B*). The adrenal cortex is devoted to the synthesis of glucocorticoids, mineralocorticoids, and androgens, and specific cell types within the cortex are associated with the synthesis of each of these steroid hormones. Examination of circulating progesterone (*P*) and estradiol (*E*) levels in *smtnl1*$^{-/-}$ mice showed that SMTNL1 deletion produced a marginal 10–15% reduction in circulating estradiol and progesterone levels, suggesting a potential role in regulating steroid biosynthesis (Fig. 3, *C* and *D*).

The finding that SMTNL1 is discretely expressed within reproductive tissues, coupled with the microarray analysis, supports links between the protein and steroid hormone action. To more fully understand this relationship, we first investigated the expression of both ER and PR in the uterus. Pregnancy induced expression of both ERα and PR-B in USM (Fig. 4*A*). The expression of both proteins increased 3–4-fold in non-pregnant USM from *smtnl1*$^{-/-}$ mice and 8–9-fold in USM from pregnant *smtnl1*$^{-/-}$ mice (Fig. 4*A*). These data suggest a direct relationship between SMTNL1 expression levels and ER and PR expression. Next, we performed IP experiments from USM isolated from pregnant WT and *smtnl1*$^{-/-}$ mice. Fig. 4*B* shows that in both tissues SMTNL1 co-immunoprecipitated with PR-B but not ERα. As observed in Western blot experiments, IP of PR-B from USM extracts prepared from *smtnl1*$^{-/-}$ mice showed a large induction of the protein. Similarly, although IP with ERα antibody confirmed the presence of ERα and PR-B in the IP as expected, Western analysis with anti-SMTNL1 antibodies indicated that SMTNL1 does not bind directly to ERα *in vivo*. Although our data do not support direct interactions of SMTNL1 with ERα, its increased expression observed after IP and Western analysis from *smtnl1*$^{-/-}$ mice may reflect either disruption of the ability of PR to suppress expression of ERα at the transcriptional level or that the increased expression of PR-B, by binding to ERα, stabilizes the protein. This notion is supported in studies by Beato and co-workers (44, 45) demonstrating an interaction of PR-B with ERα in T47D cells. Although SMTNL1 does not bind ERα

Downloaded from www.jbc.org at Duke University, on September 11, 2011

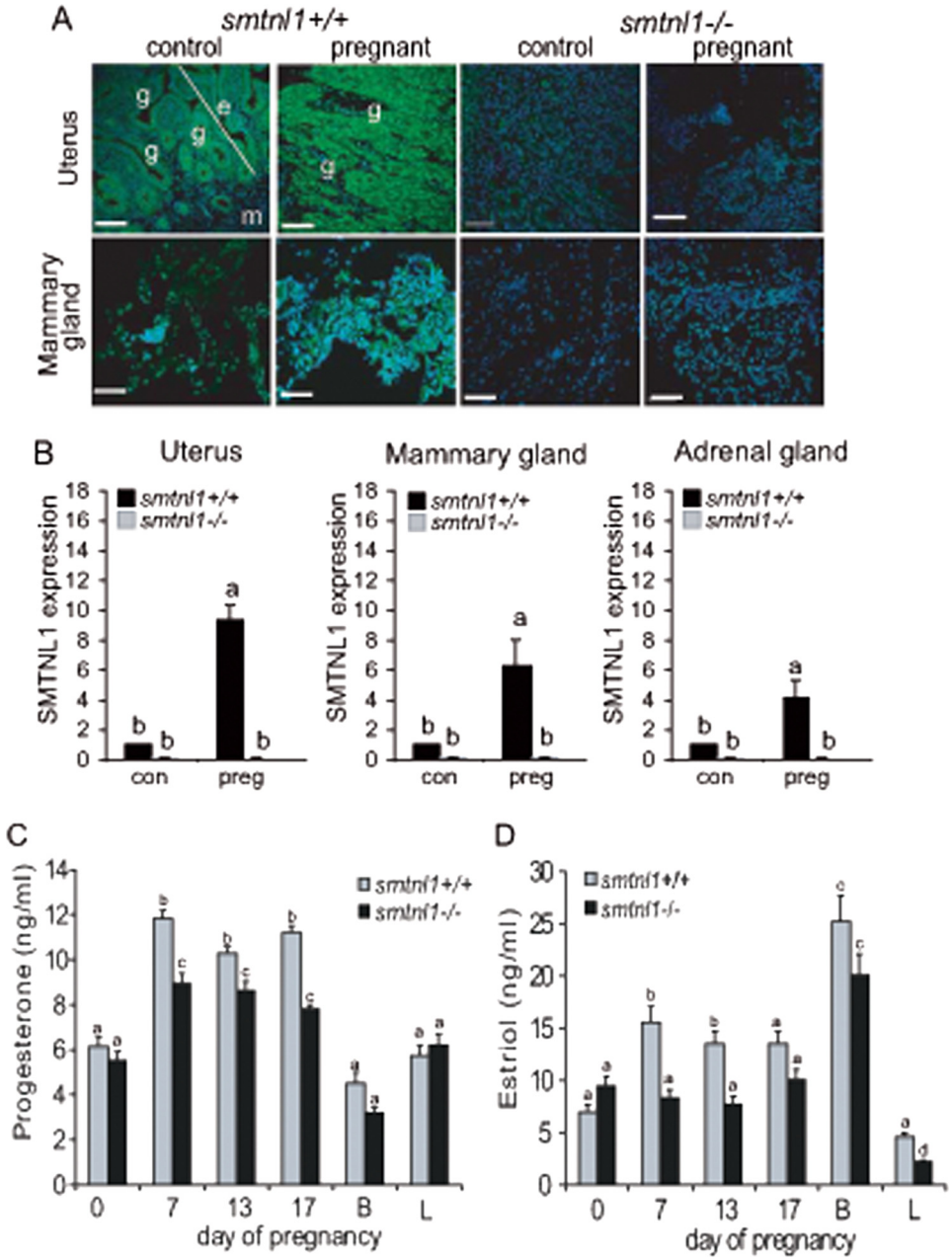


FIGURE 3. **Pregnancy regulates SMTNL1 expression in the primary genital tissues.** *A*, immunohistochemical images of SMTNL1 localization in uterus and mammary gland from control and pregnant WT and *smtnl1*$^{-/-}$ mice. *Scale bars*, 20 μm. *m*, myometrium; *e*, endometrium; *g*, endometrial glands in tunica propria of uterine mucosa. *B*, pregnancy induces significant expression of SMTNL1 relative to control (non-pregnant) in USM, mammary gland, and adrenal gland. *Insets below* show representative Western blots. Data shown are from day 0 and day 14 of pregnancy. *C* and *D*, circulating hormone concentrations of *smtnl1*$^{+/+}$ and *smtnl1*$^{-/-}$ mice during pregnancy. The circulating progesterone (*C*) and estriol (*D*) concentration is lower in *smtnl11*$^{-/-}$ mice in pregnancy. Results shown are means $\pm$ S.E. (*error bars*), $n = 4-6$ animals, general linear model with Tukey's test. *Different letters* indicate significant differences ($p < 0.05$).

directly, any effects on ER expression are likely to indirectly affect SMTNL1 expression through the feedback mechanisms between PR and ER. Next, we performed quantitative RT-PCR experiments from USM isolated from both pregnant and non-pregnant WT and *smtnl1*$^{-/-}$ mice to determine if the observed changes in PR-B could be seen at the transcriptional level. We chose a primer set directed at the sequence specific for PR-B. Fig. 4*C* shows that the mRNA levels of PR-B are up-regulated by more than 2-fold in pregnant *smtnl1*$^{-/-}$ mice when compared with WT pregnant mice. A slight, non-significant, increase in PR-B transcript was also observed in non-pregnant *smtnl1*$^{-/-}$ mice relative to the wild type non-pregnant mice (Fig. 4*C*). To further investigate the effect of SMTNL1 on the expression of PR-B *in vivo*, we developed several small interfering RNA (siRNA) constructs to knock down endogenous SMTNL1 expression. For these experiments, we chose the progestin-sensitive breast cancer cell line T47D due to the lack of well characterized USM cell lines expressing both proteins. Fig. 4*D* shows that R5020 induced the expression of both SMTNL1 and PR-B by 5–10-fold. Treatment of the cells with SMTNL1 siRNAs effectively suppresses the expression of SMTNL1 regardless of R5020 treatment. However, Western analysis of

Downloaded from www.jbc.org at Duke University, on September 11, 2011

tomtay : beata_285_24

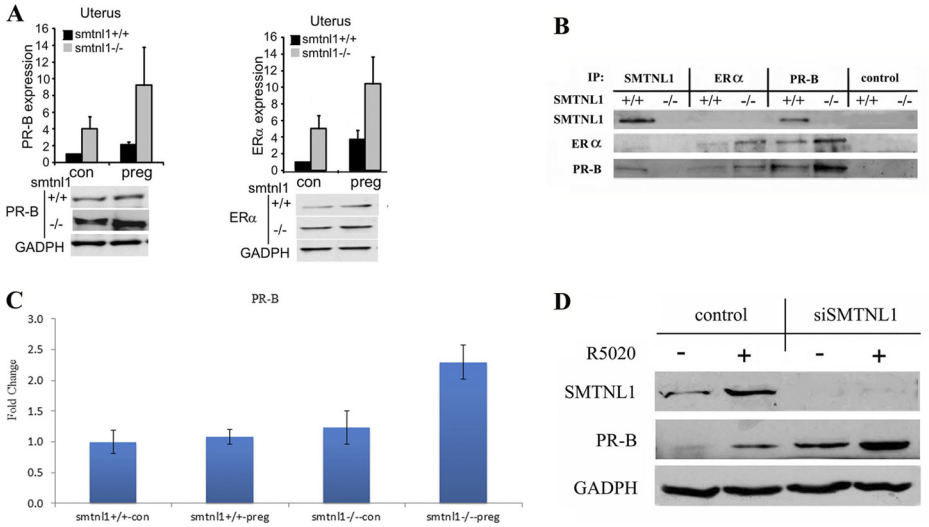


FIGURE 4. **SMTNL1 regulates the expression of ERα and PR-B in USM.** *A*, pregnancy and SMTNL1 deletion promote a higher expression of PR-B and ERα in USM. *Insets below* show representative Western blots. Data shown are from day 0 (*con.*) and day 14 of pregnancy (*preg.*). *B*, SMTNL1, PR-B, and ERα co-IP studies from uterine extracts of WT-P and *smtnl1*$^{-/-}$ pregnant. *C*, PR-B mRNA levels are up-regulated in the pregnant uteri of *smtnl1*$^{-/-}$ compared with WT mice. RT-PCR results of PR-B mRNA levels in USM from aged matched pregnant and non-pregnant WT and *smtnl*$^{-/-}$ mice, $n = 3 \pm$ S.E. (*error bars*). *D*, T47D cells were transfected with either siRNA control or siRNA directed against SMTNL1. Subsequently, cells were treated with the synthetic progestin R5020 (+) (1 nM) or ethanol (−) for 12 h, lysed, and analyzed by Western blot analysis using antibodies against SMTNL1 and PR-B.

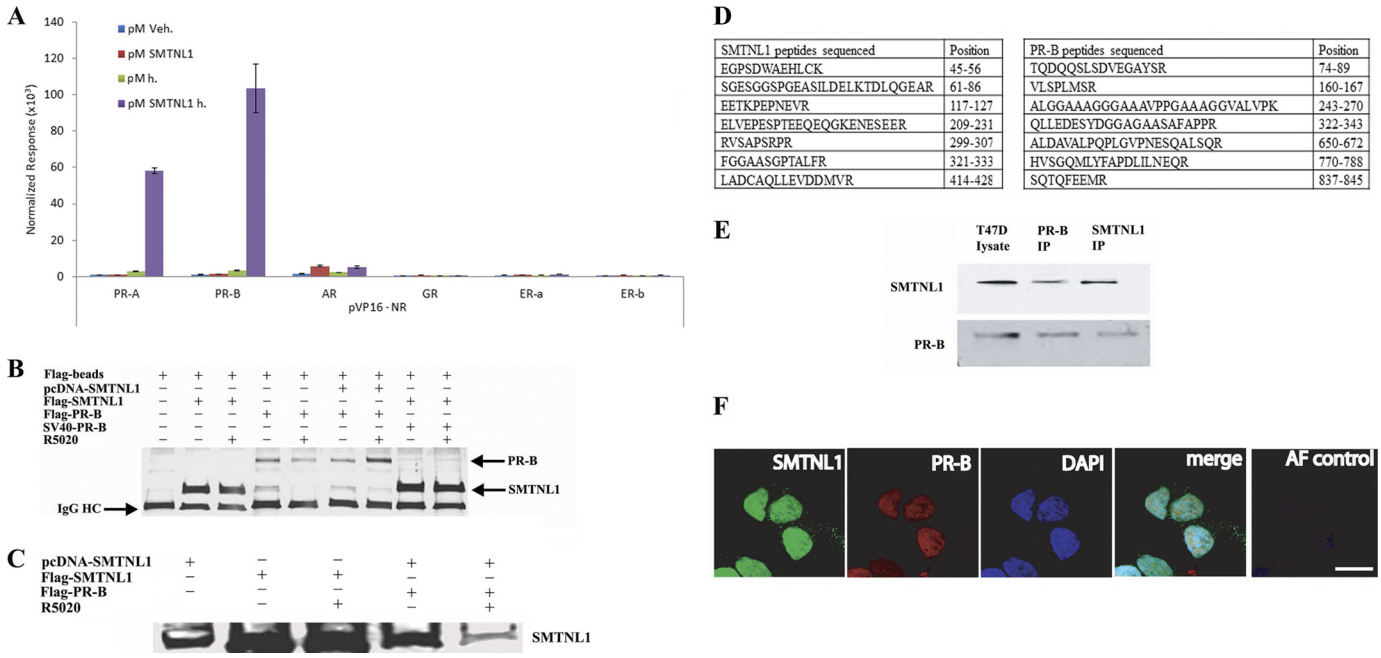
PR-B shows that SMTNL1 siRNAs dramatically induce the expression of the receptor ~10-fold above that induced by R5020 alone (Fig. 4*D*). Collectively, these data provide direct evidence that SMTNL1 directly regulates expression of PR-B *in vivo* and that the effects of SMTNL1 deletion on PR expression in *smtnl1*$^{-/-}$ mice are not the result of a nonspecific adaptive response to chronic deletion of the gene in these animals.

SMTNL1 Binds PR in Vivo and in Vitro—To determine the selectivity of SMTNL1 toward the major steroid hormone receptors (progesterone receptor-A and -B, estrogen receptor-α and -β, AR, and GR), we carried out mammalian two-hybrid analysis. SMTNL1 was fused to the C terminus of the GAL4 DNA binding domain in the pM vector, and each of the steroid receptors was fused downstream of the Gal4 activation domain in the VP16 vector. Interaction between SMTNL1 and the steroid receptors was assessed by measuring the ability of the plasmids to activate transcription from a luciferase reporter in the presence or absence of the corresponding hormones. Fig. 5*A* shows the remarkable degree of selectivity of SMTNL1 for PR-B and -A over AR, GR, ERα, and ERβ. Significantly, the interaction between SMTNL1 and both isoforms of PR is hormone-dependent. In the presence of R5020, reporter activity showed that SMTNL1 has much higher binding preference to the PR-B isoform when compared with PR-A. In contrast, SMTNL1 did not show any significant interaction with ERα, ERβ in the presence, or GR. A small, non-hormone-dependent interaction was observed between SMTNL and AR. In comparative experiments, binding of SMTNL1 to PR-B and PR-A compares favorably with the well defined co-activator steroid receptor co-activator-1 (SRC-1) NR box peptide (supplemental Fig. 1). However, unlike SMTNL1, SRC1-NR box does not discriminate between the steroid hormone receptors and binds to ERα as shown previously (46, 47). Three proteins (SRC-1, -2, and -3) have been identified in the p160 steroid hormone co-activator family, and each contains a short conserved NR interaction motif (NR box), which has the core sequence L*XX*LL (48–50). SMTNL1 is therefore discriminated from all other known steroid receptor-binding proteins in that it shows an exquisite degree of selectivity for PR-A and -B only. Additionally, SMTNL1 does not contain L*XX*LL motifs, suggesting that the protein interacts with PR at other sites and may have other functions. The finding that SMTNL1 only interacts with PR-B and A and not with either isoform of ER in two-hybrid and co-IP experiments suggests that the mechanisms of altered ER expression observed *in vivo* are likely to be mediated through PR via a feedback mechanism. Both estrogen and progesterone are known to regulate the expression of their corresponding receptors at the transcriptional level.

To further validate the observed *in vivo* interactions between SMTNL1 and PR-B, 293T cells were transfected with expression vectors for FLAG-SMTNL1 and SV40-PR-B, and cell lysates were precipitated with FLAG beads. The FLAG-SMTNL1 was able to co-immunoprecipitate SMTNL1 and PR-B (Fig. 5*B*). Likewise, when cells were transfected with expression vectors for FLAG-PR-B and pCDNA-SMTNL1, the FLAG beads were able to immunoprecipitate both FLAG-PR-B and SMTNL1 (Fig. 5*C*), and the presence of SMTNL1 was confirmed by Western blotting (Fig. 5*C*). Mass spectrometry studies confirmed the identity of the bands seen in the IP experiments (Fig. 5*D*). Additionally, endogenous SMTNL1 was found to co-IP with endogenous PR-B in T47D cell lysates as shown in Fig. 4*E*. Finally, co-localization of SMTNL1 and PR-B was observed by immunofluorescent staining in T47D cells showing discrete nuclear localization for both proteins (Fig. 5*F*).

Mapping the Interaction Sites between SMTNL1 and PR-B—Mammalian two-hybrid experiments were carried out to determine the regions(s) involved in interaction between SMTNL1 and PR-B. In the case of SMTNL1, aside from the calponin homology domain, the protein has no defined domains and is quite unique with no sequence similarities to known proteins in

Downloaded from www.jbc.org at Duke University, on September 11, 2011



SMTNL1 peptides sequenced	Position
EGPSDWAEHLCK	45-56
SGESGGSPGEASILDELKTDLQGEAR	61-86
EETKPEPNEVR	117-127
ELVEPESPTEEQEQGKENESEER	209-231
RVSAPSRPR	299-307
FGGAASGPTALFR	321-333
LADCAQLLEVDDMVR	414-428

PR-B peptides sequenced	Position
TQDQQSLSDVEGAYSR	74-89
VLSPLMSR	160-167
ALGGAAAGGGAAAVPPGAAAGGVALVPK	243-270
QLLEDESYDGGAGAASAFAPPR	322-343
ALDAVALPQPLGVPNESQALSQR	650-672
HVSGQMLYFAPDLILNEQR	770-788
SQTQFEEMR	837-845

FIGURE 5. **SMTNL1 binds PR *in vivo* and *in vitro*.** *A*, HepG2 cells were transfected with the indicated constructs. After 24 h, cells were treated with different receptor ligands as indicated and subsequently harvested for luciferase and β-gal assays. *B*, 293T cells were transfected with the indicated expression vectors. After 48 h, the culture medium was replaced with or without 10 nM R5020 for 2 h. Lysates were immunoprecipitated using FLAG beads and processed for SDS-PAGE and silver stain. *C*, IPs were subjected to the same treatment as in *B* and then probed with an antibody against SMTNL1. *D*, designated bands (SMTNL1 and PR-B) were excised and processed for mass spectrometry. Peptide sequences and their position in each protein are shown. *E*, T47D cells were lysed and lysates were incubated with SMTNL1 or PR antibodies and immunoprecipitated with protein A-Sepharose. IPs were Western blotted with SMTNL1 and PR antibodies. *F*, nuclear co-localization (*merge*, *white*) of endogenous SMTNL1 (*green*) and PR (*red*) in T47D cells. *Scale bars*, 10 μm. *Error bars*, S.E.

the database. Our approach was to create small blocks of the protein and test them for their ability to bind PR-B. Accordingly, we created several truncated pieces of SMTNL1 namely, amino acids 1–50, 1–60, 1–90, 1–150, 1–200, 1–230, and 1–345. All constructs were fused to the C terminus of the GAL4 DNA binding domain in the pM vector, sequenced, and expression-validated. Fig. 6*A* show that the first 60 amino acids of SMTNL1 are dispensable for PR-B binding, whereas amino acids between 60 and 90 are capable of restoring full binding capacity when compared with the full-length protein. No significant increase in binding was observed when additional amino acids were used; however, a significant increase in binding was observed with the 1–230 construct, indicating that amino acids 200–230 of SMTNL1 are capable of interacting with PR-B (Fig. 6*A*). Taken together, the results indicate that amino acids 60–90 and amino acids 200–230 are required for SMTNL1 interaction with PR-B, with the latter exhibiting a robust binding capacity when compared with the full-length protein. Furthermore, the results indicate that the calponin homology domain, as expected, does not play a role in mediating the interaction between the two proteins.

Next, we carried out mammalian two-hybrid experiments to determine regions of PR-B necessary for its interaction with SMTNL1. The PR-B constructs employed in the assay include the N-terminal construct (amino acids 1–555), amino acids 306–456, amino acids 456–687, amino acids 680–933, the C587A transcriptional incompetent mutant, the mutant Pro construct, the G722C mutant, the AF2 mutant (E907A/E911A), and the 1–922 construct (*i.e.* marks the end of the hormone binding domain). All constructs were fused downstream of the Gal4 activation domain in the VP16 vector, sequenced, and expression-validated. Fig. 6*B* shows that the C587A mutant abolished the interaction with SMTNL1 completely. This construct of PR-B has a point mutation in the first zinc finger of the DNA binding domain, and it disrupts the ability of PR to function as a transcription factor. When the AF2 mutant was tested, the level of the reporter activity generated was significantly reduced compared with that of the wild-type PR-B, confirming the hormone dependence of the interaction between the two proteins (Fig. 6*B*). The 1–922 construct was still capable of binding to SMTNL1, but the reporter level activity was reduced compared with that of the full-length PR-B (Fig. 6*B*). The PR-B mPro mutant showed reduced binding when compared with that of the wild type protein (Fig. 6*B*). This construct has three essential prolines (Pro-422, Pro-423, and Pro-426) changed to alanines, which results in the loss of binding to the Src homology 3 domains of signaling proteins. The G722C mutant (the 722 construct) was found to bind SMTNL1 with levels comparable with those of the wild type protein (Fig. 6*B*). This mutant generates a receptor that has lost detectable RU486 binding but retains wild-type binding affinity for progestin agonists (51, 52). The fact that SMTNL1 and PR-B are hormone-dependent prompted us to examine if the hormone binding domain of PR-B by itself is sufficient to bind SMTNL1. Fig. 6*B* shows that this is not the case, pointing to additional amino acids upstream that are required for mediating the interaction between the two proteins. Finally, as expected from the hormone dependence of the interaction, constructs missing the ligand binding domain did not show any reporter activity (Fig. 6*B*). Comparative experiments with the co-activator SRC1-NR box are shown in supplemental Fig. 2. Next, we used the mammalian two-hybrid system to examine the effects of anti-progestins (RU486 and

Downloaded from www.jbc.org at Duke University, on September 11, 2011

tomtay : beata_285_24

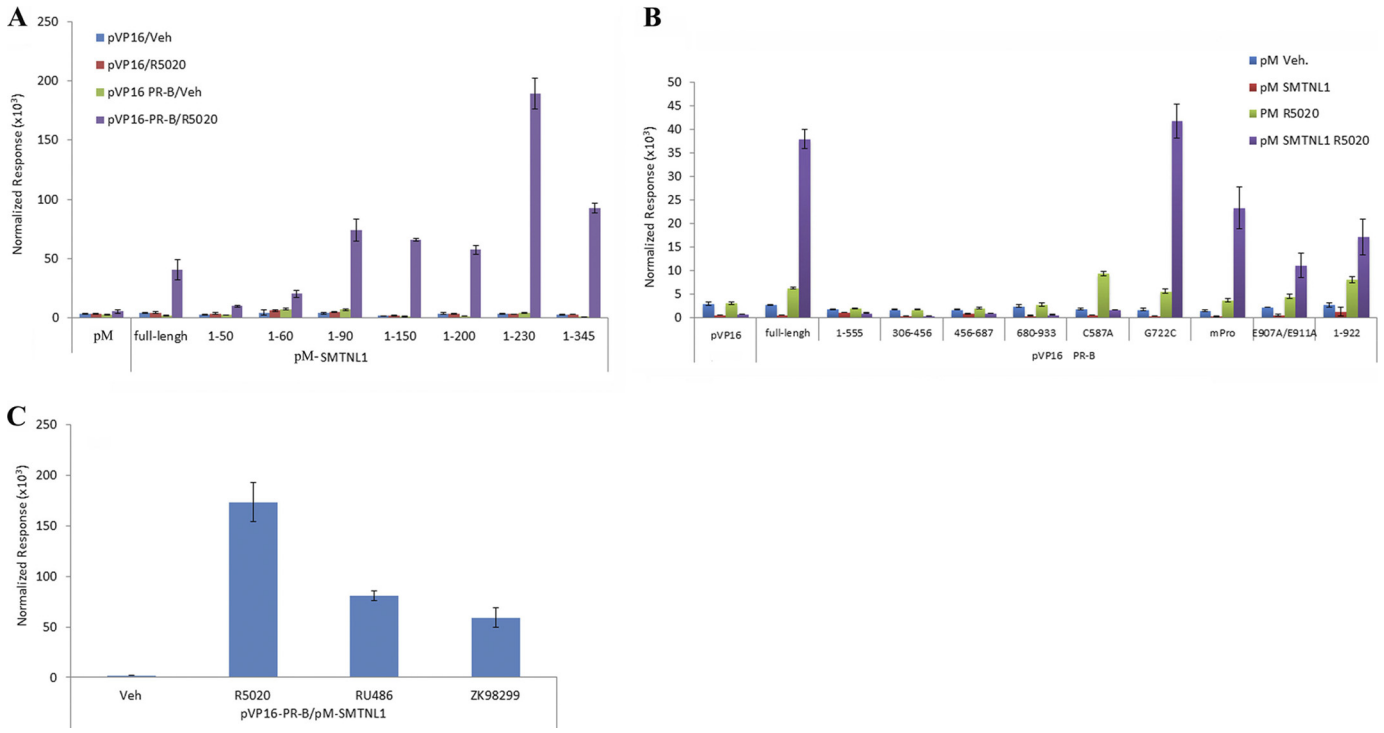


FIGURE 6. **Identification of interaction sites within SMTNL1 and PR-B.** *A*, HepG2 cells were transfected with the indicated SMTNL1 deletion constructs together with PR-B. *B*, HepG2 cells were transfected with the indicated PR-B deletion constructs and mutants together with SMTNL1. In both *A* and *B*, 24 h after, the cells were incubated with vehicle or 10 nM R5020 for 24 h and then harvested for luciferase and β-gal assays. *C*, effects of anti-progestins on SMTNL1-PR-B interaction. After transfection, the cells were incubated with vehicle (*Veh*) or 10 nM R5020, 100 nM RU486, and 100 nM ZK98299 for 24 h and harvested for luciferase and β-gal assays. *Error bars*, S.E.

ZK98299) on the interaction between SMTNL1 and PR-B. Treating the cells with anti-progestins resulted in significant reduction in the luciferase activity when compared with R5020, as shown in Fig. 6*C*. The significant reduction in the interaction of SMTNL1 with PR-B in the presence of anti-progestins suggested that binding between the two proteins is a function of the conformational changes in PR-B and further validates the hormone dependence of the interaction.

SMTNL1 Is a Transcriptional Co-regulator of PR-B Function—The significance of the interaction between SMTNL1 and PR-B was next investigated in the context of progesterone-responsive promoters and PKA-mediated signaling. SMTNL1 is phosphorylated at Ser-301 in smooth muscle cells in response to 8-Br-cAMP, resulting in translocation of the protein to the nucleus, an effect blocked by S301A substitution (11). Activators of PKA are also known to affect the transcriptional activity of PR-B (53, 54). Fig. 7*A* shows that treatment of HeLa cells, transfected with an expression vector for PR-B and MMTV-luciferase reporter plasmid, with increasing amounts of 8-Br-cAMP plus R5020 increases the transcriptional activity of PR-B in a dose-dependent manner. This assay helped us to determine the conditions for analyzing the effect of SMTNL1 on PR-B transcriptional activity at any given [8-Br-cAMP]. Thus, HeLa cells were transfected with PR-B expression vector alone or with increasing amounts of SMTNL1 expression vector together with the MMTV-luciferase reporter in the presence and/or absence of R5020 and 8-Br-cAMP. Fig. 7*B* shows that SMTNL1 inhibits PR-B transactivation in a dose-dependent manner (*i.e.* 300 ng of SMTNL1 causes a more than 50% reduction in transcriptional activity). This effect correlates precisely with 8-Br-cAMP concentrations (10 μM) required to promote nuclear translocation of SMTNL1 through Ser-301 phosphorylation (11). Increasing amounts of transfected SMTNL1 were also found to progressively repress endogenous PR-B activity by 20–30% in T47D cells (Fig. 7*C*). Taken together, these findings suggest that SMTNL1 functions as a repressor of the transcriptional activity of PR *in vivo*.

As discussed earlier, progesterone promotes USM relaxation during pregnancy by repressing the expression of specific genes encoding CAPs (55). Specifically, PR inhibits the expression of key CAPs, including oxytocin receptor, Cnx-43, and cyclooxygense-2 (21–29). Therefore, if SMTNL1 represses PR, one might predict that loss of this function in *smtnl1*$^{-/-}$ mice would lead to altered expression of PR-regulated genes. Fig. 7*D* shows that this is indeed the case. Quantitative RT-PCR studies show that mRNAs for oxytocin receptor, Cnx-43, and cyclooxygense-2 were all decreased markedly in the KO-P mice compared with their WT-P counterparts (Fig. 7*D*). These findings support SMTNL1 as a novel co-regulator of PR-B transcriptional activity in USM.

DISCUSSION

In the present study, we show that SMTNL1 plays a key role in pregnancy to promote adaptive responses in USM and that this process is mediated through interactions of SMTNL1 with the progesterone receptor PR-B. Both *in vitro* and *in vivo*, SMTNL1 specifically binds to the progesterone receptor and not other steroid hormone receptors, discriminating the protein from all other known co-regulators of this class of nuclear receptors. Both SMTNL1 and PR exhibit co-regulation of

Downloaded from www.jbc.org at Duke University, on September 11, 2011

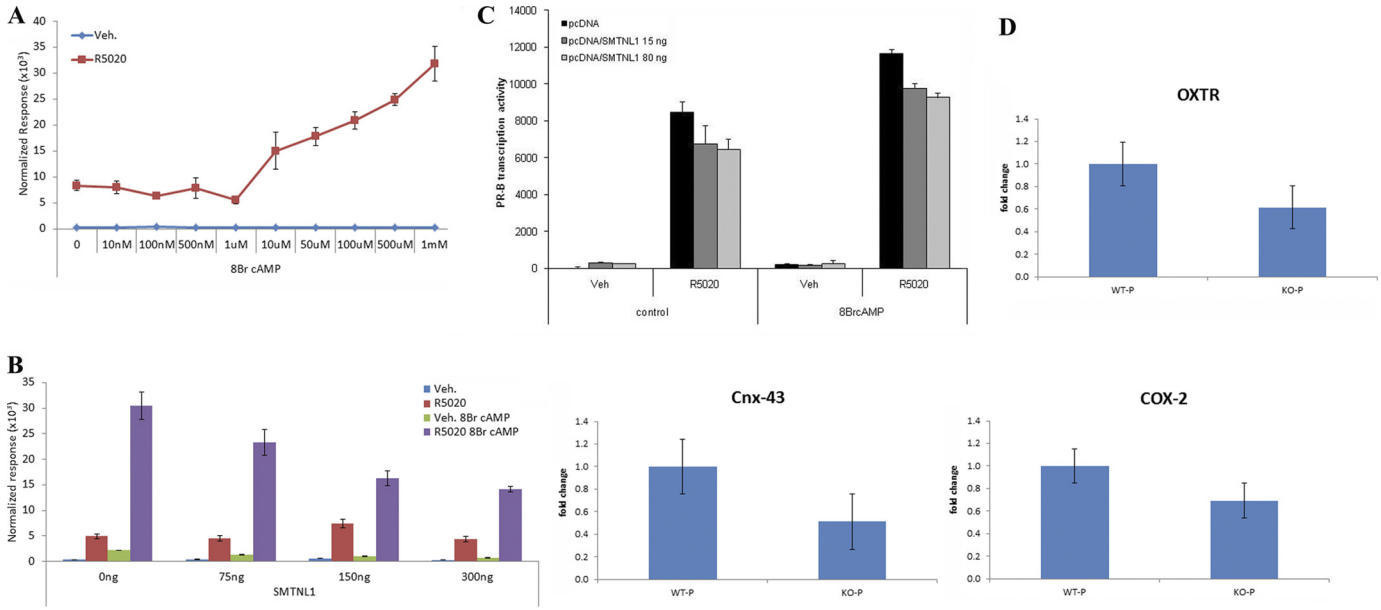


FIGURE 7. **SMTNL1 regulates PR-B expression at the transcriptional level.** *A*, effect of cAMP on the transcriptional activity of PR-B. HeLa cells were transfected with an expression vector for PR-B and an MMTV-luciferase reporter plasmid. After transfection, cells were incubated with vehicle or 10 nM R5020 in the presence of 8-Br-cAMP (10 nM to 1 mM) for 24 h and harvested for luciferase and β-gal assays. *B*, effect of SMTNL1 on PR-B transcriptional activity. HeLa cells were transfected with PR-B expression vector without (0 ng) or with increasing concentrations (75, 150, and 300 ng) of SMTNL1 expression vector together with the MMTV-luciferase reporter plasmid. The following day, cells were incubated with vehicle or 10 nM R5020 for 24 h and subsequently harvested for luciferase and β-gal assays. *C*, SMTNL1 was transfected into T47D, and the effects of increasing amounts of SMTNL1 (15 and 80 ng) on PR-B transcriptional activity with or without R5020 and with or without 10 μM 8-Br-cAMP were measured. *D*, RT-PCR analysis of oxytocin receptor (*OXTR*), Cnx-43, and cyclooxygense-2 in wild type pregnant (*WT-P*) and *smtnl1*$^{-/-}$ pregnant (*KO-P*) mouse uteri, $n = 3$ RNA sets ± S.E. (*error bars*).

expression during normal pregnancy, and there is a significant increase in PR expression at the protein level in *smtnl1*$^{-/-}$ mice in both reproductive and non-reproductive tissues. Additionally, PR expression is significantly induced in response to RNA interference of SMTNL1 in progesterone-sensitive cell lines. These observations therefore show a direct role for SMTNL1 in regulating the expression of PR itself. Additionally, transcriptional reporter assays and global gene expression analysis suggest a mechanism of action in which SMTNL1 functions as a co-regulator of PR-B transcriptional activity to regulate gene expression in reproductive tissues underlying the physiological relationship between the two proteins. Consistent with this role, quantitative RT-PCR studies of several known CAPs regulated by PR-B were greatly suppressed in USM from *smtnl1*$^{-/-}$ mice. Global gene analysis also showed that a primary target of SMTNL1 are prolactins, a well defined group of genes governing both pregnancy and lactation that are also involved in progesterone production in the late stages of pregnancy. All prolactin genes were greatly suppressed in global gene expression of tissues from *smtnl1*$^{-/-}$ mice, and these findings were also confirmed in RT-PCR studies. Clearly, our findings define SMTNL1 as a homeostatic regulator of PR function during pregnancy. Fig. 8 outlines three potential modes of action that are currently under investigation.

Our hypothesis that SMTNL1 functions as a co-regulator of PR-B stems from several lines of evidence. First, IP and Western assays of PR-B from *smtnl1*$^{-/-}$ pregnant mouse USM extracts showed a significant increase in the induction of the protein in comparison with the WT extracts. This increase is also evident at the transcript level; quantitative RT-PCR data showed a 2–3-fold up-regulation of PR-B mRNA levels in pregnant *smtnl1*$^{-/-}$ mice when compared with their WT pregnant littermates. Second, in reporter assays, SMTNL1 was found to inhibit PR-B transcriptional activation in a dose-dependent manner, and the effect was shown to be independent of cell and promoter context, ruling out the involvement of transcriptional interference. Finally, the necessity for a functional DBD and AF2 for SMTNL1 binding puts the protein at the core of PR transactivation, given the fact the primary role of the DBD is to bind to specific DNA target sequences within the promoter of responsive genes and the established functions of AF2 as a mediator of hormone-dependent transcriptional activation. It is intriguing to think that the reduction of PR-B transcription by SMTNL1 is due to the formation of an inhibitory complex that is either unable to bind DNA or is incapable of binding to the transcription machinery. Future studies will test this hypothesis by electrophoretic mobility shift and CHIP assays. Additionally, SMTNL1 phosphorylation could play a role in mediating its effects on PR-B because the S301A SMTNL1 blocks entry into the nucleus (11). Furthermore, reduction of PR-B transcriptional activity was only detected when cells were treated with PKA activators (53, 54). If SMTNL1 acts as a transcriptional co-regulator of PR *in vivo* inhibiting its function, phosphorylation of one or more sites may be similar to deleting the protein, as observed in *smtnl1*$^{-/-}$ female mice. Such a mechanism of action may imply that the default function for SMTNL1 in non-pregnant animals is to repress PR function from promoting pregnancy-like adaptive responses in USM. The observed repression of key CAPs in *smtnl1*$^{-/-}$ pregnant mice is consistent with such role. The molecular mechanism(s) by which SMTNL1 deletion promotes an increase in the transcriptional activity of PR-B *in vivo* is currently under further investigation.

Downloaded from www.jbc.org at Duke University, on September 11, 2011

tomtay : beata_285_24

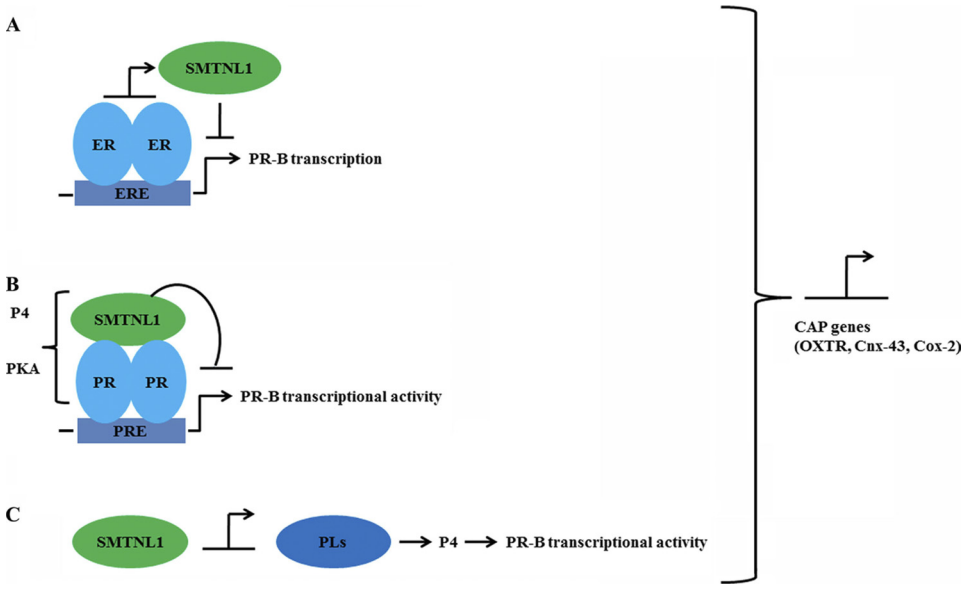


FIGURE 8. **Mechanisms by which SMTNL1 regulates PR-B to coordinately promote USM adaptations in pregnancy.** *Schematics A* and *B* show that regulation of expression of SMTNL1, PR, and ER is via two possible homeostatic feedback mechanisms. In *A*, the synthesis of PR is controlled by estrogen acting through ER. Progesterone (*P4*) abrogates estrogen induction by down-regulating ER protein concentration, decreasing circulating estrogen levels, and antagonizing ER action at the molecular level. ER may also have a direct effect on SMTNL1 transcription, a hypothesis supported by the presence of ER binding sites in the promoter region of *smtnl1*. In *B*, SMTNL1 directly and specifically binds PR-B, in a hormone-dependant manner and suppresses its transcriptional activity. A likely means by which SMTNL1 regulates PR-B is via PKA-mediated phosphorylation. Both proteins have multiple *in vivo* phosphorylation sites, and at least one of these sites, Ser-301, has the potential to affect SMTNL1 entry into the nucleus. Therefore, by phosphorylating SMTNL1, it may be possible to activate or inhibit its effects on PR function. In *C*, SMTNL1 also functions as an activator of the expression and/or release of a subset of the PRL family members (*i.e.* placental lactogens) that are involved in progesterone production in late pregnancy and thus regulating PR transcriptional activity. Taken together, we suggest that regulation of PR by SMTNL1 provides a molecular mechanism whereby PR is directed to alter gene expression patterns within USM (*i.e.* CAPs) to coordinately promote alterations in USM function during pregnancy. ⊥(inhibition) → (gene transcription).

In specific pathway analysis related to progesterone and pregnancy, most notable was the effect of SMTNL1 deletion on the PRL family members. All members of this family with observed expression on the array were found to be down-regulated in the *smtnl1*$^{-/-}$ pregnant mice. In rodents, PRLs are a large family of proteins that share extensive structural and functional homology and are synthesized in all reproductive tissues in a temporal manner (56, 57). Members of the PRL family are associated with an array of functions; however, their involvement in reproduction has received the most attention (58). Studies of *PRL*$^{-/-}$ and *PLR-R*$^{-/-}$ mice result in complete infertility in females due to failure of implantation (59, 60). These mice show a lack of functional corpus luteum and thus were unable to produce progesterone. The corpus luteum plays a central role in the maintenance of pregnancy through regulating the production of progesterone (61). In rodents, the functions of the corpus luteum are sustained throughout pregnancy by coordinating the secretion of PRLs (56, 62). The deregulation of the PRLs in *smtnl1*$^{-/-}$ pregnant mice is very interesting given our observations that deletion of SMTNL1 is associated with a slight reduction in the levels of progesterone in late pregnancy. Taken together, our results highlight a previously unrecognized role for SMTNL1 as an activator of the expression and/or release of a subset of the PRL family members during late pregnancy. Future studies will focus on elucidating the mechanism(s) of SMTNL1 activation of PRLs and their effect on progesterone production using a culture system of luteal cells from WT and *smtnl1*$^{-/-}$ pregnant mice.

Finally, analysis of an *smtnl1*$^{-/-}$ mouse breeding data base showed that the loss of SMTNL1 results in smaller litter sizes and higher embryonic lethality. Additionally, we observed that time to pregnancy was longer in *smtnl1*$^{-/-}$ mice. Collectively, our data indicate that loss of SMTNL1 results in a phenotype of lower overall reproductive fitness as a physiological effect. These phenotypic effects are distinct from those observed in PR null mice. PR-A null mice developed signs of uterine dysplasia and abnormal ovaries resulting in female infertility, whereas PR-B null mice did not show any uterine abnormalities but exhibited signs of mammary gland malformations (63–66). The differences between *smtnl1*$^{-/-}$ mice and the severity of the PR null phenotype further support the hypothesis that SMTNL1 functions to affect a subset of PR genes.

REFERENCES

1. Shynlova, O., Tsui, P., Dorogin, A., Langille, B. L., and Lye, S. J. (2007) *Biol. Reprod.* **76,** 571–578
2. Shynlova, O., Tsui, P., Jaffer, S., and Lye, S. J. (2009) *Eur. J. Obstet. Gynecol. Reprod. Biol.* **144,** Suppl. 1, S2–S10
3. Jaffer, S., Shynlova, O., and Lye, S. (2009) *Endocrinology* **150,** 4672–4680
4. Shynlova, O., Oldenhof, A., Dorogin, A., Xu, Q., Mu, J., Nashman, N., and Lye, S. J. (2006) *Biol. Reprod.* **74,** 839–849
5. Goldenberg, R. L. (2002) *Obstet. Gynecol.* **100,** 1020–1037
6. Ward, R. M., and Beachy, J. C. (2003) *BJOG* **110,** Suppl. 20, 8–16
7. Matsumura, F., and Hartshorne, D. J. (2008) *Biochem. Biophys. Res. Commun.* **369,** 149–156
8. Somlyo, A. V. (2007) *Circ. Res.* **101,** 645–647
9. Borman, M. A., MacDonald, J. A., and Haystead, T. A. (2004) *FEBS Lett.* **573,** 207–213
10. Ishida, H., Borman, M. A., Ostrander, J., Vogel, H. J., and MacDonald, J. A. (2008) *J. Biol. Chem.* **283,** 20569–20578
11. Lontay, B., Bodoor, K., Weitzel, D. H., Loiselle, D., Fortner, C., Lengyel, S., Zheng, D., Devente, J., Hickner, R., and Haystead, T. A. (2010) *J. Biol. Chem.* **285,** 29357–29366

Downloaded from www.jbc.org at Duke University, on September 11, 2011

12. Wooldridge, A. A., Fortner, C. N., Lontay, B., Akimoto, T., Neppl, R. L., Facemire, C., Datto, M. B., Kwon, A., McCook, E., Li, P., Wang, S., Thresher, R. J., Miller, S. E., Perriard, J. C., Gavin, T. P., Hickner, R. C., Coffman, T. M., Somlyo, A. V., Yan, Z., and Haystead, T. A. (2008) *J. Biol. Chem.* **283,** 11850–11859
13. Ulke-Lemée, A., Turner, S. R., Mughal, S. H., Borman, M. A., Winkfein, R. J., and MacDonald, J. A. (2011) *BMC Mol. Biol.* **12,** 10
14. Challis, J. R., and Lye, S. J. (1986) *Oxf. Rev. Reprod. Biol.* **8,** 61–129
15. Mesiano, S., and Welsh, T. N. (2007) *Semin. Cell Dev. Biol.* **18,** 321–331
16. Mesiano, S., Wang, Y., and Norwitz, E. R. (2011) *Reprod. Sci.* **18,** 6–19
17. Beato, M., Herrlich, P., and Schütz, G. (1995) *Cell* **83,** 851–857
18. Edwards, D. P. (2005) *Annu. Rev. Physiol.* **67,** 335–376
19. Giangrande, P. H., and McDonnell, D. P. (1999) *Recent Prog. Horm. Res.* **54,** 291–313
20. Kastner, P., Krust, A., Turcotte, B., Stropp, U., Tora, L., Gronemeyer, H., and Chambon, P. (1990) *EMBO J.* **9,** 1603–1614
21. Brodt-Eppley, J., and Myatt, L. (1998) *Biol. Reprod.* **59,** 878–883
22. Dong, Y. L., and Yallampalli, C. (2000) *Biol. Reprod.* **62,** 533–539
23. Fang, X., Wong, S., and Mitchell, B. F. (1997) *Endocrinology* **138,** 2763–2768
24. Hendrix, E. M., Myatt, L., Sellers, S., Russell, P. T., and Larsen, W. J. (1995) *Biol. Reprod.* **52,** 547–560
25. Ou, C. W., Chen, Z. Q., Qi, S., and Lye, S. J. (2000) *Am. J. Obstet. Gynecol.* **182,** 919–925
26. Allport, V. C., Pieber, D., Slater, D. M., Newton, R., White, J. O., and Bennett, P. R. (2001) *Mol. Hum. Reprod.* **7,** 581–586
27. Patel, F. A., Funder, J. W., and Challis, J. R. (2003) *J. Clin. Endocrinol. Metab.* **88,** 2922–2933
28. Roizen, J. D., Asada, M., Tong, M., Tai, H. H., and Muglia, L. J. (2008) *Mol. Endocrinol.* **22,** 105–112
29. Tsuboi, K., Sugimoto, Y., Iwane, A., Yamamoto, K., Yamamoto, S., and Ichikawa, A. (2000) *Endocrinology* **141,** 315–324
30. Zhao, K., Kuperman, L., Geimonen, E., and Andersen, J. (1996) *Biol. Reprod.* **54,** 607–615
31. Merlino, A. A., Welsh, T. N., Tan, H., Yi, L. J., Cannon, V., Mercer, B. M., and Mesiano, S. (2007) *J. Clin. Endocrinol. Metab.* **92,** 1927–1933
32. Mesiano, S., Chan, E. C., Fitter, J. T., Kwek, K., Yeo, G., and Smith, R. (2002) *J. Clin. Endocrinol. Metab.* **87,** 2924–2930
33. Condon, J. C., Jeyasuria, P., Faust, J. M., Wilson, J. W., and Mendelson, C. R. (2003) *Proc. Natl. Acad. Sci. U.S.A.* **100,** 9518–9523
34. Dong, X., Shylnova, O., Challis, J. R., and Lye, S. J. (2005) *J. Biol. Chem.* **280,** 13329–13340
35. Dong, X., Yu, C., Shynlova, O., Challis, J. R., Rennie, P. S., and Lye, S. J. (2009) *Mol. Endocrinol.* **23,** 1147–1160
36. Leite, R. S., Brown, A. G., and Strauss, J. F., 3rd (2004) *FASEB J.* **18,** 1418–1420
37. Renthal, N. E., Chen, C. C., Williams, K. C., Gerard, R. D., Prange-Kiel, J., and Mendelson, C. R. (2010) *Proc. Natl. Acad. Sci. U.S.A.* **107,** 20828–20833
38. Fritzsche, B., Vermot, J., Neumann, U., Schmidt, A., Schweigert, F. J., Dollé, P., and Rühl, R. (2007) *Mol. Reprod. Dev.* **74,** 258–264
39. Han, B. C., Xia, H. F., Sun, J., Yang, Y., and Peng, J. P. (2010) *J. Cell. Physiol.* **223,** 471–479
40. Xia, H. F., Ma, J. J., Sun, J., Yang, Y., and Peng, J. P. (2010) *Hum. Reprod.* **25,** 2985–2998
41. Kim, J., Kang, S. G., Kim, J. I., Park, J. H., Kim, S. K., Cho, D. J., and Kim, H. (2006) *Yonsei Med. J.* **47,** 558–567
42. Richards, J. S., Hernandez-Gonzalez, I., Gonzalez-Robayna, I., Teuling, E., Lo, Y., Boerboom, D., Falender, A. E., Doyle, K. H., LeBaron, R. G., Thompson, V., and Sandy, J. D. (2005) *Biol. Reprod.* **72,** 1241–1255
43. Alemán, G., Ortíz, V., Langley, E., Tovar, A. R., and Torres, N. (2005) *Am. J. Physiol. Endocrinol. Metab.* **289,** E172–E179
44. Ballaré, C., Uhrig, M., Bechtold, T., Sancho, E., Di Domenico, M., Migliaccio, A., Auricchio, F., and Beato, M. (2003) *Mol. Cell. Biol.* **23,** 1994–2008
45. Migliaccio, A., Piccolo, D., Castoria, G., Di Domenico, M., Bilancio, A., Lombardi, M., Gong, W., Beato, M., and Auricchio, F. (1998) *EMBO J.* **17,** 2008–2018
46. Boonyaratanakornkit, V., Scott, M. P., Ribon, V., Sherman, L., Anderson, S. M., Maller, J. L., Miller, W. T., and Edwards, D. P. (2001) *Mol. Cell* **8,** 269–280
47. Giangrande, P. H., Kimbrel, E. A., Edwards, D. P., and McDonnell, D. P. (2000) *Mol. Cell. Biol.* **20,** 3102–3115
48. Heery, D. M., Kalkhoven, E., Hoare, S., and Parker, M. G. (1997) *Nature* **387,** 733–736
49. Onate, S. A., Boonyaratanakornkit, V., Spencer, T. E., Tsai, S. Y., Tsai, M. J., Edwards, D. P., and O'Malley, B. W. (1998) *J. Biol. Chem.* **273,** 12101–12108
50. Plevin, M. J., Mills, M. M., and Ikura, M. (2005) *Trends Biochem. Sci.* **30,** 66–69
51. Vegeto, E., Allan, G. F., Schrader, W. T., Tsai, M. J., McDonnell, D. P., and O'Malley, B. W. (1992) *Cell* **69,** 703–713
52. Xu, J., Nawaz, Z., Tsai, S. Y., Tsai, M. J., and O'Malley, B. W. (1996) *Proc. Natl. Acad. Sci. U.S.A.* **93,** 12195–12199
53. Rowan, B. G., Garrison, N., Weigel, N. L., and O'Malley, B. W. (2000) *Mol. Cell. Biol.* **20,** 8720–8730
54. Weigel, N. L., Bai, W., Zhang, Y., Beck, C. A., Edwards, D. P., and Poletti, A. (1995) *J. Steroid Biochem. Mol. Biol.* **53,** 509–514
55. Smith, R. (2007) *N. Engl. J. Med.* **356,** 271–283
56. Ben-Jonathan, N., Mershon, J. L., Allen, D. L., and Steinmetz, R. W. (1996) *Endocr. Rev.* **17,** 639–669
57. Soares, M. J. (2004) *Reprod. Biol. Endocrinol.* **2,** 51
58. Bole-Feysot, C., Goffin, V., Edery, M., Binart, N., and Kelly, P. A. (1998) *Endocr. Rev.* **19,** 225–268
59. Horseman, N. D., Zhao, W., Montecino-Rodriguez, E., Tanaka, M., Nakashima, K., Engle, S. J., Smith, F., Markoff, E., and Dorshkind, K. (1997) *EMBO J.* **16,** 6926–6935
60. Ormandy, C. J., Camus, A., Barra, J., Damotte, D., Lucas, B., Buteau, H., Edery, M., Brousse, N., Babinet, C., Binart, N., and Kelly, P. A. (1997) *Genes Dev.* **11,** 167–178
61. Stocco, C., Telleria, C., and Gibori, G. (2007) *Endocr. Rev.* **28,** 117–149
62. Ogren, L., and Talamantes, F. (1988) *Int. Rev. Cytol.* **112,** 1–65
63. Chappell, P. E., Schneider, J. S., Kim, P., Xu, M., Lydon, J. P., O'Malley, B. W., and Levine, J. E. (1999) *Endocrinology* **140,** 3653–3658
64. Lydon, J. P., DeMayo, F. J., Funk, C. R., Mani, S. K., Hughes, A. R., Montgomery, C. A., Jr., Shyamala, G., Conneely, O. M., and O'Malley, B. W. (1995) *Genes Dev.* **9,** 2266–2278
65. Mulac-Jericevic, B., Mullinax, R. A., DeMayo, F. J., Lydon, J. P., and Conneely, O. M. (2000) *Science* **289,** 1751–1754
66. Mulac-Jericevic, B., Lydon, J. P., DeMayo, F. J., and Conneely, O. M. (2003) *Proc. Natl. Acad. Sci. U.S.A.* **100,** 9744–9749
67. Hagerty, L., Weitzel, D. H., Chambers, J., Fortner, C. N., Brush, M. H., Loiselle, D., Hosoya, H., and Haystead, T. A. (2007) *J. Biol. Chem.* **282,** 4884–4893

Downloaded from www.jbc.org at Duke University, on September 11, 2011

lontay.beata_285_24

Biochimica et Biophysica Acta 1852 (2015) 2238

Contents lists available at ScienceDirect

Biochimica et Biophysica Acta

journal homepage: www.elsevier.com/locate/bbadis

Protein phosphatase-1 is involved in the maintenance of normal homeostasis and in UVA irradiation-induced pathological alterations in HaCaT cells and in mouse skin

Dóra Dedinszki [a,1], Adrienn Sipos [a,1], Andrea Kiss [a], Róbert Bátori [a], Zoltán Kónya [a], László Virág [a,b], Ferenc Erdődi [a,b], Beáta Lontay [a,*]

[a] Department of Medical Chemistry, University of Debrecen, Debrecen H-4032, Hungary
[b] MTA-DE Cell Biology and Signaling Research Group, University of Debrecen, Debrecen H-4032, Hungary

ARTICLE INFO

Article history:
Received 30 June 2014
Received in revised form 27 October 2014
Accepted 4 November 2014
Available online 8 November 2014

Keywords:
Keratinocyte
Protein phosphatase-1
UV irradiation
Gene expression
Keratin 1/10
Histone 1b

ABSTRACT

The number of ultraviolet (UV) radiation-induced skin diseases such as melanomas is on the rise. The altered behavior of keratinocytes is often coupled with signaling events in which Ser/Thr specific protein kinases and phosphatases regulate various cellular functions. In the present study the role of protein phosphatase-1 (PP1) was investigated in the response of human keratinocyte (HaCaT) cells and mouse skin to UV radiation. PP1 catalytic subunit (PP1c) isoforms, PP1cα/γ and PP1cδ, are all localized to the cytoskeleton and cytosol of keratinocytes, but PP1cδ was found to be dominant over PP1α/γ in the nucleus. PP1c-silencing in HaCaT cells decreased the phosphatase activity and suppressed the viability of the cells. Exposure to a 10 J/cm^2 UVA dose induced HaCaT cell death and resulted in a 30% decrease of phosphatase activity. PP1c-silencing and UVA irradiation altered the gene expression profile of HaCaT cells and suggested that the expression of 19 genes was regulated by the combined treatments with many of these genes being involved in malignant transformation. Microarray analysis detected altered expression levels of genes coding for melanoma-associated proteins such as keratin 1/10, calcium binding protein S100A8 and histone 1b. Treatment of Balb/c mice with the PP1-specific inhibitor tautomycin (TM) exhibited increased levels of keratin 1/10 and S100A8, and a decreased level of histone 1b proteins following UVA irradiation. Moreover, TM treatment increased pigmentation of the skin which was even more apparent when TM was followed by UVA irradiation. Our data identify PP1 as a regulator of the normal homeostasis of keratinocytes and the UV-response.

© 2014 Elsevier B.V. All rights reserved.

1. Introduction

It is well established that many environmental and genetic factors contribute to the development of skin cancer, however, among these factors one of the most important causative factor is chronic exposure of the skin to solar UV radiation [1]. The solar UV spectrum includes UVA (320–400 nm), which is 90–95% of the total solar UV radiation and considered to be the "aging ray" causing benign tumor formation as well as malignant cancers [2]. UVB (280–320 nm) is thought to be responsible for a wide range of skin diseases such as non-melanoma and melanoma skin cancers. UVB acts as a tumor initiator and co-carcinogen by triggering DNA damage, immunosuppression and oxidative stress [3]. UVC radiation (200–280 nm) has no significant effect on biological systems since it is largely absorbed by stratospheric ozone [4].

UV irradiation initiates the transcription of numerous genes encoding multiple proteins, which play a role in skin cell apoptosis, malignant transformation, aging of the cells as well as collagen degradation [5]. Thus, UV light can be absorbed by several target chromophores in the skin such as nucleic acids, NADPH and heme-containing enzymes relevant for cellular signaling. DNA can absorb only UVB light, while it is affected by UVA light in an indirect manner whereby UVA-irradiated cells overproduce reactive oxygen species (ROS) resulting in ROS-induced DNA damage [6]. UV radiation can cause severe damage on many tissue components including proteins, membrane lipids and nucleic acids. It has also been recognized as a major regulator of cellular processes mediated by growth factors and cytokine-mediated signal transduction pathways. Its effects might include influence on phospholipids, protein kinases (MAP kinases, tyrosine kinases, Ser/Thr specific kinases) and protein phosphatases, leading to pathological (abnormal) gene expression [7]. The combined action of these pathways eventually

Abbreviations: PP1, protein phosphatase-1; PP1c, PP1 catalytic subunit; PP2A, protein phosphatase-2A; PP2Ac, PP2A catalytic subunit; TM, tautomycin; OA, okadaic acid; PBS, phosphate buffer saline; TBS, Tris-buffered saline solution; UV, ultraviolet; KRT, keratin; ROS, reactive oxygen species; NHEK, normal human epidermal keratinocyte; I-2, inhibitor-2; PARP, poly (ADP-ribose) polymerase

* Corresponding author at: Department of Medical Chemistry, Faculty of Medicine, University of Debrecen, H-4032 Debrecen, Egyetem tér 1, Hungary. Tel.: +36 52 412345; fax: +36 52 412566.
E-mail address: lontay@med.unideb.hu (B. Lontay).

[1] These authors contributed equally to the work.

http://dx.doi.org/10.1016/j.bbadis.2014.11.005
0925-4439/© 2014 Elsevier B.V. All rights reserved.

tontay.beata_285_24

determines the fate of UV-irradiated cells. Moreover, it is widely appreciated that the effects of UV light on certain signaling pathways are wavelength-specific [8,9] and are related mostly to the activation of MAPK, AKT/mTOR, AMPK and p53 signaling by protein phosphorylation [5]. The UV-induced changes in the phosphorylation of cellular proteins by protein kinases are relatively well established, while little is known about the regulatory role of the protein phosphatases which ensure the reversibility of these phosphorylation processes.

In the human genome almost 40 genes encode for phospho-Ser/Thr specific protein phosphatases (PP) [10] which are termed as PP1 to PP7 [11]. Among these types PP1 and PP2A are assumed to catalyze the dephosphorylation of over 90% of all eukaryotic phosphoproteins [12]. In fact, PP1 and PP2A are two of the most abundant enzymes and they are highly characterized in many cell types including skin cells [13]. Mammalian genomes contain three different genes that encode four distinct catalytic subunits termed PP1α, PP1β/δ and PP1γ1 [14], and a splice variant PP1γ2 [15] expressed ubiquitously except for the latter one. The substrate specificity and distinct subcellular localization of PP1 is regulated by various targeting subunits [16], and several of them (PNUTS, pRb, Repo-Man, GADD34, *etc.*) have recently been identified as regulators of UV-mediated pathways such as DNA damage, cell cycle, centrosome separation and apoptosis [17]. Hence, it is important to elucidate the mechanisms by which PP1 enzymes may regulate the UV radiation-induced pathologies and the underlying cellular events.

In this study, we report that PP1 enzymes play an important role in the maintenance of the homeostasis in human keratinocytes as well as in mouse skin. We also suggest that pathological processes could result from the selective regulation of PP1 enzyme activity by UVA irradiation.

2. Material and methods

2.1. Chemicals and antibodies

All chemicals were obtained from Sigma-Aldrich unless otherwise indicated. Antibodies were as follows: anti-KRT 1 (against middle region) and anti-KRT 10 (against N-terminal region) from Aviva System Biotechnology; affinity isolated anti-S100A8, horseradish-peroxidase (HRP) conjugated anti-rabbit IgG and anti-actin from Sigma-Aldrich; monoclonal anti-histone H1 (AE-4), anti-α-tubulin, anti-GAPDH and monoclonal anti-PP1 (E9) antibodies from Santa Cruz Biotechnology; affinity isolated anti-PP1cδ from Upstate Millipore; anti-PP2Ac antibody from BD Biosciences; anti-PARP, anti-cleaved PARP antibodies and HRP-linked anti-mouse IgG from Cell Signaling Technology; Alexa Fluor 488- and Alexa Fluor 546-conjugated anti-mouse and anti-rabbit IgG from Molecular Probes.

2.2. Cell culture, gene silencing and UV radiation

Human keratinocyte (HaCaT) cells (300493, CLS Cell Lines Service GmbH, Germany) were grown in high glucose DMEM supplemented with 10% heat-inactivated FBS and 2 mM L-glutamine in humidified 5% CO_2 atmosphere at 37 °C. All materials used for cell culture were purchased from PAA Laboratories, Austria. Normal human epidermal keratinocyte (NHEK) cultures were generously donated by Dr. Tamas Bíró (University of Debrecen, Department of Physiology) and maintained in Epilife medium complemented with Human Keratinocyte Growth Supplement (HKGS), 100 μg/ml streptomycin, 100 IU/ml penicillin and 50 ng/ml amphotericin B (all from Life Technologies) and were cultured on 1% collagen-coated plates. Double-stranded siRNA (100 nM) (Santa Cruz Biotechnology) was used to knock down the protein levels of endogenous PP1 isoforms (α, β/δ and γ) and a non-target sequence (Thermo Scientific Inc.) with the G–C content of the siPP1 sequence was applied in control experiments according to the manufacturer's protocol. 100 nM siRNAs were transfected into HaCaT cells using a Dharmafect 2 transfection reagent (Thermo Scientific Inc.) in serum-free medium. After 30 min, the medium was completed with 10% FBS and cells were incubated for 48 h. Then prior to UV irradiation, cells were kept in serum-free medium for 16 h in each case. UV irradiation was carried out using a Bio-Sun UV irradiation system (Vilbert Lourmat, France). After 24 hour incubation cells were either lysed for immunoblotting and microarray analysis and were fixed for immunofluorescent staining or utilized for MTT assay. 1 μM of tautomycin was applied for 1 h before UV irradiation and cells were treated as it was described before. In the case of protein phosphatase activity measurement cells were lysed and assayed right after TM treatment or UV irradiation.

2.3. Cell disruption and protein measurement

Treated cells were collected and washed by ice-cold Dulbecco's PBS without calcium, magnesium and phenol red (pH: 7.2; 2.7 mmol/l KCl, 1.5 mmol/l KH_2PO_4, 136.9 mmol/l NaCl, 8.9 mmol/l $Na_2HPO_4 \cdot 7H_2O$) and lysed in modified RIPA buffer (25 mM Tris–HCl, pH 7.6, 150 mM NaCl, 1% (v/v) Nonidet P-40, 0.1% (w/v) SDS, 1 mM DTT) containing protease inhibitor cocktail Complete Mini (Roche Diagnostics GmbH, Switzerland) followed by 3 × 15 s sonication on ice. After centrifugation (16,000 × *g* for 15 min at 4 °C), protein concentration of the supernatant was determined by the BCA method (BCA protein assay kit, Pierce Biotechnology, USA) using an ELISA reader (Labsystem Multiscan MS) at 540 nm with BSA as a standard as described before [18]. Alternatively subcellular factions of HaCaT cells were prepared as described before [19].

2.4. MTT assay

The assay was used to determine the viability of HaCaT cells. An MTT reagent was prepared by adding 5 mg of 3-(4,5-dimethylthiazol-2-yl)-2,5-diphenyltetrazolium bromide to 1 ml PBS. The cell culture medium was replaced and 20 μl of MTT was added to each well of the 96-well plate (200 μl). The plates were incubated for 1–3 h at 37 °C in 5% CO_2 atmosphere. The medium was removed and 100 μl DMSO was added to the wells for dissolving the formazan crystals in the cells and the absorbance at 540 nm was recorded.

2.5. Immunoblotting

Sodium dodecyl sulfate-polyacrylamide gel electrophoresis (SDS-PAGE) and immunoblotting were carried out as detailed before [19]. After blocking in 5% (w/v) non-fat dry milk, the membranes were washed with PBS containing 0.1% Tween 20 (PBST) and incubated with primary antibodies overnight at 4 °C, followed by application of the HRP-conjugated secondary antibodies. To determine the changes in the protein expression levels of histone 1b, keratin 1 and 10 as well as S100A8, specific antibodies were applied to detect changes. Immunoreactions were detected by enhanced chemiluminescence (ECL). Densitometry of the proteins of interest were performed by Image J. 1.46 and normalized to tubulin internal control (run on the same gel) and plotted as relative numbers (in %). To assess the extent of apoptosis of NHEK and HaCaT cells after TM treatment and UVA irradiation Western blot analysis was carried out on 30 μg of cell lysates using anti-PARP (1:500) and anti-cleaved PARP (1:500), antibodies.

2.6. Immunofluorescence microscopy

Paraformaldehyde (4%) was used for fixation (10 min) of HaCaT cells followed by three washes with ice-cold PBS. Cells were permeabilized with 0.02% (v/v) Triton X-100 dissolved in PBS for 10 min at room temperature and washed three times with PBS. After blocking in 1% (w/v) sterile BSA in PBS for 1 h, coverslips were incubated with anti-PP1c (E9), anti-PP1cδ, anti-PP2A and anti-KRT1 (all in 1:100 dilution) primary antibodies overnight at 4 °C. After extensive washing with PBS,

tontay.beata_285_24

secondary antibody was added at a 100-fold dilution (Alexa 488-conjugated anti-rabbit IgG and Alexa 596-conjugated anti-mouse IgG). Nuclear counterstaining was performed by 1 μg/ml DAPI (4′,6-diamidino-2-phenylindole). Coverslips were washed three times for 10 min in PBS and were mounted in ProLong Gold Antifade medium. Cells were observed with a 60× objective on a Zeiss Axioskop HBO50/AC microscope. Images were processed using PhotoShop Imaging software.

2.7. Immunohistochemistry

One-half of the skin samples were immediately fixed in 10% neutral-buffered formalin and embedded in paraffin. Sections (4 μm) were cut and mounted on glass slides (Superfrost/plus; A. Daigger & Company, Inc., Vernon Hills, IL), deparaffinized by xylene, dehydrated by graded ethanol and processed for hematoxylin and eosin (H&E) staining as described before [20]. Immunohistochemical staining of keratin 1, -10, S100A8 and histone 1b was also carried out incubating the sections with primary antibodies overnight at 4 °C. Sections were washed and incubated with anti-mouse or anti-rabbit HRP conjugated secondary antibody and immunosignals were developed by nickel/cobalt enhanced 3,3′-diaminobenzidine (DAB) chromogen substrate without any counterstaining. The sections were cleared with xylene before finally being mounted. The other half of the samples was used for Western blot analysis.

2.8. Protein phosphatase assay

The PP1 and PP2A activities of the HaCaT cell lysate and subcellular fractions were assayed with a 1 μM ^{32}P-labeled 20 kDa light chain of turkey gizzard myosin (^{32}P-MLC20) at 30 °C in 20 mM Tris–HCl (pH 7.4) and 0.1% 2-mercaptoethanol. To differentiate between PP1 and PP2A protein phosphatase activities by 5 nM okadaic acid (OA) subcellular fractions of the HaCaT cell lysate were diluted to 300-fold. To determine the phosphatase type specificity of inhibition by TM treatment and UVA irradiation cell lysates (1.5–2 mg/ml) were assayed in 30-fold final dilution in the absence or presence of 2 μM inhibitor-2 (I-2). The reaction was initiated by the addition of the substrate. After a 5 minute incubation the reaction was terminated by the addition of 200 μl 10% TCA and 200 μl 6 mg/ml BSA. The precipitated proteins were collected by centrifugation and the released $^{32}P_i$ was determined from the supernatant (380 μl) in a scintillation counter. Values were expressed as nmol P_i released per minute for the subcellular fractions, while in the case of TM treatment and UVA irradiation the phosphatase activity of the untreated cells was taken as 100%.

2.9. RNA and microarray processing

Total RNA was extracted from HaCaT cells using a Trizol reagent (Invitrogen). RNA integrity was checked on an Agilent Bioanalyser 2100 (Agilent Technologies), and RNA samples with >9.0 RIN value were used in the experiments. A NanoDrop ND-1000 was used to determine RNA concentration. Global expression pattern was analyzed on Affymetrix GeneChip Rat Gene 1.0 ST arrays. An Ambion WT Expression Kit (Life Technologies) and a GeneChip WT Terminal Labeling and Control Kit (Affymetrix) were used for amplifying and labeling 250 ng of total RNA samples. Samples were hybridized at 45 °C for 16 h and then the standard washing protocol was performed using an Affymetrix GeneChip Fluidics Station 450, and the arrays were scanned on a GeneChip Scanner 7G (Affymetrix). RNA labeling and hybridization was processed by UD-GenoMed Medical Genomic Technologies Ltd. (Debrecen, Hungary).

2.10. Microarray data analysis

Microarray data were analyzed by GeneSpring 12 GX software (Agilent BioTechnologies). Affymetrix CEL files were normalized with a Robust Multichip Analysis (RMA) algorithm and median normalization. Expressed genes were determined by filtering out the lowest 20th percentile of genes based on raw signal intensity. Then genes which did not show at least 1.7-fold change difference from the median, were also filtered out as non-changing genes. Statistical analysis was performed on the list of changing genes using *t* test. Statistically significant difference was considered at $p < 0.05$ and fold change cut off value was 1.5. Pathway analysis was performed using Ingenuity software (Ingenuity Systems). Statistical analysis was performed on the list of changing genes and the following comparisons were performed using *t*-test: control *vs.* UVA, control *vs.* siPP1 and siPP1 plus UVA *vs.* siRNA (no UVA). Two gene lists were generated and compared in a Venn diagram and UVA treatment specific and siRNA treatment specific genes were determined. Genes affected by both the PP1-silencing and UVA radiation treatments are listed separately (Table 1) and present the cross section in the Venn-diagram (Fig. 3a).

2.11. Mouse skin study

Six-week-old, male Balb/c mice (Charles River) were housed individually in stainless steel cages in a controlled atmosphere with a temperature range of 19.0–25.0 °C and a relative humidity of 35.0–75.0% with a 12/12 h light and dark cycle. Food and water were available *ad libitum*. All procedures were authorized by the Institutional Ethics

Table 1
Effect of UV radiation on the gene expression of PP1-silenced HaCaT cells.

Gene symbol	Gene description	FC absolute	p-Value	Regulation
SPRR1A	Small proline-rich protein 1A	1.66	0.028	Up
SYT14	Synaptotagmin XIV	1.81	0.018	Down
S100A8	S100 calcium binding protein A8	2.79	0.008	Up
PPP1CA (PP1cα)	Protein phosphatase 1, catalytic subunit, alpha isoform	2.42	0.002	Down
PPP1CB (PP1cβ/δ)	Protein phosphatase 1, catalytic subunit, beta isoform	2.41	0.015	Down
PPP1CC (PP1cγ)	Protein phosphatase 1, catalytic subunit, gamma isoform	2.83	0.008	Down
KRT1	Keratin 1	1.82	0.033	Up
KRT10	Keratin 10	2.02	0.033	Up
CSTA	Cystatin A (stefin A)	1.76	0.025	Up
SLC10A5	Solute carrier family 10	1.59	0.030	Up
CALB1	Calbindin 1, 28 kDa	2.14	0.030	Up
AKR1B10	Aldo-keto reductase family 1	1.66	0.008	Up
HIST1H2BK	Histone cluster 1, H2bk	1.59	0.030	Up
HIST1H1B	Histone cluster 1, H1b	1.58	0.043	Down
FST	Follistatin	1.51	0.040	Down
STC2	Stanniocalcin 2	1.59	0.004	Up
RNU4-1	RNA, U4 small nuclear 1	2.35	0.021	Up
HSPA6	Heat shock 70 kDa protein 6 (HSP70B')	2.45	0.039	Up
RGS2	Regulator of G-protein signaling 2, 24 kDa	2.58	0.046	Up

tontay.beata_285_24

Committee (7/2010 DE MÁB) and were conducted in accordance with the guidelines for the care and use of laboratory animals outlined in the national and European Union ethical regulations. Before UV irradiation and TM treatment [21], the hair of mice was removed by a commercially available depilating cream (Veet, Reckitt Benckiser) and the depilated areas were washed and dried immediately. 24 h after hair removal, dorsal regions of the skin were randomly selected (for vehicle and for PP1 inhibitor treatment) and labeled. Mice were divided into two groups (control (no radiation) and UVA-irradiated group) of 9 animals each. The selected areas were topically treated either with 50 μg vehicle (hydrophylic anionic cream) or with tautomycin (1 μM final concentration in vehicle) 1 h before UVA irradiation with 3.54 J/cm^2. For UVA exposure, the cages were placed in an irradiation setup equipped with Philips TL-20 W/12 lamps (Philips, Eindhoven, the Netherlands) emitted at wavelengths of 315–400 nm and the peak emission was 365 nm. The intensity of UVA rays was measured by a UVA ray meter (UVX Radiometer, Saint Gabriel, California, USA) just before irradiation. The cumulative UVA dose was 531 J/cm^2 given five-times for 30 min. Animals were killed by cervical dislocation, then the skin was excised and the subcutaneous fat removed with a scalpel blade. Tissue samples were frozen in liquid N_2 at the time of harvest, stored at −80 °C and homogenized as described [20]. Protein concentration was determined by BCA assay.

2.12. Histologic image analysis

Digital image information from the H&E-stained sections was analyzed and the depth of randomly selected areas (n = 10 in each group for each treatment) of epidermis and total skin was measured by Image J 1.41 image-analysis software (Wayne Rasband, National Institutes of Health, Washington, DC, USA).

2.13. Statistical analysis

Normalized data were analyzed by *t*-test (for two groups) or by analysis of variance (ANOVA, for >2 groups). Parametric statistical tests were used if the assumptions of such tests were met. All normalized variables used in statistical analyses were found to be normally distributed. Tests were conducted using GraphPad for Windows. All data presented in this work represent mean ± SEM.

3. Results

3.1. Distribution of protein phosphatase-1 catalytic subunit isoforms in human keratinocytes

As a first approach, we studied the subcellular localization of PP1cα, PP1cγ1, PP1cδ isoforms and PP2A to determine the expression level and the possible isoform-specific functions of PP1 and PP2A in keratinocytes. Subcellular fractions of human keratinocytes (HaCaT) were prepared using the method reported previously [19] and the purity of nuclear, cytoskeletal and cytosolic fractions was checked by identification of subcellular fraction-specific proteins such as histone, tubulin and GAPDH (Fig. 1a.). As shown on Fig. 1a, PP1cδ was identified in all fractions, whereas PP1cα and PP1cγ1 isoforms and PP2A were predominant in the cytoskeleton and cytosol, while they exhibited lower intensity signals in the nuclear fraction. The abundance of these isoforms was similar in the cytosolic and in the cytoskeletal fraction. Phosphatase activity in the HaCaT subcellular fractions was assayed using a ^{32}P-labeled myosin light chain of 20 kDa (^{32}P-MLC20) as substrate (Fig. 1b), which is known to be dephosphorylated by PP1 and PP2A in cell lysates. The highest protein phosphatase activity could be measured in the cytosolic fraction compared to that in the nuclear and cytoskeletal fractions. It has already been shown that in diluted cell lysates treatment with 5 nM okadaic acid (OA) inhibits the activity of protein phosphatase 2A (PP2A) enzymes, but does not influence PP1 [22]. We considered that

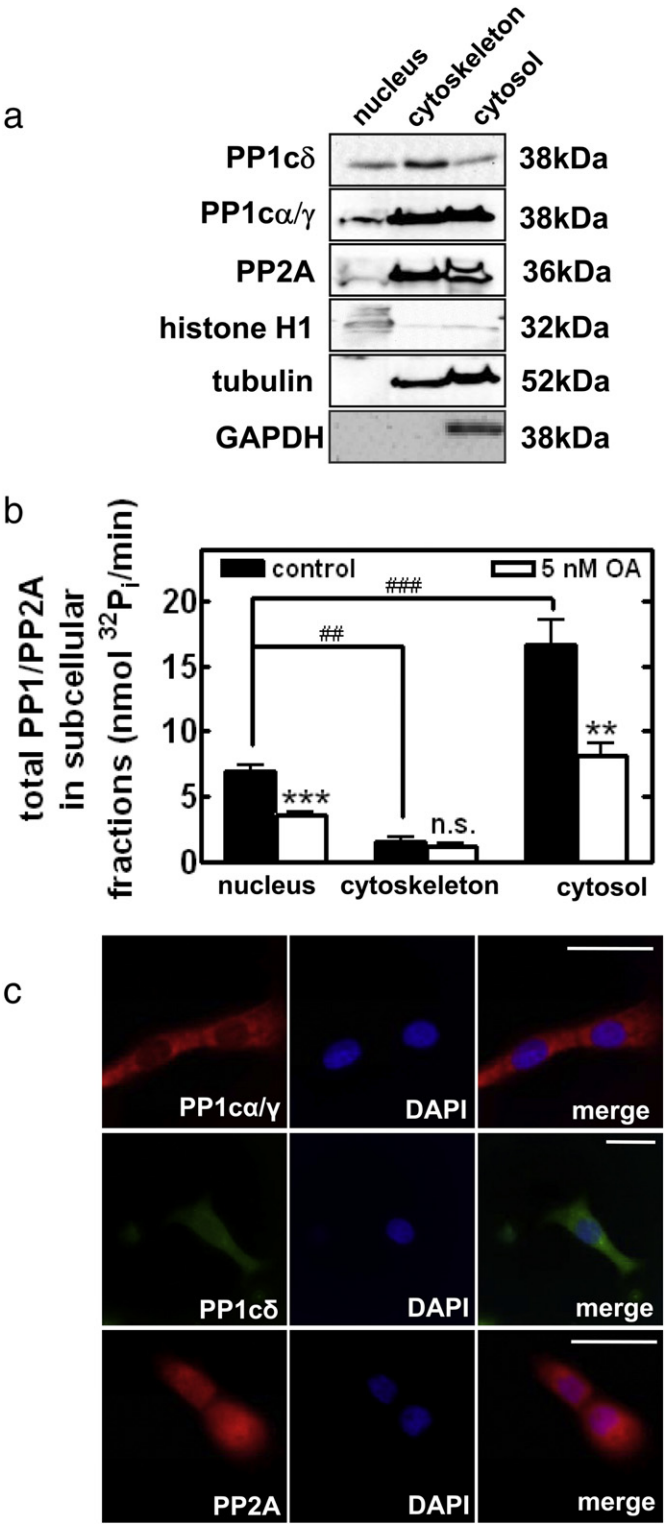


Fig. 1. Subcellular distribution of PP1 and PP2A in HaCaT cells. (a) HaCaT subcellular fractions (nucleus; cytoskeleton, cytosol) were analyzed by Western blot using antibodies specific for PP1cδ and PP1α/γ1 as well as for subcellular fraction-specific markers such as histone H1 for nucleus, tubulin for cytoskeleton and GAPDH for cytosol. (b) Protein phosphatase activity of subcellular fractions was measured using ^{32}P-MLC20 as substrate in the absence (black columns) or in the presence of 5 nM okadaic acid (OA). Values represent mean ± SEM; n = 4, ANOVA $^{***}p < 0.001$, $^{**}p < 0.01$, n.s.: non-significant and *t*-test, $^{###}p < 0.001$, $^{##}p < 0.01$. (c) Immunofluorescent microscopy of HaCaT cells stained with anti-PP1cα/γ1 (red), anti-PP1cδ (green) and anti-PP2A (red) specific antibodies. Nucleus is stained with DAPI (blue). Scale bar represents 20 μm.

tontay.beata_285_24

the phosphatase activity measured in the presence of 5 nM OA roughly equals with the PP1 activity in these fractions. Our data suggest that 50% of total phosphatase activity is related to PP2A, in both the nuclear and cytosolic fractions. In contrast, in the cytoskeletal fraction PP1 seemed to be the dominant form representing ~80% of the phosphatase activity. We also examined the distribution of PP1 isoforms in HaCaT cells by fluorescent microscopy (Fig. 1c). These data confirmed that PP1cδ was localized to both the nucleus and the cytoplasm, whereas PP1cα/γ1 was distributed throughout the cytoplasm but only speckle-like staining was detectable in the nucleus. The nucleus of the cells was stained by DAPI (Fig. 1c, middle) and the merged images (Fig. 1c, right panel) also confirmed the localization pattern of PP1c isoforms suggested above. The PP2A enzyme exhibited intensive staining throughout the cell.

3.2. Effect of UVA radiation on the phosphatase activity and survival of HaCaT cells

To investigate the effect of UV irradiation on the activity of protein phosphatases and on the viability of keratinocytes, HaCaT cells were exposed to different doses of UV radiation: 1, 5, 10, 15, 20 J/cm^2 for UVA and 0.025, 0.1, 0.05, 1 and 2 J/cm^2 for UVB. After UV irradiation the cells were incubated for 24 h then cell survival was assessed by MTT assay (Fig. 2a). Phosphatase activity of the lysates (Fig. 2b) was determined immediately after UVA irradiation with ^{32}P-MLC20 substrate in order to select an effective UV dose with respect to cell survival and phosphatase activity. The survival of HaCaT cells decreased in a dose-dependent manner as a result of exposure to UVA or UVB (Fig. 2a). UVB irradiation had no significant effect on the phosphatase activity of HaCaT cells, whereas UVA suppressed phosphatase activity in a dose-dependent manner (Fig. 2b). Based on the above results we selected the 10 J/cm^2 dose of UVA irradiation for our further experiments. To determine the role of PP1 in UVA-induced effects, PP1c was silenced by using panPP1c small interfering (si)RNA (siRNA). Forty-eight hours after siRNA transfection HaCaT cell lysates were prepared to assess the levels of PP1cδ and PP1cα/γ by Western blot analysis (Fig. 2c–d). PP1 silencing decreased the expression of PP1α/γ (Fig. 2c) and PP1cδ (Fig. 2d) by 40% and 60%, respectively. UVA irradiation did not affect PP1cδ level. Both PP1 silencing and UVA radiation decreased the phosphatase activity by 25% and 31%, respectively. When PP1 silencing was combined with UVA radiation, the phosphatase activity decreased further, although no additivity of the individual effects was observed (Fig. 2e). We assessed also the type specificity of phosphatase inhibition by TM, considered as a specific inhibitor for PP1 [22], and by UVA irradiation in HaCaT cells. We used recombinant inhibitor-2 [23] to inhibit PP1 specifically in cell lysate thereby determining the distribution of PP1 and PP2A activities. In the untreated control cell lysate inhibitor-2 (I-2) suppressed the phosphatase activity by ~60%: the remaining phosphatase activity is assumed as I-2 insensitive PP2A. Treatment of HaCaT cells by TM and UVA irradiation, or when the treatments were combined, resulted in 30%, 20% or 22% inhibition of phosphatase activity in the lysates, respectively. However, the I-2 insensitive (PP2A) activity of the lysate was not influenced by these treatments. These data suggest that TM treatment or UVA irradiation exerts a PP1 specific inhibitory effect in HaCaT cells. The survival of HaCaT cells was measured with an MTT assay (Fig. 2g). Silencing of PP1 caused an approximately 25–30% decrease in cell survival, while UVA radiation caused even more pronounced cell death (75%). PP1 silencing combined with UVA radiation did not further decrease survival compared to that of UVA radiation alone. To provide further data about the extent of apoptosis of HaCaT and primary human keratinocytes the concentration of PARP and cleaved PARP was measured by Western blot analysis. Cleavage of PARP by caspase-3 is considered as an indication of apoptosis [24], therefore a decrease of the amount of full length PARP and a parallel appearance of the cleaved fragment upon TM treatment or UVA irradiation suggest the occurrence of apoptotic cell death of HaCaT cells (Fig. 2h). TM treatment caused partial degradation of PARP while UVA irradiation with or without TM pretreatment resulted in a total loss of PARP and an increased level of cleaved PARP in both HaCaT and NHEK cell lines.

3.3. Expression analysis of genes in UVA-irradiated keratinocytes: the effect of PP1 silencing

To examine the role of PP1 silencing alone or in combination with UVA radiation microarray analysis of gene expression was carried out in control and PP1c-silenced HaCaT cells with or without UVA irradiation (10 J/cm^2). The alterations of gene expression were analyzed by an Affimetrix program and the cut-off limit was set to 1.5-fold change. Maximum variation was 2.9- and 4.1-fold compared to control, for downregulated and upregulated genes, respectively. We performed hierarchical cluster analysis on all differentially expressed genes using average linkage with Pearson's dissimilarity and the number of induced and repressed genes were presented in a heat map (Fig. 3a). UVA irradiation decreased the expression level of more than 80% of the genes (Table S1) while PP1 silencing increased the expression level of about 75% of the genes (Table S2). Since our major focus was to identify the role of PP1 in UVA-irradiated cells, the expression of genes in both PP1-silenced and UVA-irradiated HaCaT cells was further analyzed (Table 1). According to the Venn-diagram (Fig. 3a), 19 genes were affected by both treatments (Table 1): the expression of each PP1c isoform (α, β/δ and γ) was dramatically downregulated inferring the successful silencing of these genes. We also conducted Gene Ontology (GO) category enrichment analysis to determine the molecular function of GO terms (Fig. 3b). GO analysis indicated that hair, skin and embryonic development were differentially regulated by siPP1/UVA radiation treatment. In addition, the majority of these genes play a role in specific molecular and cellular functions such as cellular development, molecular transport and cell signaling. Astonishingly, 75% of these genes are strongly related to diseases and disorders such as cancer development, dermatological diseases and conditions as well as genetic disorders. These findings were also supported by the network analysis of the differentially expressed genes (Table S3). These data further support our hypothesis that PP1 plays a crucial role in the maintenance of normal dermal functions and is a potentially important modulator of the epidermal barrier.

3.4. Role of PP1c in the regulation of keratin 1, keratin 10, S100A8 and histone 1b expression in UVA-irradiated HaCaT cells

Microarray analysis of siPP1c/UVA-irradiated HaCaT cells indicated a change in the expression of genes coding for keratin 1 (KRT1) and keratin 10 (KRT10), S100A8 as well as histone 1b comparing to the control groups. In accordance with these data when HaCaT cells were silenced for PP1c, or UVA-irradiated, the protein levels of KRT1 and KRT10 were increased (Fig. 4a–b, respectively), and a slight cumulative effect of PP1c silencing and UVA irradiation was also apparent. No significant change of S100A8 protein level was detected (Fig. 4c) in PP1c-silenced cells, whereas it was elevated upon UVA irradiation. In contrast, histone 1b protein level was decreased both by PP1c silencing and UVA irradiation but these individual effects were not additive. The human HaCaT cell line displays a transformed phenotype *in vitro* and remains non-tumorigenic [25]. We also intend to test our hypothesis on NHEK cells that are resistant to transformation when grown under normal conditions *in vitro* and retain many physiological characteristics observed *in vivo* [26]. Both cell lines provided parallel lines of evidence about the effect of UVA irradiation and PP1 inhibition on apoptosis (Fig. 2h) as well as on KRT1, KRT10, S100A8 and histone 1b expression (Fig. 4 a–e). KRT1 and 10 protein expression levels were increased upon PP1 inhibition and UVA irradiation but S100A8 did not present a notable change after TM treatment. Histone 1b expression levels were mostly affected by UVA irradiation but the

tontay.beata_285_24

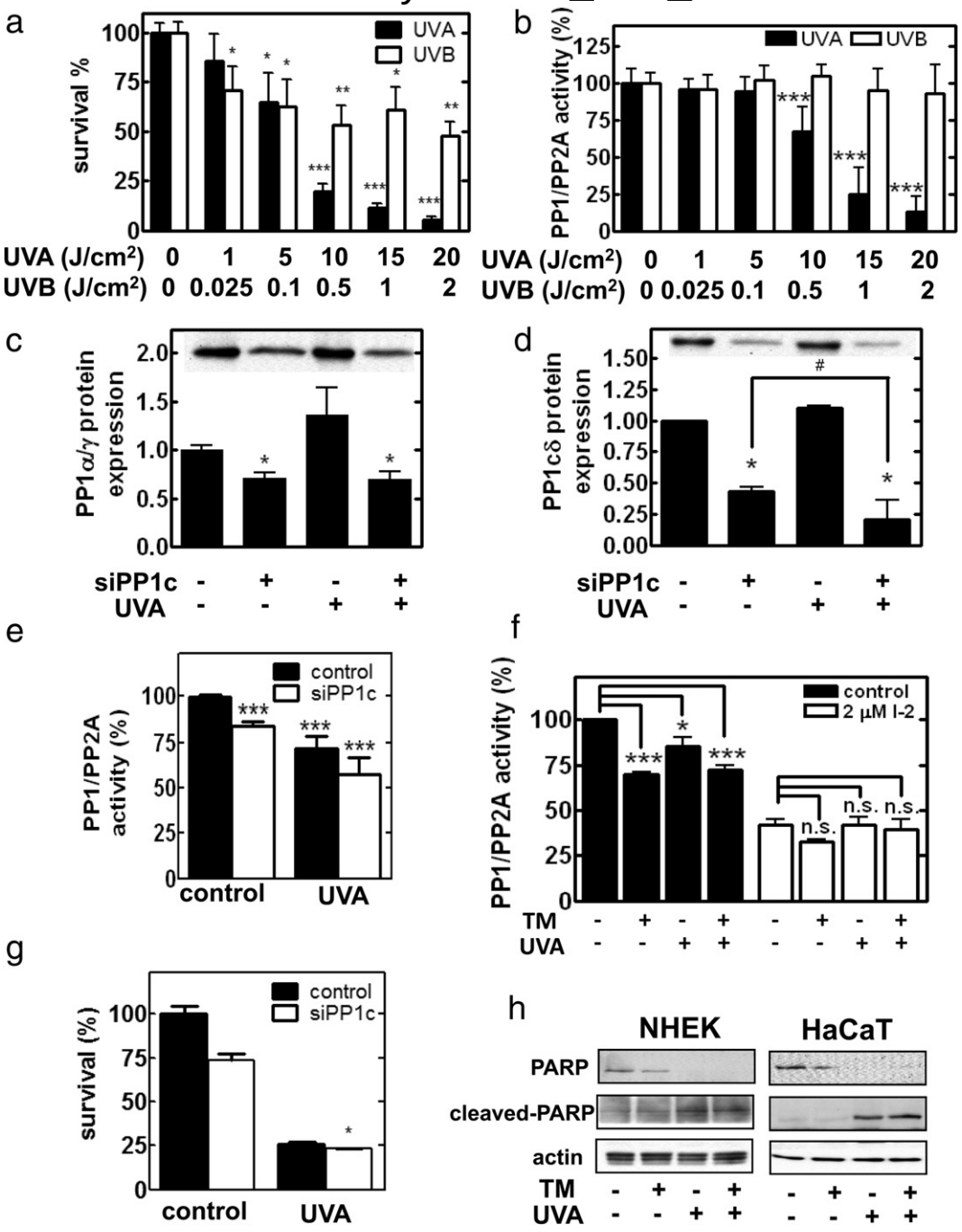


Fig. 2. Effect of PP1 silencing and UV irradiation on the viability and on the protein phosphatase activity of HaCaT cells. (a) Cells were irradiated by different UVA (1–20 J/cm^2) and UVB (0.0025–2 J/cm^2) doses. MTT assays were carried out to assess cell viability of HaCaT cells before (control) and after UVA irradiation. The optical density value of the control was taken as 100%. (b) HaCaT cells were exposed to the indicated doses of UVA or UVB radiation, and then the phosphatase activity was assayed with a ^{32}P-MLC20 substrate. Phosphatase activity of non-irradiated cells was taken as 100%. (c–f) HaCaT cells were transfected with non-target (control) or PP1-specific siRNA (siPP1), or exposed to 10 J/cm^2 of UVA radiation (UVA), or a combination of these treatments was applied. Expression levels of PP1cα/γ (c) and PP1cδ (d) was determined by Western blot analysis. (e) Phosphatase activity of the lysates was assayed and values of the non-target siRNA transfected cells without UVA irradiation was taken as 100%. (f) Phosphatase activity of the HaCaT cells treated with 1 μM of tautomycin (TM) with or without 10 J/cm^2 UVA irradiation was assayed. Activities were measured in the absence (black bars) and the presence (white bars) of 2 μM of inhibitor-2 (I-2). (g) Effect of PP1 silencing and UVA radiation on HaCaT cell viability was quantified by MTT assay. The optical density of the control was regarded as 100%. (h) Both TM-treatment and UVA irradiation induce the apoptosis of NHEK and HaCaT cells assayed by Western blot analysis using PARP and cleaved PARP specific antibodies as well as actin as loading control. Means ± SEM (n = 4), student *t*-test *p < 0.05, **p < 0.01, ***p < 0.001, n.s.: non-significant.

combined treatment of TM and UVA resulted in the elimination of histone 1b expression in NHEK cells. These results have also been confirmed by immunofluorescent staining: a decreased level of PP1 was detected after PP1c silencing and an increased level of KRT1 was observed in PP1-silenced and UVA-irradiated HaCaT cells (Fig. 4f). Not only the expression, but the cellular distribution of KRT1 (green) has changed too. Due to the results of UVA irradiation or/and siPP1c treatment, the diffuse localization of KRT1 was taken over by a strong perinuclear localization. PP1c staining (red) was substantially decreased by PP1 silencing.

tontay.beata_285_24

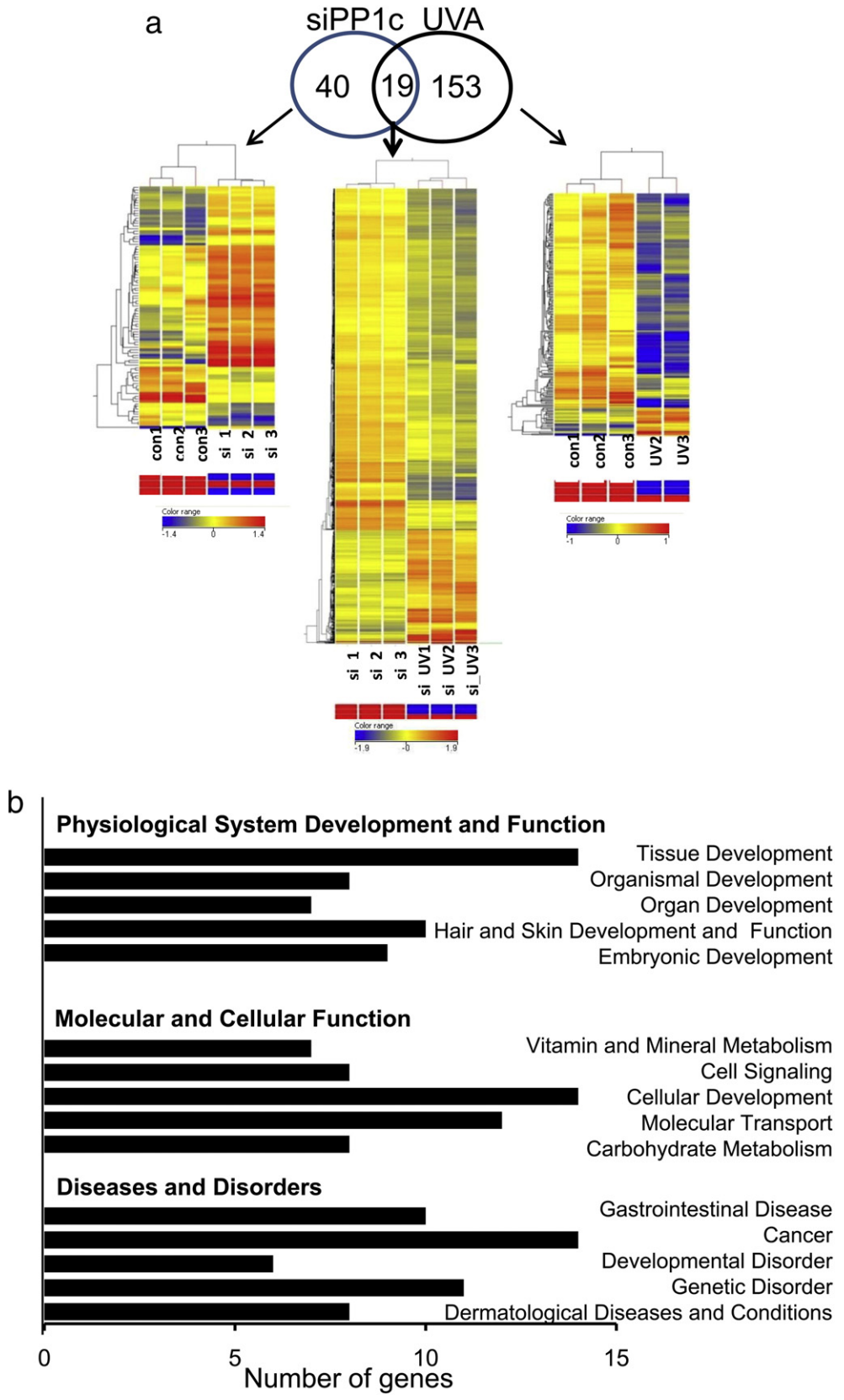


Fig. 3. Microarray analysis of PP1-silenced and UV-irradiated HaCaT cells. (a) Venn diagram demonstrating the relationship between genes differentially regulated after PP1 silencing (siPP1) and UVA irradiation in HaCaT cells. The numbers inside the circles represent the number of genes differentially regulated between the two groups. The heat map represents the hierarchical clustering analysis of the differentially expressed genes for comparing the changes in keratinocytes followed by PP1 silencing, UVA radiation and the combined treatment as indicated. The color code for the signal strength is shown in the box at the bottom of each individual column; induced genes are highlighted in red, and repressed genes in blue color. (b) Gene ontology analysis of genes related to UVA radiation and PP1 silencing.

tontay.beata_285_24

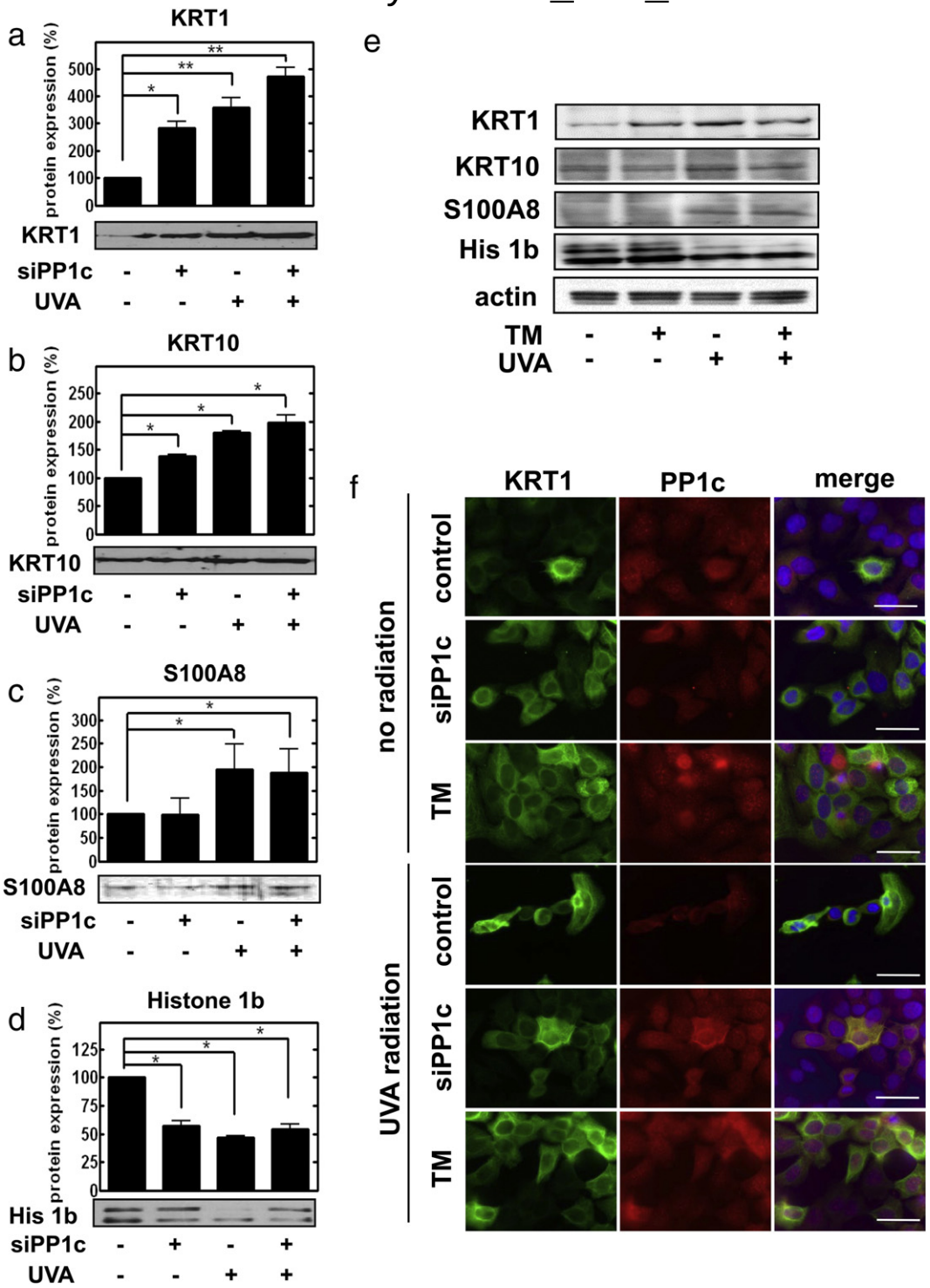


Fig. 4. Effect of PP1 silencing, PP1 inhibition and UVA radiation on the protein expression of keratin 1, keratin 10, S100A8 and histone 1b of NHEK and HaCaT cells. (a–d) Control and PP1c-silenced (siPP1) HaCaT cells were irradiated by a 10 J/cm^2 UVA dose and the protein expression of keratin 1 (KRT1) (a), keratin 10 (KRT10) (b), S100A8 (c) and histone 1b (d) were measured by Western blot analysis and the bands were subjected to densitometry and normalized to tubulin as internal control. Means ± SEM (n = 3), student *t*-test *p < 0.05, **p < 0.01. (e) Control and TM-treated NHEK cells were irradiated with UVA and KRT1, KRT10, S100A8 and histone 1b protein levels were assayed by Western blot analysis using actin as internal control. (f) Immunofluorescent staining of keratin 1 (KRT1, green, left panels) and PP1cδ (PP1, red, middle panel) in HaCaT cells. Merged images (right panel) are also shown. Scale bar = 20 μm.

3.5. PP1 inhibition and UVA irradiation cause erythemal hyperplasia and scarification of mouse skin

We carried out animal experiments treating the skins of Balb/c mice with tautomycin (TM), a PP1-specific inhibitor, and UVA irradiation, or the treatments were combined (TM followed by UVA irradiation). Analysis of skin extracts for protein expression levels of KRT1/10 (Fig. 5a–b, respectively), S100A8 (Fig. 5c) and histone 1b (Fig. 5d) showed similar features to those presented for PP1c-silenced and UVA-irradiated HaCaT cells with subtle differences. KRT1/10 was increased, while histone 1b was decreased by both TM treatments and UVA irradiation or when these challenges were combined. These results

tontay.beata_285_24

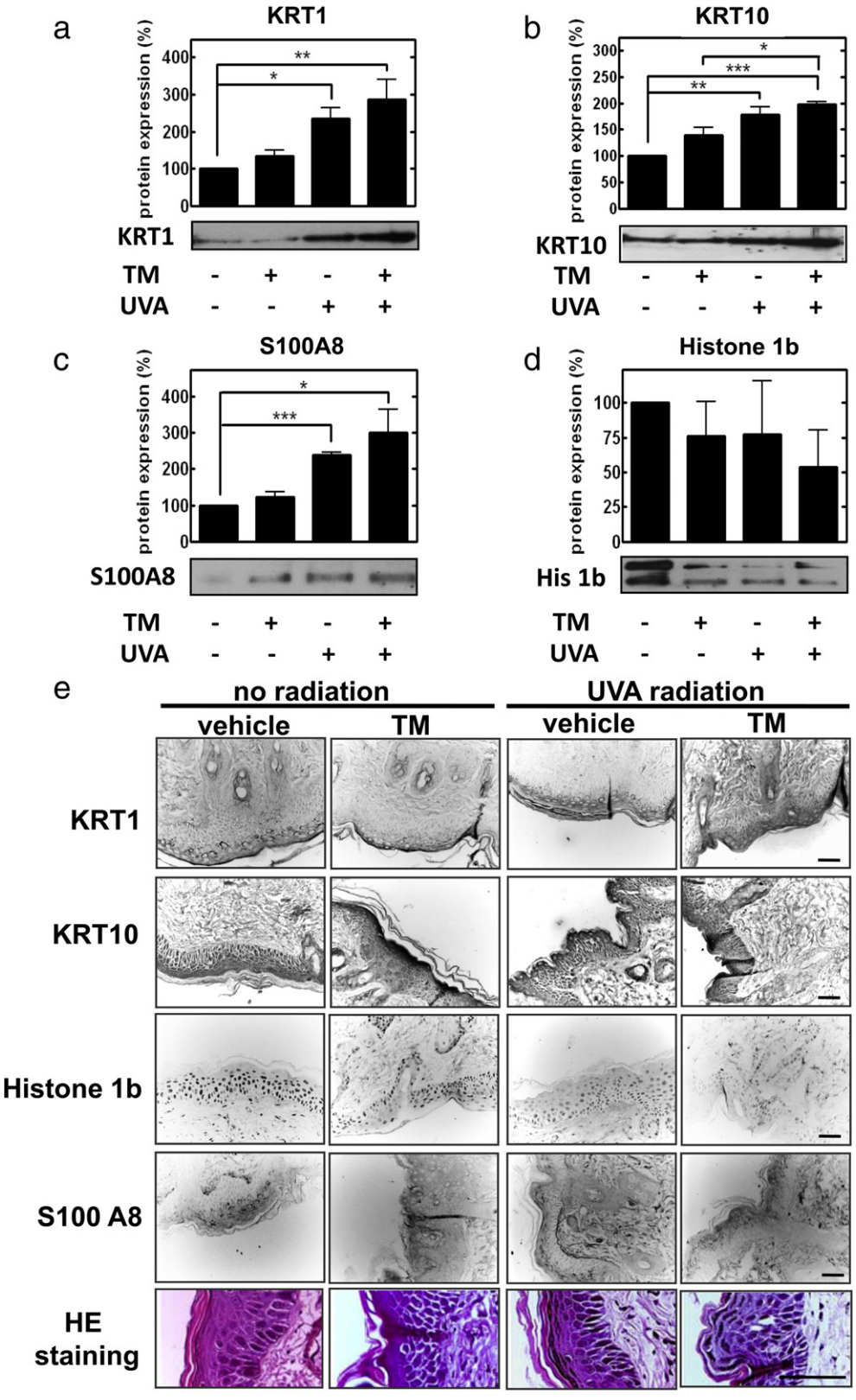


Fig. 5. Influence of PP1 inhibition and UVA radiation on keratin 1/10, S100A8 and histone 1b expression and on the thickness of murine dorsal skin. (a–g) The dorsal skin of mice was marked down the center to give a non-irradiated and a UVA-irradiated treatment group (9 mice each), all with vehicle and TM-treated areas. Western blot analysis of skin biopsies identified changes in the protein expression level of keratin 1 or 10 (KRT1 or 10) (a and b), S100A8 (c) and histone 1b (His1b) (d) which was quantified by densitometry normalized to the density of tubulin as internal control. (e) Immunohistochemical staining of mouse skin with or without UVA irradiation (no radiation), and with (TM) or without TM treatment (veh: vehicle) for keratin 1, 10 (KRT1, 10), histone 1b and S100A8. Bottom panel: histologic appearance of mouse skin with H&E staining. Scale bar = 20 μm. Means ± SEM (n = 9), paired *t*-test $^{*}p < 0.05$, $^{**}p < 0.01$, $^{***}p < 0.001$.

tontay.beata_285_24

have also been verified by immunohistochemical staining: an increased level of KRT1, KRT10 and a slight increase in S100A8 expression was detectable in the epidermal part of TM-treated and UV-irradiated mouse skin, and a significant decrease could be observed in the number of immunoreactive nucleus stained by histone 1b (Fig. 5e). Significant changes in the color and the pigmentation of the skin of Balb/c mice were observed as a result of TM treatment and UV radiation by histologic (Fig. 5e bottom panel) and macroscopic appearance of the mouse skin. Severe scarification was observed as the results of treatment with TM which was even more apparent following UVA radiation (data are not shown). H&E-stained mouse skin exhibited a significant (1.5-fold) and a marginal (1.2-fold) increase in the thickness of the viable epidermis of TM-treated and UVA-irradiated skin sections, respectively (Fig. 1Sa–b). Epidermis in the UVA-exposed TM-treated samples was thicker than either in the unirradiated control, or in UVA-irradiated sites referring to a severe epidermal hyperplasia. Prominent deposition of pigments was observed in UVA-irradiated sections. No significant change in the total thickness of mouse skin was observed (Fig. S1b).

4. Discussion

It is well established that phosphorylation and dephosphorylation of proteins are important regulatory events in the signaling pathways of keratinocytes under normal and pathological conditions [7,27]. It has also been demonstrated that the phospho-Ser/Thr-specific protein phosphatases are essential targets in these signaling pathways since they are involved in the mediation of the phosphorylation level of many proteins. In mammalian cells three major phosphatase types, PP1, PP2A and PP2B, are thought to be responsible for the dephosphorylation of more than 90% of the phospho-Ser/Thr residues. These phosphatase types are present in keratinocytes and the roles of PP2A and PP2B have been characterized in controlling differentiation, development, barrier functions and apoptosis of these cells. It appears that PP2A may influence UV irradiation-induced apoptosis of HaCaT cells [28,29] as well as epidermal barrier formation during development [30] *via* regulating the activity and phosphorylation level of Akt kinase as well as MAPK family enzymes. It is suggested that PP2B (calcineurin) is required for the normal differentiation and survival of epidermal cells. PP1 dephosphorylates the retinoblastoma protein [31]; however, other aspects of PP1 functions in physiological or pathological signaling pathways of keratinocytes have not yet been investigated in detail. In this study we characterized the subcellular distribution of PP1 and PP2A activities, and the localization of PP1c isoforms in HaCaT cells. Differential localization of PP1c isoforms in HeLa cells in nuclear fractions during mitosis has already been reported [32]. We show here the presence of all isoforms (PP1cα, PP1cγ and PP1cδ) in HaCaT cells, however regarding subcellular distribution they are all abundant in the cytosolic and cytoskeletal fractions, but PP1cδ appears to be the major isoform in the nucleus. These data are also consistent with the conclusions that PP1 isoforms are targeted to distinct subcellular compartments permitting unique and independent roles in keratinocytes. Moreover, we provide evidence here that PP1 enzymes play an important role in the maintenance of the homeostasis of keratinocytes. This conclusion is supported by the following experimental results: (i) deletion of PP1c is accompanied with decreased cell viability; (ii) cell death induced by physiologically relevant UVA irradiation of HaCaT cells was accompanied by inactivation of PP1 and (iii) both PP1 inhibition and UVA irradiation contribute to the pathological alterations of mouse skin during separate or combined treatments.

Previous studies have demonstrated contradictive results about the effect of 10–16 J/cm^2 UVA radiation on cell viability of keratinocytes. Neither cell viability nor DNA synthesis was affected, only the protein synthesis of the cells were modulated in human cultured keratinocytes [33], while cell viability of HaCaT cells decreased to 41% upon UVA irradiation [34]. Our data suggest that doses higher than the normal daily dose of UVA (10–18 J/cm^2) [35] have a more profound effect on the survival (5–25%) of HaCaT cells than that of UVB radiation (~50% survival). Another surprising distinction between these treatments is that UVA, but not UVB irradiation has an effect on protein phosphatase activity and doses higher than 10 J/cm^2 caused an almost 90% reduction of the activity. The phosphatase assay applied here measures the sum of PP1 and PP2A activities, however, assays in the presence of I-2, a specific inhibitor of PP1, have proved that PP1 is inactivated predominantly by UVA irradiation. These results are in contrast to recently published data implying that PP2A may be profoundly activated upon UV irradiation [29] when the phosphatase activity is determined using a synthesized phosphopeptide substrate. The reasons for this discrepancy is not known, however it should be noted that the UV light source and the doses applied (70 kJ/m^2 and 10 J/cm^2 UVA) are quite different in the reported study [29] and in our present work. UVA irradiation is assumed to be coupled with generation of reactive oxygen species (ROS) in keratinocytes [36]. It has been shown that ROS could induce inactivation of PP1 and PP2A by oxidizing cysteinyl residues and the metal ion(s) at the catalytic centers of PP1c and PP2Ac during cellular senescence of diploid fibroblasts [37]. These data support the hypothesis that a similar inactivation of PP1 (and PP2A) occurs during UVA irradiation of HaCaT cells which is accompanied with UVA-induced cell death. Our finding that the decreased phosphatase activity in siPP1c cells reduced cell viability further supports the vital role of PP1 in HaCaT cells as well as in human primary keratinocytes.

Using a microarray approach we explored the possible role of PP1 enzymes in the regulation of gene expression in human UVA-irradiated keratinocytes. Thereby, we observed the regulation of genes implicated in gene expression, free radical scavenging and carbohydrate metabolism. A modulated transcriptional response was also observed for some genes involved in the regulation of cell cycle, DNA replication, recombination and repair, cell morphology, assembly and organization of the cytoskeleton mainly related to intermediate filament components such as keratins and tumor marker S100A8 as well as histone 1b. The physiological system development and function analysis showed the highest number of affected genes in hair and skin development and function, in tissue development, and genes related to cancer and dermatological diseases and conditions. Expression profiling of human keratinocytes in response to UVA has already been demonstrated [38] but our study is the first to reveal the effect of PP1 silencing on gene expression under resting conditions and following UVA radiation. Nineteen genes were identified as being under the control of PP1 after UVA irradiation and all of them are known to play a crucial role in the normal development of the skin by regulating cytoskeletal elements, gene expression and protein folding and their malfunctions being associated with malignant transformation.

In order to verify data obtained by hybridization arrays, we confirmed the results for the expression of four out of the 19 genes by semi-quantitative Western blot analysis. The expression of keratin 1 and 10 intermediate filament proteins was increased in UVA-exposed and PP1-silenced HaCaT cells. In addition, the distribution and localization of keratins were also altered reminiscent of the changes observed in primary hepatocytes treated with microcystin-LR, a potent inhibitor of both PP1 and PP2A [39]. Consistent with the above data it is reasonable to assume that suppression of the phosphatase activity by PP1 silencing or by UVA irradiation has an effect on intermediate filament reorganization similar to that caused by the phosphatase inhibitory toxin microcystin-LR. Keratins serve an important role in epithelial cell protection by the formation of proteinaceous structural framework, in motility as well as in membrane trafficking. Keratin 1/10 overexpression is increased in skin cancers and is used as a diagnostic tumor marker [40]. Our data prove that the gene and protein expression of keratin 1/10 is upregulated and keratins were differentially localized after UVA irradiation and PP1 silencing indicating an essential role of PP1 enzymes in the maintenance of cytoskeletal integrity. Conversely, the decrease in PP1 activity is involved in the rearrangement of the cytoskeleton possibly contributing to the development of pathological conditions or even to skin cancer. S100A8 calcium binding protein

tontay.beata_285_24

plays a role in the regulation of cell cycle and cell differentiation, and together with keratin 1/10 proteins are upregulated in prostate, gastric and myoepithelial cancers [41]. Oppositely, histone 1b protein was found to be downregulated by PP1 silencing and UVA radiation, suggesting marked changes in chromatin structure, including a global reduction in nucleosome spacing, local reduction in chromatin compaction and changes in the modification of core histones. Moreover, histone H1 participates in the regulation of specific genes that are essential for survival [42]. Although histone 1 (H1) protein may have differential effects in various cell types, its overexpression was found to delay cell cycle progression [43] and to act as a general repressor of transcription [44].

The minimal erythemal dose (MED) of UVA has already been determined on human back skin to be 36.4 J/cm^2 [45]. In this study a total cumulative dose of 531 J/cm^2 given in non-erythemogenic 0.5 MED fractions was shown to elicit erythema response and solar damage to the skin. Applying these parameters, to investigate the long-term, cumulative effect of UVA mouse skin was irradiated with a total dose of 531 J/cm^2 in the presence or absence of the PP1 inhibitor tautomycin (TM). Instead of inflammatory symptoms, we observed increased scarification of the skin as the results of treatment with TM, which was more manifested following UVA radiation with a severe pruritogenic effect as indicated by scratch marks. This is in line with previous findings that cumulative UVA exposure had no inflammatory induction and influence on the mast cell number, but it caused pigmentation, while tumor induction even at the highest UVA dose could not be determined due to the extensive scarification that occurred [46]. The UVA-induced thickening of the epidermis has already been described [45]. We also found that PP1 inhibition by TM similar to UVA irradiation, or a combination of TM and UVA, resulted in epidermal hyperplasia. In addition, similar to our findings in HaCaT keratinocytes we have also observed increased protein levels of keratin 1/10 and S100A8 as well as the decreased protein level of histone 1b in TM-treated UVA-irradiated mouse skin.

In summary, our data imply that PP1 enzymes, besides influencing cytoskeletal and cytosolic processes, may have important roles in the regulation of gene expression in which presumably the PP1cδ isoform is involved as it is predominant in the nucleus of these cells. Moreover, PP1 appears to have important functions in the maintenance of normal homeostasis of keratinocytes since its silencing decreases viability and PP1 inhibition is accompanied with a UVA irradiation-induced decrease of survival of HaCaT cells as well as pathological skin alterations. These data suggest that PP1 is involved in the regulation of important physiological responses of keratinocytes specifically to UVA irradiation and dissecting the roles of PP1 in these signaling networks may initiate the development of novel strategies for prevention and treatment of UV-related pathologies.

Conflict of interest

The authors declare no conflict of interest.

Acknowledgement

This work was supported by grants from the Hungarian Scientific Research Fund OTKA PD104878 (B.L.) and K109249 (F.E.), and by the TÁMOP 4.2.2.-08/1-2008-0019 DERMINOVA, TAMOP 4.2.2.-08/1-2008-0019, TÁMOP 4.2.2/B-10/1-2010-0024, and TÁMOP-4.2.4.A/2-11-1-2012-0001 projects. We acknowledge the help of Szilárd Póliska (UD Genomed, Debrecen, Hungary) in microarray analysis. We are grateful to Dr. Tamás Bíró for providing us the NHEK cell line. The authors are indebted to Ágnes Németh, Andrea Docsa and Erzsébet Herbály for their excellent technical assistance.

Appendix A. Supplementary data

Supplementary data to this article can be found online at http://dx.doi.org/10.1016/j.bbadis.2014.11.005.

References

[1] T.P. Coohill, M.J. Peak, J.G. Peak, The effects of the ultraviolet wavelengths of radiation present in sunlight on human cells *in vitro*, Photochem. Photobiol. 46 (1987) 1043–1050.
[2] C.A. Cole, P.D. Forbes, R.E. Davies, An action spectrum for UV photocarcinogenesis, Photochem. Photobiol. 43 (1986) 275–284.
[3] F.R. de Gruijl, H.J. Sterenborg, P.D. Forbes, R.E. Davies, C. Cole, G. Kelfkens, H. van Weelden, H. Slaper, J.C. van der Leun, Wavelength dependence of skin cancer induction by ultraviolet irradiation of albino hairless mice, Cancer Res. 53 (1993) 53–60.
[4] M. Ichihashi, M. Ueda, A. Budiyanto, T. Bito, M. Oka, M. Fukunaga, K. Tsuru, T. Horikawa, UV-induced skin damage, Toxicology 189 (2003) 21–39.
[5] C. Cao, Y. Wan, Parameters of protection against ultraviolet radiation-induced skin cell damage, J. Cell. Physiol. 220 (2009) 277–284.
[6] B.S. Rosenstein, D.L. Mitchell, Action spectra for the induction of pyrimidine(6-4) pyrimidone photoproducts and cyclobutane pyrimidine dimers in normal human skin fibroblasts, Photochem. Photobiol. 45 (1987) 775–780.
[7] D.E. Heck, D.R. Gerecke, A.M. Vetrano, J.D. Laskin, Solar ultraviolet radiation as a trigger of cell signal transduction, Toxicol. Appl. Pharmacol. 195 (2004) 288–297.
[8] G.T. Bowden, Prevention of non-melanoma skin cancer by targeting ultraviolet-B-light signalling, Nat. Rev. Cancer 4 (2004) 23–35.
[9] W. Chen, Q. Tang, M.S. Gonzales, G.T. Bowden, Role of p38 MAP kinases and ERK in mediating ultraviolet-B induced cyclooxygenase-2 gene expression in human keratinocytes, Oncogene 20 (2001) 3921–3926.
[10] W. Peti, A.C. Nairn, R. Page, Structural basis for protein phosphatase 1 regulation and specificity, FEBS J. 280 (2013) 596–611.
[11] G.J. Barton, P.T. Cohen, D. Barford, Conservation analysis and structure prediction of the protein serine/threonine phosphatases: sequence similarity with diadenosine tetraphosphatase from *Escherichia coli* suggests homology to the protein phosphatases, Eur. J. Biochem. 220 (1994) 225–237.
[12] E. Heroes, B. Lesage, J. Gornemann, M. Beullens, L. Van Meervelt, M. Bollen, The PP1 binding code: a molecular-lego strategy that governs specificity, FEBS J. 280 (2013) 584–595.
[13] M. Bollen, W. Peti, M.J. Ragusa, M. Beullens, The extended PP1 toolkit: designed to create specificity, Trends Biochem. Sci. 35 (2010) 450–458.
[14] K. Sasaki, H. Shima, Y. Kitagawa, S. Irino, T. Sugimura, M. Nagao, Identification of members of the protein phosphatase 1 gene family in the rat and enhanced expression of protein phosphatase 1 alpha gene in rat hepatocellular carcinomas, Jpn. J. Cancer Res. 81 (1990) 1272–1280.
[15] V. Dombradi, J.M. Axton, N.D. Brewis, E.F. da Cruz e Silva, L. Alphey, P.T. Cohen, *Drosophila* contains three genes that encode distinct isoforms of protein phosphatase 1, Eur. J. Biochem. 194 (1990) 739–745.
[16] P.L. Cohen, Autoimmunity and lymphoproliferation: two genes are worse than one, Mol. Interv. 2 (2002) 427–430.
[17] T. Kuntziger, H.B. Landsverk, P. Collas, R.G. Syljuasen, Protein phosphatase 1 regulators in DNA damage signaling, Cell Cycle 10 (2011) 1356–1362.
[18] B. Lontay, Z. Serfozo, P. Gergely, M. Ito, D.J. Hartshorne, F. Erdodi, Localization of myosin phosphatase target subunit 1 in rat brain and in primary cultures of neuronal cells, J. Comp. Neurol. 478 (2004) 72–87.
[19] B. Lontay, A. Kiss, P. Gergely, D.J. Hartshorne, F. Erdodi, Okadaic acid induces phosphorylation and translocation of myosin phosphatase target subunit 1 influencing myosin phosphorylation, stress fiber assembly and cell migration in HepG2 cells, Cell. Signal. 17 (2005) 1265–1275.
[20] B. Lontay, K. Bodoor, D.H. Weitzel, D. Loiselle, C. Fortner, S. Lengyel, D. Zheng, J. Devente, R. Hickner, T.A. Haystead, Smoothelin-like 1 protein regulates myosin phosphatase-targeting subunit 1 expression during sexual development and pregnancy, J. Biol. Chem. 285 (2010) 29357–29366.
[21] A. Takai, K. Sasaki, H. Nagai, G. Mieskes, M. Isobe, K. Isono, T. Yasumoto, Inhibition of specific binding of okadaic acid to protein phosphatase 2A by microcystin-LR, calyculin-A and tautomycin: method of analysis of interactions of tight-binding ligands with target protein, Biochem. J. 306 (Pt 3) (1995) 657–665.
[22] B. Favre, P. Turowski, B.A. Hemmings, Differential inhibition and posttranslational modification of protein phosphatase 1 and 2A in MCF7 cells treated with calyculin-A, okadaic acid, and tautomycin, J. Biol. Chem. 272 (1997) 13856–13863.
[23] A. Hirschi, M. Cecchini, R.C. Steinhardt, M.R. Schamber, F.A. Dick, S.M. Rubin, An overlapping kinase and phosphatase docking site regulates activity of the retinoblastoma protein, Nat. Struct. Mol. Biol. 17 (2010) 1051–1057.
[24] S. Hur, H. Lee, Y. Kim, B.H. Lee, J. Shin, T.Y. Kim, Sargaquinoic acid and sargachromenol, extracts of *Sargassum sagamianum*, induce apoptosis in HaCaT cells and mice skin: its potentiation of UVB-induced apoptosis, Eur. J. Pharmacol. 582 (2008) 1–11.
[25] P. Boukamp, R.T. Petrussevska, D. Breitkreutz, J. Hornung, A. Markham, N.E. Fusenig, Normal keratinization in a spontaneously immortalized aneuploid human keratinocyte cell line, J. Cell Biol. 106 (1988) 761–771.
[26] P. Thraves, Z. Salehi, A. Dritschilo, J.S. Rhim, Neoplastic transformation of immortalized human epidermal keratinocytes by ionizing radiation, Proc. Natl. Acad. Sci. U. S. A. 87 (1990) 1174–1177.
[27] D.N. Syed, F. Afaq, H. Mukhtar, Differential activation of signaling pathways by UVA and UVB radiation in normal human epidermal keratinocytes, Photochem. Photobiol. 88 (2012) 1184–1190.
[28] L. Li, K. Sampat, N. Hu, J. Zakari, S.H. Yuspa, Protein kinase C negatively regulates Akt activity and modifies UVC-induced apoptosis in mouse keratinocytes, J. Biol. Chem. 281 (2006) 3237–3243.
[29] E.R. Lee, J.H. Kim, H.Y. Choi, K. Jeon, S.G. Cho, Cytoprotective effect of eriodictyol in UV-irradiated keratinocytes *via* phosphatase-dependent modulation of both the p38 MAPK and Akt signaling pathways, Cell. Physiol. Biochem. 27 (2011) 513–524.

tontay.beata_285_24

[30] R.F. O'Shaughnessy, J.C. Welti, K. Sully, C. Byrne, Akt-dependent Pp2a activity is required for epidermal barrier formation during late embryonic development, Development 136 (2009) 3423–3431.
[31] M.J. Edwards, R.C. Thomas, Protein phosphatase type 1-dependent dephosphorylation of the retinoblastoma tumor suppressor protein in ultraviolet-irradiated human skin and keratinocytes, J. Invest. Dermatol. 115 (2000) 88–94.
[32] P.R. Andreassen, F.B. Lacroix, E. Villa-Moruzzi, R.L. Margolis, Differential subcellular localization of protein phosphatase-1 alpha, gamma1, and delta isoforms during both interphase and mitosis in mammalian cells, J. Cell Biol. 141 (1998) 1207–1215.
[33] J.H. Chung, J.I. Youn, Effect of ultraviolet A on IL-1 production by ultraviolet B in cultured human keratinocytes, J. Dermatol. Sci. 9 (1995) 87–93.
[34] Y. Saitoh, A. Miyanishi, H. Mizuno, S. Kato, H. Aoshima, K. Kokubo, N. Miwa, Super-highly hydroxylated fullerene derivative protects human keratinocytes from UV-induced cell injuries together with the decreases in intracellular ROS generation and DNA damages, J. Photochem. Photobiol. B 102 (2011) 69–76.
[35] B. Staberg, H.C. Wulf, P. Klemp, T. Poulsen, H. Brodthagen, The carcinogenic effect of UVA irradiation, J. Invest. Dermatol. 81 (1983) 517–519.
[36] A. Svobodova, J. Psotova, D. Walterova, Natural phenolics in the prevention of UV-induced skin damage. A review, Biomed. Pap. Med. Fac. Univ. Palacky Olomouc 147 (2003) 137–145.
[37] H.S. Kim, M.C. Song, I.H. Kwak, T.J. Park, I.K. Lim, Constitutive induction of p-Erk1/2 accompanied by reduced activities of protein phosphatases 1 and 2A and MKP3 due to reactive oxygen species during cellular senescence, J. Biol. Chem. 278 (2003) 37497–37510.
[38] Y.Y. He, J.L. Huang, R.H. Sik, J. Liu, M.P. Waalkes, C.F. Chignell, Expression profiling of human keratinocyte response to ultraviolet A: implications in apoptosis, J. Invest. Dermatol. 122 (2004) 533–543.
[39] D.M. Toivola, R.D. Goldman, D.R. Garrod, J.E. Eriksson, Protein phosphatases maintain the organization and structural interactions of hepatic keratin intermediate filaments, J. Cell Sci. 110 (Pt 1) (1997) 23–33.
[40] V. Karantza, Keratins in health and cancer: more than mere epithelial cell markers, Oncogene 30 (2011) 127–138.
[41] I. Salama, P.S. Malone, F. Mihaimeed, J.L. Jones, A review of the S100 proteins in cancer, Eur. J. Surg. Oncol. 34 (2008) 357–364.
[42] Y. Fan, A.I. Skoultchi, Genetic analysis of H1 linker histone subtypes and their functions in mice, Methods Enzymol. 377 (2004) 85–107.
[43] D.T. Brown, B.T. Alexander, D.B. Sittman, Differential effect of H1 variant overexpression on cell cycle progression and gene expression, Nucleic Acids Res. 24 (1996) 486–493.
[44] H. Weintraub, High-resolution mapping of S1- and DNase I-hypersensitive sites in chromatin, Mol. Cell. Biol. 5 (1985) 1538–1539.
[45] R.M. Lavker, G.F. Gerberick, D. Veres, C.J. Irwin, K.H. Kaidbey, Cumulative effects from repeated exposures to suberythemal doses of UVB and UVA in human skin, J. Am. Acad. Dermatol. 32 (1995) 53–62.
[46] J.M. de Laat, S. Seite, M. Groenendijk, W.A. van Vloten, F.R. de Gruijl, Chronic UVA (365-nm) irradiation induced scratching in hairless mice: dose–time dependency and the effect of ketanserin, Exp. Dermatol. 6 (1997) 292–297.

RESEARCH ARTICLE

Myosin phosphatase and RhoA-activated kinase modulate neurotransmitter release by regulating SNAP-25 of SNARE complex

Dániel Horváth[1☯], István Tamás[1☯], Adrienn Sipos[1], Zsuzsanna Darula[2], Bálint Bécsi[1,3], Dénes Nagy[1], Judit Iván[1,3], Ferenc Erdődi[1,3], Beáta Lontay[1]*

1 Department of Medical Chemistry, Faculty of Medicine, University of Debrecen, Debrecen, Hungary, **2** Hungarian Academy of Sciences, Proteomics Research Group, Biological Research Centre, Szeged, Hungary, **3** MTA-DE Cell Biology and Signaling Research Group, Faculty of Medicine, University of Debrecen, Debrecen, Hungary

☯ These authors contributed equally to this work.
* lontay@med.unideb.hu

Check for updates

OPEN ACCESS

Citation: Horváth D, Tamás I, Sipos A, Darula Z, Bécsi B, Nagy D, et al. (2017) Myosin phosphatase and RhoA-activated kinase modulate neurotransmitter release by regulating SNAP-25 of SNARE complex. PLoS ONE 12(5): e0177046. https://doi.org/10.1371/journal.pone.0177046

Editor: Sidney Yu, Chinese University of Hong Kong, HONG KONG

Received: January 31, 2017

Accepted: April 23, 2017

Published: May 9, 2017

Copyright: © 2017 Horváth et al. This is an open access article distributed under the terms of the Creative Commons Attribution License, which permits unrestricted use, distribution, and reproduction in any medium, provided the original author and source are credited.

Data Availability Statement: All relevant data are within the paper and its Supporting Information files.

Funding: The funders had no role in study design, data collection and analysis, decision to publish, or preparation of the manuscript.

Competing interests: The authors have declared that no competing interests exist.

Abbreviations: PP1, protein phosphatase-1; PP1c, PP1 catalytic subunit; MP, myosin phosphatase;

Abstract

Reversible phosphorylation of neuronal proteins plays an important role in the regulation of neurotransmitter release. Myosin phosphatase holoenzyme (MP) consists of a protein phosphatase-1 (PP1) catalytic subunit (PP1c) and a regulatory subunit, termed myosin phosphatase targeting subunit (MYPT1). The primary function of MP is to regulate the phosphorylation level of contractile proteins; however, recent studies have shown that MP is localized to neurons, and is also involved in the mediation of neuronal processes. Our goal was to investigate the effect of RhoA-activated kinase (ROK) and MP on the phosphorylation of one potential neuronal substrate, the synaptosomal-associated protein of 25 kDa (SNAP-25). SNAP-25 is a member of the SNARE (soluble N-ethylmaleimide sensitive factor attachment protein receptor) complex, along with synaptobrevin and syntaxin, and the primary role of SNAP25 is to mediate vesicle fusion. We showed that MYPT1 interacts with SNAP-25, as revealed by immunoprecipitation and surface plasmon resonance based binding studies. Mass spectrometry analysis and *in vitro* phosphorylation/dephosphorylation assays demonstrated that ROK phosphorylates, while MP dephosphorylates, SNAP-25 at Thr138. Silencing MYPT1 in B50 neuroblastoma cells increased phosphorylation of SNAP-25 at Thr138. Inhibition of PP1 with tautomycetin increased, whereas inhibition of ROK by H1152, decreased the phosphorylation of SNAP-25 at Thr138 in B50 cells, in cortical synaptosomes, and in brain slices. In response to the transduction of the MP inhibitor, kinase-enhanced PP1 inhibitor (KEPI), into synaptosomes, an increase in phosphorylation of SNAP-25 and a decrease in the extent of neurotransmitter release were detected. The interaction between SNAP-25 and syntaxin increased with decreasing phosphorylation of SNAP-25 at Thr138, upon inhibition of ROK. Our data suggest that ROK/MP play a crucial role in vesicle trafficking, fusion, and neurotransmitter release by oppositely regulating the phosphorylation of SNAP-25 at Thr138.

MYPT1, myosin phosphatase target subunit-1; ROK, RhoA-activated kinase; TMC, tautomycetin; SNARE, soluble N-ethylmaleimide sensitive factor attachment receptor; SNAP-25, 25 kDa synaptosomal associated protein; PKA, protein kinase A; PKC, protein kinase C; CPI-17, C-kinase activated phosphatase inhibitor protein of 17 kDa; KEPI, kinase-enhanced PP1 inhibitor; H1152, (S)-(+)-2-methyl-1-[(4-methyl-5-isoquinolinyl)sulfonyl] homopiperazine·2HCl; Y27632, *trans*-4-[(1R)-1-aminoethyl]-*N*-4-pyridinylcyclohexane-carboxiamide dihydrochloride; SDS-PAGE, sodium dodecyl sulfate-polyacrylamide gel electrophoresis; PBS, phosphate buffered saline; TBS, Tris-buffered saline solution; TBST, Tris-buffered saline solution containing 0.1% Tween-20; aCSF, artificial cerebrospinal fluid; FBS, fetal bovine serum; BSA, bovine serum albumin; PAS, protein-A Sepharose; MC-LR, microcystin-LR; IP, immunoprecipitation; PEI, polyethylenimine; DMEM, Dulbecco's modified Eagle's medium; RIPA, radioimmunoprecipitation assay; TCA, trichloroacetic acid; SPR, surface plasmon resonance.

Introduction

Exocytosis is an essential component of cell signaling throughout the body and underpins a diverse array of essential physiological pathways, even though exocytosis varies considerably between cell types and can require adaptations [1]. Neurotransmitter release is a specialized mechanism of exocytosis, which includes Ca^{2+}-dependent release of neurotransmitters from synaptic vesicles [2]. The elevated calcium level is the key regulator of the process, but other regulatory elements have also been identified. In a nerve terminal, synaptic vesicle docking and release are restricted to an active zone. A pool of already docked vesicles resides at the pre-synaptic target membrane called the readily releasable pool of vesicles. A single calcium spike results in only a partial release of this pool, suggesting an additional level of regulation of neurotransmission [3]. The recycling pool contains 5–20% of all vesicles and is refilled continuously by newly synthetized vesicles depending on the physiological frequency of stimulation [4]. However, the majority of vesicles belong to the third pool type, the reserve pool, which provides a depot of synaptic vesicles from which release is triggered by intense stimulation [5].

The SNARE (soluble N-ethylmaleimide sensitive factor attachment protein receptor) complex is one of the highly conserved targets of regulated exocytosis. SNAREs are members of a family of proteins which form a complex and regulate neuronal exocytosis. The t-SNARES, such as syntaxin and synaptosomal-associated protein of 25 KDa (SNAP-25), are attached to the target membrane of the vesicles. Other components, such as synaptobrevin (VAMP), are located on the vesicle membrane (v-SNARES) and binds to its cognate t-SNARE [6, 7]. SNARE is believed to form a highly stable trimeric exocytotic complex [8] that generates a twisted bundle of four parallel α helices to bring the two membranes into close proximity and allow fusion [9]. The real number of releasable vesicles are modulated by the rate of priming and depriming of vesicles, and is related to the preassembling or the dissociation of SNARE complex, respectively [10].

Regulation of the SNARE complex, which is dependent on protein phosphorylation at serine/threonine (Ser/Thr) residues, is necessary for proper neuronal functions [11]. SNARE activation takes place in a step-wise fashion to enhance or to block its interactions. T-SNAREs must join and be delivered to the site of action before creating a complex with v-SNARE. Synaptotagmin is responsible for preventing vesicles from fusing to the membrane, even after they are docked, by interacting with SNAREs [7]. Phosphorylation of SNAREs by protein kinases also prevents the formation of the SNARE complex, when SNAREs are targeted to their site of action [12]. SNAP-25, which has multiple phosphorylation sites, is a major regulatory target of protein kinases and phosphatases [13]. SNAP-25 was found to be differentially phosphorylated by protein kinase A (PKA) and C (PKC) in neuroendocrine PC12 cell. PKC regulates refilling of the vesicle pools and recycling of SNAP-25. After the readily releasable pool has been depleted, SNAP25 phosphorylation by PKC makes elements of the complex more available to form SNARE complexes and dock more vesicles [14]. PKA phosphorylates the Thr138 residue of SNAP-25 specifically [15], and regulates the size of the readily releasable pool of vesicles, supposedly by modulating the protein binding properties of SNAP-25 [14].

Compared to the phosphorylation by protein kinases, dephosphorylation mechanisms catalyzed by protein phosphatases are poorly understood. The effects of phosphatase inhibitors on neuronal exocytosis have been investigated. Tautomycetin, a PP1-specific inhibitor, decreases depolarization-induced exocytosis, while Y27632, a ROK-specific inhibitor, has the opposite effect [16]. Myosin phosphatase (MP) first identified in smooth muscles, is a Ser/Thr specific protein phosphatase 1 (PP1) consisting of a 38 kDa catalytic subunit (PP1c) of the β/δ isoform, a 130/133 kDa myosin phosphatase target subunit-1 (MYPT1) and a 20 kDa subunit of largely unknown function [17]. MP (also termed PP1M) is involved in exocytotic processes; MYPT1

interacts and affects the dephosphorylation of several neuronal proteins [16]. Phosphorylation of Thr696 and/or Thr853 in MYPT1 by ROK results in the inhibition of MP [18, 19], and these regulatory events have also been identified in cortical synaptosomes [16]. MP is present in cortical synaptosomes in association with ROK [20], suggesting that MP is involved in synaptic signaling. ROK and MP regulate neurotransmission via phosphorylation/dephosphorylation of several presynaptic proteins (e.g., myosin-II, synapsin-I, syntaxin-1) that are involved in neurotransmitter release [16].

In the present study we tested the hypothesis that ROK and MP regulate SNAP-25 through reversible phosphorylation. Our results suggest that SNAP25 interacts with MP via binding to MYPT1. ROK phosphorylates SNAP-25 at the Thr138 and the dephosphorylation is catalyzed by MP. Phosphorylation of SNAP-25 by ROK results in a decrease in KCl-induced synaptosomal exocytosis, while dephosphorylation by MP accelerates the process. Our data suggest that ROK/MP enzymes play a crucial role in vesicle trafficking, fusion and neurotransmitter release through the regulation of the assembly of the SNARE complex.

Materials and methods

Materials

All chemicals were obtained from Sigma-Aldrich (St. Louis, MO, USA) unless otherwise indicated. Microcystin-LR was produced and purified as described previously [21].

Antibodies

Anti-SNAP-25, anti-actin, anti-Flag, anti-GST, anti-syntaxin, peroxidase conjugated anti-rabbit IgG and anti-chicken IgG were purchased from Sigma-Aldrich (St. Louis, MO, USA). Anti-SNAP-25^{pThr138} (Abgent, San Diego, CA, USA), anti-MYPT1$^{1\text{-}296}$ [20], anti-PP1cδ (Millipore, Billerica, MA, USA), anti-GAPDH (Santa Cruz, CA, USA), anti-CPI17^{pThr38} [22], horseradish peroxidase-linked anti-mouse IgG (Cell Signalling, Danvers, MA, USA), Clean-Blot IP Detection Reagent (Thermo Scientific, Waltham, MA, USA) and Texas Red-X phalloidin (Life Technologies, Carlsbad, CA, USA) were purchased as indicated. Alexa Fluor 488-conjugated anti-rabbit IgG, Alexa Fluor 546-conjugated anti-mouse IgG, Alexa Fluor 546-conjugated anti-goat IgG and To-Pro-3 iodide were obtained from Molecular Probes (Eugene, OR, USA).

Western blotting

Solubilized proteins from cells or synaptosomes were boiled with 5x SDS-PAGE (sodium dodecyl sulphate-polyacrylamide gel electrophoresis) sample buffer (50% glycerol, 10% SDS, 0.31 M Tris, 100 mM dithiothreitol, 0.01% bromophenol blue) at 100˚C for 5 min and proteins were separated by SDS-PAGE on 12% (w/V) polyacrylamide gel [23]. After gel electrophoresis, proteins were transferred to nitrocellulose membrane (Bio-Rad, Hemel Hempstead, UK). Membranes were incubated with blocking solution (5% bovine serum albumin (BSA) in Tris buffered saline (TBS: 136 mM NaCl, 2.7 mM KCl, 25 mM Tris-HCl pH 7.4) containing 0.1% Tween-20 (TBST) for 1 h at room temperature, and then with the primary antibodies overnight at 4˚C. Membranes were washed with TBST and incubated with the secondary antibodies for 1–2 h at room temperature. Primary and secondary antibodies were diluted in TBST containing 0.5% BSA. Immunoreactions were developed by enhanced chemiluminescence and visualized using FluorChem FC2 Imager (Alpha Innotech, San Leandro, CA, USA). Densitometry analysis of immunoreactive bands was carried out using Image J software (.NIH Bethesda, USA).

Immunoprecipitation

Anti-SNAP-25, anti-MYPT1$^{1\text{-}296}$ and anti-PP1cδ antibodies were bound to protein-A Sepharose (PAS) resin (GE Healthcare, Little Chalfont, UK) in the presence of immunoprecipitation (IP) buffer (50 mM Tris-HCl pH 7.4, 150 mM NaCl, 1 mM EDTA, 1% Triton X-100) by incubation for 1 h at 4˚C. Precleared (previously incubated with PAS) B50 neuroblastoma cell lysate was added to PAS-antibody complexes and incubated for 90 min at 4˚C. After centrifugation (4˚C, 900 g, 3 min) the supernatant was removed, and PAS-antibody-proteins complexes were washed with IP buffer twice, then once with phosphate buffered saline (PBS). The supernatant was removed and PAS-antibody-protein complexes were boiled at 100˚C for 5 min with SDS-PAGE sample buffer, then the samples were subjected to Western blot analysis.

Surface plasmon resonance

Interactions of MYPT1 and its mutants with SNAP-25 were analysed by surface plasmon resonance (SPR) using a Biacore 3000 instrument (GE Healthcare, Little Chalfont, UK). Anti-GST was coupled on the surface of a CM5 chip by amine-coupling, then full-length GST-MYPT1^{WT} or its C-terminal fragment (GST-MYPT1$^{667-1004}$) was captured on the surface. His-tagged MYPT1 proteins (His-MYPT1$^{1-296}$ or His-MYPT1$^{1-633}$) were immobilized directly on CM5 sensor chips by amine-coupling. Determination of the binding of Flag-SNAP-25 on these surfaces was performed as described previously [24]. Kinetic parameters and the dissociation constant (K_D) values were extracted from the sensorgrams with BIAevaluation 3.1 software using a 1:1 interaction model.

In vitro kinase assay

Phosphorylation of purified Flag-SNAP-25 by RhoA-activated protein kinase (ROK) was performed in an *in vitro* kinase assay using radioactive phosphoryl donor substrate. Flag-SNAP-25 (5 μM) was incubated with or without (control) 20 ng/μl ROK (Millipore, Billerica, MA, USA) in the presence of 1 mM γ-[^{32}P]ATP (Institute of Isotopes Co., Budapest, Hungary) and 1 μM microcystin-LR (MC-LR, a protein phosphatase inhibitor) for 120 min at 30˚C in a ROK assay buffer containing 25 mM β-glycerophosphate, 0.5 mM EGTA, 0.5 mM dithiothreitol (DTT), 5 mM $MgCl_2$, and 20 mM MOPS (pH 7.2). The reactions were terminated by the addition of hot SDS-PAGE sample buffer. After SDS-PAGE, the phosphorylation of proteins was verified by autoradiography of the gels.

Protein phosphorylation/dephosphorylation assay

The lysate of tsA201 cells expressing Flag-SNAP-25 was incubated with Anti-Flag M2 affinity gel to pull down Flag-SNAP-25. Beads were washed with TBS, and incubated with ROK (final concentration: 20 ng/μl) and ATP (final concentration: 0.5 mM) for 30 min at 30˚C in the presence 1 μM of microcystin-LR in ROK assay buffer. Control samples were handled in the same way without addition of ROK. After phosphorylation, the beads were washed twice with TBS and incubated in the presence or absence of the subunits of myosin phosphatase (purified Flag-MYPT1 and recombinant PP1cδ at a final concentration of 25 nM and 5 nM, respectively) for 15 min at 30˚C. After washing with TBS, beads were incubated with SDS-PAGE sample buffer at 100˚C for 5 min. Phosphorylation and dephosphorylation of SNAP-25 were analysed by Western blot using SNAP-25^{pThr138} phospho-specific antibody and anti-SNAP-25 for a loading control.

Mass spectrometry analysis

Bands of interest were subjected to in-gel digestion using side-chain protected porcine trypsin (37˚C, 4h). Approximately 80% of the peptide mixtures were subjected to phosphopeptide-enrichment using TiO_2 [25]. The phosphopeptide fractions, as well as the remaining 20% of the original samples, were analyzed by data-dependent LC-MS/MS using an Orbitrap Elite mass spectrometer (MS spectra acquired in the Orbitrap, MS/MS spectra in the linear ion trap). Peak lists generated from the MS/MS data by the PAVA software [26] were searched against the human subset of the Swissprot database (downloaded 06/10/2014; 20265 target sequences concatenated with a randomized sequence for each entry) using the ProteinProspector search engine (v.5.10.9.). Search parameters: enzyme: trypsin with maximum 1 missed cleavage; fixed modification: carbamidomethyl (Cys); variable modifications: acetylation (protein N-terminus), oxidation (Met), pyroglutamic acid formation (N-terminal Gln) allowing 2 variable modifications per peptide; mass accuracy: 5 ppm and 0.8 Da for precursor and fragment ions (both monoisotopic), respectively. Subsequently another search was conducted on the subset of confidently identified proteins using the same search parameters except that 2 missed cleavages were allowed, and phosphorylation on Ser/Thr was added as variable modification allowing 3 variable modifications/peptide. For all searches the following acceptance criteria were applied: score>22 and 15, and E-value<0.01 and 0.05 for protein and peptide identifications, respectively. For phosphopeptide site assignments, SLIP score threshold [27] was set to 6 (indicating 95% confidence in site localization). All phosphopeptide assignments were inspected manually.

Site-directed mutagenesis

Bacterial expression vector pReceiver-M13, which encodes wild type SNAP-25, was purchased from GeneCopoeia (Rockville, MD, USA). Point mutation of Thr138 of SNAP-25 to alanine was performed using QuickChange II XL Site-Directed Mutagenesis Kit (Qiagen, Hilden, Germany) and primers described in S1 Table. Newly synthetized mutant DNA was transformed into XL10-Blue supercompetent cells (Agilent, Santa Clara, CA, USA) and mutant plasmids were purified using EZ-10 Spin Column Plasmid DNA Minipreps Kit (Bio Basic, Markham, Canada). The sequence of the mutant was analysed and verified by DNA sequencing.

Protein production and purification

Flag-SNAP-25 or Flag-KEPI plasmids (GeneCopoeia, Rockville, MD, USA) were transfected into tsA201 cells using polyethylenimine (PEI) transfection reagent. The plasmids (15 μg) and PEI (30 μl) were diluted in 150 mM sterile NaCl solution and incubated for 30 minutes. One ml transfection mixture was added to 4 ml serum-free Dulbecco's modified Eagle's medium (DMEM) and pipetted onto the adherent tsA201 cells (50–60% confluency). Six hours later 5 ml of 20% fetal bovine serum (FBS) containing DMEM was added to the cells, which were grown for an additional 18 hours before collecting for analysis

Cell culture and treatment

B50 neuroblastoma cells (purchased from Sigma, St. Louis, MO, USA) were maintained in Dulbecco's modified Eagle's medium supplemented with 10% (V/V) FBS and 2 mM L-glutamine in a 5% CO_2-humidified atmosphere at 37˚C. Cells were plated into 6-well culture plates, the medium was removed after reaching a confluent state, and cells were synchronized via incubation in serum-free media for 24 h. To inhibit PP1 and ROK activity, tautomycetin (TMC) and H1152 (Santa Cruz Biotechnology, Santa Cruz, CA, USA) were added to the

medium at concentrations of 5 μM and 10 μM for 1 h and 30 min, respectively. Cells were harvested in radioimmunoprecipitation assay (RIPA) buffer (25 mM Tris-HCl pH 7.6, 150 mM NaCl, 0.25% sodium deoxycholate, 1% NP-40, 0.1% sodium dodecyl sulphate) containing protease inhibitors (Roche, Basel, Switzerland) and 1 μM of microcystin-LR. Proteins were solubilized by sonication and protein concentrations were determined with Pierce BCA Protein Assay Kit (Thermo Scientific, Waltham, MA, USA).

Gene silencing

The siRNA delivery was carried out with a reverse transfection protocol. Cells at 80% confluency were washed with sterile 1x PBS, trypsinized, and transfected with 100 nM double stranded siRNA (Thermo Scientific Inc., see S2 Table) consisting of a pool of 4 different siRNAs (S3 Table) targeting the endogenous MYPT1 subunit of MP. For the transfections, DharmaFECT 2 (Dharmacon, Lafayette, CO, USA) transfection reagent was used according to the manufacturer's instructions. After 48 hours, cells were either subjected to MTT or phosphatase activity assays, or lysed and prepared for Western blot analysis. Gene knock down experiments were carried out in 6-well plates ($1x10^5$ cells/well) for Western-blot and phosphatase activity assays and in a 96-well format for MTT assays (~$3x10^3$ cells/well).

Assay of protein phosphatase activity

B50 neuroblastoma cells were treated with TMC (5 μM) or H1152 (10 μM) inhibitors for 1 hour and 30 mins respectively and then lysed. Protein phosphatase activity in the lysates were measured using ^{32}P-labelled 20 kDa myosin light chain (^{32}P-MLC20) substrate in TM buffer (20 mM Tris-HCl, 0.1% β-mercaptoethanol, pH 7.4). The reaction was initiated by the addition of ^{32}P-MLC20 at a final concentration of 1 μM. After 5 min of incubation at 30˚C the reaction was terminated by the addition of 200 μl 10% trichloroacetic acid (TCA) and 200 μl 6 mg/ml BSA. After centrifugation, the $^{32}P_i$ content of the supernatant was measured in a Tri-Carb 2800TR scintillation counter (PerkinElmer, Waltham, MA, USA).

MTT assay

Viability of B50 cells were studied by MTT assay as described before [28]. Shortly, cells were synchronized in serum-free DMEM medium and were treated with TMC and H1152 as detailed before. Ten μl of MTT (3-(4,5-dimethylthiazol-2-yl)-2,5-diphenyltetrazolium bromide dissolved in PBS) solution (5 mg/ml) was added and the cells were incubated in a 5% CO_2-humidified atmosphere at 37˚C for 1 hour. The formazan crystals were dissolved in dimethyl sulfoxide (DMSO) and the absorbance was determined by a photometer (LabSystems Multiskan MS, Labsystems Diagnostics Oy, Vantaa, Finland) at 540 nm wavelength.

Synaptosome preparation and treatment

Synaptosomes were prepared from C3H mouse cerebral cortex using an established protocol [16] with modifications detailed here. Mice (3-5/experiment) were euthanized by carbon dioxide inhalation. After decapitation, the cortex was removed and immersed in homogenization buffer (0.32 M sucrose, 1.0 mM EDTA, 0.25 mM DTT, pH 7.4) in a ratio of 10 ml ice-cold buffer to 1 g of cortex. Tissue was homogenized in a glass potter and the homogenate was centrifuged at 1000 g for 10 min at 4˚C using an Allegra X-12R centrifuge (Beckman Coulter, Brea, CA, USA). The supernatant was collected into a new tube, the volume was increased to 12 ml with homogenization buffer, and two 2 ml volumes of the diluted supernatant were added slowly to the top of a Percoll gradient (2–2 ml of 23; 15; 10; 3% Percoll/homogenization

buffer) in polycarbonate tubes. Tubes were centrifuged at 32500 g for 5 min at 4˚C using Beckman L7-55 ultracentrifuge (Beckman Instruments Inc., Fullerton, CA, USA). Fractions between 10/15 and 15/23% phases were collected, diluted with four-times volume of Krebs buffer (118 mM NaCl, 5 mM KCl, 25 mM $NaHCO_3$, 1 mM $MgCl_2$, 10 mM D-glucose, pH 7.4), and centrifuged at 12600 g for 25 min at 4˚C. The supernatant was removed and the pellet was resuspended in Krebs buffer and centrifuged again at 12600 g for 20 min at 4˚C. The synaptosome pellet was resuspended in 3 ml of Krebs buffer and $CaCl_2$ was added at a final concentration of 1.2 mM, then were incubated at 30˚C for 1 h in the presence or absence of inhibitors (5 μM TMC or 10 μM H1152) and KCl.

The protocol for animal handling (5/2015/DEMÁB; 6/2011/DEMÁB) was authorized by the Animal Care and Protection Committee of the University of Debrecen, and was in accordance with the guidelines of the European Union Council, as well as the Hungarian regulations on the use of laboratory animals. Mice were given *ad libitum* access to food and water and were kept at 25˚C temperature, applying a 12 hour light/12 hour dark cycle. The veterinarian at the University of Debrecen examined the health status of the mice every month, and in case of potential sickness, microbiological examinations are conducted and the appropriate interventions (therapy, quarantine) are applied. Mice were raised in the Experimental Animal House of the University of Debrecen, Debrecen, Hungary (XV-KÁT/2000) and supplied by Dr. Balázs Pál (licence number: 6/2011/DEMÁB). The Animal House is undergoing regular authority supervision every 2 years.

Protein transduction into synaptosomes and determination of exocytosis

Purified Flag-KEPI protein [29] was introduced into synaptosomes according to a previously described protocol [30] with slight modification. Flag-peptide or Flag-KEPI (0.3 μg/μl) was added to the synaptosomes resuspended in HBS buffer (142 mM NaCl, 2.4 mM KCl, 1.2 mM K_2HPO_4, 1 mM $MgCl_2$, 5 mM D-glucose, 0.1 mM EGTA, 10 mM HEPES) containing 25% (V/V) DMSO. No proteins or peptides were added to control samples. After freezing and thawing, samples were centrifuged at 4000 *g* for 3 min at 4˚C and pellets were washed twice with Krebs buffer. Synaptosomes were resuspended in Krebs buffer at 1 mg protein/ml. After addition of 1.2 mM $CaCl_2$ and 30 mM KCl, samples were incubated at 30˚C for 30 min, then a Western blot or exocytosis assay was performed. The exocytosis assay was carried out as previously described [16]. Briefly, a water-soluble styryl dye, FM 2–10, is reversibly inserted into the outer leaflet of the cell membrane and becomes fluorescent. By endocytosis, the dye enters into the synaptosome. During subsequent exocytosis, the dye is released into the medium, so the intensity of the fluorescence decreases with neurotransmitter release ([1], [31]. Exocytosis was induced by 30 mM KCl using an established protocol according to Cousin and Robinson [32] which was modified for high-throughput as published by Lontay *et al* [16]. Synaptosomes suspended in Krebs buffer were incubated at 37˚C for 3 minutes, then FM 2–10 was added. After a 1 minute incubation at 37˚C, dye uptake was evoked by addition of 30 mM KCl. After incubating for 2 min at 37˚C, synaptosomes were washed twice with Krebs buffer, centrifuged at 1000 *g* for 1 min, and the pellet was resuspended in Krebs buffer containing 1.2 mM $CaCl_2$ and added to 96-well black plates. Exocytosis and neurotransmitter release induced by 30 mM KCl and the decrease of fluorescence was measured by Fluoroskan FL (excitation: 488 nm, emission: 540 nm).

Preparing brain slices and treatment

Experiments were performed in artificial cerebrospinal fluid (aCSF) of the following composition: 120 mM NaCl, 2.5 mM KCl, 26 mM $NaHCO_3$, 10 mM glucose, 1.25 mM NaH_2PO_4, 2

mM $CaCl_2$, 1 mM $MgCl_2$, 3 mM myo-inositol, 0.5 mM ascorbic acid, and 2 mM sodium pyruvate, pH 7.2. For the slice preparation, a modified aCSF (low sodium aCSF) was used where 95 mM NaCl was replaced by 130 mM sucrose and 60 mM glycerol. C3H mice (8 to 30 days old) of both sexes were used. After decapitation of the animal and removal of the brain, 200 μm thick coronal brain slices were prepared in ice-cold low sodium aCSF using a Microm HM 650 V vibratome (Microm International GmbH, Walldorf, Germany). After preparation, the slices were transferred into a Millicell CM culture plate insert (PICM01250; Millipore, Billerica, MA, USA) filled with aCSF. The culture plate inserts were placed in an incubating chamber which was designed for fluorescent dye loading [33]. Following the transfer, the incubating solution was slowly replaced with aCSF containing 10 μM H1152 or 5 μM tautomycetin with or without 8 mM KCl. The slices incubated for 60 min at room temperature under moderately pressurised carbogen (95% O_2 5% CO_2) conditions. After incubation, the slices were either frozen in liquid nitrogen for Western blot analysis or mounted in Mounting Medium for cryotomy (VWR, Radnor, PA, USA). The mounted samples were sliced with Leica CM 1860 Cryotom (Leica, Nussloch, Germany) and the 6 μm thick slices were prepared for immunohistochemical experiments.

Immunofluorescence staining and confocal microscopy

B50 neuroblastoma cells were grown on BioCoat Collagen Type I Cellware coverslips (Corning Inc., Corning, NY, USA). Confluent cells were washed with TBS, fixed with ascending alcohol series (70%-80%-96% ethanol for 10–10 min at -20˚C) and permeabilized in TBS containing 0.2% Triton X-100. After washing with TBS, cells were incubated in 1% horse serum/TBS (blocking solution) for 1 hour at 4˚C and with primary antibodies (diluted in blocking solution at a ratio of 1:100) overnight at 4˚C. Coverslips were washed with TBS and incubated with secondary antibodies at 1:200 dilution (Alexa Fluor 488-conjugated anti-rabbit IgG, Alexa Fluor 546-conjugated anti-mouse and anti-goat IgG). Coverslips were mounted in ProLong Gold antifade reagent (Life Technologies, Carlsbad, CA, USA). Cells were examined with a Leica X8 confocal microscope (Leica Microsystems, Wetzlar, Germany). Brain slices were also prepared for immunohistochemistry. Slices were dried, then incubated in blocking buffer consisting of 10% horse serum and 0.2% Triton X-100 in TBS for 1 hour at room temperature and the staining procedure was applied as described above using primary antibodies against $SNAP25^{pThr138}$ and syntaxin.

Statistical analysis

Normalized data were analysed by either student *t*-test or by ANOVA using GraphPad Prism 6 program and Dunnett's *t test* as post hoc test All data shown in this article represent mean ±SEM, and *n* means the number of independent experiments. The applied analysis is indicated in the figure legend.

Results

Interaction of SNAP-25 and myosin phosphatase regulatory subunit (MYPT1)

SNAP-25 was reported as an interacting protein of GST-MYPT1 identified by mass spectrometry [16]. To further study the interaction between SNAP-25 and the subunits of myosin phosphatase, we carried out reciprocal immunoprecipitations (Fig 1A) from B50 neuroblastoma cell lysates using specific anti-SNAP-25, anti-PP1cδ and anti-$MYPT1^{1-296}$ antibodies. The subunits of myosin phosphatase—MYPT1 and PP1cδ—as well as MYPT1 and SNAP-25 were

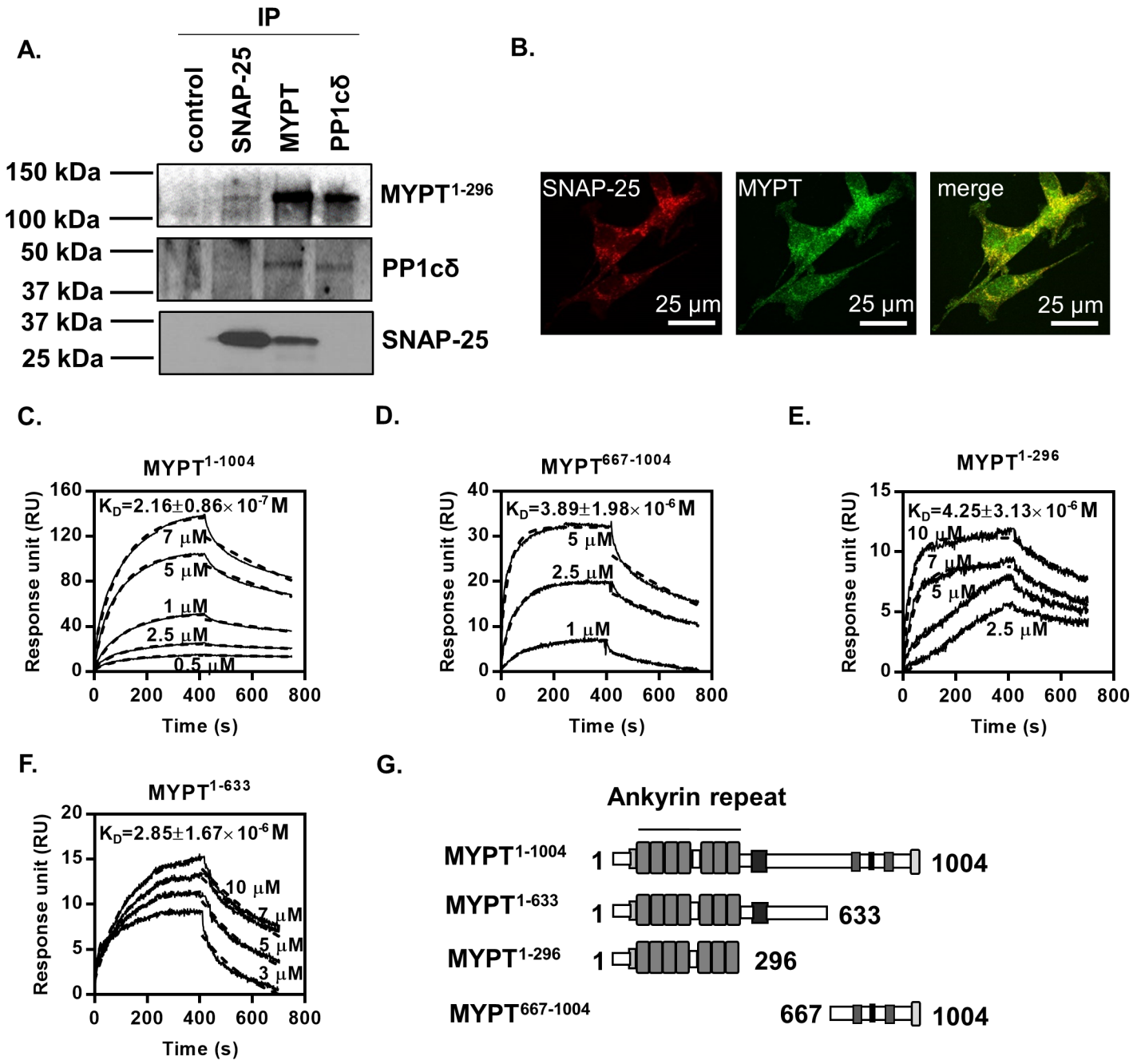


Fig 1. Interaction between SNAP-25 and the MYPT1 subunit of myosin phosphatase. (A) Immunoprecipitation was performed from B50 neuroblastoma cell lysates with antibodies specific for MYPT1, PP1cδ and SNAP-25 coupled to Protein-A Sepharose, and the precipitates were analyzed by Western blots using the indicated antibodies. In control, rabbit non-immune serum was coupled to Protein-A Sepharose. (B) Confocal microscopy of MYPT1 (green) and SNAP-25 (red). Images show the co-localization of SNAP-25 and MYPT1 in a merged image. (C-G) SPR-based binding assays of the interaction between MYPT1 and SNAP-25. Full-length GST-MYPT1$^{1-1004}$ (C) and a C-terminal GST-MYPT1$^{667-1004}$ fragment (D) were immobilized on sensor chips coupled with anti-GST. N-terminal fragments of His-MYPT1$^{1-296}$ (E) and His-MYPT1$^{1-633}$ (F) were immobilized on CM5 sensor chips by direct amine-coupling. Flag-SNAP-25 was injected over the surfaces at the concentrations indicated on the sensorgrams. Dissociation constants (K_D) derived by the BIAevaluation 3.1 software from the sensorgrams assuming a 1:1 binding model are indicated in the figures. The unit of dissociation constant values is M (n = 3). Schematic structure of the full-length, as well as the N-terminal and C-terminal fragments of MYPT1 used as ligands in the SPR measurements are shown (G).

https://doi.org/10.1371/journal.pone.0177046.g001

reciprocally co-precipitated, however SNAP-25 and PP1cδ did not show interaction. These data verify the interaction between MYPT1 and SNAP-25, and suggest that the SNAP-25 protein interacts with MP through MYPT1, but not PP1c. Co-localization of SNAP-25 and MYPT in the cytoplasm and neuronal projections of B50 neuroblastoma cells was detected using confocal microscopy (Fig 1B). The Pearson coefficient for MYPT1 and SNAP25 and for GAPDH and MYPT1 (as negative controls of non-interacting proteins) were 0.66 and 0.31, respectively. Similar values were measured in three separate experiments (n = 3), indicating partial but definite co-localization of SNAP-25 with MP in neuronal cells.

To determine the SNAP-25-interacting region of MYPT1, surface plasmon resonance (SPR) experiments were performed with full-length and truncated MYPT1 mutants and Flag-SNAP-25. Full-length wild type MYPT1 (GST-MYPT1$^{1\text{-}1004}$) (Fig 1C) and the C-terminal (GST-MYPT1$^{667\text{-}1004}$) (Fig 1D) or N-terminal fragments, MYPT1$^{1\text{-}296}$ (Fig 1E) and MYPT1$^{1\text{-}633}$ (Fig 1F), were immobilized on sensor chip surfaces to assay interaction with SNAP-25 using SPR based binding technique. The schemes of these MYPT1 mutants are shown in Fig 1G. Based on the sensorgrams obtained by injection of SNAP-25 over these MYPT1 surfaces a relatively strong interaction with the full-length MYPT1 (K_D = 2.16±0.86x10^{-7}) was detected (Fig 1C). It was also apparent that SNAP-25 binds to both the C-terminal (K_D = 4.25±3.13x 10^{-7}) and N-terminal (MYPT1$^{1\text{-}296}$: K_D = 3.89±1.98x10^{-6}; MYPT1$^{1\text{-}633}$: K_D = 2.85±1.67x10^{-6}) regions of MYPT1 with preference for the C-terminal region, based on the derived dissociation constants.

Phosphorylation/dephosphorylation of SNAP-25 by ROK/MP

Previous results have shown that RhoA-activated kinase (ROK) and MP have some common neuronal substrates, e. g. synapsin-I, syntaxin-1, and the 20 kDa light chain of myosin-II [16]. This fact motivated us to study not just the role of MP, but also the role of ROK, in the regulation of SNAP-25 by phosphorylation. To identify the potential ROK-specific phosphorylation sites, Flag-SNAP25 was phosphorylated by ROK and was subjected to LC-MS/MS analysis after tryptic digestion (Fig 2A). The following SNAP-25 Thr138 related phosphopeptides were identified in the samples: ^{136}RVT(phospho)NDAR^{142}, ^{136}RVT(phospho)NDARENEMD ENLEQVSGIIGNLR^{161}, and ^{136}RVT(phospho)NDARENEM(oxidation)DENLEQVS GIIGNLR^{161}. All of these peptides were identified in the ROK treated sample, while only the latter one was identified in the control sample (S2 Table). The phosphorylation of Thr138 residue of SNAP-25 was highly elevated in the sample in the presence of ROK. Comparison of the ion intensities of m/z 1023.4749, representing the most abundant Thr138 related phosphopeptide indicated an approximately 100-fold increase compared to the control sample. ROK phosphorylation was also verified by ^{32}P-phosphate incorporation into SNAP-25 detected by autoradiography (Fig 2B.). Flag-SNAP-25 protein was also phosphorylated by ROK and the ROK-phosphorylated Flag-SNAP25 was subjected to dephosphorylation by myosin phosphatase using i*n vitro* assays (Fig 2C). The phosphorylation state of SNAP-25 on Thr138 was analyzed by Western blot using anti-SNAP25^{pThr138} antibody. Increased phosphorylation of Thr138 was observed in response to ROK treatment compared to control samples. The addition of MP followed by ROK eliminated the phosphorylation of SNAP-25 at Thr138 residue. To verify the specificity of the phosphorylation by ROK, Thr138Ala mutant SNAP-25 (SNAP-25^{T138A}) was generated by site-directed mutagenesis and the wild type (SNAP-25^{wt}) and mutant SNAP-25 were incubated with ROK. Phosphorylation was analyzed by Western blots using anti-SNAP-25^{pThr138} antibody (Fig 2D). It was apparent that only the Flag-SNAP-25^{wt} but not the Flag-SNAP-25^{T138A} was phosphorylated by ROK. These experimental data suggest that ROK phosphorylates and MP dephosphorylates SNAP-25 on the Thr138 residue *in vitro*.

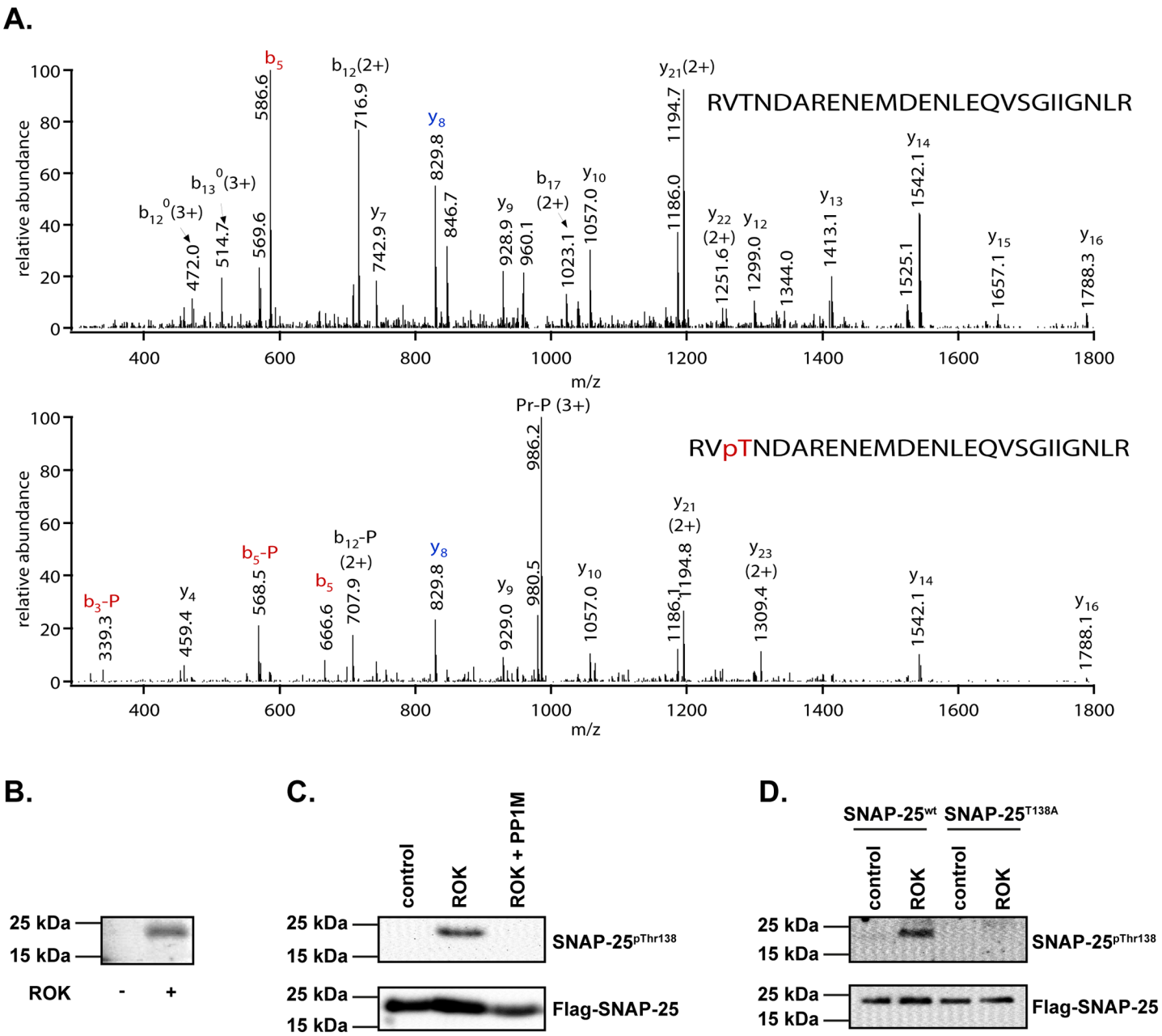


Fig 2. Phosphorylation and dephosphorylation of purified Flag-SNAP-25. (A) Mass spectrometry analysis of ROK-phosphorylated SNAP-25. Collision induced dissociation (CID) spectra representing SNAP-25 [136–161] peptides. Upper panel: m/z: 991.4868 (3+), ^{136}RVTNDARENEMDENLEQVSGII GNLR^{161}. Lower panel: m/z: 1018.1437 (3+), ^{136}RVT(Phospho)NDARENEMDENLEQVSGIIGNLR^{161}. Site of phosphorylation is Thr-138 as proven by unmodified y_8 and phosphorylated b_5 fragment ions. Peptide fragments are labeled according to the nomenclature [34]. -P stands for the 98-Da neutral loss of phosphoric acid characteristic to Ser/Thr phosphorylation, pr stands for the precursor ion and ^{0} denotes water loss of the respective fragment ions. (B) Phosphorylation of SNAP-25 by RhoA-activated kinase (ROK) in the presence of γ-^{32}P-ATP and Mg^{2+} as detailed in Materials and Methods. No ROK was introduced to control samples. Phosphorylation was detected by autoradiography. (C) Examination of SNAP-25 phosphorylation/dephosphorylation on Thr138 by *in vitro* kinase and phosphatase assays. Flag-SNAP-25 was incubated in the absence (control) or presence of ROK and then with or without MP. Phosphorylation level of Thr138 was investigated by Western blot using anti-SNAP25^{pThr138} phosphorylation site-specific antibody. The loading of Flag-SNAP-25 was verified by anti-Flag antibody. (D) *In vitro* protein kinase assay of wild type (SNAP-25^{wt}) and Thr138Ala mutant (SNAP-25^{T138A}) of SNAP-25 by ROK. The level of SNAP-25^{pThr138} was assessed by anti-SNAP-25^{pThr138} antibody by Western blot.

https://doi.org/10.1371/journal.pone.0177046.g002

Inhibition of ROK and MP influences the phosphorylation level of SNAP-25 at Thr138 in B50 neuroblastoma cells

To prove the *in vivo* regulatory effect of ROK and MP on SNAP-25, B50 neuroblastoma cells were treated with 10 μM H1152, a ROK-specific inhibitor, or 5 μM tautomycetin (TMC), a PP1-specific inhibitor. The inhibitors had no significant effect on the viability of B50 cells measured by MTT assay (Fig 3A). The protein phosphatase activity was determined using ^{32}P-labelled 20 kDa myosin light chain (^{32}P-MLC20) as substrate. Upon inhibition of PP1 with TMC the protein phosphatase activity dramatically decreased compared to the control untreated samples, suggesting that PP1 is responsible for approximately 70% of the total protein phosphatase activity in B50 cells. H1152 treatment had no significant effect on the phosphatase activity (Fig 3B). The changes in SNAP-25 Thr138 phosphorylation levels in response to inhibitory treatments were examined by Western blot using anti-SNAP-25^{pThr138}. Inhibition of ROK by H1152 decreased the phosphorylation at SNAP-25^{pThr138} by 57% compared to control, while PP1 inhibition resulted in an increase in SNAP-25^{pThr138} level to 147% (Fig 3C).

Silencing MYPT1 increases the phosphorylation level at Thr138 of SNAP-25

The fact that PP1 inhibitors influence the phosphorylation of SNAP-25 at Thr138 was proven; however, the contribution of MP inhibition to this effect remained unclear. To assess the regulatory role of MP on the dephosphorylation of SNAP-25, gene silencing of the MYPT1 regulatory subunit in B50 cells was carried out. The extent of MYPT1 silencing was verified by Western blot analysis and 43% decrease in the protein expression level of MYPT1 was detected compared to non-target controls (Fig 4A). Knocking down MYPT1 showed a 42% decrease in the viability of B50 cells compared to control as examined by MTT assay (Fig 4B). Silencing of MYPT1 showed a 50% decrease in overall phosphatase activity (Fig 4C) suggesting that MP is a predominant PP1 enzyme in B50 neuroblastoma cells. In response to knocking down MYPT1, the SNAP-25 phosphorylation on Thr138 significantly increased by 30% compared to control (Fig 4D) as assessed by semi-quantitative Western blots. This suggests that MP dephosphorylates SNAP-25 on Thr138 in B50 neuroblastoma cells and this dephosphorylation can be diminished by silencing of MYPT1, the targeting subunit of the dephosphorylation process.

MP increases the exocytosis of mouse cortical synaptosomes through the dephosphorylation of SNAP-25

Previous experiments have shown that treatment with the PP1 inhibitor, TMC, suppressed, whereas the ROK inhibitor, Y27632, increased, the level of Ca^{2+}-dependent exocytosis from rat cortical synaptosomes [16]. To determine the physiological role of SNAP-25 regulation by MP and ROK in neurotransmitter release, functional synaptosomes were prepared from mouse cortex and used as models in a high-throughput exocytosis assay. The MP-dependent physiological responses were assayed by protein transduction of a Flag-tagged kinase enhanced phosphatase inhibitor (Flag-KEPI) which specifically inhibits MP among the PP1 holoenzymes [33]. The transduction of Flag-KEPI into synaptosomes was verified by Western blot analysis using anti-Flag antibody (Fig 5A). Since the phosphorylation of KEPI at Thr73 is required for its inhibitory activity [35] the phosphorylation status was determined by using an antibody specific for the phosphorylated Thr38 of C-kinase activated phosphatase inhibitory protein of 17 kDa (CPI-17) which also recognizes the phosphorylation of KEPI^{Thr73} [29]. The transduction of Flag-KEPI into intact synaptosomes increased the phosphorylation level of KEPI compared to both the intact control and the Flag-peptide transduced samples (Fig 5A) suggesting

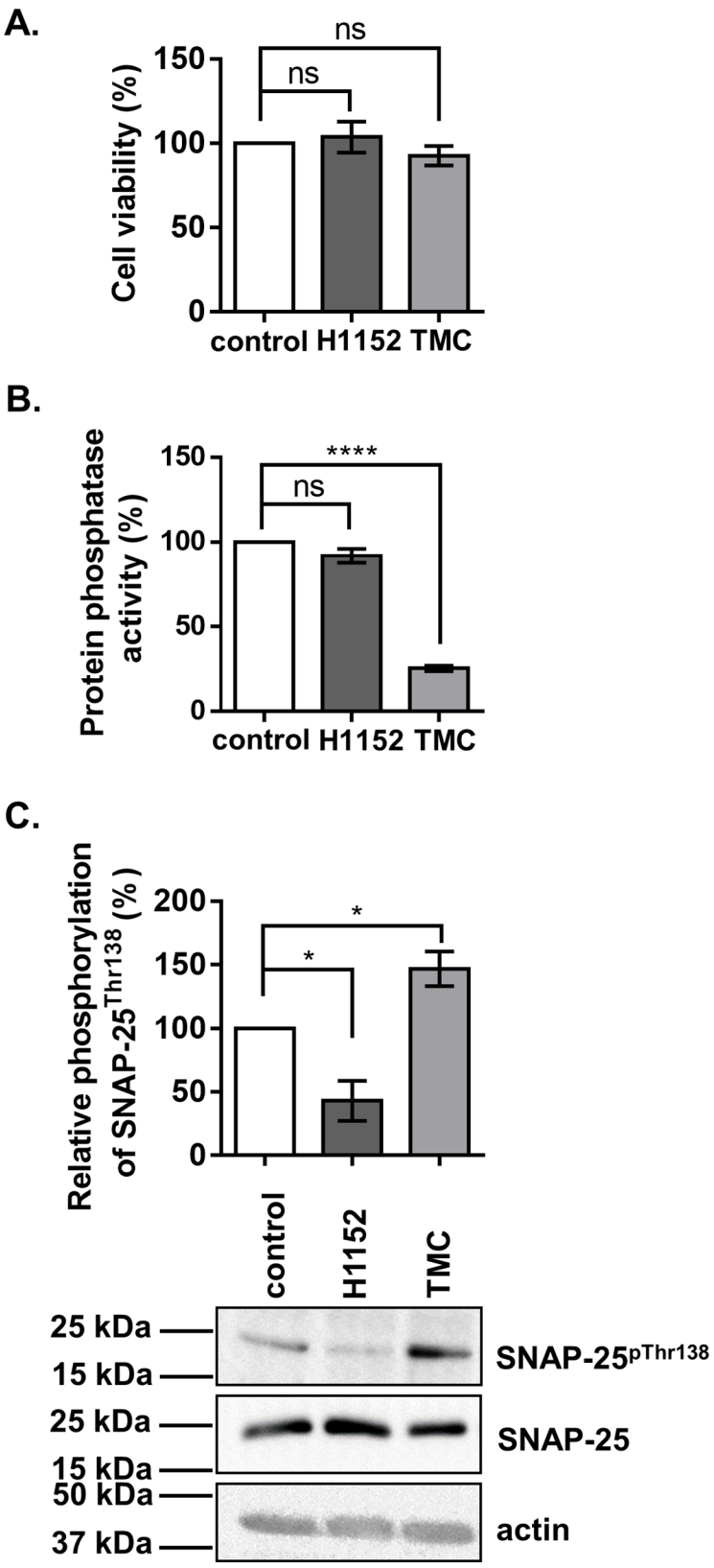


Fig 3. Treatment of B50 neuroblastoma cells with PP1 and ROK inhibitors. B50 cells were incubated with tautomycetin (TMC), a PP1 specific inhibitor, or H1152, a ROK inhibitor, for 1 hour and 30 minutes

respectively. Untreated cells served as controls. (A) Viability of B50 cells were examined using MTT assay. Values are mean±SEM (n = 6), p = 0.4645. (B) Effect of inhibitors on protein phosphatase activity. Values are mean±SEM (n = 3), p<0.0001. (C) The effect of the inhibitory treatment on the phosphorylation level of Thr138 in SNAP-25 was assessed by Western blots using anti-SNAP25^{pThr138}. Values are mean±SEM (n = 3), p = 0.0027. Amounts of SNAP-25 and actin were also determined as loading controls. Relative changes in the phosphorylation levels were determined by densitometry of the bands. Means ±SEM (n = 5), ANOVA and Dunnett's post hoc analysis, *p<0.05; **p<0.01; ***p<0.001; ****p<0.0001.

https://doi.org/10.1371/journal.pone.0177046.g003

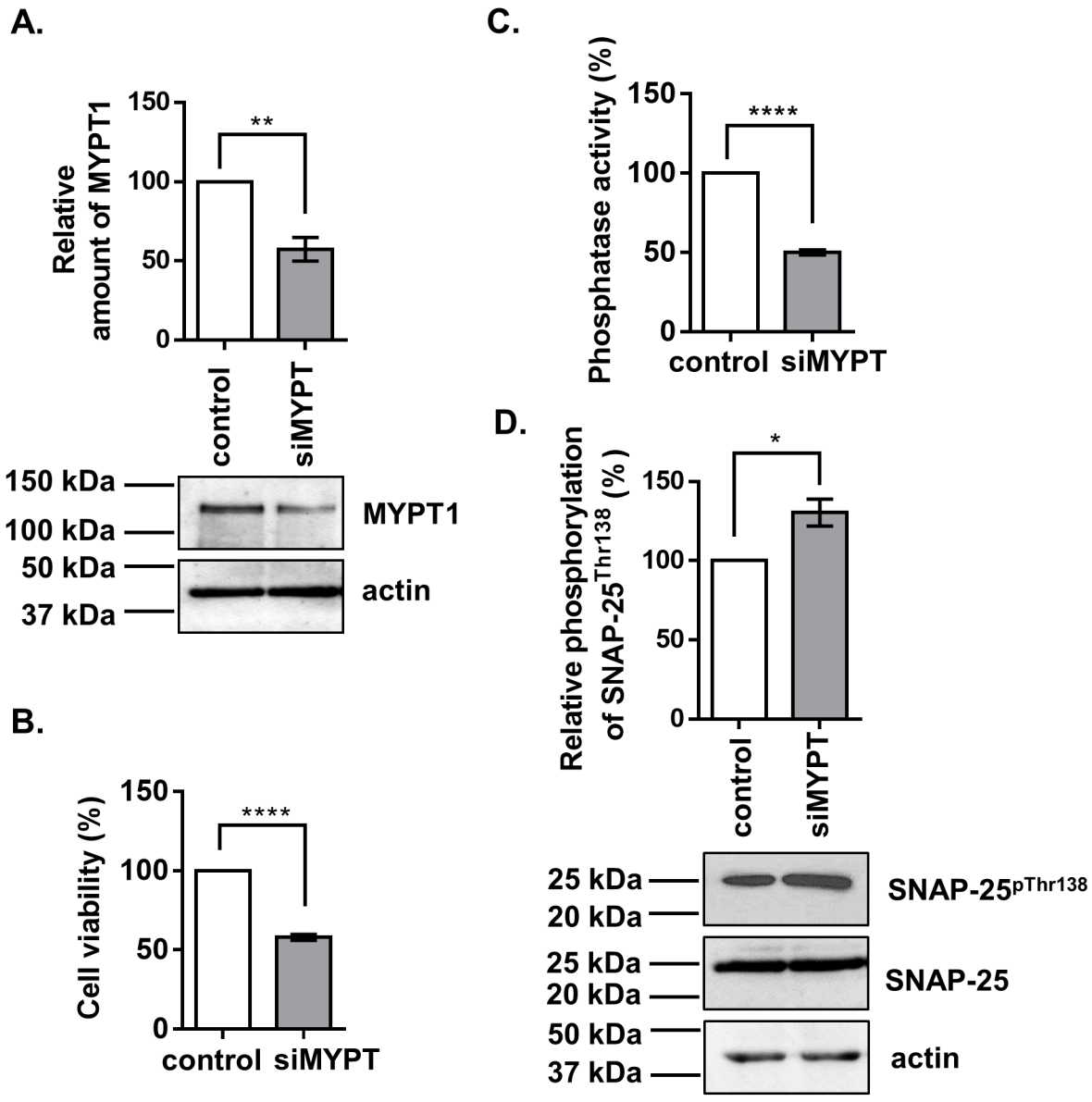


Fig 4. Silencing of MYPT1 by siRNA in B50 neuroblastoma cell line. (A) Western blot images of cell lysates after treatments with 100 nM of siRNA targeting the endogenous MYPT1 subunit. The relative amount of MYPT1 was detected and determined with anti-MYPT1$^{1-296}$ antibody. (B) MTT cell viability assays were carried out 48 hours after transfecting cells with MYPT1 specific siRNA. (C) Assay of phosphatase activity in control and siRNA transfected cell lysates with ^{32}P-MLC20 substrate. (D) The phosphorylation of SNAP-25 on Thr138 was detected by anti-SNAP25^{pThr138}, and the levels of SNAP-25 as well as actin from control and transfected cells was also determined. The changes in the level of the phosphorylated SNAP-25 was determined comparing the relative density of the bands normalized for the loading controls. Means ±SEM (n = 5), student t test, *p<0.05; **p<0.01;; ****p<0.0001.

https://doi.org/10.1371/journal.pone.0177046.g004

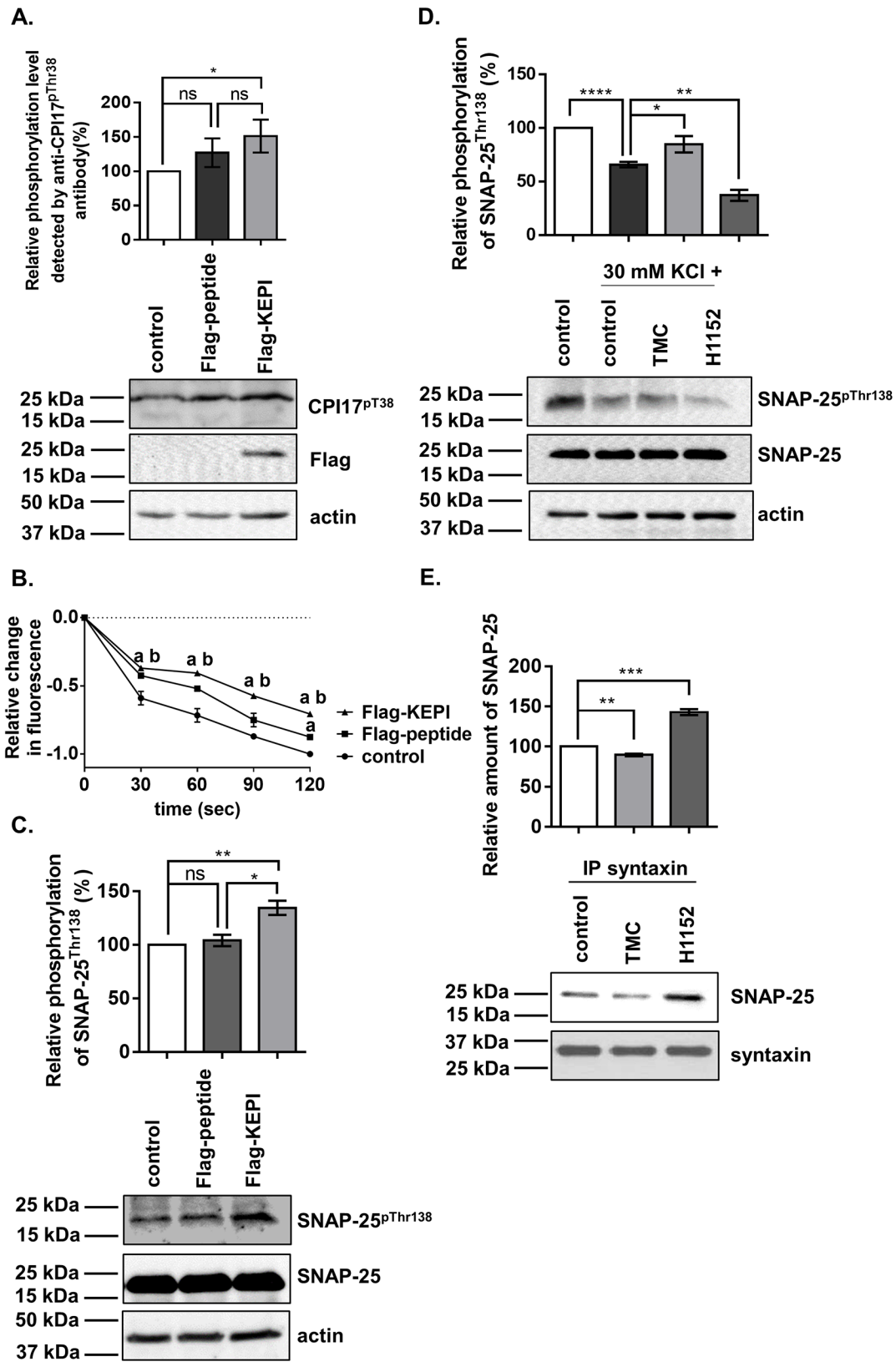


Fig 5. Effect of PP1 and ROK inhibitors on the phosphorylation level of SNAP-25 at Thr-138 and on exocytosis in mouse cortical synaptosomes. (A) Flag-KEPI, a myosin phosphatase specific inhibitor protein, was

introduced into the synaptosomes by the freeze-thaw method. To distinguish the effect of Flag-tag from Flag-KEPI, Flag-peptide was also introduced. Control synaptosomes underwent the freeze-thaw process, but no protein or peptide was added. Transduction of Flag-KEPI into synaptosomes was verified by western blot analysis using anti-Flag antibody. Relative phosphorylation levels were detected by anti-CPI17^{pThr38} antibody. C-kinase activated phosphatase inhibitor protein of 17 kDa (CPI17) and KEPI are homologous MP inhibitor proteins; both need phosphorylation to become active. As the surroundings of the phosphorylation sites of CPI17 and KEPI are similar, anti-CPI17^{pThr38} antibody can recognize the phosphorylated, active KEPI protein. ANOVA: p = 0.0389. (B) Changes in the extent of exocytosis in response to Flag-peptide or Flag-KEPI transduction was measured by incorporating FM 2–10 fluorescent dye into the synaptosomes, and determining the release of dye. Each point represents the mean ±SEM of three parallel experiments (n = 3). Symbols: *a*: significant (p<0.05) compared to control; *b*: significant compared to Flag-peptide; t-test was used. By ANOVA, we detected significant differences among treated groups (p = 0.006). (C) Effects of Flag-peptide and Flag-KEPI transduction on the phosphorylation of SNAP-25 at Thr138. ANOVA: p = 0.0050. (D) Effect of KCl depolarisation, in the absence and presence of TMC or H1152 treatments, on the phosphorylation level of Thr138 in SNAP-25 analysed by western blots using anti-SNAP25^{pThr138}. The duration of treatment was 1 hour. Actin was assessed as loading control. ANOVA: p < 0.0001. (E) Effect of TMC and H1152 treatment of synaptosomes on the interaction of SNAP-25 and syntaxin. Synaptosomes were treated with the inhibitors as mentioned above then lysed. Immunoprecipitations from synaptosome lysates were performed using anti-syntaxin antibody. The amount of Protein-A Sepharose was the same in each tube. The amounts of precipitated syntaxin and SNAP-25 were detected by Western blots. ANOVA: p<0.0001. Statistical analyses were performed using the data of n = 3–5 parallel experiments and representative blots are shown here. Means ±SEM (n = 5), ANOVA and Dunnett's post hoc analysis, *p<0.05; **p<0.01; ***p<0.001; ****p<0.0001.

https://doi.org/10.1371/journal.pone.0177046.g005

the inhibitory potential of KEPI on MP. The basal phosphorylation in control and Flag-introduced synaptosomes is suspected to be derived from the endogenous KEPI (Fig 5A). KCl-induced exocytosis was investigated in Flag-KEPI transduced synaptosomes. The synaptosomes were loaded with FM 2–10 fluorescent dye and the reduction of fluorescence intensity was recorded every 30 seconds for 3 minutes. While transduction of Flag-peptide had no significant effect on exocytosis at any time point, Flag-KEPI transduction decreased the exocytosis by 28–39% compared to untreated controls (Fig 5B) suggesting an activating role of MP in neurotransmitter release. The most significant changes were observed after the first 30 sec of the measurement. To clarify the molecular mechanism behind the physiological processes regulated by MP, the phosphorylation status of SNAP-25 on Thr138 in response to Flag or Flag-KEPI transduction was investigated by Western blot analysis. The basal level of SNAP-25^{pThr138} was not altered by the transduction of the Flag peptide, but it was significantly increased (by 34%) upon the inhibition of MP by Flag-KEPI transduction (Fig 5C). The effect of depolarization on SNAP-25^{pThr138} level was assessed in synaptosomes by Western blots (Fig 5D). The relative phosphorylation at Thr138 of SNAP-25 upon addition of KCl was lower than in the untreated controls suggesting that depolarization itself has an influence on the phosphorylation status of SNAP-25. After depolarization with KCl, the basal level of phosphorylation on Thr138 was increased in the presence of TMC, and significantly decreased by addition of H1152. Based on our previous results, we attempted to verify the effect of SNAP-25 phosphorylation at Thr138 on the SNARE complex formation by immunoprecipitation assay using an antibody specific for syntaxin, a member of the SNARE complex, in TMC or H1152-treated synaptosome lysates (Fig 5E). The relative amount of SNAP-25 in the anti-syntaxin pulled down fractions decreased upon PP1 inhibition, whereas it increased following ROK inhibition suggesting that decreasing phosphorylation level of SNAP-25 in Thr138 favors interaction between SNAP-25 and syntaxin.

ROK and MP mediate the phosphorylation level of SNAP-25^{Thr138} in brain slices

To confirm the previously described results obtained with synaptosomes on an *ex vivo* physiological model, we performed experiments using brain slices prepared from murine cortex maintained in low-Na^+ artificial cerebrospinal fluid and depolarized by KCl in a solution

containing TMC (5 μM) or H1152 (10 μM). First, the expression and phosphorylation level of SNAP-25 at Thr138 were examined. Supporting our previous observations with synaptosomes, the results in brain slices show that inhibition of PP1 by TMC increased, whereas inhibition of ROK by H1152 decreased, the level of SNAP-25^{pThr138}. Moreover, KCl-induced depolarization also caused a significant decrease in the level of SNAP-25^{pThr138} (Fig 6A). We visualized the changes of SNAP-25^{pThr138} (green) by confocal microscopy, and syntaxin (red) was also labeled as a presynaptic marker. As seen in Fig 6B, stimulation by 8 mM KCl decreased the overall SNAP-25 phosphorylation at Thr138 without influencing the expression of syntaxin. Inhibition of PP1 with TMC increased, whereas the application of H1152 almost completely eliminated phosphorylation, at Thr138 of SNAP-25 upon KCl-depolarization (Fig 6B).

Discussion

Several lines of evidences suggest that the neuronal exocytosis is regulated by the phosphorylation of the membrane fusion machinery of the SNARE complex [36, 37]. However, the precise roles of individual phosphorylation events of specific proteins are still contradictory. The SNARE-complex protein, SNAP-25 has been previously reported to be modulated by phosphorylation on multiple sites upon physiological responses [38, 39]. In this study, we identified SNAP-25 as a novel substrate of the ROK and MP enzymes and its phosphorylation at Thr138 correlates with changes in neuronal exocytosis of murine cortical synaptosomes. This work extends our previous reports showing that MP and ROK are present in both cortical synaptosomes and in giant synapses of rat auditory brain stem, and that they influence synaptosomal exocytosis and neurotransmitter release in an opposing manner: PP1 inhibition suppresses, whereas ROK inhibition stimulates exocytosis [16].

In search for the common targets of ROK/MP, mass spectrometry analysis identified several synaptosomal MYPT1-interacting proteins such as synapsin-I, calcineurin-A subunit, Ca^{2+}-calmodulin dependent kinase II, as well as syntaxin-1 and SNAP-25 of the SNARE complex [16]. Here we confirm by co-immunoprecipitation that SNAP-25 interacts with the MYPT1 regulatory subunit of MP (Fig 1A). An SPR-based *in vitro* binding assay identified a stable interaction between MYPT1 and SNAP-25 which verified that SNAP-25 binds to both the N-terminal and C-terminal regions of MYPT1 (Fig 1C–1F).

Our findings show that ROK and MP counteract each other at the Thr138 phosphorylation site of SNAP-25 *in vivo* and *in vitro* (Figs 2–4). Previous experiments showed that SNAP-25 is phosphorylated by both PKA and PKC at residues Ser28, Thr29, Thr138, and Ser187, but PKC showed higher preference toward the latter two over Ser28 and Thr29 [15, 38, 40, 41]. A recently published study showed that Thr138 of SNAP-25 is phosphorylated selectively by PKA upon ATP treatment of PC12 cells, whereas Ser187 of SNAP-25 is phosphorylated preferentially by PKC, suggesting different roles of PKA and PKC in SNAP-25 phosphorylation [42]. Here we report that ROK is a novel regulator of SNAP-25. ROK phosphorylates SNAP-25 at the Thr138 residue, but not at Ser28, Thr29, or Ser187, as revealed by mass spectrometry analysis. These data suggest a RhoA-dependent regulation of the SNARE complex through the Thr138 site of SNAP-25.

The inhibition of PP1 by TMC increased the phosphorylation of SNAP-25 at Thr138 in B50 neuroblastoma cells (Fig 3), in KCl-depolarized cortical synaptosomes (Fig 5), and in cortical thin brain slices (Fig 6). These findings also support the already well-described role of PP1 enzymes in the regulation of SNARE complex formation [43, 44]. SNAP-25 phosphorylated by PKA and PKC was dephosphorylated more efficiently by PP1 and to a lesser extent by PP2A but not by PP2B *in vitro* [42]. PP1 enzymes act equally efficiently at the Ser28, Thr 29, Thr138, and Ser187 residues of SNAP-25, and PP1 is the major phosphatase responsible for

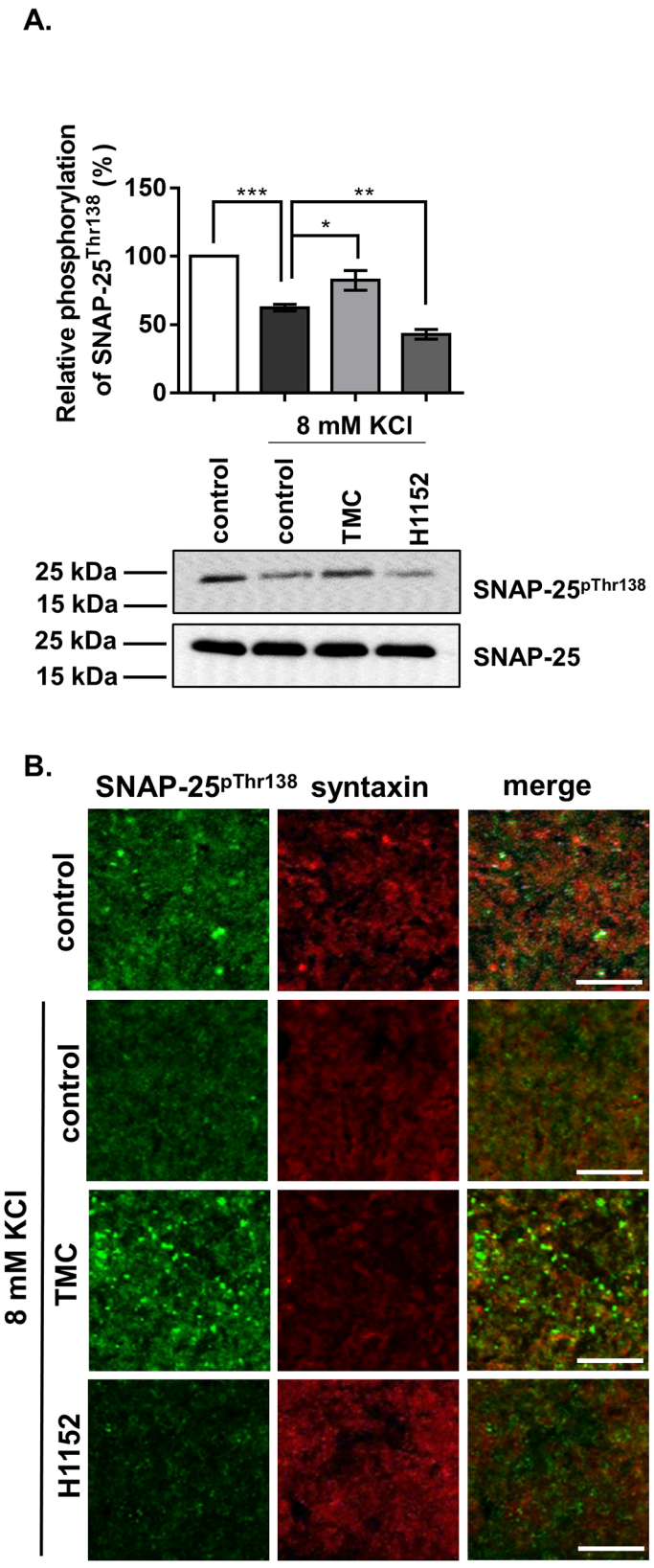


Fig 6. Effect of PP1 and ROK inhibitors on the phosphorylation of SNAP-25 at Thr138 in brain slices. (A) Mouse cortical brain slices were prepared and treated with TMC or H1152 for 1 hour. To trigger

depolarization, 8 mM KCl was added. Phosphorylation of SNAP-25 was investigated by Western blot using an anti-SNAP-25^{pThr138} antibody. Amounts of SNAP-25 protein were also determined by anti-SNAP-25 antibody. Density of bands wase determined and normalized relative phosphorylation is illustrated. Means ±SEM (n = 5), ANOVA and Dunnett's post hoc analysis, *p<0.05; **p<0.01; ***p<0.001. (B) Changes in SNAP-Thr138 phosphorylation in response to treatments as detailed in (A) were also imaged by confocal microscopy. The four sets of brain slices (control, KCl-treated, KCl + TMC treated, KCl + H1152 treated) were analysed with anti-SNAP-25^{pThr138} antibody to assess differences in phosphorylation level, and also with anti-syntaxin antibody to identify syntaxin, a typical pre-synaptic protein. Co-localizations of syntaxin and phospho-SNAP-25 are also shown on merged images. Scale bar: 10 μm.

https://doi.org/10.1371/journal.pone.0177046.g006

dephosphorylating SNAP-25 [45]. Furthermore, SNAP-25 was dephosphorylated at Thr138 by MP (the holoenzyme of PP1c and MYPT1) (Fig 2) and the selective inhibition of MP by KEPI enhanced the Thr138 phosphorylation (Fig 5C). The above data are in accordance with our previous findings that MP is the predominant PP1 holoenzyme in synaptosomes and presynaptic cells suggesting that MP is a major determinant of PP1-dependent dephosphorylation processes [20].

The final step of exocytosis, membrane fusion, is regulated by the phosphorylation of SNARE and accessory proteins. A large body of evidence show that SNAP-25 phosphorylation by PKA or PKC contributes differentially and selectively to the control of exocytosis in PC12 cells by regulating the SNARE complex formation [13, 45, 46]. Phosphorylation of SNAP-25 at The Ser187 was suggested to upregulate the binding of synaptobrevin to a pre-existing t-SNARE to increase the stability of the SNARE complex. Indeed, it was reported that PKC activation initiated an enhanced K^+-induced noradrenaline release in PC12 cells. [42]. Moreover, the phosphorylation of SNAP-25 at Ser187 by PKC was necessary for the enhancement of Ca^{2+}-triggered exocytosis by phorbol ester in an insulinoma cell line [47], and the inhibition of SNAP-25 phosphorylation at Ser187 down-regulated morphine-induced SNARE complex formation in neurons [48].

In contrast to Ser187 phosphorylation, phosphorylation of SNAP25 at Thr138 may contribute to the suppression of the SNARE complex formation [38]. Thr138 is part of the peptide region in SNAP-25 that influences SNARE complex assembly and the binding of SNAP-25 to syntaxin-1. Thus, the formation of SNARE complex was suppressed both by PKA-treatment of the purified SNAP-25 and forskolin treatment of PC12 cells [42]. Moreover, forskolin stimulation of PKA resulted in a dramatic phosphorylation of SNAP^{pThr138} without appreciable changes in neurotransmitter release [15]. On the contrary, the activation of PKA indirectly enhanced the Ca^{2+}-dependent exocytosis by maintaining the large number of vesicles in the ready-to-release pool in chromaffin cells. However, the overexpression of the T138D phosphomimic form of SNAP-25 did not modify the secretion significantly [14, 49]. It was also clarified that the phosphorylation of SNAP-25 at Thr138 inhibits noradrenaline secretion of differentiated PC12 pheochromocytoma cells [42].

Several bodies of evidence indicate the importance of ROK-dependent phosphorylation in regulated exocytosis via interference with SNARE functions. In chromaffin cells and neurons, the RhoA/ROK pathway governs the secretory response by phosphorylating syntaxin 1 and facilitating the binding of syntaxin 1 to tomosyn, thereby impairing SNARE complex formation and contributing to reduced exocytosis [50, 51]. Our results clearly confirm that the binding of SNAP-25 to syntaxin-1 and the formation of the SNARE complex were inhibited by TMC- and elevated by H1152-treatment of synaptosomes. The increase in syntaxin-SNAP25 complex formation was accompanied by the decrease of the phosphorylation of SNAP-25 at Thr138 (Fig 5E). We also observed that the modulation of the Thr138 site, as a result of the inhibition of ROK by H1152 [16] and the inhibition of MP by KEPI protein, positively and negatively regulates synaptosomal exocytosis (Fig 5), respectively. These data indicate that

ROK and MP may modulate exocytosis by directly modifying the SNARE and docking complex functions. Since the most dramatic change in KCl-induced exocytosis in control and Flag-KEPI transduced synaptosomes was observed in the first 30 seconds after depolarization, we suggest that the inhibition of myosin phosphatase predominantly impacts the formation of the SNARE complex and the process of priming rather than the fusion itself. In this study, we also clarified that selective inhibition of MP by KEPI protein suppresses KCl-induced synaptosomal exocytosis (Fig 5B). These data are reminiscent of our previous data showing that PP1 and ROK inhibition affected synaptic transmission in giant synapse in the rat auditory system; PP1 inhibition decreased, whereas ROK-inhibition increased, the release probability. Moreover, the inhibition of PP1 changed the paired-pulse ratio and it caused a significant reduction in the frequency of the relative amplitudes of the third and subsequent evoked miniature excitatory post-synaptic currents [16]. These results may be explained by the fact that several proteins related to exocytosis in intact synaptosomes are substrates of ROK and MP, including MYPT1^{Thr696}, myosin-II light chain^{Ser19}, synapsin-I^{Ser9} and syntaxin-1^{Ser14}, and the overall effect of MP and ROK on the phosphorylation status of these presynaptic proteins regulates neurotransmission. The other possible explanation is that under our experimental conditions with PP1 and ROK inhibitors, the applied [Ca^{2+}] was already high (1.2 mM, 1.8 mM and 2 mM in synaptosomal buffer, DMEM and in aCSF, respectively) which may prevent the action of PKA on SNAP-25 and on other presynaptic targets as described on chromaffin cells [14]. The RhoA signaling pathway and MP may also play a role in the regulation of SNAP-25 at Thr138 and other potential synaptosomal targets in a Ca^{2+} independent way.

In conclusion, we have shown that ROK phosphorylates and MP dephosphorylates SNAP-25 at Thr138 in synaptosomes, cortical thin slices and B50 neuroblastoma cells to regulate the assembly of the SNARE complex and neuronal exocytosis. Our findings provide an important insight into the fine-tuned balance of the action of protein kinases and phosphatases regulating neurotransmitter release in response to changes in physiological conditions.

Supporting information

S1 Table. Site-directed mutagenesis of SNAP25 primer pair.
(DOCX)

S2 Table. siRNA sequences for MYPT1 silencing.
(DOCX)

S3 Table. Thr-138 related phosphopeptides identified from LC-MS/MS data of the tryptic digest of control and ROK-treated SNAP-25.
(DOCX)

S4 Table. NC3Rs ARRIVE guidelines checklist horvath.
(PDF)

Acknowledgments

The authors are indebted to Dr. Katalin Medzihradszky (Hungarian Academy of Sciences, Proteomics Research Group), Dr Balázs Pál and Áron Kőszeghy (UD, Department of Physiology) for their support, to Dr. Karen Uray to revise the manuscript and to Ágnes Németh, Andrea Docsa and Ágota Kelemenné Szántó for their excellent technical assistance.

Author Contributions

Conceptualization: BL FE.

Formal analysis: DH IT.

Funding acquisition: BL FE.

Investigation: DH ZD AS BB IT BL DN.

Methodology: DH ZD AS BB IT BL DN.

Project administration: BL.

Resources: FE KM BL.

Software: BL KM.

Supervision: BL KM.

Validation: BL DH.

Visualization: JI DH BL.

Writing – original draft: BL DH ZD.

Writing – review & editing: DH ZD AS BB IT BL DN.

References

1. Sim AT, Baldwin ML, Rostas JA, Holst J, Ludowyke RI. The role of serine/threonine protein phosphatases in exocytosis. Biochem J. 2003; 373(Pt 3):641–59. PubMed Central PMCID: PMC1223558. https://doi.org/10.1042/BJ20030484 PMID: 12749763
2. Sudhof TC. The synaptic vesicle cycle. Annual review of neuroscience. 2004; 27:509–47. https://doi.org/10.1146/annurev.neuro.26.041002.131412 PMID: 15217342
3. Tian JH, Das S, Sheng ZH. Ca2+-dependent phosphorylation of syntaxin-1A by the death-associated protein (DAP) kinase regulates its interaction with Munc18. J Biol Chem. 2003; 278(28):26265–74. https://doi.org/10.1074/jbc.M300492200 PMID: 12730201
4. Richards DA, Guatimosim C, Rizzoli SO, Betz WJ. Synaptic vesicle pools at the frog neuromuscular junction. Neuron. 2003; 39(3):529–41. PMID: 12895425
5. Rizzoli SO, Betz WJ. Synaptic vesicle pools. Nature reviews Neuroscience. 2005; 6(1):57–69. https://doi.org/10.1038/nrn1583 PMID: 15611727
6. Pfeffer SR. Transport-vesicle targeting: tethers before SNAREs. Nature cell biology. 1999; 1(1):E17–22. https://doi.org/10.1038/8967 PMID: 10559876
7. Gerst JE. SNARE regulators: matchmakers and matchbreakers. Biochim Biophys Acta. 2003; 1641(2–3):99–110. PMID: 12914951
8. Schiavo G, Stenbeck G, Rothman JE, Sollner TH. Binding of the synaptic vesicle v-SNARE, synaptotagmin, to the plasma membrane t-SNARE, SNAP-25, can explain docked vesicles at neurotoxin-treated synapses. Proc Natl Acad Sci U S A. 1997; 94(3):997–1001. PubMed Central PMCID: PMC19628. PMID: 9023371
9. Hanson PI, Roth R, Morisaki H, Jahn R, Heuser JE. Structure and conformational changes in NSF and its membrane receptor complexes visualized by quick-freeze/deep-etch electron microscopy. Cell. 1997; 90(3):523–35. PMID: 9267032
10. Chen YA, Scales SJ, Scheller RH. Sequential SNARE assembly underlies priming and triggering of exocytosis. Neuron. 2001; 30(1):161–70. PMID: 11343652
11. Lee HK. Synaptic plasticity and phosphorylation. Pharmacology & therapeutics. 2006; 112(3):810–32. PubMed Central PMCID: PMC2748765.
12. Klenchin VA, Martin TF. Priming in exocytosis: attaining fusion-competence after vesicle docking. Biochimie. 2000; 82(5):399–407. PMID: 10865127
13. Snyder DA, Kelly ML, Woodbury DJ. SNARE complex regulation by phosphorylation. Cell biochemistry and biophysics. 2006; 45(1):111–23. https://doi.org/10.1385/CBB:45:1:111 PMID: 16679567
14. Nagy G, Reim K, Matti U, Brose N, Binz T, Rettig J, et al. Regulation of releasable vesicle pool sizes by protein kinase A-dependent phosphorylation of SNAP-25. Neuron. 2004; 41(3):417–29. PMID: 14766180

15. Hepp R, Cabaniols JP, Roche PA. Differential phosphorylation of SNAP-25 in vivo by protein kinase C and protein kinase A. FEBS Lett. 2002; 532(1–2):52–6. PMID: 12459461

16. Lontay B, Pal B, Serfozo Z, Koszeghy A, Szucs G, Rusznak Z, et al. Protein phosphatase-1M and Rho-kinase affect exocytosis from cortical synaptosomes and influence neurotransmission at a glutamatergic giant synapse of the rat auditory system. J Neurochem. 2012; 123(1):84–99. https://doi.org/10.1111/j.1471-4159.2012.07882.x PMID: 22817114

17. Hartshorne DJ, Ito M, Erdodi F. Role of protein phosphatase type 1 in contractile functions: myosin phosphatase. J Biol Chem. 2004; 279(36):37211–4. https://doi.org/10.1074/jbc.R400018200 PMID: 15136561

18. Feng J, Ito M, Ichikawa K, Isaka N, Nishikawa M, Hartshorne DJ, et al. Inhibitory phosphorylation site for Rho-associated kinase on smooth muscle myosin phosphatase. J Biol Chem. 1999; 274(52):37385–90. PMID: 10601309

19. Muranyi A, Derkach D, Erdodi F, Kiss A, Ito M, Hartshorne DJ. Phosphorylation of Thr695 and Thr850 on the myosin phosphatase target subunit: inhibitory effects and occurrence in A7r5 cells. FEBS Lett. 2005; 579(29):6611–5. https://doi.org/10.1016/j.febslet.2005.10.055 PMID: 16297917

20. Lontay B, Serfozo Z, Gergely P, Ito M, Hartshorne DJ, Erdodi F. Localization of myosin phosphatase target subunit 1 in rat brain and in primary cultures of neuronal cells. J Comp Neurol. 2004; 478(1):72–87. https://doi.org/10.1002/cne.20273 PMID: 15334650

21. Mathe C, Beyer D, Erdodi F, Serfozo Z, Szekvolgyi L, Vasas G, et al. Microcystin-LR induces abnormal root development by altering microtubule organization in tissue-cultured common reed (Phragmites australis) plantlets. Aquatic toxicology. 2009; 92(3):122–30. https://doi.org/10.1016/j.aquatox.2009.02.005 PMID: 19269700

22. Eto M, Kirkbride JA, Chugh R, Karikari NK, Kim JI. Nuclear localization of CPI-17, a protein phosphatase-1 inhibitor protein, affects histone H3 phosphorylation and corresponds to proliferation of cancer and smooth muscle cells. Biochemical and biophysical research communications. 2013; 434(1):137–42. PubMed Central PMCID: PMC3644852. https://doi.org/10.1016/j.bbrc.2013.03.055 PMID: 23541585

23. Laemmli UK. Cleavage of structural proteins during the assembly of the head of bacteriophage T4. Nature. 1970; 227(5259):680–5. PMID: 5432063

24. Kiss A, Lontay B, Becsi B, Markasz L, Olah E, Gergely P, et al. Myosin phosphatase interacts with and dephosphorylates the retinoblastoma protein in THP-1 leukemic cells: its inhibition is involved in the attenuation of daunorubicin-induced cell death by calyculin-A. Cell Signal. 2008; 20(11):2059–70. https://doi.org/10.1016/j.cellsig.2008.07.018 PMID: 18755268

25. Larsen MR, Thingholm TE, Jensen ON, Roepstorff P, Jorgensen TJ. Highly selective enrichment of phosphorylated peptides from peptide mixtures using titanium dioxide microcolumns. Molecular & cellular proteomics: MCP. 2005; 4(7):873–86.

26. Guan S, Price JC, Prusiner SB, Ghaemmaghami S, Burlingame AL. A data processing pipeline for mammalian proteome dynamics studies using stable isotope metabolic labeling. Molecular & cellular proteomics: MCP. 2011; 10(12):M111 010728. PubMed Central PMCID: PMC3237081.

27. Baker PR, Trinidad JC, Chalkley RJ. Modification site localization scoring integrated into a search engine. Molecular & cellular proteomics: MCP. 2011; 10(7):M111 008078. PubMed Central PMCID: PMC3134073.

28. Dedinszki D, Sipos A, Kiss A, Batori R, Konya Z, Virag L, et al. Protein phosphatase-1 is involved in the maintenance of normal homeostasis and in UVA irradiation-induced pathological alterations in HaCaT cells and in mouse skin. Biochim Biophys Acta. 2015; 1852(1):22–33. https://doi.org/10.1016/j.bbadis.2014.11.005 PMID: 25446992

29. Dedinszki D, Kiss A, Markasz L, Marton A, Toth E, Szekely L, et al. Inhibition of protein phosphatase-1 and -2A decreases the chemosensitivity of leukemic cells to chemotherapeutic drugs. Cell Signal. 2015; 27(2):363–72. https://doi.org/10.1016/j.cellsig.2014.11.021 PMID: 25435424

30. Nichols RA, Wu WC, Haycock JW, Greengard P. Introduction of impermeant molecules into synaptosomes using freeze/thaw permeabilization. J Neurochem. 1989; 52(2):521–9. PMID: 2536075

31. Cousin MA, Robinson PJ. Mechanisms of synaptic vesicle recycling illuminated by fluorescent dyes. J Neurochem. 1999; 73(6):2227–39. PMID: 10582580

32. Cousin MA, Robinson PJ. Two mechanisms of synaptic vesicle recycling in rat brain nerve terminals. J Neurochem. 2000; 75(4):1645–53. PMID: 10987846

33. Koszeghy A, Vincze J, Rusznak Z, Fu Y, Paxinos G, Csernoch L, et al. Activation of muscarinic receptors increases the activity of the granule neurones of the rat dorsal cochlear nucleus—a calcium imaging study. Pflugers Arch. 2012; 463(6):829–44. https://doi.org/10.1007/s00424-012-1103-1 PMID: 22547003

34. Biemann K. Appendix 5. Nomenclature for peptide fragment ions (positive ions). Methods in enzymology. 1990; 193:886–7. PMID: 2074849

35. Erdodi F, Kiss E, Walsh MP, Stefansson B, Deng JT, Eto M, et al. Phosphorylation of protein phosphatase type-1 inhibitory proteins by integrin-linked kinase and cyclic nucleotide-dependent protein kinases. Biochemical and biophysical research communications. 2003; 306(2):382–7. PMID: 12804574

36. Turner KM, Burgoyne RD, Morgan A. Protein phosphorylation and the regulation of synaptic membrane traffic. Trends in neurosciences. 1999; 22(10):459–64. PMID: 10481193

37. Morgan A, Burgoyne RD, Barclay JW, Craig TJ, Prescott GR, Ciufo LF, et al. Regulation of exocytosis by protein kinase C. Biochem Soc Trans. 2005; 33(Pt 6):1341–4. https://doi.org/10.1042/BST20051341 PMID: 16246114

38. Risinger C, Bennett MK. Differential phosphorylation of syntaxin and synaptosome-associated protein of 25 kDa (SNAP-25) isoforms. J Neurochem. 1999; 72(2):614–24. PMID: 9930733

39. Tolar LA, Pallanck L. NSF function in neurotransmitter release involves rearrangement of the SNARE complex downstream of synaptic vesicle docking. J Neurosci. 1998; 18(24):10250–6. PMID: 9852562

40. Shimazaki Y, Nishiki T, Omori A, Sekiguchi M, Kamata Y, Kozaki S, et al. Phosphorylation of 25-kDa synaptosome-associated protein. Possible involvement in protein kinase C-mediated regulation of neurotransmitter release. J Biol Chem. 1996; 271(24):14548–53. PMID: 8662851

41. Genoud S, Pralong W, Riederer BM, Eder L, Catsicas S, Muller D. Activity-dependent phosphorylation of SNAP-25 in hippocampal organotypic cultures. J Neurochem. 1999; 72(4):1699–706. PMID: 10098880

42. Gao J, Hirata M, Mizokami A, Zhao J, Takahashi I, Takeuchi H, et al. Differential role of SNAP-25 phosphorylation by protein kinases A and C in the regulation of SNARE complex formation and exocytosis in PC12 cells. Cell Signal. 2016; 28(5):425–37. https://doi.org/10.1016/j.cellsig.2015.12.014 PMID: 26721188

43. Baldwin ML, Rostas JA, Sim AT. Two modes of exocytosis from synaptosomes are differentially regulated by protein phosphatase types 2A and 2B. J Neurochem. 2003; 85(5):1190–9. PMID: 12753078

44. Mansuy IM, Shenolikar S. Protein serine/threonine phosphatases in neuronal plasticity and disorders of learning and memory. Trends in neurosciences. 2006; 29(12):679–86. https://doi.org/10.1016/j.tins.2006.10.004 PMID: 17084465

45. Gao J, Takeuchi H, Zhang Z, Fukuda M, Hirata M. Phospholipase C-related but catalytically inactive protein (PRIP) modulates synaptosomal-associated protein 25 (SNAP-25) phosphorylation and exocytosis. J Biol Chem. 2012; 287(13):10565–78. PubMed Central PMCID: PMC3322965. https://doi.org/10.1074/jbc.M111.294645 PMID: 22311984

46. Yang Y, Craig TJ, Chen X, Ciufo LF, Takahashi M, Morgan A, et al. Phosphomimetic mutation of Ser-187 of SNAP-25 increases both syntaxin binding and highly Ca2+-sensitive exocytosis. The Journal of general physiology. 2007; 129(3):233–44. PubMed Central PMCID: PMC2151612. https://doi.org/10.1085/jgp.200609685 PMID: 17325194

47. Nakata Y, Yasuda T, Fukaya M, Yamamori S, Itakura M, Nihira T, et al. Accumulation of alpha-synuclein triggered by presynaptic dysfunction. J Neurosci. 2012; 32(48):17186–96. https://doi.org/10.1523/JNEUROSCI.2220-12.2012 PMID: 23197711

48. Shu Y, Liu X, Yang Y, Takahashi M, Gillis KD. Phosphorylation of SNAP-25 at Ser187 mediates enhancement of exocytosis by a phorbol ester in INS-1 cells. J Neurosci. 2008; 28(1):21–30. https://doi.org/10.1523/JNEUROSCI.2352-07.2008 PMID: 18171919

49. Fu J, Naren AP, Gao X, Ahmmed GU, Malik AB. Protease-activated receptor-1 activation of endothelial cells induces protein kinase Calpha-dependent phosphorylation of syntaxin 4 and Munc18c: role in signaling p-selectin expression. J Biol Chem. 2005; 280(5):3178–84. https://doi.org/10.1074/jbc.M410044200 PMID: 15576373

50. Sakisaka T, Baba T, Tanaka S, Izumi G, Yasumi M, Takai Y. Regulation of SNAREs by tomosyn and ROCK: implication in extension and retraction of neurites. The Journal of cell biology. 2004; 166(1):17–25. PubMed Central PMCID: PMC2172130. https://doi.org/10.1083/jcb.200405002 PMID: 15240567

51. Gladycheva SE, Lam AD, Liu J, D'Andrea-Merrins M, Yizhar O, Lentz SI, et al. Receptor-mediated regulation of tomosyn-syntaxin 1A interactions in bovine adrenal chromaffin cells. J Biol Chem. 2007; 282(31):22887–99. https://doi.org/10.1074/jbc.M701787200 PMID: 17545156

ARTICLE IN PRESS

BBA - Molecular Basis of Disease xxx (xxxx) xxx–xxx

lontay.beata_285_24



Contents lists available at ScienceDirect

BBA - Molecular Basis of Disease

journal homepage: www.elsevier.com/locate/bbadis



Myosin phosphatase accelerates cutaneous wound healing by regulating migration and differentiation of epidermal keratinocytes via Akt signaling pathway in human and murine skin

Dániel Horváth[a], Adrienn Sipos[a], Evelin Major[a], Zoltán Kónya[a,b], Róbert Bátori[c], Dóra Dedinszki[d], Attila Szöllősi[e], István Tamás[a], Judit Iván[a,b], Andrea Kiss[a], Ferenc Erdődi[a,b], Beáta Lontay[a,*]

[a] Department of Medical Chemistry, Faculty of Medicine, University of Debrecen, Debrecen, Hungary
[b] MTA-DE Cell Biology and Signaling Research Group, Faculty of Medicine, University of Debrecen, Debrecen, Hungary
[c] Vascular Biology Center, Augusta University, Augusta, United States
[d] Institute of Enzymology, Hungarian Academy of Sciences, Budapest, Hungary
[e] Department of Physiology, Faculty of Medicine, University of Debrecen, Debrecen, Hungary

ARTICLE INFO

Keywords:
Wound healing
Myosin phosphatase
Keratinocyte
Transglutaminase 1
Ex vivo human biopsy

ABSTRACT

Wound healing is a complex sequence of cellular and molecular processes such as inflammation, cell migration, proliferation and differentiation. ROCK is a widely investigated Ser/Thr kinase with important roles in re-arranging the actomyosin cytoskeleton. ROCK inhibitors have already been approved to improve corneal endothelial wound healing. The purpose of this study was to investigate the functions of myosin phosphatase (MP or PPP1CB), a type-1 phospho-Ser/Thr-specific protein phosphatase (PP1), one of the counter enzymes of ROCK, in skin homeostasis and wound healing. To confirm our hypotheses, we applied tautomycin (TM), a selective PP1 inhibitor, on murine skin that caused the arrest of wound closure. TM suppressed scratch closure of HaCaT human keratinocytes without having influence on the survival of the cells. Silencing of, the regulatory subunit of MP (MYPT1 or PPP1R12A), had a negative impact on the migration of keratinocytes and it influenced the cell-cell adhesion properties by decreasing the impedance of HaCaT cells. We assume that MP differentially activates migration and differentiation of keratinocytes and plays a key role in the downregulation of transglutaminase-1 in lower layers of skin where no differentiation is required. MAPK Proteome Profiler analysis on human *ex vivo* biopsies with MYPT1-silencing indicated that MP contributes to the mediation of wound healing by regulating the Akt signaling pathway. Our findings suggest that MP plays a role in the maintenance of normal homeostasis of skin and the process of wound healing.

1. Introduction

Wound healing is a complex sequence of cellular and molecular processes consisting of hemostasis, inflammation, new tissue formation, re-epithelialization, and tissue remodeling [1–3]. Normal wound healing in skin is essential to reduce complications, including bacterial infection, water loss, and scar formation, that might perturb organ function and cause increased global morbidity and mortality [4,5]. Understanding the molecular, cellular, and physiologic aspects of wound healing is essential for developing new strategies to overcome impaired wound healing.

The epidermis consists of multiple layers, and cross-talk between the proliferation, migration, and differentiation processes is required for reepithelialization during wound healing [6]. Keratinocytes of the basal layer (*stratum basale*) adhere to the basement membrane and proliferate. Keratinocytes proliferate and migrate upwards through the granular and spinous layers [7], and eventually reach the cornified, outermost layers to replace cells lost through terminal differentiation [1]. In wounded skin, the keratinocytes near the damage zone respond to an array of signals, including growth factors, by activating both proliferation and migration, followed by differentiation [8]. A few days after wounding, monocytes appear in the wound and differentiate into

Abbreviations: PP1, protein phosphatase-1; PP1c, PP1 catalytic subunit; TM, tautomycin; H1152, (*S*)-(+)-2-Methyl-1-[(4-methyl-5-isoquinolinyl)sulfonyl]-hexahydro-1H-1,4-diazepine dihydrochloride; PBS, phosphate buffer saline; TBS, Tris-buffered saline solution; Tgase-1, transglutaminase-1; MP, myosin phosphatase; MYPT1, myosin phosphatase targeting subunit; NHEK, normal human keratinocyte

* Corresponding author at: Department of Medical Chemistry, Faculty of Medicine, University of Debrecen, H-4032 Debrecen, Egyetem tér 1. Hungary.
E-mail address: lontay@med.unideb.hu (B. Lontay).

https://doi.org/10.1016/j.bbadis.2018.07.013
Received 26 March 2018; Received in revised form 24 June 2018; Accepted 10 July 2018
0925-4439/ © 2018 Elsevier B.V. All rights reserved.

Please cite this article as: Horváth, D., BBA - Molecular Basis of Disease (2018), https://doi.org/10.1016/j.bbadis.2018.07.013

macrophages [9], and new tissue formation follows. At this stage, keratinocytes migrate into the injured area for primary coverage and start to proliferate and differentiate to recover the stratification and to restore the barrier function of the epithelium. Moreover, fibroblasts transform to myofibroblasts, produce extracellular matrix, and contract the tissue [10]. Remodeling, the third stage of wound healing, starts 10 days–3 weeks after injury and can last up to a year. A majority of endothelial cells, macrophages, and myofibroblasts disappear by apoptosis, leaving behind the scar containing mostly collagen, a few cells, and extracellular matrix proteins.

Many steps in wound repair are poorly characterized at the molecular level, including the underlying mechanism of reepithelialization, a major step in new tissue formation. One of the most important events is the reversible phosphorylation of proteins catalyzed by protein kinases and phosphatases. The ligands of protein tyrosine kinase receptors (*e.g.* HGF, FGF, EGF) are positive regulators of reepithelialization, initiating the migration and proliferation of keratinocytes [5]. In contrast, migration of keratinocytes from the wound edge is enhanced by protein serine(Ser)/threonine(Thr) kinase inhibitors [11]. Acetylcholine acting through muscarinic receptors or catecholamines signaling *via* β2-adrenoreceptors, lead to activation of protein kinase A and G [12] or dephosphorylation of extracellular signal-related kinases (ERK1 and ERK2) by activation of protein phosphatase 2A [13]. Another Ser/Thr kinase involved in wound healing is Rho-associated protein kinase (ROCK). ROCK is the major downstream effector of small Rho GTPases, and is involved in various cellular functions that include actin cytoskeleton organization, cell-cell adhesion [14], cell motility, and anti-apoptotic processes [15]. ROCK plays a role in epithelial regeneration, and inhibition of ROCK significantly enhances cell proliferation, chemotaxis, and wound healing of periodontal ligament stem cells [16].

The role of protein kinases has been widely described in the process of wound healing but less is known about the protein phosphatases involved in these events. Okadaic acid, the inhibitor of protein phosphatase-1 (PP1) and -2A (PP2A) enzymes, increases the phosphorylation level of myosin II resulting in decreased hepatic cell migration [17]. Although enhanced myosin II phosphorylation is needed for migration, the inhibitory influence in this case is presumably due to a maintained phosphatase inhibition that would not allow “cycling” of myosin II phosphorylation required for effective migration. On the other hand, inhibition of PP2A by 10 nM okadaic acid resulted in an increased migration [13]. Changes in the phosphorylation level of Ca^{2+}-transport and contractile proteins upon phosphatase inhibition mediates cell migration and wound healing [18].

The cytoskeletal changes in the course of wound healing are correlated with the phosphorylation state of contractile proteins such as myosin II [19], ezrin/radixin/moesin, and adducin. Phosphorylation of these proteins is primarily regulated by ROCK [20] and its counter enzyme, a type 1 Ser/Thr specific protein phosphatase, termed myosin phosphatase (MP or PPP1CB). MP consists of a 38 kDa PP1 catalytic subunit (PP1c) of the β/δ isoform, a 130/133 kDa myosin phosphatase target subunit-1 (MYPT1 or PPP1R12A), and a 20 kDa subunit of unknown function in smooth muscle [21]. MP catalyzes the dephosphorylation of a variety of ROCK-phosphorylated proteins and may be a key player in re-epithelialization [22,23]. Therefore, we investigated the involvement of MP in the cellular processes and interactions required for proper regeneration of the skin. To address this hypothesis in a physiological setting, we used well-defined *in vivo* wound healing excision injury models of murine and human origins. We used a number of reconstituted *in vitro* cellular and *ex vivo* human skin models relevant to the wound healing processes to validate the observations in healing tissue.

Our present results suggest that the inhibition of PP1 suppresses wound healing without influencing cell survival. Silencing of MP has a negative impact on the migration of keratinocytes and also influences cell-cell adhesion properties by decreasing the impedance of the monolayer of MYPT1-silenced HaCaT cells. Here, we identify the signaling mechanism by which MP regulates wound healing through the modulation of Akt signaling and Hsp27. MP differentially activates migration and differentiation of keratinocytes and plays a key role in the downregulation of transglutaminase-1 (Tgase-1) in lower layers of skin where no differentiation is required.

2. Materials and methods

2.1. Materials

Tautomycin (Merck), H1152 (Santa Cruz Biotechnology), MYPT1 siRNA, Lipofectamine 2000 (ThermoFisher Scientific), protease inhibitor cocktail tablets (Roche), Texas Red-X phalloidin and ProLong Gold Antifade medium (Life Technologies) were from the indicated sources. All other chemicals were from Sigma-Aldrich unless otherwise indicated.

2.2. Antibodies

The following antibodies were obtained from the indicated sources or described in the respective references: Anti-MYPT1$^{1\text{-}296}$ [24] and anti-PP1cδ (Merck); anti-transglutaminase-1, anti-GAPDH, and anti-α-tubulin (Santa Cruz Biotechnology); anti-β-catenin (Abcam, Cambridge, UK); anti-Akt, anti-phospho-Akt Ser473, and horseradish peroxidase (HRP)-linked anti-mouse IgG (Cell Signaling Technology); HRP-conjugated anti-rabbit IgG (Sigma-Aldrich); Alexa Fluor 488 chicken anti-rabbit IgG (Life Technologies).

2.3. Ethics statement

All procedures were authorized by the Institutional Ethics Committee of University of Debrecen (protocol number 7/2010 DE MÁB v 9/2008/DEMÁB) and were conducted in accordance with the guidelines for the care and use of laboratory animals outlined in the national and European Union ethical regulations.

2.4. Wound healing study on mouse dorsal skin and tissue processing

Male Balb/c mice (Charles River) aged 6–7 week were housed individually in a controlled atmosphere in relative humidity of 35.0–75.0% with 12/12 h light and dark cycles and at a temperature range of 19.0–25.0 °C. Food and water were available *ad libitum*. Wound incision was performed as described previously [6]. The dorsal fur of the mice was depilated using commercial hair removal cream. Mice were anaesthetized with isoflurane inhalation (Abbott Animal Health, Abbott Park, IL, USA) prior to the surgical procedures and were kept warm during anesthesia. Three full thickness 4 mm punch biopsies were made on the dorsal surface of mice and the wound beds were wiped with povidone-iodine to prevent infection. The wounds arranged lengthways were made at the same time. Tautomycin (TM), a selective PP1 inhibitor, and H1152, a ROCK inhibitor, were applied on one of the wounds in hydrophilic anionic cream in a final concentration of 1 and 10 μM, respectively (n = 6 for each treatment). Control wounds were treated with hydrophilic cream only. Treatments were repeated daily for 6 days and wounds were covered with a surgical dressing to keep the cream in place. Animals were euthanized by cervical dislocation, then the skin was excised and the subcutaneous fat removed with a scalpel blade. The wound samples were transversely cut through exactly the center of the wound in each animal and were processed for histology, while the other halves were snap frozen in liquid nitrogen and stored at −80 °C for later analysis. Wound tissue samples were lysed with lysis buffer (25 mM Tris-HCl, pH 7.5, 0.6 M NaCl, 2 mM EDTA, 1 mM DTT, 0.5%(V/V) Triton X-100) containing protease inhibitor cocktail and phenylmethylsulfonyl fluoride (PMSF) using potter homogenizer as previously described [25]. Protein concentration was determined by

BCA assay (Thermo Scientific).

2.5. Macroscopic wound observation

The wound was photographed with an Olympus camera (Olympus, Tokyo, Japan) at given intervals of healing (0, 1, 2, 3, 6 days). The size of the remaining skin defect (as the percentage of the initial wound area) was evaluated by ImageJ software (NIH, Bethesda, MD, USA) and wound closure was expressed as the ratio of actual wound area to initial wound size and was statistically analyzed.

2.6. Immunohistochemistry and histologic image analysis

After euthanasia, wounds, along with surrounding tissues, were excised, fixed with 10% phosphate-buffered (pH 7.4) formalin, and paraffin-embedded according to standard protocols [26]. Cross sections (4 μm thick) were cut, mounted on glass slides (Superfrost/plus; A. Daigger & Company, Inc., Vernon Hills, IL), deparaffinized by xylene, dehydrated by graded ethanol, and processed for hematoxylin and eosin (H&E) staining [25] using Masson-Goldner trichrome staining, as described previously. Immunohistochemical staining for transglutaminase-1 and MYPT1 was performed as follows. Sections were incubated with primary antibodies overnight at 4 °C, the sections were washed and incubated with anti-mouse or anti-rabbit HRP conjugated secondary antibody. Immunosignals were developed using 3,3′-diaminobenzidine (DAB) chromogen as a substrate without counterstaining. The sections were cleared with xylene before finally being mounted and histologic images were taken with a Leica S40 microscope.

2.7. Cell culture and treatment

Immortalized human keratinocyte HaCaT cells (Sigma-Aldrich) were maintained in DMEM supplemented with 10% (V/V) FBS and 2 mM L-glutamine in a 5% CO_2-humidified atmosphere at 37 °C. Cells were plated in 6-well or 96-well culture plates (Sarstedt) and grown to confluency. The medium was then replaced by serum-free DMEM overnight (~16–24 h) in order to synchronize cells. After synchronization, HaCaT cells were treated with 1 μM TM or 10 μM H1152 for 1 h. For differentiation, culture medium of HaCaT cells was supplemented with calcium chloride at a final concentration of 2.4 mM.

Normal human epidermal keratinocyte cell line (NHEK) was a gift from the laboratory of Tamás Bíró (Department of Physiology, University of Debrecen). NHEK cells were maintained in EpiLife medium supplemented with human keratinocyte growth supplement kit (Gibco by Life technologies, UK) in a 5% CO2-humidified atmosphere at 37 °C. Cells were plated in 6-well or 96-well culture plates (Sarstedt) and grown to confluency for differentiation. Cells growing below 80% confluency (not to let reaching total confluency) were considered as undifferentiated ones. After treatment, cells were harvested in Tris-Triton buffer (10 mM Tris-HCl pH 7.4, 100 mM NaCl, 1 mM EDTA, 1 mM EGTA, 1% Triton X-100, 10% glycerol, 0.1% SDS, 0.5% sodium deoxycholate supplemented with 1× protease inhibitor cocktail (Roche), and protein phosphatase inhibitor cocktail (1 mM NaF, 1 mM $Na_4P_2O_7$, 1 mM β-glycerophosphate, 1 mM Na_3VO_4)). Proteins were solubilized by sonication and protein concentrations were determined by BCA Protein Assay.

2.8. Gene silencing

Gene silencing of MYPT1 in HaCaT cells was carried out using double stranded siRNA (Thermo Scientific, see Table S1.) at 40 nM final concentration. Lipofectamine 2000 transfection reagent was used according to the manufacturer's instructions. 5 μl Lipofectamine 2000 and 100 pmol siMYPT1 were diluted in 250–250 μl OptiMEM medium and the mixture was incubated at room temperature for another 20 min. Cells were trypsinized, DMEM containing 10% (V/V) FBS was added, then cells were centrifuged at 1500 rpm for 3 min and resuspended in serum-free DMEM and plated onto 6-well plate. Transfection mixture was added to the cells (500 μl mixture to 2 ml serum-free DMEM), and after 4 hoursincubation 10% (V/V) FBS was added. After 48 h, the appropriate experiment was carried out. Non-targeting control RNA (NT siRNA) was used as control.

2.9. Cell viability assay (MTT assay)

Viability of HaCaT cells in response to inhibitory treatments (TM or H1152) or gene silencing of MYPT1 was measured by MTT assay. Cells were grown in 96-well plate and treated with 1 μM TM or 10 μM H1152 for 12 h (following overnight serum-starvation), or siRNA-mediated gene silencing of MYPT1 was performed for 48 h, and then the medium was removed. After addition of 100 μl serum-free DMEM and 10 μl 5 mg/ml of MTT solution (3-(4,5-dimethylthiazol-2-yl)-2,5-diphenyltetrazolium bromide dissolved in PBS), cells were incubated in a 5% CO_2-humidified atmosphere at 37 °C for 30 min, then formazan crystals were dissolved in dimethyl sulfoxide (DMSO) and the absorbance was determined by a photometer (LabSystems Multiskan MS) at 540 nm wavelength.

2.10. Caspase assay

A caspase-3 activity assay was used to investigate the effect of inhibitor treatments or MYPT1 silencing on apoptosis in human keratinocytes. HaCaT cells were cultured in 6-well plates. After treatment (1 μM TM or 10 μM H1152, 12 h) or siRNA transfection, cells were collected into Eppendorf tubes and centrifuged with maximum speed for 15 s. Supernatants were removed, cells were washed once with PBS and centrifuged again, and then pelleted cells were lysed by addition of 220 μl ice cold lysis buffer (10 mM HEPES, pH 7.4, 2 mM EDTA, 0.1% (V/V) CHAPS, 1 mM PMSF, 5 mM DTT, 1× protease inhibitor cocktail). After 10 min incubation, tubes were centrifuged (13,000 rpm, 3 min, 4 °C), supernatants were transferred into new Eppendorf tubes, and 200 μl 2× reaction buffer (200 mM HEPES, pH 7,25, 20% (w/V) sucrose, 0,1% (V/V) CHAPS, 5 mM DTT) containing 2 μl/ml Ac-DEVD-AMC caspase-3 substrate was added. Samples were incubated at 37 °C for 1 h then pipetted into white 96-well plates, in triplicate (100–100 μl). Fluorescence intensity of AMC was detected by Fluoroskan FL instrument (excitation: 360 nm, emission: 460 nm).

2.11. Western blot

Lysates, prepared from HaCaT or NHEK cell culture or from the wound tissue of mice, were boiled in 5× sodium dodecyl sulphate-polyacrylamide gel electrophoresis (SDS-PAGE) sample buffer (50% glycerol, 10% SDS, 0.31 M Tris, 100 mM dithiothreitol, 0.01% bromophenol blue) at 100 °C for 5 min. Western blot analysis was applied as described before [27]. Immunoreactions were visualized by chemiluminescence using Super Signal West Pico Chemiluminescent Substrate (Thermo Fischer) and FluorChem FC2 Imager (Alpha Innotech) or ChemiDoc Touch Imaging System (Bio-Rad).

2.12. Protein phosphatase activity assay

HaCaT or NHEK cells were treated either with TM or H1152 for 1 h, or with MYPT1-siRNA for 48 h, and then lysed in 50 mM Tris-HCl pH 7.4, 150 mM NaCl, 0.5 mM EDTA, 0.5 mM EGTA, 1% (V/V) Triton X-100 with 0.5% (V/V) protease inhibitor cocktail solution. Balb/c mice were treated with TM or H1152 and the excised skin samples were lysed as described above. The lysates were centrifuged at 15000 rpm for 10 min. The phosphatase activity of the supernatants were assayed at 30 °C in 20 mM Tris–HCl (pH 7.4) buffer containing 0.1% 2-mercaptoethanol in the presence of 1 μM ^{32}P-labeled 20 kDa light chain of turkey gizzard myosin (^{32}P-MLC20) at 3- or 300-fold final dilution for

HaCaT or NHEK cells and BALB/c mouse skin samples, respectively. The samples were prewarmed at 30 °C for 1 min, and then the reaction was initiated by addition of the substrate. After a 20 to 60 s incubation the reaction was terminated by the addition of 200 µl 10% (V/V) TCA and 200 µl 6 mg/ml BSA. The precipitated proteins were collected by centrifugation at 10,000 rpm for 3.5 min and the released $^{32}P_i$ was determined from the supernatant (370 µl) in a scintillation counter (Perkin Elmer). The phosphatase activities were normalized to the protein content of the samples and expressed as percentages of the respective non-treated samples.

2.13. Scratch assay

HaCaT cells were grown in 96-well TPP plates (Sigma-Aldrich) to confluence and scratched by a Tecan Freedom EVO 150 machine (Tecan Group Ltd., Switzerland), then cultured for an additional 24 h in the absence or presence of inhibitors or with or without transfection with MYPT-siRNA. Cells in serum-free medium were applied as negative control. To inhibit cell proliferation mitomycin was used in 30 µg/ml concentration and was applied for 30 min just before scratching the cells. Both initial and final scratch areas were determined using Leica DM IL LED microscope (Leica Camera AG, Wetzlar, Germany) and ImageJ computer image analyzing software (https://imagej.nih.gov/ij/, NIH, Bethesda, MD, USA). The final scratch area was normalized to the control surface in each case.

2.14. Electric cell-substrate impedance sensing (ECIS) measurements

Electric cell-substrate impedance sensing (ECIS, Applied BioPhysics) was applied as described previously (Keese, C. R. et al., 2004) to study the role of MYPT1 and ROCK in wound healing after MYPT1-silencing or the inhibition of PP1 and ROCK. ECIS is suitable to wound the cell monolayer and monitor the repair of the burnt area by measuring impedance of the surface. Non-target RNA treated (NT siRNA) and MYPT1-silenced (siMYPT1) HaCaT cells were plated onto 8W10E electrode arrays. After 48 h of MYPT1 silencing, electrical shock was induced in the confluent cell monolayer using the following protocol: 5 mA at 60 kHz frequency, two times for 30 s, then wound healing was monitored. Reaching maximum plateau value was considered as complete recovery. Repopulation of siMYPT1 cells was compared to migration of NT-siRNA treated cells. In another set of experiments, after wounding, healing of cells was measured in the presence of TM or H1152 compounds in a final concentration of 1 µM and 10 µM, respectively. Medium of control cells did not contain any added components except the solvent of inhibitors. Impedance of HaCat cells was also measured without any wounding in the presence of the above mentioned inhibitors or during MYPT1-silencing in the presence or absence of Ca^{2+}. Impedance was recorded in real-time on inhibitor treated and mock control cells for at least 6 h and the set of constant values are plotted. In every set of experiments, electric cell-substrate impedance was measured in three or four independent wells for every treatment.

2.15. Immunofluorescence staining

For confocal microscopy, HaCaT cells were grown on glass coverslips. After reaching 100% confluence, the cell monolayer was subjected to a scratch assay. After the assay, cells were washed with PBS and fixed for 15 min in 4% paraformaldehyde. The fixation step was followed by washing with PBS three times for 5 min. Cells were permeabilized with 0.2% (V/V) Triton X-100 in PBS for 4 min at room temperature, followed by washing with PBS two times for 5 min. The cells were blocked with 1% horse serum (V/V) in PBS for 1 h at 4 °C. Then the coverslips were incubated with anti-β-catenin primary antibody in a dilution of 1:250 in 1% horse serum-PBS overnight at 4 °C. After washing with PBS three times for 5 min, secondary antibodies were added in a 1:200 dilution in 1% horse serum-PBS solution. Following PBS washing (three times 15 min) nuclear staining was carried out with 1 µg/ml DAPI (4′, 6-diamidino-2-phenylindole). The coverslips were then washed two times with PBS for 5 min, and mounted in ProLong Gold Antifade medium. ZO-1 antibody was used in 7.5 µg/ml concentration due to manufacturer's instructions. In case of ZO-1 staining a modified protocol was used; instead of horse serum 1% BSA/PSB was applied as blocking solution and primary and secondary antibodies were also diluted in this solution. Cell permeabilization was carried out using 0.02% (V/V) Triton X-100/PBS in this experiment.

Confocal microscopy was performed with Leica X8 confocal microscope (Leica Microsystems, Wetzlar, Germany).

2.16. Akt1/Akt2 immunoprecipitation

After MYPT1 silencing HaCaT cells were harvested with ice-cold lysis buffer (50 mM Tris pH 7.4, 150 mM NaCl, 10× protease inhibitor cocktail, 1% Triton-X 100, 50× phosphatase inhibitor cocktail) then protein concentration was measured by BCA assay. Meanwhile 100 mg of protein A-coupled Sepharose beads (GE HealthCare) were incubated in 1 ml 1xTBS at 4 °C under rotary agitation for 30 min. 100 µl of bead slurry was added to the lysates and the mix was incubated at 4 °C under rotary agitation for 30 min, then were centrifuged at 4 °C, 800 *g* for 3 min and the supernatant was used for immunoprecipitation. 400 µl of precleared lysates were incubated with anti-Akt1 (Cell Signaling Technology) or anti-Akt2 (Cell Signaling Technology) antibodies in 1:50 dilution at 4 °C under rotary agitation for 2 h. Then 100 µl of bead slurry was added to the lysate-antibody mix and were incubated at 4 °C under rotary agitation for overnight. The following day the tubes were centrifuged at 4 °C, 800 *g* for 3 min, the supernatant was removed, the beads were washed twice with 1× binding buffer (300 mM Tris pH 7.4, 1,5 M NaCl, 10 mM EDTA, 1% Triton-X 100, 10× protease inhibitor cocktail, 50× phosphatase inhibitor cocktail) and once with 1xTBS. Wash buffer was removed completely from the beads and the elution was carried out by boiling the samples with 1xSDS loading buffer at 100 °C for 5 min.

2.17. JuLI™ real-time cell history recording of cell proliferation

Control, TM-, H1152-treated and NT siRNA and siMYPT1-transfected cells were cultured in 35 mm dishes and the confluent monolayer was scratched by a pipette tip. Sequential time-lapse images were recorded in each hour throughout a day by JuLI™ Br (NanoEnTek, Seoul, South Korea) to determine the rate of wound healing. Scratch sizes were measured by ImageJ software and the area of grown cells was plotted *versus* time.

2.18. Sulforhodamine B (SRB) assay

Cells were placed in a 96-well plate and subjected to inhibitory treatment or MYPT1-silencing followed by scratch assay, as previously described. After the incubation, ice-cold trichloroacetic acid (TCA) was added to the medium at 10% (V/V) final concentration. Plates were incubated for 1 h at 4 °C, and then supernatants were discarded. The plates were washed with water 5 times and then dried. To each well, 100 µl of 0.4% (w/V) sulforhodamine B (SRB)/1% acetic acid solution was added, followed by 10 min incubation at room temperature. The unbound dye was removed by washing 5 times with 1% acetic acid and the plate was dried again. Photos of the scratches were taken by Leica DM IL LED microscope (Leica Camera AG, Wetzlar, Germany), then the SRB was solubilized with 10 mM Tris base. Absorbance was read at 540 nm by Multiskan GO Microplate Spectrophotometer (ThermoFisher Scientific).

2.19. Silencing of MYPT1 in ex vivo human biopsies

NativeSkin testing kits contain biopsies prepared from surgical residue collected from adult donors with their informed consent. The biopsies exhibited normal skin barrier function and a mature *stratum corneum*. Thee biopsies had all cell types and skin appendages that are naturally present in human skin *in vivo*. The biopsies were embedded in a matrix and cultured with a maintenance medium. This set-up maintained normal tissue physiology and functions for up to seven days (Genoskin, Toulouse, France). MYPT1 was silenced by siRNA applying Lipofectamine 2000 transfection reagent topically and also by subcutaneous injection. The NT siRNA and siMYPT1-treated skin models were cultivated in an incubator (37 °C, 5% CO_2, 95% humidity) for up to 2 days by renewing the medium containing transfection mixture every day. Immunohistochemical sections of non-treated skin biopsies were collected at the day of wound production with a biopsy puncher and 6 days after healing. The sections were paraffin embedded and stained with antibodies raised against MYPT1 and transglutaminase-1 as described in Section 2.6. Skin biopsies were lysed in lysis buffer (10 mM HEPES, pH 7.9, 1.5 mM $MgCl_2$, 10 mM KCl, 1 mM EDTA, 10% (V/V) glycerol, 1% NP-40) and analyzed using a human phospho-MAPK Protein Profiler array (Research and Diagnostic Systems, Minneapolis, MN, USA) following the manufacturer's guidelines.

2.20. Statistical analysis

Normalized data were analyzed by *t*-test (for two groups) or analysis of variance (ANOVA, for > 2 groups). All normalized variables used in statistical analyses were found to be normally distributed. One and two-way ANOVAs were followed by Sidak's or Dunnett's procedure for multiple comparisons. Tests were conducted using GraphPad Prism for Windows. All data presented in this work represent mean ± SEM.

3. Results

3.1. Inhibition of PP1 slows down murine excisional wound healing

It has been shown previously that inhibition of ROCK promotes wound healing in various cell lines [28]. Therefore, we investigated the potential effect of one of the counter enzymes for ROCK phosphorylation, the PP1-type MP. Healing curves generated for control and ROCK-(10 μM H1152), and a PP1 inhibitor (1 μM TM) -treated mice demonstrated a decrease in relative wound size from day 0 to day 6 post-wounding compared to the original wound size. Up to day 2, wounds were the same size. From day 2 onwards, vehicle control and H1152-treated wounds exhibited a gradual decrease in wound size and a ~75% of healing was accomplished by day 6 (Fig. 1A and Fig. S1). In marked contrast, the wound decrease in those mice treated with TM was absent. Instead of healing, the wound area was significantly larger than the mean wound area of the controls (***$p < 0.001$, TM *vs.* control). This difference between control and TM-treated wounds was maintained until day 6. Interestingly, at 6 days post-wounding the difference between control and H1152-treated wounds was still non-significant. The wounds in control and H1152-treated groups healed at approximately the same rate (Fig. S1.). Newly formed granulation tissue in a full-thickness cutaneous wound is associated with re-epithelialization by keratinocytes. We evaluated the re-epithelialization of control, H1152- and TM-treated wounds with Masson-Goldner trichrome staining at day 6 after wounding (Fig. 1B). Re-epithelialization was almost completely inhibited in TM-treated mice. The original wound was covered completely at day 8 (picture not shown) in H1152 and control wounds. The results suggest that the inhibition of PP1 retards re-epithelialization by keratinocytes in the process of wound healing of an excision cutaneous injury.

3.2. Effect of PP1/ROCK inhibitor treatment on cell viability and phosphatase activity of human keratinocytes

To verify if the effects of PP1 and ROCK inhibitor on wound healing are related to their impact on cell viability, we conducted MTT and caspase assays on human HaCaT keratinocyte cells. Neither TM nor H1152 had a significant effect on cell viability as revealed by MTT assay (Fig. 2A). TM-treated HaCaT cells showed a slightly elevated caspase-3 activity (Fig. 2B); however, in this period, no change in the viability of the cells was detected (Fig. 2A). We also confirmed the inhibitory effect of TM on phosphatase activity of PP1 enzymes. HaCaT cells were treated with 10 μM H1152 or 1 μM TM for 1 h and the phosphatase activity of the lysates were measured using a ^{32}P-MLC20 substrate (Fig. 2C). ROCK inhibition by H1152 had no effect on phosphatase activity compared to the non-treated control samples. TM treatment significantly reduced the phosphatase activity (by 48%) in lysates of HaCaT cells.

To assess our data on primary keratinocytes, normal human keratinocytes (NHEK) from two donors were cultured and their differentiation was verified by the observation of their morphology (data not shown) or by the analysis of the protein expression level of Tgase-1, a differentiation marker (Fig. S6). Tautomycin treatment caused a decrease in the viability of non-differentiated (Fig. S2A) and differentiated (Fig. S2B) NHEK cells assessed by MTT assay. However, H1152 treatment showed no effect on cell viability (Fig. S2A, B). We detected no effect of TM and H1152 on the caspase activity of non-differentiated NHEK cells (Fig. S2C). In contrast, H1152 significantly decreased and TM increased caspase-3 activity in differentiated NHEK cells (Fig. S2D). Parallel with our findings on HaCat cells, TM treatment significantly reduced protein phosphatase activity in non-differentiated (Fig. S2E) and differentiated (Fig. S2F) NHEK cells, by 60–70% compared to control.

3.3. PP1 inhibition attenuates the proliferation and migration of human keratinocytes

We demonstrated that inhibition of PP1 had a dramatic effect between day 2 and 6 after wounding. Since this is the period characterized by extensive proliferation and migration of keratinocytes, we determined if PP1 activity was required for these processes in human keratinocytes. HaCaT cells were grown in monolayers and scratched uniformly followed by treatment with PP1 or ROCK inhibitors (Fig. 3A). All the experiments were compared to the serum-starved negative control samples. Control cells (cells with normal medium) closed the scratch by 33% compared to the negative control (Fig. 3B). Treatment with the ROCK inhibitor, H1152, accelerated the scratch closure by 19% compared to control cells ($p < 0.01$). However, no significant difference was measured between the free area of scratch of the negative control and TM-treated cells. Furthermore, TM treated cells has a significantly larger free area than control and H1152 treated cell, suggesting that TM inhibited wound healing (Fig. 3B). Proliferation of HaCaT cells was determined by an SRB assay and the rate of proliferation was compared to control cells upon H1152 and TM-treatment. PP1 inhibition with TM decreased the proliferation rate significantly (by 24%) compared to control cells, however, H1152 had no effect on the proliferation of HaCaT cells (Fig. 3C). Mitomycin was applied to inhibit cell division to verify if PP1 inhibition effects proliferation (Fig. S3B), migration (Fig. S3A) or both. The course of wound healing and the relative proliferation were hampered in response to mitomycin treatment (Fig. S3A, B). These results suggest that cell proliferation is crucial in scratch closure of HaCat monolayer and merely cell migration is not sufficient for the effective completion of the process. Addition of TM delayed scratch closure (Fig. S3A) and caused decreased proliferation rate (Fig. S3B) both in case of vehicle and mitomycin pretreated HaCaT cells.

Keratinocytes have a mesenchymal mode of migration, which

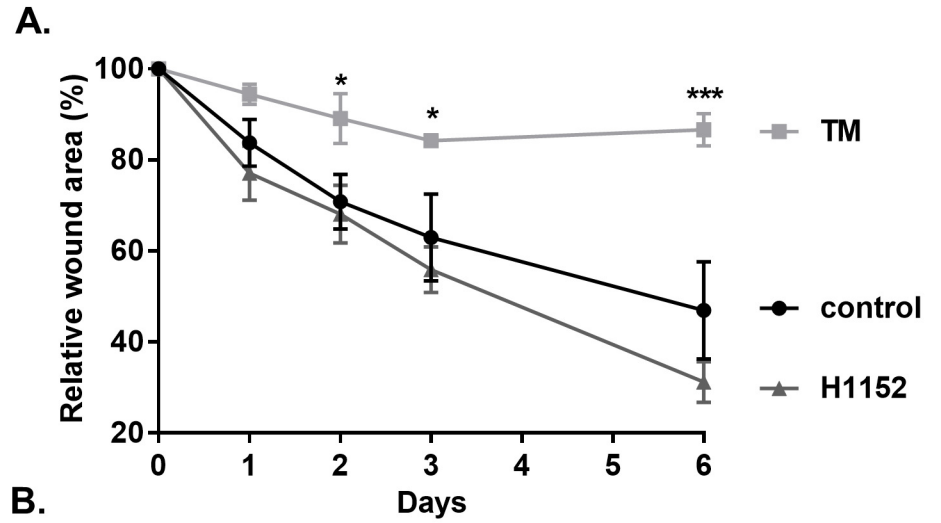
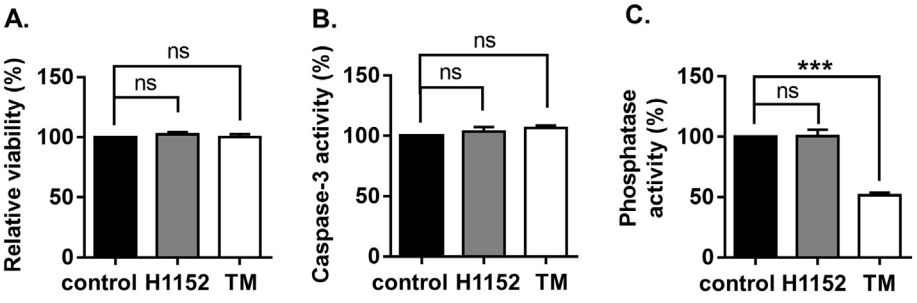


Fig. 1. Re-epithelialization was significantly delayed upon inhibition of PP1 in murine excisional wound healing. (A) *In vivo* wound closure was analyzed by full thickness wounds in the dorsal skin of control, 1 μM tautomycin (TM), and 10 μM H1152-treated mice. The relative size of the remaining wound, as a percentage of the initial wound area, is shown (n = 6, two-way ANOVA and Dunnett's *post hoc* test, control *vs.* TM, *p < 0.5, ***p < 0.001). See also photo images in Fig. S1. (B) Histology of re-epithelialization of healing wound tissue by Masson-Goldner trichrome staining of the dorsal skin at day 6 after wounding. Nuclei are dark brown, cytoplasm and muscles are brick red and connective tissue, and acidic mucus substances are represented with blue. Scale bar = 300 μm.



***p < 0.0001, and ns = non-significant.

Fig. 2. Effect of PP1 and ROCK inhibitors on cell survival and protein phosphatase activity in HaCaT cells. (A–B) HaCaT cells were treated with 10 μM H1152 or 1 μM tautomycin (TM) for 12 h after overnight serum starvation in serum-free DMEM. The effects of these inhibitors on cell viability was assessed by MTT assay (A) and caspase-3 activity measurement (B). (C) HaCaT cells were starved overnight, then treated for 1 h with 10 μM H1152 or 1 μM TM. Cell lysates were assayed for phosphatase activity in the presence of 1 μM ^{32}P-MLC20 substrate. Data represents n = 6–9 independent experiments. One-way ANOVA and Sidak's *post hoc* test,

requires protrusion formation, adhesion to the surrounding extracellular matrix, and cell contraction. As PP1 inhibition almost completely blocked the wound closure, we hypothesized that PPI inhibition will cause a reduced migration speed. To test this hypothesis experimentally, we assessed wound closure assay monitored by JuLi time-lapse microscopy and followed the kinetics of cell migration (Fig. 3D). We detected a higher migration rate compared to control when the cells were treated with H1152. However, the rate of migration of TM-treated cells was lower (Fig. 3D). To confirm these observations, electric cell impedance sensing (ECIS) measurements were applied on H1152- and TM-treated HaCaT cells. The time needed for the actual restoration of the monolayer was quantified by measuring the impedance of a HaCaT monolayer that was grown on electrodes (Fig. 3E). Electric impedance increased in time by the migration of cells. To reach constant impedance, control, H1152-, and TM-treated human keratinocytes required 2.1, 1.6, and 2.7 h, respectively. These data suggest that ROCK inhibition accelerates, while PP1 inhibition prolongs normal wound closure (Fig. 3E). These results suggest that ROCK and PP1 oppositely regulate cell migration: ROCK inhibits but PP1 stimulates this process.

3.4. Gene silencing of MYPT1 in HaCaT cells decreases the proliferation rate and delays scratch closure

To verify our data on PP1 inhibition and to determine the specific role of MP in the regulation of wound healing, gene silencing of the MP regulatory subunit (MYPT1) in HaCaT cells was performed. The efficiency of the silencing was verified by Western blot using anti-MYPT1$^{1-296}$ antibody and using tubulin as a loading control (Fig. S4A). The expression level of MYPT1 decreased in MYPT1-silenced HaCaT cells (siMYPT) compared to NT siRNA keratinocytes. The silencing of MYPT1 co-translationally has been shown to cause a decrease in the PP1c expression [29]. Accordingly, MYPT1-silenced HaCaT cells presented a significant decrease in the protein level of the PP1 catalytic subunit (Fig. S4A). We detected a slight but significant decrease (12%) in the viability of HaCaT cells in response to MYPT1 silencing by MTT assay (Fig. 4A). The caspase-3 activity did not change significantly in the MYPT1-silenced cells (Fig. 4B). Moreover, expression of cleaved PARP (cPARP), an early indicator of apoptosis, remained unaltered in the MYPT1-silenced HaCaT cells compared to those which were transfected with non-target siRNA (Fig. S4B)·We assessed the effect of MYPT1 silencing on the protein phosphatase activity of HaCaT cells. Cells were transfected with NT siRNA or MYPT1 siRNA, and 48 h later

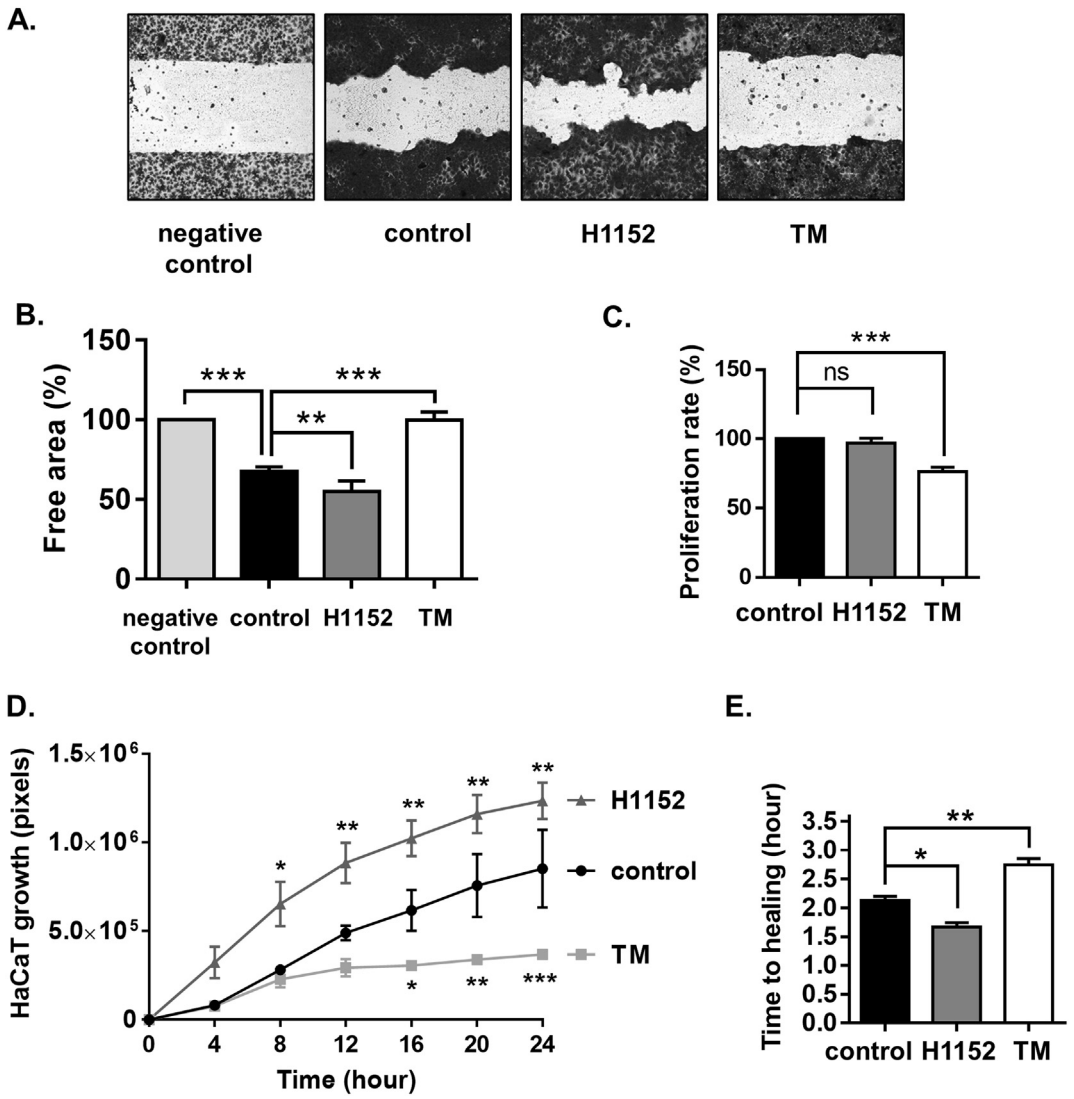


Fig. 3. Effect of PP1 and ROCK inhibitors on cell migration and proliferation of HaCaT cells. (A) HaCaT monolayers in 96-well plates were uniformly scratched, inhibitors were applied for 24 h and then the cells were stained with sulforhodamine B (SRB) and light microscope images were taken. Cells cultured in the absence of serum were applied as negative control. (B) Free areas were measured by ImageJ, a bar chart was created and statistical analysis was conducted with GraphPad Prism 6 program. (C) The proliferation rate of HaCaT cells was measured by quantification of SRB staining and expressed in %. (D) Live-cell imaging of the wound closure of HaCaT monolayers using bright field microscopy by JuLI Real-Time Cell History Recorder. HaCaT monolayers were scratched and then cultured in the presence of none, 1 μM TM, or 10 μM H1152 for 24 h. Time-lapsed images were taken every 4 h and the kinetics of cell growth was plotted. (E) Wound healing of control, H1152, and TM-treated HaCaT cells monitored by ECIS. Monolayer of HaCaT cells was burnt out on the surface of the electrodes by elevated field pulse applied twice for 30 s. H1152 or TM were applied in a concentration of 10 μM or 1 μM, respectively. Migration of the cells to the electrodes from the surrounding areas was followed until no further change in resistance was observed (complete healing) and plotted in time (hour). Data represents n = 3, (B, C and E) one-way ANOVA and Sidak's *post hoc* test. (D) Two-way ANOVA and Dunnett's *post hoc* test, ns = non-significant, *p < 0.05, **p < 0.01, ***p < 0.001.

phosphatase activity was measured using ^{32}P-MLC20 as a substrate. The siMYPT1 transfection decreased phosphatase activity in HaCaT cells by 49% compared NT siRNA transfected cells (Fig. 4C). NT siRNA and siMYPT1 transfected cells were grown to confluency and then scratched. Cells were grown for another 24 h then keratinocytes were stained with SRB and images were taken by a light microscope (Fig. 4D). The free area of the scratch after siMYPT1 transfection was three-times larger than that cells transfected with NT siRNA (Fig. 4D). In response to MYPT1 silencing, the proliferation of keratinocytes moderately decreased (Fig. 4E). Growth of cells after transfection with siRNA for MYPT1 (Fig. 4F) decreased significantly compared to cells transfected with NT siRNA. We also confirmed these data by quantifying the time to reach full closure of the scratches by ECIS (Fig. 4G) and found that silencing of MYPT1 resulted in increased time to wound closure (~1.5-times longer) compared to NT siRNA treated cells. Based on these results, we can conclude that MP facilitates keratinocyte migration.

3.5. Inhibition of PP1 and silencing of MYPT1 disrupts the barrier function of HaCaT cells

The role of ROCK in the formation of cell-cell attachments as well as the formation and maintenance of barrier integrity have been described in corneal epithelial cells [30], but the role of MP in cell-cell adhesions between keratinocytes remains unclear. Cell-cell adhesion promotes sustained migration, as cells pull neighboring cells into the wound during wound healing, accelerating the process [31]. We aimed to uncover the effect of PP1 inhibition and siMYPT1 on the barrier function of keratinocytes. HaCaT cells were transfected with NT- or MYPT1-siRNAs (Fig. 5A), or were treated with 10 μM H1152 or 1 μM TM (Fig.

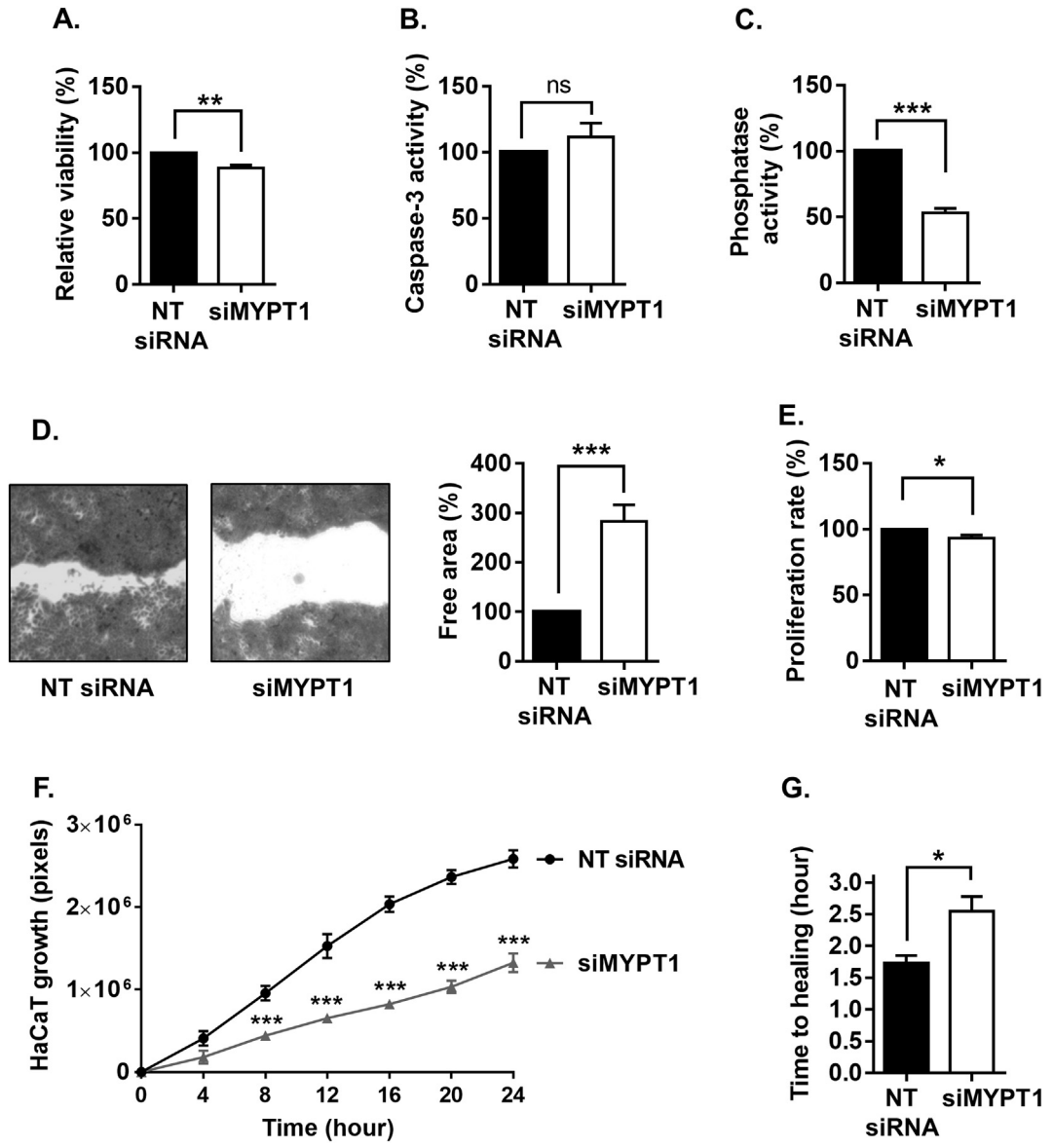


Fig. 4. Myosin phosphatase promotes proliferation and wound healing. (A-G) HaCaT cells were transfected with non-targeting control dsRNA (NT-siRNA) or with siMYPT1-dsRNA (siMYPT1). The cell viability was assayed with MTT assay (A) and caspase-3 assay (B). (C) Cell lysates were assayed for protein phosphatase activity with ^{32}P-MLC20 substrate. (D) HaCaT monolayers were scratched evenly, then culture for 24 h and investigated by light microscope after SRB staining. (E) Cell proliferation was quantified by photometric measurement of SRB product directly proportional to cell proliferation. (F) HaCaT monolayers were scratched and the wound closure (in pixel) was followed by JuLI live cell imaging. (G) Wound healing of NT-siRNA control and siMYPT1 HaCaT cells were determined by ECIS. Circular wounds were inflicted on the monolayers by elevated field pulse applied twice for 30 s, then regeneration of the cell layer was monitored up to full closure, and expressed as time to healing. n = 3, (F) two-way ANOVA and Sidak's *post hoc* test, other panels: *t*-test, ns = non-significant, *p < 0.05, **p < 0.01, *** p < 0.001. MYPT1 and PP1 expression levels verified by Western blotting are shown in Fig. S4.

S5A) followed by immunofluorescent staining to visualize F-actin (red), ZO-1 and β-catenin (green), and cell nuclei with DAPI staining (blue). No differences were observed between migrating cells parallel to the wounding edge and cells far from the wound (data not shown). In control and NT-siRNA_transfected cells, ZO-1 staining was uninterrupted at cell-cell contacts. The abundance and expression of ZO-1 at junctions was dramatically increased in confluent cells upon MYPT1 silencing demonstrating enhanced cell-cell junctions (bottom panel Fig. 5A). Since siMYPT transfection did not influence the protein expression of ZO-1 (Fig. S5C), the profound staining of ZO-1 at tight junctions (Fig. S5A) is the result of the relocalization of the protein. The presence of TM enhanced slightly the formation of actin cytoskeleton, however, H1152 prevented cell-cell adhesion formation, and triggered paracellular gap formation (Fig. S5A). To prove the effect of MYPT1-silencing and PP1 inhibition on the barrier function, HaCaT cells were allow to grow on ECIS electrodes and circular wounds were burnt. Impedance was measured every 10 min for 4 h and for another 7 h after silencing with NT- or MYPT1-siRNA (Fig. 5B) in the presence or absence of Ca^{2+} or after inhibitor treatment (Fig. S5B). The addition of Ca^{2+} by itself resulted in a significant increase in impedance due to the enhancement of cell-cell contacts. Transfection with siMYPT1-induced increased electric impedance (Fig. 5B) which was associated with the appearance of cortical F-actin and intensive ZO-1 staining (Fig. 5A). The net values in the resistance after TM treatment showed a slight change comparing to the values of control cells. Interestingly, the inhibition of ROCK by H1152 resulted in a moderate decline in impedance (Fig. S5B). Taken together, these data suggest that MP (i.e. PP1 and MYPT1) plays a role in the formation of adhesion junctions and

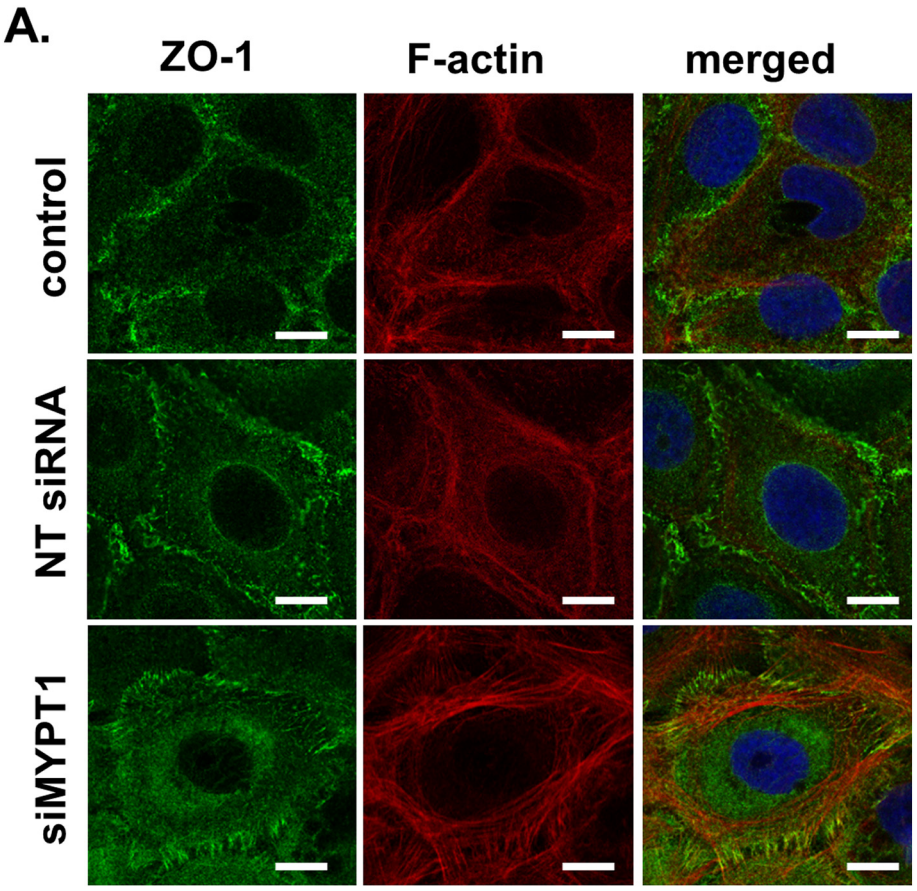
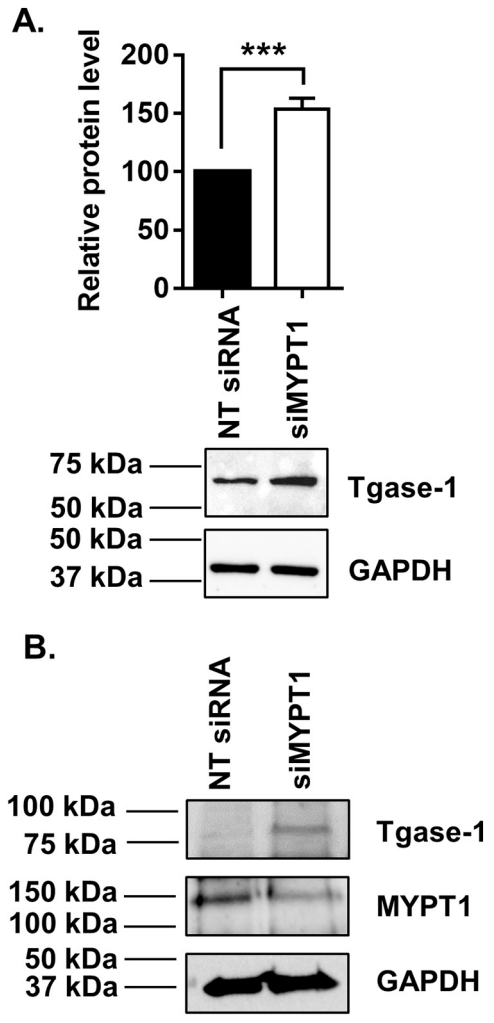


Fig. 5. Silencing of MYPT1 disrupt barrier function of HaCaT cells. (A) Immunofluorescent staining was applied on HaCaT cells transfected with non-targeting control siRNA (NT-siRNA) or with siMYPT1 using zonula occludens-1 (ZO-1) antibody (green) and fluorescent-labeled phalloidin for the visualization of F-actin (red). For nuclear staining DAPI was used. Merged images show co-localization of proteins of interest by orange. Fig. 5A shows representative images. Scale bar = 10 µm. (B). Undifferentiated or Ca^{2+}-differentiated HaCaT cells were transfected with NT siRNA or with siMYPT1. Electric impedance was quantified in real time by the ECIS label-free impedance measurement. Bars chart summarize the results after 48 h silencing. Statistical analysis was conducted by two-way ANOVA and *post hoc* Tukey's test, *p < 0,05; **p < 0.01.

maintenance of the physiological barrier function of keratinocytes.

3.6. Gene silencing of MYPT1 increases transglutaminase-1 (Tgase-1) expression in keratinocytes and in human skin

To understand the molecular mechanism regulated by MP in the process of wound healing, we examined the database of genes regulated by PP1 silencing in HaCaT cells [27] and selected six genes, including S100 A8, vanilloid receptor 1, low density lipoprotein receptor (LDLR), transglutaminase-1 (Tgase-1), and keratins 1 and 10, related to wound healing according to the available literature. To confirm that the transcriptional changes are reflected in altered protein expression,



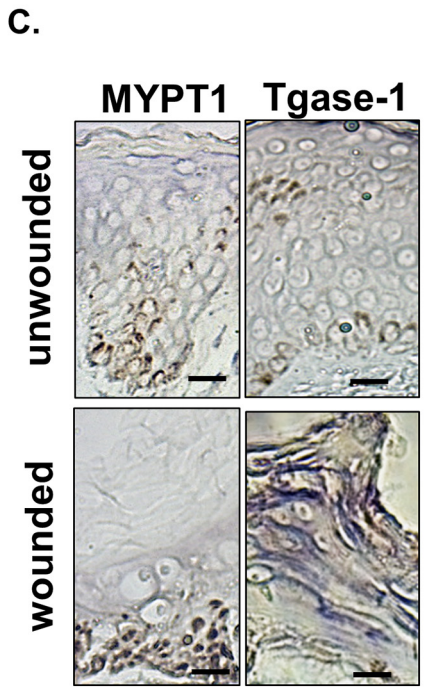


Fig. 6. Effect of MYPT1 silencing on transglutaminase-1 expression in HaCaT cells and in native human skin. Human keratinocytes (A) and *ex vivo* human native skin samples (B) were transfected with either non-targeting control RNA (NT-siRNA) or siMYPT1-RNA (siMYPT1). Western blot analysis was performed on the cell lysates using anti-transglutaminase-1 (anti-Tgase-1) or anti-MYPT1 antibodies. GAPDH was assessed as a loading control. Tgase-1 protein expressions normalized to the respective GAPDH signal were illustrated in a bar chart. (n = 3, student *t*-test, ***p < 0.001). (C) Immunohistochemistry of normal and wounded native human skin (6 day after excisional wounding) as revealed by anti-Tgase-1 and anti-MYPT1 antibodies. Scale bar = 50 μm.

human keratinocytes were transfected with NT-siRNA or siMYPT1-RNA and the cell lysates were probed with the antibodies against proteins listed above. Only Tgase-1 showed a significant increase in protein expression in response to gene silencing of MYPT1 (Fig. 6A). To test adequate responses to MYPT1-silencing in real human skin, we used native skin biopsies of human origin, which are prepared from surgical skin residue donated by adult donors. This is a standardized *ex vivo* model of human skin, which maintains physiological skin biology, skin barrier function, and metabolism during 7 days of culturing in tissue culture inserts. Indeed, the MYPT1 gene was successfully silenced in *ex vivo* skin samples as judged by Western blotting (Fig. 6B). We also verified an increase in Tgase-1 protein expression in MYPT1-silenced samples compared to the NT control (Fig. 6B). A circular wound was produced by a biopsy punch on *ex vivo* native human skin and wound healing was observed over the course of 7 days. Immunohistochemical analysis of the wound area with antibodies against MYPT1 and Tgase-1 was performed. Tgase-1 was present in the epidermis of skin, predominantly in the upper spinous and granular layers. MYPT1 showed an obvious staining at the dermal-epidermal junction in uninjured skin (Fig. 6C). In response to injury, nearly all cell layers, except the basal cell layer, stained strongly for Tgase-1, proving that physiological keratinization of the epidermis was enhanced. Surprisingly, MYPT1 staining was intensified at the *stratum basale* but in no other layers of the epidermis, suggesting its role in the migration of keratinocytes during re-epithelialization (Fig. 6C lower panels).

3.7. MYPT1 silencing regulates wound healing through the Akt signaling pathway

Mitogen-activated protein kinase (MAPK) signaling pathway is thought to play a role in the regulation of Tgase-1 gene and protein expression [32], as well as in wound healing. The effects of MYPT1 silencing on the phosphorylation level of 22 enzymes and 2 proteins related to MAPK signaling was assessed in human wounded skin using a human phospho-MAPK protein profiler array. Phosphorylation levels were normalized in each case (n = 3) to the NT siRNA-transfected human skin tissues (Fig. 7A), and the changes were compared to NT-siRNA control values. Based on these results, the elements of the Akt signaling pathway, including Akt1 Ser473, GSK-3β Ser9, as well as p70 S6 kinase Thr421/Ser424, decreased significantly, while phosphorylation of hsp27 Ser78/Ser82 increased. Regarding the MAPK pathway, the phosphorylation level of neither ERK nor p38 kinase changed but that of JNK decreased significantly on Thr183/Tyr185 upon MYPT1-silencing. The phosphorylation level of the rest of the proteins did not change significantly. Expression of Akt1 (Fig. S7B) and Akt2 (Fig. S7D) remained unaltered in MYPT1-silenced HaCaT cells compared to non-target siRNA transfected cells. However, the phosphorylation level of immunoprecipitated Akt1 was decreased in MYPT1-silenced HaCaT cells compared to those which were transfected with non-target siRNA (Fig. S4C). Phosphorylation level of Akt2 on Ser474 showed no significant change upon MYPT1 silencing in HaCaT cells (Fig. S4E). These results are well in line with our findings in MYPT1 silenced human skin tissue, where a decrease of Akt1 and a non-significant change of Akt2 phosphorylation were detected by MAPK array (Fig. 7A). These data suggest that normal homeostasis of the skin and the actions of

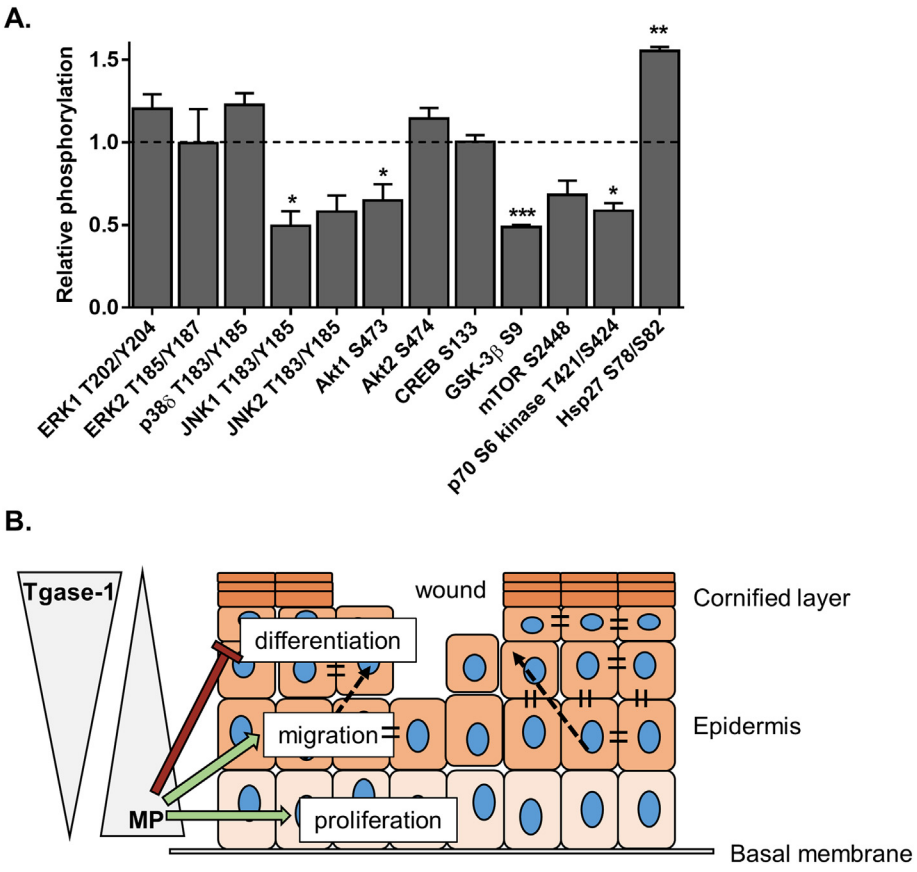


Fig. 7. Silencing of MYPT1 influences the phosphorylation of the elements of MAPK signaling pathway in human skin. (A) Native human skin was successfully transfected with non-targeting control RNA (NT-siRNA) and MYPT1-siRNA (siMYPT1) and the skin tissue lysates were applied on human phospho-MAPK Proteome Profiler array. Bar chart represents phosphorylation levels of various proteins relative to their NT siRNA pair. *$p < 0.05$; **$p < 0.01$; ***$p < 0.001$; $n = 2$, student *t*-test. (B) Complex functions of myosin phosphatase (MP) in wound healing.

keratinocytes in wound healing are regulated by the Akt and JNK pathways in an MP mediated manner.

4. Discussion

Epidermal wound healing is a complex process mediated by various factors activating parallel and sequential downstream signaling pathways [33]. Our study of the specific functions of MP in skin homeostasis and wound healing resulted in four major findings. First, we found that MP induces the migration of keratinocytes. Second, we showed that MP and ROCK regulate epidermal barrier function. Third, we demonstrated that MP was expressed differentially in various layers of human skin, and MP downregulates the expression of Tgase-1 in the proliferative and migratory layer of skin. Finally, we proposed that MP contributes to the mediation of wound healing by regulating the Akt signaling pathway and that it acts on the phosphorylation of Hsp27.

Previous studies found that the ROCK inhibitors, Y27632 [34], H1152 [30], fasudil [35] and ripasudil [36], promote corneal epithelial wound healing. Although ROCK inhibitors underwent clinical trials and are widely used [36], the effectiveness of pharmacons has been overestimated and the major target of their application is in the field of ophthalmology. To provide additional insight into the suitability of ROCK modulation in epidermal wound healing, we assessed potential therapeutic benefits of targeting MP, which serves as a counter enzyme for ROCK-phosphorylated proteins in many cases. Our excisional wound healing assay data proved that the inhibition of PP1 enzymes (such as MP) obstructed epidermal wound healing and that ROCK inhibition slightly accelerated wound closure (Fig. 1A). Since proliferation and migration are the hallmarks of healing 2 to 6 days after wounding, these data suggest that PP1 enzymes, but not ROCK play a crucial role in the process of re-epithelialization.

An increasing number of studies have supported the importance of ROCK in regulating the balance between proliferation and differentiation, however, their results seem to be contradictory and cell type dependent. Blocking ROCK function results in a decrease in the terminal differentiation of keratinocytes and an increase in their proliferation [37]. Similarly, the inactivation of the RhoA/ROCK signaling pathway by the pharmacological inhibitor, fasudil, reduces cell motility and destroys the cytoskeletal arrangement of U2OS osteosarcoma cells *in vitro* [35]. Moreover, the ROCK inhibitor, Y-27632, facilitates the proliferation and migration of human periodontal ligament stem cells [38], while H1152 exhibits a stimulatory effect on corneal endothelial cell migration and proliferation *in vitro*, promoting injury healing. In contrast, sometimes ROCK inhibition did not have any effect on cell migration [39], whereas in other studies ROCK inhibition even stimulated this process [40]. Based on our results, we suggest that ROCK inhibits cell migration but does not influence the proliferation of keratinocytes, because the inhibition of ROCK resulted in a faster scratch closure compared to its control but was not followed by increased proliferation (Fig. 3). This conclusion is also supported by a previous finding that Y-27632 has a minimal effect on basal cell proliferation in corneal epithelial cells when measured by BrdU-staining [30]. In contrast, the inhibition of PP1 completely blocked the wound and scratch closure (Figs. 1 and 3) and this inhibitory effect on wound healing is directly related to the significant decrease in both the proliferation and migration of HaCaT cells (Fig. 3 and Fig. S3). The wound healing of a circular excision in the dorsal skin was significantly impaired by the inhibition of PP1 in mice, and the histology indicated that the formation of granulation tissue and re-epithelialization were also defective (Fig. 1). Neither ROCK nor PP1 inhibition by H1152 or TM, respectively, affected cell viability or apoptosis for the period of the experiments (Fig. 2), and we believe that the defect in wound closure is the result of other mechanisms.

Gene silencing of the regulatory subunit of MP was invaluable in clarifying the specific role of MP among the other PP1 enzymes potentially playing a role in maintaining skin homeostasis and wound

healing. Surprisingly, MYPT1 phosphorylation at the inhibitory phosphorylation site has been investigated only as the target of ROCK action to verify the efficacy of ROCK inhibitors in wound healing [30, 37]. The fact that MYPT1 gene silencing exhibits an even more profound effect on cell viability, proliferation, and cell migration compared to PP1 inhibition suggests a key regulatory role of MP in skin homeostasis (Fig. 4). The crucial role of MYPT1 in cell viability is supported by several lines of evidence: (1) although PP1 inhibition has no effect, siMYPT-silencing resulted in a 12% reduction in relative viability; (2) the proliferation rate of HaCaT cells is significantly reduced by the silencing of MYPT1 (Fig. 4E); (3) the most dramatic difference in wound healing is between generic PP1-inhibited and siMYPT1-silenced cells, since the latter showed almost complete inhibition of wound closure (Figs. 3A and 4D).

Proper wound healing and homeostasis of the skin requires not only the differentiation and proliferation of cells but also the development of barrier function resulting from the physiological formation of cell-cell connections. Previous studies using ECIS found that ROCK activity was required for the maintenance of barrier properties in HCEC cells [8]. We also confirmed that the inhibition of ROCK in HaCaT cells resulted in a lower impedance (Fig. S5) accompanied by a more defined β-catenin staining and by the formation of paracellular gaps. On the other hand, silencing of MYPT1 resulted in an augmented cell-cell connection of keratinocytes and ZO-1 accumulation at the cell junctions and the formation of F-actin network, which was supported by the increased impedance values. These results suggest that MP along with ROCK are required for the assembly and maintenance of the cell-cell connections of keratinocytes, presumably *via* their effects on the F-actin organization during junction formation.

ROCK and MP may also be involved in the differentiation of epidermal keratinocytes. In human keratinocytes, ROCK inhibited cell cycle progression and led to increased expression of numerous genes associated with keratinocyte differentiation [37]. On the other hand, we found numerous proteins regulated upon PP1 silencing in HaCaT cells [27]. In the course of wound healing, the epidermal keratinocytes of *stratum spinosum* differentiate producing numerous proteins, such as involucrin and loricrin, which are cross-linked together by the action of Tgase. Tgase-1, a major enzyme that determines total Tgase activity in the epidermis, mediates post-translational modification of proteins by catalyzing ε-(γ-glutamyl)-lysine isopeptide bonds. Tgase is also implicated in differentiation [41]. We hypothesize that MP acts on the phases of wound healing differentially. This hypothesis is supported by the following results: (1) the silencing of MP decreased migration of keratinocytes, (2) MP is expressed only in stratum basale, the layer of proliferating and migrating cells of human skin, (3) MP was not expressed in the upper spinous and granular layers beneath the stratum corneum, where Tgase-1 activity was expected to be high [42]. This explains the conflicting effect of MP in wound healing: MP activates cell migration but hampers gene expression of Tgase-1, a key enzyme in keratinocyte differentiation, which is equally necessary for a normal wound closure.

MAPKs are central players in regulating keratinocyte proliferation and differentiation and have been suggested to orchestrate the process of wound healing [43]. Human skin exhibited a decrease in the phosphorylation level of several MAPK signaling proteins upon MYPT1 silencing (Fig. 7). The silencing of MYPT1 downregulated the Akt signaling pathway, presumably through the downregulation of MP. Akt is the downstream effector of PI3K and Akt activation converges on the phosphorylation of its Thr308 and Ser473 residues. Akt activates the TOR/p70 S6 kinase axis regulating protein synthesis, as well as GSK-3 acting on cell cycle [44]. Upregulation of the Akt/mTOR signaling pathway results in increased epithelial cell proliferation and migration, thereby accelerating the wound healing process. [44]. Moreover, increased phosphorylation of Akt led to an accelerated wound healing [45]. Although three isoforms of Akt (Akt1–Akt3) are encoded in mammalian cells but in the skin the activity of Akt1 and Akt2 was found to be dominant. Akt activity increased during keratinocyte differentiation and it was related to the specific activation of Akt1 and Akt2. However, only Akt1 deletion caused abnormal epidermis with increase parabasal regions and pronounced and disorganized cornified layers in organotypic skin cultures [46]. These observations support our results showing a decrease in the proliferation of keratinocytes upon MYPT1 silencing which caused a significant decrease in the phosphorylation of Akt1 at Ser473 and the downstream effectors of this pathway in human *ex vivo* biopsy (Fig. S7A) as well as in HaCaT cells (S7C).

The other potential target of MP action in epidermal wound healing and homeostasis is Hsp27, which was hyperphosphorylated upon MYPT1-silencing. Hsp27 is suggested to have a phosphorylation-activated homeostatic function at the actin cytoskeleton level [47, 48]. In addition, Hsp27 is also involved in the keratinocyte terminal differentiation and may have a role in the reorganization of the cytoskeleton and/or formation of the cornified envelope [48, 49]. However, Hsp27 had no effect on proliferation in corneal epithelial wound healing [50]. The activation of Hsp27 might explain the augmented formation of the cortical actin network and might also be related to MP-mediated differentiation through an unknown mechanism different from Akt signaling.

Although we identified Akt signaling pathway and its physiological targets to be regulated by MP, the detailed mechanism has yet to be determined in keratinocytes. We hypothesize that ROCK/MP mediates the phosphorylation of one of the upstream elements of the Akt signaling pathway. One possible explanation could be that MP regulates, indirectly, Akt activity by dephosphorylating and deactivating protein phosphatases such as protein phosphatase 2A (PP2A) and the PH domain leucine-rich repeat protein phosphatase (PHLPP) that play a role in the dephosphorylation and inhibition of Akt [51].

In summary, MP positively regulates wound healing *via* modulating cell behaviors including proliferation, cell migration, and cell-cell attachments (Fig. 7B). The successful silencing of MYPT1 in *ex vivo* human skin biopsy helped to identify the role of MP in the physiological wound healing and contributed to our understanding of the role and mechanism of MP action. The potential activation of MP might help to develop new strategies to treat diseases, which contribute significantly to the morbidity and even mortality of many patients and cause costly clinical problems such as diabetic keratopathy, fibrosis, corneal diseases or chronic ulcers.

Transparency document

The Transparency document associated with this article can be found, in online version.

Acknowledgements

The authors are indebted to Dr. László Virág (UD, Department of Medical Chemistry) for his support in the animal studies, to Dr. Csaba Hegedűs for his assistance with the scratch assay with Tecan Freedom EVO 150 liquid handling machine. We thank Ágnes Németh, Andrea Docsa, and Ágota Kelemenné Szántó for their technical assistance and Erzsébet Herbály Mihályné for her excellence in performing histological stainings. This work was supported by grants from the National Research, Development and Innovation Office (FK 125043, K108308, EFOP-3.6.2-16-2017-00006), and by the University of Debrecen (RH/751/2015). We are grateful to Dr. Karen Uray (UD, Department of Medical Chemistry) for editing the manuscript.

Conflict of interest

The authors have declared that no competing interests exist.

Contributions

BL designed the study and DH completed Figs. 1, 2 and 3. JI performed JULI kinetic measurements. AK and ZK conducted protein phosphatase activity measurements, A.S. performed the ECIS studies, EM performed immunofluorescent analysis and Fig. S3, IT completed statistical analysis and performed confocal microscopy. ASz isolated and provided NHEK cells. RB helped in scratch assays, DD performed animal experiments. BL, DH, and FE wrote the paper. All authors reviewed the manuscript.

Appendix A. Supplementary data

Supplementary data to this article can be found online at https://doi.org/10.1016/j.bbadis.2018.07.013.

References

[1] P. Martin, Wound healing–aiming for perfect skin regeneration, Science 276 (1997) 75–81.
[2] J.M. Reinke, H. Sorg, Wound repair and regeneration, Eur. Surg. Res. 49 (2012) 35–43.
[3] L.G. Hudson, R. Zeineldin, M. Silberberg, M.S. Stack, Activated epidermal growth factor receptor in ovarian cancer, Cancer Treat. Res. 149 (2009) 203–226.
[4] A.J. Singer, R.A. Clark, Cutaneous wound healing, N. Engl. J. Med. 341 (1999) 738–746.
[5] G.C. Gurtner, S. Werner, Y. Barrandon, M.T. Longaker, Wound repair and regeneration, Nature 453 (2008) 314–321.
[6] K. Muller-Decker, W. Hirschner, F. Marks, G. Furstenberger, The effects of cyclooxygenase isozyme inhibition on incisional wound healing in mouse skin, J. Invest. Dermatol. 119 (2002) 1189–1195.
[7] S. Sarkar, T. Egelhoff, H. Baskaran, Insights into the roles of non-muscle myosin Iia in human keratinocyte migration, Cell. Mol. Bioeng. 2 (2009) 486–494.
[8] V. Betapudi, V. Rai, J.R. Beach, T. Egelhoff, Novel regulation and dynamics of myosin II activation during epidermal wound responses, Exp. Cell Res. 316 (2010) 980–991.
[9] P. Martin, S.J. Leibovich, Inflammatory cells during wound repair: the good, the bad and the ugly, Trends Cell Biol. 15 (2005) 599–607.
[10] S. Werner, T. Krieg, H. Smola, Keratinocyte-fibroblast interactions in wound healing, J. Invest. Dermatol. 127 (2007) 998–1008.
[11] L. Koivisto, K. Alavian, L. Hakkinen, S. Pelech, C.A. McCulloch, H. Larjava, Glycogen synthase kinase-3 regulates formation of long lamellipodia in human keratinocytes, J. Cell Sci. 116 (2003) 3749–3760.
[12] A.I. Chernyavsky, J. Arredondo, J. Wess, E. Karlsson, S.A. Grando, Novel signaling pathways mediating reciprocal control of keratinocyte migration and wound epithelialization through M3 and M4 muscarinic receptors, J. Cell Biol. 166 (2004) 261–272.
[13] C.E. Pullar, J. Chen, R.R. Isseroff, PP2A activation by beta2-adrenergic receptor agonists: novel regulatory mechanism of keratinocyte migration, J. Biol. Chem. 278 (2003) 22555–22562.
[14] S.C. Anderson, C. Stone, L. Tkach, N. Sundarraj, Rho and Rho-kinase (ROCK) signaling in adherens and gap junction assembly in corneal epithelium, Invest. Ophthalmol. Vis. Sci. 43 (2002) 978–986.
[15] N. Lakshman, A. Kim, K.J. Bayless, G.E. Davis, W.M. Petroll, Rho plays a central role in regulating local cell-matrix mechanical interactions in 3D culture, Cell Motil. Cytoskeleton 64 (2007) 434–445.
[16] T. Wang, W. Kang, L. Du, S. Ge, Rho-kinase inhibitor Y-27632 facilitates the proliferation, migration and pluripotency of human periodontal ligament stem cells, J. Cell. Mol. Med. 21 (11) (2017) 3100–3112.
[17] B. Lontay, A. Kiss, P. Gergely, D.J. Hartshorne, F. Erdodi, Okadaic acid induces phosphorylation and translocation of myosin phosphatase target subunit 1 influencing myosin phosphorylation, stress fiber assembly and cell migration in HepG2 cells, Cell. Signal. 17 (2005) 1265–1275.
[18] O. Ruzsnavszky, B. Dienes, T. Olah, J. Vincze, T. Gall, E. Balogh, G. Nagy, R. Batori, B. Lontay, F. Erdodi, L. Csernoch, Differential effects of phosphatase inhibitors on the calcium homeostasis and migration of HaCaT keratinocytes, PLoS One 8 (2013) e61507.
[19] M. Parizi, E.W. Howard, J.J. Tomasek, Regulation of LPA-promoted myofibroblast contraction: role of Rho, myosin light chain kinase, and myosin light chain phosphatase, Exp. Cell Res. 254 (2000) 210–220.
[20] G. Loirand, P. Guerin, P. Pacaud, Rho kinases in cardiovascular physiology and pathophysiology, Circ. Res. 98 (2006) 322–334.
[21] D.J. Hartshorne, M. Ito, F. Erdodi, Role of protein phosphatase type 1 in contractile functions: myosin phosphatase, J. Biol. Chem. 279 (2004) 37211–37214.
[22] A.V. Ljubimov, M. Saghizadeh, Progress in corneal wound healing, Prog. Retin. Eye Res. 49 (2015) 17–45.
[23] A. Mediero, A. Guzman-Aranguez, A. Crooke, A. Peral, J. Pintor, Corneal re-epithelialization stimulated by diadenosine polyphosphates recruits RhoA/ROCK and ERK1/2 pathways, Invest. Ophthalmol. Vis. Sci. 49 (2008) 4982–4992.
[24] B. Lontay, Z. Serfozo, P. Gergely, M. Ito, D.J. Hartshorne, F. Erdodi, Localization of myosin phosphatase target subunit 1 in rat brain and in primary cultures of neuronal cells, J. Comp. Neurol. 478 (2004) 72–87.
[25] B. Lontay, K. Bodoor, D.H. Weitzel, D. Loiselle, C. Fortner, S. Lengyel, D. Zheng, J. Devente, R. Hickner, T.A. Haystead, Smoothelin-like 1 protein regulates myosin phosphatase-targeting subunit 1 expression during sexual development and pregnancy, J. Biol. Chem. 285 (2010) 29357–29366.
[26] B. Lontay, K. Bodoor, A. Sipos, D.H. Weitzel, D. Loiselle, R. Safi, D. Zheng, J. Devente, R.C. Hickner, D.P. McDonnell, T. Ribar, T.A. Haystead, Pregnancy and smoothelin-like protein 1 (SMTNL1) deletion promote the switching of skeletal muscle to a glycolytic phenotype in human and mice, J. Biol. Chem. 290 (2015) 17985–17998.
[27] D. Dedinszki, A. Sipos, A. Kiss, R. Batori, Z. Konya, L. Virag, F. Erdodi, B. Lontay, Protein phosphatase-1 is involved in the maintenance of normal homeostasis and in UVA irradiation-induced pathological alterations in HaCaT cells and in mouse skin, Biochim. Biophys. Acta 1852 (2015) 22–33.
[28] R.H. Croze, W.J. Thi, D.O. Clegg, ROCK inhibition promotes attachment, proliferation, and wound closure in human embryonic stem cell-derived retinal pigmented epithelium, Transl. Vis. Sci. Technol. 5 (2016) 7.
[29] K. Bodoor, B. Lontay, R. Safi, D.H. Weitzel, D. Loiselle, Z. Wei, S. Lengyel, D.P. McDonnell, T.A. Haystead, Smoothelin-like 1 protein is a bifunctional regulator of the progesterone receptor during pregnancy, J. Biol. Chem. 286 (2011) 31839–31851.
[30] J. Yin, F.S. Yu, Rho kinases regulate corneal epithelial wound healing, Am. J. Phys. Cell Phys. 295 (2008) C378–C387.
[31] J.T. Nardini, D.A. Chapnick, X. Liu, D.M. Bortz, Modeling keratinocyte wound healing dynamics: cell-cell adhesion promotes sustained collective migration, J. Theor. Biol. 400 (2016) 103–117.
[32] C. Jonak, M. Mildner, G. Klosner, V. Paulitschke, R. Kunstfeld, H. Pehamberger, E. Tschachler, F. Trautinger, The hsp27kD heat shock protein and p38-MAPK signaling are required for regular epidermal differentiation, J. Dermatol. Sci. 61 (2011) 32–37.
[33] A.A. Kramerov, M. Saghizadeh, A.V. Ljubimov, Adenoviral gene therapy for diabetic keratopathy: effects on wound healing and stem cell marker expression in human organ-cultured corneas and limbal epithelial cells, J. Vis. Exp. (110) (2016) 54058.
[34] N. Okumura, M. Ueno, N. Koizumi, Y. Sakamoto, K. Hirata, J. Hamuro, S. Kinoshita, Enhancement on primate corneal endothelial cell survival in vitro by a ROCK inhibitor, Invest. Ophthalmol. Vis. Sci. 50 (2009) 3680–3687.
[35] Y. Xia, X. Cai, J. Fan, L. Zhang, Z. Li, J. Ren, G. Wu, F. Zhu, RhoA/ROCK pathway inhibition by fasudil suppresses the vasculogenic mimicry of U2OS osteosarcoma cells in vitro, Anti-Cancer Drugs 28 (2017) 514–521.
[36] K.P. Garnock-Jones, Ripasudil: first global approval, Drugs 74 (2014) 2211–2215.
[37] R. McMullan, S. Lax, V.H. Robertson, D.J. Radford, S. Broad, F.M. Watt, A. Rowles, D.R. Croft, M.F. Olson, N.A. Hotchin, Keratinocyte differentiation is regulated by the Rho and ROCK signaling pathway, Curr. Biol. 13 (2003) 2185–2189.
[38] T. Wang, W. Kang, L. Du, S. Ge, Rho-kinase inhibitor Y-27632 facilitates the proliferation, migration and pluripotency of human periodontal ligament stem cells, J. Cell. Mol. Med. 21 (2017) 3100–3112.
[39] W.T. Arthur, K. Burridge, RhoA inactivation by p190RhoGAP regulates cell spreading and migration by promoting membrane protrusion and polarity, Mol. Biol. Cell 12 (2001) 2711–2720.
[40] C.D. Nobes, A. Hall, Rho GTPases control polarity, protrusion, and adhesion during cell movement, J. Cell Biol. 144 (1999) 1235–1244.
[41] D.S. Lee, G. Quan, J.Y. Choi, S.Y. Kim, S.C. Lee, Chronic ultraviolet radiation modulates epidermal differentiation as it up-regulates transglutaminase 1 and its substrates, Photodermatol. Photoimmunol. Photomed. 21 (2005) 45–52.
[42] T. Nakamura, K. Nishida, A. Dota, M. Matsuki, K. Yamanishi, S. Kinoshita, Elevated expression of transglutaminase 1 and keratinization-related proteins in conjunctiva in severe ocular surface disease, Invest. Ophthalmol. Vis. Sci. 42 (2001) 549–556.
[43] R.L. Eckert, T. Efimova, S.R. Dashti, S. Balasubramanian, A. Deucher, J.F. Crish, M. Sturniolo, F. Bone, Keratinocyte survival, differentiation, and death: many roads lead to mitogen-activated protein kinase, J. Investig. Dermatol. Symp. Proc. 7 (2002) 36–40.
[44] R.M. Castilho, C.H. Squarize, J.S. Gutkind, Exploiting PI3K/mTOR signaling to accelerate epithelial wound healing, Oral Dis. 19 (2013) 551–558.
[45] C.H. Squarize, R.M. Castilho, T.H. Bugge, J.S. Gutkind, Accelerated wound healing by mTOR activation in genetically defined mouse models, PLoS One 5 (2010) e10643.
[46] B.R. Thrash, C.W. Menges, R.H. Pierce, D.J. McCance, AKT1 provides an essential survival signal required for differentiation and stratification of primary human keratinocytes, J. Biol. Chem. 281 (2006) 12155–12162.
[47] J. Guay, H. Lambert, G. Gingras-Breton, J.N. Lavoie, J. Huot, J. Landry, Regulation of actin filament dynamics by p38 map kinase-mediated phosphorylation of heat shock protein 27, J. Cell Sci. 110 (Pt 3) (1997) 357–368.
[48] J.N. Lavoie, G. Gingras-Breton, R.M. Tanguay, J. Landry, Induction of Chinese hamster HSP27 gene expression in mouse cells confers resistance to heat shock. HSP27 stabilization of the microfilament organization, J. Biol. Chem. 268 (1993) 3420–3429.
[49] M. Bektas, D.S. Rubenstein, What's in a name?: heat shock protein 27 and keratinocyte differentiation, J. Invest. Dermatol. 130 (2010) 10–12.
[50] I.S. Song, S.S. Kang, E.S. Kim, H.M. Park, C.Y. Choi, H. Tchah, J.Y. Kim, Heat shock protein 27 phosphorylation is involved in epithelial cell apoptosis as well as epithelial migration during corneal epithelial wound healing, Exp. Eye Res. 118 (2014) 36–41.
[51] J.R. Bayascas, D.R. Alessi, Regulation of Akt/PKB Ser473 phosphorylation, Mol. Cell 18 (2005) 143–145.

frontiers | Frontiers in Endocrinology

lontay.beata_285_24

TYPE Original Research
PUBLISHED 31 May 2024
DOI 10.3389/fendo.2024.1375771

Check for updates

OPEN ACCESS

EDITED BY
Toshio Takahashi,
Suntory Foundation for Life Sciences, Japan

REVIEWED BY
Hiroyasu Kamei,
Kanazawa University, Japan
Rabab Al-Lahham,
University of Texas Medical Branch at Galveston, United States
Yue Zhao,
Nanjing University, China

*CORRESPONDENCE
Beáta Lontay
lontay@med.unideb.hu

RECEIVED 24 January 2024
ACCEPTED 10 May 2024
PUBLISHED 31 May 2024

CITATION
Keller I, Ungvári Á, Kinter R, Szalmás F, Kókai E and Lontay B (2024) Smoothelin-like protein 1 promotes insulin sensitivity and modulates the contractile properties of endometrial epithelial cells with insulin resistance. *Front. Endocrinol.* 15:1375771. doi: 10.3389/fendo.2024.1375771

COPYRIGHT
© 2024 Keller, Ungvári, Kinter, Szalmás, Kókai and Lontay. This is an open-access article distributed under the terms of the Creative Commons Attribution License (CC BY). The use, distribution or reproduction in other forums is permitted, provided the original author(s) and the copyright owner(s) are credited and that the original publication in this journal is cited, in accordance with accepted academic practice. No use, distribution or reproduction is permitted which does not comply with these terms.

Smoothelin-like protein 1 promotes insulin sensitivity and modulates the contractile properties of endometrial epithelial cells with insulin resistance

Ilka Keller, Ádám Ungvári, Richárd Kinter, Fanni Szalmás, Endre Kókai and Beáta Lontay*

Department of Medical Chemistry, Faculty of Medicine, University of Debrecen, Debrecen, Hungary

Introduction: The incidence of infertility is significantly higher in women with diseases linked to impaired glucose homeostasis, such as insulin resistance. Defective glucose metabolism interferes with fertilization; however, the molecular mechanism underlying this interference is unclear. Smoothelin-like protein 1 (SMTNL1) was isolated from muscle and steroid hormone-responsive tissues and regulates the contractile functions of various cell types through the inhibition of myosin phosphatase (MP) holoenzyme. In addition, SMTNL-1 after phosphorylation at Ser301 by protein kinase A translocates to the nucleus and functions as a transcriptional co-activator of the progesterone receptor-B. SMTNL1 null mice exhibit reduced reproductive fitness and are more prone to type 2 diabetes mellitus. However, the role of SMTNL1 in endometrial epithelial cells is not known.

Methods: The effect of SMTNL1 overexpression was investigated in pregnancy and in gestational diabetic endometrial epithelial cell models by immunofluorescent staining, cell migration, and semi quantitative Western blot analysis and glucose uptake assay.

Results: We show that SMTNL1 promotes the differentiation of endometrial epithelial cells in a progesterone-dependent manner to attenuate insulin resistance. Furthermore, SMTNL1 hampers the migration capacity of epithelial cells in a gestational diabetes model by inhibiting the expression of MYPT1, the regulatory subunit of MP, and the activity of the holoenzyme, resulting in increased phosphorylation of the 20 kDa regulatory myosin light chain. SMTNL1 also acts as an insulin-sensitizing agent by increasing the gene expression of PP2A and DUPS9 protein phosphatases, resulting in decreased ERK1/2 activity and, hence, decreasing the phosphorylation of IRS-1 at Ser612 under gestational diabetes conditions.

Conclusion: SMTNL1 may have therapeutic relevance to the progesterone-dependent inhibition of endometrial epithelial cell migration under hyperglycemic conditions and insulin sensitivity in the endometrium in gestational diabetes or other metabolic disorders.

KEYWORDS

endometrium, insulin resistance, insulin signaling, migration, gene expression

Highlights

- SMTNL1 induces differentiation of endometrial epithelial cells
- SMTNL1 hampers migration of epithelial cells in a gestational diabetes model
- SMTNL1 promotes insulin sensitivity in insulin-resistant endometrial epithelial cells by decreasing IRS Ser612 phosphorylation
- SMTNL1 regulates the expression of PP2A and DUSP9, which regulate ERK1/2
- SMTNL1 increases glucose uptake and glycogen storage

1 Introduction

Morphological changes in the uterine epithelium are essential for the female reproductive cycle and the process of implantation. Secretory cells in the uterine epithelium undergo morphological changes during the luteal phase of the female cycle. The expression of cell surface molecules such as Mucin-1 (MUC-1) indicates successful differentiation and receptive endometrium (1). Aberrations in the single-layered columnar epithelium and secretory cells lead to inadequate trophoblast-to-endometrium communication, leading to implantation failure before cell-cell interaction can occur. Imbalances in steroid hormones and other pathological processes such as insulin resistance and the resulting metabolic syndrome can cause severe deformities, differentiation disorders, and pathological changes in the integrity of the endometrial epithelium (2). These defects are associated with various infertility disorders such as polycystic ovarian syndrome and may be the underlying cause of several aberrances leading to oligo-anovulation (3). Defective ovulation, sexual steroid hormone homeostasis, or blastocyst implantation induce a variety of clinical symptoms, including infertility. Infertility occurs in 5–10% of the reproductive-age female population (4). Additionally, high insulin and glucose levels and stimuli promoting epithelial cell proliferation and differentiation increase the risks of endometriosis and endometrial hyperplasia leading to endometrial cancer (5–7).

The underlying molecular mechanism of insulin resistance is multifactorial and includes the depletion of cell surface receptors, loss of function mutations, and unbalanced posttranslational modifications of molecules in the insulin receptor signaling pathway, including phosphorylation, enhanced Ser phosphorylation and reduced Tyr phosphorylation by Ser/Thr protein kinases (8). Serine phosphorylation of the insulin receptor substrate 1 (IRS-1) results in inhibition of its binding to the insulin receptor and tyrosine phosphorylation, therefore inhibition of binding of the downstream phosphatidyl-inosotol-3-kinase (PI3K) and activation of protein kinase B/Akt (9). Akt binds to GLUT4-containing vesicles and mediates insulin-stimulated glucose transport (10).

SMTNL1 is expressed in rabbit ileum (11), steroid hormone-responsive tissues, smooth muscle, and skeletal muscle (12). In addition, SMTNL1 regulates contractile functions in smooth muscle cells by inhibiting MP holoenzyme via binding to the MYPT1 regulatory subunit of MP, resulting in elevated phosphorylation of the 20 kDa regulatory subunit (MLC20) (12). Furthermore, phosphorylation on SMTNL1 Ser301 by protein kinase A and G results in SMTNL1 translocation to the nucleus where it functions as a transcriptional coregulator of progesterone receptor (PR) to regulate the expression of cytoskeletal elements, steroid receptors, and metabolic enzymes (13).

SMTNL1 is a potent regulator of insulin signaling, as shown in an *in vitro* insulin-resistant C2C12 rodent cell line skeletal muscle model. In mouse and differentiated skeletal muscle cell culture models of insulin resistance, SMTNL1 can attenuate the effects of altered IRS-1 serine phosphorylation induced by the over-activation of Ser/Thr protein kinases (14, 15). By reducing the expression of novel type PKCε (nPKCε), SMTNL1 can downregulate the activity of ERK 1/2 MAPK, resulting in decreased IRS-1 Ser612 phosphorylation, which was boosted by *in vitro* hyperinsulinemic-hyperglycemic conditions (14, 16). Thus, SMTNL1 prevents the dissociation of the IRS-1-PI3K-Akt-mTOR pathway and acts as an insulin-sensitizing agent in our *in vitro* rodent model. Moreover, SMTNL1 can induce GLUT4-mediated glucose uptake in C2C12 cells (14). In *Smtnl1* $^{-/-}$ mice, fitness is reduced, including reduced litter size, elongated times between pregnancies, and glucose intolerance, especially in pregnant animals (15). Interestingly, endometrial prolactin (PRL) levels are reduced in late pregnancy in *smtnl1* $^{-/-}$ mice (12). Although the insulin-sensitizing role of SMTNL1 has been characterized in skeletal muscle, the molecular explanation of the above-mentioned SMTNL1 KO reproductive phenotype and the correlation of it with the insulin-resistant conditions was not yet known, nor was its effect on endometrial epithelial cells. The aim of this study was to determine the effects of SMTNL1 on insulin sensitivity and the contractile properties of human endometrial adenocarcinoma cells under pregnant and hyperglycemic/hyperinsulinemic conditions.

2 Materials and methods

2.1 Chemicals

All chemicals were obtained from Sigma-Aldrich (St. Louis, MO, USA) unless indicated otherwise.

2.2 Antibodies

All antibodies are listed in Supplementary Table S2.

2.3 Cell culture and maintenance of Ishikawa cells

The human endometrial adenocarcinoma Ishikawa cell line (ECACC, #99040201) was maintained in Dulbecco's modified Eagle's medium (DMEM) with phenol red supplemented with 1000 mg/L glucose, 5% fetal bovine serum (FBS), 2 mM L-glutamine (Lonza,

Basel, Switzerland), and 1% non-essential amino acids (NEAA). Cells were grown in a humidified incubator in an atmosphere of 5% CO_2 at 37°C and passaged every 3 days at a 3:1 ratio.

2.4 Transient transfection and differentiation

The full-length human SMTNL1 construct (pcDNA-3.1-M11-FT-SMTNL1 plasmid expression vector, referred to as FT-SMTNL1, GeneCopoeia Rockville, USA) and the empty pcDNA-3.1 plasmid as a transfection control (MOCK) were overexpressed in Ishikawa cells. Both the FT-SMTNL1 plasmid and the MOCK plasmid (used in 2.5x10^{-3} µg/µl concentrations) were supplemented by Gene Juice transfection reagent (4 µl per well) and were suspended in 400 µl/well serum-free DMEM, then incubated for 15 minutes. After incubation mixture was added to adhered cells, previously seeded on 6 well plates in 2x10^5/well density, and then culture was incubated at room temperature for another 15 minutes. After incubation serum free DMEM was further completed by 900 µl of serum containing complete growth medium to reach 1500 µl/well final volume. Cells were cultured for 72 hours after transfection.

2.5 *In vitro* pregnancy and gestational diabetes model of Ishikawa cells

The day after culturing or transfection, cells were washed with 1x PBS and complete growth medium was replaced by DMEM without phenol red, supplemented with 1000 mg/L glucose, 5% FBS, 2 mM L-glutamine, and 1% NEAA. For the pregnancy model, the medium was supplemented with 1 µM medroxy-progesterone-acetate, 10 nM 17-β-oestradiol, and 0.5 mM 8-Br-cAMP to represent physiological hormones of gestation (P4). For the gestational diabetes group (GDB), P4 cells were supplemented with 100 nM insulin and 0.025 mM glucose. Cells were lysed 72 hours after treatment.

2.6 Viability assay

Cells were seeded and transfected as described above. Cultures were maintained for 72 hours, and then 20 µM/well AlamarBlue (Invitrogen™, Waltham, Massachusetts, USA) reagent was added. Plates were incubated at 37°C for 90 minutes or until color change was evident. Fluorescence was measured at 530/590 nm with a fluorimeter (Tecan Group Ltd, Switzerland). The fluorescence of blank samples was subtracted, and the results were normalized to the average of control values.

2.7 Cell migration assay

Transfected Ishikawa cells were labeled with Vybrant™ DiD Cell-Labeling Solution (Invitrogen™, Waltham, Massachusetts, USA, Catalog number: V22887), seeded into collagen-coated OptiPlate-96 Black plates (PerkinElmer; Waltham, MA, USA), and cultured for 48 hours under control, P4, or GDB conditions. Each well was scratched by a Tecan Freedom EVO 150 machine (Tecan Group Ltd, Switzerland), and then cultured for an additional 24 hours; migratory potential was measured during this period. Cells were monitored using real-time screening for 24 hours with a 10x air objective (NA: 1.15) using the Opera Phoenix™ High Content Confocal System (HCS) instrument (PerkinElmer; Waltham, MA, USA). Free surface areas and cell numbers were analyzed using the built-in Harmony software (version 4.8). Results were normalized to the average of MOCK samples.

2.8 Immunofluorescence staining

The confocal microscopy protocol was previously described (16). Briefly, the actin cytoskeleton was stained with Texas-Red Phalloidin (yellow) and nuclei were labeled with DAPI (4′, 6-diamidino-2-phenylindole) (blue). Anti-MUC-1, anti-MYPT1, anti-MYPT1^{pT696}, anti-MLC, and anti-MLC^{pS18} antibodies were used at 1:100 dilutions and labeled with Alexa488 fluorophore in 1:1000 dilution (green). Visualization was carried out using the Opera Phoenix™ HCS. A total of 14–16 fields with 3x 10^4 cells were acquired per well and laser-based autofocus was performed for each imaging position. Images of DAPI, Alexa-488 and Alexa-647 channels were collected at the 0 µm position of the Z image plane relative to the bottom of the optical plate using a 10x objective. Intensity of Alexa 488 fluorophore has been calculated as follows: Analysis have been conducted by measuring sum of Alexa 488 fluorophore intensity of 9 fields of each well, 3 independent wells per groups, by built in intelligent software of high content screening instrument. Analyzed intensity have been filtered to autofluorescence, and intensity of secondary antibody control was subtracted from each well's sum intensity. Data was normalized to cell number obtained from nuclei number stained with DAPI. Control MOCK group value was taken as 100%, and all other groups were expressed as ratios.

2.9 Protein extraction

Protein extraction was conducted as previously described (17). Total protein concentrations were determined using the bicinchoninic acid (BCA) Protein Assay Kit (Thermo Scientific, Waltham, MA, USA).

2.10 Western blot analysis

Semi-quantitative Western blot analyses were conducted, as previously described (16) with modifications as follows. Protein (50 µg) was loaded onto 4–20% precast Criterion gel (Bio-Rad Laboratories) and separated at 200 V. Nitrocellulose membranes were blocked in 5% (w/v) bovine serum albumin/tris-buffered saline containing 0.1% (v/v) Tween 20 (BSA/TBST) for at least 1.5 hours.

The membranes were incubated with primary and secondary antibodies diluted in blocking solution. Antibody binding was detected with enhanced chemiluminescence (WesternBright ECL or WesternBright Sirius and WesternBright Peroxide reagents, Advansta Inc.; San Jose, CA, USA) at a ratio of 1:1 in a ChemiDoc Touch Imaging System (Bio-Rad Laboratories; Hercules, CA, USA).

2.11 Glycogen content measurement

Cells were seeded on 6-well plates, grown to 70% confluency, and transfected with FT-SMTNL1 or MOCK vector. After 72 hours, cells were trypsinized for 5 mins; the reaction was terminated by adding 6 times volume of complete growth media. Cells were centrifuged for 4 minutes at 2000 g at 4°C. Pellets were solubilized in 0.1 M KH_2PO_4 followed by sonication at 10% output (Branson Sonifier 250. Fisher Scientific). After adding 25% TCA, the lysate was vortexed and centrifuged at 16000 g for 5 minutes at 4°C. After adding concentrated H_2SO_4, the supernatants were incubated for 30 minutes at room temperature. The mixture was incubated with 6% phenol for 5 minutes at 90°C. The glycogen content was measured based on absorbance at 490 nm, and concentration was calculated against standard curve, consisting of glycogen stock of the following concentrations: 0.00625 g/100 ml, 0.025 g/100 ml, 0.1 g/100 ml and reagent blank. Blank absorbance was subtracted from each wells value. Results of glycogen concentration in g/100 ml were normalized to protein concentration, measured by BCA assay from each sample, protein concentration expressed as g/100 ml unit. Normalized results had a unit of glycogen/protein (g/g). MOCK control group value was taken as 100%, and all other groups were expressed as ratios as bar chart.

2.12 Glucose uptake assay

The 2-NBDG (2-N-7-Nitrobenz-2-oxa-1,3-diazol-4-yl-Amino-2-Deoxyglucose) uptake was assessed as described previously (14). Ishikawa cells were cultured, transfected, treated as previously described, washed with PBS, and incubated in complete growth media (glucose-free DMEM) for 1 hour. After adding 100 µM 2-NBDG dissolved in complete growth media, cells were washed with PBS and lysed in 0.1 M KH_2PO_4 (pH 11.0) lysis buffer supplemented with 1% Triton X-100. Fluorescence was measured at an excitation of 485 nm and an emission of 535 nm using a Tecan Spark Multimode microplate reader (Tecan Treading AG, Mannedorf, Germany). Fluorescence was normalized to protein concentrations.

2.13 RNA isolation and semi-quantitative RT-PCR analysis

Total RNA was extracted from Ishikawa cell culture after P4 and GDB treatment with or without FT-SMTNL1. TRIzol reagent (1 ml, Life Technologies, Carlsbad, CA) was added to each well. Cell lysates were treated with 200 µl chloroform and centrifuged at 13000 rpm at 4°C for 15 minutes. Isopropanol (500 µl) was added to the RNA fraction, and the mixture was centrifuged at 13000 rpm at 4°C for 10 minutes. The pellet was resuspended in 75% ethanol and centrifuged again at 13000 rpm at 4°C for 5 minutes. The pellet was resuspended in 10 µl of nuclease-free water. Concentration was measured using a NanoDrop Fluorospectrometer (Thermo Fisher Scientific, Waltham, Massachusetts, USA). Reverse transcription was carried out using 0.6 µg RNA/sample at 37°C for 120 minutes using a cDNA Synthesis Kit (Thermo Fisher Scientific, Waltham, Massachusetts, USA). The cDNA was used for PCR amplification with a 2x Xceed qPCR SyberGreen Master mix (Institute of Applied Biotechnologies, Prague – Strašnice, Czech Republic). The PCR primers are listed in Supplementary Table S1. The PCR protocol is as follows: 95°C for 3 minutes for denaturation; 50 cycles of 95°C for 3 seconds, 60°C for 30 seconds, 72°C for 90 seconds. PCR was performed using a LightCycler 480 (Roche Applied Science, Penzberg, Germany) machine. The Cp values of each sample were normalized to the geometric mean of housekeeping genes, including GAPDH and Cyclophilin A. Data was normalized to the value of MOCK vector treatment.

2.14 Statistical analysis

Image J software was used to quantify Western blot images. Data were plotted as bar charts and statistical analyses were calculated using GraphPad Prism 8 software. Phosphorylated proteins were normalized to non-phosphorylated protein expression, while non-phosphorylated protein expression was normalized to loading controls. All groups were normalized to the MOCK vector, which was set at 100%. Data are presented as mean ± SD for n = 3–6 independent experiments. Differences were considered statistically significant at $p < 0.05$ using unpaired two-tailed t-tests to compare two groups.

3 Results

3.1 SMTNL1 overexpression facilitates the differentiation of endometrial epithelial cells

SMTNL1 acts as a key regulator in steroid hormone-sensitive tissues such as the uterus; however, the detailed mechanism is unclear. To assess the effect of SMTNL1 on cell differentiation and cell viability, Ishikawa endometrial epithelial cells were transfected with the empty vector (MOCK control) or the FT-SMTNL1 plasmid. In our experiments, we used Ishikawa cell line modelling the inner columnar epithelium of the endometrium, which differs in function and structure from the underlying endometrial stromal cells (18). Validation of overexpression was conducted by immunofluorescence (Supplementary Figures S1A, C, D, F) and Western blot analysis (Supplementary Figure S1B) applying anti-Flag (Supplementary Figures S1A–C) and anti-SMTNL1 antibodies (Supplementary

Figures S1D–F). Immunofluorescence staining with the Flag-tag antibody showed cytosolic localization of SMTNL1 expression with lower nuclear SMTNL1 expression, staining with anti-SMTNL1 antibody resulted in same peripherial, homogenous arrangement (Supplementary Figure S1D). Analysis of Alexa 488 intensity labelling anti-Flag-tag antibody shown an elevation of 171% (p=0.012) comparing FT-SMTNL1 overexpressed group to MOCK control, and elevation by 165% (p=0.0141) compared with untreated control group (Supplementary Figure S1C). SMTNL1 fluorescence intensity was elevated by 128.67% (p=0.0025) and by 150% (p=0.0055) in FT-SMTNL1 overexpressed group compared to control and MOCK (Supplementary Figure S1F). Investigating the endogenous SMTNL1 expression in the applied control, P4 and GDB environments a decrement of expression was seen in GDB group, by 56.75% (p=0.034) and by 48% (p=0.0290) compared with control and P4 groups, respectively (Supplementary Figure S1E). FT-SMTNL1 expression increased by 177% (p = 0.0002) and 191.5% (p<0.0001) in cells transfected with FT-SMTNL1 compared with control (untreated control) and MOCK group, respectively (Supplementary Figure S1B). FT-SMTNL1 transfection in Ishikawa cells did not affect cell viability quantified by Alamar Blue assay (Supplementary Figure S1G). The effects of SMTNL1 on differentiation of Ishikawa cells were assessed by HCS screening microscopy and RT-PCR. To investigate morphological changes in Ishikawa cells, the actin cytoskeleton was labeled with Texas Red phalloidin (yellow) and MUC-1 differentiation marker was labeled with Alexa 488 fluorophore (green) (Figures 1A, B). The mRNA expression of MUC-1 was assessed by RT-PCR (Figure 1C). Ischikawa cells were subjected to progesterone treatment (P4) and hyperglycaemic/hyperinsulinaemic treatment (GDB) modeling insulin resistance in the presence of progesterone mimicking disorders such as gestational diabetes based on the protocols of previous publications (19, 20). These results are summarized in Supplementary Figure S2. showing that the expression levels of Akt remained unchanged (Supplementary Figure S2A). Although Akt^{pS473} phosphorylation was increased in the control group upon acute insulin treatment (Supplementary Figure S2B) but there was no increase in Akt phosphorylation in the GDB samples proving the insulin resistant state of the epithelial cells. P4 and GDB treatments induced cytoskeletal changes; the undifferentiated cuboidal morphology shifted towards an elongated, columnar shape. SMTNL1 overexpression further promoted these changes in a non-progesterone-dependent manner (Figures 1A, B). The synergic effects of SMTNL1 and progesterone were indicated in the P4 and GDB groups as prominent morphological changes. MUC-1 expression was evoked by both SMNTL1 and progesterone. SMTNL1 overexpression enhanced MUC-1 intensity the most in P4 environment, to which decrement was detectable in control FT-SMTNL1 overexpressed group by 143.33% (p<0.0001) and by 149% (p<0.0001) in GDB environment overexpressed group. The MUC-1 differentiation and mRNA expression were most prominent in the P4 SMTNL1-overexpressed group (Figures 1B–D), suggesting the positive effect of SMTNL1 on the differentiation of endometrial epithelial cells in the presence of P4. SMTNL1 overexpression increased MUC-1 mRNA expression levels by 554.67% (p=0.0036) in the P4 SMTNL1 supplemented group, compared to the P4 MOCK control. SMNTL1 enhanced MUC-1 mRNA expression by 170% (p=0.026) in the GBD-transfected group compared to the GDB MOCK control. The expression of MUC-1 was increased by 90.67% (p=0.0551) in P4 MOCK cells compared with MUC-1 expression in the control MOCK group, indicating differentiation of Ishikawa cells in the P4 environment. In the GDB environment, MUC-1 mRNA expression decreased by 104.16% (p=0.0307) compared to P4 MOCK group, indicating that the hyperinsulinemic-hyperglycemic environment hampers differentiation. Comparing the SMTNL1 overexpressed groups the P4 treated environment evoked the highest expression of MUC-1 mRNA, which was decreased by 611.958% (p=0.0001) in control, and by 488.83% (p=0.0064) in GDB samples with FT-SMTNL1 overexpression (Figure 1C). Analyzing immunofluorescence images MUC-1 intensity labelled with Alexa 488 fluorophore elevated significantly in P4 MOCK group by 47.33% (p=0.0315) compared with untreated MOCK control. SMTNL1 overexpression elevated MUC-1 intensity by 90.67% (p=0.0031) and by 33% (p=0.0391) compared with P4 and GDB MOCK groups, respectively. GDB treatment hindered MUC-1 intensity by 91.33% (p=0.0029) compared to P4 MOCK samples (Figure 1D).

3.2 SMTNL1 overexpression decreases MYPT1 expression and inhibits MP activity

Changes in the expression of cytoskeletal proteins and their modifying enzymes contribute to changes in cell shape and differentiation. Therefore, the effects of SMTNL1 on its major interacting partner, MYPT1, were investigated (12, 13) (Figure 2). Ishikawa cells were cultured in control environment, in control environment further supplemented with P4 (P4), and P4 with the addition of high glucose and insulin (pathological GDB). MYPT1 activity was measured by quantifying the inhibitory phosphorylation site in Ishikawa cells after control, P4 and GDB treatment for 72 hours, with or without FT-SMTNL1 overexpression. Immunofluorescent staining (Figure 2A) and its image analysis (Figure 2C) shows reduction in MYPT1 expression based on fluorescence intensity in both P4 an GDB groups upon FT-SMTNL1 overexpression by 35.34% (p=0.0079) and by 38.66% (p=0.0445) in P4 in GDB groups, respectively compared to their untransfected MOCK controls. The FT-SMTNL1 overexpression resulted in a 96.33% (p=0.0132) and a 85% (p=0.0301) decrease in P4 and GDB treatments, respectively compared to non-treated FT-SMTNL1 overexpressed group (Figure 2C). Changes in MYPT1 expression were also assessed by Western blot analysis and the results aligned with the HCS analysis data (Figures 2A, C). SMTNL1 overexpression reduced MYPT1 expression in the P4 and GDB groups by 39.49% (p=0.0187) and 50.91% (p=0.0175), respectively, compared to P4 MOCK and GDB MOCK groups, respectively (Figure 2B). These findings correlate with previously characterized ability of SMTNL1 to reduce MYPT1 expression in smooth and skeletal muscle as the coactivator of PR (12). Assessing MYPT1 activity, by measuring its inhibitory phosphorylation, SMTNL1 overexpression significantly increased $MYPT1^{pT696}$ inhibitory phosphorylation in the GDB group by 113.66% (p=0.0002), compared to GDB MOCK. The inhibitory

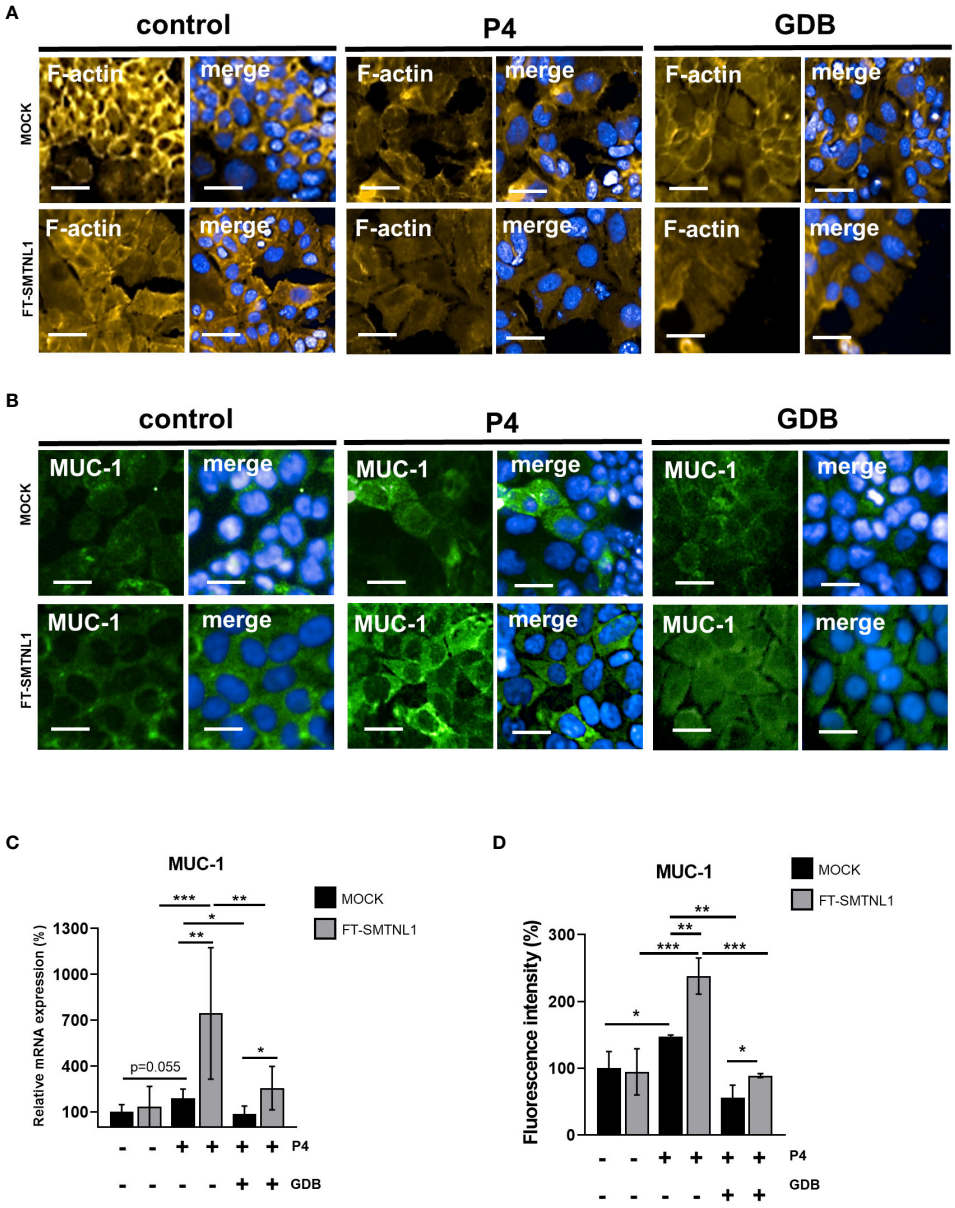


FIGURE 1
SMTNL1 overexpression facilitates the differentiation of Ishikawa cells. Differentiation was assessed by staining of F-actin of Ishikawa cells using Texas-Red Phalloidin dye (yellow) in control/P4/GDB groups. Nuclei were stained with DAPI (blue). Scale bars: 100 µm **(A)**. Differentiation of Ishikawa cells in control/P4/GDB groups was followed by high-content microscopy by staining for the MUC-1 differentiation marker with Alexa 488 fluorophore (green). Nuclei were stained by DAPI (blue). Scale bars: 100 µm **(B)**. MUC-1 differentiation marker mRNA expression was followed by RT-PCR. Cp values were normalized to housekeeping genes GAPDH and Cyclophilin A and were expressed as ratios of untreated MOCK control taken as 100%. Data was plotted as bar charts, where values represent n=3–8 +/- SD **(C)**. Muc-1 protein fluorescent intensity was assessed by HCS system **(D)** Two groups were compared by unpaired two-tailed t-test, and four groups or more were compared by two-way ANOVA where: $p< 0.05$ (*), $p<0.01$ (**) and $p<0.0001$ (***) **(C, D)**. P4: progesterone, GDB: insulin resistance with P4, gestational diabetes.

phosphorylation on MYPT1^{pT696} was decreased by 31.8% (p=0.0406) implementing P4 MOCK treatment compared to the control MOCK group, indicating MYPT1 activation in P4 environment, which was further hindered by FT-SMTNL1 transfection. It also elevated MYPT1 inhibitory phosphorylation by 50.3% (p=0.0286) in P4 FT-SMTNL1 treated group (Figure 2E). GDB treatment caused inactivation of MYPT1 by elevating Thr696 phosphorylation by 30.94% (p=0.0304) compared to P4 MOCK group, which inactivation was further increased upon FT-SMTNL1 overexpression by 113.66% (p=0.0002) in SMTNL1 overexpressed GDB group. SMTNL1 overexpression evoked the most potent inhibition of MYPT1 in GDB environment, compared to which decrement was detectable in control SMTNL1 overexpressed group by 124.675% (p<0.0001), and by 94.3% (p=0.036) in P4 treated SMTNL1 overexpressed group. Western Blot analysis data were supported by immunofluorescent staining where nuclei were labelled by DAPI (blue), MYPT1^{pT696} was visualized using Alexa 488 fluorophore (green) (Figure 2D). Analyzing the intensity of

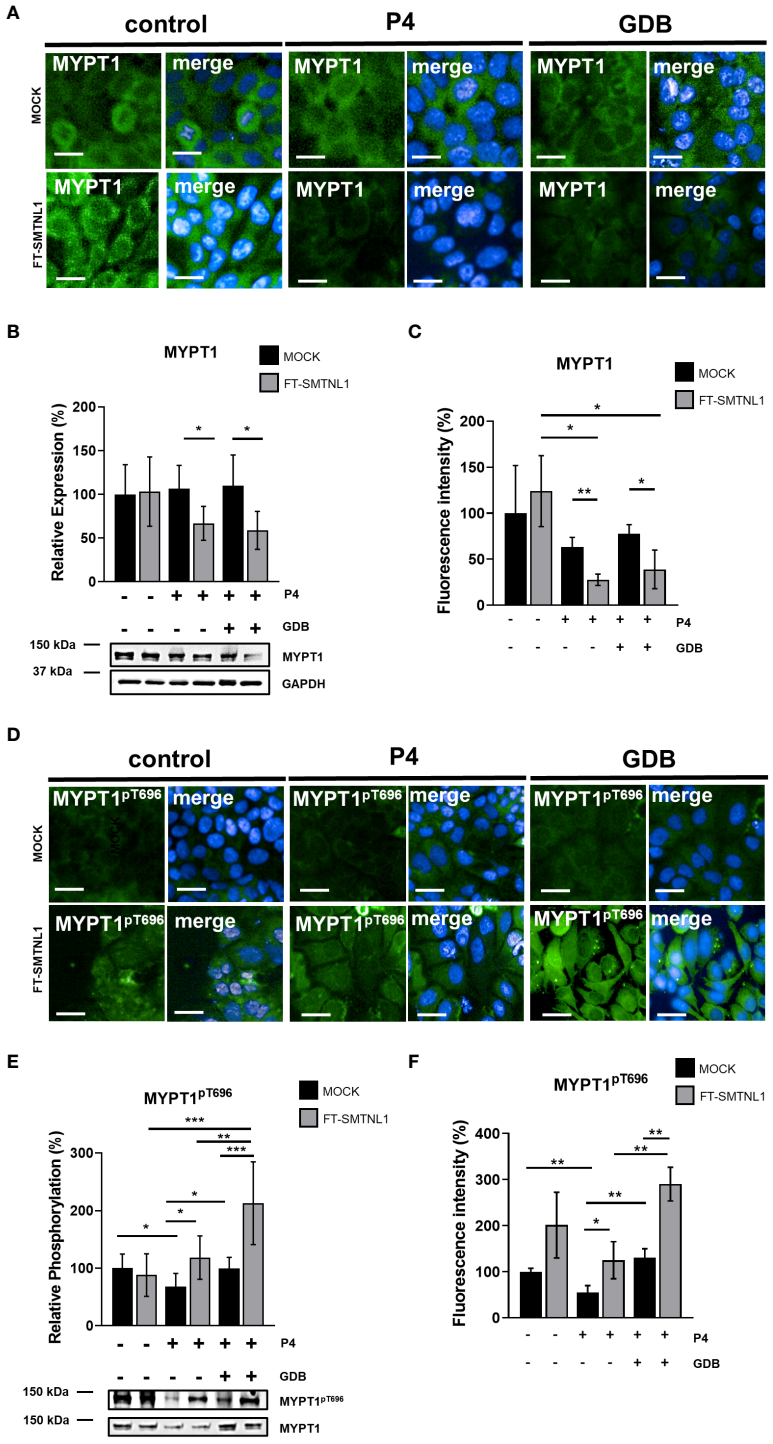


FIGURE 2
SMTNL1 inhibits the expression and the activity of MP in GDP in endometrial epithelial cells. Ishikawa cells were transfected with empty vector (MOCK) or FT-SMTNL1 in each of the control/P4/GDB treatments. Immunofluorescent staining was conducted using antibodies against MYPT1 **(A)** and MYPT1^{pT696} **(D)**, crosslinked with Alexa 488 fluorophore (green), nuclei were stained by DAPI (blue). Images were captured by Opera Phoenix^{TM} HCS. Scale bar: 20µm. **(A, D)** The intensity of Alexa 488 Fluorophore labelling anti-MYPT1 **(C)** and anti-MYPT1p^{T696} **(F)** primary antibodies have been measured, by built in intelligent software of high content screening instrument. Data was normalized to cell number obtained from nuclei number stained with DAPI. Protein samples from whole-cell lysates were analyzed using Western blot analysis with anti-MYPT1 **(B)**, anti-MYPT1^{pT696} **(E)** antibodies. Values represent n =5–8, mean ± SD. Data represents the ratio to control MOCK group, which was considered to be 100%. Two groups were compared by unpaired two-tailed t-test, and four groups or more were compared by two-way ANOVA, where: $p< 0.05$ (*), $p<0.01$ (**) and $p<0.0001$ (***).

MYPT1^{pT696} labelled with Alexa 488, inhibitory phosphorylation of MYPT1 was elevated by FT-SMTNL1 overexpression by 70% (p=0.0473) in P4 and by 159.67% (p=0.0026) in GDB groups. Applying P4 treatment has reduced MYPT1 inhibitory phosphorylation by 45% (p=0.0098) compared with control MOCK group, and GDB environment resulted in an increase of phosphorylation by 75.66% (p=0.0059) compared to P4 MOCK group (Figure 2F). Our data verified the regulatory effects of SMTNL1 on MYPT1 expression and activity in Ishikawa cells. The cytoplasmatic and nuclear localization of MYPT1 did not change in the P4 and GDB groups.

3.3 SMTNL1 overexpression regulates MLC20 phosphorylation via inhibition of MP

The overexpression of SMTNL1 reduced MYPT1 expression level in both P4 and GDB cells (Figure 2) and influenced MP activity via inhibitory phosphorylation in the GDB group (Figure 2). Because of these facts, we assessed the effect of SMTNL1 overexpression on the substrate of MP, the 20 kDa myosin light chain (MLC20). Neither the hormone treatments nor the SMTNL1 overexpression evoked any significant effects on MLC20 expression (Figures 3A–C). MLC expression and phosphorylation were measured by HCS microscopy after labeling nuclei with DAPI and MLC and MLC20^{pS19} with Alexa 488 fluorophore (green) (Figures 3A, D). Analyzing the intensity of Alexa488 fluorophore MLC has shown no changes in expression in any of the applied treatments (Figure 3C), and FT-SMTNL1 overexpression elevated the phosphorylation of MLC on the Ser19 residue by 31% (p=0.0014) in P4 and by 9% (p=0.0327) in GDB group compared with their untreated MOCK control (Figure 3F). MLC was predominantly localized in the cytoplasm in Ishikawa cells, and neither its localization nor expression changed in any of the experimental groups. MLC20^{pS19} phosphorylation was elevated in response to SMTNL1 overexpression in both the P4 and GDB groups, presumably due to the inhibition of MP. The decreased MYPT1 expression and elevated inhibitory phosphorylation of MYPT1 in response to SMTNL1 overexpression was accompanied by an increase in the phosphorylation of MLC20 at the Ser19 residue (Figure 3E) exclusively in the progesterone-supplemented groups. MLC20^{pS19} phosphorylation increased by 37.78% (p=0.0342) in the P4 group and by 40.91% (p=0.0315) in the GDB group comparing the effects of SMTNL1 overexpression to their MOCK controls. Progesterone decreased MLC20^{pS19} phosphorylation by 27% (p=0.0305) compared with MLC20^{pS19} phosphorylation in the non-treated MOCK control group. Comparing P4 MOCK group to GDB MOCK a 47.89% (p=0.0187) elevation of MLC20^{pS19} phosphorylation was detectable. Comparing SMTNL1 overexpressed groups, MLC phosphorylation was the most elevated in GDB environment, to which a decrease was detectable compared to both P4 and control environments by 51.02% (p=0.0306), and by 48.1% (p=0.0406), respectively (Figure 3E).

3.4 SMTNL1 inhibits the migration of endometrial epithelial cells

SMTNL1 regulates MP regulatory subunit MYPT1 expression and activity on a progesterone-dependent manner in endometrial epithelial cells resulting in the altered regulatory phosphorylation of MLC20. Since MP and MLC20 are crucial key elements of the cellular contractile functions, affecting migration as well, we aimed to determine the effects of SMTNL1 overexpression on the migration of Ishikawa cells in the control, P4 and GDB groups (Figure 4A) using scratch assays. Changes in covered surface area were monitored for 24 h in real-time with HCS microscopy (Figure 4B). SMTNL1 overexpression in the control environment reduced the migration of Ishikawa cells by 28.67% (p=0.0227). The reduction of migration in response to SMTNL1 overexpression was more pronounced in the P4 and GDB groups by 59.68% (p=0.0003) and by 32.14% (p=0.0153), compared to the corresponding MOCK controls, respectively. P4 treatment increased the migration of Ishikawa cells by 25.8% (p=0.0355) compared to the MOCK-transfected cells, correlating with the natural induction of endometrial epithelial cell migration during pregnancy. Moreover, comparing FT-SMTNL1 overexpressed groups there was a 45.33% (p=0.0349) decrease between GDB and control treatments. However, GDB treatment reduced the migration of Ishikawa cells by 41.85% (p=0.0067), compared to untreated MOCK control, and by 67.66% (p<0.0001) compared to P4 MOCK group, indicating the pathological effects of impaired glucose homeostasis in gestational diabetes during hyperglycemia.

3.5 SMTNL1 regulates IRS-1 and Akt-1 Ser phosphorylation and activity in Ishikawa cells

Fertility disorders are often linked to insulin resistance. In addition, the incidences of type two diabetes mellitus and metabolic syndrome are higher in *smtnl1 -/- null* mice (12). A previous study suggests that SMTNL1 plays a crucial role in the regulation of insulin signaling in skeletal muscle (14). To elucidate the effect of SMTNL1 on insulin signaling in endometrial epithelial cells, we determined the protein and phosphorylation levels of IRS-1 and Akt-1 under P4 and GDB conditions (Figure 5). None of the treatments significantly affected the expression of IRS-1 (Figure 5A); however, IRS-1^{pS612} phosphorylation, the hallmark of insulin resistance, was elevated in MOCK-transfected cells in GDB groups by 34.87% (p=0.0203) compared with control conditions. SMTNL1 overexpression in combination with both P4 and GDB treatment decreased IRS-1^{pS612} phosphorylation compared with P4 and GDP MOCK cells by 23.62% (p=0.0228) and by 31.375% (p=0.0305), respectively (Figure 5B). In addition, Akt-1 expression was unaltered under any treatments (Figure 5C). P4 and GDB treatments decreased the phosphorylation of Akt-1^{pS473} by 21.33% (p=0.0034) and 17.66% (p=0.089), respectively, indicating the successful establishment of an insulin-resistant model (Figure 5D). Upon SMTNL1 overexpression, Akt-1^{pS473} phosphorylation was elevated by 57.33% (p=0.0110) and by 53% (p=0.0209) in the P4 and GBD groups, compared with the corresponding MOCK-transfected groups, respectively (Figure 5D).

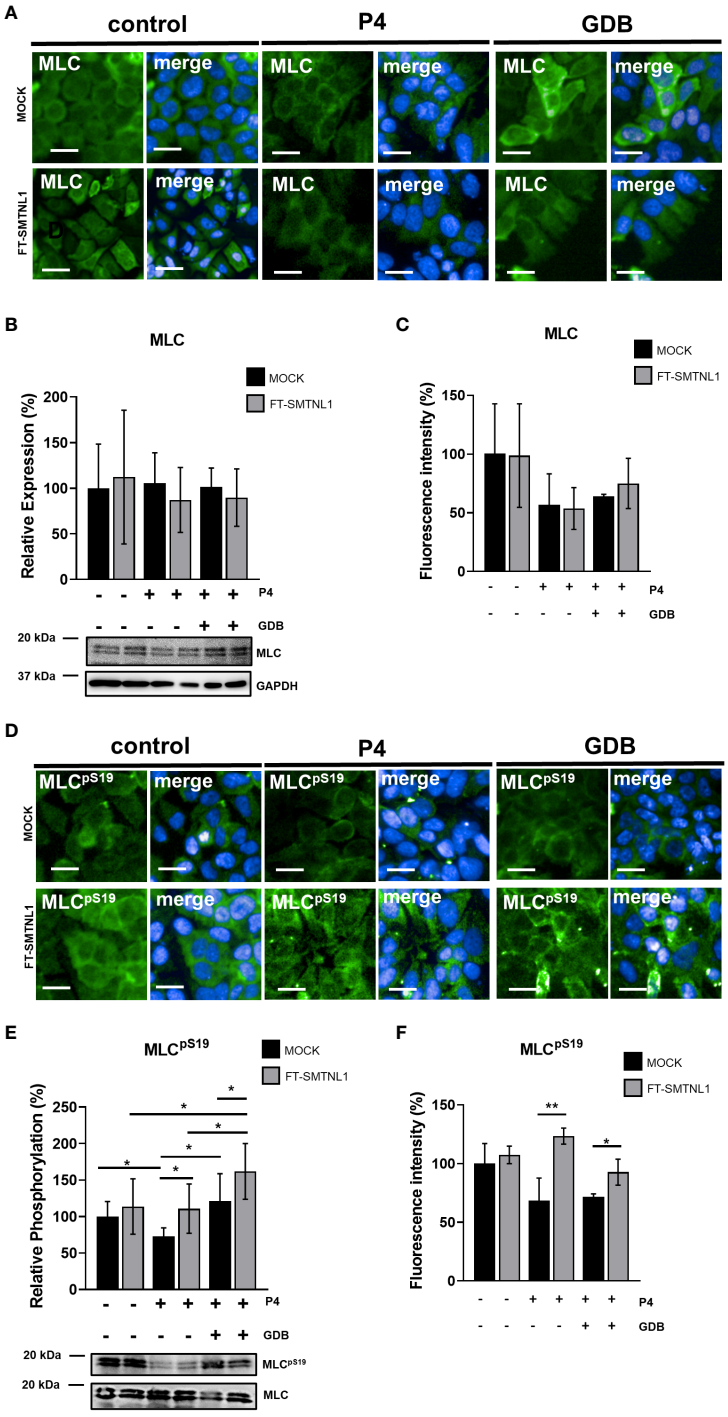


FIGURE 3
Effect of SMTNL1 on the regulatory 20kDa myosin light chain phosphorylation. Ishikawa cells were transfected with empty vector (MOCK) or FT-SMTNL1 in each of control, progesterone (P4) and insulin resistant (gestational diabetes; GDB) treatments. Immunofluorescent staining was conducted using antibodies against anti-MLC **(A)** and anti-MLCpS19 **(D)** detected with Alexa 488 fluorophore (green). Nuclei were stained by DAPI (blue). Pictures were captured by Opera Phoenix™ high-content screening microscopy. Scale bar: 20 µm. The intensity of Alexa 488 Fluorophore labelling anti-MLC **(C)** and anti-MLCp^{S19} **(F)** primary antibodies have been measured, by built in intelligent software of high content screening instrument. Data was normalized to cell number obtained from nuclei number stained with DAPI. Protein samples from whole-cell lysates were analyzed using Western blot with anti-MLC **(B)**, anti-MLCpS19 antibodies **(E)**. Values represent n =5–8, mean ± SD. Data represents the ratio of control MOCK group taken as 100%. Two groups were compared by unpaired two-tailed t-test, and four groups or more were compared by two-way ANOVA, where: $p < 0.05$ (*) and $p < 0.01$ (**).

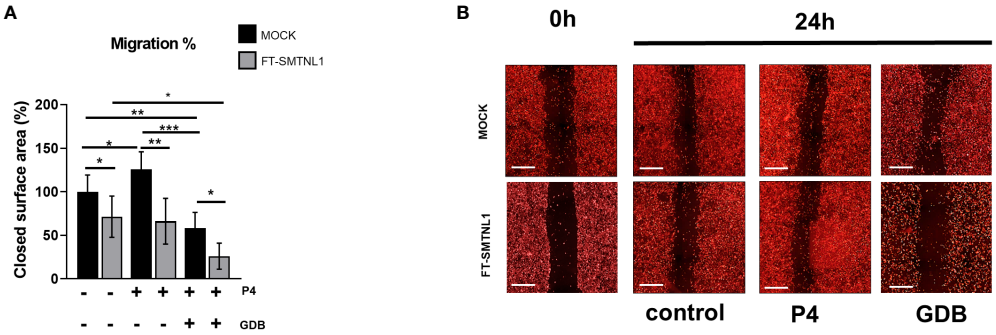


FIGURE 4
SMTNL1 hampers the migration capacity of endometrial epithelial cells. Scratch assay of DiD fluorescent dye-labeled Ishikawa cells transfected with either empty vector (MOCK) or FT-SMTNL1 and maintained in control, progesterone (P4), or gestational diabetes (GDB) environment. After 48 hours of treatment cells were scratched and were grown for an additional 24 h. Surface area of the closed territory was analyzed, and values were normalized and expressed as the ratio of the control MOCK group. Data was plotted as bar charts, where each column represents n=4-9, mean ± SD. Two groups were compared by unpaired two-tailed t-test, and four groups or more were compared by two-way ANOVA, where: p< 0.05 (*), p<0.01 (**) and p<0.0001 (***). **(A)** Photos of scratch areas were taken at the indicated times. Scale bars: 500 μm **(B)**.

Collectively, these data demonstrated that pregnancy and hyperinsulinemia/hyperglycemia modeling gestational diabetes induced insulin resistance, and the overexpression of SMTNL1 attenuated this effect.

3.6 SMTNL1 regulates MAPK kinases and phosphatases to influence insulin resistance

The effects of SMTNL1 on potential upstream regulators of insulin signaling were examined. Effector proteins of the insulin signaling pathway are regulated through a complex signaling cascade. MAPKs are significantly altered in insulin resistance and ERK1/2 regulates IRS-1 phosphorylation at Ser612. Thus, we investigated the expression and activity of ERK1/2 in MOCK and SMTNL1-transfected Ishikawa cells under control, P4, and GDB conditions. We evaluated the effects of SMTNL1 overexpression on ERK1/2 and the upstream regulator of ERK1/2 activity, nPKCε. No changes in ERK1/2 expression were detected under any experimental condition (Figure 6A). However, the activating phosphorylation of ERK1/2 at Thr202/Tyr204 increased by 184.33% (p=0.0337) and 158.67% (p=0.0369) in the MOCK GDB group compared with the control MOCK and P4 MOCK groups, respectively. The elevated ERK1/2 phosphorylation was attenuated by 153% (p=0.0451) in the FT-SMTNL1 GDB group compared to the MOCK GDB group (Figure 6B).

The expression of potent regulators of ERK1/2 activity was evaluated. Novel PKCε contributes to phosphorylation and activation of ERK1/2 MAPK by elevating ERK1/2 phosphorylation. Similarly to ERK1/2 activity, the GDB environment increased nPKCε activity by 46.125% (p=0.059) compared to the MOCK control, and nPKCε expression was reduced by 67.125% (p=0.0190) in response to SMTNL1 overexpression in GDB environment (Figure 6C). Further elements that contribute to the regulation of ERK1/2 by decreasing its activating phosphorylation site are protein phosphatase 2A (PP2A) and dual-specific phosphatase 9 (DUSP9). The expression of PP2A, a Ser/Thr protein phosphatase dephosphorylating ERK1/2, was elevated by 68.67% (p=0.0420) in response to P4. In addition, the PP2A level was increased by 131.33% (p=0.0180) in response to SMTNL1 overexpression in the GDB group compared to the GDB MOCK control group (Figure 6D). Comparing FT-SMTNL1 overexpressed groups the control group shown a decrement by 118.75% (p=0.0228) compared with the GDB SMTNL1 overexpressed group, regarding PP2A expression. Expression of the DUSP9, another potential regulator of ERK1/2, was enhanced by 346,66% (p=0.0104) in the GDB environment, and by 208,17% (p=0.0231) in P4 treatment upon SMTNL1 transfection (Figure 6E). Comparing the SMTNL1 overexpressed groups there was an elevation of DUSP9 expression by 279% (p=0.0443) comparing control and GDB samples. Our data suggests that SMTNL1 can attenuate the activity of ERK1/2 MAPK indirectly by decreasing the expression of nPKCε and increasing the expression of PP2A and DUSP9 in insulin-resistant endometrial epithelial cells.

To clarify that the MAPK pathway assumed by us really affects IRS-1, we used the selective inhibitor of ERK1/2, U0126. Based on our results, without any change in the expression of ERK1/2 (Supplementary Figure S5A), the phosphorylation of ERK1/2$^{pT202/Y204}$ decreased under all conditions with U0126 inhibition (Supplementary Figure S5B). In parallel with the inhibition of ERK1/2, the phosphorylation of IRS-1^{pS612} decreased (Supplementary Figures S5C, D), and the glucose uptake measured by the NBGD assay increased in parallel (Supplementary Figure S5E), which clearly proves the insulin-sensitizing role of ERK1/2 inhibition.

3.7 SMTNL1 promotes progesterone-dependent glycogen storage and glucose uptake in endometrial epithelial cells

The requirement for excess glycogen storage is crucial for uterine endometrium homeostasis. SMTNL1 promotes glycogen synthesis and supports essential functional changes during endometrial differentiation. To validate the effects of SMTNL1 on glycogen storage, glucose metabolic status was assessed in Ishikawa

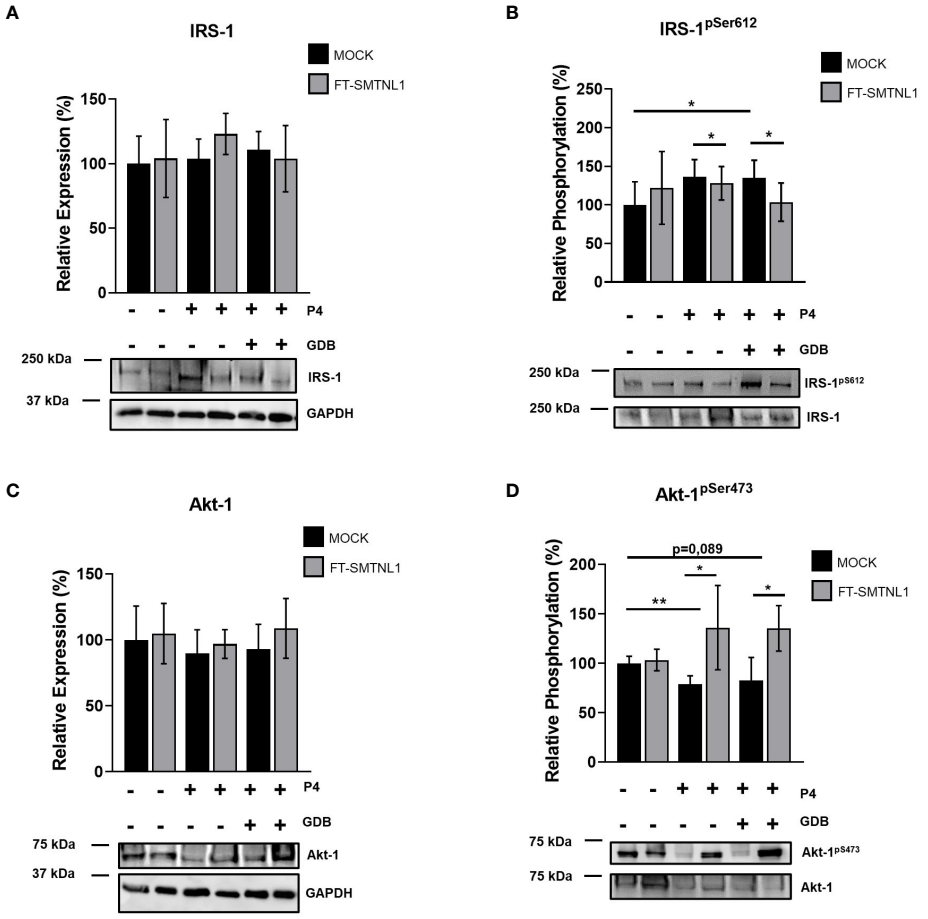


FIGURE 5
SMTNL1 overexpression affects the phosphorylation of insulin receptor substrate 1 and Akt-1 in Ishikawa cells. Empty vector (MOCK) or FT-SMTNL1-transfected Ishikawa cells were cultured under control, control pregnant (P4), or gestational diabetes (GDB) environments. Proteins were separated by SDS-PAGE followed by Western blot analysis using anti-IRS-1 **(A)**, anti-IRS-1pS612 **(B)**, anti-Akt-1 **(C)**, and anti-Akt-1pS473 antibodies **(D)**. Values represent n=3–8, mean +/- SD, expressed as the ratio of the control MOCK group. Two groups were compared by unpaired two-tailed t-test, and four groups or more were compared by two-way ANOVA, where: p< 0.05 (*) and p<0.01 (**).

cells in control, P4, and GDB conditions, with or without SMTNL1 overexpression (Figure 7A). SMTNL1 transfection significantly increased glycogen content in the P4 and GDB groups by 52,5% (p=0.0002) and by 44.55% (p=0.0024) compared to the corresponding MOCK controls, respectively. Glycogen storage was decreased in the P4 and GDB environments in Ishikawa cells by 32.5% (p=0.0091) and 61.25% (p<0.0001), in MOCK-transfected samples compared to untreated MOCK samples, respectively. GDB treatment reduced the glycogen content by 28.75% (p=0.01) compared to P4 MOCK. Comparing SMTNL1 overexpressing samples, a 36.67% (p=0.0226) decrease in glycogen content was detectable in GDB group compared to values of P4 treatment. The depletion of glycogen content in the P4 group corresponds to a physiological phenomenon; pregnant women also show mild signs of insulin resistance during pregnancy. The even more pronounced depletion of glycogen storage in the GDB group is due to the hyperglycemic-hyperinsulinemic environment. Glycogen depletion in both the P4 and GDB groups was restored by expressing FT-SMTNL1. Thus, SMTNL-1 exhibits a potent insulin-sensitizing effect in both the P4 and GDB conditions (Figure 7A).

To further evaluate the effects of SMTNL1 on glucose homeostasis in endometrial epithelial cells, 2-NDBG glucose uptake was measured. Ishikawa cells were incubated with 2-NDBG glucose for 1 hour, and the utilized glucose content was quantified by the 2-NDBG fluorescence intensity. SMTNL1 significantly increased glucose uptake in Ishikawa cells (Figure 7B) by 59.13% (p=0.0459) and 92.47% (p=0.0037) in the P4 and GDB environments, compared with their corresponding MOCK groups, respectively. The amount of utilized glucose decreased by 41.33% (p=0.0376) and 76.67% (p=0.0125) in the P4 MOCK and GDB MOCK transfected groups compared with the control MOCK group, respectively. GDB treated group show a decreased uptake of 2-NDBG glucose compared with P4 MOCK group by a decrement of 33.34% (p=0.0127). The downregulation of glucose uptake in response to P4 and GDB and the elevation of glucose uptake upon FT-SMTNL1 overexpression correlates with the glycogen storage results (Figures 7A, B), indicating that SMTNL1 sensitized the cells to insulin. Regarding expression of Glut4 transporter, neither of the applied treatments evoked significant change in the expression of the protein (Supplementary Figure S4A), hence the indicated change in the glycogen storage and

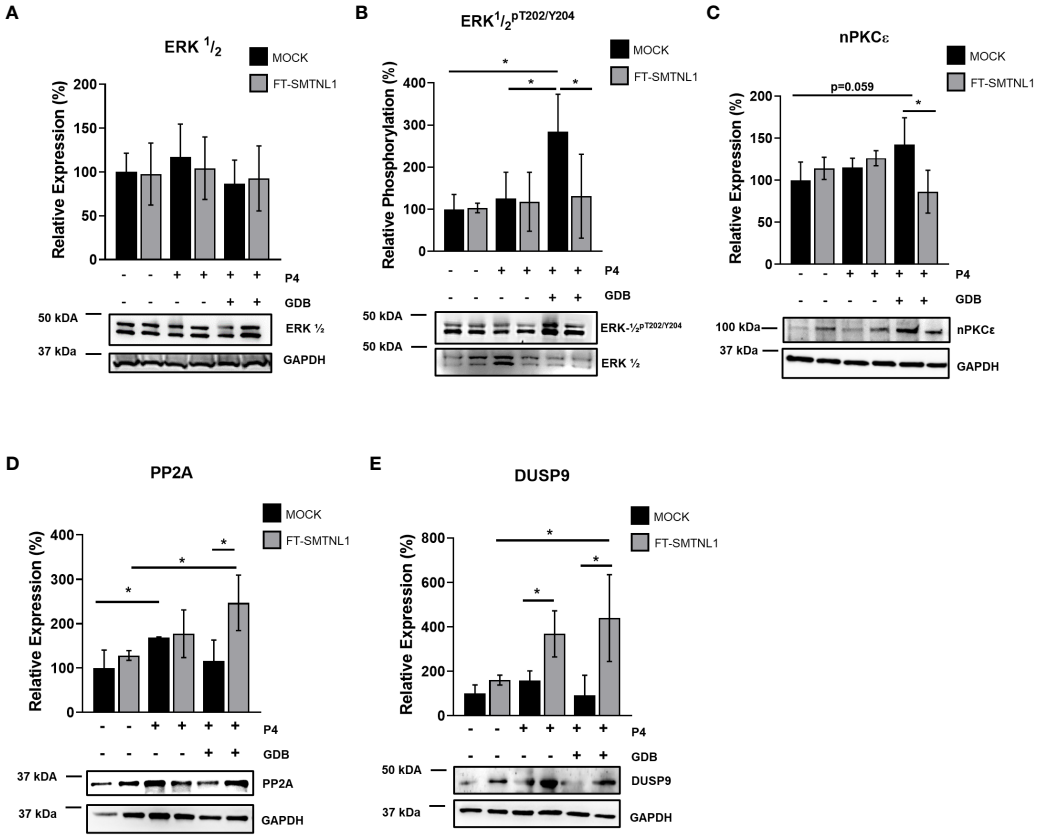


FIGURE 6
SMTNL1 overexpression affects ERK1/2 phosphorylation by regulating PP2A and DUSP9 expression in Ishikawa cells. Empty vector (MOCK) or FT-transfected Ishikawa cells were cultured in either control, control pregnant (P4), or gestational diabetes (GDB) environments. Proteins were separated by SDS-PAGE followed by Western blot analysis using anti-ERK½ **(A)**, anti-ERK ½ pT202/Y204 **(B)**, anti-nPKCε **(C)**, anti-PP2A **(D)**, and anti-DUSP9 **(E)**. Values represent n=3–7, mean +/- SD, expressed as the ratio of control MOCK group, which was considered 100%. Two groups were compared by unpaired two-tailed t-test, and four groups or more were compared by two-way ANOVA, where: $p < 0.05$ (*).

the 2-NDBG uptake might be regarded to the altered localization of the transporter, which is caused by the FT-SMTNL1 overexpression.

4 Discussion

The importance of endometrial epithelial cells in the initial stages of embryo implantation and uterine growth has been well established. Endometrial cells provide the first contact site for blastocysts (21). Both the synchronized dialogue between epithelial cells and blastocyst and the homeostasis and differentiation of endometrial cells are crucial. Dysfunctional or defective epithelium may result in reproductive failure. However, the pathomechanisms of accompanying disorders, such as insulin resistance and gestational diabetes, are unclear. We hypothesized that one of the major orchestrating hormone-dependent proteins is SMTNL1. SMTNL1 KO animals exhibit a defective reproductive phenotype with high embryonal lethality, low embryo numbers after implantation, and longer intervals between pregnancies compared to WT littermates. In addition, SMTNL1 KO mice exhibit a gestational insulin-resistant phenotype, indicating crosstalk between signaling pathways regulated by SMTNL1.

In the present study, we used Ishikawa cells, a well-described cellular model of endometrial cells derived from a human endometrial epithelial adenocarcinoma (18, 22). Ishikawa cells represent the luminal epithelium on the surface of the uterine cavity and the glandular epithelium, which makes up the tubular glands and reaches deeply into the endometrial stroma (23). Control and MOCK transfected Ishikawa cells appear botryoidal, with polygonal and pleomorphic features, irregularly shaped nuclei, and small prominent nucleoli with high nuclei/cytoplasmic ratio, as observed in previous studies (23). The addition of progesterone triggers differentiation, with lower cell count and enlarged cells with small vacuoles and pleomorphic nuclei. The hyperglycemic state with progesterone prevented the morphological transformation of Ishikawa cells, and the cuboidal structure was maintained (Figure 1). This is in line with previous publications showing that changes in the luminal surface of rat endometrium in response to progesterone and estradiol are progressive, leading to the formation of dense microvilli and numerous droplets (24). Interestingly, the overexpression of SMTNL1 initiated the differentiation of endometrial cells, and these changes were more prominent in the presence of progesterone. Strikingly, elevated SMTNL1 rescued the differentiation arrest of Ishikawa cells in GDB environment and promoted morphological changes. Differentiation was assessed by

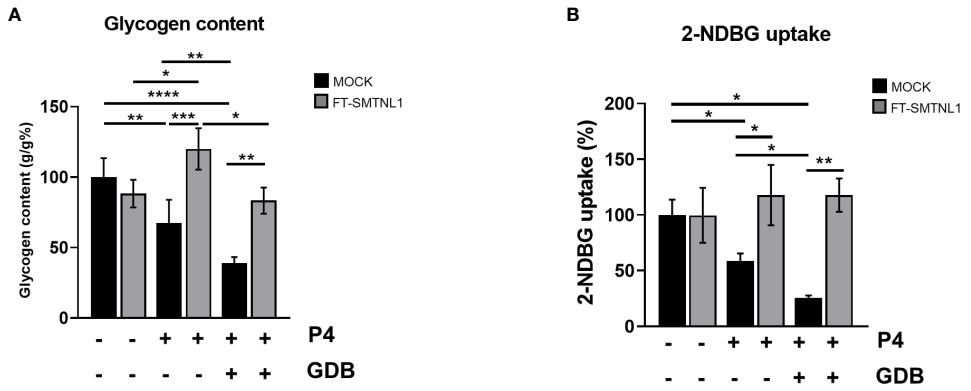


FIGURE 7
SMTNL1 facilitates glucose uptake and glycogen storage of Ishikawa cells. Glycogen content of control/P4/GDB treated Ishikawa cells were normalized to protein concentration. Control MOCK group value was taken as 100% and all other all other values were compared to that and expressed as ratio. Data are displayed as bar charts, values represent n=3-9 mean +/- SD. Groups were compared by two-tailed t-test. Bars represent n=3, mean +/- SD. p< 0.05 (*), p<0.01 (**), p<0.001 (***) and p<0.0001 (****) **(A)**. 2-NDBG glucose uptake of Ishikawa cells were assessed in control, progesterone (P4), and gestational diabetes (GDB) conditions with or without SMTNL1 overexpression. Values were normalized and expressed as the ratio of the control MOCK group, which was considered 100%. Bars represent n=3, mean +/- SD. Two groups were compared by unpaired two-tailed t-test, and four groups or more were compared by two-way ANOVA, where: p< 0.05 (*) and p<0.01 (**) **(B)**.

measuring the gene expression of MUC-1, a differentiation marker. MUC-1 may also be a fertility and differentiation marker during the implantation period of the female cycle and its timely activation and inhibition is vital (1, 25) (Supplementary Figure S6).

To determine the mechanism for the cytoskeletal changes elicited by SMTNL1, SMTNL1-dependent enzymes regulating cell motility and shape were investigated. Our data suggests that SMTNL1 reduces the expression of MYPT1, the regulatory subunit of MP, in the presence of progesterone, and these changes are more prominent in the presence of progesterone and hyperglycemia (Figure 2A). MYPT1 expression decreased significantly in response to SMTNL1 overexpression in endometrial epithelial cells. This result is in line with a previous study showing that SMTNL1 downregulates MYPT1 gene expression in skeletal muscle and the smooth muscle of the thoracic aorta and uterus (15).

The major target of MP is non-muscle myosin, which plays crucial roles in processes requiring cellular remodeling, differentiation, movement, cell adhesion, cell migration, morphogenesis, and development via actin cross-linking and contractile functions (26). Based on our data and studies in murine endometrial tissues (27), we suggest that the role of MP is inevitable in endometrial epithelial cells and MYPT1 is the major isoform in the MP present in Ishikawa cells (28). In addition, SMTNL1 can inhibit MP activity in both smooth muscle (12) and endometrial epithelial cells by altering MYPT1 expression, which affects MLC20 phosphorylation (Figures 2A, 3C).

SMTNL1 negatively influences the migration of endometrial epithelial cells; SMTNL1 overexpression decreases MP activity and increases the phosphorylation of MLC20 (Figures 2A, C, 3C), especially in the P4 and GDB models. This finding is in agreement with a previous study showing that SMTNL1 overexpression in C2C12 myoblasts hampers cell migration, possibly through inhibition of MP (16). Moreover, inhibition of MP also reduced cell migration in HepG2 cells (15). MP may be involved in cell body contraction and tail detachment (29, 30). One suggested mechanism is a slower turnover rate of MLC20 phosphorylation in the cell center in response to the inhibition of MP, resulting in more stable adhesive structures and, hence, a slower migration rate. Overall, our results and previous studies indicate that MP facilitates Ishikawa cell migration, and cell migration is reduced in the insulin-resistant state by SMTNL1 (Figure 4A). This finding is important because an imbalance in steroid hormones can affect epithelial integrity and the migration capacity of endometrial cells, and numerous reports have shown a correlation between steroid hormone imbalance and metabolic disorders. The expression of the diabetes-obesity syndrome in C57BL/KsJ (*db/db*) mice is accompanied by progressive cellular atrophy and dysfunction of the female reproductive tract (31), characterized by a marked depression in uterine epithelial cellular integrity (32) and decreased responsiveness to ovarian steroid hormone therapy (32, 33). In addition, obesity and insulin resistance initiate endometrial cancer formation (5–7, 34, 35).

Several lines of evidence in isolated uterine cell cultures suggest that insulin ligands and insulin receptor activity affect cellular proliferation and differentiation of endometrial cells. The metabolic consequences of endometrial hyperglycemic/hyperinsulinemia are associated with reproductive dysfunction and tissue atrophy (7). Our findings show that SMTNL1 plays a detrimental role in the insulin-related regulation of endometrial cells. IRS-1 phosphorylation at Ser612 was upregulated in the progesterone and hyperglycemic models without affecting the expression of IRS-1 (Figures 5A, B). SMTNL1 overexpression decreased the phosphorylation at Ser612, in P4 and in the GDB model. Under insulin-resistant conditions, the shift from Tyr to Ser phosphorylation of IRS-1 prevent the binding of IRS-1 to PI3K, which accounts for insulin signaling defects (36). The

phosphorylation of the Ser612 residue of IRS-1, located proximal to the regulatory Tyr residues, suppresses the insulin signaling pathway via ERK1/2 regulation. ERK1/2 activation plays a major role in maintaining insulin-induced PI3K-dependent InR (37).

In our model, ERK1/2 was phosphorylated after chronic insulin treatment and overexpression of SMTNL1 suppressed ERK1/2 activity, especially in the presence of progesterone (Figure 6B). In addition, IRS-1 Ser612 phosphorylation was reduced, likely due to SMTNL1-dependent reduction of ERK1/2 activity. We suggest that ERK1/2 exerts insulin-desensitizing effects in endometrial epithelial cells through Ser612 phosphorylation and the regulation of IRS-1, as chronic activation of ERK1/2 leads to the downregulation of GLUT4 expression and decreased insulin-induced glucose transport (38).

ERK1/2 gene expression did not change but ERK1/2 phosphorylation and, presumably, activity decreased in response to SMTNL1 overexpression. These changes are likely due to the altered expression of upstream regulators such as Ser/Thr kinases or phosphatases. PKC isoforms play a critical role in ERK1/2 regulation in the endometrium (39). PKCe expression was decreased in the skeletal muscle of SMTNL1 KO animals (13), and decreased PKCε expression suppressed ERK1/2 activity and IRS-1 Ser612 phosphorylation in C2C12 cells (14). However, PKCe expression was affected by SMTNL1 in GDB condition in Ishikawa cells (Figure 6C). Uterine MAP kinase kinases were not altered in a microarray analysis of pregnant *smtnl1* KO mice compared to WT mice (13). Thus, we investigated protein phosphatases as potential regulators. Protein phosphatase 2A (PP2A), a Ser/Thr specific protein phosphatase, is a negative regulator of ERK1/2 (37), and the expression of the catalytic subunit of PP2A increased upon progesterone treatment but the increase was eliminated in the insulin resistance model (Figure 6D). Surprisingly, SMTNL1 overexpression dramatically increased the expression and presumably the activity of PP2A (Figure 6D). This result contradicts data in skeletal muscle where PP2A expression was not regulated by SMTNL1 (14). Endometrial cell progesterone sensitivity might be the key to this phenomenon.

We also investigated the expression of another potential regulator, DUSP9, that dephosphorylates and inactivates ERK1/2 (40, 41). DUSP9 is positively regulated by SMTNL1 (13). The expression of DUSP9 was independent of progesterone but SMTNL1 overexpression in the insulin-resistant state significantly increased DUSP expression (Figure 6E). This finding is in line with previous findings showing that DUSP9 can impede insulin resistance *in vivo* in the *ob/ob* murine model by lowering blood glucose levels via dephosphorylation and inactivation of ERK1/2 (42). DUSP9 expression can be differentially modulated in an insulin-sensitive model by both the type of diet and tissue (41, 43). Finally, the fact that the treatment with the selective inhibitor of ERK1/2, U0126, had a clear insulin-sensitizing effect on both IRS-1 phosphorylation and glucose uptake. It is in line with previous findings in T lymphocytes showing the induction of glucose metabolism upon U0126 (44). It supports our hypothesis that SMTNL1 induces insulin sensitization through the inhibition of ERK1/2 by modulating PP2A and DUSP9.

Glucose uptake and glycogen content in endometrial epithelial cells were significantly lower in the hyperglycemic model combined with progesterone (Figures 7A, B). These findings agree with a previous study in *db/db* mutant diabetic mice showing that elevated systemic glucose and insulin concentrations and lower glycogen levels correlated with the severity and specificity of progressive cellular changes in uterine epithelial cells (35). In addition, insulin, but not progesterone, directly regulates glycogen synthesis through canonical acute inactivation of GSKα/β and noncanonical stimulation of GYS2 transcription in endometrial epithelial cells (45). SMTNL1 promoted glucose uptake in a progesterone-dependent manner and increased glycogen content in Ishikawa cells, compensating for insulin resistance (Figures 7A, B). This phenomenon was previously described in insulin-resistant myotubules; SMTNL1-overexpression initiated glycolysis (14) and regulated hexokinase at the gene expression level (16).

Taken together, the results of the present study indicate that the disordered proliferation of endometrial cells, which can lead to the development of endometriosis, embryonal implantation disorders, and endometrial cancer, occurs in the insulin-resistant condition. SMTNL1 acts as a unique progesterone-dependent cytoskeletal and gene expression regulator to prevent or dampen insulin resistant defects. Thus, SMTNL1 is a promising therapeutic target for drug development. SMTNL1 enhances the differentiation of endometrial epithelial cells in a progesterone-dependent manner and prevents cellular transformation during insulin resistance. SMTNL1 regulates the phosphorylation of MLC20 through inhibition of myosin phosphatase to inhibit cell migration in the insulin-resistant state in the presence of progesterone. These effects may be relevant to the treatment of endometrial dysfunction in metabolic diseases, in the treatment of endometriosis, and in the control of metastasis during the early stages of endometrial tumors. SNTNL1 may also play a role in preventing insulin resistance by contributing to progesterone-dependent insulin sensitization via decreasing Ser phosphorylation of IRS. Therefore, SMTNL1 may be a feasible therapeutic target for progesterone-dependent inhibition of endometrial epithelial cells during hyperglycemia and insulin-sensitizing endometrium in gestational diabetes or other metabolic disorders.

Data availability statement

The original contributions presented in the study are included in the article/Supplementary Material, further inquiries can be directed to the corresponding author/s.

Author contributions

IK: Data curation, Formal analysis, Investigation, Software, Validation, Writing – original draft. ÁU: Investigation, Validation, Writing – review & editing. RK: Data curation, Investigation, Writing – review & editing. FS: Investigation, Visualization, Writing – original draft. EK: Visualization, Writing

– review & editing. BL: Conceptualization, Formal analysis, Funding acquisition, Project administration, Resources, Supervision, Writing – original draft.

Funding

The author(s) declare financial support was received for the research, authorship, and/or publication of this article. Funding: This work was supported by grants from the National Research, Development and Innovation Office FK125043 and K143533 (to B. L.), the University of Debrecen, Faculty of Medicine Research Fund (1G3DBKJ0BFTK 247) for B. L. and from the EU co-financed by the European Regional Development Fund under project EFOP-3.6.2-16-2017-00006 and from the EFOP-3.6.3-VEKOP-16-2017-00009 project co-financed by EU. ÚNKP-22-3-1.

Acknowledgments

We thank Dr. Karen Uray for revising the manuscript. We also thank Andrea Docsa and Ágota Kelemenné Szántó for their technical assistance.

Conflict of interest

The authors declare that the research was conducted in the absence of any commercial or financial relationships that could be construed as a potential conflict of interest.

Publisher's note

All claims expressed in this article are solely those of the authors and do not necessarily represent those of their affiliated organizations, or those of the publisher, the editors and the reviewers. Any product that may be evaluated in this article, or claim that may be made by its manufacturer, is not guaranteed or endorsed by the publisher.

Supplementary material

The Supplementary Material for this article can be found online at: https://www.frontiersin.org/articles/10.3389/fendo.2024.1375771/full#supplementary-material

References

1. Wu F, Mao D, Liu Y, Chen X, Xu H, Li TC, et al. Localization of Mucin 1 in endometrial luminal epithelium and its expression in women with reproductive failure during implantation window. *J Mol Histol.* (2019) 50:563–72. doi: 10.1007/s10735-019-09848-6

2. Sancakli Usta C, Turan G, Hocaoglu M, Bulbul CB, Kilic K, Usta A, et al. Differential expressions of ki-67, bcl-2, and apoptosis index in endometrial cells of women with and without type II diabetes mellitus and their correlation with clinicopathological variables. *Reprod Sci.* (2021) 28:1447–56. doi: 10.1007/s43032-020-00423-z

3. Sharpe A, Morley LC, Tang T, Norman RJ, Balen AH. Metformin for ovulation induction (excluding gonadotrophins) in women with polycystic ovary syndrome. *Cochrane Database Syst Rev.* (2019) 12:CD013505. doi: 10.1002/14651858

4. Kara M, Ozcan SS, Aran T, Kara O, Yilmaz N. Evaluation of endometrial receptivity by measuring HOXA-10, HOXA-11, and leukemia inhibitory factor expression in patients with polycystic ovary syndrome. *Gynecol Minim Invasive Ther.* (2019) 8:118–22. doi: 10.4103/GMIT.GMIT_112_18

5. Dai M, Zhu XL, Liu F, Xu QY, Ge QL, Jiang SH, et al. Cholesterol synthetase DHCR24 induced by insulin aggravates cancer invasion and progesterone resistance in endometrial carcinoma. *Sci Rep.* (2017) 7:41404. doi: 10.1038/srep41404

6. Xie BY, Lv QY, Ning CC, Yang BY, Shan WW, Cheng YL, et al. TET1-GPER-PI3K/AKT pathway is involved in insulin-driven endometrial cancer cell proliferation. *Biochem Biophys Res Commun.* (2017) 482:857–62. doi: 10.1016/j.bbrc.2016.11.124

7. Wang C, Jeong K, Jiang H, Guo W, Gu C, Lu Y, et al. YAP/TAZ regulates the insulin signaling *via* IRS1/2 in endometrial cancer. *Am J Cancer Res.* (2016) 6:996–1010.

8. Galicia-Garcia U, Benito-Vicente A, Jebari S, Larrea-Sebal A, Siddiqi H, Uribe KB, et al. Pathophysiology of type 2 diabetes mellitus. *Int J Mol Sci.* (2020) 21. doi: 10.3390/ijms21176275

9. Boucher J, Kleinridders A, Kahn CR. Insulin receptor signaling in normal and insulin-resistant states. *Cold Spring Harb Perspect Biol.* (2014) 6. doi: 10.1101/cshperspect.a009191

10. Kupriyanova TA, Kandror KV. Akt-2 binds to Glut4-containing vesicles and phosphorylates their component proteins in response to insulin. *J Biol Chem.* (1999) 274:1458–64. doi: 10.1074/jbc.274.3.1458

11. Borman MA, MacDonald JA, Haystead TA. Modulation of smooth muscle contractility by CHASM, a novel member of the smoothelin family of proteins. *FEBS Lett.* (2004) 573:207–13. doi: 10.1016/j.febslet.2004.08.002

12. Lontay B, Bodoor K, Weitzel DH, Loiselle D, Fortner C, Lengyel S, et al. Smoothelin-like 1 protein regulates myosin phosphatase-targeting subunit 1 expression during sexual development and pregnancy. *J Biol Chem.* (2010) 285:29357–66. doi: 10.1074/jbc.M110.143966

13. Bodoor K, Lontay B, Safi R, Weitzel DH, Loiselle D, Wei Z, et al. Smoothelin-like 1 protein is a bifunctional regulator of the progesterone receptor during pregnancy. *J Biol Chem.* (2011) 286:31839–51. doi: 10.1074/jbc.M111.270397

14. Tamas I, Major E, Horvath D, Keller I, Ungvari A, Haystead TA, et al. Mechanisms by which smoothelin-like protein 1 reverses insulin resistance in myotubules and mice. *Mol Cell Endocrinol.* (2022) 551:111663. doi: 10.1016/j.mce.2022.111663

15. Lontay B, Bodoor K, Sipos A, Weitzel DH, Loiselle D, Safi R, et al. Pregnancy and smoothelin-like protein 1 (SMTNL1) deletion promote the switching of skeletal muscle to a glycolytic phenotype in human and mice. *J Biol Chem.* (2015) 290:17985–98. doi: 10.1074/jbc.M115.658120

16. Major E, Keller I, Horvath D, Tamas I, Erdodi F, Lontay B. Smoothelin-like protein 1 regulates the thyroid hormone-induced homeostasis and remodeling of C2C12 cells *via* the modulation of myosin phosphatase. *Int J Mol Sci.* (2021) 22. doi: 10.3390/ijms221910293

17. Major E, Gyory F, Horvath D, Keller I, Tamas I, Uray K, et al. Smoothelin-like protein 1 regulates development and metabolic transformation of skeletal muscle in hyperthyroidism. *Front Endocrinol (Lausanne).* (2021) 12:751488. doi: 10.3389/fendo.2021.751488

18. Nishida M. The Ishikawa cells from birth to the present. *Hum Cell.* (2002) 15:104–17. doi: 10.1111/huc.2002.15.issue-3

19. Ormazabal P, Romero C, Gabler F, Quest AF, Vega M. Decreased phosphorylation of Y(1)(4)caveolin-1 in endometrial tissue of polycystic ovary syndrome patients may be related with an insulin resistant state in this tissue. *Horm Metab Res.* (2013) 45:291–6.

20. Ormazabal P, Romero C, Quest AF, Vega M. Testosterone modulates the expression of molecules linked to insulin action and glucose uptake in endometrial cells. *Horm Metab Res.* (2013) 45:640–5. doi: 10.1055/s-00000025

21. Lejeune B, Van Hoeck J, Leroy F. Transmitter role of the luminal uterine epithelium in the induction of decidualization in rats. *J Reprod Fertil.* (1981) 61:235–40. doi: 10.1530/jrf.0.0610235

22. Hannan NJ, Paiva P, Dimitriadis E, Salamonsen LA. Models for study of human embryo implantation: choice of cell lines? *Biol Reprod.* (2010) 82:235–45. doi: 10.1095/biolreprod.109.077800

23. Arnold JT, Lessey BA, Seppala M, Kaufman DG. Effect of normal endometrial stroma on growth and differentiation in Ishikawa endometrial adenocarcinoma cells. *Cancer Res.* (2002) 62:79–88.

24. Stavreus-Evers A, Nikas G, Sahlin L, Eriksson H, Landgren BM. Formation of pinopodes in human endometrium is associated with the concentrations of progesterone and progesterone receptors. *Fertil Steril*. (2001) 76:782–91. doi: 10.1016/S0015-0282(01)01993-8

25. Jeschke U, Walzel H, Mylonas I, Papadopoulos P, Shabani N, Kuhn C, et al. The human endometrium expresses the glycoprotein mucin-1 and shows positive correlation for Thomsen-Friedenreich epitope expression and galectin-1 binding. *J Histochem Cytochem*. (2009) 57:871–81. doi: 10.1369/jhc.2009.952085

26. Vicente-Manzanares M, Horwitz AR. Myosin light chain mono- and di-phosphorylation differentially regulate adhesion and polarity in migrating cells. *Biochem Biophys Res Commun*. (2010) 402:537–42. doi: 10.1016/j.bbrc.2010.10.071

27. Tullio AN, Accili D, Ferrans VJ, Yu ZX, Takeda K, Grinberg A, et al. Nonmuscle myosin II-B is required for normal development of the mouse heart. *Proc Natl Acad Sci USA*. (1997) 94:12407–12. doi: 10.1073/pnas.94.23.12407

28. Yotova I, Quan P, Gaba A, Leditznig N, Pateisky P, Kurz C, et al. Raf-1 levels determine the migration rate of primary endometrial stromal cells of patients with endometriosis. *J Cell Mol Med*. (2012) 16:2127–39. doi: 10.1111/j.1582-4934.2011.01520.x

29. Totsukawa G, Wu Y, Sasaki Y, Hartshorne DJ, Yamakita Y, Yamashiro S, et al. Distinct roles of MLCK and ROCK in the regulation of membrane protrusions and focal adhesion dynamics during cell migration of fibroblasts. *J Cell Biol*. (2004) 164:427–39. doi: 10.1083/jcb.200306172

30. Ridley AJ. Rho GTPases and cell migration. *J Cell Sci*. (2001) 114:2713–22. doi: 10.1242/jcs.114.15.2713

31. Garris DR. Deciduoma growth in the ovariectomized Guinea pig: steroid hormone-mediated vascular support of endometrial differentiation. *Endocrinology*. (1988) 122:2183–90. doi: 10.1210/endo-122-5-2183

32. Garris DR. The effects of estradiol and progesterone on reproductive tract atrophy and tissue adrenergic indices in diabetic C57BL/KsJ mice. *Proc Soc Exp Biol Med*. (1990) 193:39–45. doi: 10.3181/00379727-193-42987

33. Garris DR, Coleman DL, Morgan CR. Age- and diabetes-related changes in tissue glucose uptake and estradiol accumulation in the C57BL/KsJ mouse. *Diabetes*. (1985) 34:47–52. doi: 10.2337/diabetes.34.1.47

34. Mu N, Zhu Y, Wang Y, Zhang H, Xue F. Insulin resistance: a significant risk factor of endometrial cancer. *Gynecol Oncol*. (2012) 125:751–7. doi: 10.1016/j.ygyno.2012.03.032

35. Garris DR, Garris BL. Diabetes-induced, progressive endometrial involution characterization of periluminal epithelial lipoatrophy. *Diabetes*. (2003) 52:51–8. doi: 10.2337/diabetes.52.1.51

36. Morino K, Petersen KF, Shulman GI. Molecular mechanisms of insulin resistance in humans and their potential links with mitochondrial dysfunction. *Diabetes*. (2006) 55 Suppl 2:S9–S15. doi: 10.2337/db06-S002

37. Gual P, Gremeaux T, Gonzalez T, Le Marchand-Brustel Y, Tanti JF. MAP kinases and mTOR mediate insulin-induced phosphorylation of insulin receptor substrate-1 on serine residues 307, 612 and 632. *Diabetologia*. (2003) 46:1532–42. doi: 10.1007/s00125-003-1223-4

38. Krook A, Bjornholm M, Galuska D, Jiang XJ, Fahlman R, Myers MG Jr., et al. Characterization of signal transduction and glucose transport in skeletal muscle from type 2 diabetic patients. *Diabetes*. (2000) 49:284–92. doi: 10.2337/diabetes.49.2.284

39. Haughian JM, Jackson TA, Koterwas DM, Bradford AP. Endometrial cancer cell survival and apoptosis is regulated by protein kinase C alpha and delta. *Endocr Relat Cancer*. (2006) 13:1251–67. doi: 10.1677/erc.1.01278

40. Shen Z, Zhang C, Qu L, Lu C, Xiao M, Ni R, et al. MKP-4 suppresses hepatocarcinogenesis by targeting ERK1/2 pathway. *Cancer Cell Int*. (2019) 19:61. doi: 10.1186/s12935-019-0776-3

41. Khoubai FZ, Grosset CF. DUSP9, a dual-specificity phosphatase with a key role in cell biology and human diseases. *Int J Mol Sci*. (2021) 22. doi: 10.3390/ijms222111538

42. Ye P, Xiang M, Liao H, Liu J, Luo H, Wang Y, et al. Dual-specificity phosphatase 9 protects against nonalcoholic fatty liver disease in mice through ASK1 suppression. *Hepatology*. (2019) 69:76–93. doi: 10.1002/hep.30198

43. Emanuelli B, Eberle D, Suzuki R, Kahn CR. Overexpression of the dual-specificity phosphatase MKP-4/DUSP-9 protects against stress-induced insulin resistance. *Proc Natl Acad Sci USA*. (2008) 105:3545–50. doi: 10.1073/pnas.0712275105

44. Marko AJ, Miller RA, Kelman A, Frauwirth KA. Induction of glucose metabolism in stimulated T lymphocytes is regulated by mitogen-activated protein kinase signaling. *PloS One*. (2010) 5:e15425. doi: 10.1371/journal.pone.0015425

45. Flannery CA, Choe GH, Cooke KM, Fleming AG, Radford CC, Kodaman PH, et al. Insulin regulates glycogen synthesis in human endometrial glands through increased GYS2. *J Clin Endocrinol Metab*. (2018) 103:2843–50. doi: 10.1210/jc.2017-01759

Glossary

2-NBDG	2-N-7-Nitrobenz-2-oxa-1,3-diazol-4-yl-Amino-2-Deoxyglucose
Akt1	Protein kinase B
DAPI	4′, 6-diamidino-2-phenylindole
DMEM	Dulbecco's Modified Eagle's Medium
ERK ½	Extracellular signal-regulated kinase
FBS	Fetal Bovine Serum
GDB	gestational diabetes
GLUT4	Glucose transporter type 4
HCS	High Content Screening
IR	insulin resistance
IRS-1	Insulin Receptor Substrate 1
MAPK	mitogen-activated protein kinase
MLC20	20 kDa myosin light chain
MP	myosin phosphatase
MPA	medroxy-progesterone-acetate
mTOR	Mammalian target of rapamycin
MUC-1	Mucin 1
MYPT1	myosin phosphatase target subunit 1
NEAA	Non-Essential-Amino-Acids
nPKCε	novel type protein kinase C ε
OD	17-β-oestradiol
PBS	phosphate-buffered saline
PI3K	phosphatidyl-inositol-3-kinase
PIC	Phosphatase Inhibitor Cocktail
PMSF	phenylmethylsulfonyl fluoride
P4	progesterone
PRL	prolactin
RIPA	radioimmunoprecipitation assay buffer
SD	standard deviation
SDS	sodium dodecyl-sulfate
SDS-PAGE	Sodium dodecyl-sulfate polyacrylamide gel electrophoresis
SMTNL1	Smoothelin-like protein 1.

Magnesium-dependent-protein phosphatase 1B regulates the protein arginine methyltransferase 5 through the modulation of myosin phosphatase

Received for publication, July 10, 2024, and in revised form, December 8, 2024 Published, Papers in Press, December 18, 2024,
https://doi.org/10.1016/j.jbc.2024.108107

Ilka Keller, Ádám Ungvári, Evelin Major, Dániel Horváth, Zoltán Kónya, Emese Tóth, Ferenc Erdődi, Andrea Kiss, and Beáta Lontay*

From the Department of Medical Chemistry, Faculty of Medicine, University of Debrecen, Debrecen, Hungary

Reviewed by members of the JBC Editorial Board. Edited by Philip A. Cole

Dysregulation of the expression levels and the activity of kinases/phosphatases is an intrinsic hallmark of tumor transformation and progression, as either as a primary cause or consequence. The myosin phosphatase (MP)/protein arginine methyltransferase 5 (PRMT5)/histone (H4) pathway is an oncogenic signaling pathway downregulating the gene expression of tumor suppressors. However, the upstream regulators of the pathway are unknown. We show that the Mg^{2+}-dependent protein phosphatase 1 B (PP2Cb or PPM1B) interacts and regulates MP through the MYPT1 regulatory subunit, and this interplay results in the inactivation of the tumorigenic pathway driven by PRMT5. The phospho-Thr696 inhibitory residues of the MYPT1 regulatory subunit of MP was dephosphorylated by PPM1B. The inhibition of PPM1B by sanguinarine resulted in the deactivation of MP and the increased activity of PRMT5 leading to increased symmetric dimethylation of histone H4 in HeLa cells. The overexpression of the PPM1B had the opposite action. The overexpression of PPM1B decreased the colonization activity of HeLa cells through modulation of MP. Finally, human cervical carcinoma biopsies showed almost complete elimination of PPM1B compared to their healthy control counterparts. The phosphorylation of the inhibitory $MYPT1^{pT696}$ and the regulatory $PRMT5^{pT80}$ residues and the symmetric dimethylation of H4 were elevated in the cancer biopsies and it resulted in a decrease in retinoblastoma protein expression. The results indicate a tumor suppressor role of the PPM1B/MP axis *via* inhibition of PRMT5, thereby regulating gene expression through H4 arginine dimethylation. Collectively, PPM1B is a tumor suppressor and a possible tumor marker for cervical carcinoma.

Oncogenesis is a complex process associated with accumulation of genetic and epigenetic defects and converged into aberrant regulation of intracellular and extracellular signaling pathways leading to the alteration of the transcriptional program (1). High throughput "omics" analysis of gene expression in cancer patients led to the identification of key genes and signaling pathways that drive cancer progression (2, 3). However, relatively little is known about the mechanisms that underlie the deregulation of signaling pathways in cancers.

One of the oncogenic signaling pathways is the myosin phosphatase (MP)/protein arginine methyltransferase 5 (PRMT5)/histone pathway downregulating the gene expression of tumor suppressors (4). Arginine-methylated proteins function in a number of key cellular processes required for maintenance of tissue homeostasis as well as disease phenotypes such as cancer and catalyzed by protein arginine methyltransferases (5). Methylation modifies the hydrogen bonding of the side chain of the targeted protein arginine amino acid, resulting in changes in protein function and molecular properties (5). PRMT5 is the major enzyme that catalyzes specifically symmetric dimethylation by using S-adenosylmethionine as a methyl donor (6). In human cells, PRMT5 performs its methylation activity as part of a heterooctameric methylosome enzyme complex that consists of four PRMT5 and four methylosome protein 50 (MEP50), which, in addition to stabilizing PRMT5, contributes to its activity by targeting its substrates to the holoenzyme and functions as a positive allosteric regulator (7, 8). Substrates for the enzyme include transcriptional regulators (*e.g.* tumor protein p53 (p53), E2F transcription factor 1 (E2F1), tumor protein p65 (p65), Kruppel like factor 4 (KLF4), sterol regulatory element binding protein (SREBP1) and molecules involved in signal transduction (*e.g.* epidermal growth factor receptor and platelet-derived growth factor receptor) and by symmetrically dimethylating some Sm proteins present in snRNP complexes (*e.g.* small nuclear ribonucleoprotein-associated protein B (SmB) and small nuclear ribonucleoprotein-associated protein D1 (SmD1)), thereby PRMT5 contributes to the maturation of mRNA by promoting their splicing. However, its most important substrates are histone proteins, of which it performs symmetric dimethylation on arginine 8 of H2A and arginine 3 of H3 and H4, leading to epigenetic modification and regulating the expression of several genes implicated in both tumor promotion and suppression (5). These include tumor suppressor genes (*e.g.* retinoblastoma protein (pRb), p53, protein tyrosine phosphatase B and protooncogenes (*e.g.* ras-proximate-1 (RAP), mitogen-activated protein kinase (MAPK) (9). In several types of tumors, overactivation of PRMT5 protein has

* For correspondence: Beáta Lontay, lontay@med.unideb.hu.

© 2024 THE AUTHORS. Published by Elsevier Inc on behalf of American Society for Biochemistry and Molecular Biology. This is an open access article under the CC BY-NC-ND license (http://creativecommons.org/licenses/by-nc-nd/4.0/).

tontay:beata_285_24

been described, resulting in silencing of the tumor suppressors (4, 10).

Several phosphorylation sites involved in the PRMT5 regulation have been described. These include phosphorylation of the side chains Tyr297, Tyr304, and Tyr306 by the mutant kinase janus kinase 2 (JAK2), which inhibits the formation of the methylosome complex by interfering with the interaction of PRMT5 with methylosome protein 50, thereby reducing the methylation of histone proteins. This, in turn, contributes to the development of myeloproliferative diseases (11, 12). Our group has described another phosphorylation site, Thr80, in hepatocellular carcinoma samples. The site is phosphorylated by Rho A activated kinase (ROK) and dephosphorylated by MP, the former therefore activates and the latter inhibits PRMT5 (4).

MP is a Ser/Thr specific protein phosphatase composed of protein phosphatase catalytic subunit β isoform (PP1β/δ or PPP1CB or PP1 catalytic subunit (PP1c)) and a myosin phosphatase target subunit 1 (MYPT1) regulatory subunit (MYPT1 or PPP1R12A) that determines the substrate specificity of the enzyme (13). MP is a key enzyme involved not only in the regulation of the activity of myosin in muscle contraction and cell motility, but in various cellular processes other substrates have also been identified (14). Phosphorylation of MYPT1 on Ser/Thr residues by a variety of protein Ser/Thr kinases is one of the principal regulatory mechanisms of MP's functions causing activation or inhibition of this enzyme. There are two major and well-characterized inhibitory sites in MYPT1, namely Thr696 and Thr853 (15). ROK was first identified as the kinase for the phosphorylation of both inhibitory phosphorylation sites [19], but later several other kinases including zipper-interacting protein kinase (ZIPK), integrin-linked kinase (ILK), myotonic dystrophy kinase, protooncogene serine/threonine-protein kinase (Raf-1 [20] and p21-activated protein kinases were also shown to act on Thr696 (16). Phosphorylation of MYPT1 on Thr696 or on Thr853 attenuated the activity of MP by inducing structural movements that allows the interaction of the inhibitory phosphorylated region of MYPT1 with the substrate binding groove of the catalytic center of PP1c. The role of the MYPT Thr853 phosphorylation site in the regulation of the MP holoenzyme is not clear. Some of the studies found that MYPT1 Thr853 phosphorylation does not inhibit MP activity in smooth muscle (16), while others described an equivalent effect with the phosphorylation of MYPT1 at Thr696 and found the MYPT1 Thr853 as a primary ROK phosphorylation site using a ROK-selective inhibitor (17). *Khasnis at al* suggested that the phosphorylation at Thr696 facilitated the phosphorylation at Thr853 in ileal smooth muscle (18). The phosphorylation of the two sites appears to be independent and each site is accessible to a different kinase(s) and there is also the possibility that in different cells the accessibility of these two sites to distinct kinases may vary (17, 19) but based on the contradictory data, we focused on the role of MYPT1 Thr696, the major MP regulatory site, in our study.

Since only MP and PRMT5 but not ROK, the upstream regulator of these enzymes, shows nuclear localization, the question arose as to what the upstream regulator of the MP/PRMT5/histone signal transduction pathway is. Based on our previous findings several proteins in the MYPT1 nuclear interactome have been described in addition to histone and the members of methylosome complex. Strikingly, the only MYPT1 interacting partner with catalytic activity identified by mass spectrometry analysis was Mg^{2+}/Mn^{2+} -dependent protein phosphatase 1 B isoform (PPM1B or PP2C beta isoform or PP2Cβ) (20). Therefore, we aimed to investigate the role of this PPM1B in the regulation of the oncogenic signaling regulated by PRMT5.

Results

Interaction of PPM1B with MYPT1

Initial reports have already described the presence of MP in the nucleus and its role in the regulation of gene expression through the dephosphorylation of PRMT5 (4, 14). However, there is no information about the upstream regulators of MP in the nucleus. One of the candidates is the Mg^{2+}/Mn^{2+}-dependent protein phosphatase 1B (PPM1B) but its exact function and correlation to the MP/PRMT5/histone proto-oncogene axis remained unknown. PPM1B was reported as an interacting protein of MYPT1 when GST-MYPT1 pull-down fraction was analyzed by mass spectrometry [20], and it was the only potential MYPT1 regulating enzyme in the MYPT1-interactome. Our goal was to further support our omics-related data on the interaction between PPM1B and the MYPT1 subunit, and we carried out reciprocal immunoprecipitations (Fig. 1*A*), pull-down assays (Fig. 1*B*), and Duolink proximity ligation assay (Fig. 1*C*).

First, an immunoprecipitation assay was conducted by using FT-PPM1B and FT-MYPT1 overexpressing tsA201 cell lysates with anti-MYPT1 and anti-PPM1B antibodies. MYPT1 and PPM1B were coprecipitated and the interaction was documented in the PPM1B precipitate; however, PPM1B was also presented in the FT-MYPT1 precipitate. Protein A sepharose (PAS) bead crosslinked with anti-MYPT1 coprecipitate both MYPT1 and PPM1B, but PAS bead cross-linked with PPM1B antibody did not presented binding of MYPT1, which might be explained by the overlap of the PPM1B binding region of MYPT1 with the anti-MYPT1 antibody epitope. Since the Mg^{2+}/Mn^{2+}-dependent protein phosphatase 1 A (PPM1A) shows the highest sequence homology with PPM1B, and one out of the six identified peptides in the MYPT1 interactome presented 100% homology with PPM1A isoform, we also assayed the immunoprecipitate for PPM1A (Fig. 1*A*). Based on our result, although all the investigated proteins were present in the input lysates, PPM1A did not show protein-protein interaction with MYPT1.

Second, to further support the interaction between PPM1B and MYPT1, pull-down assays were also carried out using GST-MYPT1 or GST (as negative control). Untransfected or FT-PPM1B overexpressed tsA201 lysates, or recombinant PP1c as positive controls were applied. The GST and GST-MYPT1 binding proteins were eluted from the Glutathione Sepharose beads, separated by SDS-PAGE and assayed by

ASBMB

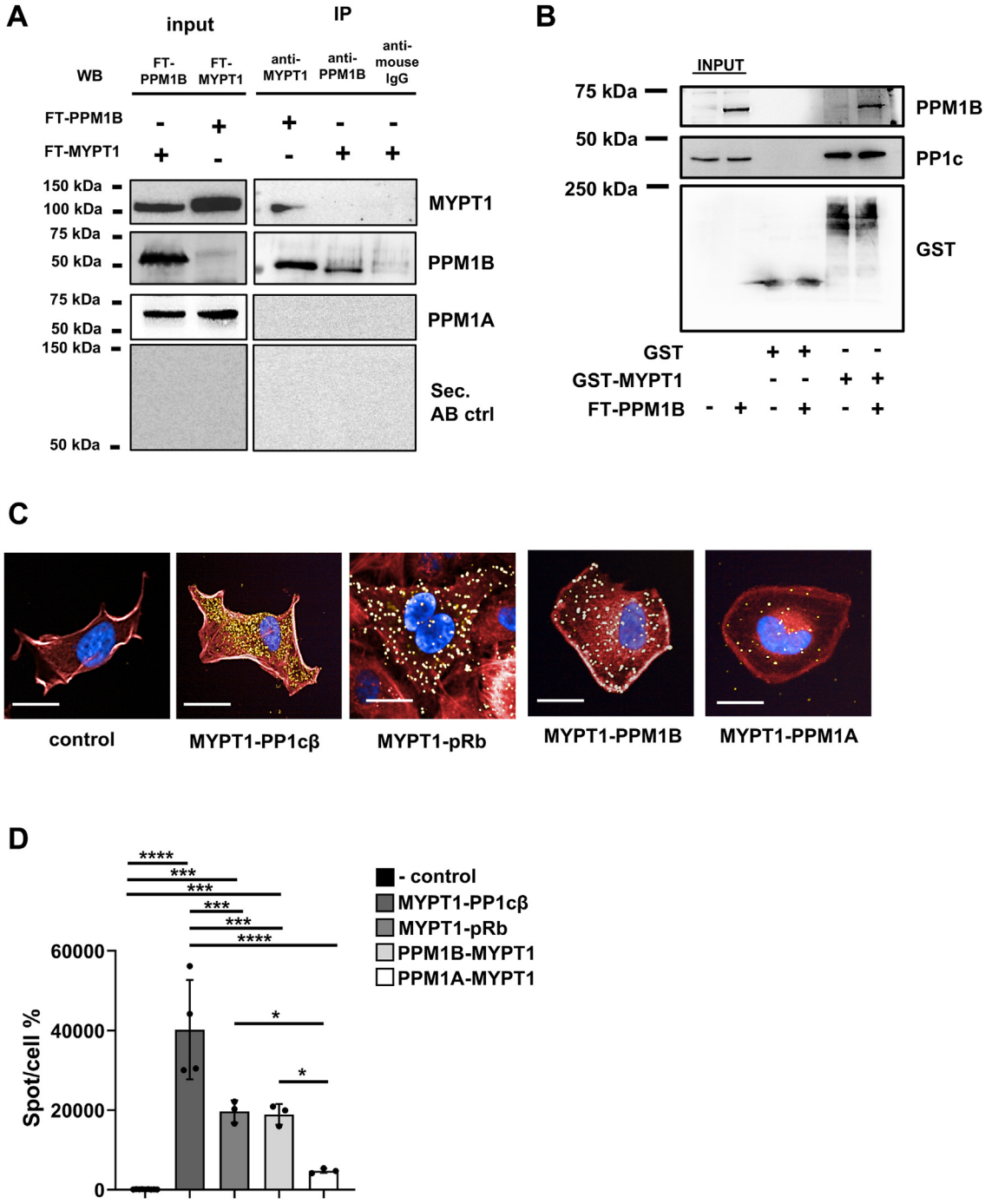


Figure 1. Protein-protein interaction of PPM1B and MYPT1. *A*, immunoprecipitation was performed from tsA201 cell lysate with antibodies specific for MYPT1 and PPM1B and coupled to Protein-A sepharose, and the precipitates were analyzed by Western blot using the indicated antibodies. *B*, pull-down of Flag-PPM1B by GST-MYPT1. GST, or GST-MYPT1 coupled glutathione-sepharose 4B beads were incubated with untransfected or Flag-PPM1B overexpressing tsA201 cell lysates. The interaction was detected by Western blot analysis using anti-GST and anti-Flag antibodies. PP1cβ was identified as a positive control using anti-PP1c antibody. *C*, quantitative analysis of MYPT1 and PPM1B interactions evaluated by Duolink protein-protein interaction assay. Antibodies against the retinoblastoma protein (pRb) were applied as positive control. Interaction of MYPT1 was assayed with PPM1A antibody, as well. F-actin was stained by Alexa688 Phalloidin (*red*), nuclei were visualized by DAPI (*blue*). Protein-protein interaction is indicated as a *yellow* signal. The scale bar represents 10 μm. *D*, bars represent spots/cell. Negative control group value was taken as a 100%, and all other groups are expressed as a ratio. Values represents mean ± SD; n = 3 to 9; groups were compared by one way ANOVA followed by Tukey *post hoc* test, where (*) $p < 0.05$, $p < 0.01$ (**), $p < 0.001$ (***) and $p \leq 0.0001$ (****).DAPI, 4′,6-diamidino-2-phenylindole; MYPT1: myosin phosphatase target subunit 1, PPM1B: protein phosphatase, Mg^{2+}/Mn^{2+} -dependent 1 B or PP2Cβ.

Western blot analysis using antibodies against GST, PP1c, and PPM1B. GST-MYPT1 but no GST showed interaction with PPM1B and the interaction between the subunits of MP, namely PP1c and MYPT1 was verified (Fig. 1*B*). Third, the interaction of PPM1B with MYPT1 was analyzed in HeLa human cervical carcinoma cells by Duolink proximity ligation assay (PLA) (Fig. 1, *C* and *D*). Samples labeled with anti-MYPT1 and anti-PP1β antibodies (specific for PP1β catalytic

tontay:beata_285_24

subunit of MP) served as positive control showing the interaction of the holoenzyme. We also presented the interaction between MYPT1 and its already known interacting partner and the substrate of MP, the pRb as another positive control. For investigating PPM1B-MYPT1 interaction, samples were incubated with anti-MYPT1 and anti-PPM1B antibodies, while unlabeled group acted as negative control (Fig. 1*C*). The negative control spot number normalized to cell number was considered as 100%, to which we compared the values of interaction between PP1c and MYPT1, pRb, and MYPT1, as well as PPM1B and MYPT1. The analysis proved the mutual and strong interaction between the subunits of the MP holoenzyme and revealed a significant number of interactions per cell between not only the pRb (the substrate of MP) and MYPT1 (p = 0.0004) but also between PPM1B and MYPT1 (p = 0.0006) in total cell area compared to negative control (Fig. 1*D*). To elucidate the difference in the interaction between MYPT1 and PPM1B and MYPT1 and PPM1A, an interaction group labeled with anti-MYPT1 and anti-PPM1A antibodies were also established, which shown no significant spot number per cell compared to negative control group (p =) (Fig. 1*D*). In addition, the degree of interaction between PPM1A and MYPT1 was significantly lower (p = 0.0363) compared to the PPM1B-MYPT1 interaction. We found no difference in the spot number per cell between the PPM1A-MYPT1 group compared to the negative control (p = 0.7012) (Fig. 1*D*) All these data verify the interaction between MYPT1 and PPM1B and indicate their localization and interaction not exclusively in the nucleus but in the cytoplasm, as well.

MP is the substrate of PPM1B

To prove the regulatory role of PPM1B on MP through the regulation of its MYPT1 subunit, GST-MYPT1 was phosphorylated by ROK, and *in vitro* phosphatase assay was carried out using recombinant PPM1B (Fig. 2*A*). Western blot data using anti-MYPT1^{pT696} showed that ROK successfully phosphorylated the inhibitory sites, and the relative phosphorylation of Thr696 residues increased by 8.61-fold (p = 0.0004) compared to GST-MYPT1 group. Addition of recombinant, purified, enzymatically active PPM1B caused a substantial decrease in the phosphorylation of MYPT^{pT696} and from a relative value 1.99 to 0.404 (p = 0.0031) (4.8-fold decrease) indicating that phospho-MYPT1 is a substrate of PPM1B. To assess the PPM1B activity sanguinarine (SNG)-dependency, we completed our phosphatase assay with or without the addition of 1 μM SNG to the assay. The phosphorylation of MYPT1 at the Thr696 inhibitory residues showed 2.76-fold (p = 0.0062) elevation compared to ROK and PPM1B-treated samples. The Thr696 phosphorylation level of SNG treated samples was significantly different from only the ROK-phosphorylated ones. To investigate the Mn^{2+}/Mg^{2+} ion dependency of PPM1B, we repeated the experiments without Mn^{2+} and Mg^{2+} ions. The phosphorylation of MYPT1 at Thr696 increased 2.738-fold (p = 0.006) compared to ROK- and PPM1B-treated group. The MP activity in HeLa cell lysates was quantified upon PPM1B inhibition using SNG that is a plant benzo(c)phenanthridine alkaloid, which was identified as a potent and specific inhibitor of PPM1 enzymes (21). SNG was applied on cell culture system since there is no commercially available PPM1B-specific inhibitor and it was

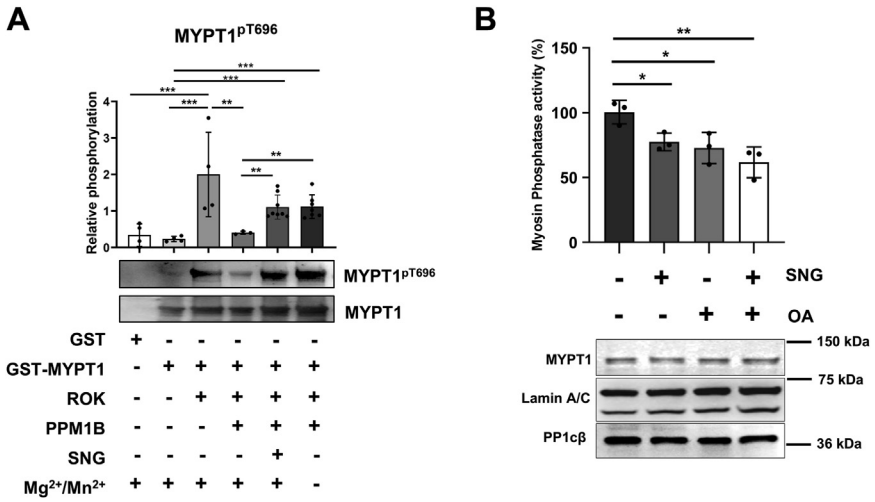


Figure 2. PPM1B activates MP by dephosphorylating Thr696 and Thr853 inhibitory phosphorylation of MYPT1. Purified GST or GST-MYPT1 were coupled with glutathione-sepharose 4B beads. Resin-bound GST-MYPT1 was phosphorylated by ROK, and then incubated with PPM1B in the presence of Mg^{2+} and Mn^{2+} ions, or Mg^{2+} and Mn^{2+} ions plus 1 μM sanguinarine, or in the absence of Mg^{2+} and Mn^{2+}. Phosphorylation of GST-MYPT1 was tested by Western blot using anti-MYPT1-^{pT696} antibody (*A*). The amount of GST-MYPT1 in each sample was detected by anti-MYPT1 antibody. Multiple columns were compared by one-way ANOVA followed by Tukey *post hoc* test, two columns were compared by unpaired two-tailed *t* test, where $p < 0.05$ (*), $p < 0.01$ (**) and $p < 0.001$ (***).Columns represent mean ± SD, n = 3 to 11. *B*, HeLa cells were treated with 1 μM SNG or 50 nM OA, or with their combination. Myosin phosphatase activity was assessed using 1 μM ^{32}P-myosin substrate. The liberated $^{32}P_i$ of the samples were measured and normalized to the MYPT1 protein content calculated by a calibration curve using GST-MYPT1 recombinant protein and displayed as percent values of the control counts (100%). Values represent mean ± SD; n = 3. Groups were compared using one way ANOVA followed by Tukey *post hoc* test, where $p < 0.05$ (*) and $p < 0.01$ (**). Cell lysates were assessed by Western blot analysis for MYPT1, PP1cβ, and lamin A/C as loading control. MP, myosin phosphatase; MYPT1: myosin phosphatase target subunit 1; OA, okadaic acid; PP1c, PP1 catalytic subunit; PPM1B: protein phosphatase, Mg^{2+}/Mn^{2+} -dependent 1 B or PP2Cβ; ROK, Rho A activated kinase; SNG, sanguinarine.

widely applied for the inhibition of PPM1B. *Yu et al., 2020* (22), showed that 4 μM SNG treatment for 24 h significantly inhibited cell proliferation and promoted apoptosis of THP-1 cells. *Aburai et al., 2010* (21), also showed an increased caspase 3/7 activity upon 1 μM SNG treatment even after 6 h. Therefore, it was necessary to conduct experiments on the effect of SNG on HeLa cells. Fig. S2*A* shows a 11.42% (p = 0.0105) reduction in the viability of HeLa cells upon 1 μM SNG treatment for 60 min by Alamar Blue assay.

Phosphatase activity in the HeLa lysates was assayed using gizzard ^{32}P-myosin as substrate (23) (Fig. 2*B*). Previously, it was shown that MYPT1 dramatically increases the activity of PP1c toward phosphorylated myosin and it is accepted that smooth muscle myosin (or heavy-meromyosin) is effectively dephosphorylated only by the MP holoenzyme in cell lysates or tissue extracts (24). Therefore, assays conducted using ^{32}P-myosin should reflect only the MP activity. In our assay, none of the subunits of the MP holoenzyme showed a change in the protein content (Fig. 1*B* immunoblots). Fig. 2*B*. illustrates that upon inhibition of PPM1 with SNG the MP activity, that was normalized to the MYPT1 content of the cell lysate, decreased by 23% (p = 0.02) compared to the control untreated samples indicating the involvement of PPM1B in the regulation of MP activity. Treatments with okadaic acid (OA), the potent protein phosphatase 1 and 2A inhibitor toxin, induced a 29% reduction (p = 0.04) in the total MP activity in HeLa cells and the combined application of the inhibitors appeared to be additive showing a 40% decrease (p = 0.007) compared to the untreated control. Briefly, 50 nM OA only inhibits protein phosphatase-2A (PP2A), and PP1 is not influenced (25), and PP1 activity in cells was not affected even with 1 μM OA (26). Therefore, we assume that the MP holoenzyme, containing PP1c is not influenced directly but indirectly through other phosphatase such as protein phosphatase-2A (PP2A) and PPM1B dephosphorylating the MYPT1 subunit.

PPM1B inhibition results in increased phosphorylation of the MYPT1 inhibitory phosphorylation sites in the subcellular fractions of HeLa cells

To validate the *in vivo* regulatory effect of PPM1B on MP, HeLa cells were treated with 1 μM SNG to inhibit the activity of PPM1B. Since the interaction was suggested to be mainly nuclear, subcellular fractions of the vehicle and SNG-treated cells were generated to gain total cell lysate, cytoplasmatic, and nuclear fractions. Furthermore, to exclude the effect of SNG on the PPM1B expression and localization, total cell lysate, nuclear and cytosolic fractions of HeLa cells were prepared with or without SNG treatment, and significant changes in the expression was not observed in any experimental condition either by Western blot analysis in subcellular fractions (Fig. S2*B*) or by immunofluorescent staining (Fig. S2*C*). The purity of the fractions was validated in each case by tubulin and lamin A/C as cytoplasmic and nuclear markers, respectively. Based on our results, SNG did not affect PPM1B expression and localization in HeLa cells. The effect of 1 μM SNG was also assessed by semiquantitative Western blot analysis. SNG had no effect on the expression of MYPT1 but elevated the amount of nuclear MYPT1 by 1.58-fold (p = 0.0233) suggesting the translocation of the enzyme into the nucleus upon PPM1B inhibition (Fig. 3*A*). This effect was also verified by immunofluorescent staining (Fig. 3*B*) where MYPT1 was present with a higher intensity in the 4′,6-diamidino-2-phenylindole (DAPI) labeled area of HeLa cells. We also investigated the phosphorylation of the T696 residue of MYPT1 (Fig. 3*C*), and it was elevated upon SNG-treatment in the total lysates by 2.048-fold (p = 0.0119). The nuclear phosphorylation was significantly elevated at MYPT1^{pT696} upon SNG treatment by 2.137-fold (p = 0.0201) (Fig. 3*C*) and the MYPT1^{pT696} fluorescent staining (green) also indicates a remarkable increase specifically in the nuclei (Fig. 3*D*). Concluding these observations, we suggest the translocation of MYPT1 from the cytoplasm to the nucleus as the results of the elevated phosphorylation level on Thr696 residue because of PPM1B inhibition (Fig. 3, *A* and *C*).

PPM1B inhibition by sanguinarine affects the PRMT5 activity and the gene expression

MP is known to inhibit PRMT5 by dephosphorylating its Thr80 regulatory residue (27). We examined the effect of PPM1B inhibition by SNG on the expression and post-translational modifications of PRMT5 and its substrate H4 in HeLa cells by semiquantitative Western blot analysis (Fig. 4, *A*, *C*, *E* and *G*) and immunofluorescent staining (Fig. 4, *B*, *D*, F and H). Our data demonstrate that expression of PRMT5 was not affected in any of the investigated cell fractions (Fig. A and B), but the Thr80 phosphorylation was significantly elevated in each of the examined cellular compartments upon the SNG treatment (Fig. 4, *C* and *D*). The relative phosphorylation level of PRMT5 at Thr80 elevated in the total cell lysates, cytoplasm as well as in the nuclear fraction by 1.96-fold (p = 0.0493), 1.5-fold (p = 0.0437), and 2.36-fold (p = 0.0208), respectively compared to untreated control sample upon SNG treatment (Fig. 4, *C* and *D*). We also examined H4 expression (Fig. 4, *E* and *F*), along with its symmetrical dimethylation (Fig. 4, *G* and *H*). In correlation with our previous findings, we have perceived elevated symmetrical dimethylation in total cell lysate by 1.54-fold (p = 0.0339), and elevation by 3.25-fold in the nuclear compartment (p = 0.0035) (Fig. 4, *G* and *H*) without any changes at gene expression level (Fig. 4, *E* and *F*).

Overexpression of FT-PPM1B impedes PRMT5 activity through the activation of myosin phosphatase

Since SNG inhibits all the members of the Mg^{2+}/Mn^{2+}-dependent phosphatases (21), and there are no commercially available selective inhibitors for PPM1B, we aimed to demonstrate specific effects related to the PPM1B isoform. The specific knockdown of this isoform was challenging and biologically questionable since its expression level was already decreased or almost eliminated in many cancer tissues compared to control ones (28). For this, the Flag-tagged PPM1B isoform was overexpressed in HeLa cells. The efficiency of PPM1B overexpression was validated by confocal

tontay:beata_285_24

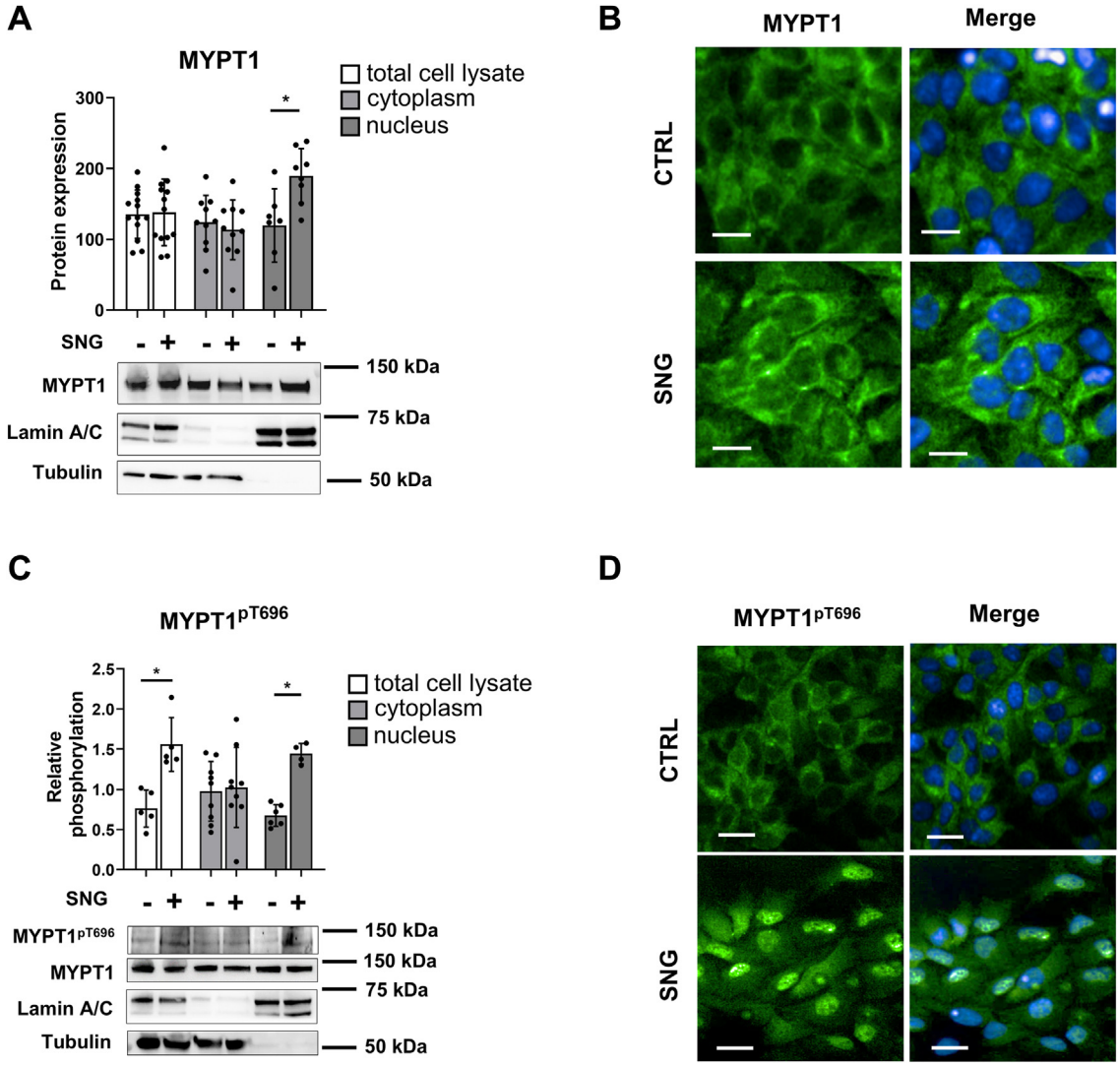


Figure 3. Effect of SNG on MYPT1 expression and MP activity in HeLa cells. Total cell lysates, nuclear and cytoplasmic fractions from control and SNG-treated cells were examined by Western blot analysis using anti-MYPT1 (*A*) and anti-MYPT1^{pT696} (*C*) antibodies. Values represent mean ± SD, n = 3 to 13. Columns display the expression of MYPT1, along with phosphorylation at MYPT1 ^{pT696} residue. For comparison of multiple groups two way ANOVA was used, followed by Tukey *post hoc* test, for comparison of two groups two tailed unpaired *t* test was used where $p < 0.05$ (*) and $p < 0.001$ (***). Immunofluorescent staining of control and SNG-treated HeLa cells using antibodies specific for MYPT1 (*B*) and MYPT1^{pT696} (*D*) are shown. Nuclei are stained with DAPI. The scale bar represents 10 μm. DAPI, 4′,6-diamidino-2-phenylindole; MP, myosin phosphatase; MYPT1: myosin phosphatase target subunit 1; SNG, sanguinarine.

microscopy, labeling Flag-tag with Alexa488 fluorophore (Fig. S3*D*) as well as by semiquantitative Western blot analysis using anti-Flag antibody (Fig. S3*B*), as well as anti-PPM1B antibody (Fig. S3*A*). Transfection evoked a significant decrease of viability of mock transfected cells compared to control by 25.25% ($p = 0.021$), but interestingly no significant viability changes were detectable between the control and PPM1B-overexpressing cells (Fig. S3*C*). Overexpression of PPM1B did not affect the expression of either MYPT1 (Fig. 5*A*) or PRMT5 (Fig. 5*C*) compared to HeLa cells transfected with empty vector, suggesting that PPM1B has no effect on their gene expression. On the other hand, upon PPM1B overexpression, Thr696 phosphorylation of MYPT1 exhibited a 0.7-fold ($p = 0.0425$) decrease compared to the mock control, and the transfection had no effect in any investigated cases on the phosphorylation levels. The downstream substrate of MP, PRMT5 showed a significant reduction by 0.61-fold ($p = 0.0158$) compared to the control, and a 0.68-fold decrease ($p = 0.0354$) compared to the mock, in the level of its Thr80 phosphorylation indicating that MYPT1 activity is indirectly correlated to PRMT5 activity and depends on PPM1B expression (Fig. 5*D*). Along with these findings, the major nuclear PRMT5 substrate, namely H4 and its symmetric dimethylation was investigated. While the protein level of histone proteins was not altered (Fig. 5*E*), the symmetric dimethylation of H4 decreased by 0.64-fold ($p = 0.0413$) and by 0.74-fold ($p = 0.0312$) comparing to control and mock transfected cells, respectively (Fig. 5*F*). Immunofluorescence staining was used to track the expression and posttranslational modification of MYPT1, PRMT5, and H4. The obtained results were consistent with those from Western blot analysis (Fig. S4, *A*–*G*).

ASBMB

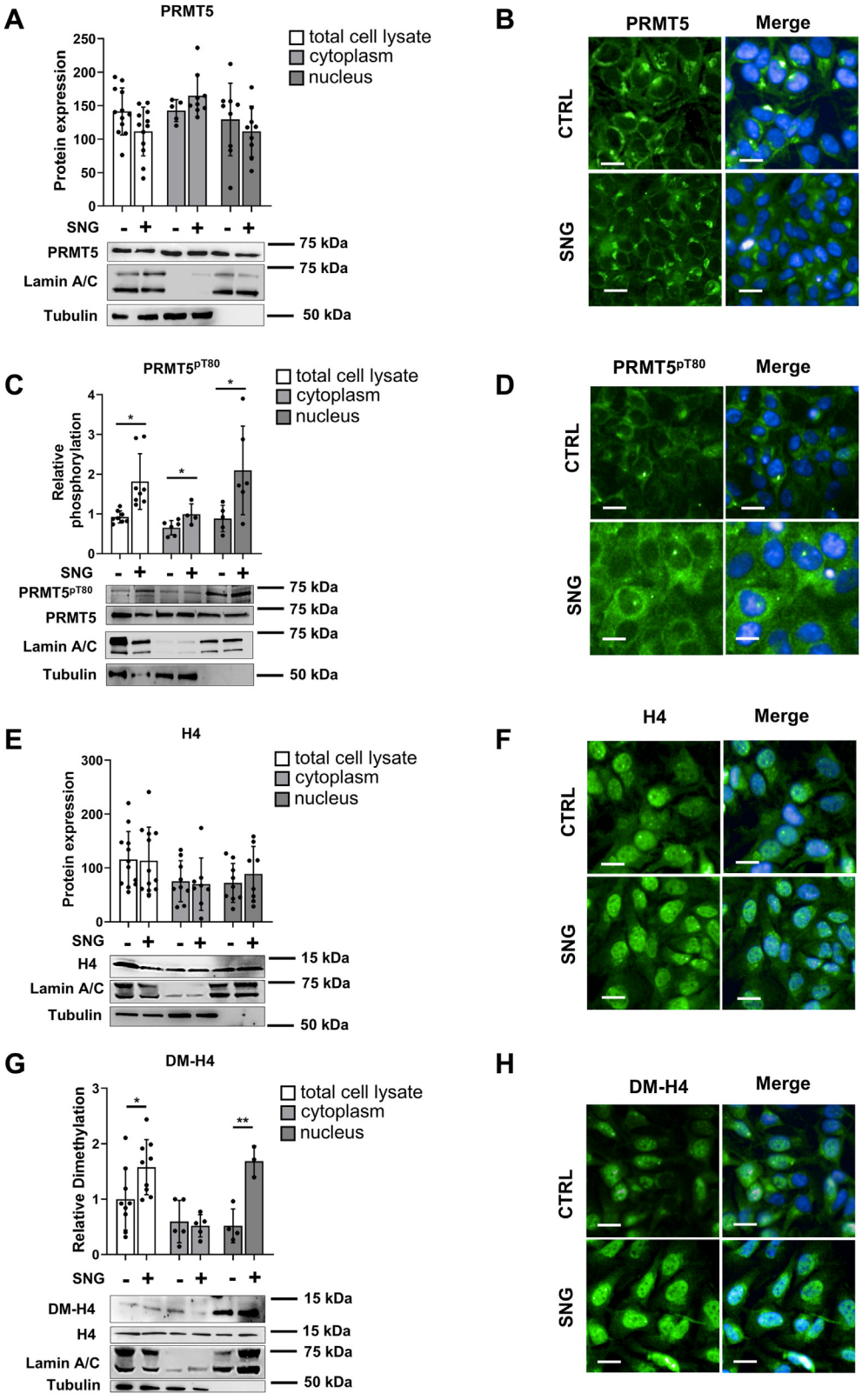


Figure 4. Effect of treatment by SNG on PRMT5 and H4 in HeLa cells revealed by Western blot. Total cell lysates, nuclear, and cytoplasmic fractions from control and SNG-treated cells were assessed by Western blot analysis using anti-PRMT5 (*A*), anti-PRMT5^{pT80} (*C*), anti-H4 (*E*) and anti-DM-H4 (*G*) antibodies. Values are mean ± SD, n = 3 to 12. Columns display the expression of PRMT5 and H4, along with phosphorylation at PRMT5^{T80} residue, and symmetric dimethylation of H4. For comparison of multiple groups two way ANOVA was used followed by Tukey *post hoc* test, or for comparison of two groups two tailed unpaired *t* test was used where $p < 0.05$ (*) and $p < 0.01$ (**). Immunofluorescent staining of control and SNG-treated HeLa cells using antibodies specific for PRMT5 (*B*), anti-PRMT5-P^{T80} (*D*), anti-H4 (*F*), and anti-DM-H4 (*H*) antibodies. Nuclei are stained with DAPI. The scale bar represents 10 μm. DAPI, 4′,6-diamidino-2-phenylindole; PRMT, protein arginine methyltransferase 5; SNG, sanguinarine.

tontay:beata_285_24

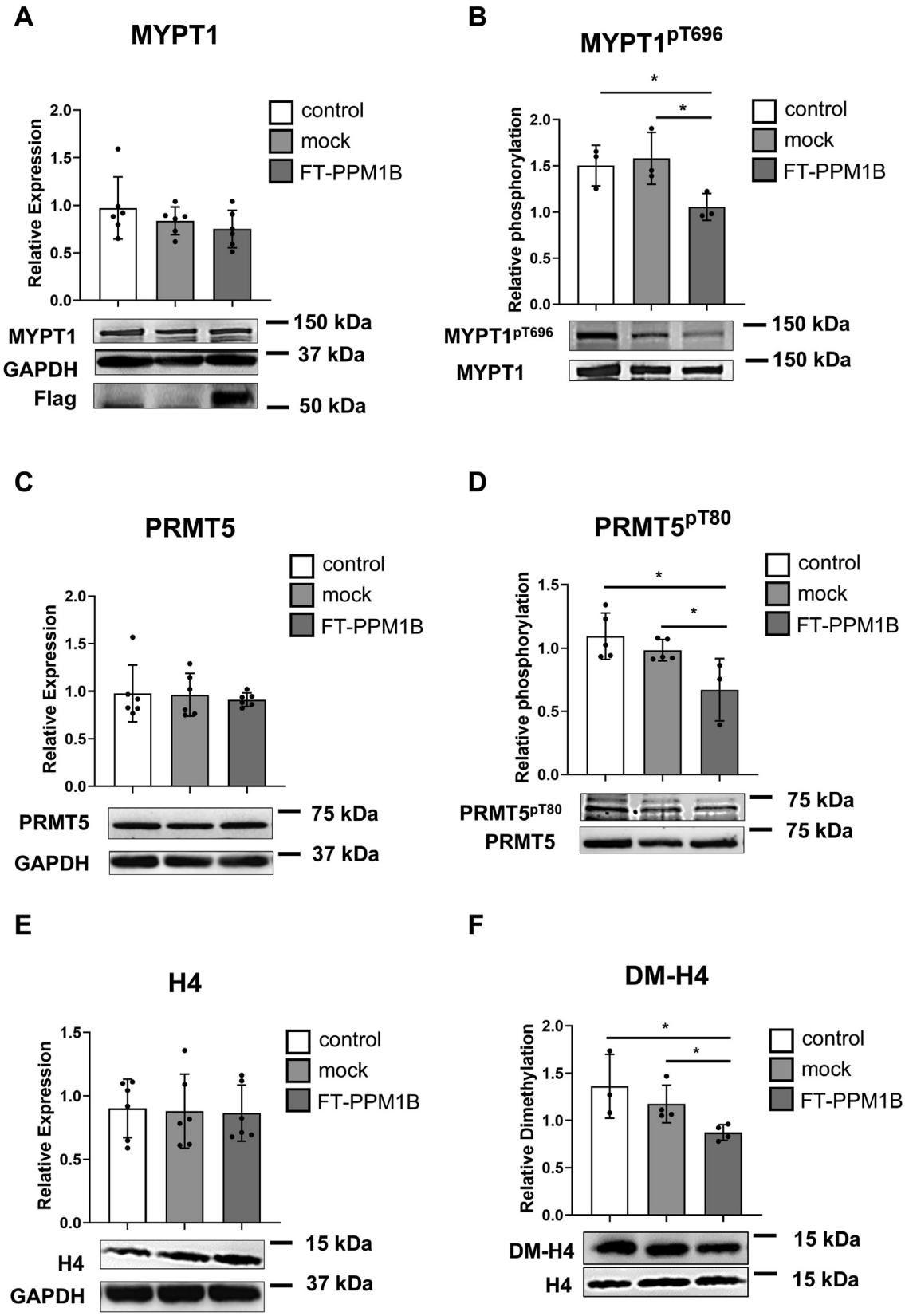


Figure 5. Effect of PPM1B overexpression on the expression and activity of MP and PRMT5. Proteins from untransfected (control), empty vector (mock), and Flag-PPM1B (FT-PPM1B) transfected HeLa cells were assessed by Western blot analysis using anti-MYPT1 (*A*), anti-MYPT1^{pT696} (*B*), anti-PRMT5 (*C*), anti-PRMT5^{pT80} (*D*), anti-H4 (*E*), and anti-DM-H4 (*F*) antibodies. Values mean ± SD, n = 3 to 6. Groups were compared using either unpaired two-tailed t-tests or one way ANOVA for comparison of multiple groups followed by Tukey *post hoc* test, where $p < 0.05$ (*). MP, myosin phosphatase; MYPT1: myosin phosphatase target subunit 1; PPM1B: protein phosphatase, Mg^{2+}/Mn^{2+} -dependent 1 B or PP2Cβ, PRMT, protein arginine methyltransferase 5.

lontay.beata_285_24

PPM1B WT but not its phosphatase-deficient R179G mutant inhibits PRMT5 activity through the activation of myosin phosphatase

To further validate the role of PPM1B in the activation of MP by the dephosphorylation of its regulatory subunit MYPT1 on Thr 696, we generated the phosphatase deficient mutant of PPM1B (mutant R179G) based on previous publications (29). HeLa cells were transfected with the with WT (FT-PPM1B) and the phosphatase-inactive R179G mutant form of Flag-PPM1B (R179G PPM1B) and the expression and phosphorylation levels were compared to mock controls (Fig. 6). Flag tag expression compared to empty vector transfected mock control group validated successful overexpression of both mutant and WT PPM1B (Fig. 6*B*), and none of the overexpression conditions affected expression of MYPT1 (Fig. 6*A*). Phosphorylation of MYPT1 on Thr696 sidechain showed a decrease from 1.14 to 0.68 (p = 0.021) in the samples overexpressing FT-PPM1B compared to MOCK-transfected samples. In

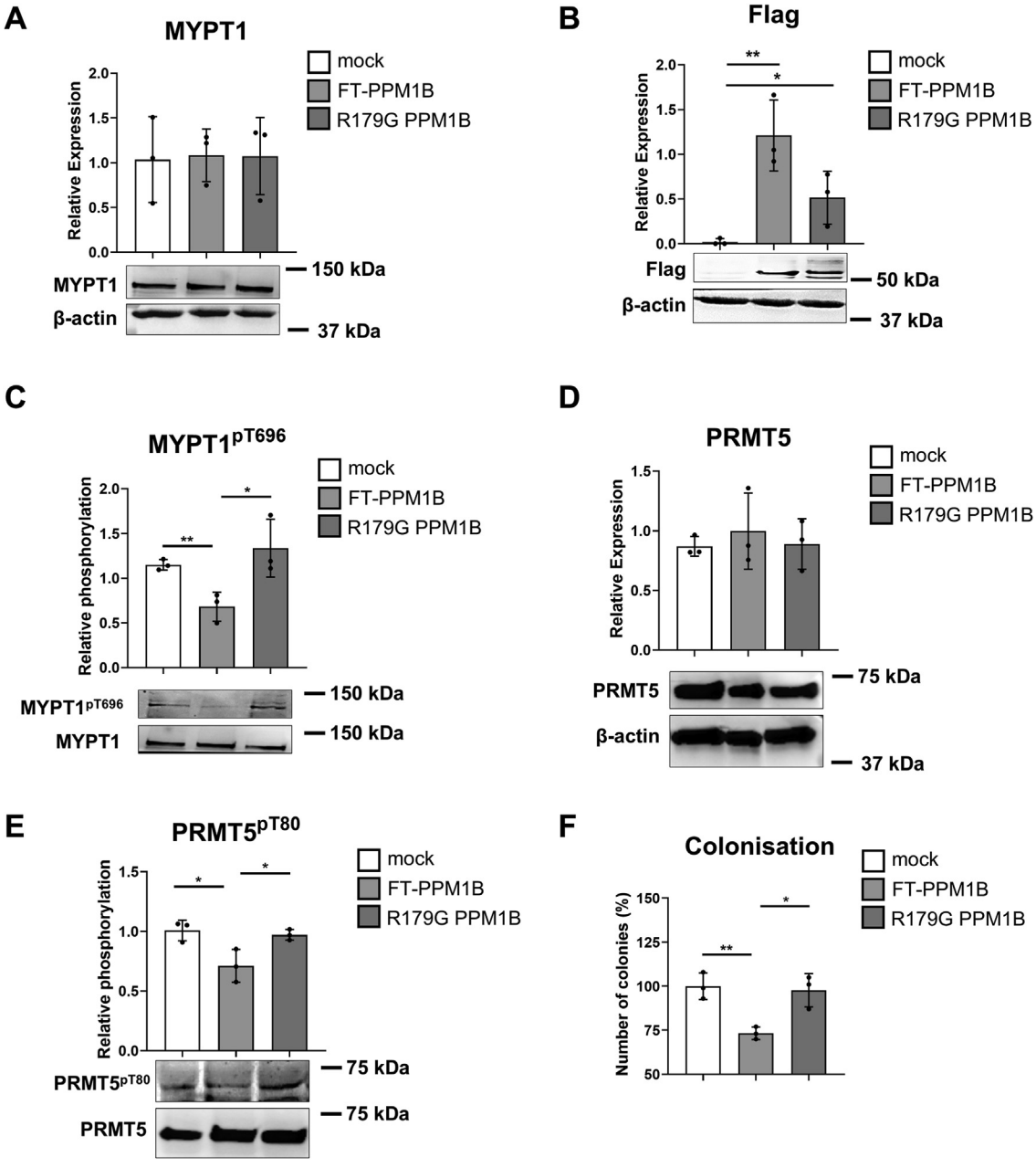


Figure 6. The effect of PPM1B^{R179G} inactive mutant on the expression and activity of MYPT1 and on the colonization capacity of HeLa cells. Proteins from empty vector (mock), WT Flag-PPM1B (WT PPM1B), and Flag-R179G inactive mutant PPM1B (R179G PPM1B) transfected HeLa cells were assessed by Western blot analysis using anti-MYPT1 (*A*), anti-Flag (*B*), anti-MYPT1^{pT696} (*C*), anti-PRMT5 (*D*), and anti-PRMT5^{pT80} (*E*) antibodies. Values are mean ± SD, n = 3. Groups were compared using either unpaired two-tailed *t* tests for comparison of two groups, or one way ANOVA for comparison of multiple groups followed by Tukey *post hoc* test, where $p < 0.05$ (*) and $p < 0.01$ (**).(*F*) Mock control, FT-PPM1B, and R179G mutant PPM1B overexpressed HeLa cells were seeded onto six well plates, and were cultured for 12 days. Survival factor was calculated and represented as *bar* chart, where values are mean ± SD, and n = 3. Groups were compared by one way ANOVA, followed by Tukey multiple comparison test, where $p < 0.05$ (*), and $p < 0.01$ (**). PRMT, protein arginine methyltransferase 5; MYPT1: myosin phosphatase target subunit 1; PPM1B, protein phosphatase, Mg^{2+}/Mn^{2+} -dependent 1 B or PP2Cβ.

tontay:beata_285_24

addition, MYPT phosphorylation increased 1.67-fold (p = 0.0097) in the phosphatase-deficient PPM1B overexpressed samples compared to WT PPM1B values (Fig. 6*C*). The activity of the PRMT5, the substrate of MP was also affected by the overexpression of PPM1B activity. The relative phosphorylation of PRMT5 at Thr80 showed a decrease from 1.007 to 0.71 (p = 0.0022) upon the overexpression of FT-PPM1B while the overexpression of the R179G PPM1B mutant had no significant effect compared to the control (p = 0.89) but showed a 1.95-fold increase (p = 0.039) compared to the FT-PPM1B overexpressing cell lysates (Fig. 6*E*). The expression level of PRMT5 was not altered in either the FT-PPM1B or the R179G PPM1B groups compared to mock control (p = 0.77 and 0.99, respectively) (Fig. 6*D*). These results suggest the *in vivo* role of PPM1B in the dephosphorylation of MYPT1 at Thr696 inhibitory residue and its indirect effect on the activity of PRMT5.

To further investigate the difference between the effects of WT PPM1B (FT-PPM1B) and its phosphatase deficient mutant R179G overexpression, colonogenic assay for 12 days were established, in which empty vector transfected mock served as control. The colonization activity of WT PPM1B overexpressed group was reduced by 27% (p = 0.0098) compared to mock control and the overexpression of mutant R179G PPM1B elevated it back by 25% (p = 0.0150) (Fig. 6*F*) suggesting the inhibitory role of PPM1B on the colony formation of HeLa cells.

In vitro *findings of PPM1B-MYPT1-PRMT5-H4 axis are detectable in human cellular carcinoma lysates*

As our results showed the existence of the PPM1B/MP/PRMT5 axis in HeLa cervical carcinoma cells, our goal was to investigate this protooncogenic signaling pathway in human cervical carcinoma and nontumorous tissues as well. We subjected the lysates of human biopsies to semi-quantitative Western blot analysis, and cancer tissues were compared to control tissue lysates. Our results demonstrate that PPM1B and MYPT1 expression were significantly decreased to 0.44-fold (p = 0.0452) and 0.26-fold (p = 0.0244) in the tumor samples compared to the healthy control, respectively (Fig. 7, *A* and *B*). The inhibitory phosphorylation of MYPT1^{pT696} showed a strong, 2.52-fold (p = 0.0012) elevation in the tumor samples (Fig. 7*C*). PRMT5 phosphorylation on Thr^{80} residue changed significantly by 2.325-fold (p = 0.0498), while the relative PRMT5 expression decreased from 2.76 to 0.97 (p = 0.022) in the tumor samples compared to the normal samples (Fig. 7, *D* and *E*). Regarding H4, its expression showed no change (p = 0.34), while the symmetric dimethylation increased significantly by 1.327-fold (p = 0.0499) in the tumor samples compared to controls (Fig. 7, *F* and *G*). To investigate a well-known tumor suppressor that is reportedly altered by the MP/PRMT5/H4 tumorigenic pathway, we assessed pRb expression in the cervical carcinoma lysates, where expression of pRb decreased by 0.38-fold (p = 0.0435) comparing control lysates to tumorous ones (Fig. 7*H*).

Discussion

In the present study, we have characterized PPM1B as the upstream regulator of the MP/PRMT5/histone signaling pathway providing a novel mechanism of tumorigenesis in HeLa cells and cervical carcinoma. We have identified the phospho-Thr696 inhibitory residue of MYPT1 regulatory subunit of MP as the target of PPM1B. The dephosphorylation of this site was shown to decrease the activity of PRMT5, the downstream substrate of MP assessed by its regulatory Thr80 phosphorylation and histone symmetric dimethylation analysis. The interaction between MP and PPM1B was also supported by multiple interaction analyses (Fig. 1, *A–D*). The chemical inhibition of PPM1B by SNG resulted in the deactivation of MP and the increased activity of PRMT5 leading to increased symmetric dimethylation of histone H4 (Figs. 3, *A–F* and 4, *A–H*). The overexpression of the PPM1B isoform had opposite action (Fig. 5, *A–G*). The cervical carcinoma biopsies and their healthy control counterparts supported the almost complete elimination of PPM1B accompanied by tumorigenesis (Fig. 7, *A–I*). Therefore, PPM1B could be assumed as a tumor suppressor in cervical carcinoma.

We found that MP interacts with PPM1B through its MYPT1 regulatory subunit, and this interplay is supported not only by immunoprecipitation and pull-down assay but by proximity ligation assay (Fig. 1, *A–D*). It is well in line with a previous report suggesting the interaction of nuclear MYPT1 with the members of the methylosome complex as well as PPM1B isoform by mass spectrometry analysis (4). Although nuclear protein-protein interactions between the enzymes have been demonstrated, the results of the proximity ligation assay do not exclude the possibility that the interplay exists outside the nucleus and regulates possible cytosolic signal transduction processes. PPM1B exhibited cytosolic and nuclear localization, and it was supported by findings showing endogenous PPM1B localized in the nucleus of mature 3T3-L1 adipocytes where it can bind to peroxisome proliferator-activated receptor gamma (PPARγ) (30) but it was also reported as the regulator of major cytosolic signaling pathways such as mitogen-activated protein kinase and AMPK signaling (31). MYPT1 was also found in the nuclear and microsomal fraction of HepG2 cells (25) and in the nucleus of neuronal cells (32) and it was shown that nuclear MP regulated gene expression through the modulation of the PRMT5 enzyme of the methylosome complex (4).

The question arises as to what is the importance of the interaction between PPM1B and MP? The answer lies in the regulatory processes of myosin phosphatase. MYPT1 includes several consensus sites for a number of protein kinases and among these phosphorylations at Thr696 results in the inhibition of MP activity (13, 15, 33). Strikingly, none of the potent myosin phosphatase kinases is present in the nucleus (25, 34, 35). To our recent knowledge, MYPT1 is not phosphorylated in the nucleus, raising the possibility that it is translocated to the nucleus in an already phosphorylated status (36).

Our data suggest directly that MP is a substrate of PPM1B and the latter dephosphorylates the MYPT1 Thr696 inhibitory

ASBMB

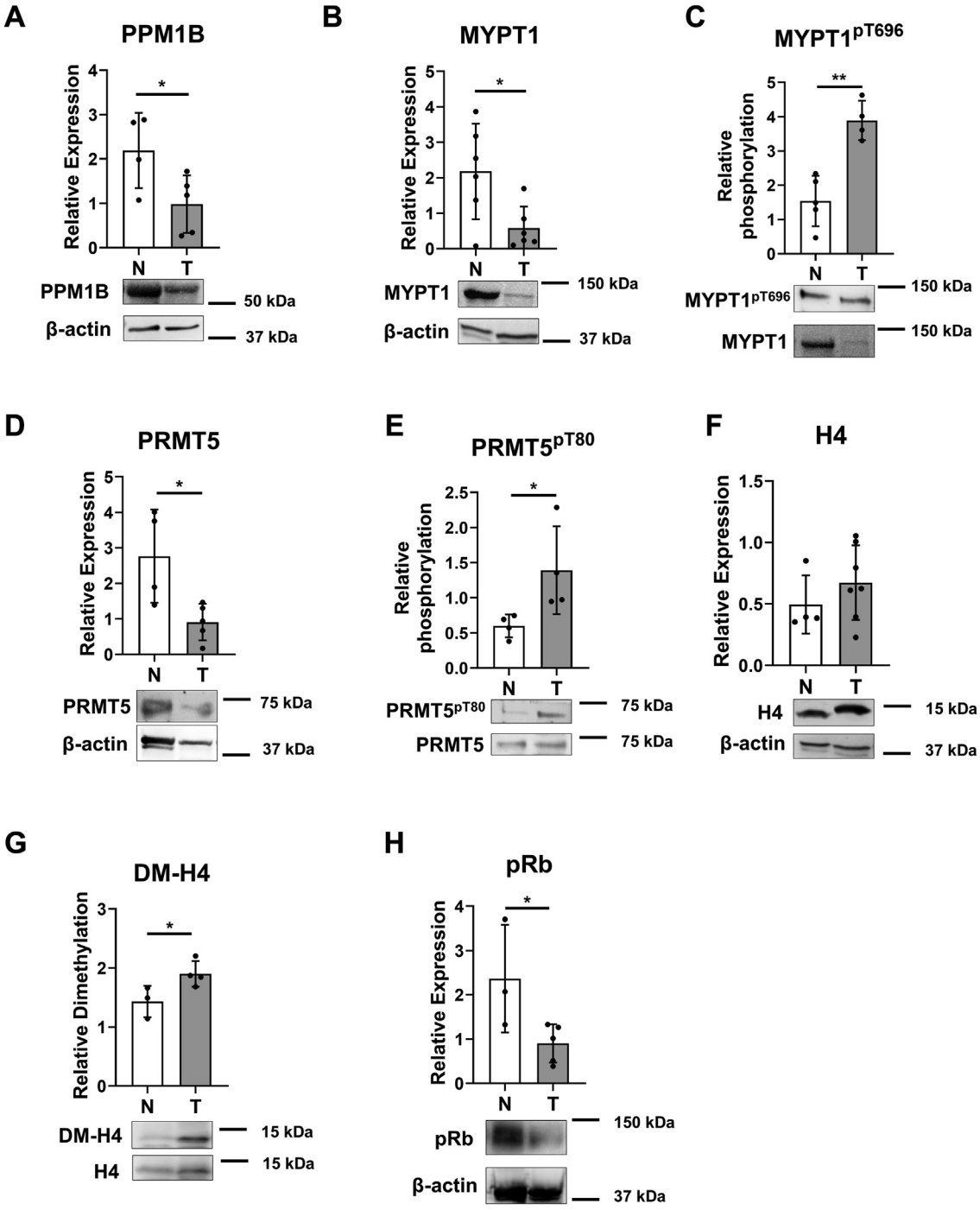


Figure 7. Expression and activity of the elements of the PPM1B/MP/PRMT5/H4 oncogenic signaling in human cervical cancer. Normal (N) and tumor (T) tissue lysates were analyzed by Western blot using anti-PPM1B (*A*), anti-MYPT1 (*B*), anti-MYPT1^{pT696} (*C*), anti-PRMT5 (*D*), anti- PRMT5^{pT80} (*E*), anti-H4 (*F*), anti-DM-H4 (*G*), and anti-pRb (*H*) antibodies. Values are mean ± SD, n = 3 to 8. Data were normalized to the healthy control. Differences between groups were analyzed by unpaired two-tailed *t* test, $p < 0.05$ (*) and $p < 0{,}01$ (**).MP, myosin phosphatase; MYPT1, myosin phosphatase target subunit 1; PPM1B, protein phosphatase, Mg2+/Mn2+ -dependent 1 B or PP2Cβ;pRb, retinoblastoma protein; PRMT, protein arginine methyltransferase 5.

phosphorylation site using recombinant active enzymes in *in vitro* kinase and phosphatase assays. These findings are also supported by our MP activity measurement in the presence of SNG, a PPM1 specific phosphatase inhibitor, and by *in vitro* kinase assay using ROK and recombinant active PPM1B (Fig. 2*A*). Aspecific effects beyond the inhibitory effects of SNG on PPM1 enzymes were excluded based on preliminary data, as the mitogen-activated protein kinase phosphatase-1 enzyme was only inhibited in the SNG cellular system at 17 μM IC50 value (37). Since inhibition of PPM1B did not cause a complete inhibition of MP activity, it is therefore thought that PPM1B is not the sole MYPT1 phosphatase, but rather acts in concert with other previously described regulatory protein phosphatases (17) to regulate MP holoenzyme.

tontay:beata_285_24

Our finding that PPM1B is the major upstream regulator of nuclear MP can rely on the finding that no other protein phosphatase was present in the nuclear MYPT1 interactome (4) and the inhibitory phosphorylation levels of MYPT1 were significantly changed only in the nuclear fraction of SNG-treated HeLa cells (Fig. 3). Consistent with this, both PPM1B overexpression (Fig. 5) and chemical inhibition (Figs. 3 and 4) experiments indicate that PPM1B activates MP activity by dephosphorylating its MYPT^{pT696} inhibitory phosphorylation site that results in the inhibition of PRMT5 by the decreased phosphorylation at the Thr80 activating phosphorylation site (Figs. 4*C* and 5*E*). This led to a decrease in symmetric dimethylation of histone 4 (Figs. 4*G* and 5*G*) in the nuclear fraction of HeLa cells. Our previous observations have already shown the significant upregulation of cancer-related pathways in hepatocellular carcinoma upon MYPT1 silencing that suppressed the gene and protein expression of several tumor suppressors or increased that of potential oncogenes (4).

To support our results on HeLa cells, we also analyzed the PPM1B-regulated signaling elements in human cervical tumor biopsies (Fig. 7). Recent studies have revealed tumor-suppressing roles for PPM1B; however, the Human Protein Atlas data suggested low cancer specificity. Data obtained by overexpression of WT and phosphatase dead mutant suggest that PPM1B regulates tumor cell colonization through modulation of MP and indirectly PRMT5, suggesting the tumor suppressor nature of PPM1B. (Fig. 6*F*). PPM1B inhibited gastric cancer migration and invasion *in vitro* and tumor metastasis *in vivo* by dephosphorylating Rho GDP-dissociation inhibitor (RhoGDI1) and was identified as a favorable diagnostic biomarker (28). In addition, the expression of PPM1B remarkably decreased due to the high expression of miR-186, and the overexpression of PPM1B inhibited the proliferation and tumorigenicity of bladder cancer cells (38). Moreover, the degradation of PPM1B led to the upregulation of its substrate, CDK2, and increased the proliferation and migration of hepatocellular carcinoma cells (39) and PPM1B downregulation was also was associated with more advanced clinical stages of human colorectal cancer (40). These results are fully consistent with our findings that the PPM1B expression was massively downregulated in cervical carcinoma compared to healthy controls (Fig. 7*A*).

Although most previous findings suggested the role of MP as a downstream effector of ROK signaling, more and more results suggest its ROK-independent action in the inhibition of cancer formation. The unbalanced and constant phosphorylation of MYPT1 at Thr696 was suggested to be related to cancer formation and mutations as well as altered phosphorylation and expression of MYPT1 were documented in various cancer types (14). Interestingly, decreased expression of MYPT1 did not always accompany tumor development, but increased phosphorylation of MYPT. This phenomenon may be explained, at least in part, by the regulation of MP with PPM1B. Interestingly, in those cancer types where PPM1B downregulation was detected such as bladder, gastric, and hepatocellular carcinoma, only the inhibitory phosphorylation of MYPT1 showed correlation but not the MYPT1 protein expression (4) which explains the tumor suppressor activity of MP without any changes in its protein expression. Although this is a favorable explanation, the possibility of regulation by miRNA cannot be ruled out.

Taken together, the present study has identified PPM1B as a novel phosphatase of MP and as an upstream regulator of the MP/PRMT5/histone signaling pathway. It provides new insight into the molecular mechanism by which PPM1B regulates cancer cell formation through activation of myosin phosphatase. MP and PPM1B clearly serve tumor suppressive functions, and are inactivated in human cancer patients. Beyond their prognostic feature in most cancer types—such as in cervical carcinoma—their reactivation by small pharmacologic compounds is rather important but remains challenging. The mere inhibition of the upstream kinases is not sufficient, but also requires the activation of counteracting phosphatase(s) in targeting oncogenic phosphorylations to increase the efficiency of kinase inhibitor therapies.

Experimental procedures

Chemicals

All chemicals were obtained from Sigma-Aldrich unless indicated otherwise.

Antibodies

All antibodies are described in Table S1.

Cell culture maintenance

Human epithelioid cervix carcinoma HeLa cell line and SV40 transformed human embryonal kidney cells (purchased from ECACC, cat. number 99040201 and 85120602, respectively), were maintained according to the manufacturer's instructions in Dulbecco's modified Eagle's medium (DMEM) with phenol red, supplemented by 10% fetal bovine serum (FBS), and 2 mM L-glutamine (further referred as complete growth medium). Cells were incubated at 37 °C in a humidified atmosphere containing 5% CO_2. Cell lines were tested for *mycoplasma* and they were free from *mycoplasma* contamination for all experiments. The authenticity of the cell lines were validated and documented by the manufacturer. Cell lines were tested and they were free from *mycoplasma* contamination for all experiments.

Overexpression of PPM1B protein

Mg^{2+}/Mn^{2+} dependent protein phosphatase 1B (PPM1B) was overexpressed in HeLa cells using 1.7 ng/μl human pRec-M11-FT-PPM1B plasmid (GeneCopoeia) and Gene Juice transfection reagent (5.32 μg dissolved in 1500 μl serum free DMEM) according to the manufacturer's protocol (labeled as FT-PPM1B group). Mock control group was established by the same amount of transfection reagent and equal concentration of empty vector (further referred as mock group). Cells were cultured for 72 h after transfection then lysed as it is described in "Protein extraction" section.

ASBMB

Site-directed mutagenesis of R179G inactive mutant of PPM1B

Expression vector pReceiver-M11 encoding WT human full-length PPM1B (NM_002706.6) transcript variant 1 was purchased from GeneCopoeia Inc. Point mutations of PPM1BR179G/pReceiver-M11 were performed using QuickChange II XL Site-Directed Mutagenesis Kit according to the manufacturer's instructions (Agilent Technologies) and is further referred to as R179G mutant PPM1B. Primer pairs are listed in Table S2. The sequence of mutants was verified by DNA sequencing, performed by GenoMed Medical Genomic Technologies Ltd. Primers for sequencing are listed in Table S2. Vectors containing mutant protein sequence were produced by *Escherichia coli* cultures then HeLa cells were transfected with the mutant plasmid with the same conditions as described in the "Overexpression of PPM1B protein" section.

SNG treatment and subcellular fractionation

Prior to SNG treatment, HeLa cell culture was incubated in incomplete DMEM containing 0.1% FBS for 24 h and then treated with 1 μM SNG dissolved in complete media for 1 h to inhibit the activity of PPM1B. Serum-starved cells without any treatment served as the control group. Cells were either processed according to the protocol described in "Protein Extraction" section or were handled as follows. Cells were washed with 1x PBS, then centrifuged at 800*g* for 3 min and were solubilized in 400 μl of "Buffer A" consisting of: 10 mM 4-(2-hydroxyethyl)-1-piperazineethanesulphonic acid (Hepes pH 7.9), 10 mM potassium chloride (KCl), 0.1 mM EDTA, 0.1 mM ethylene glycol-bis(β-aminoethyl ether)-N,N,N′,N′-tetraacetic acid (EGTA) supplemented with 1 mM DTT, and 10x dilution of phosphatase inhibitor cocktail (1 mM sodium fluoride (NaF), 1 mM tetrasodium pyrophosphate ($Na_4P_2O_7$), 1 mM β-glycerophosphate, and 1 mM sodium orthovanadate (Na_3VO_4), mixture further referred to as 10x phosphatase inhibitor cocktail (PIC)) plus 1 μM Microcystin-LR (McαR). Samples were homogenized using Hamilton needle, then the mixture was centrifuged at 16,000*g* for 1 min, and the supernatant was saved as the cytoplasmic fraction. The pellet was suspended in 50 μl "Buffer B" (20 mM Hepes pH 7.9, 420 mM sodium chloride (NaCl), 0.5 mM EDTA, and 0.5 mM EGTA) supplemented by 10xPIC and 1 μM McαR as described above, then the mixture was incubated on ice for 25 min and centrifuged at 12,000*g* for 10 min. The supernatants were considered as nuclear fraction. Protein concentrations were determined with Pierce BCA Protein Assay Kit (Thermo Fisher Scientific,) as described before (32).

Protein extraction

Cells were washed once with 1xPBS (pH 7.4) and then lysed in radioimmunoprecipitation assay buffer (25 mM Tris, 150 mM NaCl, 1% Na-deoxycholate, 0.1% SDS) supplemented with 1% Triton-X-100, protease inhibitor, and PIC. Proteins were solubilized by sonication and were centrifuged at 13,000*g* at 4 °C for 10 min, supernatant was considered as total protein extract. Protein concentrations were determined with Pierce BCA Protein Assay Kit (Thermo Fisher Scientific) as described before (32).

Alamar Blue cell viability assay

HeLa cells were plated on 96-well plates and were transfected by FT-PPM1B as described above, and were incubated for 72 h, or were grown for 24 h, then serum starved in 0.1% FBS-containing media for 24 h prior to 1 h long 1 μM SNG treatment. Then, resazurin was added at a 20 μM final concentration for 2 h, and the fluorescence intensity was measured using a Tecan Spark 10M multimode plate reader (Tecan Group Ltd) at 560/590 nm. Viability was expressed as the percentage of untreated cells.

Human cervix tissue lysates

Normal and tumor tissue lysates were obtained from Protein Biotechnologies solubilized in radioimmunoprecipitation assay buffer. After centrifugation at 16,000*g*, at 4 °C for 4 min, supernatants were incubated in SDS sample buffer (Bio-Rad Laboratories) for 5 min at 100 °C and the samples were applied for Western blot analysis.

Western blot analysis

Lysates (20 μg of protein per sample) were loaded onto 4 to 20% precast Criterion gels (Bio-Rad Laboratories) and were separated by size, then transferred to nitrocellulose membrane at 200 V as described previously using a Criterion blotter (Bio-Rad Laboratories) at 100 V for 75 min and handled as described previously (41). Bands were visualized in a ChemiDoc Touch Imaging System (Bio-Rad Laboratories) using Western Bright enhanced chemiluminescence reagents (Advansta Inc).

Immunofluorescent staining and confocal microscopy by high content screening

HeLa cells were added to 96-well Cell Carrier Ultra glass bottom plates (PerkinElmer) for 24 h then were incubated in 0.1% FBS-containing DMEM for 24 h followed by treatment with 1 μM SNG for 1 h. In case of PPM1B overexpression, cells were transfected as described previously. In both cases untreated cells served as control group. Cells were fixed with 300 μl/well 4% (v/v) paraformaldehyde/Tris-buffered saline (TBS) (50 mM Tris, pH 7.4, 150 mM NaCl, 1 mM EDTA, 1x PIC, 1x phosphatase inhibitor cocktail, 1% (v/v) Triton X-100) for 10 min at room temperature (RT), permeabilized with 300 μl/well 0.25% Triton X-100/TBS solution for 15 min and the nonspecific binding sites were blocked with 300 μl/well 1% bovine serum albumin (BSA)/TBS solution for 1 h. After blocking, the cells were labeled with antibodies raised against MYPT1, MYPT1^{pT696}, PRMT5, PRMT5^{pT80}, H4, dimethyl-H4, PPM1B, or Flag antibodies in 1:100 dilution in blocking solution at 4 °C overnight, followed by Alexa Fluor 488-conjugated chicken anti-rabbit or anti-mouse antibody in 1:1000 dilution in blocking solution for 1.5 h at RT. Actin was visualized by Texas Red Phalloidin and nuclei were stained with DAPI for 2 min. Finally, the cells were washed three times with 1xPBS. The visualization was conducted in each case by

tontay:beata_285_24

Opera Phenix High Content Analysis equipment (PerkinElmer) using a 40x water objective in confocal mode. The nuclear region of the cells was segmented based on DAPI staining and was analyzed with the built-in Harmony software (version 4.8; http://www.perkinelmer.com/product/harmony-4-2office-hh17000001).

Immunoprecipitation

Flag-PPM1B (FT-PPM1B) and Flag-MYPT1 (FT-MYPT1) proteins were expressed in tsA201 cell line as described before, and cells were lysed in TBS-EDTA buffer. PAS) resin (GE HealthCare, #17–0780–01) was blocked with 5% (w/V) BSA/TBS for one night (∼16 h) at 4 °C. Then antibodies (anti-PPM1B, anti-MYPT1, or anti-mouse) were coupled to PAS in binding buffer (50 mM Tris, pH 7.0) in 1:67 dilution by gentle rotation for 3 h at 4 °C. The tsA201 lysates (1 mg/ml) were precleared with PAS and then were added to the PAS-antibody complex for 2 h and were washed three times with 1xTBS. Then PAS-anti-MYPT1-FT-MYPT1 particles were incubated with FT-PPM1B containing precleared tsA201 lysate, while PAS-anti-PPM1B-FT-PPM1B complexes with FT-MYPT1 for 3 h. Finally, beads were washed with 1xTBS and were incubated at 100 °C for 5 min in 1x SDS sample buffer. Samples were investigated by SDS-PAGE followed by Western blot analysis.

Pull-down assay

Glutathione Sepharose 4B beads (P1743-1VL, Merck) (30 μl/sample) were incubated with 400 μl binding buffer (50 mM Tris, 150 mM NaCl, 1 mM EDTA, 1% (V/V) Triton X-100, pH 7.4, and 1 x PIC) containing 1 μM purified GST or GST-MYPT1 in for 60 min at 4 °C. The resin-GST/GST-MYPT1 complexes were washed with TBS and then were incubated either with untransfected or Flag-PPM1B over-expressing tsA201 lysates (previously precleared with uncoupled Glutathione Sepharose 4B) for 120 min at 4 °C. The resins were washed three times with TBS then incubated with 2x SDS sample buffer for 5 min at 100 °C (32). The samples were analyzed by Western blotting using antibodies against PPM1B, PP1c, and GST. GST-MYPT1 were expressed in *E. coli* and purified as described before (42, 43).

Duolink PLA protein-protein interaction assay

Duolink PLA protein-protein interaction assay (DUO92007, Sigma-Aldrich) was conducted according to the instructions of the manufacturer. Cells were plated on CellCarrier Ultra glass bottom plates (PerkinElmer), and were fixed by 300 μl/well 4%(v/v) paraformaldehyde/TBS, and permeabilized in 300 μl/well 0.2% Triton-X-100 in TBS. Samples were incubated with primary antibodies in 1:100 dilution, specific for MYPT1 and PPM1B, or with anti-PP1cβ and anti-MYPT1 for positive control group, or with anti-pRb and anti-MYPT1 and with anti-PPM1A and anti-MYPT1. In negative control group no primary antibodies were applied. Total volume used of the primary antibody was 100 μl/well, and the samples were incubated for O/N at 4 °C. Duolink PLA probe was then ligated to primary antibodies, and then amplification buffer was added to the system in 40 μl/well volume, enabling fluorescent oligonucleotide sequences to be polymerized in between PLA probes linked to proteins by primary antibodies, which were in optimal physical proximity to each other. Fluorescent signal of polymerized oligonucleotides was read by Opera Phoenix High Content Screening instrument built-in Harmony software (version 4.8), at an excitation of 554 nm, and emission of 576 nm, by 40x water objective. Registered signals of interacting proteins showed up as fluorescent spots. To determine cell area and nuclei area, cytoplasm and nuclei were stained by Alexa688 Phalloidin and DAPI, respectively. Fluorescent spots indicating the interactions were counted and determined by built in intelligent Harmony software (version 4.8), and the spot number was normalized to cell number obtained by DAPI nuclei staining. For each interaction group at least triplicates of wells were visualized, by at least 9 pixels per well density. Negative control group values were expressed as spot/cell, and were taken as 100%. The values of all other groups were taken as a ratio to the control value.

Assay of MP activity

HeLa cells were subcultured then serum starved in 0.1% FBS DMEM for 24 h then were treated with 1 μM SNG or 50 nM OA, as well as combined treatments with 50 nM OA and 1 μM SNG suspended in complete media for 1 h. Cells were washed and lysed in 50 mM Tris–HCl pH 7.4, 150 mM NaCl, 0.15%(m/V) buffer with 1x PIC, 1 mM PMSF, and 50 mM 2-mercaptoethanol with ultrasound. After centrifugation (16,000*g*, 20 min), the supernatants were preincubated for 1 min at 30 °C and assayed in presence of 1 μM phosphorylated smooth muscle myosin substrate (^{32}P-myosin) for 1 min as described earlier (25). The values were normalized to the MYPT1 content of the samples assessed by a standard curve using GST-MYPT1 recombinant protein. MP activity values were expressed as ratio to the control group. Columns represent mean ± SD, n = 3. Comparison of groups were conducted by one-way ANOVA with Tukey post hoc analysis, and two samples were compared by unpaired two-tailed *t* test, where statistical significance was validated upon $p < 0.05$.

RhoA kinase assay and PPM1B phosphatase assay

Glutathione Sepharose 4B beads (30 μl/sample) coupled with GST or GST-MYPT1 were washed with TBS and incubated with ROK (20 ng/μl) and ATP (1 mM) for 45 min at 30 °C in ROK assay buffer (20 mM Mops pH 7.2 25 mM GlicP, 0.5 mM EGTA, 5 mM $MgCl_2$, and 0.5 mM DTT) in the presence of 1 μM of McαR and 1 x PIC. Control samples were handled in the same way without the addition of ROK. After phosphorylation, the beads were washed three times with TBS and incubated in the presence or absence of PPM1B in a buffer containing 20 mM Tris pH 7.4, 150 mM NaCl, 1 mM DTT, 1 mg/ml BSA, 0.1% Tween, protease inhibitors, 5 mM $MgCl_2$, and 5 mM $MnCl_2$ for 45 min at 30 °C. PPM1B activity was also tested in the presence of 1 μM SNG or without the addition of $MgCl_2$ and $MnCl_2$. After washing with TBS, beads were incubated with SDS sample buffer at 100 °C for 5 min.

ASBMB

lontay.beata_285_24

Phosphorylation level of MYPT1 were analyzed by Western blot using MYPT1-^{pT853} and MYPT1-^{pT696} phospho-specific antibodies and anti-MYPT1 as a loading control.

Colonogenic assay

HeLa cells were seeded at a density of 10^3 cells/well in six well plates, and were transfected as it was previously described, either with FT-PPM1B (WT PPM1B) or R179G mutant PPM1B (inactive phosphatase) plasmid. Empty vector treated mock served as control. Cells were cultured for 12 days, after which cultures were washed with 1X PBS, and were dried at RT for 30 min. Cells were stained with 0.27 m/m% Coomassie Brilliant Blue R250 dye (B0149), were visualized, and colonies were counted by ImageJ software (https://imagej.net/ij/). Colony numbers were normalized to plated cell number. The average colony number of Mock groups was taken as 100%, and all other groups were expressed as ratio and results were represented as bar charts.

Statistical analysis

Immunoblots were analyzed by ImageJ software. All data were represented as bar charts, created by GraphPad Prism 8 software. Statistical analyses were also performed using GraphPad Prism 8 software (https://www.graphpad.com/updates/prism-10-1-1-release-notes). Phosphorylated proteins were normalized to non-phosphorylated protein expression, and expressed as relative numbers, while nonphosphorylated protein expression was normalized to the loading control, either GAPDH or β-actin, and were represented as relative numbers, except for SNG treatment, where raw data are presented for total proteins. Results of MP activity, Duolink, Alamar Blue viability, and Colonogenic assay values were expressed as ratio to the control group. All data are presented as mean ± SD, where n is the number of independently performed experiments. Differences were considered statistically significant at $p < 0.05$ using unpaired two-tailed t tests to compare two groups, and one-way or two-way ANOVA to compare multiple groups, followed by Tukey multiple comparison test. Data were tested for normal distribution and outliers were defined by Grubbs's test.

Data availability

All data are contained within the manuscript. Data are to be shared upon request (contact: lontay@med.unideb.hu). No datasets were deposited into a publicly accessible repository.

Supporting information—This article contains supporting information.

Acknowledgments—We thank Andrea Docsa and Ágota Kelemenné Szántó for their excellent technical assistance and for Vy Nhat Huynh for his technical help to cell viability assay.

Author contributions—I. K., A. U., E. M., D. H, Z. K., E. T., A. K., and B. L. methodology; I. K., A. U., and Z. K. investigation; I. K. and A. U., software; I. K., E. M., and D. H., validation; I. K., E. M., F. E., A. K. and B. L. writing–review and editing; I. K., Z. K., A. K., and B. L. formal analysis; I. K., A. U., and E. T. visualization; I. K. and B. L. data curation; I. K. and B. L. writing–original draft; I. K. project administration; B. L. funding acquisition; B. L. conceptualization.

Funding and additional information—This work was supported by grants from the National Research, Development and Innovation Office FK125043 and K143430 (to B. L), K129104 (to F. E), the University of Debrecen, Faculty of Medicine Research Fund (1G3DBKJ0BFTK247).

Conflict of interest—The authors declare that they have no conflicts of interest with the contents of this article.

Abbreviations—The abbreviations used are: BSA, bovine serum albumin; DAPI, 4′,6-diamidino-2-phenylindole; DMEM, Dulbecco's modified Eagle's medium; EGTA, ethylene glycol-bis(β-aminoethyl ether)-N,N,N′,N′-tetraacetic acid; FBS, fetal bovine serum; MP, myosin phosphatase; MYPT1, myosin phosphatase target subunit 1; OA, okadaic acid; PAS, protein A sepharose; PIC, phosphatase inhibitor cocktail; PLA, proximity ligation assay; PP1c, protein phosphatase 1 catalytic subunit; PPM1, Mg^{2+}/Mn^{2+} dependent protein phosphatase M1; PPM1A, protein phosphatase, $Mg^{2+/}Mn^{2+}$ -dependent 1 A or PP2Cα; PPM1B, protein phosphatase, $Mg^{2+/}Mn^{2+}$ -dependent 1 B or PP2Cβ; PPP1CB, protein phosphatase catalytic subunit β/δ isoform or PP1c; pRb, retinoblastoma protein; PRMT5, protein arginine methyltransferase 5; ROK, Rho A activated kinase; RT, room temperature; SNG, sanguinarine; TBS, Tis-buffered saline.

References

1. Tsang, D. P., and Cheng, A. S. (2011) Epigenetic regulation of signaling pathways in cancer: role of the histone methyltransferase EZH2. *J. Gastroenterol. Hepatol.* **26**, 19–27
2. Geffen, Y., Anand, S., Akiyama, Y., Yaron, T. M., Song, Y., Johnson, J. L., *et al.* (2023) Pan-cancer analysis of post-translational modifications reveals shared patterns of protein regulation. *Cell* **186**, 3945–3967. e3926
3. Wang, H., Yang, L., Liu, M., and Luo, J. (2023) Protein post-translational modifications in the regulation of cancer hallmarks. *Cancer Gene Ther.* **30**, 529–547
4. Sipos, A., Ivan, J., Becsi, B., Darula, Z., Tamas, I., Horvath, D., *et al.* (2017) Myosin phosphatase and RhoA-activated kinase modulate arginine methylation by the regulation of protein arginine methyltransferase 5 in hepatocellular carcinoma cells. *Sci. Rep.* **7**, 40590
5. Kim, H., and Ronai, Z. A. (2020) PRMT5 function and targeting in cancer. *Cell Stress* **4**, 199–215
6. Al-Hamashi, A. A., Diaz, K., and Huang, R. (2020) Non-histone arginine methylation by protein arginine methyltransferases. *Curr. Protein Pept. Sci.* **21**, 699–712
7. Antonysamy, S., Bonday, Z., Campbell, R. M., Doyle, B., Druzina, Z., Gheyi, T., *et al.* (2012) Crystal structure of the human PRMT5:MEP50 complex. *Proc. Natl. Acad. Sci. U. S. A.* **109**, 17960–17965
8. Ho, M. C., Wilczek, C., Bonanno, J. B., Xing, L., Seznec, J., Matsui, T., *et al.* (2013) Structure of the arginine methyltransferase PRMT5-MEP50 reveals a mechanism for substrate specificity. *PLoS One* **8**, e57008
9. Stopa, N., Krebs, J. E., and Shechter, D. (2015) The PRMT5 arginine methyltransferase: many roles in development, cancer and beyond. *Cell. Mol. Life. Sci.* **72**, 2041–2059
10. Lattouf, H., Kassem, L., Jacquemetton, J., Choucair, A., Poulard, C., Tredan, O., *et al.* (2019) LKB1 regulates PRMT5 activity in breast cancer. *Int. J. Cancer* **144**, 595–606
11. Liu, F., Zhao, X., Perna, F., Wang, L., Koppikar, P., Abdel-Wahab, O., *et al.* (2011) JAK2V617F-mediated phosphorylation of PRMT5

lontay:beata_285_24

downregulates its methyltransferase activity and promotes myeloproliferation. *Cancer Cell* **19**, 283–294
12. Zhu, F., and Rui, L. (2019) PRMT5 in gene regulation and hematologic malignancies. *Genes Dis.* **6**, 247–257
13. Hartshorne, D. J., Ito, M., and Erdodi, F. (1998) Myosin light chain phosphatase: subunit composition, interactions and regulation. *J. Muscle Res. Cell Motil* **19**, 325–341
14. Kiss, A., Erdodi, F., and Lontay, B. (2019) Myosin phosphatase: unexpected functions of a long-known enzyme. *Biochim. Biophys. Acta Mol. Cell Res* **1866**, 2–15
15. Kimura, K., Ito, M., Amano, M., Chihara, K., Fukata, Y., Nakafuku, M., *et al.* (1996) Regulation of myosin phosphatase by Rho and rho-associated kinase (Rho-kinase). *Science* **273**, 245–248
16. Feng, J., Ito, M., Ichikawa, K., Isaka, N., Nishikawa, M., Hartshorne, D. J., *et al.* (1999) Inhibitory phosphorylation site for Rho-associated kinase on smooth muscle myosin phosphatase. *J. Biol. Chem.* **274**, 37385–37390
17. Muranyi, A., Derkach, D., Erdodi, F., Kiss, A., Ito, M., and Hartshorne, D. J. (2005) Phosphorylation of Thr695 and Thr850 on the myosin phosphatase target subunit: inhibitory effects and occurrence in A7r5 cells. *FEBS Lett.* **579**, 6611–6615
18. Khasnis, M., Nakatomi, A., Gumpper, K., and Eto, M. (2014) Reconstituted human myosin light chain phosphatase reveals distinct roles of two inhibitory phosphorylation sites of the regulatory subunit, MYPT1. *Biochemistry* **53**, 2701–2709
19. Ichikawa, K., Ito, M., and Hartshorne, D. J. (1996) Phosphorylation of the large subunit of myosin phosphatase and inhibition of phosphatase activity. *J. Biol. Chem.* **271**, 4733–4740
20. Lontay, B., Pal, B., Serfozo, Z., Koszeghy, A., Szucs, G., Rusznak, Z., *et al.* (2012) Protein phosphatase-1M and Rho-kinase affect exocytosis from cortical synaptosomes and influence neurotransmission at a glutamatergic giant synapse of the rat auditory system. *J. Neurochem.* **123**, 84–99
21. Aburai, N., Yoshida, M., Ohnishi, M., and Kimura, K. (2010) Sanguinarine as a potent and specific inhibitor of protein phosphatase 2C in vitro and induces apoptosis via phosphorylation of p38 in HL60 cells. *Biosci. Biotechnol. Biochem.* **74**, 548–552
22. Yu, Y., Luo, Y., Fang, Z., Teng, W., Yu, Y., Tian, J., *et al.* (2020) Mechanism of sanguinarine in inhibiting macrophages to promote metastasis and proliferation of lung cancer via modulating the exosomes in A549 cells. *Onco Targets Ther.* **13**, 8989–9003
23. Wu, Y., Erdodi, F., Muranyi, A., Nullmeyer, K. D., Lynch, R. M., and Hartshorne, D. J. (2003) Myosin phosphatase and myosin phosphorylation in differentiating C2C12 cells. *J. Muscle Res. Cell Motil* **24**, 499–511
24. Alessi, D., MacDougall, L. K., Sola, M. M., Ikebe, M., and Cohen, P. (1992) The control of protein phosphatase-1 by targetting subunits. The major myosin phosphatase in avian smooth muscle is a novel form of protein phosphatase-1. *Eur. J. Biochem.* **210**, 1023–1035
25. Lontay, B., Kiss, A., Gergely, P., Hartshorne, D. J., and Erdodi, F. (2005) Okadaic acid induces phosphorylation and translocation of myosin phosphatase target subunit 1 influencing myosin phosphorylation, stress fiber assembly and cell migration in HepG2 cells. *Cell Signal* **17**, 1265–1275
26. Favre, B., Turowski, P., and Hemmings, B. A. (1997) Differential inhibition and posttranslational modification of protein phosphatase 1 and 2A in MCF7 cells treated with calyculin-A, okadaic acid, and tautomycin. *J. Biol. Chem.* **272**, 13856–13863
27. Lontay, B., Bodoor, K., Sipos, A., Weitzel, D. H., Loiselle, D., Safi, R., *et al.* (2015) Pregnancy and smoothelin-like protein 1 (SMTNL1) deletion promote the switching of skeletal muscle to a glycolytic phenotype in human and mice. *J. Biol. Chem.* **290**, 17985–17998
28. Li, R., Dou, J., Bai, T., Cai, B., and Liu, Y. (2022) Protein phosphatase PPM1B inhibits gastric cancer progression and serves as a favorable prognostic biomarker. *Appl. Immunohistochem. Mol. Morphol.* **30**, 366–374
29. Zhao, Y., Liang, L., Fan, Y., Sun, S., An, L., Shi, Z., *et al.* (2012) PPM1B negatively regulates antiviral response via dephosphorylating TBK1. *Cell. Signal.* **24**, 2197–2204
30. Tasdelen, I., van Beekum, O., Gorbenko, O., Fleskens, V., van den Broek, N. J., Koppen, A., *et al.* (2013) The serine/threonine phosphatase PPM1B (PP2Cbeta) selectively modulates PPARgamma activity. *Biochem. J.* **451**, 45–53
31. Li, Z., Chen, R., Li, Y., Zhou, Q., Zhao, H., Zeng, K., *et al.* (2023) A comprehensive overview of PPM1B: from biological functions to diseases. *Eur. J. Pharmacol.* **947**, 175633
32. Lontay, B., Serfozo, Z., Gergely, P., Ito, M., Hartshorne, D. J., and Erdodi, F. (2004) Localization of myosin phosphatase target subunit 1 in rat brain and in primary cultures of neuronal cells. *J. Comp. Neurol.* **478**, 72–87
33. Broustas, C. G., Grammatikakis, N., Eto, M., Dent, P., Brautigan, D. L., and Kasid, U. (2002) Phosphorylation of the myosin-binding subunit of myosin phosphatase by Raf-1 and inhibition of phosphatase activity. *J. Biol. Chem.* **277**, 3053–3059
34. Acconcia, F., Barnes, C. J., Singh, R. R., Talukder, A. H., and Kumar, R. (2007) Phosphorylation-dependent regulation of nuclear localization and functions of integrin-linked kinase. *Proc. Natl. Acad. Sci. U. S. A.* **104**, 6782–6787
35. Surve, S. V., Myers, P. J., Clayton, S. A., Watkins, S. C., Lazzara, M. J., and Sorkin, A. (2019) Localization dynamics of endogenous fluorescently labeled RAF1 in EGF-stimulated cells. *Mol. Biol. Cell* **30**, 506–523
36. Ryan, T., Shelton, M., Lambert, J. P., Malecova, B., Boisvenue, S., Ruel, M., *et al.* (2013) Myosin phosphatase modulates the cardiac cell fate by regulating the subcellular localization of Nkx2.5 in a Wnt/Rho-associated protein kinase-dependent pathway. *Circ. Res.* **112**, 257–266
37. Vogt, A., Tamewitz, A., Skoko, J., Sikorski, R. P., Giuliano, K. A., and Lazo, J. S. (2005) The benzo[c]phenanthridine alkaloid, sanguinarine, is a selective, cell-active inhibitor of mitogen-activated protein kinase phosphatase-1. *J. Biol. Chem.* **280**, 19078–19086
38. Yang, Z., Xu, G., Wang, B., Liu, Y., Zhang, L., Jing, T., *et al.* (2021) USP12 downregulation orchestrates a protumourigenic microenvironment and enhances lung tumour resistance to PD-1 blockade. *Nat. Commun.* **12**, 4852
39. Ying, H., Ji, L., Xu, Z., Fan, X., Tong, Y., Liu, H., *et al.* (2020) TRIM59 promotes tumor growth in hepatocellular carcinoma and regulates the cell cycle by degradation of protein phosphatase 1B. *Cancer Lett.* **473**, 13–24
40. Wang, H., Chen, Y., Han, J., Meng, Q., Xi, Q., Wu, G., *et al.* (2016) DCAF4L2 promotes colorectal cancer invasion and metastasis via mediating degradation of NFkappab negative regulator PPM1B. *Am. J. Transl Res.* **8**, 405–418
41. Horvath, D., Sipos, A., Major, E., Konya, Z., Batori, R., Dedinszki, D., *et al.* (2018) Myosin phosphatase accelerates cutaneous wound healing by regulating migration and differentiation of epidermal keratinocytes via Akt signaling pathway in human and murine skin. *Biochim. Biophys. Acta Mol. Basis Dis.* **1864**, 3268–3280
42. Kiss, E., Muranyi, A., Csortos, C., Gergely, P., Ito, M., Hartshorne, D. J., *et al.* (2002) Integrin-linked kinase phosphorylates the myosin phosphatase target subunit at the inhibitory site in platelet cytoskeleton. *Biochem. J.* **365**, 79–87
43. Toth, A., Kiss, E., Herberg, F. W., Gergely, P., Hartshorne, D. J., and Erdodi, F. (2000) Study of the subunit interactions in myosin phosphatase by surface plasmon resonance. *Eur. J. Biochem.* **267**, 1687–1697

ASBMB

ARTICLE IN PRESS

BBA - Molecular Cell Research xxx (xxxx) xxx–xxx

lontay.beata_285_24

Contents lists available at ScienceDirect

BBA - Molecular Cell Research

journal homepage: www.elsevier.com/locate/bbamcr

Review

Myosin phosphatase: Unexpected functions of a long-known enzyme☆

Andrea Kiss[a], Ferenc Erdődi[a,b], Beáta Lontay[a,*]

[a] Department of Medical Chemistry, Faculty of Medicine, University of Debrecen, Debrecen, Hungary
[b] MTA-DE Cell Biology and Signaling Research Group, Faculty of Medicine, University of Debrecen, Debrecen, Hungary

ARTICLE INFO

Keywords:
Protein phosphatase 1
Myosin phosphatase
MYPT1/PPP1R12A
Insulin resistance
Cancer
Cell cycle
Neurotransmitter release
Development
Dephosphorylation
Interactome
Gene expression

ABSTRACT

Myosin phosphatase (MP) holoenzyme is a Ser/Thr specific enzyme, which is the member of protein phosphatase type 1 (PP1) family and composed of a PP1 catalytic subunit (PP1c/PPP1CB) and a myosin phosphatase targeting subunit (MYPT1/PPP1R12A). PP1c is required for the catalytic activity of the holoenzyme, while MYPT1 regulates MP through targeting the holoenzyme to its substrates. Above the well-characterized function of MP, as the major regulator of smooth muscle contractility mediating the dephosphorylation of 20 kDa myosin light chain, accumulating data support its role in other, non-contractile functions. In this review, we summarize the scaffold function of MP holoenzyme and its roles in processes such as cell cycle, development, gene expression regulation and neurotransmitter release. In particular, we highlight novel interacting proteins of MYPT1 and pathophysiological functions of MP relevant to tumorigenesis, insulin resistance and neurodegenerative disorders.

This article is part of a Special Issue entitled: Protein Phosphatases as Critical Regulators for Cellular Homeostasis edited by Prof. Peter Ruvolo and Dr. Veerle Janssens.

1. Introduction

Reversible phosphorylation of proteins on serine (Ser), threonine (Thr) and tyrosine (Tyr) residues is one of the most common mechanisms by which coordinated regulation of cellular processes occurs [1]. The phosphorylation status of the cells is determined by the balance between the activities of protein kinases and protein phosphatases, therefore, the identification of the specific kinase(s) and phosphatase(s) implicated in the given cellular process is essential to uncover regulatory tools. Both types of enzyme are equally important in maintaining the physiologically relevant phosphorylation status of proteins, but they affect the phosphorylation signal differently. It is assumed that phosphatases may determine the time of the transduction of the signal to its intracellular target as well as the duration of the signal, while kinases have more influence over the strength of the signal [2]. There are hundreds of protein kinases and phosphatases as possible regulators of cellular events, however, these enzymes are interrelated too, as phosphatase mediation involves phosphorylation of phosphatase inhibitory and regulatory proteins, while dephosphorylation of kinases by phosphatases also contribute to their activation/inhibition. This

Abbreviations: AR, androgen receptor; CDK, cyclin dependent kinase; Chk1, Check point kinase 1; CLA, calyculin-A; CPI-17, C-kinase-activated protein phosphatase-1 inhibitor of 17 kDa; EGCG, epigallocatechin-gallate; eNOS, endothelial nitrogen monoxide synthase; iNOS, inducible nitrogen monoxide synthase; ERM, ezrin radixin moesin; FIH, factor inhibiting hypoxia inducible factor; HDAC7, histone deacetylase 7; GBPI, gastrointestinal-and brain-specific PP1 inhibitor; ILK, integrin linked kinase; IP3K, inositolphosphatae 3 kinase; IR, insulin receptor; IRS1, insulin receptor substrate 1; KEPI, kinase enhanced PP1 inhibitor; LATS1, large tumor suppressor kinase 1; LPS, lipopolysaccharide; 67LR, 67 kDa laminin receptor; M20/21, small subunit of myosin phosphatase of 20/21 kDa; MLC20, 20 kDa regulatory light chain of myosin II; MLCK, MLC20 kinase; MLCP, myosin light chain phosphatase; MP, myosin phosphatase; M-RIP/p116RIP, myosin phosphatase-Rho interacting protein; microRNA-30d, miR-30d; MYPT1, myosin phosphatase target subunit 1; Nkx2.5, NK2 homeobox 5; OA, okadaic acid; Par-4, prostate apoptosis response protein; NUAK1, NUAK family SnF1-like kinase-1; PDK, pyruvate dehydrogenase kinase; PHI-1 and -2, phosphatase holoenzyme inhibitor-1 and -2; PI3K, phosphatidylinositide 3 kinase; PKA, cyclic AMP-dependent protein kinases/protein kinase A; PKC, protein kinase C; PKGIα, cGMP-dependent protein kinase Iα/protein kinase G; PLK1, polo-like kinase 1; PP1c, protein phosphatase 1 (PP1) catalytic subunit; pRb, retinoblastoma protein; PP2Ac, protein phosphatase-2A (PP2A) catalytic subunit; PP2B, protein phosphatase-2B; PRMT5, protein arginine methyltransferase 5; ROCK, Rho A associated kinase; SIAH2, Seven in absentia homolog 2; SMTNL1, smoothelin like 1 protein; SNARE, soluble *N*-ethylmaleimide sensitive factor attachment protein receptor; SNAP-25, synaptosomal-associated protein of 25 kDa; SKM, skeletal muscle; VSMC, vascular smooth muscle cell; ZIPK, zipper-interacting protein kinase

☆ This article is part of a Special Issue entitled: Protein Phosphatases as Critical Regulators for Cellular Homeostasis edited by Prof. Peter Ruvolo and Dr. Veerle Janssens.

* Corresponding author at: Department of Medical Chemistry, Faculty of Medicine, University of Debrecen, H-4032 Debrecen, Egyetem tér 1, Hungary.
E-mail address: lontay@med.unideb.hu (B. Lontay).

https://doi.org/10.1016/j.bbamcr.2018.07.023
Received 13 May 2018; Received in revised form 9 July 2018; Accepted 26 July 2018
0167-4889/ © 2018 Elsevier B.V. All rights reserved.

Please cite this article as: Kiss, A., BBA - Molecular Cell Research (2018), https://doi.org/10.1016/j.bbamcr.2018.07.023

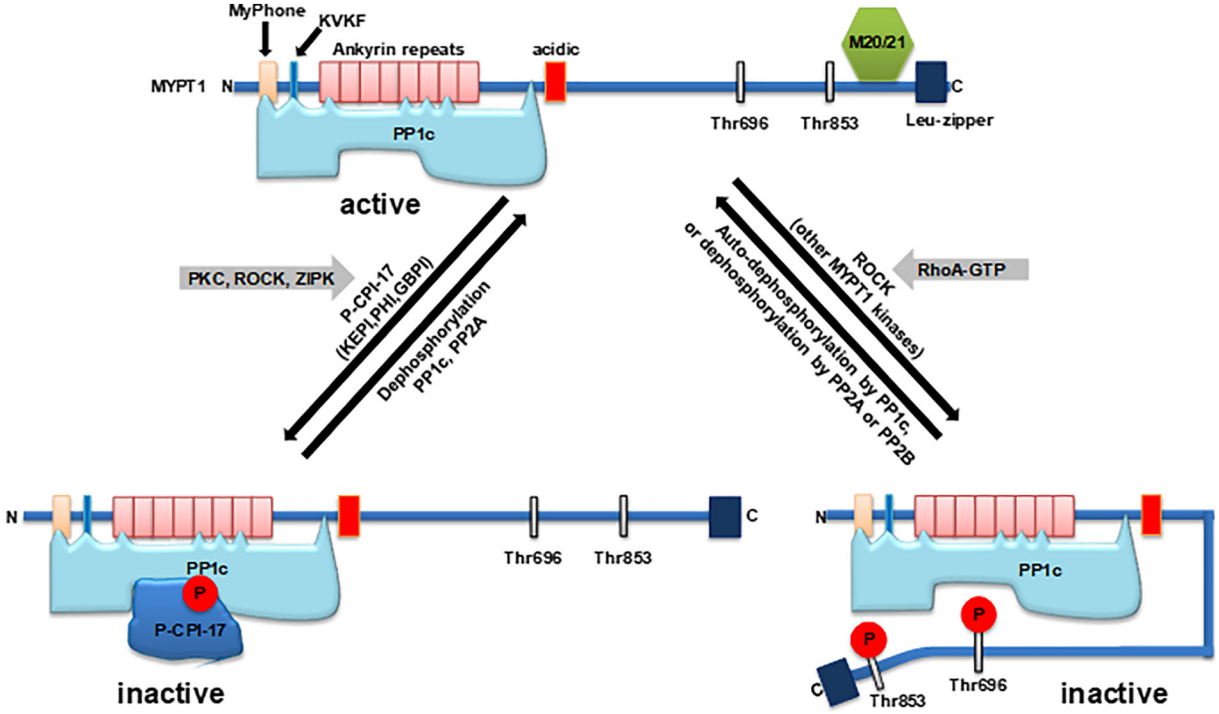


Fig. 1. The structure and regulation of MP by phosphorylation. The upper part of the figure depicts the major structural regions of MYPT1 and its interaction with PP1c and M20/21. The lower part represents the inhibition of MP by direct phosphorylation of its MYPT1 regulatory subunit at Thr696 and Thr853 (right). A scheme for inhibition by phosphorylated CPI-17 is also shown. Possible dephosphorylating phosphatases are also indicated under the reverse arrows. See text for more details for the phosphorylation dependent regulation of MP activity.

review mainly focuses on the regulatory possibilities of the phospho-serine/threonine (P-Ser/Thr) specific protein phosphatases with a special emphasis on the cellular roles of myosin phosphatase (MP). The major aims are to reveal primarily the novel, non-contractile functions of this enzyme as it has received also considerable attention for the past few years. Even though, this introduction may not disregard a brief retrospective summary of studies on MP in relation to myosin phosphorylation and smooth muscle contraction as well as the structure and regulation of MP.

Besides the definite physiological significance, smooth muscle has been the tissue in which numerous signaling pathways (Ca^{2+}-signal, NO/cGMP effects, etc.) are studied in connection with the changes in contractile features. Even in protein phosphorylation history, the regulation of smooth muscle contraction via phosphorylation-dephosphorylation of the 20 kDa regulatory light chain of myosin II (MLC20) was investigated soon after the recognition that the active form of glycogen phosphorylase required covalently bound phosphate (reviewed in [1]). The first studies were focused on the MLC20 kinase (MLCK) [3], and the phosphatase was thought to ensure only the reversibility of the modification by dephosphorylation. The role of MLC20 phosphatase (MLCP) in smooth muscle contraction was clearly revealed when okadaic acid (OA), a potent membrane permeable phosphatase inhibitor was discovered. OA induced muscle contraction parallel with MLC20 phosphorylation in skinned gizzard preparation even in the absence of Ca^{2+} [4]. These data indicated that phosphorylation of MLC20 may occur via the possible involvement of Ca^{2+}-independent kinase(s) distinct from the classical Ca^{2+}-calmodulin dependent MLC20 kinase (MLCK) if the phosphatase is suppressed in the system. At about the same time Ca^{2+}-senzitization of smooth muscle contraction in G-protein coupled pathways was also demonstrated with the possible involvement of MLCP (reviewed in [5]). These findings directed attention to the structure and regulation of MLCP, and although there were attempts before to isolate this enzyme, many distinct forms had been reported even without a consensus in the type of the phosphatase.

The myosin phosphatase (MP) was isolated first from chicken gizzard [6,7] and later from pig bladder [8]. These independent groups confirmed that the MP/MLCP holoenzyme consists of three subunits: a protein phosphatase-1 catalytic subunit (PP1c) of about 38 kDa; a large myosin binding subunit of 110–133 kDa (later defined as myosin phosphatase target subunit-1, MYPT1); and a smaller subunit of about 20/21 kDa (M20/21). It is to note that the myosin phosphatase is named by different acronyms such as MP, MLCP or PP1M. We use MP in further description of the structure and the function of this enzyme in the cellular processes and the name PP1cβ/δ (PPP1CB) for the catalytic subunit and MYPT1 (PPP1R12A) for the 130–133 kDa major regulatory subunit. The latter protein is also termed as M110, myosin binding subunit (MBS), and M130/M133 in earlier publications.

1.1. The structure and regulation of MP

The interactions of the subunits in the trimeric holoenzyme of MP have been a great interest for the past three decades and identified by distinct binding techniques and structural analysis. It was apparent that PP1c was responsible for the catalytic activity and it interacted with MYPT1, which plays a targeting role in the dephosphorylation process as it also binds to myosin directing PP1c toward the phosphorylated residues in MLC20. The M20/21 subunit binds to the C-terminal region of MYPT1 and had no direct influence on phosphatase activity. While MYPT1 is ubiquitously expressed in mammalian cells, M20/21 is found, besides smooth muscle, mainly in cardiac muscle. The physiologic role of M20/21 is largely unrevealed yet, but the data have gained so far suggest that it increases Rho-A associated kinase (ROCK) dependent inhibitory phosphorylation of MYPT2 (the heart specific MYPT isoform) in cardiomyocytes resulting in suppression of MP activity [9]. It has also been shown that M20/21 regulates microtubule dynamics [10]. It was established that out of three major PP1c isoforms (α, β/δ, γ1) expressed in mammalian cells MYPT1 exclusively interacted with PP1cβ/δ [11] and this specificity was determined by residues in PP1c located

at the central region. The structure of MYPT1 and its isoforms has been described in several reviews [12,13] together with other MYPT family proteins such as MYPT2 [14], MBS85, MYPT3 and TIMAP [15]. Our present review focuses on the physiological roles of the ubiquitously expressed MYPT1 complexed with PP1cβ/δ in distinct cell types.

The schematic structure of MYPT1 in association with PP1c and M20/21 is shown in Fig. 1. MYPT1 includes an RVxF (consensus sequence RxxQV/I/LK/RxY/W) PP1c-binding motif ($K^{35}VKF^{38}$) which appears to be essential for the interaction of MYPT1 with PP1c [16]. Additional binding sites are: (i) a region N-terminal to the RVxF motif (residues 10–17 in MYPT1 termed the myosin phosphatase N-terminal element or MyPhoNE); (ii) repeats 1, 5, 6 and 7 of the ankyrin repeat region [17]; and (iii) region(s) (not identified) between residues 301 to 511 close to the central region [16].

It has been an attractive idea that the interaction of PP1c and MYPT1 might be regulated by the phosphorylation of MYPT1 in the N-terminal region. Thr34 at the proximity of the PP1c-binding motif (^{35}KVK^{38}F) was a good candidate to disrupt subunit interactions after phosphorylation. However, Thr34 phosphorylated by PKC did not either strengthen or weaken the interaction of MYPT1 with PP1c [16]. Recently, Hu et al. [18] identified Ser20 as a phosphorylation site for CHK1 (Check point kinase 1) and this phosphorylation event is claimed to be essential to the interaction of MYPT1 with PP1c as well as to the dephosphorylation of PLK1 by MP. On the other hand, phosphorylation of Ser20 decreases the stability of MYPT1 rendering it more susceptible for proteasome degradation. It is unclear yet how these opposite effects, i.e. promoting activity of MP toward PLK1 and at the same time decreasing activity by MYPT1 degradation, are balanced to reach beneficial physiological responses.

A binding site for PP1c in the C-terminal half of MYPT1 has not been identified. Nevertheless, this MYPT1 region plays an important role in the phosphorylation-dependent inhibition of MP activity. MYPT1 includes several consensus sites for a number of protein kinases and among these phosphorylation at Thr696 and/or Thr853 (numbering is for the human isoform) results in inhibition of MP activity (Fig. 1). ROCK was first identified as the kinase for the phosphorylation of both Thr696 and Thr853 [19], but later several other kinases including zipper-interacting protein kinase (ZIPK), integrin-linked kinase (ILK), myotonic dystrophy kinase, Raf-1 [20] and p21-activated protein kinases were also shown to act on Thr696 (reviewed in [12,13,21] and see references therein). Using Thr696Ala and Thr853Ala mutants of MYPT1 it was also established that phosphorylation of either Thr696 or Thr853 resulted in inhibition of PP1c in a reconstituted PP1c-MYPT1 complex in vitro [22]. The current hypothesis is that phosphorylation of these sites induces such structural movements in MYPT1 which allows the inhibitory phosphorylation peptide to interact with the substrate binding groove and the catalytic center of PP1c (Fig. 1). These suggested conformational changes might be helped by the hypothesized, partly “unstructured” nature of the C-terminal regions of MYPT1. However, around the inhibitory phosphorylation site (Thr696) the protein is structured. It was demonstrated in a study by NMR [23] of a MYPT1 peptide (658–714) including Thr696 that the average structure of this peptide is relatively extended and consists of three helices. The Thr696 is located at the end of the middle helix and the loops connecting the helices are thought to be quite flexible, therefore, they may allow the necessary movements upon phosphorylation leading to inhibition. The sequence around P-Thr696 or P-Thr853 are similar to that of P-Ser19 in MLC20 [17] therefore these MYPT1 regions may act as substrate analogues which are dephosphorylated by PP1c at a very slow rate compared to P-Ser19 of MLC20.

Thr696 and Thr853 inhibitory phosphorylation sites are preceded by Ser695 and Ser852, residues in MYPT1 which are phosphorylated by cyclic AMP- and cGMP-dependent protein kinases (PKA and PKG). First, it was demonstrated that PKA or PKG dependent phosphorylation of Ser695 counteracted with phosphorylation of Thr696 protecting MP from ROCK- or other MYPT1 kinase dependent inhibition [24]. These phosphorylation assays were further developed to identify cross-talk between the PKA and ROCK-dependent phosphorylation events [25,26] and suggested that PKA phosphorylation at Ser852 also abolish subsequent phosphorylation at Thr853, while an interesting finding was that PKA is able to phosphorylate simultaneously all four residues (Ser695, Thr696, Ser852, Thr853) but this MYPT1 form is not inhibitory on PP1c.

Besides the direct inhibition of MP activity by phosphorylation of MYPT1, MP activity could also be suppressed by inhibitory proteins in an indirect manner (Fig. 1). The best known MP inhibitor is the C-kinase-dependent phosphatase inhibitor of 17 kDa (CPI-17) which is active following phosphorylation at Thr38 by protein kinase C (PKC). Other kinases (ROCK, ZIPK) may also be involved in Thr38 phosphorylation (reviewed in [27]). CPI-17, unlike other PP1 inhibitors, such as inibitor-1 and -2, can inhibit both PP1c and MP (PP1c-MYPT1 complex) with high effectiveness, and although it does not contain a canonical PP1c binding motif, its interaction with both PP1c and MYPT1 is apparent. Other CPI-17 family members: phosphatase holoenzyme inhibitor-1 and -2 (PHI-1 and -2), kinase enhanced PP1 inhibitor (KEPI) and gastrointestinal-and brain-specific PP1 inhibitor (GBPI) include PP1c-binding RVxF motif and an inhibitory phosphorylation sequence very similar to that of in CPI-17 [27]. KEPI also inhibits both PP1c and MP [28] and its phosphorylation and inhibitory action on MP in THP-1 and in MCF-7 cells is also considered [29].

An important question with respect to the regulation of MP which phosphatase(s) can relieve MP from the inhibition by phosphorylated MYPT1 or CPI-17. Isolated PP1c, protein phosphatase-2A (PP2A) catalytic subunit (PP2Ac) and protein phosphatase-2B (PP2B, also termed calcineurin) dephosphorylated the phospho-Thr696 and -Thr853 in MYPT1 (Fig. 1). It was also established that cyclosporin A, a calcineurin/PP2B inhibitor, increased the phosphorylation level of both Thr696 and Thr853 in MYPT1 as well as influenced the barrier function in endothelial cells suggesting that PP2B plays an important role in the dephosphorylation of these inhibitory sites in cellular systems [30]. Similarly, calyculin-A in a PP2A inhibitory concentration resulted in significant elevation in the phosphorylation of Thr696 of MYPT1 and suppression of the barrier function in endothelial cells implicating PP2A in MYPT1^{pThr696} dephosphorylation [31]. These are indications for the roles of PP2B and PP2A in dephosphorylation of MYPT1 and activation of MP and imply a specific interplay between the distinct types of phosphatase in cellular regulation. In recent works 67 kDa laminin receptor (67LR) mediated activation of MP was reported in melanoma cell lines [32] and in endothelial cells [31] by epigallocatechin-gallate (EGCG), a green tea ingredient. In an EGCG/67LR → PKA → PP2A → MP pathway activation of PP2A (containing Bδ subunit) by PKA phosphorylation results in enhanced dephosphorylation of both MYPT1^{pThr696} and CPI-17^{pThr38} thereby activation of MP.

The above results point to the possibility that PP2A may also be a CPI-17^{pThr38} phosphatase. However, a recent model has been worked out stating that the inhibitory action of CPI-17 ^{pThr38} on MP could be due to “unfair competition” with the substrates, implying that the inhibitor binds tightly excluding interactions of PP1c (or MP) with the substrates and on the other hand interaction of CPI-17^{pThr38} with a dephosphorylating phosphatase [33]. In addition, CPI-17^{pThr38} is a “bad” substrate for MP, it is dephosphorylated slowly and this also contributes to a sustained inhibitory action. Nonetheless, the dephosphorylation of CPI-17^{pThr38} by PP1c is considered to be sufficient and necessary for the reactivation of MP. Based on this suggested model, a similar “autodephosphorylation” mechanism may play a role in the reactivation of MP from inhibition caused by phosphorylation of MYPT1 at Thr696 and/or Thr853. The MYPT1 subunit of MP is subject to posttranslational modifications other than phosphorylation also and these events may affect the physiological role of this enzyme. MYPT1 is a substrate for the asparaginyl hydroxylase FIH [factor inhibiting HIF (hypoxia inducible factor)] and it is hydroxylated in the ankyrin repeat region in cultured cells and in vitro using purified proteins [34]. The

physiological consequence of this modification with respect to MP activity is unclear. It is suggested that MYPT1 serving as an alternative substrate of HIF may influence HIF/hypoxia signaling.

It has also been shown that MYPT1 is subject to reversible methylation by histone lysine methyltransferase SETD7 and histone demethylase LSD1 [35] at Lys442. As methylation stabilizes MYPT1, increased demethylation activity which is quite common in malignant cells results in degradation of MYPT1 by the ubiquitin-proteasome pathway, favoring retinoblastoma protein phosphorylation and cell cycle progression of cancer cells. These data suggest that MYPT1 protein stability is regulated by its methylation status influencing the phosphorylation level of protein(s) dephosphorylated by MP involving the targeting function of MYPT1.

Molecular interaction between Seven in absentia homolog 2 (SIAH2) and MYPT1 has been shown to be necessary for the proteasomal degradation of MYPT1 in mammalian cells [36]. This interaction involved the substrate binding domain of SIAH2 (116–324) and a central region of MYPT1 (445–632) which included a degenerate consensus SIAH-binding motif of RLAYVAP (493–499). SIAH2 is an E3-ligase capable of directing proteins for degradation by the ubiquitin–-proteasome system. These data confirm that the cellular level of MYPT1 and thereby the activity of MP is regulated by proteolytic degradation. In this regard it is interesting that MYPT1 is also subject to proteolytic cleavage by caspase-3 during apoptosis of cells [37]. Caspase-3 cleavage at the C-terminal region (Asp884) results in loss of the myosin binding ability of MYPT1 concomitant with increased inhibitory phosphorylation at Thr696 and Thr853. As a consequence of cleavage of the myosin binding region, MYPT1 dissociated from actin stress fibers and this delocalization together with enhanced inhibitory phosphorylation led to hyperphosphorylation of myosin-II.

1.2. Interactions of MYPT1

The unique structure of MYPT1 provides platforms for multiple interaction with numerous proteins and other biological macromolecules (Fig. 2 and Table S1). It is also important that which region(s) of MYPT1 is/are responsible for the binding of these interactive partners (Fig. 2). First, the binding of the major substrate, P-myosin, was probed and although these experiments led to controversial results from different groups the consensus is that P-myosin interacts with both the N-terminal and C-terminal regions in a way that P-MLC20 bind at the second half of the ankyrin repeat region while the heavy chain associates with the C-terminal part [12]. A similar binding pattern is established for the retinoblastoma protein (pRb) [38] and also hypothesized for the interaction of MYPT1 with the endothelial nitric oxide synthase (eNOS) [31].

Binding of the other MYPT1 partners are more region selective (reviewed in [12,13]). Adducin, Tau, MAP2, protein methyltransferase 5 (PRMT5) and SNAP-25 all bind to the N-terminal region and they are phosphorylated by ROCK and dephosphorylated by MP. Smoothelin-like protein-1 (SMTLN1) as well as calcineurin (PP2B), a MYPT1 phosphatase, binds preferentially also to the N-terminal half which contains a specific PIxIT motif for its binding. In contrast, GTP-RhoA, moesin (and ezrin), interleukin-16 precursor protein [39], prostate apoptosis response (Par-4) protein [40], myosin phosphatase-Rho interacting protein (M-RIP/p116RIP) and cGMP-dependent kinase (cGKIα) bind to the C-terminus and within this group interleukin-16 precursor protein, Par-4, M-RIP and cGKIα specifically interact with the leucine-zipper motifs. The diversity of these interactions predicts the role of MP in a great deal of cellular processes and the significance of these protein-protein interactions will be highlighted in the upcoming sections (Table 1).

2. Diverse functions of myosin phosphatase

2.1. Basic role of myosin phosphatase in cytoskeletal processes

MP has an established role in the control of actomyosin contractility via dephosphorylation of MLC20 but it also contributes to the regulation of cell migration [41] or cell adhesion [42]. MP also plays a role in the regulation of cytoskeletal organization by dephosphorylation of the ERM proteins. The ERM family consists of three structurally related proteins, ezrin, radixin, and moesin, which function as linkers between transmembrane proteins and the underlying cytoskeleton, and fulfill many cellular functions in cell adhesion, migration, or proliferation. Inactive, ERM proteins reside in the cytoplasm in a closed conformation, while phosphorylation at a conserved threonine residue (Thr567 in ezrin, Thr564 in radixin, and Thr558 in moesin) by ROCK or PKC induces the formation of an open and active conformation enabling them to bind to their target molecules [43,44]. Several reports suggest that MP is responsible for dephosphorylation of ERM in different cell types [44–46]. Direct interaction between C-terminal part of MYPT1 (rat sequence) and the N-terminal domain of ezrin and moesin was identified, and MP was shown to dephosphorylate the C-terminal part

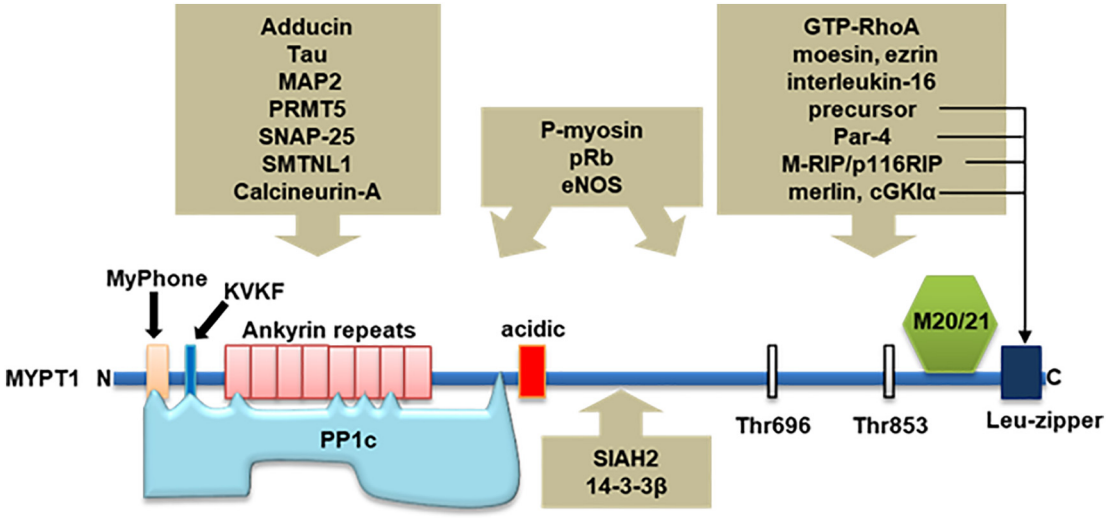


Fig. 2. Protein-protein interactions of MYPT1. Besides PP1c a few major interacting partners of MYPT1 are shown classified as binding to the N-terminal region (left panel above the MYPT1 scheme), to both the N-terminal and C-terminal region (middle panel) and to the C-terminal regions (right panel). Arrows in the right panel indicate proteins which interact with the leucine zipper motifs. Proteins binding to the central region are indicated below the MYPT1 scheme.

Table 1
Substrates of myosin phosphatase.

MP substrate	Tissue/cell type	Regulated P-site	Protein kinase	Citation
MLC20	VSM	Thr18	MLCK/ROK	[5,6]
ERM				
Ezrin	HPAEC	Thr567	ROK	[44]
Radixin	HPAEC	Thr564 (direct dephosphorylation was not proven)	ROK	[44]
Moesin	HPAEC, MDCK	Thr558	ROK	[43,44]
Adducin	MDCK (only interaction was proven)	Not identified	ROK	[48]
Tau	Brain	Thr245/Thr377/Ser409 (direct dephosphorylation was not proven)	ROK	[45]
pRb	THP-1	Thr826	CDK4	[38]
	SBC-5	Thr807/811	CDK4	[35]
eNOS	BPAEC	Thr497	PKC/ROK	[31]
SNAP25	Mouse cortex, B50	Thr138	ROK, PKA, PKC	[74,75]
Syntaxin	Mouse cortex, B50	Ser14	ROK	[74]
Synapsin	Mouse cortex, B50	Ser9	ROK	[74]
PRMT5	Human hepatocarcinoma cell	Thr80	ROK	[54]
IRS1	Skeletal muscle, L6	Ser522	AKT?	[125]
Polo-like kinase 1	SW962, HeLa	Thr210	Aurora A	[62]
HDAC7	Thymocytes	Ser155	PKD1	[90]
		Ser318		
		Ser448		

of moesin phosphorylated by ROCK in vitro [44]. In another study, selective association of ERM proteins and MP subunits were revealed by coimmunoprecipitation: ezrin and moesin directly interacted with PP1cδ, while radixin was bound to MYPT1 only [45]. MYPT1 was found to colocalize with moesin at membrane ruffling area in MDCK epithelial cells suggesting that MP may play a role in the regulation of moesin phosphorylation in vivo [44]. Dephosphorylation of ezrin by MP was demonstrated by MYPT1-depletion or CPI-17 overexpression experiments in different cell lines [47]. MP-catalyzed dephosphorylation of ERM proteins has a protective effect against LPS-induced endothelial permeability [46]. Overexpression of CPI-17 in human melanomas showed Ras activation and tumorigenic transformation via inhibition of MP and subsequent activation of ERM proteins [47]. MP together with ROCK was identified as a regulator of the phosphorylation state of adducin, which mediates the interaction of adducin with F-actin [48].

The microtubule associated proteins, Tau and MAP2 were also found to interact with both ROCK and MYPT1, and MP was shown to dephosphorylate ROCK-phosphorylated Tau in vitro in PC12 pheochromocytoma cells proposing that MP may also regulate microtubule dynamics in neuroblastoma cells [49].

2.2. Role of MP in the control of cell proliferation and cell division

2.2.1. Dephosphorylation of retinoblastoma protein

MP contributes to the control of cell proliferation by distinct mechanisms [50]. One remarkable cell cycle-related interactor of MYPT1 is retinoblastoma protein (pRb), a tumor suppressor that is dis-regulated in many types of cancer. pRb regulates cell cycle and proliferation by repressing transcription of E2F-mediated genes. Phosphorylation by cyclin-dependent kinases inactivates pRb and promotes cell cycle progression. PP1 or PP2A are responsible for dephosphorylation and activation of pRb [51,52]. MYPT1 was identified as a possible PP1-targeting subunit acting on phosphorylated pRb in leukemic cells [38]. The interaction of MYPT1 and pRb was confirmed at cellular level, and surface plasmon resonance (SPR) studies revealed that the C-terminal fragment of pRb binds to both the N- and C-terminal part of MYPT1. The MYPT1-PP1c complex enhanced the catalytic activity toward phosphorylated pRb compared to PP1c alone, supporting the targeting function of MYPT1 during pRb dephosphorylation. Inhibition of MP either by CLA or by the overexpression of the endogenous MP inhibitory protein KEPI [29] results in an increased phosphorylation of pRb-Thr826, and this may contribute to the chemoresistance of leukemic cells caused by phosphatase inhibition. In another study, overexpression of MYPT1 resulted in a decrease in the phosphorylation of pRb at Ser807/811 residues, suggesting that MP may modulate pRb activity via dephosphorylation at multiple sites [35]. MP-catalyzed dephosphorylation of pRb was proposed to play a role in the regulation of androgen receptor (AR) which plays a pivotal role in the development and progression of prostate cancer [53]. Analysis of clinical datasets showed downregulation of MYPT1 and upregulation of KEPI in human prostate cancer cells. Restoring MP activity in prostate cancer cells by KEPI depletion was able to repress aberrant AR activity by the following mechanism: activated MP dephosphorylates pRb at Ser807/811 residues causing repression of E2F1 mediated cell cycle progression and subsequent AR phosphorylation by CDKs and a significant inhibition of AR target gene expression leading to reduced proliferative and migratory capacity. In addition to dephosphorylation-dependent regulation, MP was also implicated in the control of protein expression of pRb via dephosphorylation and inhibition of arginine methyltransferase PRMT5 ([54], see in details later in this review). These data imply that MP may be involved in the regulation of cell cycle progression by controlling the activity of pRb at multiple levels.

2.2.2. Dephosphorylation and activation of merlin

The NF2 tumor suppressor gene product, merlin was also reported to be dephosphorylated and activated by MP [55]. Merlin has similar domain organization as the ERM family proteins, but it is regulated in an opposing manner, that is, phosphorylated merlin is inactive, while the dephosphorylated form is active and functions in contact inhibition and growth suppression. Merlin inhibits cell proliferation via multiple mechanism, it initiates anti-mitogenic signaling and suppresses oncogenic gene expression [56,57]. MP was identified as the decisive phosphatase that renders merlin active in its closed conformation by dephosphorylation at Ser518 residue. MYPT1 binds through its leucine zipper domain to the amino-terminal part of the alpha-helical coiled coil region of merlin, and L339 side chain of merlin was shown to be critical for the interaction. Depletion of MYPT1 elevates merlin phosphorylation and supports Ras activation. CPI-17, the specific inhibitor of MP, is upregulated in many cancer cells, and causes the loss of merlin function in tumor suppression [55]. ILK was identified as the specific kinase responsible for the inhibition of MP in cancer cells. By direct phosphorylation of MYPT1 ILK promotes the inactivation of merlin and concomitant suppression of the Hippo tumor suppressor pathway which leads to the activation of YAP/TAZ/TEAD-mediated transcription of growth-promoting genes. [58]. Recently, nuclear association of MYPT1 and merlin in cardiomyocytes was reported. MP was shown to be activated in response to oxidative stress mediating the dephosphorylation and activation of merlin, thereby modulating Hippo signaling in

cardiomyocytes [59]. Interestingly, curcumin – a natural compound with anti-inflammatory and anti-tumorigenic effects – seems to assist the activation of merlin by dephosphorylation-dependent activation of MP [60].

2.2.3. Regulation of the dephosphorylation of polo-like kinase 1 by MP during mitosis

MYPT1 is specifically phosphorylated during the course of mitosis by proline-directed kinases, and phospho-MYPT1 was shown to associate with the mitotic polo-like kinase 1 (PLK1) on centromeres and on kinetochores [61,62]. PLK1 is a Ser/Thr kinase that controls a variety of mitotic events including G2/M transition, maturation of centrosomes, mitotic spindle assembly, sister chromatid segregation, mitotic exit, and cytokinesis. Silencing of MYPT1 results in an elevated phosphorylation of PLK1 at its activation site, Thr210, suggesting that MP may antagonize the function of PLK1 during mitosis. Accordingly, simultaneous reduction of MYPT1 and PLK1 protein level rescue cells from mitotic arrest caused by inhibition of PLK1 alone [62]. Studies in the last few years have demonstrated that via spatial and temporal coordination of PLK1 activity MYPT1 contributes to the control of mitotic progression. For example, MYPT1-depleted cells enter M phase more quickly, implicating MP in G2 checkpoint regulation [63]. Loss of MYPT1 also results in precocious sister chromatid segregation [64] as well as the reversal of the step-wise increase in the kinetochore-microtubule assembly stability between prometaphase and metaphase [65]. Binding and activity of MP toward PLK1 is modulated by multiple phosphorylation sites and several kinases (Fig. 3). Proline-directed kinases, CDK1 (cdc2) and MAPK were shown to phosphorylate Ser432, Ser473 and Ser601 residues in MYPT1 during mitosis. Phosphorylation of Ser473 by Cyclin A/Cdk1 complex constitutes a recognition site in MYPT1 for the Polo-box domain of PLK1, which is crucial for the association of MYPT1 and PLK1 [62,65]. An adaptor protein, optineurin was shown to be required too for bringing CDK1 in the vicinity of MYPT1 and stimulate CDK1-mediated MYPT1-Ser473 phosphorylation and subsequent PLK1 dephosphorylation during mitosis [66]. It was suggested that phosphorylation of MYPT1-Ser473 alone is not sufficient for proper activation, but Ser445 phosphorylation is also required to stimulate MP activity toward PLK1. The latter phosphorylation is mediated by LATS1, another mitotic kinase [63]. Upon cell detachment, NUAK1 phosphorylates MYPT1 at Ser472 along with Ser445 and Ser910 residues, which was shown to trigger binding of MYPT1 to 14–3-3 protein thereby inhibiting the activity of MP [39,42]. In addition, the phosphorylation of these side chains, most notably Ser472, may also interfere with the "priming" phosphorylation of MYPT1 at the PLK1 docking site, Ser473. Consistent with this, NUAK1 activation leads to increased PLK1 phosphorylation, presumably by weakening the association between MYPT1 and its substrate [67]. No discussion is given by the authors on the contradictory effect of Ser445 phosphorylation on MP activity. NUAK is activated by Liver kinase 1 (LKB1), and it was reported that shRNA-mediated inhibition of LKB1 strengthens the association between MYPT1 and PLK1, providing further evidence for the negative regulatory role of NUAK1 in MYPT1-mediated dephosphorylation of PLK1 [68]. It is concluded that LKB1 stabilizes the MYPT1-PP1c- PLK1 complex, however this is not fully consistent with the observed experimental data. In addition, it was proposed recently that CHK1-mediated phosphorylation of MYPT1 at Ser20 is also required to target MP to PLK1 [18].

2.3. Novel role of MP in neurotransmitter release

Recent studies have shown that MP is localized in neurons and it is also involved in the mediation of neuronal processes. Neuronal myosin phosphatase target subunit 1 was first identified from brain cDNA library screened with a cDNA fragment of rat MYPT1 [69]. The global mapping of rat brain revealed that expression of MYPT1 was detectable in each brain region but showed higher concentration and greater enzyme activity in cortex, olfactory bulb, striatum, hippocampus, and diencephalon with a concentration of 30–78 nmol/g total protein [70].

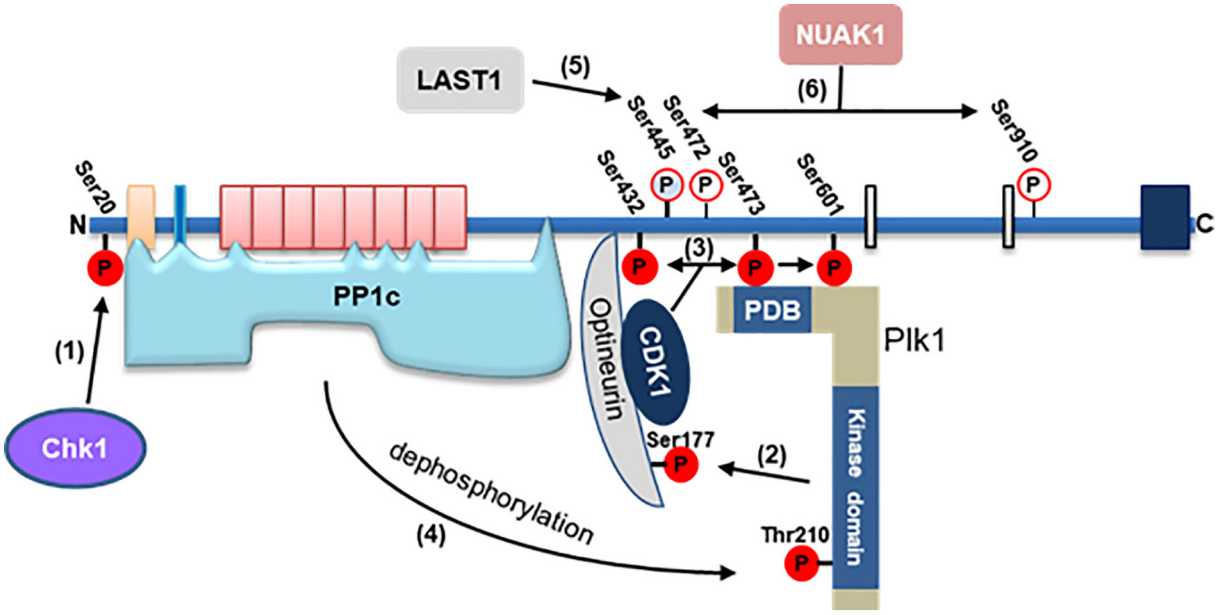


Fig. 3. Regulation of myosin phosphatase in mitosis.
Modulation of MP activity toward Plk1 by phosphorylation and protein-protein interaction. (1) Check point kinase 1 (Chk1) phosphorylates MYPT1 at Ser20 which was suggested to be necessary for MYPT1-PP1cδ interaction. (2) Optineurin is phosphorylated by PLK1 at Ser177, stimulating the binding of optineurin to both MYPT1 and CDK1, and (3) allowing CDK1 to phosphorylate MYPT1-Ser473 (as well as Ser432 and Ser601). This phosphorylation creates a polo-box domain binding pattern in MYPT1, required for the interaction between MYPT1 and Plk1, and (4) subsequently targets MP toward Thr210 in Plk1. (5) Phosphorylation of MYPT1-Ser445 by LATS1 was also suggested to promote MP-catalyzed dephosphorylation of Plk1. (6) NUAK1 has a negative role in the regulation of MP-mediated activation of Plk1 by phosphorylation of Ser445, Ser472, and Ser910 residues in MYPT1 and thereby weakening the association between MYPT1 and Plk1. *Plk1*: *polo-like kinase-1*; *PBD*: *polo-box domain*; *CDK1*: *cyclin-dependent kinase 1*; *Chk1*: *checkpoint kinase 1*; *NUAK1*: *NUAK family SnF1-like kinase-1 LATS1*: *large tumor suppressor kinase 1*.

These values were comparable to the MYPT1 concentrations found in C2C12 myoblast cells (40–48 nmol/g total protein) [71]. The presence of MYPT1 was also observed in cortical synaptosomes and in primary neuronal cells. The complex of MYPT1 and PP1cδ was colocalized and coprecipitated with synaptophysin, a presynaptic marker protein [70]. Mass spectrometry analysis identified several additional MYPT1-bound synaptosomal proteins (Table 1) such as synapsin-I, calcineurin-A subunit, Ca^{2+}-calmodulin dependent kinase II and the SNARE (soluble *N*-ethylmaleimide sensitive factor attachment protein receptor) complex elements such as syntaxin, and the synaptosomal-associated protein of 25 kDa (SNAP-25). The phosphorylation of syntaxin-1 at Ser14 by casein kinase-2 was already described [72] and it was suggested that the phosphorylation of synapsin-I by PKA at Ser9 modulates neurotransmitter release through docking actin to synaptic vesicles [73]. SNAP-25 was also identified as a substrate of ROCK that acts on the Thr138 phosphorylation site of SNAP-25. Dephosphorylation of all the previously mentioned ROCK-specific sites was catalyzed by MP [74]. The application of PP1-specific inhibitors on cortical synaptosome preparations resulted in the suppression of the depolarization-induced exocytosis and neurotransmitter release supporting the previous findings [74]. Moreover, the transduction of MP inhibitor KEPI protein into synaptosomes resulted in an increase of SNAP-25 phosphorylation and a decrease in the extent of neurotransmitter release and the interaction between SNAP-25 and syntaxin increased with decreasing phosphorylation level of SNAP-25 on Thr138 [75] suggesting that MP positively regulates neurotransmitter release through the initiation of the formation of SNARE complex (Fig. 4).

2.4. Functions of MP during development

Embryonic development is the subsequent sequence of regional specification, morphogenesis, cell differentiation and growth. Regional specification involves the action of cytoplasmic components that are located within the fertilized egg and it does not generate functional differentiated cells. Morphogenesis relates to the formation of three-dimensional shape and it involves the synchronized movements of cells creating the three germ layers of the early embryo. Cell differentiation relates specifically to the formation of functional cells. Growth mostly occurs through cell division but also through changes of cell size and the deposition of extracellular materials [76].

The role of MP in embryogenesis has been already suggested since *MYPT1*-deletion caused embryonal lethality at stage e7.5 days [77]. The majority of publication documented MP action on development through the modulation of the actomyosin complex that generates forces driving tissue morphogenesis [78]. Live imaging studies demonstrated that in adult Drosophila ovary during egg formation MP via its MYPT1 subunit (flw Drosophila form) is the key regulator of the morphogenesis of follicle cells. MP was required for the initiation and periodicity of basal myosin oscillation that creates egg chamber elongation [79].

Pregnancy and the implantation of the zygote is one of the key step in embryogenesis and during this process tissues coordinately adapts in order to accommodate the developing fetus and then prepare for delivery. One of the inhibitory molecule of MP, namely smoothelin like protein 1 (SMTNL1) was identified as a target of PKA and PKG in the course of smooth muscle contraction [80]. It was characterized as a protein with a dual function: it serves as the negative regulator of MP in the cytoplasm but upon phosphorylation by PKA/PKG at the Ser301 phosphorylation site, SMTNL1 translocates to the nucleus and acts as a cofactor of progesterone receptor. During pregnancy and aging the expression of SMTNL1 increased and it was correlated with MYPT1 expression [81]. MYPT1 expression increased drastically during development and sexual maturation and it was sex-dependent since it was 30% higher in males than females in VSM and skeletal muscle.

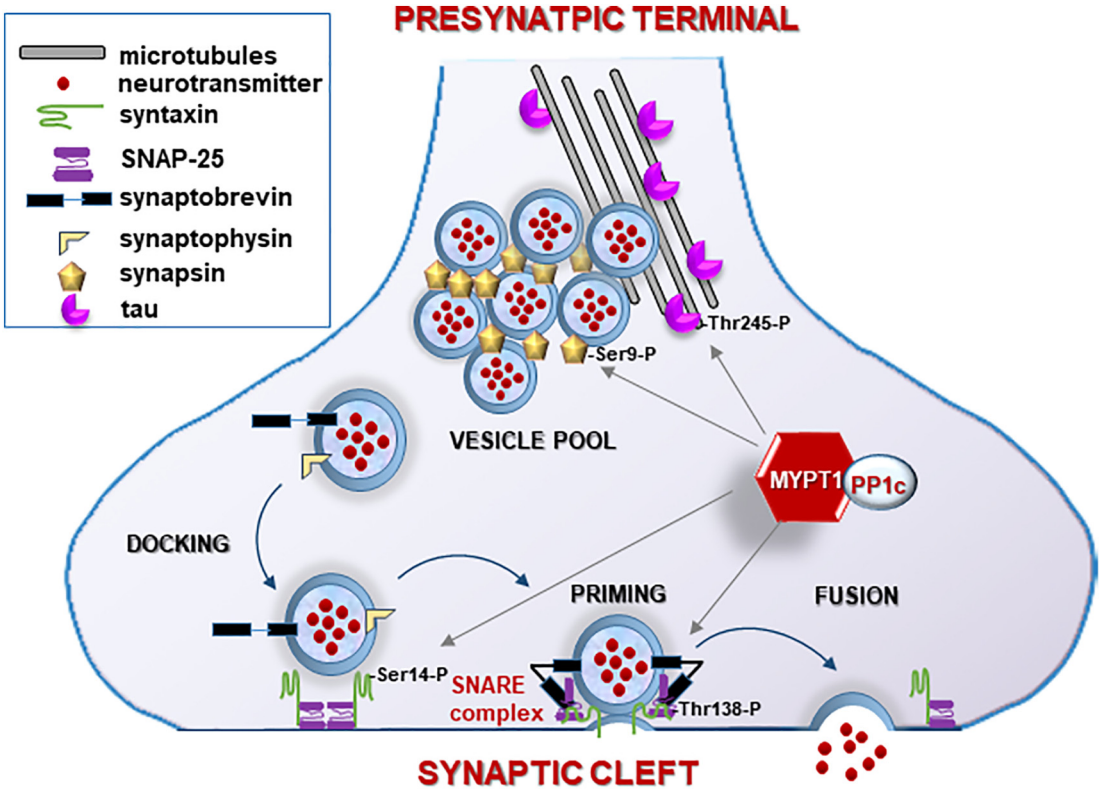


Fig. 4. MP regulates neurotransmitter release.
MP dephosphorylates syntaxin at Ser14 and SNAP-25 at Thr138 which initiates the priming of synaptic vesicles. The phosphorylation level at Ser9 of synapsin modulates its affinity to the synaptic reserve of vesicles regulating their transport to the active zone. Tau phosphorylation regulates microtubules assembly and vesicle trafficking.

However, *SMTNL1*-deletion caused a reciprocal age-dependent pattern of expression of MYPT1 as well as a change in MP activity. Pregnancy as well as SMTNL1 deletion significantly increased the expression of MYPT1 in smooth muscle suggesting a pregnancy-related Ca^{2+}-desensitization and relaxation regulating blood pressure. [82]. SMTNL1 regulated the expression of MYPT1 at transcriptional level in various sex-hormone sensitive tissues as well as in smooth and skeletal muscle where it induced an isotype switch of muscle fibers to a more glycolytic phenotype causing global metabolic shift toward insulin resistance [83]. Based on these findings it is clear that SMTNL1 regulates metabolic, contractile and reproductive properties, and known mechanisms are through the regulation of MP at the transcriptional level and also by inhibiting its enzymatic activity in development and pregnancy.

During development the tight coordination of adjacent tissues are required. Such coordination was characterized in the motor neuron positioning in Zebrafish during axonogenesis. The cell bodies of neurons in developing vertebral column and the axons in the cord exiting to the surrounding tissues shift relative to each other because of their differential growth rate. MP was identified as a regulator of the motor neuron adjustment in their position and it was believed to be a conserved feature in development. *Mypt1* mutants exhibited motor neuron defects and it was found to modulate caudal primary axon branching through a common, muscle intrinsic mechanism [84].

MP was also affected in human embryonic stem cells. Administration of H89 PKA inhibitor resulted in an increased cell viability, suppressed cell blebbing and colony formation of the dissociated stem cells, however, the pluripotency of hESCs and their ability to differentiate were not affected. PKA inhibition likely led to a decrease in ROCK activity and caused changes in the adherent properties of hESCs were accompanied by a decrease in MYPT1 and MLC20 phosphorylation [85]. Therefore, both the cell differentiation and the embryogenetic contributions of MP should be further investigated to clarify its role in developmental stages.

2.5. Regulation of gene expression by MP

MYPT1 was also found in the nuclear and microsomal fraction of HepG2 cells [86], and in the nucleus of neuronal cells [70] proving its role beyond the regulation of cytoskeletal elements and contractility. One of the unconventional nuclear substrates of MP is histone deacetylase 7 (HDAC7), which belongs to the class IIa HDACs. This is a member of a transcriptional complex involved in gene expression regulation and it acts as a repressor of numerous genes such as *Nur77* that involved in T-lymphocyte differentiation [87]. HDAC7 translocates upon its phosphorylation on the Ser155, Ser318 and Ser448 sites by protein kinase D to the cytoplasm where it associates with 14–3-3 proteins [88,89]. HDAC7 attaches in the cytoplasm to MP holoenzyme [90], which dephosphorylates the phospho-Ser residues of HDAC7 and promotes its nuclear redistribution [91]. Subsequent attenuation of Nur77 (an orphan nuclear receptor also known as NR4A) expression inhibits apoptosis of thymocytes implicating a regulatory role of MYPT1 in the survival of thymocytes (Fig. 5).

Another regulatory action of MP on gene expression is via the regulation of the subcellular localization of Nkx2.5 transcription factor. Nkx2.5 is one of the earliest markers of cardiomyogenic differentiation and its activity is required for cardiac differentiation [92]. It regulates many targets through direct interactions with other transcription factors including GATA4, Tbx5 and MEF2C [93]. MYPT1 was identified as a putative cofactor of Nkx2.5 and their interaction has been verified. Wnt3a-signaling activates ROCK, which phosphorylates MYPT1 at Thr853 causing the translocation of MP to the nucleus, where it can form a complex with Nkx2.5. MYPT1 induces exclusion of Nkx2.5 from the nucleus to the cytoplasm in a chromosome region maintenance 1 (Crm1)-dependent pathway. The translocation of Nkx2.5 apparently results in the inhibition of its transcriptional activity [94].

Numerous other MYPT1-interacting proteins such as RNA helicase, protein phosphatase 1B and replication protein A have been identified from human hepatocellular carcinoma cells and the interaction of MYPT1 with the members of the methylosome complex consisting of the protein arginine methyltransferase 5 (PRMT5), MEP50 and PCln was also verified [54]. PRMT5 plays roles in the regulation of transcription, RNA transport and cellular signaling by the generation of the ω-NG, NG-symmetric dimethylarginine. The molecular mechanism how MP regulates gene expression is through the inhibition of PRMT5 activity by its dephosphorylation at the Thr80 residue antagonizing the effect of ROCK. PRMT5 symmetrically dimethylates histone 2AR3 and − 4R3 and shifts the balance from an activating to a suppressive symmetric dimethylarginine mark at these motifs with respect to gene expression. The lack of MYPT1 results in the altered gene expression of 2627 genes involved in cell cycle, tumor morphology and metabolism [54] (Fig. 5).

The fact that the thyroid-hormone stimulation induced the phosphorylation of MYPT1 at Thr853 inhibitory phosphorylation site through the ROCK signaling pathway and caused a decrease of the osteocalcin expression in osteoblasts also support the diverse nuclear role of MP [95]. These lines of evidence support the role of MP in regulating gene expression through MP-mediated dephosphorylation and the identification of target genes opens new perspectives on the function of ROCK/MP signaling at the nuclear level.

2.6. The role of MP in the regulation of endothelial and epithelial barrier function

Vascular endothelium forms a selective permeable barrier between blood and the interstitial space of all organs and participates in the regulation of macromolecule transport and blood cell trafficking through the vessel wall. Endothelial MYPT1 was first cloned from porcine aortic endothelial cells [96]. The involvement of MP in endothelial cell barrier enhancement/protection was directly proved since ROCK-induced phosphorylation of MYPT1 at the inhibitory phosphorylation sites resulted in MP inactivation concomitant with accumulation of phosphorylated MLC20, actin remodeling and cell contraction of the endothelial cells [97].

Nitric oxide (NO) is a soluble gas synthesized from L-arginine in endothelial cells by the endothelial nitric oxide synthase (eNOS). This molecule has a wide range of biological roles such as the modulation of vascular tone by regulating the underlying smooth muscle layer [98]. The activity of eNOS depends on its phosphorylation state as well as its interacting partners and subcellular localization [99]. The major regulatory action is its reversible phosphorylation by PKC or ROCK at its inhibitory Thr497 site. The protein-protein interaction of eNOS and MYPT1 was established, and MYPT1 targeted PP1c to the phosphorylated eNOS-Thr497 substrate. The inhibition of MP, as an eNOS-pThr497-phosphatase suppressed the NO-production and the transendothelial resistance [31] underlying the physiological importance of MP in the maintenance of endothelial integrity and vascular tone.

The expression of full-length MYPT1 isoform was detected in intestinal epithelial cells and it was distributed at the cell-cell contacts and along F-actin [100]. Moreover, airborne particulate induced stress fiber formation in lung epithelial cells via the activation of ROCK and the increased phosphorylation of MYPT1 at Thr853 [101]. Another physiological relevance of MP on barrier function was described in the outer layer of the glomerular filtration barrier consisting of podocytes [102]. These differentiated insulin-dependent epithelial cells prevent protein excretion into the urine by the regulation of their actin cytoskeleton. Insulin increased glomerular filtration barrier permeability through the stimulation of NADPH oxidase that generated reactive oxygen species increasing the dimerization of PKGIα and the phosphorylation of MYPT1 at the inhibitory Thr696 site [103]. These findings support the view of the role of MP in the modulation of barrier integrity through the regulation of the actomyosin complex as well as the production of NO.

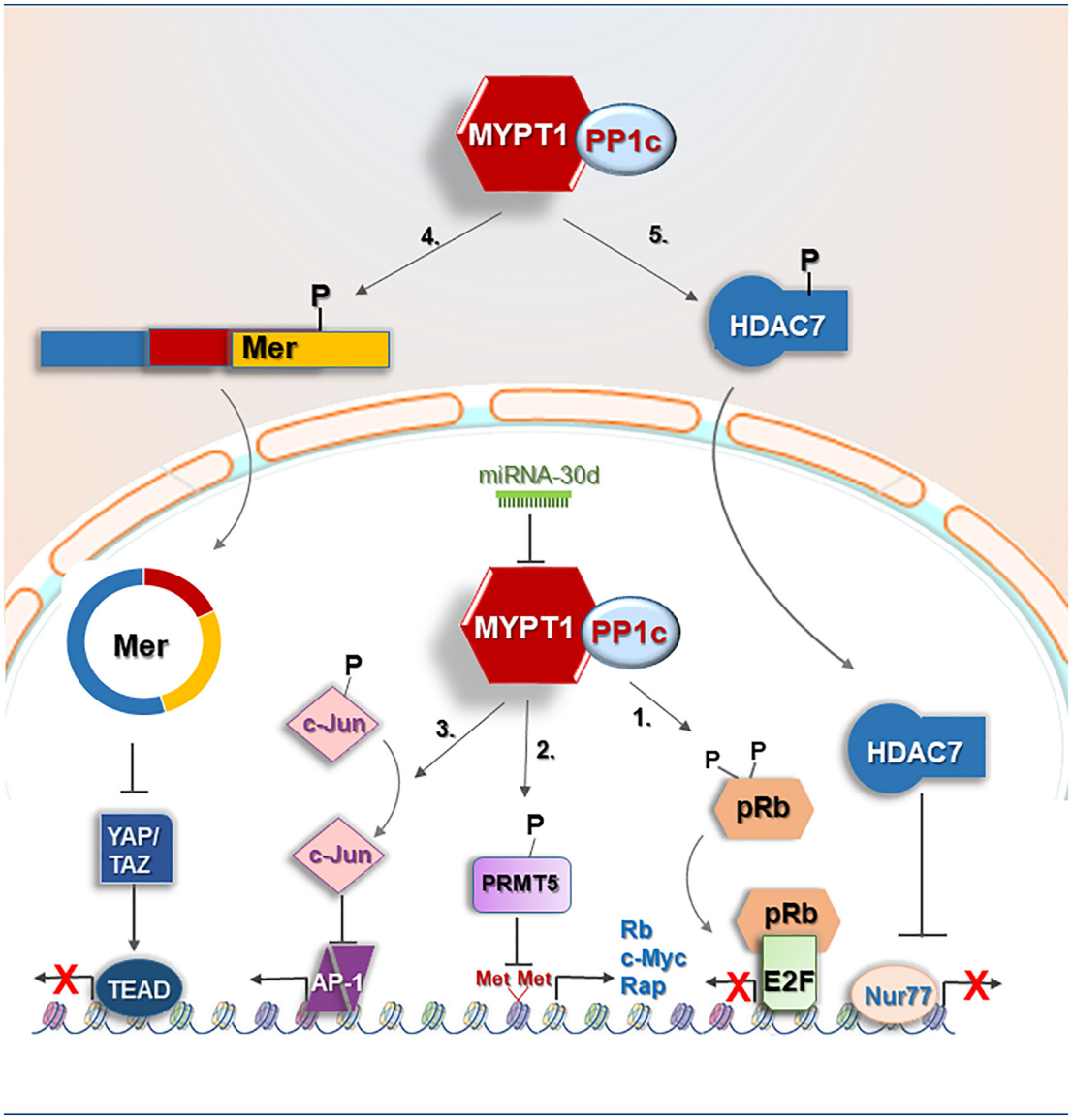


Fig. 5. Anti-tumorigenic signaling pathways regulated by MP.
1. Repression of E2F-mediated cell cycle progression. Activation of pRb by dephosphorylation at Ser807/811 residues causes repression of E2F-mediated cell cycle progression. 2. Activation of the gene expression of tumor-suppressor Rb, Rap and c-Myc. PRMT5 symmetric dimethyltransferase activity is reduced via dephosphorylation catalyzed by MP and results in increased gene expression of tumor suppressors. 3. Inhibition of c-Jun-VEGFA pathway and angiogenesis. MP antagonizes the effect of JNK signaling regulating the phosphorylation of c-Jun at Ser63/73, which increases the AP-1 transcriptional activity enhancing tumorigenic transformation. 4. Activation of anti-mitogenic and tumor suppressor signaling through merlin. Dephosphorylation of merlin at the Ser518 site induces its conformational change, activation and translocation to the nucleus. Active merlin initiates the Hippo pathway (YAP/TAZ/TED) resulting in the degradation of YAP/TAZ oncogenes and inhibition of tumor growth. 5. HDAC7 attaches in the cytoplasm to myosin phosphatase holoenzyme, which dephosphorylates the phospho-Ser residues of HDAC7 and promotes its nuclear redistribution. *E2F1 transcription factor*; *HDAC7*: *histone deacetylase 7*; *Mer*: *merlin*; *miR-30d*: *microRNA-30d*; *MP*: *myosin phosphatase*; *MYPT1*: *myosin targeting subunit 1*; *PP1c*: *protein phosphatase 1 catalytic subunit*; *pRb*: *retinoblastoma protein*; *PRMT5*: *protein arginine methyltransferase 5*; *VEGFA*: *vascular endothelial growth factor A*; *YAP/TAZ*: *transcriptional regulators*.

3. Pathophysiological role of myosin phosphatase

3.1. Anti-tumorigenic action of MP

Several publications have been released recently to elucidate the contribution of the ROCK/MP axis in tumorigenesis beyond their already described role in angiogenesis. Suppression of the RhoA/ROCK signaling pathway with ROCK inhibitors was found to inhibit VEGF-induced angiogenesis and the ability of endothelial cells to organize into capillary networks [104]. It was accompanied by the change of MYPT1 phosphorylation and MP enzyme activity and manifested in the alteration of cytoskeletal reorganization including formation of stress fibers and focal adhesions [105,106]. Although the majority of previous findings suggested the role of MP as a downstream effector of ROCK signaling, more and more results suggest its ROCK-independent action in the inhibition of cancer formation. The unbalanced and constant phosphorylation of MYPT1 at Thr853 was suggested to be related to cancer formation and mutations, in addition altered phosphorylation and expression of MYPT1 were documented in various cancer types [107]. MYPT1 was downregulated in gastric cancer and functional studies revealed that the overexpression of MYPT1 inhibited tumor progression and metastasis formation [108].

MYPT1 phosphorylation and MP activity correlated with the clinical stage of cancers in the case of gastric cancer and in human

hepatocellular carcinoma [54], and the higher MYPT1 expression level resulted in longer survival time and also a higher expression of MYPT1 was observed in postoperative patients [108]. c-Myc as a global transcriptional regulator can activate genes involved in cell proliferation and growth but it is also able to repress genes involved in cell cycle and adhesion [109] raising the possibility of a yet-unexplored mechanism used by tumors to suppress differentiation and potentiate aggressiveness. c-Myc expression is significantly lower in HCC than in non-tumor tissues [54]. The overexpression of MYPT1 in gastric cancer cells dramatically improved the expression levels of c-myc and cyclin D suggesting that MYPT1 inhibits cell proliferation and induces cancer cell cycle arrest via cyclin D and c-myc. We found that MYPT1-silencing resulted in a decrease in c-Myc gene and protein expression suggesting again the tumor suppressor effect of this MYPT1 subunit, and presumably MP itself, in HCC (Fig. 5).

Insertional mutations of MYPT1 were also reported to be the drivers of invasive lobular breast cancer (ILC). The majority of ILC is characterized by the functional loss of E-cadherin but mutations of additional genes are also required for the tumorigenesis. Among these genes *mypt*1 was characterized. *Mypt1* gene is located in chromosome 1 q locus, which is frequently gained or amplified in ILC producing truncated MYPT1 subunits. These mutant proteins lacked various regulatory domains altering its scaffolding ability but preserved their PP1c binding feature [110].

Aberrant microRNA 30d (miR30d), a small non-coding RNA molecule, has been associated with cancer progression and its overexpression was observed in prostate cancer cells and in human specimens. MiR-30d enhanced proliferation, migration, invasion, angiogenesis and tumor growth due to downregulation of its target gene, *MYPT1*, which subsequently led to the activation of c-Jun and VEGFA proteins, which are proangiogenic factors. MP signaling activation by inducing MYPT1 expression antagonized the effect of miR-30d, implying that MYPT1 serves as an anti-oncogenic factor in prostate cancer cells and may be a potential drug target [111] (Fig. 5).

Downregulation of *MYPT1* in human hepatocellular carcinoma cells resulted in the upregulation of cancer-related pathways. Above all, MYPT1 inhibitory phosphorylation was significantly increased and in parallel, its nuclear target, PRMT5 enzyme activity (suggested by the elevation of its Thr80 phosphorylation) increased in human hepatocellular carcinoma biopsies and 15 other tumorous cell lines. Hyperactivation of PRMT5 suppressed gene and protein expression of several tumor suppressors such as pRb and RAP1. [54].

In contrast to the previously mentioned anti-oncogenic potential of MP, the Serum Antibodies based SILAC-Immunoprecipitation approach identified MYPT1 as a pancreatic cancer associated antigen upon the application of pancreatic cancer vaccine (GVAX) in phase II clinical trial. Significant MYPT1 expression was detected in malignant compared to normal duct epithelium. Interestingly, tissue microarray revealed significantly higher amount of cytoplasmic and membrane-bound MYPT1 compared to other cancer types [112]. This controversial finding could be resolved by suggesting a pancreatic cancer-specific phenomenon.

Nevertheless, the regulation of protein stability of MYPT1 was also indicated to play a crucial role in cancer formation. The stability of PP1c and MYPT1 is interdependent and knocking down one of the subunits decreases the expression level of the other associated with changes in cell shape and cell survival. [11] Moreover, the protein stability of MYPT1 and its affinity for the ubiquitin-proteasome pathway also play a role in cancer formation through its modification by histone demethylase LSD1 (as it was detailed in the Introduction). LSD1 overexpression and activation in cancer cells induces the destabilization of MYPT1 protein resulting in the activation of pRb phosphorylation and inducing E2F activity [35]. Retinoblastoma protein and merlin also play a key role in cancer formation by modulating gene expression as it was discussed earlier (“Role of MP in the control of cell proliferation and cell division” and Fig. 5). These trends collectively lead to the conclusion that MP is an anti-tumorigenic effector by regulating the gene expression of tumor suppressors in various cancer types. Possible ROCK-independent mechanisms are either through the gene expression regulation of MYPT1 or through the modulation of protein stability of MYPT1 resulting in a decreased level of proteins in cancer cells. However, the regulation of MP holoenzyme by the inhibitory phosphorylation of MYPT1 is another possibility.

3.2. MP in neurodegenerative disorders

MYPT1 was identified as one of the peripheral markers in Huntington's disease (HD) patients and in HD mouse models. The presence of mutant huntingtin caused an increase in the expression level of MYPT1 in human blood leukocytes, postmortem brain as well as in HD mouse tissues. Stimulation of ROCK pathway including MP mainly regulated the cytoskeletal rearrangement and triggered caspase-mediated cell death [113].

Interestingly, MYPT1 was also described as a biomarker in cerebrospinal fluid of patients with Parkinson's disease and its expression was downregulated but its neurological role yet needs to be clarified [114].

3.3. MP in insulin signaling: novel drug target of insulin resistance?

Insulin mediates a wide spectrum of biological processes via the phosphatidylinositide 3 kinase (PI3K) and the MAPK-signaling pathways [115], and the malfunctions of insulin signaling could contribute to the development of insulin resistance, metabolic syndrome and type 2 diabetes [116]. Insulin acts through insulin receptor substrate (IRS-1) that interacts with p85 and Grb2 and they associated with the PI3K and MAPK pathways, respectively, leading to the activation of a number of downstream kinases, such as AKT/PKB, mTOR/raptor, S6K1, GSK3 and PDK1.

In the early 2000s the major function of MP was recognized only as an element of a complex signaling network of insulin that controls the phosphorylation of 20 kDa MLC and VSMC contraction [117]. Insulin-induced IRS-1 tyrosine phosphorylation activates PI3K/AKT signaling and the vasodilatory effect is mediated through NO activating cGKI and resulting in the dephosphorylation of MYPT1 at the inhibitory phosphorylation site. The phosphorylation of MYPT1 was negatively regulated by AKT (protein kinase B) phosphorylation in response to insulin, therefore, phosphorylation and activation of AKT, downstream of IRS-1 and PI3-K, were impaired in diabetic VSMC [118]. Besides that, insulin triggered serotonin-induced contraction through the IR/PI3K/PDK1 pathway and PDK was suggested to directly phosphorylate MYPT1 in a ROCK-independent manner [119]. Interestingly, the hyper-reactivity of diabetic patients' VSMC was the consequence both the enhanced phosphorylation of MP but also the decreased expression level of MYPT1 [120].

A relatively new component of the MYPT1-PP1cδ complex, myosin phosphatase-Rho interacting protein (M-RIP) also plays a role in the regulation of MP in insulin signaling. M-RIP is a smooth muscle protein [121] that binds to actin filaments through its amino-terminal domain and acts as a scaffold to RhoA/ROCK to regulate MP on the actomyosin complex [122]. Insulin stimulation initiated the binding of M-RIP to MYPT1 resulting in an insulin-induced vasodilation in vascular smooth muscle [123] (Fig. 6).

In skeletal muscle, insulin stimulation leads to the activation of PI3K/PDK1/Akt signaling initiating mTOR that required for the interaction of MYPT1 with IRS1. MP dephosphorylate IRS1 at the phospo-Ser residues counterbalancing the effect of the insulin-activated protein kinases. MYPT1 was identified as a novel endogenous insulin-stimulated interaction partner of IRS-1 in L6 myotubes [124]. Insulin initiated an interaction between the IRS1/p85 complex and MYPT1, and it was suggested to be dependent on the activation of PI3K, PDK1, AKT/PKB and mTOR/raptor (mTORC1) but not MAPK signaling. Based on

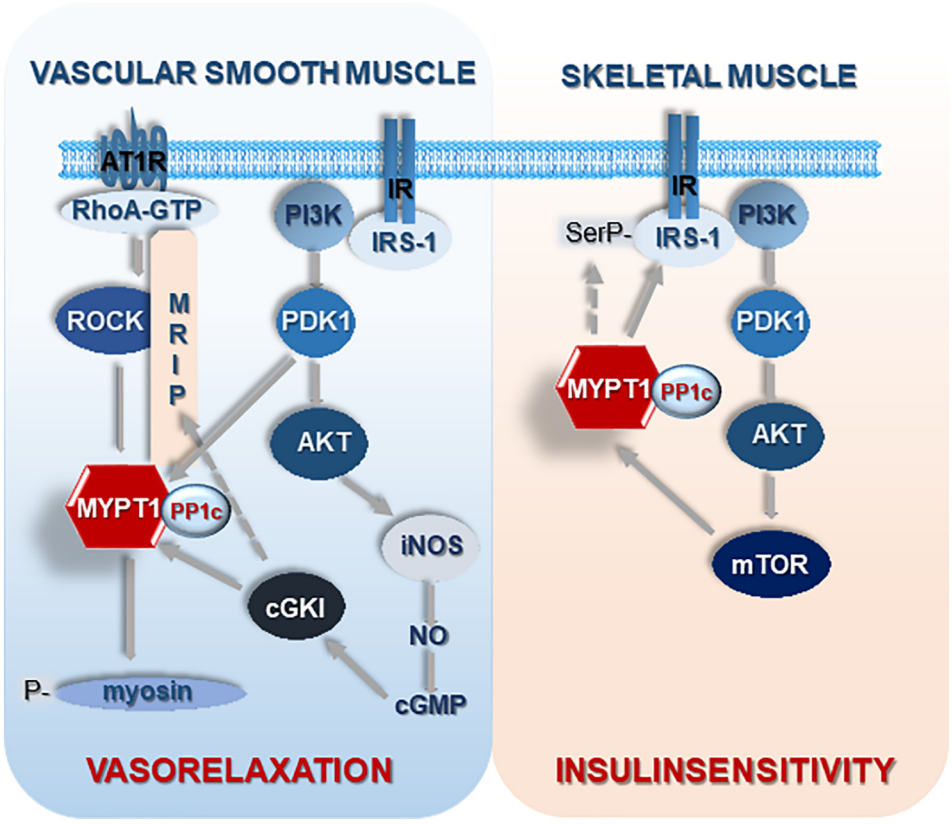


Fig. 6. Hypothetic function of MP in insulin signaling.
Insulin-induced IRS1 tyrosine phosphorylation activates PI3K/Akt signaling and the vasodilatory effect is mediated through NO activating cGKI and resulting in the dephosphorylation of MYPT1 at the inhibitory phosphorylation site. Upon insulin stimulation, M-RIP binds to MYPT1 causing vasodilatation in vascular smooth muscle. In skeletal muscle, insulin stimulation leads to the activation of PI3K/PDK1/Akt signaling initiating mTOR that is required for the interaction of MYPT1 with IRS1. MP dephosphorylates IRS1 at the phospho-Ser residues counterbalancing the effect of the insulin-activated protein kinases.
cGKI: *cyclic guanosine-3′,5′-monophosphate-dependent protein kinase*; *iNOS*: *inducible nitric oxide synthase*; *IR*: *insulin receptor*; *IRS1*: *insulin-receptor substrate 1*; *mTOR*: *mammalian target of rapamycin*; *MRIP*: *myosin phosphatase-Rho interacting protein*; *PDK1*: *phosphoinositide-dependent kinase-1*; *PI3K*: *phosphatidylinositide 3 kinase*.

these results, the hypothetic function of MP is the dephosphorylation of IRS-1 to counterbalance the effect of insulin-activated Ser/Thr kinases, resulting in balanced phosphorylation of IRS-1 on Ser and Thr residues and proper insulin action through IRS1 (Fig. 6). Insulin stimulation led to increased interaction between IRS-1 and MYPT1/PP1cδ, and to the greater ability of MP to dephosphorylate IRS-1 [125]. These lines of evidence were supported by quantitative phosphoproteomics assay using *MYPT1* knock down L6 skeletal muscle cell lines and 295 phosphoproteins were documented to be related in insulin signaling to mTOR or RhoA signaling [126].

4. Conclusions

Recent publications highlighted the diverse and unexpected functions of myosin phosphatase, the well-characterized enzyme in smooth muscle contractility. It has already been documented that the MYPT1 regulatory subunit of MP is ubiquitously expressed and it exhibits diverse subcellular localization in eukaryotic cells. The fact that besides the cytoplasm and cytoskeleton MYPT1 and PP1c both localized in nuclear, mitochondrial and plasma membrane fractions of the cells, and that the majority of identified proteins in MYPT1-interactomes are not relevant to cytoskeletal regulation suggest that MP is more than the regulator of myosin light chain dephosphorylation only.

One key observation highlighted in this review is that MYPT1 functions not simply as a substrate targeting subunit in MP, but it could also serve as a scaffold protein or provides a nucleocytoplasmic shuttle mechanism for other proteins and PP1c activation/inhibition are not always coupled with these events. On the other hand, MP has been considered for decades as the downstream target of the RhoA /ROCK signaling, nevertheless its therapeutic potential has been deeply ignored. Several reports have now described the ROCK-independent action and regulation of MP, therefore this review has intended to focus on the importance of MP in distinct signaling mechanisms.

Based on the findings on the role of MP in distinct pathways, the modulation of MP by designing MP holoenzyme-specific activator(s) provides plausible way of repressing tumorigenesis or initiating insulin sensitivity, while enhancing dephosphorylation of crucial downstream molecules such as pRb, PRMT5 or PLK may also provide a novel therapeutic approach. The combination of genetic and pharmacological tools will allow exploration of these relationships and it may contribute to a more complete understanding of the molecular events regulated by dephosphorylation processes.

Transparency document

The Transparency document associated with this article can be found, in online version.

Acknowledgements

This work was supported by grants from the National Research, Development and Innovation Office (FK 125043, K108308, PD111715) and from the EU co-financed by the European Regional Development Fund under projects GINOP-2.3.2-15-2016-00044 and EFOP-3.6.2-16-2017-00006.

Conflict of interest

The authors have declared that no competing interests exist.

Appendix A. Supplementary data

Supplementary data to this article can be found online at https://doi.org/10.1016/j.bbamcr.2018.07.023.

References

[1] P. Cohen, The origins of protein phosphorylation, Nat. Cell Biol. 4 (2002) E127–E130.

[2] R. Heinrich, B.G. Neel, T.A. Rapoport, Mathematical models of protein kinase signal transduction, Mol. Cell 9 (2002) 957–970.
[3] K.E. Kamm, J.T. Stull, Dedicated myosin light chain kinases with diverse cellular functions, J. Biol. Chem. 276 (2001) 4527–4530.
[4] A. Takai, C. Bialojan, M. Troschka, J.C. Ruegg, Smooth muscle myosin phosphatase inhibition and force enhancement by black sponge toxin, FEBS Lett. 217 (1987) 81–84.
[5] A.P. Somlyo, A.V. Somlyo, Signal transduction and regulation in smooth muscle, Nature 372 (1994) 231–236.
[6] D. Alessi, L.K. MacDougall, M.M. Sola, M. Ikebe, P. Cohen, The control of protein phosphatase-1 by targetting subunits. The major myosin phosphatase in avian smooth muscle is a novel form of protein phosphatase-1, Eur. J. Biochem. 210 (1992) 1023–1035.
[7] H. Shimizu, M. Ito, M. Miyahara, K. Ichikawa, S. Okubo, T. Konishi, M. Naka, T. Tanaka, K. Hirano, D.J. Hartshorne, et al., Characterization of the myosin-binding subunit of smooth muscle myosin phosphatase, J. Biol. Chem. 269 (1994) 30407–30411.
[8] A. Shirazi, K. Iizuka, P. Fadden, C. Mosse, A.P. Somlyo, A.V. Somlyo, T.A. Haystead, Purification and characterization of the mammalian myosin light chain phosphatase holoenzyme. The differential effects of the holoenzyme and its subunits on smooth muscle, J. Biol. Chem. 269 (1994) 31598–31606.
[9] D. Shichi, T. Arimura, T. Ishikawa, A. Kimura, Heart-specific small subunit of myosin light chain phosphatase activates rho-associated kinase and regulates phosphorylation of myosin phosphatase target subunit 1, J. Biol. Chem. 285 (2010) 33680–33690.
[10] N. Takizawa, D.J. Schmidt, K. Mabuchi, E. Villa-Moruzzi, R.A. Tuft, M. Ikebe, M20, the small subunit of PP1M, binds to microtubules, Am. J. Phys. Cell Physiol. 284 (2003) C250–C262.
[11] E. Scotto-Lavino, M. Garcia-Diaz, G. Du, M.A. Frohman, Basis for the isoform-specific interaction of myosin phosphatase subunits protein phosphatase 1c beta and myosin phosphatase targeting subunit 1, J. Biol. Chem. 285 (2010) 6419–6424.
[12] D.J. Hartshorne, M. Ito, F. Erdodi, Role of protein phosphatase type 1 in contractile functions: myosin phosphatase, J. Biol. Chem. 279 (2004) 37211–37214.
[13] M.E. Grassie, L.D. Moffat, M.P. Walsh, J.A. MacDonald, The myosin phosphatase targeting protein (MYPT) family: a regulated mechanism for achieving substrate specificity of the catalytic subunit of protein phosphatase type 1delta, Arch. Biochem. Biophys. 510 (2011) 147–159.
[14] A.N. Chang, K.E. Kamm, J.T. Stull, Role of myosin light chain phosphatase in cardiac physiology and pathophysiology, J. Mol. Cell. Cardiol. 101 (2016) 35–43.
[15] A. Boratko, C. Csortos, TIMAP, the versatile protein phosphatase 1 regulator in endothelial cells, IUBMB Life 69 (2017) 918–928.
[16] A. Toth, E. Kiss, F.W. Herberg, P. Gergely, D.J. Hartshorne, F. Erdodi, Study of the subunit interactions in myosin phosphatase by surface plasmon resonance, Eur. J. Biochem. 267 (2000) 1687–1697.
[17] M. Terrak, F. Kerff, K. Langsetmo, T. Tao, R. Dominguez, Structural basis of protein phosphatase 1 regulation, Nature 429 (2004) 780–784.
[18] X. Hu, Z. Li, Y. Ding, Q. Geng, Z. Xiahou, H. Ru, M.Q. Dong, X. Xu, J. Li, Chk1 modulates the interaction between myosin phosphatase targeting protein 1 (MYPT1) and protein phosphatase 1cbeta (PP1cbeta), Cell Cycle 17 (2018) 421–427.
[19] K. Kimura, M. Ito, M. Amano, K. Chihara, Y. Fukata, M. Nakafuku, B. Yamamori, J. Feng, T. Nakano, K. Okawa, A. Iwamatsu, K. Kaibuchi, Regulation of myosin phosphatase by Rho and Rho-associated kinase (Rho-kinase), Science 273 (1996) 245–248.
[20] C.G. Broustas, N. Grammatikakis, M. Eto, P. Dent, D.L. Brautigan, U. Kasid, Phosphorylation of the myosin-binding subunit of myosin phosphatase by Raf-1 and inhibition of phosphatase activity, J. Biol. Chem. 277 (2002) 3053–3059.
[21] M. Ito, T. Nakano, F. Erdodi, D.J. Hartshorne, Myosin phosphatase: structure, regulation and function, Mol. Cell. Biochem. 259 (2004) 197–209.
[22] A. Muranyi, D. Derkach, F. Erdodi, A. Kiss, M. Ito, D.J. Hartshorne, Phosphorylation of Thr695 and Thr850 on the myosin phosphatase target subunit: inhibitory effects and occurrence in A7r5 cells, FEBS Lett. 579 (2005) 6611–6615.
[23] S. Mori, R. Iwaoka, M. Eto, S.Y. Ohki, Solution structure of the inhibitory phosphorylation domain of myosin phosphatase targeting subunit 1, Proteins 77 (2009) 732–735.
[24] A.A. Wooldridge, J.A. MacDonald, F. Erdodi, C. Ma, M.A. Borman, D.J. Hartshorne, T.A. Haystead, Smooth muscle phosphatase is regulated in vivo by exclusion of phosphorylation of threonine 696 of MYPT1 by phosphorylation of serine 695 in response to cyclic nucleotides, J. Biol. Chem. 279 (2004) 34496–34504.
[25] M.E. Grassie, C. Sutherland, A. Ulke-Lemee, M. Chappellaz, E. Kiss, M.P. Walsh, J.A. MacDonald, Cross-talk between Rho-associated kinase and cyclic nucleotide-dependent kinase signaling pathways in the regulation of smooth muscle myosin light chain phosphatase, J. Biol. Chem. 287 (2012) 36356–36369.
[26] C. Sutherland, J.A. MacDonald, M.P. Walsh, Analysis of phosphorylation of the myosin-targeting subunit of myosin light chain phosphatase by Phos-tag SDS-PAGE, Am. J. Phys. Cell Physiol. 310 (2016) C681–C691.
[27] M. Eto, Regulation of cellular protein phosphatase-1 (PP1) by phosphorylation of the CPI-17 family, C-kinase-activated PP1 inhibitors, J. Biol. Chem. 284 (2009) 35273–35277.
[28] F. Erdodi, E. Kiss, M.P. Walsh, B. Stefansson, J.T. Deng, M. Eto, D.L. Brautigan, D.J. Hartshorne, Phosphorylation of protein phosphatase type-1 inhibitory proteins by integrin-linked kinase and cyclic nucleotide-dependent protein kinases, Biochem. Biophys. Res. Commun. 306 (2003) 382–387.
[29] D. Dedinszki, A. Kiss, L. Markasz, A. Marton, E. Toth, L. Szekely, F. Erdodi, Inhibition of protein phosphatase-1 and -2A decreases the chemosensitivity of leukemic cells to chemotherapeutic drugs, Cell. Signal. 27 (2015) 363–372.
[30] B. Kolozsvari, E. Bako, B. Becsi, A. Kiss, A. Czikora, A. Toth, G. Vamosi, P. Gergely, F. Erdodi, Calcineurin regulates endothelial barrier function by interaction with and dephosphorylation of myosin phosphatase, Cardiovasc. Res. 96 (2012) 494–503.
[31] R. Batori, B. Becsi, D. Nagy, Z. Konya, C. Hegedus, Z. Bordan, A. Verin, B. Lontay, F. Erdodi, Interplay of myosin phosphatase and protein phosphatase-2A in the regulation of endothelial nitric-oxide synthase phosphorylation and nitric oxide production, Sci. Rep. 7 (2017) 44698.
[32] S. Tsukamoto, Y. Huang, D. Umeda, S. Yamada, S. Yamashita, M. Kumazoe, Y. Kim, M. Murata, K. Yamada, H. Tachibana, 67-kDa laminin receptor-dependent protein phosphatase 2A (PP2A) activation elicits melanoma-specific antitumor activity overcoming drug resistance, J. Biol. Chem. 289 (2014) 32671–32681.
[33] J.J. Filter, B.C. Williams, M. Eto, D. Shalloway, M.L. Goldberg, Unfair competition governs the interaction of pCPI-17 with myosin phosphatase (PP1-MYPT1), elife 6 (2017).
[34] J.D. Webb, A. Muranyi, C.W. Pugh, P.J. Ratcliffe, M.L. Coleman, MYPT1, the targeting subunit of smooth-muscle myosin phosphatase, is a substrate for the asparaginyl hydroxylase factor inhibiting hypoxia-inducible factor (FIH), Biochem. J. 420 (2009) 327–333.
[35] H.S. Cho, T. Suzuki, N. Dohmae, S. Hayami, M. Unoki, M. Yoshimatsu, G. Toyokawa, M. Takawa, T. Chen, J.K. Kurash, H.I. Field, B.A. Ponder, Y. Nakamura, R. Hamamoto, Demethylation of RB regulator MYPT1 by histone demethylase LSD1 promotes cell cycle progression in cancer cells, Cancer Res. 71 (2011) 655–660.
[36] E. Twomey, Y. Li, J. Lei, C. Sodja, M. Ribecco-Lutkiewicz, B. Smith, H. Fang, M. Bani-Yaghoub, I. McKinnell, M. Sikorska, Regulation of MYPT1 stability by the E3 ubiquitin ligase SIAH2, Exp. Cell Res. 316 (2010) 68–77.
[37] T. Iwasaki, T. Katayama, K. Kohama, Y. Endo, T. Sawasaki, Myosin phosphatase is inactivated by caspase-3 cleavage and phosphorylation of myosin phosphatase targeting subunit 1 during apoptosis, Mol. Biol. Cell 24 (2013) 748–756.
[38] A. Kiss, B. Lontay, B. Becsi, L. Markasz, E. Olah, P. Gergely, F. Erdodi, Myosin phosphatase interacts with and dephosphorylates the retinoblastoma protein in THP-1 leukemic cells: its inhibition is involved in the attenuation of daunorubicin-induced cell death by calyculin-A, Cell. Signal. 20 (2008) 2059–2070.
[39] Y. Koga, M. Ikebe, A novel regulatory mechanism of myosin light chain phosphorylation via binding of 14-3-3 to myosin phosphatase, Mol. Biol. Cell 19 (2008) 1062–1071.
[40] S. Vetterkind, E. Lee, E. Sundberg, R.H. Poythress, T.C. Tao, U. Preuss, K.G. Morgan, Par-4: a new activator of myosin phosphatase, Mol. Biol. Cell 21 (2010) 1214–1224.
[41] D. Xia, J.T. Stull, K.E. Kamm, Myosin phosphatase targeting subunit 1 affects cell migration by regulating myosin phosphorylation and actin assembly, Exp. Cell Res. 304 (2005) 506–517.
[42] A. Zagorska, M. Deak, D.G. Campbell, S. Banerjee, M. Hirano, S. Aizawa, A.R. Prescott, D.R. Alessi, New roles for the LKB1-NUAK pathway in controlling myosin phosphatase complexes and cell adhesion, Sci. Signal. 3 (2010) ra25.
[43] R.G. Fehon, A.I. McClatchey, A. Bretscher, Organizing the cell cortex: the role of ERM proteins, Nat. Rev. Mol. Cell Biol. 11 (2010) 276–287.
[44] Y. Fukata, K. Kimura, N. Oshiro, H. Saya, Y. Matsuura, K. Kaibuchi, Association of the myosin-binding subunit of myosin phosphatase and moesin: dual regulation of moesin phosphorylation by Rho-associated kinase and myosin phosphatase, J. Cell Biol. 141 (1998) 409–418.
[45] K.M. Kim, C. Csortos, I. Czikora, D. Fulton, N.S. Umapathy, G. Olah, A.D. Verin, Molecular characterization of myosin phosphatase in endothelium, J. Cell. Physiol. 227 (2012) 1701–1708.
[46] A. Kovacs-Kasa, B.A. Gorshkov, K.M. Kim, S. Kumar, S.M. Black, D.J. Fulton, C. Dimitropoulou, J.D. Catravas, A.D. Verin, The protective role of MLCP-mediated ERM dephosphorylation in endotoxin-induced lung injury in vitro and in vivo, Sci. Rep. 6 (2016) 39018.
[47] L.B. Riecken, A. Zoch, U. Wiehl, S. Reichert, I. Scholl, Y. Cui, M. Ziemer, U. Anderegg, C. Hagel, H. Morrison, CPI-17 drives oncogenic Ras signaling in human melanomas via Ezrin-Radixin-Moesin family proteins, Oncotarget 7 (2016) 78242–78254.
[48] K. Kimura, Y. Fukata, Y. Matsuoka, V. Bennett, Y. Matsuura, K. Okawa, A. Iwamatsu, K. Kaibuchi, Regulation of the association of adducin with actin filaments by Rho-associated kinase (Rho-kinase) and myosin phosphatase, J. Biol. Chem. 273 (1998) 5542–5548.
[49] M. Amano, T. Kaneko, A. Maeda, M. Nakayama, M. Ito, T. Yamauchi, H. Goto, Y. Fukata, N. Oshiro, A. Shinohara, A. Iwamatsu, K. Kaibuchi, Identification of Tau and MAP2 as novel substrates of Rho-kinase and myosin phosphatase, J. Neurochem. 87 (2003) 780–790.
[50] F. Matsumura, Y. Yamakita, S. Yamashiro, Myosin light chain kinases and phosphatase in mitosis and cytokinesis, Arch. Biochem. Biophys. 510 (2011) 76–82.
[51] V. Kolupaeva, V. Janssens, PP1 and PP2A phosphatases—cooperating partners in modulating retinoblastoma protein activation, FEBS J. 280 (2013) 627–643.
[52] T. Izawa, Y. Fukata, T. Kimura, A. Iwamatsu, K. Dohi, K. Kaibuchi, Elongation factor-1 alpha is a novel substrate of rho-associated kinase, Biochem. Biophys. Res. Commun. 278 (2000) 72–78.
[53] J. Grey, D. Jones, L. Wilson, S. Nakjang, J. Clayton, R. Temperley, E. Clark, L. Gaughan, C. Robson, Differential regulation of the androgen receptor by protein phosphatase regulatory subunits, Oncotarget 9 (2018) 3922–3935.
[54] A. Sipos, J. Ivan, B. Becsi, Z. Darula, I. Tamas, D. Horvath, K.F. Medzihradszky, F. Erdodi, B. Lontay, Myosin phosphatase and RhoA-activated kinase modulate arginine methylation by the regulation of protein arginine methyltransferase 5 in

hepatocellular carcinoma cells, Sci. Rep. 7 (2017) 40590.
[55] H. Jin, T. Sperka, P. Herrlich, H. Morrison, Tumorigenic transformation by CPI-17 through inhibition of a merlin phosphatase, Nature 442 (2006) 576–579.
[56] W. Li, J. Cooper, M.A. Karajannis, F.G. Giancotti, Merlin: a tumour suppressor with functions at the cell cortex and in the nucleus, EMBO Rep. 13 (2012) 204–215.
[57] J. Cooper, F.G. Giancotti, Molecular insights into NF2/Merlin tumor suppressor function, FEBS Lett. 588 (2014) 2743–2752.
[58] I. Serrano, P.C. McDonald, F. Lock, W.J. Muller, S. Dedhar, Inactivation of the Hippo tumour suppressor pathway by integrin-linked kinase, Nat. Commun. 4 (2013) 2976.
[59] T. Matsuda, P. Zhai, S. Sciarretta, Y. Zhang, J.I. Jeong, S. Ikeda, J. Park, C.P. Hsu, B. Tian, D. Pan, J. Sadoshima, D.P. Del Re, NF2 activates Hippo Signaling And Promotes ischemia/reperfusion injury in the heart, Circ. Res. 119 (2016) 596–606.
[60] L.S. Angelo, J.Y. Wu, F. Meng, M. Sun, S. Kopetz, I.E. McCutcheon, J.M. Slopis, R. Kurzrock, Combining curcumin (diferuloylmethane) and heat shock protein inhibition for neurofibromatosis 2 treatment: analysis of response and resistance pathways, Mol. Cancer Ther. 10 (2011) 2094–2103.
[61] G. Totsukawa, Y. Yamakita, S. Yamashiro, H. Hosoya, D.J. Hartshorne, F. Matsumura, Activation of myosin phosphatase targeting subunit by mitosis-specific phosphorylation, J. Cell Biol. 144 (1999) 735–744.
[62] S. Yamashiro, Y. Yamakita, G. Totsukawa, H. Goto, K. Kaibuchi, M. Ito, D.J. Hartshorne, F. Matsumura, Myosin phosphatase-targeting subunit 1 regulates mitosis by antagonizing polo-like kinase 1, Dev. Cell 14 (2008) 787–797.
[63] T. Chiyoda, N. Sugiyama, T. Shimizu, H. Naoe, Y. Kobayashi, J. Ishizawa, Y. Arima, H. Tsuda, M. Ito, K. Kaibuchi, D. Aoki, Y. Ishihama, H. Saya, S. Kuninaka, LATS1/WARTS phosphorylates MYPT1 to counteract PLK1 and regulate mammalian mitotic progression, J. Cell Biol. 197 (2012) 625–641.
[64] J. Li, X. Liu, J. Liao, J. Tian, J. Wang, X. Wang, J. Zhang, X. Xu, MYPT1 sustains centromeric cohesion and the spindle-assembly checkpoint, J. Genet. Genomics 40 (2013) 575–578.
[65] A.M.G. Dumitru, S.F. Rusin, A.E.M. Clark, A.N. Kettenbach, D.A. Compton, Cyclin A/Cdk1 modulates Plk1 activity in prometaphase to regulate kinetochore-microtubule attachment stability, elife 6 (2017).
[66] D. Kachaner, J. Filipe, E. Laplantine, A. Bauch, K.L. Bennett, G. Superti-Furga, A. Israel, R. Weil, Plk1-dependent phosphorylation of optineurin provides a negative feedback mechanism for mitotic progression, Mol. Cell 45 (2012) 553–566.
[67] S. Banerjee, A. Zagorska, M. Deak, D.G. Campbell, A.R. Prescott, D.R. Alessi, Interplay between Polo kinase, LKB1-activated NUAK1 kinase, PP1betaMYPT1 phosphatase complex and the SCFbetaTrCP E3 ubiquitin ligase, Biochem. J. 461 (2014) 233–245.
[68] K. Werle, J. Chen, H.G. Xu, R.X. Zhao, Q. He, C. Lu, R. Cui, J. Liang, Y.L. Li, Z.X. Xu, Liver kinase B1 regulates the centrosome via PLK1, Cell Death Dis. 5 (2014) e1157.
[69] M. Fujioka, N. Takahashi, H. Odai, S. Araki, K. Ichikawa, J. Feng, M. Nakamura, K. Kaibuchi, D.J. Hartshorne, T. Nakano, M. Ito, A new isoform of human myosin phosphatase targeting/regulatory subunit (MYPT2): cDNA cloning, tissue expression, and chromosomal mapping, Genomics 49 (1998) 59–68.
[70] B. Lontay, Z. Serfozo, P. Gergely, M. Ito, D.J. Hartshorne, F. Erdodi, Localization of myosin phosphatase target subunit 1 in rat brain and in primary cultures of neuronal cells, J. Comp. Neurol. 478 (2004) 72–87.
[71] Y. Wu, F. Erdodi, A. Muranyi, K.D. Nullmeyer, R.M. Lynch, D.J. Hartshorne, Myosin phosphatase and myosin phosphorylation in differentiating C2C12 cells, J. Muscle Res. Cell Motil. 24 (2003) 499–511.
[72] C. Gil, A. Falques, E. Sarro, R. Cubi, J. Blasi, J. Aguilera, E. Itarte, Protein kinase CK2 associates to lipid rafts and its pharmacological inhibition enhances neurotransmitter release, FEBS Lett. 585 (2011) 414–420.
[73] S. Hilfiker, F. Benfenati, F. Doussau, A.C. Nairn, A.J. Czernik, G.J. Augustine, P. Greengard, Structural domains involved in the regulation of transmitter release by synapsins, J. Neurosci. 25 (2005) 2658–2669.
[74] B. Lontay, B. Pal, Z. Serfozo, A. Koszeghy, G. Szucs, Z. Rusznak, F. Erdodi, Protein phosphatase-1M and Rho-kinase affect exocytosis from cortical synaptosomes and influence neurotransmission at a glutamatergic giant synapse of the rat auditory system, J. Neurochem. 123 (2012) 84–99.
[75] D. Horvath, I. Tamas, A. Sipos, Z. Darula, B. Becsi, D. Nagy, J. Ivan, F. Erdodi, B. Lontay, Myosin phosphatase and RhoA-activated kinase modulate neurotransmitter release by regulating SNAP-25 of SNARE complex, PLoS One 12 (2017) e0177046.
[76] S. Menchero, T. Rayon, M.J. Andreu, M. Manzanares, Signaling pathways in mammalian preimplantation development: linking cellular phenotypes to lineage decisions, Dev. Dyn. 246 (2017) 245–261.
[77] R. Okamoto, M. Ito, N. Suzuki, M. Kongo, N. Moriki, H. Saito, H. Tsumura, K. Imanaka-Yoshida, K. Kimura, A. Mizoguchi, D.J. Hartshorne, T. Nakano, The targeted disruption of the MYPT1 gene results in embryonic lethality, Transgenic Res. 14 (2005) 337–340.
[78] R.C. King, The meiotic behavior of the Drosophila oocyte, Int. Rev. Cytol. 28 (1970) 125–168.
[79] A. Valencia-Exposito, I. Grosheva, D.G. Miguez, A. Gonzalez-Reyes, M.D. Martin-Bermudo, Myosin light-chain phosphatase regulates basal actomyosin oscillations during morphogenesis, Nat. Commun. 7 (2016) 10746.
[80] M.A. Borman, J.A. MacDonald, T.A. Haystead, Modulation of smooth muscle contractility by CHASM, a novel member of the smoothelin family of proteins, FEBS Lett. 573 (2004) 207–213.
[81] B. Lontay, K. Bodoor, D.H. Weitzel, D. Loiselle, C. Fortner, S. Lengyel, D. Zheng, J. Devente, R. Hickner, T.A. Haystead, Smoothelin-like 1 protein regulates myosin phosphatase-targeting subunit 1 expression during sexual development and pregnancy, J. Biol. Chem. 285 (2010) 29357–29366.
[82] K. Bodoor, B. Lontay, R. Safi, D.H. Weitzel, D. Loiselle, Z. Wei, S. Lengyel, D.P. McDonnell, T.A. Haystead, Smoothelin-like 1 protein is a bifunctional regulator of the progesterone receptor during pregnancy, J. Biol. Chem. 286 (2011) 31839–31851.
[83] B. Lontay, K. Bodoor, A. Sipos, D.H. Weitzel, D. Loiselle, R. Safi, D. Zheng, J. Devente, R.C. Hickner, D.P. McDonnell, T. Ribar, T.A. Haystead, Pregnancy and smoothelin-like protein 1 (SMTNL1) deletion promote the switching of skeletal muscle to a glycolytic phenotype in human and mice, J. Biol. Chem. 290 (2015) 17985–17998.
[84] J. Bremer, M. Granato, Myosin phosphatase fine-tunes zebrafish motoneuron position during axonogenesis, PLoS Genet. 12 (2016) e1006440.
[85] L. Zhang, Y. Xu, J. Xu, Y. Wei, X. Xu, Protein kinase A inhibitor, H89, enhances survival and clonogenicity of dissociated human embryonic stem cells through Rho-associated coiled-coil containing protein kinase (ROCK) inhibition, Hum. Reprod. 31 (2016) 832–843.
[86] B. Lontay, A. Kiss, P. Gergely, D.J. Hartshorne, F. Erdodi, Okadaic acid induces phosphorylation and translocation of myosin phosphatase target subunit 1 influencing myosin phosphorylation, stress fiber assembly and cell migration in HepG2 cells, Cell. Signal. 17 (2005) 1265–1275.
[87] M. Parra, H. Kasler, T.A. McKinsey, E.N. Olson, E. Verdin, Protein kinase D1 phosphorylates HDAC7 and induces its nuclear export after T-cell receptor activation, J. Biol. Chem. 280 (2005) 13762–13770.
[88] T.A. McKinsey, C.L. Zhang, E.N. Olson, Identification of a signal-responsive nuclear export sequence in class II histone deacetylases, Mol. Cell. Biol. 21 (2001) 6312–6321.
[89] H.Y. Kao, A. Verdel, C.C. Tsai, C. Simon, H. Juguilon, S. Khochbin, Mechanism for nucleocytoplasmic shuttling of histone deacetylase 7, J. Biol. Chem. 276 (2001) 47496–47507.
[90] M. Parra, T. Mahmoudi, E. Verdin, Myosin phosphatase dephosphorylates HDAC7, controls its nucleocytoplasmic shuttling, and inhibits apoptosis in thymocytes, Genes Dev. 21 (2007) 638–643.
[91] C. Compagnucci, S. Barresi, S. Petrini, E. Bertini, G. Zanni, Rho-kinase signaling controls nucleocytoplasmic shuttling of class IIa histone deacetylase (HDAC7) and transcriptional activation of orphan nuclear receptor NR4A1, Biochem. Biophys. Res. Commun. 459 (2015) 179–183.
[92] M. Jamali, P.J. Rogerson, S. Wilton, I.S. Skerjanc, Nkx2-5 activity is essential for cardiomyogenesis, J. Biol. Chem. 276 (2001) 42252–42258.
[93] J. Savage, A.J. Conley, A. Blais, I.S. Skerjanc, SOX15 and SOX7 differentially regulate the myogenic program in P19 cells, Stem Cells 27 (2009) 1231–1243.
[94] T. Ryan, M. Shelton, J.P. Lambert, B. Malecova, S. Boisvenue, M. Ruel, D. Figeys, P.L. Puri, I.S. Skerjanc, Myosin phosphatase modulates the cardiac cell fate by regulating the subcellular localization of Nkx2.5 in a Wnt/Rho-associated protein kinase-dependent pathway, Circ. Res. 112 (2013) 257–266.
[95] A. Kondo, H. Tokuda, K. Kato, R. Matsushima-Nishiwaki, G. Kuroyanagi, J. Mizutani, O. Kozawa, T. Otsuka, Rho-kinase negatively regulates thyroid hormone-stimulated osteocalcin synthesis in osteoblasts, Biochimie 95 (2013) 719–724.
[96] M. Hirano, N. Niiro, K. Hirano, J. Nishimura, D.J. Hartshorne, H. Kanaide, Expression, subcellular localization, and cloning of the 130-kDa regulatory subunit of myosin phosphatase in porcine aortic endothelial cells, Biochem. Biophys. Res. Commun. 254 (1999) 490–496.
[97] A.A. Birukova, K. Smurova, K.G. Birukov, K. Kaibuchi, J.G. Garcia, A.D. Verin, Role of Rho GTPases in thrombin-induced lung vascular endothelial cells barrier dysfunction, Microvasc. Res. 67 (2004) 64–77.
[98] D. Tousoulis, A.M. Kampoli, C. Tentolouris, N. Papageorgiou, C. Stefanadis, The role of nitric oxide on endothelial function, Curr. Vasc. Pharmacol. 10 (2012) 4–18.
[99] E.H. Heiss, V.M. Dirsch, Regulation of eNOS enzyme activity by posttranslational modification, Curr. Pharm. Des. 20 (2014) 3503–3513.
[100] J.M. Zha, H.S. Li, Y.T. Wang, Q. Lin, M. Tao, W.Q. He, Characterization of isoform expression and subcellular distribution of MYPT1 in intestinal epithelial cells, Gene 588 (2016) 1–6.
[101] Y.I. Chirino, C.M. Garcia-Cuellar, C. Garcia-Garcia, E. Soto-Reyes, A.R. Osornio-Vargas, L.A. Herrera, A. Lopez-Saavedra, J. Miranda, R. Quintana-Belmares, I.R. Perez, Y. Sanchez-Perez, Airborne particulate matter in vitro exposure induces cytoskeleton remodeling through activation of the ROCK-MYPT1-MLC pathway in A549 epithelial lung cells, Toxicol. Lett. 272 (2017) 29–37.
[102] G.I. Welsh, R.J. Coward, Podocytes, glucose and insulin, Curr. Opin. Nephrol. Hypertens. 19 (2010) 379–384.
[103] A. Piwkowska, D. Rogacka, M. Kasztan, S. Angielski, M. Jankowski, Insulin increases glomerular filtration barrier permeability through dimerization of protein kinase G type Ialpha subunits, Biochim. Biophys. Acta 1832 (2013) 791–804.
[104] G.P. van Nieuw Amerongen, P. Koolwijk, A. Versteilen, V.W. van Hinsbergh, Involvement of RhoA/Rho kinase signaling in VEGF-induced endothelial cell migration and angiogenesis in vitro, Arterioscler. Thromb. Vasc. Biol. 23 (2003) 211–217.
[105] X. Yang, F. Zheng, S. Zhang, J. Lu, Loss of RhoA expression prevents proliferation and metastasis of SPCA1 lung cancer cells in vitro, Biomed. Pharmacother. 69 (2015) 361–366.
[106] J.G. Zhang, D.D. Zhang, X. Wu, Y.Z. Wang, S.Y. Gu, G.H. Zhu, X.Y. Li, Q. Li, G.L. Liu, Incarvine C suppresses proliferation and vasculogenic mimicry of hepatocellular carcinoma cells via targeting ROCK inhibition, BMC Cancer 15 (2015) 814.
[107] C.C. Wong, C.M. Wong, F.C. Ko, L.K. Chan, Y.P. Ching, J.W. Yam, I.O. Ng, Deleted in liver cancer 1 (DLC1) negatively regulates Rho/ROCK/MLC pathway in hepatocellular carcinoma, PLoS One 3 (2008) e2779.

[108] F. Wang, Y. Sun, Overexpression of myosin phosphatase target subunit 1 (MYPT1) inhibits tumor progression and metastasis of gastric cancer, Med. Sci. Monit. 24 (2018) 2508–2517.
[109] I. Uribesalgo, S.A. Benitah, L. Di Croce, From oncogene to tumor suppressor: the dual role of Myc in leukemia, Cell Cycle 11 (2012) 1757–1764.
[110] S.M. Kas, J.R. de Ruiter, K. Schipper, S. Annunziato, E. Schut, S. Klarenbeek, A.P. Drenth, E. van der Burg, C. Klijn, J.J. Ten Hoeve, D.J. Adams, M.J. Koudijs, J. Wesseling, M. Nethe, L.F.A. Wessels, J. Jonkers, Insertional mutagenesis identifies drivers of a novel oncogenic pathway in invasive lobular breast carcinoma, Nat. Genet. 49 (2017) 1219–1230.
[111] Z.Y. Lin, G. Chen, Y.Q. Zhang, H.C. He, Y.X. Liang, J.H. Ye, Y.K. Liang, R.J. Mo, J.M. Lu, Y.J. Zhuo, Y. Zheng, F.N. Jiang, Z.D. Han, S.L. Wu, W.D. Zhong, C.L. Wu, MicroRNA-30d promotes angiogenesis and tumor growth via MYPT1/c-JUN/VEGFA pathway and predicts aggressive outcome in prostate cancer, Mol. Cancer 16 (2017) 48.
[112] D.T. Jhaveri, M.S. Kim, E.D. Thompson, L. Huang, R. Sharma, A.P. Klein, L. Zheng, D.T. Le, D.A. Laheru, A. Pandey, E.M. Jaffee, R.A. Anders, Using quantitative seroproteomics to identify antibody biomarkers in pancreatic cancer, Cancer Immunol. Res. 4 (2016) 225–233.
[113] K.L. Narayanan, V. Chopra, H.D. Rosas, K. Malarick, S. Hersch, Rho kinase pathway alterations in the brain and leukocytes in Huntington's disease, Mol. Neurobiol. 53 (2016) 2132–2140.
[114] E.S. Wang, Y. Sun, J.G. Guo, X. Gao, J.W. Hu, L. Zhou, J. Hu, C.C. Jiang, Tetranectin and apolipoprotein A-I in cerebrospinal fluid as potential biomarkers for Parkinson's disease, Acta Neurol. Scand. 122 (2010) 350–359.
[115] K. Siddle, Signalling by insulin and IGF receptors: supporting acts and new players, J. Mol. Endocrinol. 47 (2011) R1–10.
[116] K. Bouzakri, H.A. Koistinen, J.R. Zierath, Molecular mechanisms of skeletal muscle insulin resistance in type 2 diabetes, Curr. Diabetes Rev. 1 (2005) 167–174.
[117] N. Begum, N. Duddy, O. Sandu, J. Reinzie, L. Ragolia, Regulation of myosin-bound protein phosphatase by insulin in vascular smooth muscle cells: evaluation of the role of Rho kinase and phosphatidylinositol-3-kinase-dependent signaling pathways, Mol. Endocrinol. 14 (2000) 1365–1376.
[118] J.H. Lee, T. Palaia, L. Ragolia, Impaired insulin-mediated vasorelaxation in diabetic Goto-Kakizaki rats is caused by impaired Akt phosphorylation, Am. J. Phys. Cell Physiol. 296 (2009) C327–C338.
[119] S. Watanabe, T. Matsumoto, M. Oda, K. Yamada, J. Takagi, K. Taguchi, T. Kobayashi, Insulin augments serotonin-induced contraction via activation of the IR/PI3K/PDK1 pathway in the rat carotid artery, Pflugers Arch. 468 (2016) 667–677.
[120] Y. Matsuo, M. Kuwabara, N. Tanaka-Totoribe, T. Kanai, E. Nakamura, S. Gamoh, A. Suzuki, Y. Asada, H. Hisa, R. Yamamoto, The defective protein level of myosin light chain phosphatase (MLCP) in the isolated saphenous vein, as a vascular conduit in coronary artery bypass grafting (CABG), harvested from patients with diabetes mellitus (DM), Biochem. Biophys. Res. Commun. 412 (2011) 323–327.
[121] H.K. Surks, C.T. Richards, M.E. Mendelsohn, Myosin phosphatase-Rho interacting protein. A new member of the myosin phosphatase complex that directly binds RhoA, J. Biol. Chem. 278 (2003) 51484–51493.
[122] N. Riddick, K. Ohtani, H.K. Surks, Targeting by myosin phosphatase-RhoA interacting protein mediates RhoA/ROCK regulation of myosin phosphatase, J. Cell. Biochem. 103 (2008) 1158–1170.
[123] J.H. Lee, T. Palaia, L. Ragolia, Impaired insulin-stimulated myosin phosphatase Rho-interacting protein signaling in diabetic Goto-Kakizaki vascular smooth muscle cells, Am. J. Phys. Cell Physiol. 302 (2012) C1371–C1381.
[124] T. Geetha, P. Langlais, M. Luo, R. Mapes, N. Lefort, S.C. Chen, L.J. Mandarino, Z. Yi, Label-free proteomic identification of endogenous, insulin-stimulated interaction partners of insulin receptor substrate-1, J. Am. Soc. Mass Spectrom. 22 (2011) 457–466.
[125] T. Geetha, P. Langlais, M. Caruso, Z. Yi, Protein phosphatase 1 regulatory subunit 12A and catalytic subunit delta, new members in the phosphatidylinositide 3 kinase insulin-signaling pathway, J. Endocrinol. 214 (2012) 437–443.
[126] X. Zhang, D. Ma, M. Caruso, M. Lewis, Y. Qi, Z. Yi, Quantitative phosphoproteomics reveals novel phosphorylation events in insulin signaling regulated by protein phosphatase 1 regulatory subunit 12A, J. Proteome 109 (2014) 63–75.

lontay.beata_285_24

THE JOURNAL OF BIOLOGICAL CHEMISTRY VOL. 290, NO. 29, pp. 17985–17998, July 17, 2015
© 2015 by The American Society for Biochemistry and Molecular Biology, Inc. Published in the U.S.A.

Pregnancy and Smoothelin-like Protein 1 (SMTNL1) Deletion Promote the Switching of Skeletal Muscle to a Glycolytic Phenotype in Human and Mice*[S]

Received for publication, April 14, 2015, and in revised form, June 3, 2015 Published, JBC Papers in Press, June 5, 2015, DOI 10.1074/jbc.M115.658120

Beata Lontay[‡§], Khaldon Bodoor[‡1], Adrienn Sipos[§], Douglas H. Weitzel[‡], David Loiselle[‡], Rachid Safi[‡], Donghai Zheng[¶], James Devente[‖], Robert C. Hickner[¶], Donald P. McDonnell[‡], Thomas Ribar[‡‡], and Timothy A. Haystead[‡2]**

*From the [‡]Department of Pharmacology, Duke University Medical Center, Durham, North Carolina 27710, [§]Department of Medical Chemistry, Faculty of Medicine, University of Debrecen, Debrecen-4032, Hungary, [¶]Departments of Kinesiology, East Carolina University, Greenville, North Carolina 27858, [‖]Department of Obstetrics and Gynecology, East Carolina University, Greenville, North Carolina 27834, **Department of Biokinetics, Exercise, and Leisure Sciences, University of KwaZulu-Natal, Durban 4000, South Africa, and [‡‡]Duke iPSC Shared Resource Facility, Duke University Medical Center, Durham, North Carolina 27710*

Background: Pregnancy promotes physiological adaptations throughout the body mediated by the female sex hormones.
Results: Pregnancy promotes switching of skeletal muscle to a glycolytic phenotype through the smoothelin-like protein 1 transcriptional cofactor.
Conclusion: Deletion of SMTNL1 is able to mimic the effect of pregnancy in mice.
Significance: Novel mechanism to explain insulin resistance during pregnancy.

Pregnancy promotes physiological adaptations throughout the body, mediated by the female sex hormones progesterone and estrogen. Changes in the metabolic properties of skeletal muscle enable the female body to cope with the physiological challenges of pregnancy and may also be linked to the development of insulin resistance. We conducted global microarray, proteomic, and metabolic analyses to study the role of the progesterone receptor and its transcriptional regulator, smoothelin-like protein 1 (SMTNL1) in the adaptation of skeletal muscle to pregnancy. We demonstrate that pregnancy promotes fiber-type changes from an oxidative to glycolytic isoform in skeletal muscle. This phenomenon is regulated through an interaction between SMTNL1 and progesterone receptor, which alters the expression of contractile and metabolic proteins. *smtnl1*$^{-/-}$ mice are metabolically less efficient and show impaired glucose tolerance. Pregnancy antagonizes these effects by inducing metabolic activity and increasing glucose tolerance. Our results suggest that SMTNL1 has a role in mediating the actions of steroid hormones to promote fiber switching in skeletal muscle during pregnancy. Our findings also bear on the management of gestational diabetes that develops as a complication of pregnancy in ~4% of women.

Skeletal muscle (SKM)[3] shows plasticity and is able to adapt its contractile phenotype in response to physiological stress, including exercise training, hormonal shifts, aging, and pathological stress (1). Skeletal muscle plasticity has been studied extensively in endurance exercise training in both humans and animals and shown to promote the switching of SKM fiber content to a more oxidative phenotype characterized by an increase in the relative numbers of type I slow-twitch and type2a fast-twitch fibers and a decrease in type2b fast-twitch glycolytic fibers (2, 3). Alternatively, intermittent bursting effort promotes transformation of type2a/b fibers to a more glycolytic type2b phenotype, with fewer mitochondria and increased expression of the MHC2b isoform as well as enzymes associated with glycolysis. SKM is also the primary site for the caloric disposal of glucose and long chain fatty acids, which is profoundly affected by the composition and the metabolic and enzymatic properties of its fibers. Switching of SKM to an oxidative phenotype is associated with a decreased susceptibility to the development of insulin resistance. Exercise training alone can reverse obesity-induced insulin resistance by increasing the oxidative capacity of muscle through the enhancement of mitochondrial density and glucose transporter content (4, 5). Conversely, reduced oxidative capacity of SKM is associated with predisposition to the development of insulin resistance and increased weight gain.

Pregnancy is also a physiological state that can promote major changes in SKM, mainly mediated by the female sex ste-

* This work was supported, in whole or in part, by National Institutes of Health Grant R01DK065954-05 (to T. A. H.). This work was also supported by Grants OTKA PD107898, TÁMOP-4.2.2.A-11/1/KONV-2012-0025, and TÁMOP 4.2.4.A/2-11-1-2012-0001, the University of Debrecen (RH/751/2015) (to B. L.), and by The King Hussein fellowship (to K. B.). The authors declare that they have no conflicts of interest with the contents of this article.
[S] This article contains supplemental Table 1.
[1] A Duke University School of Medicine visiting scholar.
[2] To whom correspondence should be addressed: Duke University School of Medicine, C118 LSRC Box 3813, Durham, NC 27710. Tel./Fax: 919-613-8606; E-mail: timothy.haystead@duke.edu.

[3] The abbreviations used are: SKM, skeletal muscle; smoothelin-like protein 1, SMTNL1; NP, non-pregnant; PR, progesterone receptor; ERα/β, estrogen receptor α/β; IHC, immunohistochemistry; SQ-WB, semi quantitative Western blot analysis; MHC1, -2a, -2B, myosin heavy chain 1, 2a, 2b; IRS, insulin receptor substrate; CLAMS, comprehensive laboratory animal monitoring system; GLM, general linear models; RER, respiratory exchange ratio; Glut4, glucose transporter 4; IRS1, insulin receptor substrate 1; IP, immunoprecipitation; WN, WT non-pregnant; KN, KO-non-pregnant; KP, KO-pregnant.

Downloaded from http://www.jbc.org/ at UNIVERSITY OF DEBRECEN on July 21, 2015

tontay:beata_285_24

roid hormones estrogen and progesterone (6). Both progesterone receptors (PR) and estrogen receptors (ER) are expressed in SKM, but their function and relevance have yet to be defined (7). Some direct links between the effect of progesterone and estrogen on SKM come from studies on pregnancy-induced insulin resistance. The increased glucose requirements of the gravid uterus during pregnancy are thought to necessitate major adjustments in glucose production and utilization by maternal SKM, adipose, and other tissues. This is the reason why normal pregnancy is associated with the development of insulin resistance, which is thought of as a means by which the mother can supply the developing fetus with sufficient glucose for growth. However, in 2–4% of all pregnancies, this condition progresses to a type II diabetic state known as gestational diabetes and becomes a complication of pregnancy. At the midterm of pregnancy both SKM and adipose tissues show insulin resistance (8), but the underlying molecular mechanisms that promote this response are unknown. These mechanisms have been speculated to be linked to increased circulating insulin levels promoted by an increase in the number and mass of pancreatic β cells induced by progesterone (9).

Smoothelin-like protein 1 (SMTNL1) plays a role in mediating exercise-induced adaptations in both smooth and SKM that are sex-dependent (10). For example, striated muscle in male *smntl*$^{-/-}$ mice exhibit an endurance phenotype, whereas female null mice exhibit a more glycolytic phenotype (11). Pregnancy was also found to induce the expression of SMTNL1 in tissues such as uterine and vascular smooth muscle and sex hormone-related tissues. In uterine smooth muscle, SMTNL1 plays a major role in pregnancy to promote adaptive responses, and this process is specifically mediated through interactions of SMTNL1 with the steroid hormone receptor PR-B. *In vitro* and *in vivo* SMTNL1 selectively binds PR and does not bind other steroid hormone receptors. This suggests that SMTNL1 is a bifunctional co-regulator of PR-B signaling and thus provides a molecular mechanism whereby PR-B is targeted to alter gene expression patterns to coordinately promote alterations in uterine smooth muscle function during pregnancy (12). Based on these observations we have speculated that SMTNL1 could function as a transcriptional regulator of SKM differentiation and plasticity; this putative role is evident by the nuclear localization of the protein upon phosphorylation at serine 301 by protein kinase G/A and by the presence of a number of regulatory transcription factor binding sites in the promoter region of *smtnl1* (13). In this study we show that pregnancy induces switching of SKM to a glycolytic phenotype and this effect is mediated through SMTNL1. A range of proteomic, global gene array, and metabolic studies in wild type (WT) and *smtnl1*$^{-/-}$ mice support this hypothesis. The finding that deletion of SMTNL1 promotes fiber specific expression of both ER and PR suggests that these events are likely to be mediated through progesterone or estrogen during pregnancy. We suggest that in SKM, these events are natural adaptations of normal pregnancy and potentially infer evolutionary advantages to the mother by increasing her ability to store fat and her physical strength to carry the developing fetus.

Experimental Procedures

Antibodies—Semi-quantitative Western blotting (SQ-WB) was performed with antibodies specific for PR (Abcam), ERα (Santa Cruz), SMTNL1, SMTNL1^{S301A} (Proteintech Inc.), MYPT1 (D. J. Hartshorne, University of Arizona), tubulin (Sigma), anti-Glut4 (Santa Cruz Biotechnology), anti-IRS1 (Cell Signaling Technology), anti-MHCI (14), anti-MHC2a, anti-MHC2b (14), and Developmental Studies Hybridoma Bank, University of Iowa). The specificity of MHC antibodies has been established before (10, 14).

Mouse Colony Maintenance and Pregnancy Studies—Congenic 129 SvEv *smtnl1*$^{-/-}$ mouse were created as described (10). Pregnancy and pseudo-pregnancy studies were conducted as described (11). For pregnancy studies 8-week-old mice were sacrificed at days 14–17. Animal studies were approved by the Duke University Institutional Animal Care and Use Committee. ERKO mice were housed, and tissue sections were dissected at NIEHS/National Institutes of Health, Research Triangle Park, NC. Procedures involving humans were approved by the University and Medical Center Institutional Review Board at East Carolina University.

Intraperitoneal Glucose Tolerance Test—An intraperitoneal glucose tolerance test was performed at 5–6-week-old animals using *smtnl*$^{+/+}$ and *smtnl*$^{-/-}$ non-pregnant and 14-day pregnant animals. After a 12-h fast, mice were injected intraperitoneally with glucose (2 mg/kg body weight). Blood glucose levels were determined from tail vein blood at 0, 30, 60, and 120 min after the glucose injection by Ascensia Breeze Blood Glucose Monitoring System.

Microarray—RNeasy Lipid Tissue Mini kit (Qiagen) was used to isolate total RNA from the plantarus skeletal muscle of wild type and/or *smtnl1*$^{-/-}$ of pregnant (day 17) and/or non-pregnant mice according to the manufacturer's protocol, and RNA were stored in liquid N_2 at −80 °C until further processing. The quantity and quality of RNA were assessed using a NanoDrop ND-1000 spectrophotometer and an Agilent Bioanalyzer and samples with an RNA Integrity number (RIN) >7 were only used for further analysis. For microarray hybridizations, 100 ng of total RNA was amplified and labeled using the MessageAmp Premier Kit (Ambion). Equal amounts of labeled cRNA were hybridized to the Affymetrix Mouse Genome 430 2.0 microarray (Affymetrix) according to the manufacturer's protocol. Partek Genomics Suite 6.4 (Partek Inc., St. Louis, MO) was used to perform data analysis. Robust multi-chip analysis normalization was done on the entire data set. Multiway analysis of variance and -fold change were performed to select target genes that were differentially expressed between the different comparisons (*i.e.* WN *versus* KN, KN *versus* KP, WP *versus* KP, WN *versus* WP). Top differentially expressed genes were selected with a p value cut-off of 0.05 based on the analysis of variance test and -fold change cutoff of ≥2. Gene Ontology Enrichment analysis on the gene lists was performed with χ^2 test and limited to functional groups with more than two genes. Hierarchical Clustering was performed on differentially expressed genes based on Average Linkage with Pearson's Dissimilarity. Additionally, the gene lists were analyzed using the GeneGo software for obtaining pathway maps, biological

Downloaded from http://www.jbc.org/ at UNIVERSITY OF DEBRECEN on July 21, 2015

networks, and diseases relevant to the list. All microarray experimental results are available at the Duke Microarray facility website.

Biochemical Assays and Semi-quantitative Western blot Analysis—Tissue samples were frozen in liquid N_2 at the time of harvest, stored at −80 °C, and homogenized as described (10). Densitometry of the blots was performed, and scans were analyzed by the Volume Analyze feature of the Molecular Analyst Software (Bio-Rad) and Image J. The density of the protein of interest was normalized to tubulin and plotted as relative numbers except for the Western blot analysis of $SMTNL1^{Ser\text{-}301}$ phosphorylation when density data were also normalized to the SMTNL1 expression. All IP procedures using anti-ERα, -PR-B, and SMTNL1 antibodies were carried out as described (15).

Immunohistochemistry and Fiber Typing—Immunohistochemistry and fiber typing of mouse tissues were performed as described previously (10, 14). Human rectus abdominis samples of premenopausal patients of hysterectomy (non-pregnant) or C-sectioning (pregnant) and sections of vastus lateralis biopsies of age-matched healthy women were treated similarly. Images taken on a Zeiss LSM 510 confocal laser scanning microscope were processed using LSM 5 Examiner software program. For detection of glycogen, Periodic Acid Schiff staining (Sigma) was applied on mouse and human skeletal muscle tissues following the instructions of manufacturer, and the density was measured by Image J software and normalized to the data of WT non-pregnant tissues. A representative set of images of $n = 5–7$ experiments is shown in the figures.

Proteomic Studies—Plantaris samples of WT and SMTNL null mice in days 0 and 14 of pregnancy, for proteomic analysis as described in samples of WT and SMTNL null mice in days 0 and 14 of pregnancy, were homogenized in a glass homogenizer in sample buffer (5 M urea, 4% CHAPS, 1 mM DTT) and centrifuged at 15,000 × *g* for 15 min as described before (16). Samples were subjected parallel to multi-dimensional proteomic analysis using micro anion-exchange separation, one-dimensional SDS-PAGE, and LC-MALDI TOF-TOF MS/MS analysis. Proteins were visualized with silver-staining, and gels were dried. Proteins showing increased recovery between each condition were excised for identification by MALDI-TOF TOF mass spectrometry (supplemental Table S1). Changes in individual proteins were determined using a combination of densitometry and iTRAQ (17, 18) (supplemental Table S1).

Comprehensive Laboratory Animal Monitoring System (CLAMS)—Seven- to eight-week-old either pregnant or non-pregnant 129 WT and $smtnl1^{-/-}$ mice were fed a normal diet (5001 chow) and were individually housed for 1 week to acclimate them to individual housing. Mice were then placed into individual CLAMS (Columbus Instruments, Columbus, OH) cages and acclimated for 24 h. Data collection consisted of 48-h feeding/24-h fasting/24-h re-feeding phases. Mice were monitored over 4 days. File displays were collected every 20 min for oxygen consumption (VO_2, volume of oxygen consumed; ml/kg/h), VCO_2 (volume of carbon dioxide produced, ml/kg/h), RER (respiratory exchange ratio, the respiratory quotient of VCO_2/VO_2, indicative of macronutrient utilization), heat (kcal/h), accumulated food (g), accumulated drink (g), XY total activity (all horizontal beam breaks in counts), XY and Z activity, and substrate utilization, estimated by the RER in fasting or feeding conditions.

Statistical Analysis—Data were normalized by taking values obtained for WT males as 1 and by calculating a corresponding proportional value for WT females and both sexes of KO mice. Normalized data were analyzed by *t* tests (for two groups) or by general linear models (GLM, for >2 groups). Parametric statistical tests were used if the assumptions of such tests were met; otherwise, we log-transformed data for analyses. In GLMs, we tested all possible interaction terms and report here the final models obtained by excluding non-significant ($p > 0.05$) interactions. When any covariate or factor was significant in GLMs, we applied Tukey's HSD procedure to test for pairwise differences in group means. Tests were conducted in the R statistical environment (R Development Core Team 2008).

Results

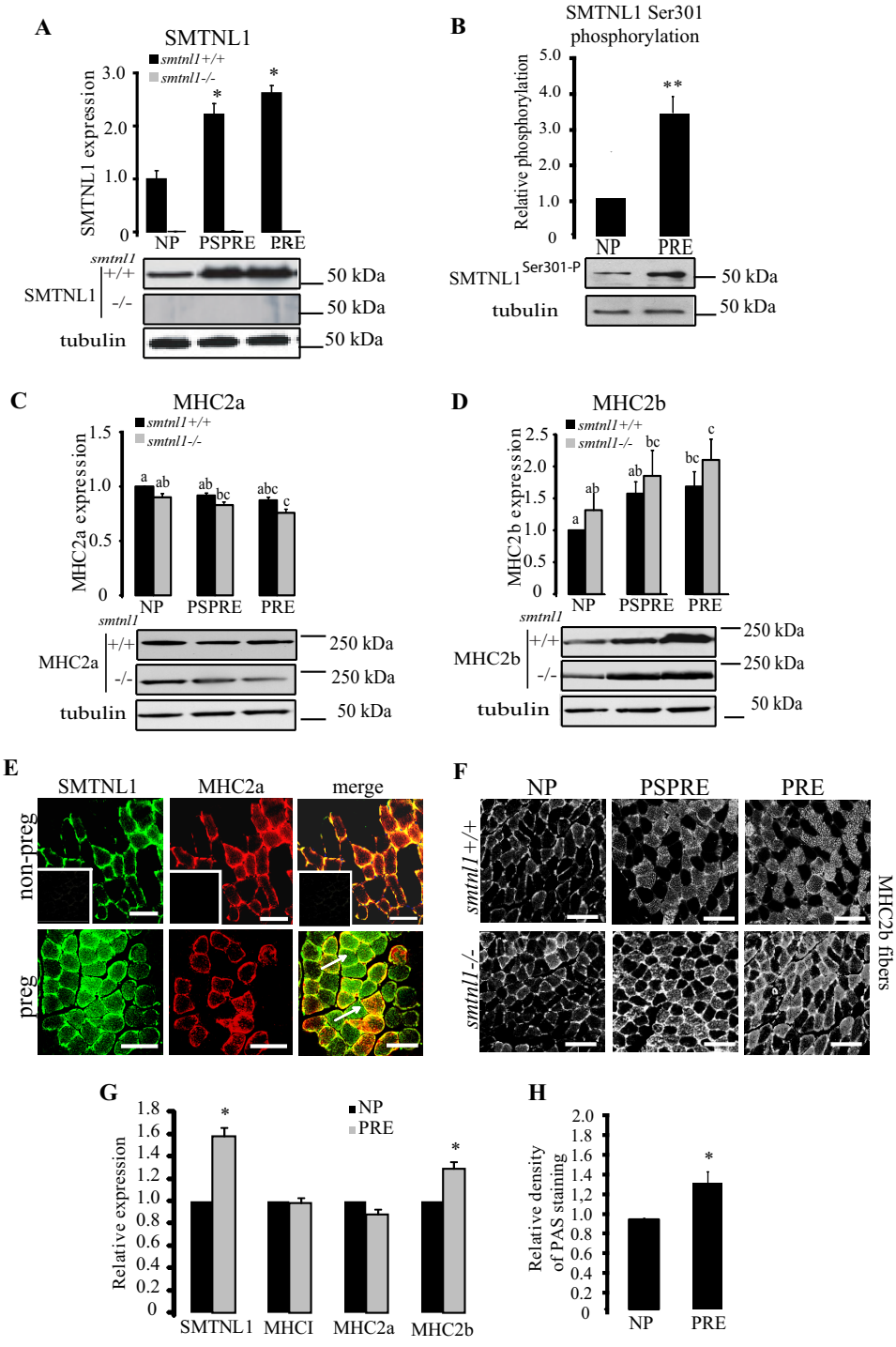
Pregnancy and SMTNL1 Regulate Glycolytic Fiber Switching in Mice and Humans—To investigate the sex-related differences in female $smtnl1^{-/-}$ mice, we conducted Western blot analysis and fiber typing experiments in pregnant animals. Because exercise induces fiber transformation in non-pregnant animals, pseudo-pregnant mice were also examined to discriminate between the physical effects of increased weight gain of the pregnant mother from the effects of hormonal regulation of SKM. Pseudo-pregnant mice proceed with the normal hormonal changes observed in fully pregnant animals but do not experience weight gain from the developing fetal mice *in utero*. Pregnancy and pseudo-pregnancy promote a 2.2-fold increase of SMTNL1 expression within the mixed fiber plantaris muscle compared with non-pregnant females (t_{max} day 16 ± 2) (Fig. 1*A*). Fig. 1*B* shows that pregnancy induces the phosphorylation (t_{max} day 12 ± 2) of SMTNL1 at Ser-301. Previously we demonstrated that *in vivo* SMTNL1 localization is highly regulated, and phosphorylation at Ser-301 promotes translocation from the cytosol to the nucleus (11), suggesting its potential role as transcriptional cofactor (12). Western analysis of MHC2a and -2b levels showed increased expression of MHC2b in response to both pregnancy and SMTNL1 deletion with concomitant reduction in MHC2a expression (Fig. 1, *C* and *D*). These expression changes were also mimicked in pseudo-pregnant mice, suggesting that these effects are regulated by the primary sex hormones rather than to physical stress arising from the developing fetal mice (Fig. 1, *C* and *D*). Detailed fiber typing of MHC isoform expression by immunohistochemistry (IHC) of SKM from non-pregnant WT females showed that SMTNL1 expression was confined only to type2a muscle fibers in murine plantaris muscle (Fig. 1*E*), which was also confirmed in human SKM (Fig. 1*G*). By day 13 of pregnancy, SMTNL1 expression was greatly increased, which implied that pregnancy promoted increased numbers of type2a fibers. However, IHC of MHC2a expression showed a decline in the mean proportion of type2a fibers (Fig. 1*E*). This phenomenon was more pronounced in SKM from pregnant female $smtnl1^{-/-}$ mice, which showed a >10% decline in type2a fibers relative to WT littermates (Fig. 1, *E–I*). Although SMTNL1 is not expressed in "*bona fide*" type2b fibers, co-staining experiments with anti-MHC2a and -MHC2b

Downloaded from http://www.jbc.org/ at UNIVERSITY OF DEBRECEN on July 21, 2015

tontay:beata_285_24

suggested that staining of SMTNL1 can also be found in fibers undergoing type2a/type2b transition (see *arrows* in Fig. 1*E*).

If pregnancy and SMTNL1 deletion reduces MHC2a expression, this raises the question of whether these conditions concomitantly increase MHC2b levels and numbers of type2b fibers? Quantitative Western blot analysis and IHC with anti-MHC2b suggested that pregnancy and pseudo-pregnancy induced a 15–20% increase in proportion of type2b glycolytic



I

	Non-pregnant		Pseudopregnant		Pregnant	
GENOTYPE	*smtnl1* +/+	*smtnl1* -/-	*smtnl1* +/+	*smtnl1* -/-	*smtnl1* +/+	*smtnl1* -/-
2a fiber type %	34.77±1.9	32.22±2.5	24.84±2.2 *	26.00±2.5 #	25.29±1.8 *	24.45±2.1 **
2b fiber type %	45.58 ±2.7	49.22 ±2.7	58.44 ±1.9	60.96±3.3*	61.12±2.4 *	65.32±3.0 **
SMTNL1 positive fibers %	36.06±1.6	N/A	39.77±1.9	N/A	42.87±1.9 #	N/A
Relative PAS density	1.00 ±0.0	1.18 ±0.2	1.25 ±0.03	1.32 ±0.1 #	1.26 ±0.04 #	1.39 ±0.2 *

Downloaded from http://www.jbc.org/ at UNIVERSITY OF DEBRECEN on July 21, 2015

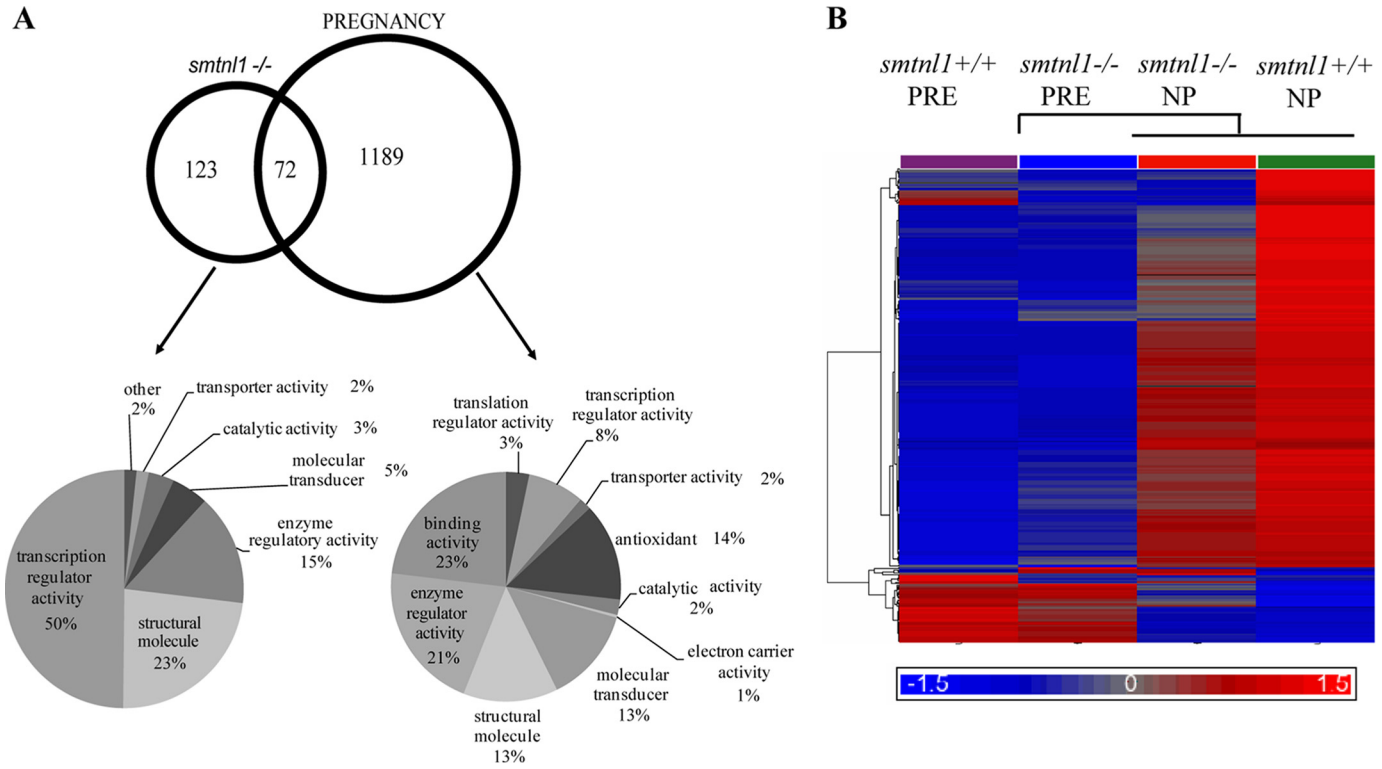


FIGURE 2. **The relationship between genes differentially regulated in the comparisons of pregnancy and SMTNL deletion and the ontology of the related genes.** *A*, Venn diagram; the *numbers within the intersections of the circles* indicate the common genes between the different groups (*NP*, non-pregnant; *PRE*, pregnant) compared to the *smtnl1+/+* non-pregnant data. The *numbers outside the circles* indicate the number of genes differentially regulated between the two groups as indicated. The molecular function of the pregnancy and *smtnl1*$^{-/-}$ deletion-related genes are represented. *B*, the color code for the signal strength is shown in the *box at the bottom* in which induced genes are indicated by *red*, and repressed genes are indicated by *blue*.

fibers (Fig. 1, *F* and *I*). IHC examination of the expression of SMTNL1, MHC1, and MHC2a/2b in abdominis rectus muscle isolated from women undergoing hysterectomy (non-pregnant control) or C-section (as pregnant) suggested that pregnancy was also likely to promote similar fiber switching in humans (Fig. 1*G*). Pregnancy or pseudo-pregnancy did not affect the expression of MHCI, the marker of oxidative slow type 1 fibers. The decrease of protein expression of type2a marker MHC2a was only tendentious significant, whereas that of MHC2b increased by 20%, indicating that fibers switched from oxidative to the more glycolytic phenotype in human pregnant SKM. The increased type2b content in pregnancy is accompanied by a 24% increase in glycogen content (Fig. 1*H*). These data suggest that pregnancy promotes the transformation of SKM fiber type to a more glycolytic phenotype in mice and humans and that SMTNL1 may play a regulatory role in this process.

The Effects of SMTNL1 Deletion and Pregnancy on Global Gene Expression in Skeletal Muscle—Given the observations that both SMTNL1 and pregnancy promote changes in the mean total fiber composition of SKM, we carried out global gene analysis to determine the extent of this switch in four experimental groups (*smtnl1*$^{-/-}$, pregnant WT, and pregnant *smtnl1*$^{-/-}$ groups were compared with non-pregnant WT). A total of 1384 genes were differentially expressed between the groups. Specifically, the comparison of WT non-pregnant mice *versus* *smtnl1*$^{-/-}$ non-pregnant mice identified 195 genes, whereas the comparison of WT non-pregnant mice and WT pregnant mice resulted in 1261 genes expressed differently. The expression of 72 genes was related specifically to both pregnancy and SMTNL1 deletion (Fig. 2*A*). Complete lists of genes for all four comparisons are available at the Duke Microarray facility website. We also conducted Gene Ontology (GO) category enrichment analyses to determine the molecular function of GO terms (Fig. 2*A*). Based on their biological functions, these genes play a role in cytoskeleton organization, calcium binding, regulation of metabolic processes and steroid synthesis, immune function, and growth regulation. Fifty percent of the genes altered by SMTNL1 deletion were related to transcrip-

FIGURE 1. **Pregnancy induced a fiber type switch to a glycolytic phenotype in SKM, and it is enhanced by SMTNL1 deletion.** *A*, expression of SMTNL1 in non-pregnant (*NP*), pregnant (*PRE*), and pseudopregnant (*PSPRE*) plantaris muscle by SQ-WB. *B*, phosphorylation of SMTNL1 Ser-301 in non-pregnant (*NP*) and pregnant (*PRE*) plantaris muscle. Means + SEM ($n = 4–5$/group), *t* test, *, $p < 0.05$. *C* and *D*, pregnancy reduces MHC2a expression (*C*) and increases expression of MHC2b (*D*) in SKM. Protein expression levels in non-pregnant, pregnant, and pseudopregnant by SQ-WB. $n = 4–13$/group, data are presented as the mean ± S.E., GLM with Tukey's test. Different letters indicate significant differences, $p < 0.05$. *E*, fiber typing by IHC and confocal microscopy of plantaris muscle. SMTNL1 (*green*) is expressed in type2a fibers (*red*) in control SKM. SMTNL1 expression shows localization in fibers different from type2a (*arrows*). *Insets* show secondary antibody controls. *Scale bars* = 20 μm. *F*, analysis of MHC2b expression (*white*) in plantaris muscle. *Scale bar* = 10 μm. *G*, SMTNL1, MHCI, MHC2a, and MHC2b expression in human SKM in pregnancy. *H*, quantitative Periodic Acid Schiff staining for glycogen content of human rectus abdominis sections. *G* and *H*, means ± S.E. ($n = 4–5$/group), *t* test. *, $p < 0.05$. *I*, quantitative fiber counting of plantaris muscle of non-pregnant, pregnant, and pseudopregnant (*smtnl1*$^{+/+}$ and *smtnl1*$^{-/-}$ animals. *PAS*, Periodic Acid Schiff. Data are the means ± S.E. ($n = 14–15$/group), *t* test. #, $p < 0.1$; *, $p < 0.05$; **, $p < 0.001$.

Downloaded from http://www.jbc.org/ at UNIVERSITY OF DEBRECEN on July 21, 2015

tontay:beata_285_24

tional regulators, and the remaining 50% included structural molecules (23%) and enzyme regulators (15%) (Fig. 2*A*). We performed hierarchical clustering on all differentially expressed genes using average linkage with Pearson's dissimilarity and present the number of induced and repressed genes in a heat map (Fig. 2*B*). Genes with significant changes in expression were assigned to different canonical pathways and subjected to GeneGo Analysis. Pregnancy was found to be largely related either to metabolism such as glycolysis-glyconeogenesis, fatty acid synthesis, or contractile proteins or signaling pathways involving prostaglandin and steroid synthesis and nuclear hormone receptor signaling (Table 1). SMTNL1 deletion caused mostly the up-regulation of signaling pathways of nuclear receptors and skeletal/smooth muscle contraction. The altered canonical pathways and the up- and down- regulated genes of signaling are listed in Table 1.

Proteomic Analysis Confirms Switching of SKM to a Glycolytic Phenotype in Response to Pregnancy and SMTNL1 Deletion—Multidimensional proteomic analysis showed that pregnancy promoted a striking and specific induction of several glycolytic enzymes and contractile proteins, the expression of which is specifically associated with type2b fibers (Fig. 3). In particular, 32% of the induced proteins are required for glycolysis (*i.e.* hexokinase, 6-phosphofructokinase, and aldolase), whereas others are associated with glycogen storage, *e.g.* glycogen phosphorylase and amylo-1,6-glucosidase. Additionally, ~42% of the induced proteins were contractile proteins associated with fast twitch fibers such as MHC2b, fast twitch forms of troponins, fast twitch myosin light chains, and fast-type myosin-binding protein C, established markers of type2b fibers (supplemental Table S1 and Figshare/SMTNL1). Our proteomic data are consistent with the result of the microarray analysis and support the hypothesis that during pregnancy female mice adapt their skeletal muscle to a glycolytic phenotype. The finding that these pregnancy-induced adaptations are less emphasized in SMTNL1-deleted tissues suggests that the protein may regulate this process.

SMTNL1 Regulates the Expression of ERα and PR-B—It has been established that SMTNL1 is expressed in smooth muscle as well as in reproductive tissues and that it is regulated through pregnancy (12). This observation supports links between the protein and steroid hormone action. Although both estrogen and progesterone clearly mediate adaptations in vascular and uterine smooth muscle, SKM is not generally recognized as a target of these hormones. We, therefore, examined PR and ER expression in SKM from *smntl1*$^{-/-}$ and WT mice. Western blot analysis of WT plantaris muscles showed that pregnancy induced a 1.5-fold increase in ERα expression by day 13. Remarkably, basal levels of ERα were induced 4–5-fold over WT levels in SKM isolated from non-pregnant *smtnl1*$^{-/-}$ and 10–15-fold over WT levels in pregnant *smtnl1*$^{-/-}$ mice (Fig. 4*A*). PR (A or B) was barely detectable in the muscle from either non-pregnant or pregnant WT mice using PR-B-specific antibody, but the PR-B isoform showed a dramatic increase in expression in SKM isolated from *smtnl1*$^{-/-}$ mice (Fig. 4*A*). In fiber typing experiments, PR-B expression was marginal in non-pregnant WT mice but showed discrete staining in all muscle fibers, including both type2a and type2b fibers in muscles isolated from pregnant animals (Fig. 4*C*). In contrast, ERα expression was confined only to type2b fibers in both non-pregnant and pregnant SKM (Fig. 4*D*). Notably, the expression of ERα was greatly enhanced in type2b fibers in muscles isolated from pregnant *smtnl1*$^{-/-}$ mice (Fig. 4*D*). A similar staining pattern was also observed in human SKM (Fig. 2*E*). Moreover, the deletion of either ERα or ERβ in mouse plantaris caused a significant increase in the protein expression level of SMTNL1 (Fig. 4*F*), suggesting the regulatory role of estrogen on SMTNL1 gene expression. The discrete expression of ERα in type2b fibers-only implies a role for estrogen in mediating the fiber switching process during pregnancy.

To investigate whether SMTNL1 mediates many of its cellular effects on skeletal muscle adaptation through direct interactions with either ER or PR, we carried out co-immunoprecipitation experiments from skeletal (Fig. 4*G*) muscle isolated from WT and *smtnl1*$^{-/-}$ mice. SMTNL1 co-precipitated with native PR-B but not ERα. *In vivo* interactions between these proteins were confirmed by repeating the IP experiments with antibodies to each of these proteins and Western blotting the IPs with anti-SMTNL1. Besides using SKM, we applied uterine smooth muscle extract as a positive control (data shown in our previous work in Bodoor *et al.* (12), as it expresses both ERα and PR under normal conditions). *Smtnl1*-deleted tissues did not present any interaction with SMTNL1 itself by IP. IP of PR-B or ERα from skeletal and uterine smooth muscle extracts prepared from *smtnl1*$^{-/-}$ mice showed an induction of both proteins. Similarly, although IP with ERα antibody demonstrated the presence of ERα and PR-B in the IP as expected, Western analysis with anti-SMTNL1 confirmed that it did not associate directly with ERα *in vivo* (Fig. 4*G*). Although our data do not support direct interactions of SMTNL1 with ERα, its increased expression observed after IP and Western analysis from *smtnl1*$^{-/-}$ mice may reflect that PR suppresses the expression of ERα at the transcriptional level. In accordance with this mechanism, it was reported that both ER and PR mutually regulate each others' expression through transcriptionally controlled feedback mechanisms (19).

Pregnancy Induces Metabolic Activity and Reduces Oxygen Consumption—One objective of this study was to determine whether the effects of pregnancy and SMTNL1 deletion on SKM phenotype in mice resulted in any changes of energy expenditure and/or feeding behavior. Pregnant or non-pregnant WT and *smtnl1*$^{-/-}$ mice were housed in CLAMS apparatus, and metabolic measurements taken daily (Fig. 5, *A*–*F*). During the study there was no significant difference in food intake among the four experimental groups (pregnant and non-pregnant WT and *smtnl1*$^{-/-}$ mice; data not shown). Energy expenditure (VO_2), or the amount of energy an individual uses daily to complete all regular body activities, of fed and fasted non-pregnant WT and *smtnl1*$^{-/-}$ mice was not significantly different among groups (Fig. 5, *A* and *B*). VO_2 however, was significantly lower in the fed pregnant mice than in the fed non-pregnant mice. Interestingly, in fasted pregnant mice, both WT and *smtnl1*$^{-/-}$ animals showed a smaller decrease in VO_2 than did those fed, suggesting an overall rescuing effect of pregnancy (Fig. 5, *A* and *B*). Normally, increases in the RER indicates increased utilization of carbohydrates for fuel. Conversely,

Downloaded from http://www.jbc.org/ at UNIVERSITY OF DEBRECEN on July 21, 2015

TABLE 1

The involvement of pregnancy and SMTNL1 regulated genes in metabolic and canonical signaling pathways

Genes were analyzed using the GeneGo software for obtaining pathway maps, biological networks, and diseases relevant to the study.

Metabolic pathways	Genes	Gene symbol	Name	Regulation in pregnancy	Regulation in *smtnl1-/-*
Glycolysis	NM_009657	Aldoc	Aldolase	2.2	1.4
	NM_133232	Pfkfb3	6-Phosphofructo-2-kinase	4.02	1.4
Glyconeogenesis	NM_007994	Fbp2	Fructosebisphosphatase 2	-2.54	-1.66
	NM_008797	Pcx	Pyruvatecarboxylase	-2.5	-1.2
Glycogenolysis	NM_153781	Pyg	Glycogenphosphorylase	2.32	1.4
Glycogenesis	NM_010292	Gck	Glucokinase	-3.65	1.26
	NM_028132	Pgm2	Phosphoglucomutase 2	-2.24	-1.6
TCA Cycle	NM_007861	Dld	Dihydrolipoamidedehydrogenase	2.3	1.2
Fatty Acid Synthesis	NM_009128	Scd2	Stearoyl-coenzymeAdesaturase	2.57	1.2
	NM_133904	Acacb	Acetyl-coenzymeAcarboxylase	-2.1	-1.2
Fatty Acid Degradation	NM_001033600	Acsl4	Acyl-CoAsynthetase family memb. 4	2.6	1.2
	NM_008194	Gyk	Glycerolkinase	2.6	1.2
Canonical signaling pathways	**Genes**	**Gene symbol**	**Name**	**Regulation in pregnancy**	**Regulation in *smtnl1-/-***
Striated/smooth Muscle Contraction	NM_09610	Actg2	Actin, alpha	3.8	1.32
	NM_007392	Acta2	Actin, alpha 2	5.42	1.93
	NM_011586	Myo18	Myosin, heavy polypeptide XVIII	-2.2	-1.2
	NM_ 01039545	Myh2	Myosin, heavy polypeptide 2	3.1	1.29
	NM_028021	Myh14	Myosin, heavy polypeptide 14 IIA	-2.3	-1.06
	XM_485171	Myl9	Myosin, light chain polypeptide 9, reg.	2.28	1.25
	NM_009922	Cnn1	Calponin 1	4.97	1.51
	NM_031170	Chd7	Keratin 8	6.8	1.97
	NM_008712	Nos1	Nitricoxidesynthase 1, neuronal	-2.83	-1.97
	NM_010518	Igfbp5	Insulin-likegrowthfact. bind. prot.	2.13	1.15
	NM_145571	Cald1	Caldesmon 1	2.35	1.12
	NM_011652	Ttn	Titin	2.17	1.22
	NM_139300	Mylk	Myosin light polypeptidekinase	2.26	1.43
Nuclear Receptors	NM_008829	Pgr	Progesterone receptor	12.1	1.8
	NM_007956	Esr1	Estrogen receptor 1	2.2	1.2
	NM_008173	Nr3a2	Nuclear receptor subfamily 3	2.4	-1.09
	NM_013613	Nr4a2	Nuclear receptor subfamily 4	3.9	2.1
	NM_030676	Nr5a2	Nuclear receptor subfamily 5	2.3	1.7
	NM_011935	Esrrg	Estrogenrelated receptor gamma	2.4	1.6
	NM_001111267	Ncoa7	Nuclear receptor coactivator	2.7	1.3
Calcium Regulation G Protein Signaling	NM_009061	Rgs2	Regulator of G-protein signaling 2	3.07	1.3
	NM_009063	Rgs5	Regulator of G-protein signaling 5	2.5	-1.4
	NM_011158	Prkar2b	Protein kinase, cAMP dependent	2.8	2.0
	NM_001039079	Prkcz	Protein kinase C zeta	-2.2	-1.3
	NM_008803	Pde8a	Phosphodiesterase 8A	-2.4	-1.2
	NM_001122759	Pde7a	Phosphodiesterase 7A	-2.2	-1.2
	NM_031185	Akap12	A kinase anchor protein 12	2.2	1.2
	NM_001037723	Adcy7	Adenylatecyclase 7	2.6	1.2
	NM_009109	Ryr1	Ryanodinerceptor 1	-2.1	-1.1
Steroid Biosynthesis	NM_008293	Hsd3b1	Hydroxy-delta-5-steroid dehydrogenase andsteroidisomerase	3.7	5.6

decreased RER indicates a shift toward fatty acid utilization. The RER of both non-pregnant and pregnant *smtnl1*$^{-/-}$ mice was elevated in the fed state during the dark cycle (period of normal activity and feeding) compared with WT mice (Fig. 5, *C* and *D*), suggesting a hyper-metabolic shift toward carbohydrate utilization as fuel. RER was reduced in both the *smtnl1*$^{-/-}$ and WT pregnant animals compared to non-pregnant animals, demonstrating that the *smtnl1*$^{-/-}$ mice are able to efficiently shift substrate utilization (fats *versus* carbohydrates). RER data (Fig. 5, *C* and *D*) also revealed that there was an enhanced shift in substrate utilization in pregnant *smtnl1*$^{-/-}$ mice because the shift in metabolism between fatty acids and carbohydrates dur-

Downloaded from http://www.jbc.org/ at UNIVERSITY OF DEBRECEN on July 21, 2015

tontay:beata_285_24

TABLE 1—*continued*

Prostaglandin Synthesis	NM_008289	Hsd11b2	Hydroxysteroiddehydrogenase	2.6	1.3
	NM_008278	Hpgd	Hydroxyprostagl.dehydroxygen. 15	4.5	1.4
	NM_008869	Pla2g4a	Phospholypase A2	2.9	1.2
Inflammatory Response Pathway	NM_007743	Col1a2	Collagen, type I, alpha 2	2.5	-1.1
	NM_010559	Il6ra	Interleukin 6 receptor	-4.0	-1.2
	NM_011580	Thbs1	Thrombospondin 1	2.5	-1.0
	NM_007642	Cd28	CD28 antigen	3.3	1.3
	NM_010683	Lamc1	Laminin gamma	2.0	1.6
	NM_008482	Lamb1-1	Laminin B1 subunit	3.7	1.6
Blood Clotting Cascade	NM_008872	Plat	Plasminogen activator	3.4	1.1
	NM_0080013	Fgl2	Fibrinogen-like protein 2	3.0	-1.1
	NM_001111048	Fga	Fibrinogen, alpha	-2.1	-1.1
Apoptosis	NM_016851	Irf6	Interferon regulatoryfactor 6	4.1	1.7
	NM_009810	Casp3	Caspase 3	2.6	1.2
	NM_001042558	Apaf1	Apoptotic peptidase activating factor 1	2.1	1.3
Cell Cycle	NM_009828	Ccna2	Cyclin A2	2.6	2.0
	NM_009873	Cdk6	Cyclin dependent kinase 6	2.5	1.5
	NM_007630	Ccnb2	Cyclin B2	2.1	2.2
	NM_007631	Ccnd1	Cyclin D1	2.4	1.1
	NM_011249	Rbl1	Retinoblastome-like 1	2.4	1.2
	NM_008229	Hdac2	Hystonedeacetylase 2	2.1	1.3
MAPK Cascade	NM_001039934	Mtap2	Microtubule-associated protein 2	4.3	1.6
	NM_001025245	Mbp	Myelinbasic protein	2.3	1.8
TGF Beta Signaling_Pathway	NM_009263	Spp1	Secreted phosphoprotein 1	2.8	1.6
	NM_007614	Ctnnb1	Catenin beta1	2.1	-1.1
	NM_008046	Fst	Follistatin	2.6	1.6
Matrix Metalloproteinases	NM_011985	Mmp23	Matrixmetallopeptidase 23	2.3	1.4
	NM_008608	Mmp14	Matrixmetallopeptidase 14	2.3	1.4
Statin Pathway	NM_009230	Soat1	SterolO-acyltransferase 1	2.3	1.6
	NM_023114	Apoc3	Apolipoprotein C-III	-3.9	-1.1
	NM_009692	Apoa1	Apolipoprotein A-I	-3.4	-1.1
Pentose Phosphate Pathway	NM_025683	Rpe	Ribulose-5-phosphatase-3-epimerase	2.0	-1.1
Biogenic Amine Synthesis	NM_009538	Ddc	Dopadecarboxylase	3.0	1.1
	NM_008230	Hdc	Histidinedecarboxylase	2.4	2.3
Cholesterol Biosynthesis	NM_020010	Cyp51	Cytochrome P450, family 51	2.0	1.2
	NM_025436	Sc4mol	Sterol-C4-methyl oxidase-like	2.6	-1.0
	NM_145360	Idi1	Isopentenyl-diphosphateisomerase	2.8	-1.1
	NM_008255	Hmgcr	3-hydroxy-3-meth.glutaryl-Coenzyme A reductase	2.6	1.3
	NM_010191	Fdft1	Farnesyldiphosphatase farnesyltrasnferase 1	-2.0	-1.1

ing the diurnal cycles was more pronounced in the *smtnl1*$^{-/-}$ pregnant mice. Non-pregnant *smtnl1*$^{-/-}$ mice showed a marked decrease in activity during the dark cycle compared with WT mice, and this difference was more pronounced in the pregnant pairings (Fig. 5, *E* and *F*). These findings suggest that although the *smtnl1*$^{-/-}$ mice can shift their metabolic pathways, their metabolism is less efficient than WT littermates as they preferentially utilize carbohydrates for fuel. This preference was enhanced when the *smtnl1*$^{-/-}$ mice become pregnant.

Effect of Pregnancy and SMTNL1 Deletion on Glucose Tolerance and on Insulin Signaling—To address the response to glucose administration, we performed an intraperitoneal glucose tolerance test. We analyzed data from the glucose tolerance test by repeated measures of analysis of variance. Pregnant mice had higher blood glucose levels at the start of the experiment (87.5 ± 29.95 mg/dl) than non-pregnant animals (57.0 ± 17.55 mg/dl, $p = 0.007$). Blood glucose levels increased sharply in *smtnl1*$^{-/-}$ non-pregnant mice, whereas the increase was more moderate in *smtnl1*$^{-/-}$ pregnant and WT mice (Fig. 5*G*). The interaction terms were significant both between genotype and time ($F = 5.587$, $p < 0.001$) and between status and time ($F = 6.996$, $p < 0.001$), confirming that the effect of time on blood glucose levels differed between individuals of different genotype and status. In the genotype-time interaction, the linear term was significant ($F = 7.433$, $p = 0.014$), indicating that the

Downloaded from http://www.jbc.org/ at UNIVERSITY OF DEBRECEN on July 21, 2015

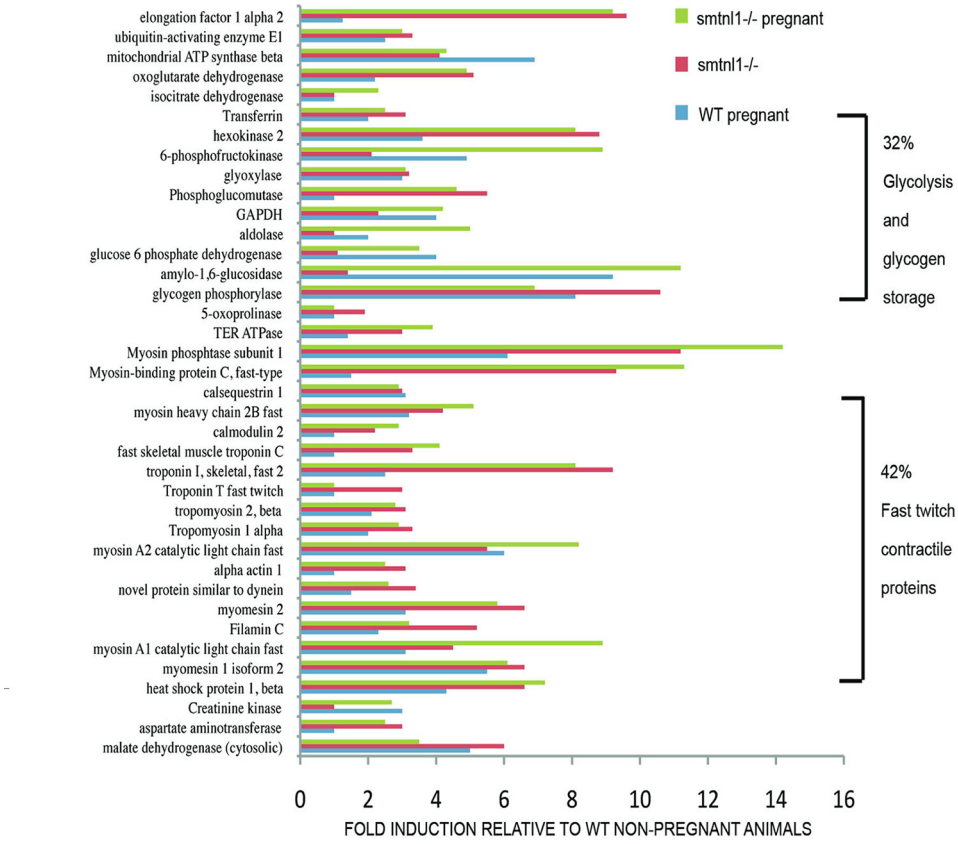


FIGURE 3. **Proteomic analysis shows that pregnancy and SMTNL1 deletion induces expression of glycolytic enzymes and contractile proteins associated with Type2b fibers.** Plantaris muscle extracts were subjected to proteomic analysis prepared from *smtnl1*$^{+/+}$ (WT), *smtnl1*$^{+/+}$, pregnant (*WP*), *smntl1*$^{-/-}$ (KO), and *smtnl1*$^{-/-}$ pregnant (KOP) animals. The data show -fold induction of proteins in WP, KO, and KOP samples compared with WT. *TER ATPase*, transitional endoplasmic reticulum ATPase. See the related data in supplemental Table S1.

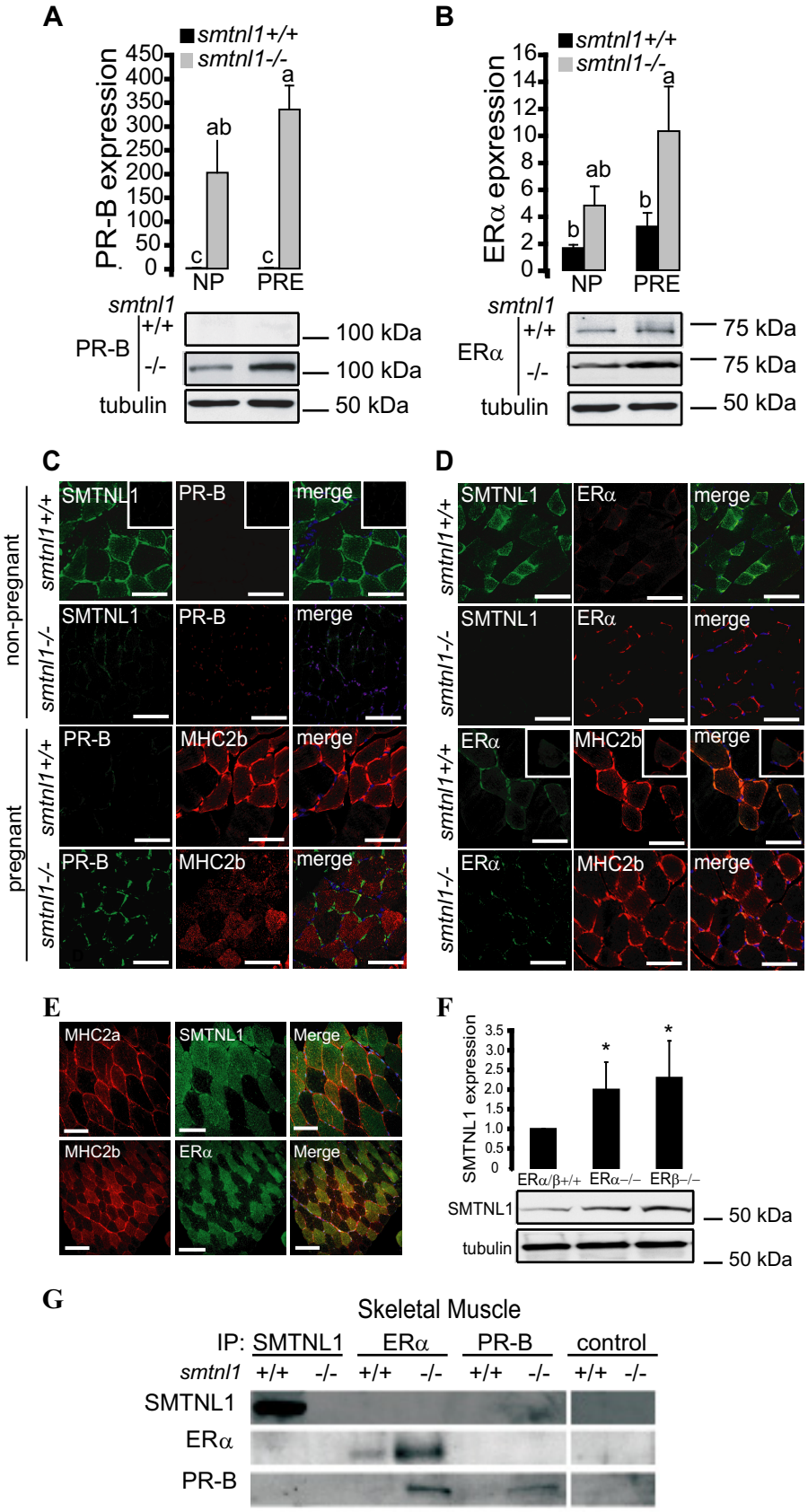
differences between KO and WT genotypes were similar at each measurement (Fig. 5*G*). WT pregnant mice also had slightly but not significantly lower blood glucose levels than WT non-pregnant mice between 15 and 60 min. These results show that *smtnl1*$^{-/-}$ non-pregnant mice have much lower glucose tolerance than *smtnl1*$^{-/-}$ pregnant or WT mice, indicating that pregnancy increases glucose tolerance in KO mice to the level of tolerance in WT mice. Impaired glucose tolerance is associated with pronounced insulin resistance and at cellular level occurs in tandem with changes in key steps in the insulin-signaling cascade that regulates glucose uptake by SKM. Insulin receptor substrate 1 (IRS1) and the insulin-sensitive glucose transporter 4 (Glut4) are believed to be key elements of insulin-signaling in SKM (20) To verify the importance of pregnancy and SMTNL1 deletion in the development of insulin resistance, SQ-WB analysis was conducted on non-pregnant and pregnant plantaris tissues of WT and *smtnl1*$^{-/-}$ mice, determining the protein expression of Glut4 and IRS1 (Fig. 5, *H–I*). SMTNL1 deletion decreased the expression of Glut4 and IRS1 by 53 and 58%, respectively. Pregnancy attenuated IRS1 expression significantly but had no effect on the Glut4 expression level in WT animals. However, pregnant *smtnl1*$^{-/-}$ animals exhibited an increase in both Glut4 and IRS1 expression in *smtnl1*$^{-/-}$ animals. Our results suggest that the impaired glucose tolerance of *smtnl1*$^{-/-}$ is the consequence of decreased Glut4 and IRS1 expression.

Discussion

Data presented herein suggest that pregnancy hormones such as progesterone and estrogen trigger the switching of SKM to a glycolytic phenotype through their respective nuclear receptors (Fig. 6). We hypothesize that SMTNL1 plays a negative regulatory role on the transcriptional activity of PR and ER in SKM and that protein kinase A- or G-mediated signaling can influence this process specifically through the phosphorylation of SMTNL1 at Ser-301 (11). Functionally, therefore, SMTNL1 acts as a transcriptional repressor of PR *in vivo*, and the phosphorylation of SMTNL1 specifically inhibits this function (12). Mechanistically this implies that the default function for SMTNL1 in non-pregnant animals is to repress PR function from promoting pregnancy-like adaptive responses in female SKM. Conversely, pregnancy (or adrenergic-induced signals) through Ser-301 phosphorylation relieves SMTNL1 inhibition of PR to promote appropriate changes in SKM gene expression resulting in switching to a more glycolytic phenotype. Intriguingly, protein kinase A-mediated signaling pathways have long been known to greatly affect both progesterone and estrogen signaling *in vivo* (21, 22). However, our study is the first to suggest that cyclic nucleotide-mediated signaling pathways in SKM may also be related to the regulation of gene expression by SMTNL1 acting through PR and ER.

Downloaded from http://www.jbc.org/ at UNIVERSITY OF DEBRECEN on July 21, 2015

tontay:beata_285_24



Downloaded from http://www.jbc.org/ at UNIVERSITY OF DEBRECEN on July 21, 2015

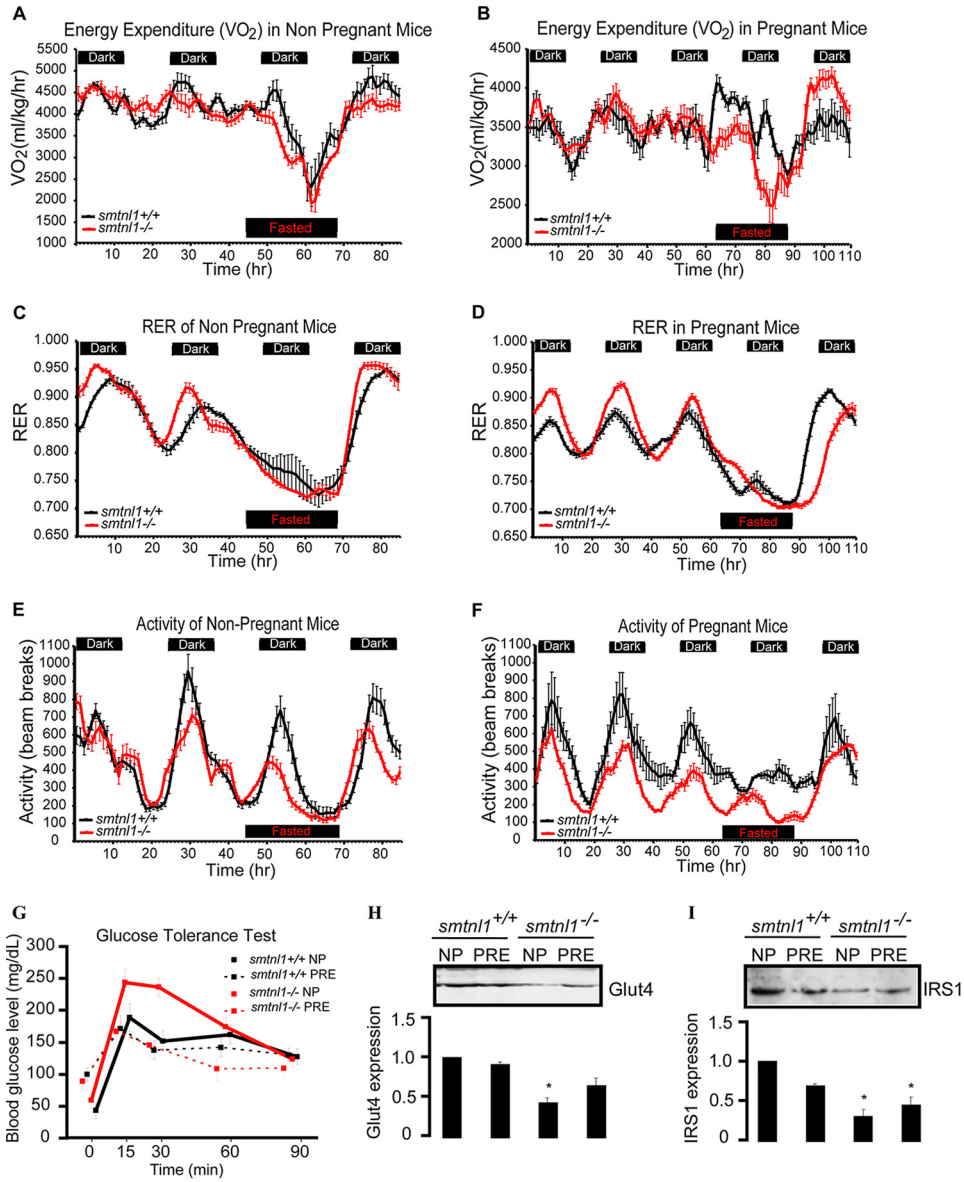


FIGURE 5. **Effect of pregnancy and SMTNL1 deletion on metabolic parameters of animals.** *A* and *B*, energy expenditure in non-pregnant (*A*) and pregnant (*B*) mice. The volume of oxygen consumed, ml/kg/h (VO_2) was measured over time. *C* and *D*, the RER is the respiratory quotient of the consumed oxygen and exhaled carbon dioxide (VO_2/VCO_2), was calculated *versus* time of non-pregnant (*C*) and pregnant (*D*) mice. Heat production was measured (kcal/h) in light and dark cycles. *E* and *F*, the activities of non-pregnant (*E*) and pregnant (*F*) animals were measured as the unit of beam breaks. *G*, changes in blood glucose levels (mean ± 1 S.E.) in *smtnl1*$^{+/+}$ and -$^{-/-}$, either pregnant or non-pregnant mice in increasing times followed by intraperitoneal glucose injection. *H* and *I*, expression of Glut4 (*H*) and IRS1 (*I*) in non-pregnant (*NP*) and pregnant (*PRE*) plantaris muscle. SMTNL1 deletion caused decreases in Glut4 and IRS1 expression and pregnancy partially rescued its effect. Protein expression levels were determined in non-pregnant and pregnant mice plantaris muscle by SQ-WB. $n = 4$–13/group. Data are presented as the mean ± S.E. Results are expressed as the means ± S.E. ($n > 6$ mice/group). #, $p < 0.05$; ***, $p < 0.001$ (repeated measures analysis of variance).

The SMTNL1/PR-B Complex Presents a Homeostatic Feedback Mechanism Regulating the Expression of Each Other and of ERα—Expression studies in *smtnl1*$^{-/-}$ mice showed that PR-B and ER expression levels are strikingly regulated by intracellular levels of SMTNL1. Similarly, studies in ERα null mice showed that SMTNL1 expression was elevated in most tissues normally expressing the protein. Furthermore, SMTNL1 levels also closely followed progesterone levels throughout pregnancy. Together these findings suggest that SMTNL1 expression is closely linked to PR and ER and vice versa. The extent of

FIGURE 4. **The effects of pregnancy and SMTNL1 deletion on ER and PR expression in skeletal muscle.** *A* and *B*, SMTNL1 deletion and pregnancy (*PRE*) induce expression of PR-B (*A*) and ERα (*B*) in SKM comparing to non-pregnant (*NP*) animals. Data are the mean ± S. E. for $n = 4$, GLM with Tukey's test; different letters indicate significant differences. $p < 0.05$. *C*, analysis of PR-B (*red*) in MHC2a (co-staining for SMTNL1 (*green*)) and MHC2b (*red*, staining for MHC2b) in plantaris. *Scale bars* = 20 μm. *D*, immunohistochemistry shows discrete expression of ERα (*red*) in type2b fibers in plantaris muscle. *Scale bars* = 20 μm. *E*, SMTNL1 and ERα localization in human skeletal muscle. Shown is localization of SMTNL1 (*green*) in type2a (*red*) and ERα (*green*) in type2b fibers (*red*) in human skeletal muscle by confocal microscopy. *Scale bars* represent 20 μm. *F*, SMTNL1 expression in plantaris of ERα$^{-/-}$ and ERβ$^{-/-}$ mice. Plantaris muscle of ERα/β$^{+/+}$, ERα$^{-/-}$, and ERβ$^{-/-}$ were lysed and analyzed by WB analysis using SMTNL1 antibody and anti-tubulin for loading control. Data were normalized, and values are relative changes compared with that obtained in ERα/β$^{+/+}$. Data are the mean ± S.E., $n = 4$ each group. GLM: *, $p > 0.05$. *G*, SMTNL1 binds to PR-B but not to ERα *in vivo* in skeletal muscle. SMTNL, PR-B, and ERα were immunoprecipitated from skeletal muscle and uterine muscle (see positive control as shown in Ref. 12) extracts.

Downloaded from http://www.jbc.org/ at UNIVERSITY OF DEBRECEN on July 21, 2015

tontay:beata_285_24

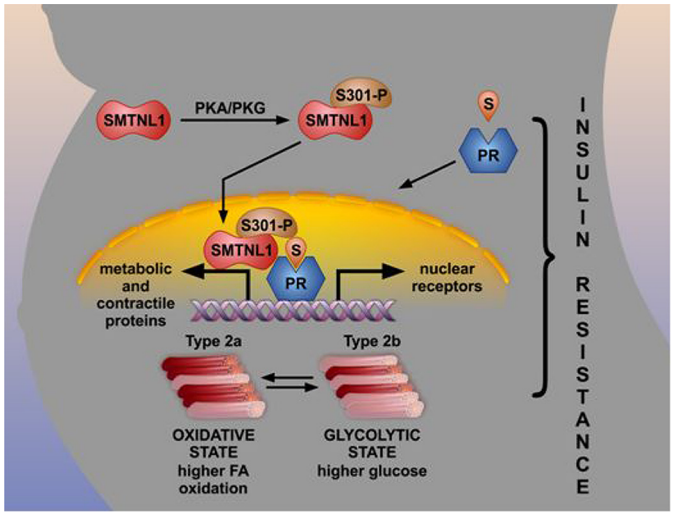


FIGURE 6. **Schematic showing the molecular mechanism by which SMTNL1 regulates PR-B to coordinately promote skeletal muscle adaptations in response to pregnancy.** In response to elevated steroid hormone, progesterone (*S*) levels SMTNL1 and PR-B enter the nucleus. In the non-pregnant state, SMTNL1 functions to repress PR-B activity; however, during pregnancy this inhibition is relieved and promotes activation of skeletal muscle-specific genes regulating the expression of metabolic and contractile proteins. This coordinated response adapts the mother's physiological state to support the weight gain originating from developing fetus. Switching to a glycolytic phenotype in skeletal muscle reduces the oxidative capacity of SKM, promoting increased storage of fatty acid (*FA*) and inducing an insulin-resistant state resulting in increased circulating glucose. *PKA/PKG*, protein kinase A/G.

SMTNL1 involvement in this feedback mechanism is most dramatic in *smtnl1*$^{-/-}$ mice with the observation that the expression of both PR and ER are greatly increased within specific muscle fibers in response to SMTNL1 deletion. The finding that ERα is specifically localized in type2b fibers suggests that these fibers are likely to be sensitive to estrogen when transitioned to glycolytic fibers. Interestingly, earlier work by others suggested that the expression of ER in SKM has a role in the development of muscle strength in humans (23, 24). Because prior work from our group showed that SMTNL1 only interacts with PR-B and-A and not with either isoform of ER (12), the altered ER expression observed in *smtnl1*$^{-/-}$ mice most likely must be mediated through PR via a homeostatic feedback mechanism (25), as PR and ER are known to mutually regulate the expression of each other. We, therefore, hypothesize that the differential localization and expression of SMTNL1, PR, and ER are key to the adaptation to pregnancy. We propose that under normal physiological conditions SMTNL1 is expressed in type2a fibers, where it represses the activity of PR. Because ER shows type2b-specific localization, this provides fiber-selective estrogen sensitivity. On one hand, circulating estrogen bound to ER might bind and repress the promoter of *smtnl1*, which provides an explanation to the low expression of SMTNL1 in type2b fibers in normal conditions and the increased SMTNL1 expression in ERα- or β-deleted animals (Fig. 4*F*). On the other hand, the increased number of type2b but a slight decreased number of 2a fibers detected in *smtnl1*$^{-/-}$ SKM could be explained by the release of PR repression by SMTNL1 in type2a fibers.

The Effects of Pregnancy on Metabolic Pathways Related to Insulin Resistance—Bioinformatics analysis of data from global gene expression and multidimensional proteomic analyses showed that pregnancy highly regulates sets of genes related to canonical pathways that play a role in glycolysis, gluconeogenesis, muscle contraction, and steroid biosynthesis as well as inflammatory responses, supporting our hypothesis of the manifestation of a glycolytic phenotype in pregnant SKM. The main profile of genes induced in *smtnl1*$^{-/-}$ deletion was transcriptional regulation, suggesting a primary role of SMTNL1 in gene expression as genes such as PR and nuclear receptor subfamily 3–4 are regulated. The majority of pathways regulated in pregnancy were related to the mediation of insulin resistance (26). During the progression of normal pregnancies, insulin resistance arises. Pronounced insulin resistance is associated with impaired glucose tolerance and with a high risk of gestational diabetes; however, the underlying mechanisms are not very well understood (27). Redundant control mechanisms operate to maintain normal glucose homeostasis in SKM. Insulin activates the insulin receptor tyrosine kinase, which activates signaling partners such as PKB/Akt and stimulates the translocation of GLUT4 vesicles to the plasma. IRS1 protein expression was increased in *smtnl1*$^{-/-}$ mice; moreover, pregnancy itself had a negative effect on IRS expression. Importantly, IRS expression is increased postpartum (20), and overexpression of the protein in a spontaneous gestational diabetes is associated with the reversal of insulin resistance (28). Pregnancy and SMTNL1 deletion are likely to regulate Glut4 expression through different pathways because *smtnl1*$^{-/-}$ tissues showed significantly lower levels of the Glut4 protein, an effect rescued by pregnancy. Our results showed that ER and PR expression levels had a robust increase in pregnant and *smtnl1*$^{-/-}$ tissues. Moreover, ER expression was related to a more efficient metabolic state, and ER KO animals presented overt insulin resistance (29). Although these findings strongly suggest a better metabolic status of SMTNL1 knock-out mice, we found impaired metabolism in *smtnl1*$^{-/-}$ mice. This controversy may be explained by the observation that circulating hormone levels influence the improvement of insulin resistance (26) and that the levels of circulating progesterone and estrogen decreased significantly during pregnancy (12).

How Might Pregnancy-induced Glycolytic Fiber Switching in Skeletal Muscle Contribute to Insulin Resistance—In Fig. 6 we suggest that pregnancy-induced fiber switching to a more glycolytic phenotype is a coordinated physiological response that may be at the heart of increased weight gain and generalized insulin resistance associated with normal pregnancy (Fig. 6). By virtue of its mass, SKM dictates the overall caloric disposal of both glucose and free fatty acids. If the oxidative capacity of SKM is increased through endurance exercise, one reduces the risk of developing insulin resistance, and exercise alone can reverse the symptoms of obesity-induced type II diabetes. This is because the primary sites of free fatty acid oxidation in mammals are oxidative type I and Type2a SKM fibers. Conversely, if the type2a content of SKM is reduced, the ability to oxidize free fatty acid is also reduced, thereby increasing storage of fatty acid (FA) as triglyceride in adipose tissue. When oxidative capacity is reduced, the storage of FA as triglyceride is further exacerbated in the presence of high carbohydrate levels. This is because humans and most mammals derive much of their stored triglyceride via pathways of *de novo* FA synthesis

Downloaded from http://www.jbc.org/ at UNIVERSITY OF DEBRECEN on July 21, 2015

through the metabolism of glucose in adipose tissue and liver (30). Excess fat and carbohydrate in the diet, therefore, provides an optimal environment for excessive weight gain, especially in sedentary individuals. We hypothesize that switching to a glycolytic phenotype in pregnancy, with a reduced oxidative fiber content of SKM, therefore, provides a molecular basis to explain increased weight gain and insulin resistance in pregnant females. We suggest that this is a normal response to pregnancy and infers the evolutionary advantage of enabling the mother to increase circulating glucose levels for proper fetal development as well as store fat more efficiently to meet the caloric demands of lactation. Our results also suggest that switching to a glycolytic phenotype infers an advantage by increasing the mother's physical strength. Type2b muscle fibers are associated with strength and resistance training such as seen with weight lifting. An increase in the mother's physical strength would much better enable her to manage the increased weight of the fetus in the latter stages of pregnancy. Importantly, in ~4% of all pregnancies, pregnancy-induced insulin resistance progresses to gestational diabetes. If pregnancy, therefore, promotes the transition to a more glycolytic phenotype as an evolutionary benefit, then this may render some women even more susceptible to developing gestational diabetes, especially under the influence of high energy Western diets.

Finally, considering all our understanding of muscle physiology and its importance to health and well being, one might ask why pregnancy-induced fiber switching has not already been reported in the literature. A search of the current literature suggests that this may be because the majority of muscle studies to date have been carried out in males only. The experimental bias of studies toward male over female physiology is likely attributable to the commonly held belief that the estrous cycle introduces hard-to-explain variability in physiological processes in female animals. Indeed, in studies of female physiology, ovariectomized females are typically used to remove the oestrus-related aspects of physiology from the inquiry. As a result, many normal physiological responses relevant to female physiology get purposefully ignored. Although further investigation is certainly warranted, particularly non-invasive studies of SKM in pregnant women, our findings could indicate that important aspects of women's health are being missed due to an experimental bias.

Author Contributions—B. L. designed, performed, and analyzed the experiments shown in Figs. 1 and in part in Figs. 2, 3, 4, and 6 and wrote the paper. K. B. analyzed the experiments in Fig. 2. S. A. performed the experiments in Figs. 1 and 5. D. H. W. assisted in the CLAMS study. D. L. performed the proteomic analysis. D. P. M. and R. S. helped in ER and PR studies. D. Z. provided MHC-specific antibodies. J. D. and R. C. H. provided human biopsies and performed the human study. T. R. performed CLAMS experiments. T. A. H. conceived and coordinated the study and wrote the paper.

Acknowledgments—We are grateful to Dr. Ferenc Erdődi (University of Debrecen, Debrecen, Hungary) for revising the paper and Dr. Kennet Korach (Reproductive and Developmental Toxicology Laboratory, Research Triangle Park, NC) for providing the ERKO mice as well as to Dr. Szabolcs Lengyel (Hungarian National Academy of Science, Ecology Research Center, Debrecen, Hungary) for helping in statistical analyses.

Note Added in Proof—Supplemental Table S1 was missing in the version of this article that was published as a Paper in Press on April 14, 2015. The supplemental table is now available.

References

1. Halayko, A. J., and Solway, J. (2001) Molecular mechanisms of phenotypic plasticity in smooth muscle cells. *J. Appl Physiol.* **90,** 358–368
2. Booth, F. W., and Thomason, D. B. (1991) Molecular and cellular adaptation of muscle in response to exercise: perspectives of various models. *Physiol. Rev.* **71,** 541–585
3. Fitts, R. H. (2003) Effects of regular exercise training on skeletal muscle contractile function. *Am. J. Phys. Med. Rehabil.* **82,** 320–331
4. Carey, A. L., and Kingwell, B. A. (2009) Novel pharmacological approaches to combat obesity and insulin resistance: targeting skeletal muscle with "exercise mimetics." *Diabetologia* **52,** 2015–2026
5. Hamilton, M. T., and Booth, F. W. (2000) Skeletal muscle adaptation to exercise: a century of progress. *J. Appl. Physiol.* **88,** 327–331
6. Edwards, D. P. (2005) Regulation of signal transduction pathways by estrogen and progesterone. *Annu. Rev. Physiol.* **67,** 335–376
7. Barros, R. P., Morani, A., Moriscot, A., and Machado, U. F. (2008) Insulin resistance of pregnancy involves estrogen-induced repression of muscle GLUT4. *Mol. Cell. Endocrinol.* **295,** 24–31
8. Sugaya, A., Sugiyama, T., Yanase, S., Shen, X. X., Minoura, H., and Toyoda, N. (2000) Expression of glucose transporter 4 mRNA in adipose tissue and skeletal muscle of ovariectomized rats treated with sex steroid hormones. *Life Sci.* **66,** 641–648
9. Brănişteanu, D. D., and Mathieu, C. (2003) Progesterone in gestational diabetes mellitus: guilty or not guilty? *Trends Endocrinol. Metab.* **14,** 54–56
10. Wooldridge, A. A., Fortner, C. N., Lontay, B., Akimoto, T., Neppl, R. L., Facemire, C., Datto, M. B., Kwon, A., McCook, E., Li, P., Wang, S., Thresher, R. J., Miller, S. E., Perriard, J. C., Gavin, T. P., Hickner, R. C., Coffman, T. M., Somlyo, A. V., Yan, Z., and Haystead, T. A. (2008) Deletion of the protein kinase A/protein kinase G target SMTNL1 promotes an exercise-adapted phenotype in vascular smooth muscle. *J. Biol. Chem.* **283,** 11850–11859
11. Lontay, B., Bodoor, K., Weitzel, D. H., Loiselle, D., Fortner, C., Lengyel, S., Zheng, D., Devente, J., Hickner, R., and Haystead, T. A. (2010) Smoothelin-like 1 protein regulates myosin phosphatase-targeting subunit 1 expression during sexual development and pregnancy. *J. Biol. Chem.* **285,** 29357–29366
12. Bodoor, K., Lontay, B., Safi, R., Weitzel, D. H., Loiselle, D., Wei, Z., Lengyel, S., McDonnell, D. P., and Haystead, T. A. (2011) Smoothelin-like 1 protein is a bifunctional regulator of the progesterone receptor during pregnancy. *J. Biol. Chem.* **286,** 31839–31851
13. Ulke-Lemée, A., Turner, S. R., Mughal, S. H., Borman, M. A., Winkfein, R. J., and MacDonald, J. A. (2011) Mapping and functional characterization of the murine smoothelin-like 1 promoter. *BMC Mol. Biol.* **12,** 10
14. Akimoto, T., Ribar, T. J., Williams, R. S., and Yan, Z. (2004) Skeletal muscle adaptation in response to voluntary running in Ca^{2+}/calmodulin-dependent protein kinase IV-deficient mice. *Am. J. Physiol. Cell Physiol.* **287,** C1311–C1319
15. Lontay, B., Serfozo, Z., Gergely, P., Ito, M., Hartshorne, D. J., and Erdodi, F. (2004) Localization of myosin phosphatase target subunit 1 in rat brain and in primary cultures of neuronal cells. *J. Comp. Neurol.* **478,** 72–87
16. Borman, M. A., MacDonald, J. A., and Haystead, T. A. (2004) Modulation of smooth muscle contractility by CHASM, a novel member of the smoothelin family of proteins. *FEBS Lett.* **573,** 207–213
17. Schmidt, C., and Urlaub, H. (2009) iTRAQ-labeling of in-gel digested proteins for relative quantification. *Methods Mol. Biol.* **564,** 207–226
18. Shadforth, I. P., Dunkley, T. P., Lilley, K. S., and Bessant, C. (2005) i-Tracker: for quantitative proteomics using iTRAQ. *BMC Genomics* **6,** 145
19. Clarke, C. L., and Sutherland, R. L. (1990) Progestin regulation of cellular proliferation. *Endocr. Rev.* **11,** 266–301
20. Kirwan, J. P., Varastehpour, A., Jing, M., Presley, L., Shao, J., Friedman, J. E., and Catalano, P. M. (2004) Reversal of insulin resistance postpartum is linked to enhanced skeletal muscle insulin signaling. *J. Clin. Endocrinol.*

Downloaded from http://www.jbc.org/ at UNIVERSITY OF DEBRECEN on July 21, 2015

tontay:beata_285_24

Metab. **89,** 4678–4684
21. Coleman, K. M., Dutertre, M., El-Gharbawy, A., Rowan, B. G., Weigel, N. L., and Smith, C. L. (2003) Mechanistic differences in the activation of estrogen receptor-α (ERα)- and ERβ-dependent gene expression by cAMP signaling pathway (s). *J. Biol. Chem.* **278,** 12834–12845
22. Rowan, B. G., Garrison, N., Weigel, N. L., and O'Malley, B. W. (2000) 8-Bromo-cyclic AMP induces phosphorylation of two sites in SRC-1 that facilitate ligand-independent activation of the chicken progesterone receptor and are critical for functional cooperation between SRC-1 and CREB binding protein. *Mol. Cell. Biol.* **20,** 8720–8730
23. Onambele, N. G., Skelton, D. A., Bruce, S. A., and Woledge, R. C. (2001) Follow-up study of the benefits of hormone replacement therapy on isometric muscle strength of adductor pollicis in postmenopausal women. *Clin. Sci.* **100,** 421–422
24. Skelton, D. A., Phillips, S. K., Bruce, S. A., Naylor, C. H., and Woledge, R. C. (1999) Hormone replacement therapy increases isometric muscle strength of adductor pollicis in post-menopausal women. *Clin. Sci.* **96,** 357–364
25. Bradshaw, M. S., Tsai, S. Y., Leng, X. H., Dobson, A. D., Conneely, O. M., O'Malley, B. W., and Tsai, M. J. (1991) Studies on the mechanism of functional cooperativity between progesterone and estrogen receptors. *J. Biol. Chem.* **266,** 16684–16690
26. Catalano, P. M. (2010) Obesity, insulin resistance, and pregnancy outcome. *Reproduction* **140,** 365–371
27. Solomon, C. G., and Seely, E. W. (2001) Brief review: hypertension in pregnancy: a manifestation of the insulin resistance syndrome? *Hypertension* **37,** 232–239
28. Shao, J., Yamashita, H., Qiao, L., Draznin, B., and Friedman, J. E. (2002) Phosphatidylinositol 3-kinase redistribution is associated with skeletal muscle insulin resistance in gestational diabetes mellitus. *Diabetes* **51,** 19–29
29. Bryzgalova, G., Gao, H., Ahren, B., Zierath, J. R., Galuska, D., Steiler, T. L., Dahlman-Wright, K., Nilsson, S., Gustafsson, J. A., Efendic, S., and Khan, A. (2006) Evidence that oestrogen receptor-α plays an important role in the regulation of glucose homeostasis in mice: insulin sensitivity in the liver. *Diabetologia* **49,** 588–597
30. Towler, M. C., and Hardie, D. G. (2007) AMP-activated protein kinase in metabolic control and insulin signaling. *Circ. Res.* **100,** 328–341

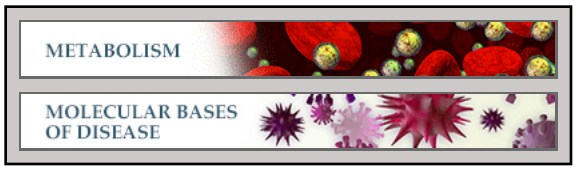
Downloaded from http://www.jbc.org/ at UNIVERSITY OF DEBRECEN on July 21, 2015

lontay.beata_285_24

jbc The Journal of Biological Chemistry
AFFINITY SITES
ASBMB American Society for Biochemistry and Molecular Biology

Metabolism:

Pregnancy and Smoothelin-like Protein 1 (SMTNL1) Deletion Promote the Switching of Skeletal Muscle to a Glycolytic Phenotype in Human and Mice



Beata Lontay, Khaldon Bodoor, Adrienn Sipos, Douglas H. Weitzel, David Loiselle, Rachid Safi, Donghai Zheng, James Devente, Robert C. Hickner, Donald P. McDonnell, Thomas Ribar and Timothy A. Haystead

J. Biol. Chem. 2015, 290:17985-17998.
doi: 10.1074/jbc.M115.658120 originally published online June 5, 2015

Access the most updated version of this article at doi: 10.1074/jbc.M115.658120

Find articles, minireviews, Reflections and Classics on similar topics on the JBC Affinity Sites.

Alerts:
- When this article is cited
- When a correction for this article is posted

Click here to choose from all of JBC's e-mail alerts

Supplemental material:
http://www.jbc.org/content/suppl/2015/06/11/M115.658120.DC1.html

This article cites 30 references, 15 of which can be accessed free at
http://www.jbc.org/content/290/29/17985.full.html#ref-list-1

Downloaded from http://www.jbc.org/ at UNIVERSITY OF DEBRECEN on July 21, 2015

Journal of Neurochemistry lontay.beata_285_24 JNC

JOURNAL OF NEUROCHEMISTRY | 2012 | 123 | 84–99 doi: 10.1111/j.1471-4159.2012.07882.x

ORIGINAL ARTICLE

Protein phosphatase-1M and Rho-kinase affect exocytosis from cortical synaptosomes and influence neurotransmission at a glutamatergic giant synapse of the rat auditory system

Beáta Lontay,* Balázs Pál,† Zoltán Serfőző,‡ Áron Kőszeghy,† Géza Szücs,† Zoltán Rusznák†,§ and Ferenc Erdődi*

*Department of Medical Chemistry and Cell Biology and Signaling Research Group of the Hungarian Academy of Sciences, Medical and Health Science Center, University of Debrecen, Debrecen, Hungary
†Department of Physiology, Medical and Health Science Center, University of Debrecen, Debrecen, Hungary
‡Department of Experimental Zoology, Centre for Ecological Research, Balaton Limnological Institute, Hungarian Academy of Sciences, Tihany, Hungary
§Neuroscience Research Australia, Sydney, Australia

Abstract

Protein phosphatase-1M (PP1M, myosin phosphatase) consists of a PP1 catalytic subunit (PP1c) and the myosin phosphatase target subunit-1 (MYPT1). RhoA-activated kinase (ROK) regulates PP1M via inhibitory phosphorylation of MYPT1. Using multidisciplinary approaches, we have studied the roles of PP1M and ROK in neurotransmission. Electron microscopy demonstrated the presence of MYPT1 and ROK in both pre- and post-synaptic terminals. Tautomycetin (TMC), a PP1-specific inhibitor, decreased the depolarization-induced exocytosis from cortical synaptosomes. *trans*-4-[(1*R*)-1-aminoethyl]-*N*-4-pyridinylcyclohexanecarboxamide dihydrochloride, a ROK-specific inhibitor, had the opposite effect. Mass spectrometry analysis identified several MYPT1-bound synaptosomal proteins, of which interactions of synapsin-I, syntaxin-1, calcineurin-A subunit, and Ca^{2+}/calmodulin-dependent kinase II with MYPT1 were confirmed. In intact synaptosomes, TMC increased, whereas Y27632 decreased the phosphorylation levels of $MYPT1^{Thr696}$, myosin-II light $chain^{Ser19}$, synapsin-I^{Ser9}, and syntaxin-1^{Ser14}, indicating that PP1M and ROK influence their phosphorylation status. Confocal microscopy indicated that MYPT1 and ROK are present in the rat ventral cochlear nucleus both pre- and post-synaptically. Analysis of the neurotransmission in an auditory glutamatergic giant synapse demonstrated that PP1M and ROK affect neurotransmission via both pre- and post-synaptic mechanisms. Our data suggest that both PP1M and ROK influence synaptic transmission, but further studies are needed to give a full account of their mechanism of action.

Keywords: EPSC, giant synapse, myosin phosphatase target subunit (MYPT), protein phosphatase-1, Rho-kinase (ROK), synaptosome.

J. Neurochem. (2012) **123**, 84–99.

Received May 6, 2012; revised manuscript received July 12, 2012, accepted July 18, 2012.

Address correspondence and reprint requests to Dr. Ferenc Erdődi, Department of Medical Chemistry, Medical and Health Science Center, University of Debrecen, H-4032 Debrecen, Nagyerdei krt. 98. Hungary. E-mail: erdodi@med.unideb.hu

Abbreviations used: CaMKII, Ca^{2+}/calmodulin-dependent kinase II; EPSC, excitatory post-synaptic current; GF109203X, Bisindolylmaleinimide I; Gö6976, 5,6,7,13-Tetrahydro-13-methyl-5-oxo-12H-indolo [2,3-a]pyrrolo[3,4-c]carbazole-12-propane-nitrile; GST, glutathion-S-transferase; H1152, (S)-(+)-2-methyl-1-[(4-methyl-5-isoquinolinyl) sulfonyl] homopiperazine 2HCl; ICQ, intensity correlation quotient; IG, immunogold; MC-LR, microcystin-LR; mEPSC, miniature EPSC; MLC20, 20 kDa light chain of myosin-II; $MLC20^{pS19}$, MLC20 phosphorylated at Ser19; MS, mass spectrometry; MYPT1, myosin phosphatase target subunit-1; $MYPT1^{pThr696}$, MYPT1 phosphorylated at Thr696; OA, okadaic acid; P-CPI-17, phosphorylated form of CPI-17; PKA, protein kinase A; PKC, protein kinase C; PP1, protein phosphatase-1; PP1c, PP1 catalytic subunit; PP1M, myosin phosphatase; PP2A, protein phosphatase-2A; PP2Ac, PP2A catalytic subunit; PP2B, protein phosphatase-2B (calcineurin); ROK, RhoA-activated kinase; SNAP-25, 25 kDa synaptosomal-associated protein; SNARE, soluble N-ethylmaleimide-sensitive factor attachment protein receptor; $synapsin^{pSer9}$, synapsin-I phosphorylated at Ser9; $syntaxin^{pSer14}$, syntaxin-1 phosphorylated at Ser14; TMC, tautomycetin; Y27632, *trans*-4-[(1*R*)-1-aminoethyl]-*N*-4-pyridinylcyclohexanecarboxamide dihydrochloride.

© 2012 The Authors

lontay.beata_285_24

The Ca^{2+}-dependent release of neurotransmitters from synaptic vesicles is a crucial event in neurotransmission (Sudhof 2004). Neurotransmitter release occurs after the Ca^{2+}-mediated fusion of synaptic vesicles with the target membrane, involving the formation of a complex between soluble N-ethylmaleimide-sensitive factor attachment protein receptor (SNARE) proteins. This complex includes the 25 kDa synaptosomal-associated protein (SNAP-25), syntaxin-1, and synaptobrevin. The Ca^{2+} sensor synaptotagmin completes the SNARE-induced fusion by promoting fusion pore formation. Following exocytosis, vesicles are recycled and refilled with transmitters to form newly releasable pools.

Ser/Thr-specific phosphorylation of SNAREs and their interacting partners are important tools in these regulatory processes (Turner *et al.* 1999; Snyder *et al.* 2006). For example, phosphorylation of SNAP-25 by protein kinase A (PKA, EC 2.7.11.11) or protein kinase C (PKC, EC 2.7.11.13) (Nagy *et al.* 2002, 2004), and phosphorylation of tomosyn (a syntaxin-1-binding protein) by PKA (Baba *et al.* 2005) facilitated the SNARE complex formation and neurotransmitter release. In contrast, syntaxin-1 phosphorylation by RhoA-activated kinase (ROK, EC 2.7.11.1) had a negative impact (Sakisaka *et al.* 2004) on these events. Synapsins, the major vesicle-binding phosphoproteins, may play crucial roles in synaptic vesicle mobilization and recycling (Chi *et al.* 2001). Distinct protein kinases catalyze the phosphorylation of synapsin-I at multiple sites (Cesca *et al.* 2010), but the physiological significance of this process is not fully understood yet.

Although less is known of the roles of protein phosphatases in neurotransmission, some aspects of their significance have already been described. Protein phosphatase-1 (PP1, EC 3.1.3.53), -2A (PP2A, EC 3.1.3.53), and calcineurin (PP2B, EC 3.1.3.16) appear to be responsible for the dephosphorylation of > 90% of neuronal phosphoproteins (Mansuy and Shenolikar 2006). PP2B initiates synaptic vesicle endocytosis by dephosphorylation of a group of proteins termed dephosphins (Cousin and Robinson 2001). Moreover, PP1 and PP2A catalytic subunits (PP1c and PP2Ac, respectively), as well as PP2B exhibited certain specificities in the dephosphorylation of different phosphorylation sites on synapsin-I (Jovanovic *et al.* 2001). However, the dephosphorylation of synapsin-I and other pre-synaptic phosphoproteins has been largely unexplored with respect to the regulatory (targeting) subunits of the protein phosphatases involved.

Protein phosphatase-1M (PP1M or myosin phosphatase) consists of the 38 kDa PP1cδ (also termed PP1cβ) isoform, a 130/133 kDa myosin phosphatase target subunit-1 (MYPT1), and a 20 kDa subunit of unknown function (Hartshorne *et al.* 2004). Phosphorylation of MYPT1 by ROK at Thr696 and/or Thr853 results in the inhibition of PP1M (Feng *et al.* 1999; Murányi *et al.* 2005). We have shown previously that PP1M is present in cortical synaptosomes where it is associated with ROK (Lontay *et al.* 2004), suggesting that both PP1M and ROK may be involved in the regulation of synaptic transmission. In this work, we used specific inhibitors of ROK and PP1 to study their functions in synaptosome exocytosis and neurotransmitter release, sought novel targets of PP1M in synaptosomes, and identified several MYPT1-interacting neuronal proteins. We conclude that both ROK and PP1M influence neurotransmitter release via interacting with and phosphorylation/dephoshorylation of several pre-synaptic proteins (e.g., myosin-II, synapsin-I, syntaxin-1). Finally, using a thin-slice preparation, we demonstrate that ROK and PP1M act on both pre- and post-synaptic targets when regulating neurotransmission.

Materials and methods

Synaptosome preparation

Synaptosomes were prepared from Wistar rat cerebral cortex as described earlier (Dunkley *et al.* 1986; Lontay *et al.* 2004) and used in the experiments as detailed in Supplementary Information. The protocol for animal handling was authorized by the Animal Care and Protection Committee of the University of Debrecen, and it was in accordance with the guidelines of the European Union Council and with the Hungarian regulations. The rats were bred in the departmental animal house. For the preparation of brain slices, 10–14-day-old Wistar rats of both sexes were used (n = 23).

Electron microscopy

The synaptosomes were isolated, concentrated, and prepared for ultrathin sectioning using an established protocol (Moring *et al.* 1990). The pellets were fixed and immunogold (IG) labeling of the ultrathin sections applying anti-MYPT1 and anti-ROK antibodies was conducted using a previously described protocol (Brorson and Nguyen 2001). Further details of the procedure are given in Supporting information.

High-throughput fluorescent plate assay of exocytosis

Synaptic vesicle exocytosis was assessed by monitoring the release of the fluorescent dye FM 2-10 from synaptosomes using a previously described technique (Baldwin *et al.* 2003) that was modified to adopt it to a high-throughput assay. Synaptosomes loaded with FM 2-10 styryl dye were applied onto 96-well plates (Multifluor-1, Thermo Labsystem, Philadelphia, PA, USA) and samples (in triplicates) were pre-incubated in Krebs buffer — either alone (control) or in the presence of the kinase and phosphatase inhibitors. Each effector was applied for 5 min before inducing depolarization. In control experiments, only the buffers that were used to dissolve the effectors were applied. The experiments were conducted in the presence of 1.2 mM Ca^{2+} or 1.2 mM EGTA, so that the EGTA-treated samples could be used as controls for their parallel (Ca^{2+}-containing) wells. Neurotransmitter release was induced by adding KCl solution with the automatic injector of Fluoroskan FL to achieve a final K^+ concentration of 30 mM. Exocytosis from the synaptosomes was measured as the decrease of fluorescence (excitation: 488 nm; emission: 540 nm) using the kinetic measurement feature of the Ascent Software 2.6. The extent of the Ca^{2+}-dependent exocytosis was calculated as the difference

© 2012 The Authors

lontay.beata_285_24

between the release measured in the presence of Ca^{2+} and EGTA (i.e., without added Ca^{2+}). The relevant data were determined between 0 and 6 min after the stimulation at 30-s intervals and expressed in arbitrary units.

Immunoblotting

Protein determination, sodium dodecyl sulfate–polyacrylamide gel electrophoresis, and immunoblotting were carried out as described before (Lontay *et al.* 2004). Details of other procedures and the antibodies used are given in Supporting information. To assess and compare changes in the extent of phosphorylation, densitometric analysis of the blots was performed (ImageJ, NIH, Bethesda, MD, USA). The density of the phosphorylated proteins was normalized to that of the loading controls.

In vitro phosphorylation/dephosphorylation assays

The endogenous PP1 and PP2A were irreversibly inactivated by pre-incubation with 1 μM microcystin-LR (MC-LR) for 5 min in synaptosome lysates (0.33 mg/mL) containing 20 mM Tris-HCl (pH 7.4), 1 mM (*2S,3S*)-1,4-bis(sulfanyl)butane-2,3-diol, and 5 mM $MgCl_2$. Phosphorylation of synapsin-I^{Ser9} and syntaxin-1^{Ser14} was initiated with the addition of 0.2 mM ATP in the absence (control) or presence of 0.4 mU/mL ROK (Upstate, Lake Placid, NY, USA) and incubated for 15 min. Buffer exchange was performed using Protein Desalting Spin Columns (Pierce, Rockford, IL, USA) to remove MC-LR, ATP, and Mg^{2+}. The ROK-phosphorylated samples were divided into three equal parts and were incubated for 10 min alone, or with adding either 5 nM purified skeletal muscle PP1c (Tóth *et al.* 2000) or 5 nM PP1c plus 25 nM Flag-MYPT1. Flag-MYPT1 was expressed in HEK293 cells and purified on anti-Flag-peptide-coupled Sepharose (Sigma, St. Louis, MO, USA) according to the manufacturer's recommendations. The reactions were stopped by adding hot SDS sample buffer followed by boiling. The samples were analyzed by immunoblotting using anti-synapsin-I^{pSer9} and anti-syntaxin-1^{pSer14} antibodies.

Immunoprecipitation and GST-MYPT pull-down assay

Immunoprecipitations of synaptosome lysate (100 μg protein) were carried out using anti-$MYPT1^{1-296}$, anti-ROK, anti-syntaxin (Sigma), or anti-synapsin (Santa Cruz Biotechnology Inc., Santa Cruz, CA, USA) antibodies covalently coupled to Protein A Sepharose using Seize X Protein A immunoprecipitation kit (Pierce) (Lontay *et al.* 2004). Details of immunoblotting procedures and isolation of glutathion-S-transferase (GST)-MYPT1 bound synaptosomal proteins are described in Supporting information.

Protein identification by mass spectrometry

Desalted and concentrated protein samples (20 μL) obtained from the pull-down experiments were digested with 100 ng trypsin overnight. The reaction was stopped by addition of 10% formic acid and the mixture was injected to an Agilent 1100 nano-HPLC system. The peptides were eluted from a Zorbax 300SB-C18 column (Agilent Technologies, Santa Clara, CA, USA) at 300 nL/min flow rate using a 2-h gradient (0–30% acetonitrile in 0.1% formic acid) and subjected to mass spectrometry (MS) using an ESI-4000 QTRAP mass spectrometer (Applied Biosystems MDS Sciex, Carlsbad, CA, USA). MS/MS spectra were acquired in an information-dependent acquisition mode that automatically selected and fragmented the two most intensive peaks from each MS spectrum. Protein identification was based on the MS/MS spectra using the MASCOT (http://www3.interscience.wiley.com/journal/68500773/abstract?CRETRY=1&SRETRY=0) search engine and the SwissProt/NCBI database. Proteins that were present in three repetitive experiments and gave 99% or higher confidence in the sequence analysis were selected. Those synaptosome proteins were considered as MYPT1-binding partners that were identified from the GST-MYPT1 pull-down fractions, but were not present in the GST ones.

Immunolabeling and confocal microscopy

Detailed description of the preparation and the major steps of the immunolabelling have been presented elsewhere (Pál *et al.* 2005; Rusznák *et al.* 2008) and detailed in Supporting information. Immunolabelling was performed with the combined application of monoclonal synaptophysin (1 : 2000; BioGenex, San Ramon, CA, USA) and either $MYPT1^{1-296}$- (1 : 100) or ROK-specific (1 : 50) antibodies. The immunolabeling was visualized using a confocal microscope (Zeiss LSM 510; Oberkochen, Germany) equipped with a 40× oil immersion objective. The optical thickness was 1 μm. For the colocalization analysis, the 'Co-localization highlighter' and 'Intensity Correlation Analysis' plug-ins of ImageJ were used.

Recording and analysis of excitatory post-synaptic currents

All electrophysiological experiments were performed in artificial cerebrospinal fluid (for its composition and other details, see Supporting information). The experiments were conducted on 200-μm-thick brain slices. Neurons were viewed using an Axioskop microscope (Zeiss) equipped with differential interference contrast optics and a 63× water immersion objective. Slices were incubated with tautomycetin (TMC; 5 μM), *trans*-4-[(1*R*)-1-aminoethyl]-*N*-4-pyridinylcyclohexanecarboxamide dihydrochloride (10 μM), or both drugs for 1 h. The recordings were performed within the following 2 h. All experiments were conducted at a holding potential of −60 mV. Excitatory post-synaptic currents (EPSCs) were evoked using a monopolar stimulating electrode that was connected to a BioStim STC-7a stimulator (Supertech, Pécs, Hungary). During stimulation, the pulses were delivered with a frequency of 50 Hz. 'Minimal stimulation' was employed in all experiments. In some cases, miniature EPSCs (mEPSCs) were recorded in the presence of 1 μM tetrodotoxin.

Statistical analysis

Normalized data were analyzed by *t*-tests (for two groups) or by analysis of variance (ANOVA, for > two groups). Parametric statistical tests were used if the assumptions of such tests were met. Normality of the data was tested by Kolmogorov–Smirnov tests. All normalized variables used in statistical analyses were found to be normally distributed. Tests were conducted using SPSS (IBM, Armonk, NY, USA) for Windows. All data represent mean ± SEM.

Results

Electron microscopic localization of MYPT1 and ROK in synaptosomes

Synaptosome fractions were satisfactorily pure and dense for performing immunolabeling (Fig. 1). In most cases, synaptosomes were situated in close proximity of each other (Fig. 1a, b and d) or, less frequently, at specialized appositions. In the

© 2012 The Authors

lontay.beata_285_24

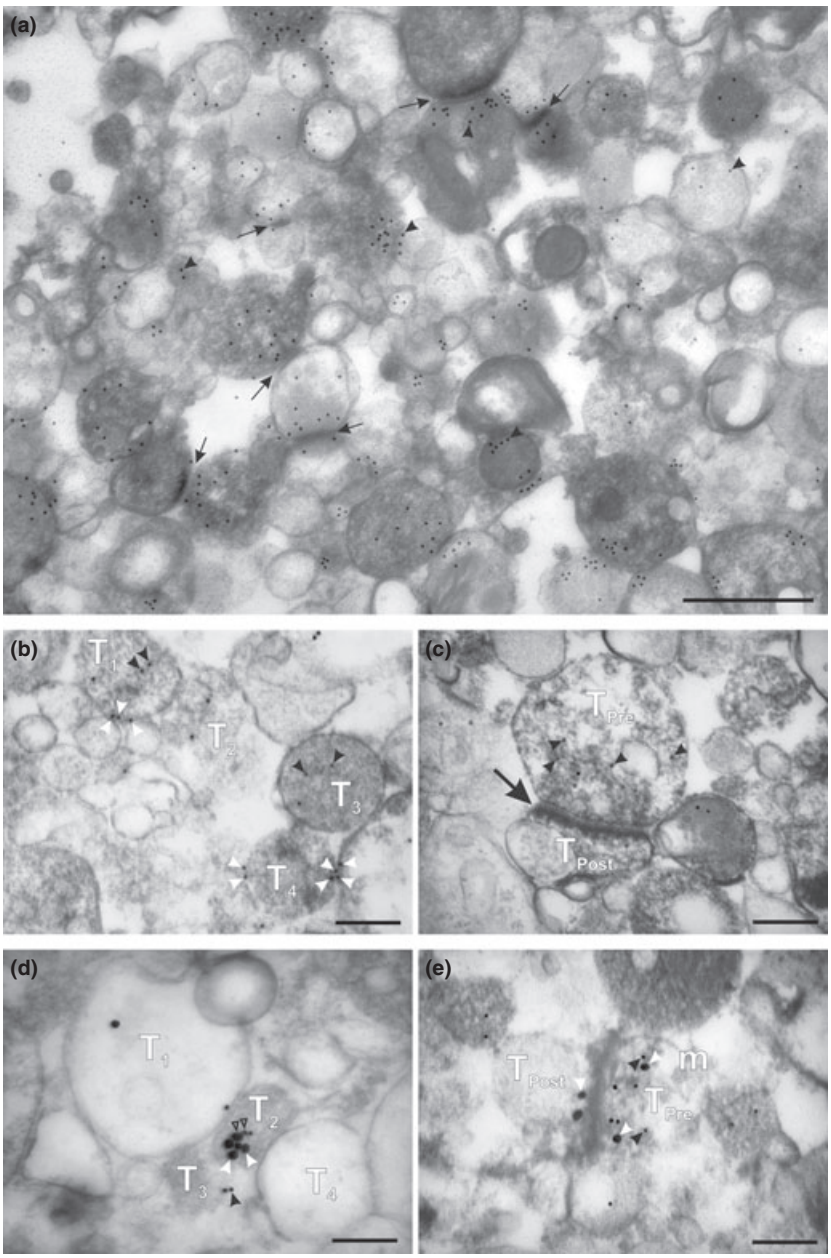


Fig. 1 Electron microscopy of myosin phosphatase target subunit-1 (MYPT1)- and ROK-IG labeling in cortical synaptosome preparations. (a) Low-magnification micrograph of the distribution of MYPT-IG particles (diameter: 15 nm). Note the accumulation of the particles nearby the synaptic contacts (arrows). (b) MYPT-IG particles in synaptosomes (T_1–T_4) connected to electron-dense material in synaptosome plasma (black arrowheads) and localizing close to or at synaptosome membranes (white arrowheads). (c) MYPT-IG particles (arrowheads) are seen in the pre-synaptic terminal (T_{pre}) only. Arrow: post-synaptic density; T_{post}: post-synaptic terminal. (d) A group of mixed MYPT-IG (diameter: 15 nm, black arrowhead) and ROK-IG (diameter: 25 nm, white arrowheads) particles in a synaptosome (T_2), which is situated close to but forming no specialized apposition with other labeled (T_1, T_3) and unlabeled (T_4) synaptosomes. Open arrowheads indicate a pair of different-sized IG particles that are in neighboring (coupled) position. (e) MYPT- (black arrowheads) and ROK-IG (white arrowheads) particles in a pair of synaptosomes associated with an asymmetric contact. MYPT-IG particles are seen at the pre-synaptic site (T_{pre}), whereas ROK-IG particles are situated at both sites of the synapse. m: mitochondrion; T_{post}: post-synaptic terminal. (a)–(c): single-labeled preparations for MYPT1, (d)–(e): double-labeled (MYPT1 and ROK) preparations. (a–c), (e), preparations were contrasted with uranyl acetate and lead citrate. Calibration: 500 nm (a), 200 nm (b–e).

latter case, synaptosomes were in contact with typical—symmetric or asymmetric—synaptic appositions (Fig. 1a, c and e). Anti-MYPT1$^{1-38}$ and anti-MYPT1$^{1-296}$ antibodies were equally effective for immunolabeling. The quality of the immunolabeling was enhanced when the glutaraldehyde content of the fixative was reduced to 0.1% and an appropriate antigen-retrieval technique (Brorson and Nguyen 2001) was employed. MYPT1-immunogold (MYPT1-IG) particles appeared as highly electron-dense spheres connected to electron-dense material within the synaptosomes or in their membranes (Fig. 1b). Similar to the MYPT1-IG particles, ROK-IG particles appeared as electron-dense dots in the synaptosomes (Fig. 1d and e). In single-labeled preparations, 27% of the synaptosomes (n = 304) were associated with other synaptosomes at specialized synaptic appositions. MYPT1-IG particles were localized to pre-synaptic terminals in 62% and to both sites (i.e., to pre- and post-synaptic terminals) in 2–3% of these 'associated' synaptosomes. In double-labeled preparations (n = 125), ROK-IG particles were found at pre-synaptic and at both terminals in 37% and 44% of the associated synaptosome pairs, respectively. In colabeled synaptosomes, MYPT1-IG and ROK-IG particles were detected together in 38% of the labeled synaptosomes. They were also found separately (Fig. 1d and e) or at neighboring positions (Fig. 1d). In most synaptosomes containing both MYPT1-IG and ROK-IG particles, the number of MYPT1-IG particles

© 2012 The Authors

lontay.beata_285_24

exceeded that of the ROK-IG ones, with a typical MYPT1-IG/ROK-IG ratio of 4 : 2. Possible coupling of MYPT1 and ROK was assessed on the basis of the number of MYPT1- and ROK-IG particles being closer to each other than 10 nm. This way, the MYPT1-/ROK-IG particles were coupled in 13% of the double-labeled synaptosomes (n = 125).

Effects of PP1 and ROK inhibitors on synaptosomal exocytosis

To determine the role of PP1M and ROK in the exocytosis from synaptosomes and in neurotransmitter release, TMC and Y27632 were applied as specific inhibitors of PP1 and ROK, respectively. Y27632 has been shown to be a selective ROK inhibitor when tested against a plethora of kinases (Davies *et al.* 2000), whereas TMC and okadaic acid (OA) selectively inhibited PP1 and PP2A, respectively, in COS-7 cells (Mitsuhashi *et al.* 2003). In our experiments, TMC (5 μM) and OA (50 or 100 nM) selectively inhibited synaptosomal PP1 and PP2A (Figure S1a, Supporting information). PP1 activity was ~63% of the total phosphatase activity. Phosphatase activity was also determined in the presence of a PP1M-specific inhibitor—thiophosphorylated C-kinase-activated phosphatase inhibitor protein of 17 kDa (P-CPI-17; (Erdődi *et al.* 2003), Eto *et al.* 2004). These experiments suggested that ~50% of the total phosphatase activity is attributable to PP1M, implying that PP1M has predominance over both other PP1 holoenzymes and PP2A in synaptosomes. The relative amounts of PP1 and PP2A in the synaptosomal lysate corresponded to an estimated concentration of PP1 and PP2A of 3.2 and 1.6 μM, respectively, in intact synaptosomes (Figure S1b). These amounts were also in accordance with the MC-LR-induced, dose-dependent inactivation pattern of phosphatases observed in synaptosomal lysates (Figure S1c).

To assess synaptosome exocytosis, a high-throughput assay was employed. The synaptosomes were loaded with FM 2-10 and the reduction of the fluorescence intensity was recorded, which was the result of the exocytosis of the dye. Application of TMC (i.e., inhibition of PP1) markedly suppressed, whereas the ROK inhibitor Y27632 profoundly increased synaptosome exocytosis (Fig. 2a). When applied simultaneously, Y27632 prevented the inhibitory effects of TMC, but this was accompanied with a substantial decrease of its own stimulatory effect (Fig. 2a). The time course of the kinetic curves characterizing the decrease of FM 2-10 fluorescence (i.e., the increase of the rate of the synaptosome exocytosis) had a rapidly declining part and a slower phase leading to a plateau, but this biphasic character was obvious in slow exocytotic processes only. The effects of other phosphatase and kinase inhibitors on synaptosomal exocytosis were also assessed by examining the relative decrease of fluorescence recorded at 30 s into the stimulation (Fig. 2b, lower part). Tautomycin (TM; 0.5–1 μM), which relates structurally to TMC and is also considered as a PP1-specific

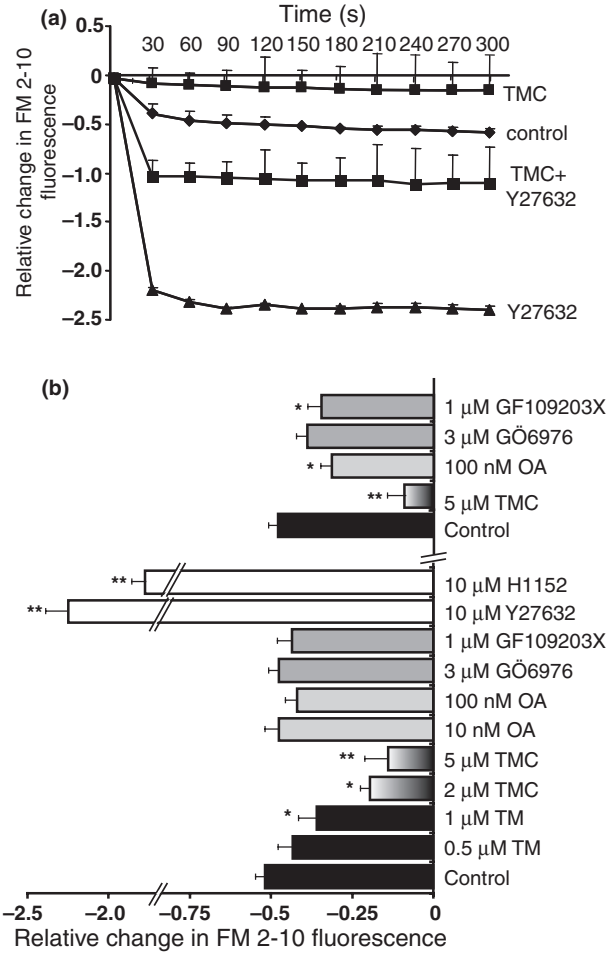


Fig. 2 Effect of PP1 and ROK inhibitors on KCl-induced, Ca^{2+}-dependent exocytosis from cortical synaptosomes. (a) Effects of 10 μM Y27632 and 5 μM tautomycetin (TMC) alone or their combined application on the Ca^{2+}-dependent exocytosis from cortical synaptosomes measured as the relative change in FM 2-10 fluorescence. (b) Effects of the indicated effectors on the KCl-induced, Ca^{2+}-dependent exocytosis from cortical synaptosomes. The rate of exocytosis was expressed as the relative change in FM 2-10 fluorescence measured at 30 s (lower part) and 180 s (upper part) after initiating the depolarization. n = 3–5. $^{**}p < 0.01$, $^{*}p < 0.05$.

inhibitor *in vivo* (Favre *et al.* 1997), inhibited exocytosis in a concentration-dependent manner, although its inhibitory effect was less pronounced than that of the TMC. OA did not have a significant influence on this rapid phase of exocytosis at the concentrations tested (10–100 nM). However, 100 nM OA exerted a moderate (~28%)—but statistically significant—inhibitory effect at 180 s (Fig. 2b, upper part). Y27632 (10 μM) was slightly more effective than (S)-(+)-2-methyl-1-[(4-methyl-5-isoquinolinyl)sulfonyl]homopiperazine 2HCl (10 μM H1152; another ROK inhibitor) in stimulating the exocytosis from synaptosomes (Fig. 2b). As it has been reported that Y27632 might inhibit

© 2012 The Authors

lontay.beata_285_24

smooth muscle PKCδ *in vitro* (Eto *et al.* 2001), two established PKC inhibitors, GF109303 (Bisindolylmaleinimide I) and Gö6976 (5,6,7,13-Tetrahydro-13-methyl-5-oxo-12H-indolo[2,3-a]pyrrolo[3,4-c]carbazole-12-propane-nitrile) were also tested to assess the significance of PKC inhibition in synaptosomal exocytosis. Neither inhibitor stimulated the exocytosis or exerted appreciable effect on the rapid phase, while a ~27% suppression of exocytosis was observed at 180 s when 1 μM Bisindolylmaleinimide I was applied (Fig. 2b, upper part).

Identification of MYPT1-binding proteins and potential substrates of PP1M and ROK in synaptosomes

We carried out pull-down assays with GST-MYPT1 and GST (as control) to separate potential MYPT1-interacting proteins from synaptosome lysate. The potential interacting proteins were subjected to mass spectrometry analysis for identification. Table 1 lists the MYPT1-interacting proteins identified by the peptide sequences obtained from the mass spectrometry analysis. These proteins included neuron-specific (synapsin-I, syntaxin, syntaxin-binding protein, synaptotagmin-1, and -2, SNAP25, or brain-specific polypeptide PEP19) or ubiquitously expressed proteins (sodium/potassium-transporting ATPase 1-3, ATP synthase, and the guanine nucleotide-binding protein G_0) as well as enzymes with important roles in neuronal signal transduction pathways and in neurotransmitter release [Ca^{2+}/calmodulin-dependent kinase II (CaMKII) and PP2B)]. Known MYPT1-interacting proteins, such as isoforms of the 14-3-3 protein (Koga and Ikebe 2008) and the microtubule-associated protein tau (Amano *et al.* 2003), also showed up in the bound fraction. Many of these neuronal MYPT1-binding proteins are thought to function as mediators of neurotransmitter release and synaptic vesicle trafficking (e.g., synapsin-I, syntaxin-1, and SNAP-25) and are regulated by phosphorylation/dephosphorylation. We conducted reciprocal immunoprecipitation experiments with antibodies specific for synapsin-I, syntaxin-1 as well as MYPT1 and ROK. MYPT1 reciprocally coprecipitated with ROK and synapsin-I (Fig. 3a). MYPT1 and syntaxin-1 coprecipitated when anti-MYPT1 was used for immunoprecipitation, but not when anti-syntaxin was the precipitating antibody. ROK reciprocally coprecipitated with all of these proteins. The binding of CaMKII (presumably the α isoform) and PP2B to MYPT1 was confirmed by positive identification of these proteins on western blots in the GST-MYPT1 pull-down fractions (Fig. 3b). These results confirmed some of the major interactions identified by mass spectrometry analyses of the GST-MYPT1 pull-down fractions.

The presence of PP1M and ROK in synaptosomes and their interactions with synaptosomal proteins suggest that common substrates of these two enzymes may exist among the neuronal proteins. To confirm this, PP1-specific dephosphorylation was selectively inhibited (by TMC) followed by an assessment of the phosphorylation patterns of proteins present in synaptosome lysate (Fig. 3c). PP1 inhibition led to a substantial increase of the phosphorylation of many proteins—catalyzed by endogenous kinases present in the synaptosome lysate—as judged by autoradiography of the gels containing separated proteins. Four bands at ~75 kDa, ~45–50 kDa, ~37 kDa, and ~25 kDa (bands 1–4, respectively) were selected for further analysis, as their apparent molecular masses were very similar to those of certain neuronal MYPT1-interacting proteins that were identified by mass spectrometry (e.g., synapsin-I, synaptotagmin, syntaxin-1, and SNAP-25). When proteins excised from these bands were subjected to mass spectrometry analysis, specific phosphopeptides were not unambiguously detected, but bands 1, 3, and 4 included the MYPT1-interacting synapsin-I, syntaxin-1, and SNAP-25, respectively (data not shown). Selective inhibition of PP1M (by P-CPI-17) increased the phosphorylation level of the proteins in all bands (Fig. 3d), suggesting that PP1M was involved in their dephosphorylation. The basal phosphorylation in synaptosome lysate was profoundly suppressed by Y27632, indicating that ROK is one of the major endogenous kinases that phosphorylate the proteins in bands 1–4.

ROK and PP1M mediate the phosphorylation levels of MLC20^{Ser19}, synapsin-I^{Ser9}, and syntaxin-1^{Ser14} in cortical synaptosomes

We assessed how TMC and Y27632 influence the phosphorylation status of MYPT1^{Thr696} and the 20 kDa light chain of myosin-II (MLC20) at Ser19 in intact synaptosomes during KCl depolarization (Fig. 4a and b). The depolarization slightly decreased both phosphorylation levels compared with control (data not shown). In depolarized synaptosomes, phosphorylation of MYPT1^{Thr696} (yielding MYPT1^{pThr696}) was moderately increased by TMC and profoundly decreased by Y27632 (Fig. 4a). Similarly, direct inhibition of PP1c (by TMC) resulted in a significant increase in the amount of phosphorylated MLC20^{Ser19} (MLC20^{pSer19}). ROK inhibition (by Y27632) almost completely diminished the amount of MLC20^{pSer19} when TMC was absent (Fig. 4b), implying that ROK is responsible for the phosphorylation of MLC20^{Ser19}. The relative decrease of the amounts of both MYPT1^{pThr696} and MLC20^{pSer19} upon combined application of Y27632 and TMC was substantially less than that induced by Y27632 alone. This observation suggests that inhibition of PP1 (by TMC) permits the activity of other kinase(s), distinct from ROK, which could also participate in MYPT1^{Thr696} and MLC20^{Ser19} phosphorylation. These unidentified kinase(s) may correspond to the integrin-linked kinase or zipper-interacting protein kinase, especially as these kinases have been shown to phosphorylate both MYPT1^{Thr696} and MLC20^{Ser19} (Hartshorne *et al.* 2004). Proving their actual roles in synaptosomes, however, is yet to be achieved.

As ROK was previously reported to phosphorylate syntaxin-1^{Ser14} (Sakisaka *et al.* 2004), changes in the

© 2012 The Authors

lontay.beata_285_24

Table 1 GST-MYPT-binding proteins of rat cortical synaptosomes

Accession number	Protein	MW	Peptides[a]	Function
O14974 (MYPT1_HUM)	Protein phosphatase 1 regulatory subunit 12A (MYPT1)	115669	669 SYLTPVRDEESEQR 683 162 QGVDIEAAR 170 494 LAYVAPTIPR 503 934 LYEQILAENEK 947 443 TGSYGALAEITASK 456 17 WIGSETDLEPPVVK 30 696 STQGVTLTDLQEAEK 710 950 AQLHDTNMELTDLK 963 695 RSTQGVTLTDLQEAEK 710 264VGQTAFDVADEDILGYLEELQK285	signal transduction
P09951 (SYN1_RAT)	Synapsin-1 (Synapsin I)	74114	564 QASISGPAPPK 574 257 EMLSSTTYPVVVK 269 586 QGPPQKPPGPAGPIR 600 429 GSHSQTPSPGALPLGR 444	reserve pool regulation
P61765 (STXB1_RAT	Syntaxin-binding protein 1 (Unc-18 homolog) (Unc-18A) (Unc-18-1)	67925	468 ISEQTYQLSR 477 506 SSASFSTTAVSAR 518 30 VLVVDQLSMR 39	docking/priming
P06686 (AT1A2_RAT)	Sodium/ potassium-transporting ATPase alpha-2 chain precursor (Sodium pump 2)	113457	44 LSLDELGR 51 470 DRNPKVAEIPFNSTNK 485 176 MQINAEEVVVGDLVEVK 192 DRNPKVAEIPFNSTNK 645 LNIPVSQVNPR 655 542VAEIPFNSTNK553	sodium/potassium pump
P06687 (AT1A3_RAT)	Sodium/ potassium-transporting ATPase alpha-3 chain (Sodium pump 3)	113032	467 VAEIPFNSTNK 477 436 DVAGDASESALLK 448 603 VIMVTGDHPITAK 615 734 QAADMILLDDNFASIVTVGEEVR 756 203 VDNSSLTGESEPQTR 217 638 LNIPVSQVNPR 648 153 NMVPQQALVIR 163 620 GVGIISEGNETVEDIAAR 637 168 MQINAEEVVVGDLVEVK 184	sodium/potassium pump
P63329 (PP2BA_RAT)	Serine/threonine protein phosphatase 2B catalytic subunit, alpha isoform	59291	101 LFEVGGSPANTR 112 391 ARKEVIRNKIRAI 403	signal transduction
P62260 (1433E_RAT)	14-3-3 protein epsilon (Mitochondrial import stimulation factor L subunit)	29274	197 AAFDDAIAELDTLSEESYK 215 20 YDEMVESM 28 131 YLAEFATGNDR 141 62 IISSIEQK 69 5 EDLVYQAK 12 87 QMVETELK 94 107 HLIPAANTGESK 118 245 EALQDVEDENQ 255 43 NLSSVAYKNVIGAR 56 216 DSTEIIMQLLR 225	docking/priming
P63102 (1433Z_RAT)	14-3-3 protein zeta/delta (Protein kinase C inhibitor protein-1)	27955	42 NLLSVAYK 49 1 MDKNELVQK 9 28 SVTEQGAELSNEER 41 213 DSTLIMQLLR 222 140 GIVDQSQQAYQEAFEISK 157 194 TAFDEAIAELDTLSEESYK 212 128 YLAEVAAGDDK 138 159 EMQPTHPIR 167 140 GIVDQSQQAYQEAFEISK 157	docking/priming

© 2012 The Authors

lontay.beata_285_24

Table 1 (Continued)

Accession number	Protein	MW	Peptides[a]	Function
P19332 (TAU_RAT)	Microtubule-associated protein tau	39233	145 TPSLPTPPTR 154 329 SPVVSGDTSPR 339 319 TDHGAEIVYK 328 176 LQTAPVPMPDLK 187 287 IGSLDNITHVPGGGNK 302	cytoskeleton
P61265 (STX1B_RAT)	Syntaxin-1B	33452	72 QELEDLTADIK 82 158 TTTNEELEDMLESGK 172 232 IEYNVEHSVDYVER 245	docking/priming
P60881 (SNP25_RAT)	Synaptosomal-associated protein 25 (SNAP-25)	20800	51 IEEGMDQINK 60 23 MLQLVEESK 31 116 EQMAISGGFIR 126 37 TLVMLDEQGEQLER 50 153 HMALDMGNEIDTQNR 167 9 ADQLADESLESTR 21 134 ENEMDENLEQVSGIIGNLR 152 22 RMLQLVEESK 31 8 RADQLADESLESTRR 22	exocytosis
P63055 (PCP4_RAT)	Neuron-specific polypeptide PEP-19	10893	74 AAVAIQFR 83	signal transduction
P38406 (GNAL_RAT)	Guanine nucleotide-binding protein G(o) subunit	44734	45 LLLLGAGESGK 55	signal transduction
P21707 (SYT1_RAT)	Synaptotagmin-1 (Synaptotagmin I) (SytI) (p65)	47711	302 MDVGGLSDPYVK 313	exocytosis
P62161 (CALM_RAT)	Calmodulin (CaM)	16515	91VFDKDGNGYISAAELR 106 1 ADQLTEEQIAEFK 13 14 EAFSLFDKDGDGTITTK 30 107 HVMTNLGEKLTDEEVDEMIR 126 127 EADIDGDGQVNYEEFVQMMTAK 148 95 DGNGYISAAELR 106 76 MKDTDSEEEIR 86	signal transduction
P10719 (ATPB_RAT)	ATP synthase beta chain	51171	110 TIAMDGTEGLVR 121 144 IMNVIGEPIDER 155 407 IMDPNIVGSEHYDVAR 422 189 VVDLLAPYAK 198 144 IMNVIGEPIDER 155 282 VALTGLTVAEYFR 294 213 TVLIMELINNVAK 225 125 VLDSGAPIKIPVGPETLGR 143	proton pump
P05065 (ALDOA_RAT)	Fructose-bisphosphate aldolase A	39783	112 GVVPLAGTNGETTTQGLDGLSER 134 29 GILAADSTGSIAK 42 244 FSNEEIAMATVTALR 258	glycolysis
P11275 (KCC2A_RAT)	CaM kinase II subunit alpha	54651	75 VTEQLIEAISNGDFESYTK 93 302 AILTTMLATR 311	signal transduction

[a]The MASCOT peptide scores ranged from 31 to 253 for the interacting proteins identified.

phosphorylation status of candidate pre-synaptic substrates of PP1M and ROK (e.g., synapsin-I and syntaxin-1) were also determined (Fig. 4c and d) during KCl-evoked depolarization of synaptosomes. A search for consensus ROK site(s) in synapsin (using the Kinexus PhosphoNET database—www.phosphonet.ca) indicated Ser9 as a possible phosphorylation site for this kinase with a relatively high score. Depolarization resulted in 2- and 1.5-fold increase in the levels of phosphorylated synapsin-I^{Ser9} (synapsin-I^{pSer9}) and syntaxin-1^{Ser14} (syntaxin-1^{pSer14}), respectively (data not shown). This elevated synapsin-I^{pSer9} level was further increased upon treatment with TMC (~two-fold; Fig. 4c), whereas ROK inhibition markedly decreased the amount of synapsin-I^{pSer9}. The pattern of changes of the amounts of

© 2012 The Authors

lontay.beata_285_24

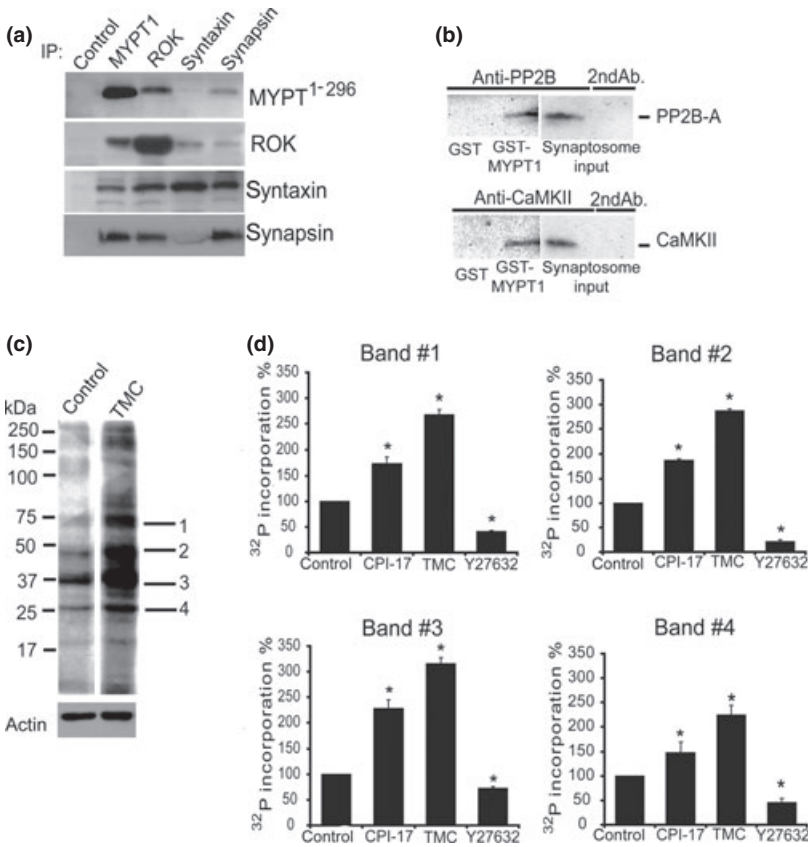


Fig. 3 Identification of myosin phosphatase target subunit-1 (MYPT1)- and ROK-interacting proteins and potential PP1M and ROK substrates in synaptosomes. (a) Immunoprecipitation (IP) of MYPT1, ROK, syntaxin, and synapsin from synaptosome lysates. Immunoprecipitations were carried out and the immunoprecipitates were analyzed with the antibodies indicated or with non-immune rabbit serum (as control) using protein A Sepharose. (b) Western blots of whole synaptosome lysate (input) as control and GST- or GST-MYPT1 pull-down fractions from the lysate were developed with anti-CaMKII or anti-PP2B-A antibodies. The secondary antibody was used as control for non-specific signals (2ndAb). (c) Synaptosome lysate containing 5 mM Mg^{2+} was pre-incubated in the absence or in the presence of 5 μM tautomycetin (TMC) prior to initiation of the phosphorylation reaction with 0.2 mM [γ-^{32}P]ATP. The proteins were separated by sodium dodecyl sulfate-polyacrylamide gel electrophoresis and the gel was subjected to autoradiography. Alternatively, samples were subjected to western blot by anti-actin antibody to verify similarity in protein loading. (d) The effect of P-CPI-17, TMC, and Y27632 on the *in vitro* phosphorylation of synaptosomal proteins in synaptosome lysate. Phosphorylation reactions were carried out as described above in the absence and in the presence of 5 μM TMC, 2 μM P-CPI-17, or 10 μM Y27632 and the changes in the extent of phosphorylation were assessed by scintillation counting of the excised gel pieces of bands 1–4 indicated in (c). Alternatively, proteins were eluted from the excised gel pieces and subjected to mass spectrometry analysis (data not shown). $n = 3$, $^*p < 0.05$.

syntaxin-1^{pSer14} and synapsin-I^{pSer9} was similar upon the different treatments (Fig. 5d). ROK inhibition decreased both the basal and TMC-induced synapsin-I^{pSer9} and syntaxin-1^{pSer14} amounts to similarly low levels, indicating the predominant involvement of ROK in these phosphorylation processes.

The identity of the phosphatase holoenzyme that may act on synapsin-I^{pSer9} and syntaxin-1^{pSer14} is not known. To assess the possible roles of PP1c and PP1M, we generated phosphosubstrates by phosphorylating synapsin-I^{Ser9} (Fig. 4e) and syntaxin-1^{Ser14} (Fig. 4f) in synaptosome lysates. In these experiments, the endogenous PP1 and PP2A were irreversibly inactivated by covalently coupling PP1c and PP2Ac with MC-LR (Fig. 4e–f, controls). Addition of exogenous ROK to these lysates resulted in a 3–3.5-fold increase of the extent of synapsin-I^{Ser9} and syntaxin-1^{Ser14} phosphorylation when compared with control (i.e., without ROK), providing further evidence that these sites are phosphorylated by ROK. Following buffer exchange to remove MC-LR, ATP, and Mg^{2+}, purified PP1c was added to the ROK-phosphorylated samples with or without purified Flag-MYPT1. When PP1c was added alone, it dephosphorylated both synapsin-I^{pSer9} and syntaxin-1^{pSer14}. The extent of dephosphorylation of both phosphoproteins increased when PP1c and Flag-MYPT1 were added together (i.e., PP1M holoenzyme was formed), suggesting that MYPT1 had a PP1c-targeting role under these conditions.

© 2012 The Authors

lontay.beata_285_24

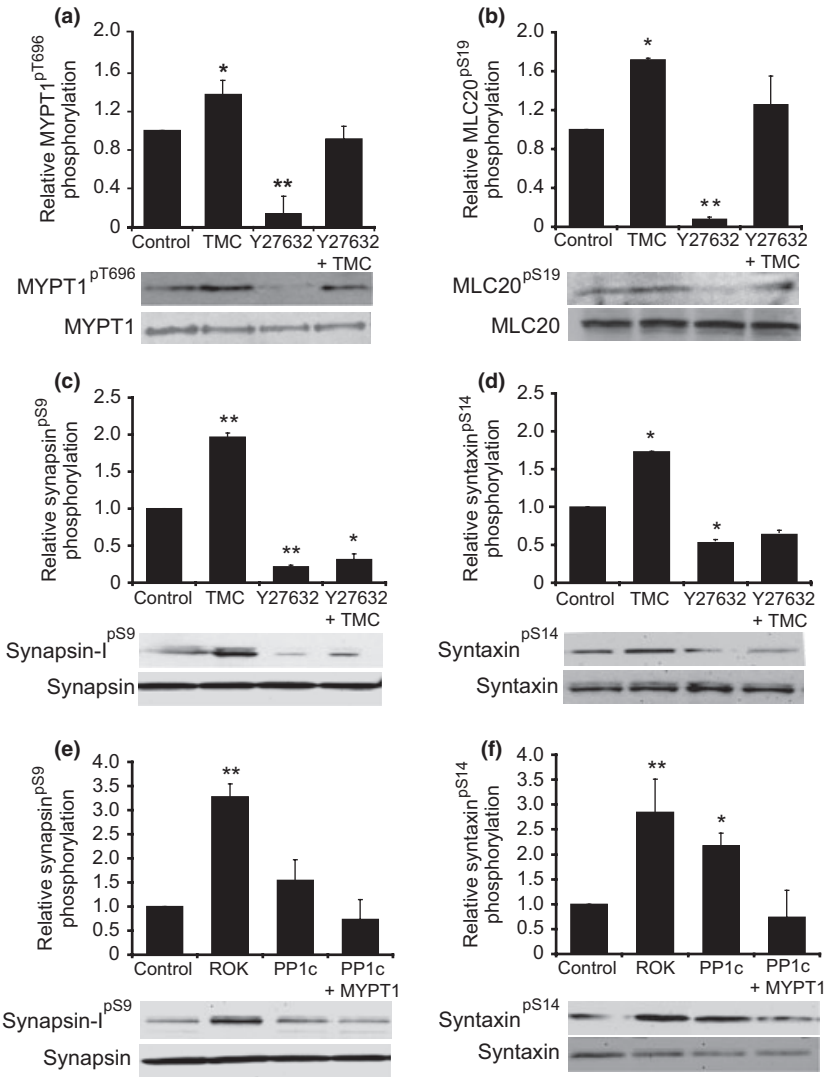


Fig. 4. The effects of PP1 and ROK inhibitors on MYPT^{Thr696}, 20 kDa myosin light chain^{Ser19} (MLC20^{Ser19}), synapsin^{Ser9}, and syntaxin^{Ser14} phosphorylation. (a)–(d): Effect of 5 μM tautomycetin (TMC), 10 μM Y27632, or their combination on the phosphorylation levels of MYPT1^{Thr696} (a), MLC20^{Ser19} (b), synapsin^{Ser9} (c), and syntaxin^{Ser14} (d) in intact synaptosomes as judged by western blots using phosphorylation site-specific antibodies. Representative western blots with anti-MYPT1^{pThr696} (a), MLC20^{pSer19} (b), anti-synapsin^{pSer9} (c), and anti-syntaxin^{pSer14} (d) antibodies are shown. Anti-MYPT1 (a), anti-MLC20 (b), anti-synapsin (c), and anti-syntaxin (d) were used for loading controls. Relative changes in the phosphorylation were determined by densitometric analysis of the blots. (e)–(f): Phosphorylation of synapsin-I^{Ser9} and syntaxin-1^{Ser14} in synaptosome lysate by exogenous ROK, and dephosphorylation of the ROK-phosphorylated synapsin-I^{pSer9} and syntaxin-1^{pSer14} by PP1c or by PP1c plus Flag-MYPT was carried out as described in Materials and methods. Data represent mean ± SEM obtained from $n = 5–9$ independent experiments, $^{*}p < 0.05$; $^{**}p < 0.01$.

Localization and function of MYPT1 and ROK in the ventral cochlear nucleus

Brain slices accommodating the glutamatergic 'giant synapse' formed between the acoustic nerve (endbulbs of Held) and the cell bodies of the bushy cells were also examined. The expression and localization of PP1M (by identifying MYPT1) and ROK were studied using confocal microscopy. The possible pre- or post-synaptic localization of either protein was assessed by simultaneous synaptophysin-specific immunolabeling. As demonstrated in Fig. 5, MYPT1-specific immunoreaction was present within the cell bodies of the bushy neurons (Fig. 5a1), indicating its post-synaptic expression. Colocalization with the synaptophysin-specific labeling (Fig. 5a2) was also noted (Fig. 5a3 and a4). To assess the degree of colocalization, parameters allowing objective characterization of the extent of colocalization were determined. In the presented case, the Pearson's coefficient was 0.121, the overlap coefficient was 0.443, while the intensity correlation quotient (ICQ) was 0.121. Similar results were obtained in four more images (taken from different locations), indicating a relatively high degree of overlap between the synaptophysin- and MYPT1-specific immunolabelings. Based on its morphology and size (~5 μm in diameter), the circular structure marked with an asterisk in Fig. 5a1–a4 was identified as the cross-section of a capillary (Sposito and Gross 1987). As the endothelium expresses MYPT1 (e.g., Hirano *et al.* 1999; Birukova *et al.* 2004), its strong immunopositivity was regarded as an internal positive control.

The ROK-specific immunoreactivity (Fig. 5b1) was not prominent within the cell bodies of the bushy neurons, although immunopositive puncta corresponding to intracellular ROK could be identified (arrows in Fig. 5b1). Rather, the ROK-specific immunolabeling mainly appeared as a ring-like pattern around the cell bodies and demonstrated partial colocalization with synaptophysin (Fig. 5b3 and b4). In the

© 2012 The Authors

lontay.beata_285_24

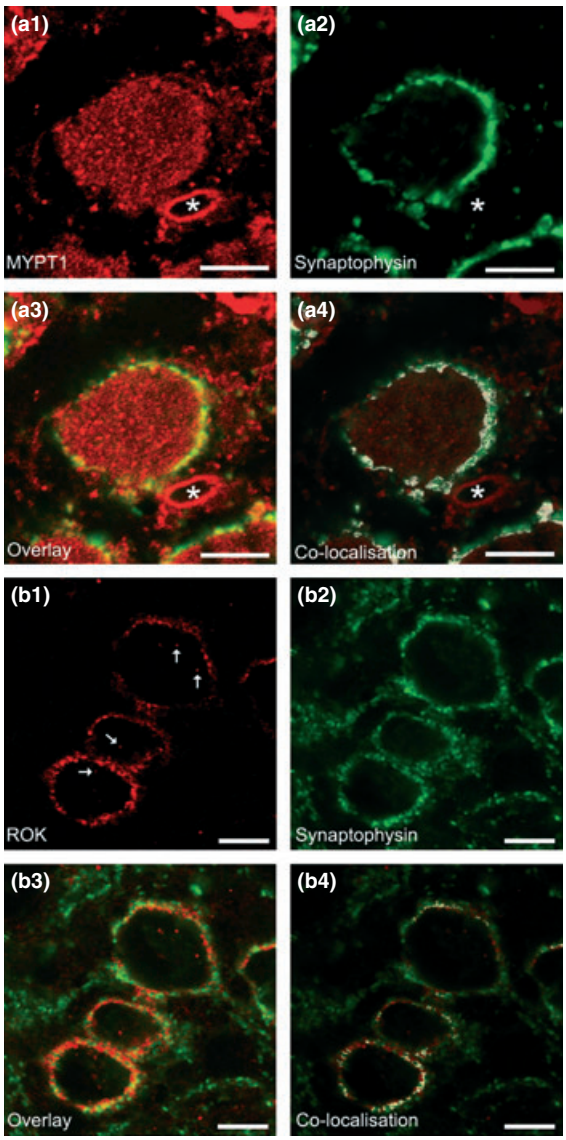


Fig. 5 Confocal investigation of the presence and distribution of myosin phosphatase target subunit-1 (MYPT1)- and ROK-specific immunoreactions in the acoustic nerve terminal-bushy cell synapse. (a1) MYPT1$^{1-296}$-specific immunolabelling of a bushy cell. *: cross-section of a capillary. Note the strong MYPT1-specific labeling of the endothelium. (a2) Synaptophysin-specific immunolabeling of the same area. (a3) Overlay of (a1) and (a2). To enhance visibility of the colocalized pixels, the intensities of the red and green channels were optimized. (a4) Distribution of the colocalized MYPT1- and synaptophysin-specific labeling. Pixels showing colocalization were sought using the 'Co-localization highlighter' plug-in of the ImageJ software. To ensure better visibility, the intensity of the original overlay image was reduced. Bright pixels indicate colocalization. (b1) ROK-specific immunolabeling of three bushy cells. Arrows indicate some examples of immunopositive puncta with clearly intracellular localization. (b2) Synaptophysin-specific immunolabeling of the same area. (b3) Overlay of (b1) and (b2) using the same images, but with optimized red and green intensities. (b4) Distribution of the colocalized pixels. Scale bars represent 10 μm.

presented case, the Pearsons' coefficient, overlap coefficient, and ICQ were 0.264, 0.461, and 0.236, respectively. Similar values were yielded in all other cases (n = 4), indicating partial but definite colocalization.

Functional experiments were also conducted, in which minimal stimulation of the acoustic nerve fibers was performed in combination with paired-pulse protocols (v = 50 Hz). The resulted EPSCs were recorded from the cell bodies of the bushy neurons under control conditions or after the application of TMC and/or Y27632 (Figure S2a1). To quantify the observed effects, the amplitude of the first EPSC (A_1) and the paired-pulse ratio (PPR) was determined (Figure S2a2 and a3). Under control conditions, A_1 and PPR were 0.87 ± 0.18 nA and 0.95 ± 0.08, respectively (n = 10). After 1-h pre-incubation with TMC, A_1 was reduced to 0.52 ± 0.22 nA, whereas PPR was increased to 1.47 ± 0.32 (n = 6). In contrast, when Y27632 was applied, A_1 and PPR were 1.04 ± 0.27 nA and 0.91 ± 0.03, respectively (n = 7). If the two inhibitors were simultaneously applied, they seemed to counter-balance each other's action (A_1: 0.59 ± 0.18 nA; PPR: 1.15 ± 0.10; n = 6). Although the trends of the changes were noteworthy—TMC decreased A_1 and increased PPR, whereas inhibition of ROK exerted the opposite effect—only the effect of TMC on the PPR was statistically significant.

Trains of stimuli (v = 50 Hz) were also applied. This stimulus protocol is more sensitive than the application of paired-pulse stimuli (Srinivasan *et al.* 2008), thus it was more likely that any effect of TMC or Y27632 could be revealed. To quantify the changes, the relative amplitudes of consecutive stimuli were monitored (Fig. 6). TMC reduced the amplitude of the first EPSC and increased the relative amplitudes of the second and subsequent EPSCs (Fig. 6a1). Pre-incubation with Y27632 caused the opposite effect: it increased the amplitude of the first EPSC and decreased the relative amplitudes of the third and further EPSCs (Fig. 6a2). When the slices were pre-incubated with both inhibitors simultaneously, no significant change occurred (Fig. 6a3).

TMC and Y27632 altered the time course of the EPSCs as well. This effect was quantified by fitting the falling phase of the EPSCs to a single exponential function. TMC markedly slowed down the falling phase: the decay time constant changed from 1.91 ± 0.35 ms (n = 8) to 3.39 ± 0.67 ms (n = 6; Figure S2b1 and b2). Y27632 reduced the time constant to 0.820 ± 0.095 ms (n = 6). When both inhibitors were present, the decay time constant became 4.86 ± 1.26 ms (n = 6)—a finding that cannot be explained by the possible antagonistic effects of the PP1 and ROK inhibitors. However, as detailed characterization of the kinetic changes was outside the scope of this work, no further experiments were performed addressing the possible background of this phenomenon.

mEPSCs were also recorded and analyzed (Fig. 6b and c). mEPSCs are the consequences of non-action potential-related,

© 2012 The Authors

lontay.beata_285_24

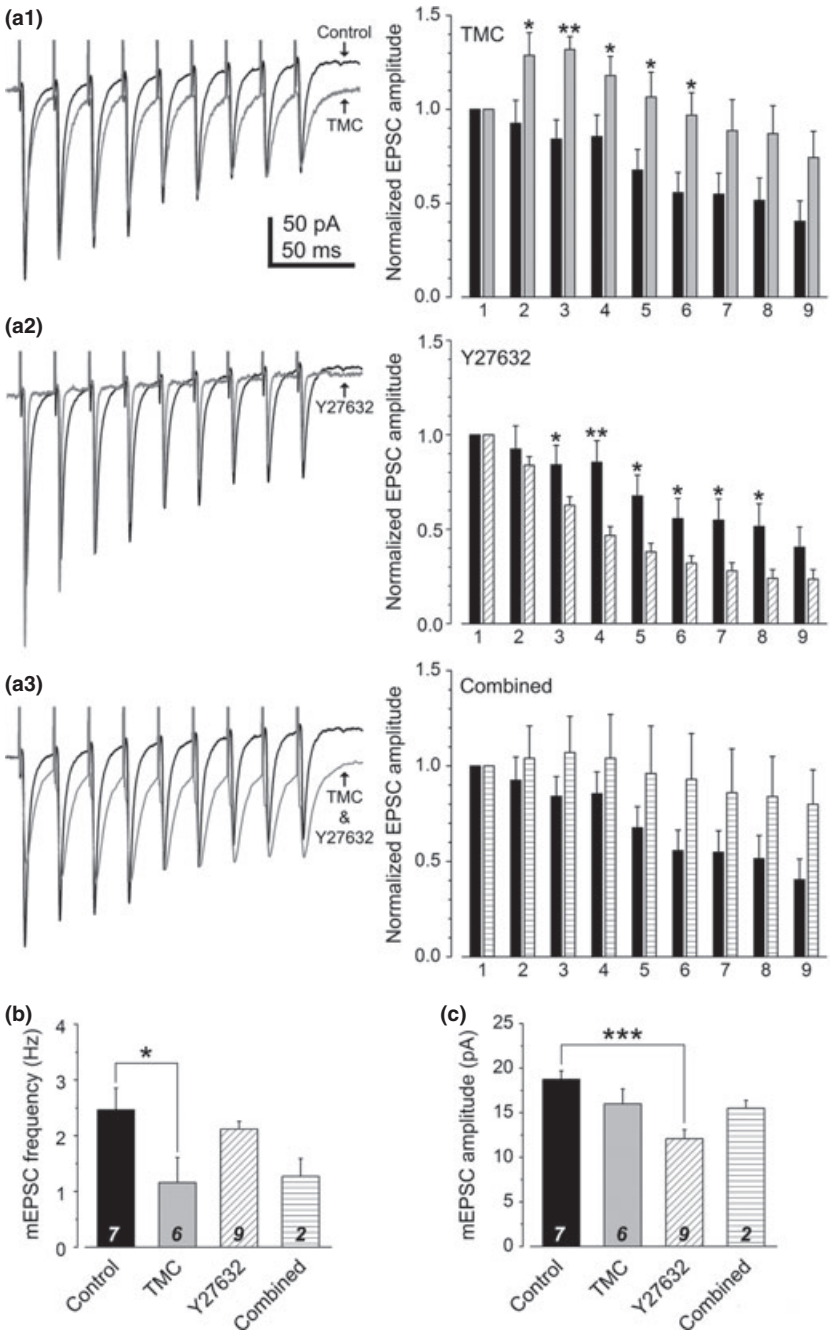


Fig. 6 Effects of the PP1 inhibitor tautomycetin (TMC) and ROK inhibitor Y27632 on the neurotransmission occurring in the acoustic nerve terminal-bushy cell synapse. (a1) EPSCs evoked by a train of stimuli (v = 50 Hz). Black trace represents the control situation, gray trace demonstrates the effect of TMC. All traces are the averages of 10 subsequent current sweeps. The narrow positive components of the EPSCs are stimulatory artifacts, which were partially removed from the figures. The column diagram in the right panel represents EPSC amplitudes normalized to that of the first EPSC. Numbers (1–9) on the X axis indicate the number of the elevant EPSC. Control: black columns (n = 8), TMC: gray columns (n = 6). (a2) Demonstration of the effect of Y27632 (n = 6). (a3) Demonstration of the combined effect of TMC and Y27632 (n = 6). (b–c) Effects of TMC and Y27632 on the frequency (b) and amplitude (c) of miniature EPSCs. To record mEPSCs, action potential firing (thus synchronized vesicle release) was prevented by the application of the Na^+ channel antagonist tetrodotoxin. Numbers in the columns indicate the number of cells investigated. Error bars indicate SEM. *p < 0.05; **p < 0.01; ***p < 0.001.

stochastic vesicular release from the pre-synaptic terminal. TMC pre-incubation significantly reduced the frequency (from 2.46 ± 0.39 Hz to 1.15 ± 0.45 Hz), but did not change the amplitude of the mEPSCs. In contrast, when Y27632 was applied, the frequency remained unchanged but the amplitude was significantly reduced (from 18.7 ± 1.0 pA to 12.1 ± 1 pA). TMC significantly reduced the coefficient of variation of the mEPSC amplitudes (from 0.54 ± 0.07 to 0.37 ± 0.03; p < 0.05), whereas pre-incubation with Y27632 had no appreciable effects (0.58 ± 0.02).

Discussion

Our results indicate that PP1M and ROK are present in both cortical synaptosomes and in a giant synapse of the rat auditory brain stem. PP1M and ROK affect synaptosomal exocytosis and influence neurotransmission by acting on both pre- and post-synaptic targets. Selective inhibition of PP1 and ROK exert opposite effects: the former suppresses, the latter stimulates exocytosis and neurotransmitter release. As PP1c is assumed to exert its effect complexed with regulatory/targeting proteins (Cohen 2002; Mansuy and

© 2012 The Authors

Shenolikar 2006), we assessed the significance of PP1M (i.e., the PP1c-MYPT1 complex) in synaptic transmission. PP1M is the predominant holoenzyme in synaptosomes (see Figure S1a) and it may be the major determinant of PP1-dependent dephosphorylation processes. It has already been suggested that PP2A regulates neurotransmission: PP2A-specific inhibitors (OA, fostreicin) reduced glutamate release or depolarization-induced exocytosis of synaptosomes (Baldwin *et al.* 2003) and OA blocked basal synaptic transmission in hippocampal slices (Koss *et al.* 2007). In this study, inhibition of PP1 decreased the extent of KCl-induced exocytosis, indicating that PP1-type phosphatases are involved in the regulation of synaptic exocytosis. PP1M activity is regulated via a ROK-mediated inhibitory phosphorylation of Thr696 in MYPT1 (Hartshorne *et al.* 2004). This mechanism is present in synaptosomes too, as indicated by the Y27632-mediated suppression of MYPT1^{Thr696} phosphorylation. We have previously shown that PP2A-specific phosphatase inhibition increases the phosphorylation level of MYPT1 at Thr696 and Thr850 (Lontay *et al.* 2005; Kiss *et al.* 2008), resulting in an inhibition of PP1M. We propose that the inhibitory effect of OA on synaptosomal exocytosis is exerted via suppression of PP2A (a MYPT1 phosphatase) thereby increasing the inhibitory phosphorylation of MYPT1.

Beside MLC20, a well-known substrate of both ROK and PP1M, synapsin-I, and syntaxin-1 have emerged as possible novel interactive partners and substrates for PP1M and ROK in synaptosomes. An obvious question is how the phosphorylation of these substrates relates to synaptic exocytosis and neurotransmitter release. The information available in the literature is controversial about the effects of myosin phosphorylation on neurotransmitter release. Myosin phosphorylation increased acetylcholine release in cultured superior cervical ganglion neurons (Mochida 1995) and it also contributed to fusion pore expansion during exocytosis in chromaffin cells (Neco *et al.* 2008). Moreover, it has also been indicated that actomyosin-based contraction coupled with MLC20 phosphorylation may stabilize the cortical actin network, leading to inhibition of exocytosis (Vitale *et al.* 1995; van Leeuwen *et al.* 1999). In addition, ROK-dependent MLC20 phosphorylation is involved in synapse loss under neuropathological conditions (Sunico *et al.* 2010). In this work, the phosphorylation levels of MYPT1 and MLC20 were diminished by the inhibition of ROK during KCl-evoked depolarization of synaptosomes, whereas PP1 inhibition increased the phosphorylation levels of both proteins. These results suggest that myosin phosphorylation and ROK activity correlate inversely with synaptosomal exocytosis.

We provide evidence that ROK phosphorylates synapsin-I^{Ser9} and syntaxin-1^{Ser14}, and these phosphorylated proteins are the substrates of PP1. MYPT1 increased the activity of PP1c toward these substrates *in vitro*, suggesting that MYPT1 has a targeting role in the PP1M-mediated dephosphorylation of synapsin-I^{pSer9} and syntaxin-1^{pSer14}. It has been shown that phosphorylation of Ser9 in an N-terminal peptide of synapsin-I by PKA counteracts the suppressive effect of the dephosphorylated peptide on synaptic transmission (Hilfiker *et al.* 2005). Synapsin-I^{Ser9} phosphorylation by PKA influences synaptic vesicle life cycle during synaptogenesis (Bonanomi *et al.* 2005) and promotes synapsin-I dissociation from vesicles, allowing its dispersion (Chi *et al.* 2001) and enhancing the rate of synaptic vesicle exocytosis (Menegon *et al.* 2006). Our results show that the amount of synapsin-I^{pSer9} increases during KCl-evoked exocytosis. However, further increase in the amount of synapsin-I^{pSer9} upon PP1 inhibition or its decrease by ROK inhibition correlates inversely with the observed changes in exocytosis and this controversy cannot be resolved at this point. Nevertheless, it has been shown that caseine kinase-2-dependent phosphorylation of syntaxin-1^{Ser14} suppresses glutamate release from synaptosomes (Gil *et al.* 2011). ROK-dependent phosphorylation of syntaxin-1^{Ser14} has been shown to increase the affinity of syntaxin-1^{pSer14} to tomosyn and this interaction impairs SNARE complex formation, thereby it could contribute to reduced exocytosis (Sakisaka *et al.* 2004). This regulatory feature of ROK was not observed in cells overexpressing a Ser14 → Ala mutant of syntaxin-1, indicating the significance of syntaxin^{Ser14} phosphorylation in this process. Our results show that increase in syntaxin-1^{pSer14} by PP1 inhibition and decrease of syntaxin-1^{pSer14} upon ROK inhibition are accompanied with suppressed or stimulated synaptosomal exocytosis, respectively. Although more work is needed to determine the significance of the changes in the phosphorylation levels of different proteins (e.g., MLC20, synapsin-I, and syntaxin-1) in synaptic transmission, we propose that the regulation of syntaxin-1^{Ser14} phosphorylation by ROK and PP1M is a major factor controlling synaptic exocytosis and neurotransmitter release.

PP1 and ROK inhibition affected synaptic transmission in a thin-slice preparation. The giant synapse studied here is often utilized for the investigation of synaptic transmission (Cant and Morest 1979; Ryugo and Sento 1991; Isaacson and Walmsley 1996; Ryugo *et al.* 1996; Oleskevich and Walmsley 2002; Oleskevich *et al.* 2004). Our results demonstrate that MYPT1 and ROK are present pre- and post-synaptically in the endbulb of Held-bushy cell synapse. Consistent with these data, both of them were found in pre-and post-synaptic locations in synaptosomes, too (Fig. 1). In addition, MYPT1 was found in association with PP1c and ROK in the pre-synaptic fraction (Lontay *et al.* 2004), while other neuronal-targeting subunits of PP1 (e.g., neurabin, neurofilament-L) were identified in the post-synaptic densities of synaptosomes (Terry-Lorenzo *et al.* 2002). Our present findings indicating that PP1M interacts with and may be involved in the dephosphorylation of several pre-synaptic proteins are in accord with the conclusion that PP1M is the major phosphatase in the pre-synaptic terminal.

© 2012 The Authors

lontay.beata_285_24

We demonstrate that inhibition of either PP1M or ROK influences neurotransmission. To identify the most likely mechanism(s) of action, the following considerations should be made.

(a) Several bodies of evidence indicate that pre-synaptic mechanisms are involved in the mediation of the effects. (i) Both TMC and Y27632 altered the relative amplitudes of the third and subsequent evoked EPSCs. Considering the direction of the changes, we conclude that TMC reduces, whereas Y27632 increases the release probability. (ii) TMC changed the paired-pulse ratio (the slight depression was transformed to facilitation) and it caused a significant reduction of the frequency of the mEPSCs. These effects provide additional support to the hypothesis that TMC is capable of reducing the release probability, although they do not give information about possible changes of the size of the readily releasable pool (Stevens and Wesseling 1999). (iii) TMC significantly reduced the coefficient of variation of the mEPSC amplitudes. As reduced release probability is associated with a reduced variance (Silver *et al.* 1998; Oleskevich *et al.* 2000), this observation is another argument for the release probability reducing effect of TMC.

(b) There is strong evidence for the involvement of a post-synaptic mechanism in mediating the effects of both TMC and Y27632, as the former increased, whereas the latter decreased the decay tau. An alteration of the decay of the EPSCs may have three reasons: change of the amount of neurotransmitter released, change of the rate of neurotransmitter removal from the synaptic cleft, and change of post-synaptic receptor desensitization/deactivation. However, under point (a) it was concluded that TMC reduces, whereas Y27632 increases the release probability—in other words, TMC reduces the amount of glutamate released into the synaptic cleft and Y27632 has the opposite effect. If only the amount of neurotransmitter was reduced in the synaptic cleft, the decay tau would be reduced (Takahashi *et al.* 1995). Therefore, our observation (i.e., the combination of reduced release probability and increased decay tau) can only be explained if an effect on the post-synaptic receptors is assumed. We conclude that TMC reduces, whereas Y27632 increases the rate of desensitization (or deactivation) of post-synaptic non-NMDA receptors.

(c) Y27632 caused a significant decrease of the mEPSC amplitude, which may be explained by either pre- or post-synaptic mechanisms. Decreased mEPSC amplitude may be the consequence of an effect on the post-synaptic receptors, resulting in, inter alia, their reduced sensitivity. Alternatively, reduced mEPSC amplitude may also occur because of pre-synaptic changes (e.g., reduced neurotransmitter content of the vesicles). However, as Y27632 did not change significantly the coefficient of variation of the mEPSC amplitudes, a strictly pre-synaptic mechanism of reducing mEPSC amplitude is unlikely.

Taken together, we conclude that both PP1M and ROK participate in the regulation of neurotransmission by acting via both pre- and post-synaptic mechanisms. Our observations provide further evidence that phosphorylation/dephosphorylation processes play important roles in the regulation of neurotransmission by, inter alia, determining the response features of the non-NMDA receptors (Swope *et al.* 1992; Wang *et al.* 2005; Lee 2006; Derkach *et al.* 2007; Santos *et al.* 2009) or controlling the phosphorylation status of post-synaptic proteins (Lee 2006). In fact, post-synaptic localization of ROK and its involvement in the control of dendritic spine morphology (Schubert *et al.* 2006) and protrusive motility (Tashiro and Yuste 2004) were evident in previous studies, although the phosphorylation targets of this kinase have remained elusive. The involvement of PP1M in post-synaptic processes is also supported by a previous article, demonstrating that the PP1M-specific inhibitor CPI-17 is present post-synaptically and it is required for long-term depression (Eto *et al.* 2002). Our present data reveal binding of CaMKII to MYPT1. The facts that—beside their pre-synaptic occurrence—both CaMKII and MYPT1 are present post-synaptically, suggests functional significance of this interaction. Binding of autophosphorylated CaMKII to post-synaptic densities switches the dephosphorylating phosphatase from PP2A to PP1 (Strack *et al.* 1997), but the targeting subunit for PP1c in this process has not been identified yet. Our data support the hypothesis that the PP1M holoenzyme acts as a potential CaMKII phosphatase and MYPT1 targets PP1c toward the CaMKII autophosphorylation site. However, further studies are required to uncover the exact targets and functions of both ROK and PP1M in post-synaptic phosphorylation.

Acknowledgements

This work was supported by grants from the Hungarian Scientific Research Fund OTKA K68416, K72812, PD 75276, CNK 80709, from the Ministry of Health of Hungary ETT 244/2006, by TÁMOP 4.2.2.-08/1-2008-0019 DERMINOVA, TÁMOP-4.2.2/B-10/1-2010-0024 and TÁMOP-4.2.1./B-09/1/KONV-2010-0007. B.L. and Z.S. are recipients of the J. Bolyai Fellowship. The authors are indebted to Krisztina Pocsai, Ágnes Németh, and Zsuzsanna N. Fekete for their excellent technical assistance.

The authors declare no conflict of interest.

Supporting information

Additional supporting information may be found in the online version of this article:

Appendix S1. Materials and methods.

Figure S1. Effects of phosphatase inhibitors on the total synaptosomal phosphatase activity and estimation of the synaptosomal PP1, PP2A, and PP2B concentrations.

Figure S2. Changes of the EPSC amplitude, paired-pulse ratio, and time course of evoked EPSCs in the acoustic nerve fiber-bushy cell synapse of the cochlear nucleus after preincubation of the brain slices with TMC and/or Y27632.

© 2012 The Authors

lontay.beata_285_24

As a service to our authors and readers, this journal provides supporting information supplied by the authors. Such materials are peer-reviewed and may be re-organized for online delivery, but are not copy-edited or typeset. Technical support issues arising from supporting information (other than missing files) should be addressed to the authors.

References

Amano M., Kaneko T., Maeda A. *et al.* (2003) Identification of Tau and MAP2 as novel substrates of Rho-kinase and myosin phosphatase. *J. Neurochem.* **87**, 780–790.

Baba T., Sakisaka T., Mochida S. and Takai Y. (2005) PKA-catalyzed phosphorylation of tomosyn and its implication in Ca^{2+}-dependent exocytosis of neurotransmitter. *J. Cell Biol.* **170**, 1113–1125.

Baldwin M. L., Rostas J. A. and Sim A. T. (2003) Two modes of exocytosis from synaptosomes are differentially regulated by protein phosphatase types 2A and 2B. *J. Neurochem.* **85**, 1190–1199.

Birukova A. A., Smurova K., Birukov K. G., Kaibuchi K., Garcia J. G. and Verin A. D. (2004) Role of Rho GTPases in thrombin-induced lung vascular endothelial cells barrier dysfunction. *Microvasc. Res.* **67**, 64–77.

Bonanomi D., Menegon A., Miccio A., Ferrari G., Corradi A., Kao H. T., Benfenati F. and Valtorta F. (2005) Phosphorylation of synapsin I by cAMP-dependent protein kinase controls synaptic vesicle dynamics in developing neurons. *J. Neurosci.* **25**, 7299–7308.

Brorson S. H. and Nguyen G. H. (2001) Increased level of immunogold labeling of epoxy sections by rising the temperature significantly beyond 100 degrees C in the antigen retrieval medium. *Micron* **32**, 591–597.

Cant N. B. and Morest D. K. (1979) The bushy cells in the anteroventral cochlear nucleus of the cat. A study with the electron microscope. *Neuroscience* **4**, 1925–1945.

Cesca F., Baldelli P., Valtorta F. and Benfenati F. (2010) The synapsins: key actors of synapse function and plasticity. *Prog. Neurobiol.* **91**, 313–348.

Chi P., Greengard P. and Ryan T. A. (2001) Synapsin dispersion and reclustering during synaptic activity. *Nat. Neurosci.* **4**, 1187–1193.

Cohen P. T. (2002) Protein phosphatase 1–targeted in many directions. *J. Cell Sci.* **115**, 241–256.

Cousin M. A. and Robinson P. J. (2001) The dephosphins: dephosphorylation by calcineurin triggers synaptic vesicle endocytosis. *Trends Neurosci.* **24**, 659–665.

Davies S. P., Reddy H., Caivano M. and Cohen P. (2000) Specificity and mechanism of action of some commonly used protein kinase inhibitors. *Biochem. J.* **351**, 95–105.

Derkach V. A., Oh M. C., Guire E. S. and Soderling T. R. (2007) Regulatory mechanisms of AMPA receptors in synaptic plasticity. *Nat. Rev. Neurosci.* **8**, 101–113.

Dunkley P. R., Jarvie P. E., Heath J. W., Kidd G. J. and Rostas J. A. (1986) A rapid method for isolation of synaptosomes on Percoll gradients. *Brain Res.* **372**, 115–129.

Erdődi F., Kiss E., Walsh M. P., Stefansson B., Deng J. T., Eto M., Brautigan D. L. and Hartshorne D. J. (2003) Phosphorylation of protein phosphatase type-1 inhibitory proteins by integrin-linked kinase and cyclic nucleotide-dependent protein kinases. *Biochem. Biophys. Res. Commun.* **306**, 382–387.

Eto M., Kitazawa T., Yazawa M., Mukai H., Ono Y. and Brautigan D. L. (2001) Histamine-induced vasoconstriction involves phosphorylation of a specific inhibitor protein for myosin phosphatase by protein kinase C alpha and delta isoforms. *J. Biol. Chem.* **276**, 29072–29078.

Eto M., Bock R., Brautigan D. L. and Linden D. J. (2002) Cerebellar long-term synaptic depression requires PKC-mediated activation of CPI-17, a myosin/moesin phosphatase inhibitor. *Neuron* **36**, 1145–1158.

Eto M., Kitazawa T. and Brautigan D. L. (2004) Phosphoprotein inhibitor CPI-17 specificity depends on allosteric regulation of protein phosphatase-1 by regulatory subunits. *Proc. Natl Acad. Sci. USA* **101**, 8888–8893.

Favre B., Turowski P. and Hemmings B. A. (1997) Differential inhibition and posttranslational modification of protein phosphatase 1 and 2A in MCF7 cells treated with calyculin-A, okadaic acid, and tautomycin. *J. Biol. Chem.* **272**, 13856–13863.

Feng J., Ito M., Ichikawa K., Isaka N., Nishikawa M., Hartshorne D. J. and Nakano T. (1999) Inhibitory phosphorylation site for Rho-associated kinase on smooth muscle myosin phosphatase. *J. Biol. Chem.* **274**, 37385–37390.

Gil C., Falques A., Sarro E., Cubi R., Blasi J., Aguilera J. and Itarte E. (2011) Protein kinase CK2 associates to lipid rafts and its pharmacological inhibition enhances neurotransmitter release. *FEBS Lett.* **585**, 414–420.

Hartshorne D. J., Ito M. and Erdodi F. (2004) Role of protein phosphatase type 1 in contractile functions: myosin phosphatase. *J. Biol. Chem.* **279**, 37211–37214.

Hilfiker S., Benfenati F., Doussau F., Nairn A. C., Czernik A. J., Augustine G. J. and Greengard P. (2005) Structural domains involved in the regulation of transmitter release by synapsins. *J. Neurosci.* **25**, 2658–2669.

Hirano M., Niiro N., Hirano K., Nishimura J., Hartshorne D. J. and Kanaide H. (1999) Expression, subcellular localization, and cloning of the 130-kDa regulatory subunit of myosin phosphatase in porcine aortic endothelial cells. *Biochem. Biophys. Res. Commun.* **254**, 490–496.

Isaacson J. S. and Walmsley B. (1996) Amplitude and time course of spontaneous and evoked excitatory postsynaptic currents in bushy cells of the anteroventral cochlear nucleus. *J. Neurophysiol.* **76**, 1566–1571.

Jovanovic J. N., Sihra T. S., Nairn A. C., Hemmings Jr H. C., Greengard P. and Czernik A. J. (2001) Opposing changes in phosphorylation of specific sites in synapsin I during Ca^{2+}-dependent glutamate release in isolated nerve terminals. *J. Neurosci.* **21**, 7944–7953.

Kiss A., Lontay B., Bécsi B., Márkász L., Oláh É., Gergely P. and Erdődi F. (2008) Myosin phosphatase interacts with and dephosphorylates the retinoblastoma protein in THP-1 leukemic cells: its inhibition is involved in the attenuation of daunorubicin-induced cell death by calyculin-A. *Cell. Signal.* **20**, 2059–2070.

Koga Y. and Ikebe M. (2008) A novel regulatory mechanism of myosin light chain phosphorylation via binding of 14-3-3 to myosin phosphatase. *Mol. Biol. Cell* **19**, 1062–1071.

Koss D. J., Hindley K. P., Riedel G. and Platt B. (2007) Modulation of hippocampal calcium signalling and plasticity by serine/threonine protein phosphatases. *J. Neurochem.* **102**, 1009–1023.

Lee H. K. (2006) Synaptic plasticity and phosphorylation. *Pharmacol. Ther.* **112**, 810–832.

van Leeuwen F. N., van Delft S., Kain H. E., van der Kammen R. A. and Collard J. G. (1999) Rac regulates phosphorylation of the myosin-II heavy chain, actinomyosin disassembly and cell spreading. *Nat. Cell Biol.* **1**, 242–248.

Lontay B., Serfőző Z., Gergely P., Ito M., Hartshorne D. J. and Erdődi F. (2004) Localization of myosin phosphatase target subunit 1 in rat brain and in primary cultures of neuronal cells. *J. Comp. Neurol.* **478**, 72–87.

Lontay B., Kiss A., Gergely P., Hartshorne D. J. and Erdődi F. (2005) Okadaic acid induces phosphorylation and translocation of myosin phosphatase target subunit 1 influencing myosin phosphorylation, stress fiber assembly and cell migration in HepG2 cells. *Cell. Signal.* **17**, 1265–1275.

© 2012 The Authors

lontay.beata_285_24

Mansuy I. M. and Shenolikar S. (2006) Protein serine/threonine phosphatases in neuronal plasticity and disorders of learning and memory. *Trends Neurosci.* **29**, 679–686.

Menegon A., Bonanomi D., Albertinazzi C., Lotti F., Ferrari G., Kao H. T., Benfenati F., Baldelli P. and Valtorta F. (2006) Protein kinase A-mediated synapsin I phosphorylation is a central modulator of Ca^{2+}-dependent synaptic activity. *J. Neurosci.* **26**, 11670–11681.

Mitsuhashi S., Shima H., Tanuma N., Matsuura N., Takekawa M., Urano T., Kataoka T., Ubukata M. and Kikuchi K. (2003) Usage of tautomycetin, a novel inhibitor of protein phosphatase 1 (PP1), reveals that PP1 is a positive regulator of Raf-1 in vivo. *J. Biol. Chem.* **278**, 82–88.

Mochida S. (1995) Role of myosin in neurotransmitter release: functional studies at synapses formed in culture. *J. Physiol. Paris* **89**, 83–94.

Moring J., Shoemaker W. J., Skita V., Mason R. P., Hayden H. C., Salomon R. M. and Herbette L. G. (1990) Rat cerebral cortical synaptoneurosomal membranes. Structure and interactions with imidazobenzodiazepine and 1,4-dihydropyridine calcium channel drugs. *Biophys. J.* **58**, 513–531.

Murányi A., Derkach D., Erdődi F., Kiss A., Ito M. and Hartshorne D. J. (2005) Phosphorylation of Thr695 and Thr850 on the myosin phosphatase target subunit: inhibitory effects and occurrence in A7r5 cells. *FEBS Lett.* **579**, 6611–6615.

Nagy G., Matti U., Nehring R. B., Binz T., Rettig J., Neher E. and Sorensen J. B. (2002) Protein kinase C-dependent phosphorylation of synaptosome-associated protein of 25 kDa at Ser187 potentiates vesicle recruitment. *J. Neurosci.* **22**, 9278–9286.

Nagy G., Reim K., Matti U., Brose N., Binz T., Rettig J., Neher E. and Sorensen J. B. (2004) Regulation of releasable vesicle pool sizes by protein kinase A-dependent phosphorylation of SNAP-25. *Neuron*, **41**, 417–429.

Neco P., Fernandez-Peruchena C., Navas S., Gutierrez L. M., de Toledo G. A. and Ales E. (2008) Myosin II contributes to fusion pore expansion during exocytosis. *J. Biol. Chem.* **283**, 10949–10957.

Oleskevich S. and Walmsley B. (2002) Synaptic transmission in the auditory brainstem of normal and congenitally deaf mice. *J. Physiol.* **540**, 447–455.

Oleskevich S., Clements J. and Walmsley B. (2000) Release probability modulates short-term plasticity at a rat giant terminal. *J. Physiol.* **524**, 513–523.

Oleskevich S., Youssoufian M. and Walmsley B. (2004) Presynaptic plasticity at two giant auditory synapses in normal and deaf mice. *J. Physiol.* **560**, 709–719.

Pál B., Pór A., Pocsai K., Szücs G. and Rusznák Z. (2005) Voltage-gated and background K^+ channel subunits expressed by the bushy cells of the rat cochlear nucleus. *Hear. Res.* **199**, 57–70.

Rusznák Z., Bakondi G., Pocsai K., Pór A., Kosztka L., Pál B., Nagy D. and Szücs G. (2008) Voltage-gated potassium channel (Kv) subunits expressed in the rat cochlear nucleus. *J. Histochem. Cytochem.* **56**, 443–465.

Ryugo D. K. and Sento S. (1991) Synaptic connections of the auditory nerve in cats: relationship between endbulbs of held and spherical bushy cells. *J. Comp. Neurol.* **305**, 35–48.

Ryugo D. K., Wu M. M. and Pongstaporn T. (1996) Activity-related features of synapse morphology: a study of endbulbs of held. *J. Comp. Neurol.* **365**, 141–158.

Sakisaka T., Baba T., Tanaka S., Izumi G., Yasumi M. and Takai Y. (2004) Regulation of SNAREs by tomosyn and ROCK: implication in extension and retraction of neurites. *J. Cell Biol.* **166**, 17–25.

Santos S. D., Carvalho A. L., Caldeira M. V. and Duarte C. B. (2009) Regulation of AMPA receptors and synaptic plasticity. *Neuroscience* **158**, 105–125.

Schubert V., Da Silva J. S. and Dotti C. G. (2006) Localized recruitment and activation of RhoA underlies dendritic spine morphology in a glutamate receptor-dependent manner. *J. Cell Biol.* **172**, 453–467.

Silver R. A., Momiyama A. and Cull-Candy S. G. (1998) Locus of frequency-dependent depression identified with multiple-probability fluctuation analysis at rat climbing fibre-Purkinje cell synapses. *J. Physiol.* **510**, 881–902.

Snyder D. A., Kelly M. L. and Woodbury D. J. (2006) SNARE complex regulation by phosphorylation. *Cell Biochem. Biophys.* **45**, 111–123.

Sposito N. M. and Gross P. M. (1987) Topography and morphometry of capillaries in the rat subfornical organ. *J. Comp. Neurol.* **260**, 36–46.

Srinivasan G., Kim J. H. and von Gersdorff H. (2008) The pool of fast releasing vesicles is augmented by myosin light chain kinase inhibition at the calyx of Held synapse. *J. Neurophysiol.* **99**, 1810–1824.

Stevens C. F. and Wesseling J. F. (1999) Augmentation is a potentiation of the exocytotic process. *Neuron* **22**, 139–146.

Strack S., Choi S., Lovinger D. M. and Colbran R. J. (1997) Translocation of autophosphorylated calcium/calmodulin-dependent protein kinase II to the postsynaptic density. *J. Biol. Chem.* **272**, 13467–13470.

Sudhof T. C. (2004) The synaptic vesicle cycle. *Annu. Rev. Neurosci.* **27**, 509–547.

Sunico C. R., Gonzalez-Forero D., Dominguez G., Garcia-Verdugo J. M. and Moreno-Lopez B. (2010) Nitric oxide induces pathological synapse loss by a protein kinase G-, Rho kinase-dependent mechanism preceded by myosin light chain phosphorylation. *J. Neurosci.* **30**, 973–984.

Swope S. L., Moss S. J., Blackstone C. D. and Huganir R. L. (1992) Phosphorylation of ligand-gated ion channels: a possible mode of synaptic plasticity. *FASEB J.* **6**, 2514–2523.

Takahashi M., Kovalchuk Y. and Attwell D. (1995) Pre- and postsynaptic determinants of EPSC waveform at cerebellar climbing fiber and parallel fiber to Purkinje cell synapses. *J. Neurosci.* **15**, 5693–5702.

Tashiro A. and Yuste R. (2004) Regulation of dendritic spine motility and stability by Rac1 and Rho kinase: evidence for two forms of spine motility. *Mol. Cell. Neurosci.* **26**, 429–440.

Terry-Lorenzo R. T., Carmody L. C., Voltz J. W., Connor J. H., Li S., Smith F. D., Milgram S. L., Colbran R. J. and Shenolikar S. (2002) The neuronal actin-binding proteins, neurabin I and neurabin II, recruit specific isoforms of protein phosphatase-1 catalytic subunits. *J. Biol. Chem.* **277**, 27716–27724.

Tóth A., Kiss E., Herberg F. W., Gergely P., Hartshorne D. J. and Erdődi F. (2000) Study of the subunit interactions in myosin phosphatase by surface plasmon resonance. *Eur. J. Biochem.* **267**, 1687–1697.

Turner K. M., Burgoyne R. D. and Morgan A. (1999) Protein phosphorylation and the regulation of synaptic membrane traffic. *Trends Neurosci.* **22**, 459–464.

Vitale M. L., Seward E. P. and Trifaro J. M. (1995) Chromaffin cell cortical actin network dynamics control the size of the release-ready vesicle pool and the initial rate of exocytosis. *Neuron* **14**, 353–363.

Wang J. Q., Arora A., Yang L., Parelkar N. K., Zhang G., Liu X., Choe E. S. and Mao L. (2005) Phosphorylation of AMPA receptors: mechanisms and synaptic plasticity. *Mol. Neurobiol.* **32**, 237–249.

© 2012 The Authors

frontiers in Endocrinology

lontay.beata_285_24

ORIGINAL RESEARCH
published: 05 October 2021
doi: 10.3389/fendo.2021.751488

Smoothelin-Like Protein 1 Regulates Development and Metabolic Transformation of Skeletal Muscle in Hyperthyroidism

*Evelin Major[1], Ferenc Győry[2], Dániel Horváth[1], Ilka Keller[1], István Tamás[1], Karen Uray[1], Péter Fülöp[3] and Beáta Lontay[1]**

[1] Department of Medical Chemistry, Faculty of Medicine, University of Debrecen, Debrecen, Hungary, [2] Department of Surgery, Faculty of Medicine, University of Debrecen, Debrecen, Hungary, [3] Department of Internal Medicine, Division of Metabolism, Faculty of Medicine, University of Debrecen, Debrecen, Hungary

OPEN ACCESS

Edited by:
Pieter de Lange, University of Campania Luigi Vanvitelli, Italy

Reviewed by:
Flavia Fonseca Bloise, Federal University of Rio de Janeiro, Brazil
Justin A MacDonald, University of Calgary, Canada

***Correspondence:**
Beáta Lontay
lontay@med.unideb.hu

Specialty section:
This article was submitted to Cellular Endocrinology, a section of the journal Frontiers in Endocrinology

Received: *01 August 2021*
Accepted: *14 September 2021*
Published: *05 October 2021*

Citation:
Major E, Győry F, Horváth D, Keller I, Tamás I, Uray K, Fülöp P and Lontay B (2021) Smoothelin-Like Protein 1 Regulates Development and Metabolic Transformation of Skeletal Muscle in Hyperthyroidism. Front. Endocrinol. 12:751488. doi: 10.3389/fendo.2021.751488

Hyperthyroidism triggers a glycolytic shift in skeletal muscle (SKM) by altering the expression of metabolic proteins, which is often accompanied by peripheral insulin resistance. Our previous results show that smoothelin-like protein 1 (SMTNL1), a transcriptional co-regulator, promotes insulin sensitivity in SKM. Our aim was to elucidate the role of SMTNL1 in SKM under physiological and pathological 3,3′,5-Triiodo-L-thyronine (T3) concentrations. Human hyper- and euthyroid SKM biopsies were used for microarray analysis and proteome profiler arrays. Expression of genes related to energy production, nucleic acid- and lipid metabolism was changed significantly in hyperthyroid samples. The phosphorylation levels and activity of AMPKα2 and JNK were increased by 15% and 23%, respectively, in the hyperthyroid samples compared to control. Moreover, SMTNL1 expression showed a 6-fold decrease in the hyperthyroid samples and in T3-treated C2C12 cells. Physiological and supraphysiological concentrations of T3 were applied on differentiated C2C12 cells upon SMTNL1 overexpression to assess the activity and expression level of the elements of thyroid hormone signaling, insulin signaling and glucose metabolism. Our results demonstrate that SMTNL1 selectively regulated TRα expression. Overexpression of SMTNL1 induced insulin sensitivity through the inhibition of JNK activity by 40% and hampered the non-genomic effects of T3 by decreasing the activity of ERK1/2 through PKCδ. SMTNL1 overexpression reduced IRS1 Ser307 and Ser612 phosphorylation by 52% and 53%, respectively, in hyperthyroid model to restore the normal responsiveness of glucose transport to insulin. SMTNL1 regulated glucose phosphorylation and balances glycolysis and glycogen synthesis *via* the downregulation of hexokinase II by 1.3-fold. Additionally, mitochondrial respiration and glycolysis were measured by SeaHorse analysis to determine cellular metabolic function/phenotype of our model system in real-time. T3 overload strongly increased the rate of acidification and a shift to glycolysis, while SMTNL1 overexpression antagonizes the T3 effects. These lines of evidence suggest that SMTNL1

lontay.beata_285_24

potentially prevents hyperthyroidism-induced changes in SKM, and it holds great promise as a novel therapeutic target in insulin resistance.

Keywords: insulin sensitivity, skeletal muscle, hyperthyroidism, insulin signaling, insulin receptor substrate 1, phosphorylation, glucose metabolism

INTRODUCTION

Hyperthyroidism is a pathological disorder in which excess thyroid hormone (TH) is produced and secreted by the thyroid gland (1). Thyroid hormones are key regulators of metabolism and development and have diverse effects. Thyroxine (T4) is the main product of thyroid secretion. Thyroxine is deiodinated in peripheral tissues to produce 3,3′,5-Triiodo-L-thyronine (T3), the biologically active TH (2). The biological effects of THs are mediated through the interaction of T3 with high-affinity thyroid receptors (TRs). TRs are ligand-dependent nuclear transcription factors that interact with thyroid-responsive elements (TREs) located in the promoter of T3-responsive genes (3). Five different subtypes of TRs (α1, α2, β1, β2, and β3) are encoded by two genes, TRα (*NR1A1*) and TRβ (*NR1A2*). All subtypes except TRα2 bind T3 (4, 5).

THs have profound effects on skeletal muscle (SKM), affecting contractile function, metabolic properties, myogenesis, and muscle regeneration *via* altered gene expression (6, 7). THs cross the plasma membrane by facilitated diffusion that is primarily mediated by monocarboxylate transporters 10 and 8 (MCT10 and 8) in SKM (8, 9). Intracellular TH levels are also modulated by iodothyronine deiodinase type 2 (DIO2), which converts T4 to T3 to increase intracellular T3 availability and effects (10). T3 regulates gene expression in SKM by interacting with TRα and TRβ at specific promoter regions (11, 12). In addition, THs elicit short-term effects in SKM by regulating membrane transporter activity (13), phospholipase C (14), and the kinase activity of p38 and AMP-activated protein kinase (AMPK), which are important in mitochondrial biogenesis (15).

SKM represents 40% of the human body mass and is one of the most important tissues regulating energy expenditure and lipid and glucose homeostasis (16). Changes in the energetic profile of SKM significantly affect systemic physiology (17). Insulin-mediated glucose uptake by SKM is regulated through the phosphatidylinositol 3-kinase (PI3K) and protein kinase B (PKB/Akt) pathways and the heterologous MAPKs and AMPK pathways. Insulin binds to the insulin receptor (IR) triggering an intracellular signaling cascade that includes the phosphorylation and binding of insulin receptor substrate 1 (IRS1), PI3K, and Akt. IRS1 provides an interacting surface for both IR and PI3K; thus, the regulation of IRS1 is crucial (18). As the target of insulin-dependent cascades, glucose disposal is increased by the translocation of glucose transport molecule 4 (GLUT4) from the intracellular vesicles to the surface and by the regulation of glucose transport, glucose phosphorylation, glycogen synthesis, glycolysis, and glucose oxidation (19). T3 promotes an elevation in basal and some extent insulin-mediated glucose uptake primarily increasing GLUT4 protein expression and insulin-independent translocation of GLUT4 (20). Interestingly, T3 also exerts acute, non-genomic action by activating GLUT4 already present on the plasmamembrane (21).

One potential regulator of insulin resistance in SKM is the smoothelin-like protein 1 (SMTNL1). SMTNL1 was identified as an early target of protein kinase A and G (PKA/PKG) in gastrointestinal smooth muscle (22) and is expressed in skeletal muscle and steroid hormone-sensitive tissues. SMTNL1 translocates to the nucleus after phosphorylation at Ser301 by PKA/PKG. In the nucleus, SMTNL1 functions as a transcriptional regulator of progesterone receptors, leading to subsequent gene regulation of numerous metabolic enzymes, cytoskeletal elements, steroid receptors, and cytokines (23). We previously showed that SMTNL1 regulates insulin signaling by promoting the gene expression of GLUT4 and IRS1 in murine skeletal muscle. Moreover, SKM fiber type shifts from oxidative to glycolytic phenotype in *SMTNL1* KO mice; consequently, *SMTNL1*$^{-/-}$ mice are metabolically less efficient and exhibit impaired glucose tolerance (24).

SMTNL1 is the major metabolic regulator in SKM and SMTNL1 KO mice mimic the pathophysiological processes of hyperthyroidism (24). Thus, our aim was to determine the role of SMTNL1 in SKM under physiological and pathological TH concentrations. We found that THs play diverse roles in the regulation of SKM development and homeostasis through the downregulation of SMTNL1 expression. SMTNL1 overexpression prevented the metabolic shift of SKM during insulin resistance induced by supraphysiological TH levels.

MATERIALS AND METHODS

Chemicals

All chemicals were obtained from Sigma-Aldrich (St. Louis, MO, USA) unless otherwise indicated.

Antibodies

See **Table 1** in the **Supplementary Materials and Methods** for a list of antibodies used in Western blot analyses. See **Figure S7** for evidence that β-actin is an applicable loading control in our model.

Cell Culture Maintenance and Transfection

C2C12 mouse myoblast cells (*ECACC 91031101*) were grown in Dulbecco's Modified Eagle's Medium (DMEM) supplemented with 1000 mg/L glucose, 2 mM L-glutamine (Lonza), 10% (v/v) fetal bovine serum (FBS; Sigma-Aldrich; St. Louis, MO, USA; Cat. No. F9665, batch number: BCBW5069), and phenol red at 37°C and 5% CO_2. Transient transfection was conducted using

lontay.beata_285_24

GeneJuice reagent with pM13-NT-FT-SMTNL1 (NT-FT: N-terminal Flag tagged SMTNL1) as described in **Supplementary Materials and Methods**. Myoblasts at passage number 6-9 were seeded into collagen-coated tissue culture plates or dishes (VWR International; West Chester, PA, USA) and incubated overnight (O/N). Transfection with empty vector (MOCK) acted as the control in all experiments.

Differentiation and Treatment of C2C12 Cells

The day after transfection, myogenic differentiation was induced at 90% confluency. Cells were washed with 1x Phosphate buffered saline (PBS) and the growth medium was replaced by phenol red-free DMEM supplemented with 1000 mg/L glucose, 2 mM L-glutamine and 2% (v/v) horse serum (HS) (differentiation medium). 10 nM T3 dissolved in 1 M HCl : EtOH (1:4) was added from the first day (**Figure 4**) or from the beginning of the fourth day (**Figures 5**–**8**) of differentiation. The non-treated control cells were treated with 1 M HCl : EtOH and are called 'vehicle' in the figures. Differentiation medium supplemented with either T3 or vehicle was changed daily for 6 days (**Figure 4**) and for 72 hours (**Figures 5**–**8**).

SeaHorse Analysis

Myoblasts were transfected with empty vector or NT-FT-SMTNL1 and were seeded at a density of 10 000 cells per well in collagen-coated XF96 microplates (Agilent Technologies; Santa Clara, CA, USA). Following a 72-hour T3 treatment of cells, 180 µl of assay media (Agilent Technologies; Santa Clara, CA, USA) containing 1000 mg/L glucose was added. Myoblasts were incubated for 1 hour in a non-CO_2 incubator along with the previously hydrated sensor cartridge (Agilent Technologies; Santa Clara, CA, USA) loaded with the following inhibitors: 50 µM etomoxir (carnitine palmitoyltransferase-1 inhibitor); 2 µM oligomycin (ATP synthase inhibitor); 4 µM FCCP (carbonyl cyanide-p-trifluoromethoxyphenylhydrazone; mitochondrial oxidative phosphorylation uncoupler), or 10 µM antimycin (mitochondrial electron transport chain complex III inhibitor) + 100 mM 2-deoxy-D-glucose (glycolysis inhibitor). Five measurement points were taken for the baseline and after each injection. Finally, cells were solubilized in 1 N NaOH and total protein concentration was measured using a Bicinchoninic acid (BCA) assay kit (Thermo Fisher Scientific; Waltham, MA, USA).

Cell Lysis

On the last day of differentiation combined with SMTNL1 overexpression and/or hormone treatment, myotubes were washed with 1x PBS and were harvested in ice-cold RIPA buffer [25 mM Tris-HCl (pH 7.6), 150 mM NaCl, 1% sodium deoxycholate, 0.1% SDS, 1% Triton-X 100, 1mM PMSF, 10x PIC, 50x PPIC, 1 µM MC-LR] on ice. Cell suspensions were sonicated for 30 seconds with a 10% pulse using a Branson Sonifier sonicator and were centrifuged for 10 minutes at 16 000 x *g*, 4° C. Then supernatants were transferred to fresh tubes. Total protein concentrations were measured by Bicinchoninic acid (BCA) assay kit (Thermo Fisher Scientific; Waltham, MA, USA).

Western Blot Analysis

After harvesting and lysing cells, whole-cell lysates were boiled in 4x sodium dodecyl sulphate (SDS) sample buffer (Bio-Rad Laboratories; Hercules, CA, USA) for 5 minutes. Western blot analyses were conducted as described previously (25) with the following modifications: 30 µg of protein was loaded onto 4-20% precast Criterion gels (Bio-Rad Laboratories; Hercules, CA, USA) and separated at 200 V. After a 75-minute transfer at 100 V, nitrocellulose membranes were blocked in 5% (w/v) bovine serum albumin (BSA)/Tris-buffered saline (TBS) containing 0.1% (v/v) Tween 20 for 1.5 hours. The blots were incubated with primary antibodies at 4°C, O/N and secondary antibodies at room temperature (RT) for 1.5 hours, diluted in the blocking solution. In phospho-blots, membranes were stripped or HRP-inactivated as described in **Supplementary Materials and Methods** and were re-probed with non-phospho antibodies.

Human Euthyroid and Hyperthyroid Skeletal Muscle (SKM) Biopsies

Sternohyoid muscle biopsies from euthyroid (eu) and hyperthyroid (hyper) donors were frozen in liquid N_2 at the time of harvest and were stored at -70°C. Donors were selected based on their gender and disease. All biopsies were derived from female patients with struma nodosa (euthyroid) or with Basedow or struma nodosa colloides (hyperthyroid). We strove to select female patients not older than 60 years (**Figure S1**). Samples were homogenized in modified RIPA buffer [25 mM Tris (pH 7.6), 150 mM NaCl, 0.1% SDS, 1% Triton X-100, 1 mM EDTA, 1 mM DTT, 1 mM PMSF, 10x PIC, 50x PPIC, 1 µM MC-LR] on ice using a glass Potter-Elvehjem tissue grinder. After centrifugation at 16 000 x *g*, 4°C, supernatants were transferred to fresh tubes and were subjected to Western blot analysis. Statistical analysis was performed using data from 73 patients, as shown in **Supplementary Figures**.

Total RNA Isolation for Microarray Analysis of Human SKM Biopsies

An RNeasy Fibrous Tissue kit (cat. no. 74704, Qiagen; Hilden, Germany) was used according to the manufacturer's instructions. Euthyroid and hyperthyroid SKM samples (3 of each) were homogenized in a guanidine-isothiocyanate buffer using the TissueRuptor (Qiagen; Hilden, Germany) and were treated with proteinase K at 55°C for 10 minutes. Cell debris was removed by centrifugation at 10 000 x *g* for 3 minutes and supernatants were transferred to fresh tubes. Then 96-100% ethanol was added to the cleared lysates and was mixed thoroughly. After RNA was bound to the RNeasy silica membrane, traces of DNA were eliminated by DNase I treatment on the RNeasy column at 30°C for 15 minutes. DNase I and any possible contaminants were washed away, and RNA was eluted in RNase-free water. Total RNA concentration and purity were determined using a NanoDrop ND-1000 spectrophotometer (Thermo Fisher Scientific; Waltham, MA, USA). The microarray analysis was performed using an Affymetrix Human Gene 1.0 ST Array as previously described (26). All of the raw DNA chip data is available in the

Gene Expression Omnibus (GEO; http://www.ncbi.nlm.nih.gov/geo/) under the following accession number: GSE178996.

Proteome Profiler Human Phospho-Kinase and Phospho-MAPK Arrays

Human Phospho-Kinase (cat. no. ARY003B) and Phospho-MAPK (cat. no. ARY002B) array kits (R&D Systems; Minneapolis, MN, USA) were used according to the manufacturer's instructions. Briefly, human euthyroid and hyperthyroid SKM biopsies were homogenized in Lysis Buffer 6 supplemented with protease and phosphatase inhibitors. For the Phospho-Kinase Array, samples were diluted in Array Buffer 1 and were incubated with the membranes at 4°C O/N. On the next day, membranes were incubated in a cocktail of biotinylated detection antibodies at RT for 2 hours. For the Phospho-MAPK Array, samples were diluted in Array Buffer 1 and were incubated with Detection Antibody Cocktail at RT for 1 hour. Then the prepared sample/antibody mixtures were added to the membranes which were incubated at 4°C O/N. Membranes were then incubated in diluted Streptavidin-HRP and the signal was detected by ECL with the provided Chemi-Reagent Mix in both arrays.

Statistical Analysis

Immunoblots were analyzed using ImageJ. Bar charts were created and statistical analyses were performed using GraphPad Prism8. Phosphorylated proteins were normalized to non-phosphorylated protein expression, while non-phosphorylated protein expression was normalized to the loading control. Normalized data were checked for normality and were analyzed using unpaired two-tailed t-test for the comparison of two groups, and One-way ANOVA or Two-way ANOVA for the comparison of four or more groups followed by their corresponding parametric or non-parametric *post hoc* test. All data are presented as mean +/- SEM, where n is the number of independently performed experiments. Outliers were identified using the Thompson Tau-test and Grubbs's test. Differences were considered statistically significant at $p < 0.05$.

RESULTS

Microarray Analysis of Euthyroid and Hyperthyroid Human Skeletal Muscle Tissues and a Gene Ontology Analysis

A tissue bank with 73 samples of sternohyoid muscle from 44 euthyroid and 29 hyperthyroid patients undergoing thyroid surgery was established. Using patient data, statistical analysis was performed based on the classification of donors (**Figure S1**). Over 39,000 transcripts were examined, encompassing the entire expressed human genome. Comparing the euthyroid and hyperthyroid samples, 393 differentially regulated genes were identified. **Figure 1** shows a list of genes that were up- or downregulated ($p<0.05$; $n = 3$) in the hyperthyroid samples compared with gene expression in the euthyroid samples. Hierarchical cluster analysis was performed on all differentially expressed genes using average linkage with Pearson's dissimilarity and the numbers of induced or repressed genes are presented in a heat map (**Figure 1A**). Hyperthyroidism influenced molecular cellular functions and their related diseases, including disorders of metabolism and energy production, lipid metabolism, cellular and tissue development, endocrine system, skeletal and muscular function, and gene expression regulation (**Figure 1B**). Bioinformatics analysis identified differentially regulated canonical pathways; the most profound changes were found in mTOR, p70S6K, AMPK, PI3K/Akt and MAPK signaling pathways (**Figure S2**). Taken together, the signaling pathways identified by microarray analysis showed altered expression of genes involved in metabolism, development, and cytoskeletal function in SKM upon the clinical manifestations of hyperthyroidism.

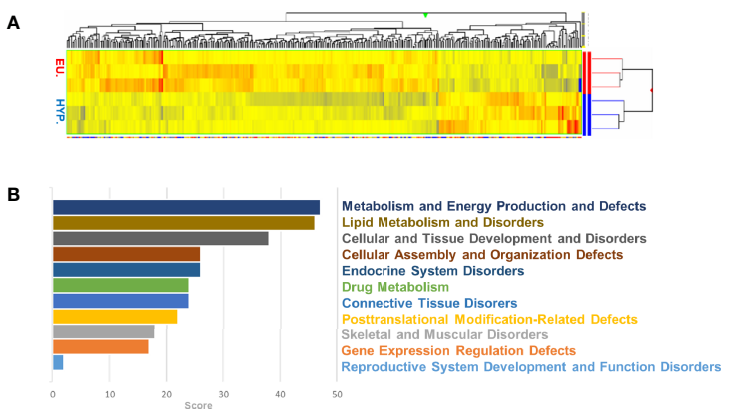


FIGURE 1 | Microarray analysis of human euthyroid and hyperthyroid skeletal muscle biopsies. Euthyroid and hyperthyroid SKM samples were analyzed by microarray. The color code for the signal strength is shown in which induced genes are indicated by red and repressed genes are indicated by blue **(A)**. Ontology of the related genes and their classification by GO terms **(B)**.

Hyperthyroidism Affects Key Metabolic Pathways in Human Skeletal Muscle

To investigate hyperthyroidism-induced changes in human SKM, we analyzed the phosphorylation profiles of an array of kinases. The comparison of hyperthyroid and euthyroid samples were visualized using heat maps and graphs (**Figures 2A, B**). Phosphorylation levels of transcription factors, including STAT2^{Y689}, STAT5a^{Y694}, STAT5b^{Y699} were markedly increased in hyperthyroidism (**Figure 2B**). Among Ser/Thr kinases, phosphorylation of MSK1/2$^{S376/S360}$, Akt2^{S474}, WNK1^{T60} and MKK3$^{S218/T222}$ was significantly reduced and phosphorylation of ERK1/2$^{T202/Y204,T185/Y187}$, AMPKα2^{T172} and JNK$_{pan}$ $^{T183/Y185,T221/Y223}$ was strongly elevated in hyperthyroid samples compared with phosphorylation in euthyroid samples (**Figure 2B**). Interestingly, phosphorylation of mTOR^{S2448}, p70S6K$^{T421/S424}$, PLC-γ1^{Y783}, eNOS^{S1177}, and HSP60 was considerably diminished in the hyperthyroid samples compared with phosphorylation in the euthyroid samples (**Figure 2A**). Regarding cell cycle and apoptosis, hyperthyroidism decreased the phosphorylation of p27^{T198} only (**Figure 2A**). These results suggest that hyperthyroidism has a huge impact on key metabolic pathways through posttranslational regulation of their members in SKM. We also further validated our results on differentiated "hyperthyroid" C2C12 cell model by semi-quantitative Western blot analysis (**Figure 6E** and **Figures 7A–C**).

SMTNL1 Expression Is Changed in Skeletal Muscle During Hyperthyroidism

To investigate the role of SMTNL1 in hyperthyroidism, human euthyroid and hyperthyroid SKM samples were analyzed by Western blot. SMTNL1 expression decreased 6-fold in the hyperthyroid samples (**Figure 3A**), indicating that SMTNL1 may play a role in the pathophysiology of hyperthyroidism in SKM. This change was accompanied by a significant decrease in the expression of type IIa fiber marker MyHC IIa (**Figure 3B**) and a considerable decrease in type I fiber marker MyHC I expression (**Figure 3C**), suggesting an SKM isotype switch and metabolic shift from an oxidative to a glycolytic fiber type induced by hyperthyroidism.

Effects of Supraphysiological T3 Exposure on C2C12 Differentiation

The C2C12 mouse myoblast cell line was used to validate the results from the human SKM biopsies and explore the molecular mechanisms behind the effects of SMTNL in hyperthyroidism. C2C12 mouse myoblast cells are widely used to study skeletal muscle metabolism *in vitro* (27). In our model system, myoblasts were differentiated for 6 days in the presence of physiological or supraphysiological T3 (10 nM) (28, 29). Differentiation was confirmed by Western blot analysis of early (desmin) and late (MyHC) myogenic markers. Neither physiological nor

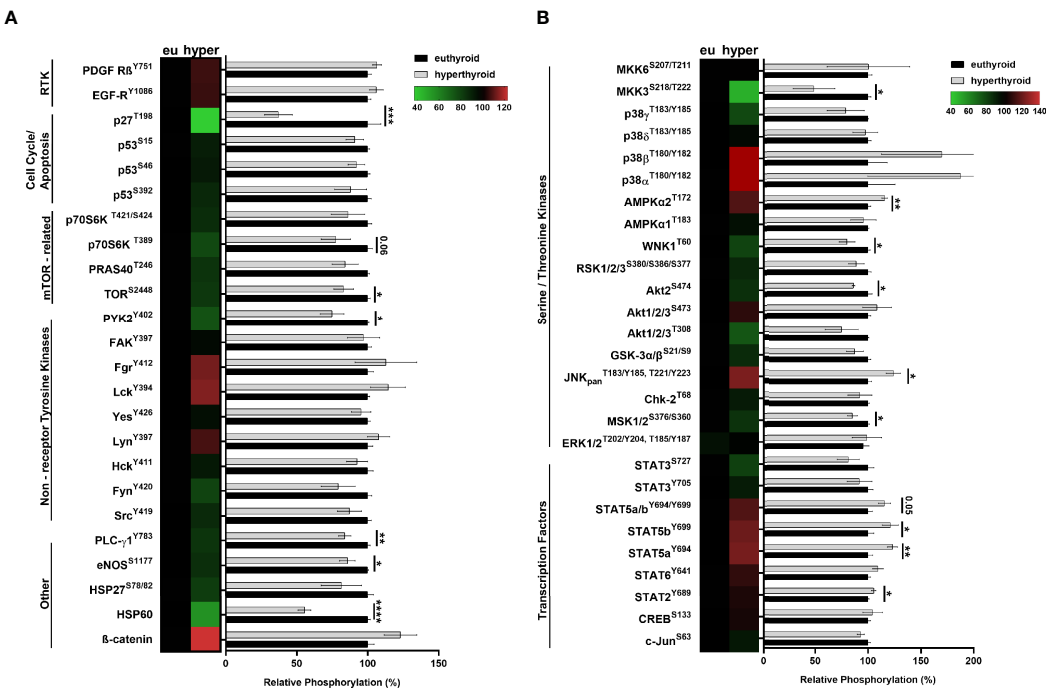


FIGURE 2 | Analysis of human euthyroid and hyperthyroid skeletal muscle biopsies with proteome profiler phospho-kinase and phospho-MAPK arrays. **(A, B)** Euthyroid and hyperthyroid SKM samples were analyzed by human Phospho-Kinase array and by Human Phospho-MAPK Array. Results were visualized by a combination of heat maps and graphs. Bar charts show the phosphorylation levels of various proteins in hyperthyroid samples relative to their corresponding euthyroid pairs. In case of the heat maps, increased phosphorylation levels are indicated by red and decreased phosphorylation levels are indicated by green. Values represent n=2-3, mean +/- SEM. Groups were compared using unpaired two-tailed t-tests, $p < 0.05$ (*), $p < 0.01$ (**), $p < 0.001$ (***), and $p < 0.0001$ (****).

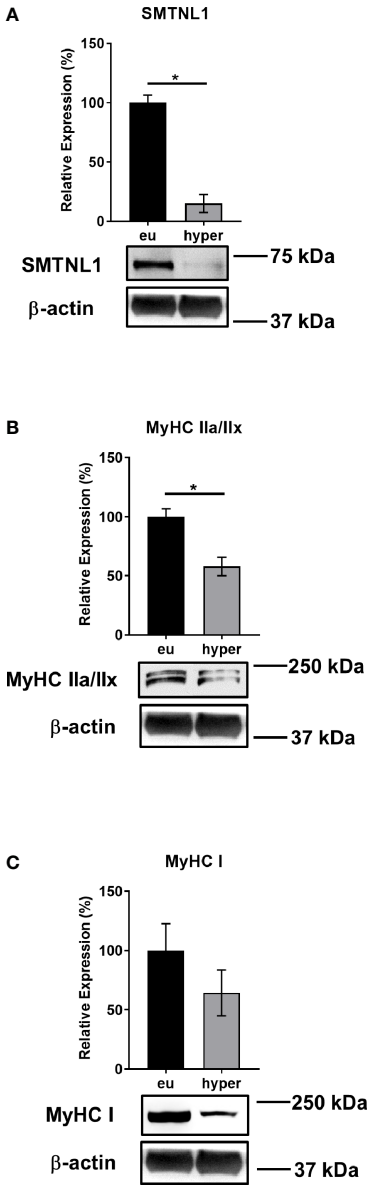


FIGURE 3 | SMTNL1, MyHC IIa/IIx, and MyHC I Expression during Hyperthyroidism. Proteins from skeletal muscle biopsies were separated by SDS-PAGE followed by Western blot analysis using anti-SMTNL1 **(A)**, anti-MyHC IIa/IIx **(B),** and anti-MyHC I **(C)** antibodies. Values represent n=3, mean +/- SEM. Bar charts display the expression levels of SMTNL1, MyHC IIa/IIx, and MyHC I in hyperthyroid samples normalized to their euthyroid counterparts. Groups were compared using unpaired two-tailed t-tests, $p < 0.05$ (*).

supraphysiological T3 condition altered the expression of myogenic markers after Day 4. Desmin expression was significantly upregulated by 57% on Day 4, and MyHC expression was significantly upregulated by 46% on Day 6 of T3 treatment (**Figures 4A, B**). Thus, T3 promotes the myogenesis of C2C12 myoblasts into multinucleated, fiber-shaped myotubes. We also examined the effects of differentiation and T3 treatment on endogenous SMTNL1 expression. SMTNL1 expression was increased during regular differentiation; however, it was not significant. Upon T3 treatment, SMTNL1 levels were significantly increased on Day 1 but then progressively decreased 4-fold by the end of differentiation compared to the vehicle (**Figure 4C**). SMTNL1 was transiently overexpressed in C2C12 myoblasts, which were differentiated for 6 days. On the beginning of Day 4, differentiating myoblasts were treated with 10 nM of T3 for 72 hours. SMTNL1 overexpression was confirmed by Western blot analysis (**Figure S3A**). Based on these data, SMTNL1 levels were inversely altered upon T3-treatment suggesting the regulatory effect of T3 on SMTNL1 expression. We examined the effects of the previously described treatments on the viability of C2C12 cells using the alamarBlue assay. Neither SMTNL1 overexpression nor T3 treatment affected the viability of myotubes (**Figure S3B**). These results are in agreement with our Proteome Profiler data showing that hyperthyroidism does not induce apoptosis in SKM.

T3 Treatment and SMTNL1 Overexpression Influence the Expression of Regulatory Proteins Involved in T3 Signaling/Action in C2C12 Myotubes

The effects of THs are primarily determined by the presence of TH transporters in the plasma membrane, the expression of TH receptors, and intracellular hormone availability, which depend on the activity of iodothyronine deiodinases. To elucidate the effects of SMTNL1 on MCT8, DIO2, TRα, and TRβ expression upon T3 treatment, we carried out Western blot analyses on NT-FT-SMTNL1-transfected and/or T3-treated myotubes. MCT8 and DIO2 expression did not change significantly (**Figures 5A, B**). However, TRα expression was dramatically reduced by 67% and 52% in response to T3 treatment and SMTNL1 overexpression, respectively. Initially, our hypothesis was that SMTNL1 can antagonize the effects of T3. Remarkably, the combined treatment with T3 and SMTNL1 caused a further decrease in TRα expression by 37% compared to SMTNL1 overexpression but it was not significant compared to T3 treatment (**Figure 5C**). These data are in line with a previous study demonstrating that THs lower TRα levels *via* proteasomal degradation in SKM (30). In contrast, T3 treatment led to a significant increase in TRβ expression (**Figure 5D**). SMTNL1 overexpression did not significantly change TRβ protein expression (**Figure 5D**) or boost the effect of T3 on TRα expression (**Figure 5C**). Thus, SMTNL1 does not appear to antagonize the effects of T3 at TRs. Furthermore, SMTNL1 does not directly interact with TRα or TRβ, based on the immunoprecipitation of NT-FT-SMTNL1 (**Figure S4A**). Treatment of NT-FT-SMTNL1-transfected myotubes with a membrane-permeable cAMP analog, 8BrcAMP, significantly reduced TRα expression by 42% compared to SMTNL1 overexpression alone (**Figure S4B**), suggesting that SMTNL1 may regulate TRα expression at the transcriptional level. MyoD1, one of the master proteins controlling myogenesis, is positively regulated by T3 (31, 32) and our data are in agreement with this notion; T3 treatment alone or in combination with

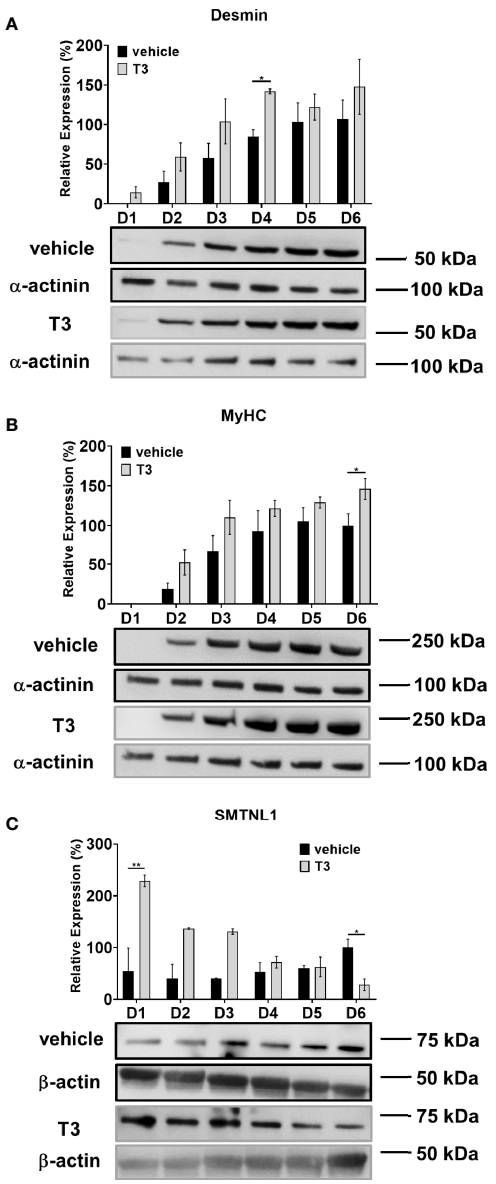


FIGURE 4 | Effect of T3 treatment on SMTNL1 expression during C2C12 myogenesis. **(A–C)** Myoblasts were seeded on a collagen-coated plate and differentiation was induced in the presence of 2% HS and supraphysiological (10 nM) T3. Equal amounts of 1 M HCl : EtOH solution was added to the non-treated control, indicated as 'vehicle' which contains physiological (approximately 1 nM) T3. The differentiation medium was changed daily for 6 days. Myotubes were harvested and lysates were analyzed by Western blot using anti-desmin **(A)**, anti-MyHC **(B),** and anti-SMTNL1 **(C)** antibodies. Values represent n=3-4, mean +/- SEM. Data were normalized to the D6 vehicle control. Groups were compared using Two-way ANOVA and Tukey's *post hoc* test, $p < 0.05$ (*), $p < 0.01$ (**).

SMTNL1 overexpression induced a 55% and a 49% increase in MyoD1 expression in myotubes, respectively (**Figure 5E**). These data indicate that T3 has a positive effect on C2C12 myogenesis through the regulation of MyoD1.

SMTNL1 Overexpression Decreases Ser Phosphorylation of IRS1 in the Presence of Excess T3 in C2C12 Myotubes

Hyperthyroidism is often accompanied by insulin resistance (33). In addition, *SMTNL1*$^{-/-}$ mice have impaired glucose tolerance associated with pronounced insulin resistance (24). Therefore, the effects of SMTNL1 on crucial members of insulin signaling were investigated. Although IRS1 expression did not change under any conditions (**Figure 6A**), IRS1 phosphorylation at Ser307 (**Figure 6B**) and Ser612 (**Figure 6C**) was increased following T3 treatment by 1.6-fold and 1.8-fold, respectively. SMTNL1 overexpression alone and in combination with T3 treatment reduced IRS1-P^{S307} to 48% and 73%, respectively. IRS1-P^{S612} decreased by 53% in response to combined treatment compared with IRS1-P^{S612} in the T3-treated cells (**Figures 6B, C**). Another important member of the insulin signaling pathway is PI3K. T3 treatment significantly decreased expression of the p85 subunit of PI3K but the other treatments did not significantly change p85 expression (**Figure 6D**). T3 treatment caused a negligible decrease in the phosphorylation of mTOR-P^{S2448} and overexpression of SMTNL1 had no effects. However, mTOR-P^{S2448} was increased significantly after combined treatment with T3 and SMTNL1 overexpression compared to the T3-treated cells (**Figure 6E**). Besides that, expression of mTOR remained unchanged under all conditions (**Figure S5A**). Collectively, these data provide evidence that T3 excess triggers the development of insulin resistance while overexpression of SMTNL1 can moderate these effects.

Regulation of Ser/Thr Kinases Involved in Insulin Signaling by SMTNL1 Under Supraphysiological T3 Exposure in C2C12 Myotubes

The involvement of SMTNL1 in hyperthyroidism-induced posttranslational alterations was determined using Western blot analyses of NT-FT-SMTNL1-transfected and/or T3-treated myotubes. The expression of AMPK, ERK1/2 and SAPK/JNK did not change significantly (**Figure S5B–D**). AMPK-P^{T172} significantly increased by approximately 30% in response to T3 treatment alone or in combination with SMTNL1 overexpression (**Figure 7A**). In parallel, ERK1/2$^{T202/Y204}$ phosphorylation increased by 57% in response to T3 treatment, while SMTNL1 overexpression induced a 27% decrease compared with phosphorylation in the non-treated control (**Figure 7B**). Although SAPK/JNK-P$^{T183/Y185,T221/Y223}$ was elevated after T3 treatment, SMTNL1 overexpression alone reduced SAPK/JNK-P$^{T183/Y185,T221/Y223}$ by 40%. Moreover, SMTNL1 overexpression was able to prevent the increased SAPK/JNK-P$^{T183/Y185,T221/Y223}$ induced by T3 (**Figure 7C**). PKCδ expression did not change in response to T3 treatment, but decreased by 38% and 50% in response to SMTNL1 overexpression in the absence or presence of T3, respectively (**Figure 7D**). Finally, PP2Acα expression showed a marginally significant decrease in response to prolonged T3 treatment; SMTNL1 overexpression alone or in combination with T3 did not change PP2Acα expression (**Figure 7E**). Since IRS1 is a target of the previously mentioned

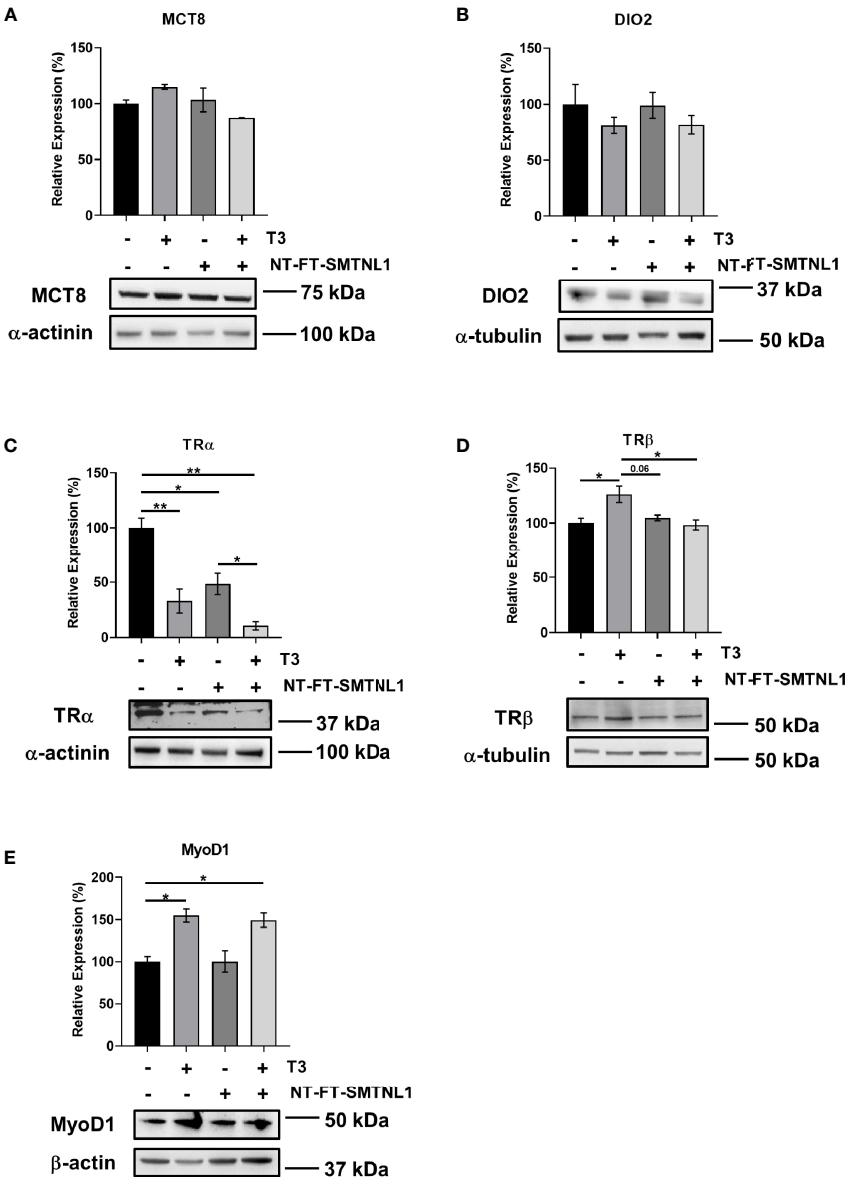


FIGURE 5 | T3 treatment and SMTNL1 overexpression influence the expression of regulatory proteins involved in T3 signaling/action. **(A–C)** Myoblasts were transfected with either empty vector or NT-FT-SMTNL1 and were differentiated with a simultaneous 72-hour T3 treatment starting from Day 4. Proteins from whole-cell lysates were analyzed by Western blot using anti-MCT8 **(A)**, anti-DIO2 **(B)**, anti-TRα **(C),** anti-TRβ **(D),** and anti-MyoD1 **(E)**. Values represent n=3-5, mean +/- SEM. Data were normalized to the empty vector-transfected control. Groups were compared using One-way ANOVA and Tukey's post hoc test, $p < 0.05$ (*), $p < 0.01$ (**).

Ser/Thr kinases, these data explain the elevated Ser phosphorylation levels of IRS1 in response to excess T3 and confirm the insulin-sensitizing effect of SMTNL1.

SMTNL1 Overexpression Induces GLUT4 and Decreases Hexokinase II Expression in the Presence of Excess T3 in C2C12 Myotubes

Hyperthyroidism is a hypermetabolic state associated with elevated glucose utilization (33). Furthermore, deletion of *SMTNL1* causes impaired glucose tolerance *via* decreased GLUT4 levels (24). Therefore, we investigated the effects of SMTNL1 on important contributors to glucose metabolism. GLUT4 expression was markedly elevated under each condition (**Figure 8A**). In addition, T3 treatment significantly enhanced hexokinase II (HK II) expression by 43%. In contrast, HK II protein levels fell by 25% in response to SMTNL1 overexpression alone or in combination with T3 compared with the expression in the non-treated control (**Figure 8B**) suggesting that SMTNL1 plays a role in the regulation of glycolysis.

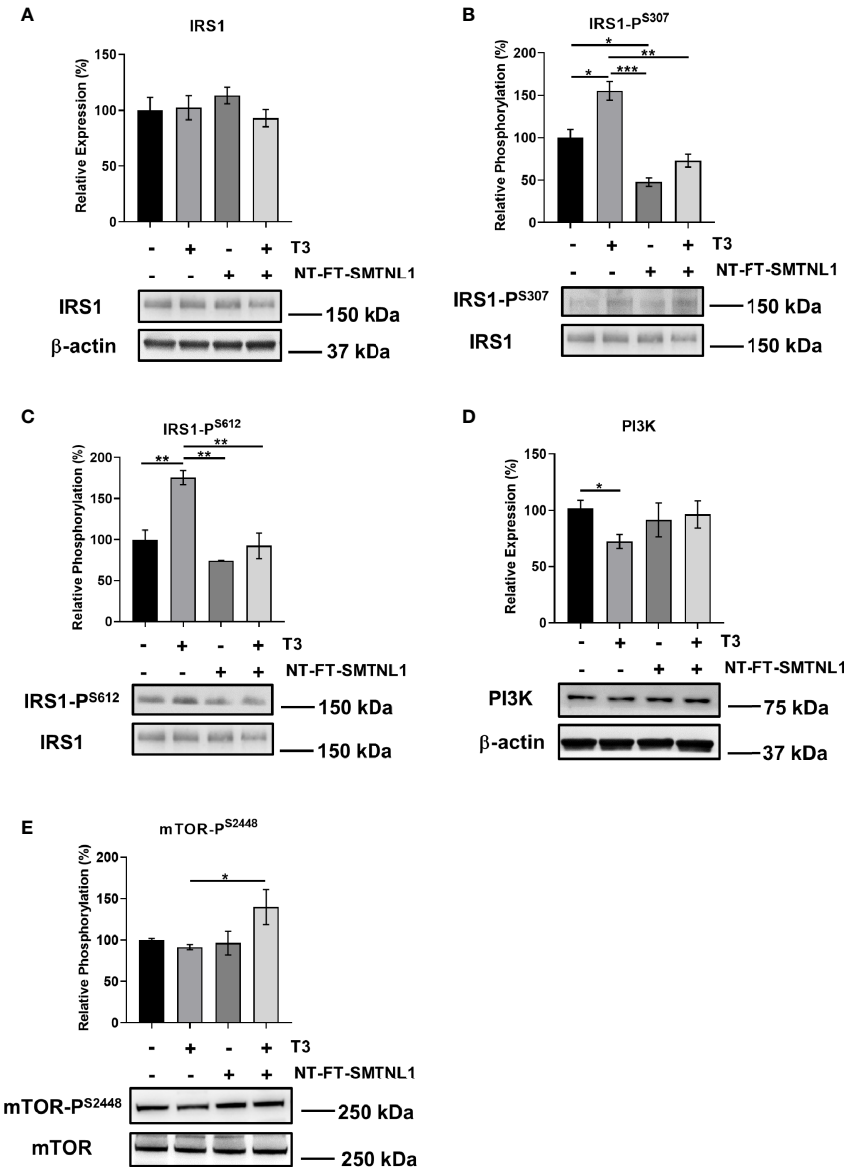


FIGURE 6 | T3 overload and SMTNL1 overexpression affect the phosphorylation of key members of insulin signaling. **(A–E)** Empty vector or NT-FT-SMTNL1-transfected myoblasts were differentiated with a simultaneous 72-hour T3 treatment starting from Day 4. Proteins from whole-cell lysates were analyzed by Western blot using anti-IRS1 **(A)**, anti-IRS1-P^{S307} **(B)**, anti-IRS1-P^{S612} **(C)**, anti-PI3K **(D),** and anti-mTOR-P^{S2448} **(E)**. Values represent n=3-6, mean +/- SEM. Data were normalized to the empty vector-transfected control. Groups were compared using One-way ANOVA and Tukey's *post hoc* test, $p < 0.05$ (*), $p < 0.01$ (**), $p < 0.001$ (***).

Antagonistic Effects of SMTNL1 Overexpression on the Acidification Rate Upon T3 Overload in C2C12 Myoblasts

The rate of lactate production and mitochondrial respiration was investigated using the rate of increase in proton concentration by measuring the extracellular acidification rate (ECAR) or the rate of decrease in oxygen concentration (OCR). Three key parameters of cell energy metabolism were examined: baseline phenotype, stressed phenotype, and metabolic potential (**Figure S6A, B**). ECAR was markedly increased in response to T3 treatment, while SMTNL1 overexpression alone or in combination with T3 strongly decreased ECAR (**Figure 9A**). Similarly, anaerobic glycolysis was increased in response to excess T3, but decreased by half in response to SMTNL1 overexpression compared with the non-treated control. Moreover, SMTNL1 overexpression was able to prevent anaerobic glycolysis from increasing in response to excess T3

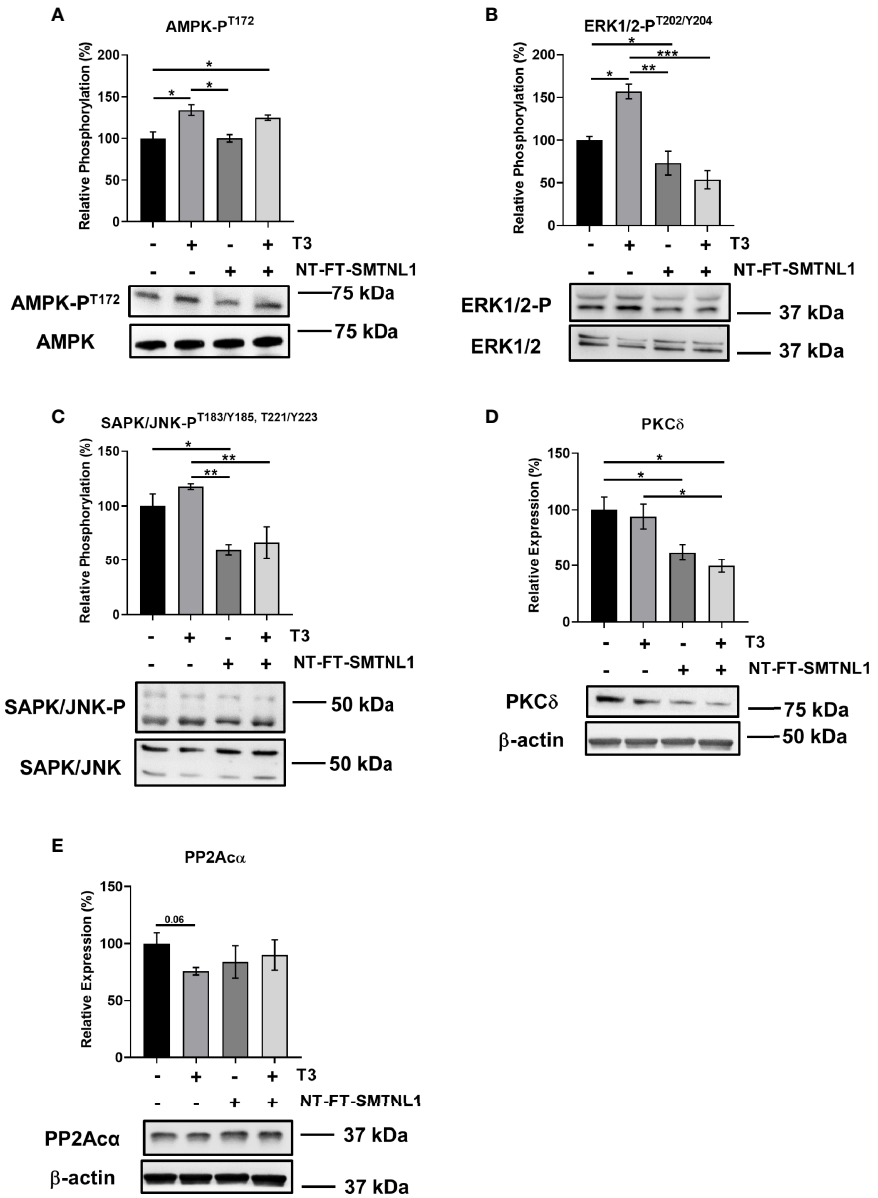


FIGURE 7 | T3 excess and SMTNL1 overexpression regulate the phosphorylation and expression of various Ser/Thr kinases and phosphatases. **(A–E)** Myoblasts were transfected with either empty vector or NT-FT-SMTNL1 and were differentiated in parallel with a 72-hour T3 treatment from Day 4 onwards. Whole-cell lysates were separated by SDS-PAGE followed by Western blot analysis using anti-AMPK-P^{T172} **(A)**, anti- ERK1/2-P$^{T202/Y204}$ **(B)**, anti-SAPK/JNK-P$^{T183/Y185,T221/Y223}$ **(C)**, anti-PKCδ **(D),** and anti-PP2Acα **(E)** antibodies. Values represent n=4-6, mean +/- SEM. Data were normalized to the empty vector-transfected control. Groups were compared using One-way ANOVA and Tukey's post hoc test, $p < 0.05$ (*), $p < 0.01$ (**), $p < 0.001$ (***).

(**Figure 9B**). Excess T3 did not affect maximal glycolysis but SMTNL1 overexpression alone or in combination with T3 reduced maximal glycolysis (**Figure 9C**). Interestingly, the glycolytic reserve was diminished under each condition (**Figure 9D**). T3 treatment did not affect basal OCR, while SMTNL1 overexpression significantly reduced basal OCR (**Figure 9E**). The rate of mitochondrial respiration did not change in response to T3 treatment; however, SMTNL1 overexpression caused a 46% decrease in the rate of mitochondrial respiration (**Figures 9G–I**). Fatty acids can also be metabolized to pyruvate, acetyl CoA, and other intermediates for ATP production. Our results show that fatty acid oxidation (FAO) increased in response to excess T3, while SMTNL1 overexpression significantly reduced fatty acid oxidation by 58% (**Figure 9F**). Taken together, these data suggest that T3 overload strongly increases the rate of acidification (ECAR),

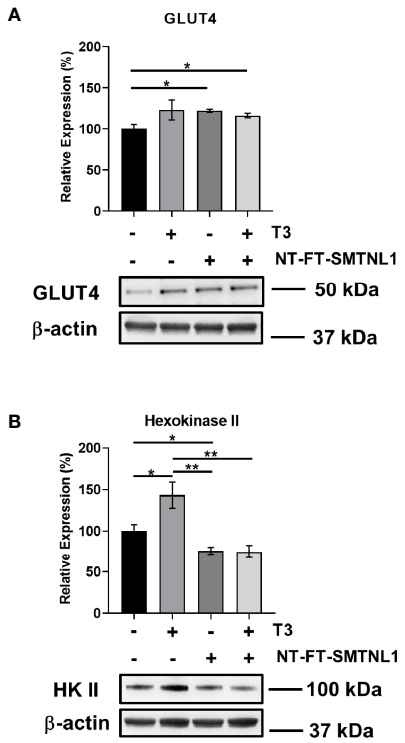


FIGURE 8 | T3 treatment and SMTNL1 overexpression affect the expression of crucial members of glucose metabolism. Myoblasts were transfected with empty vector or NT-FT-SMTNL1 and were differentiated with a 72-hour T3 treatment starting from Day 4. Proteins from whole-cell lysates were analyzed by Western blot using anti-GLUT4 **(A)** and anti-hexokinase II **(B)** antibodies. Values represent n=3-4, mean +/- SEM. Data were normalized to the empty vector-transfected control. Groups were compared using One-way ANOVA and Tukey's *post hoc* test, $p < 0.05$ (*), $p < 0.01$ (**).

while SMTNL1 overexpression antagonizes the T3 effects preventing glycolytic metabolism.

DISCUSSION

Our study is the first to compare global SKM gene expression in hyperthyroid and euthyroid patients. This screen revealed the role of a major regulator, SMTNL1, in thyroid homeostasis in SKM. In this study, we characterize the role of SMTNL1 in the molecular mechanism of hyperthyroidism in human skeletal muscle and the effect of supraphysiological T3 exposure on differentiated C2C12 muscle cells.

A Gene Ontology functional enrichment analysis of microarray data comparing SKM from euthyroid and hyperthyroid patients showed that hyperthyroidism negatively associated with mTOR, AMPK, PI3K/Akt, p70S6K and MAPK signaling (**Figure S2**). Moreover, hyperthyroidism-related differentially expressed genes were significantly involved in metabolic and energy production diseases, cellular and tissue development disorders, and defects in gene expression regulation. These results are in line with the results of Clément et al., who conducted a microarray analysis of five healthy men after a 14-day treatment with THs (34). However, our data are the first to describe changes in patients with long-standing hyperthyroid disease (**Figures 1** and **2**).

SMTNL1, as a transcriptional cofactor, regulates primarily progesterone and androgen receptors (35). No protein-protein interactions between TRα/β and SMTNL1 were detected in the presence of T3 (**Figure S4A**); thus, we ruled out the possibility of SMTNL1 being a member of the coregulatory complex of TH receptors. Data on human euthyroid and hyperthyroid samples demonstrated that elevated T3 levels drastically decreased SMTNL1 expression (**Figure 3A**). In addition, SMTNL1 expression was inversely proportional to T3 during the course of C2C12 differentiation (**Figure 4C**) but T3 caused a significant decrease in SMTNL1 expression only in differentiated myotubes (**Figure 4C** and **Figure S3C**) suggesting a mechanism related to developed SKM. Moreover, the activation of PKA resulted in a significant decrease in TRα expression, especially in cells overexpressing SMTNL1 (**Figure S4B**), suggesting that PKA-related SMTNL1 phosphorylation induced the translocation of SMTNL1 to the nucleus as it was described before (23) and triggered its transcriptional activity towards TRα expression. One possible explanation is that T3 acts through a non-genomic activation of kinases, which phosphorylate and activate transcription factors resulting in transcriptional regulation (15). The promoter of SMTNL1 contains binding sites for GR, AP-1, RXR, MyoD, and ER transcription factors (36). Thus, another possible explanation is that TR is tethered to DNA by other proteins, as the DNA-binding capacity of TR is dispensable and T3-bound TRs can modulate the function of AP-1 complexes without binding to DNA (37, 38). TRα downregulation by SMTNL1 overexpression and T3 treatment suggests that TRβ may be a potential transcription factor for SMTNL1. Lastly, MyoD could interact with TRs affecting the expression of SMTNL1 through an interaction as an extensive "regulatory lattice" through which different pathways communicate and influence one another (38).

The role of SMTNL1 in SKM homeostasis and development is supported by several lines of evidence. First, adult skeletal muscle undergoes interconversion between types I, IIa, IIx and IIb fibers in response to physiological and pathological signals (39). In the absence of SMTNL1, which is expressed mainly in type IIa fibers, SKM transforms into type IIx/IIb fibers with a glycolytic phenotype in humans and rodents, leading to a drastic change in global metabolic properties (24). Hyperthyroidism also initiates a shift in expression to the next faster MyHC isoform, that is, MyHC I switches to IIa, IIa to IIx, or IIx to IIb, depending on the initial fiber type and this isoform switch is regulated by many factors including T3 (40, 41). We observed a significant decrease in MyHC IIa/IIx fiber markers in hyperthyroid human SKM (**Figure 3B**), while MyHCIIb were not investigated due to its absence in human SKM (42). MyHC I changes were not significant, probably due to the very low of type I fibers under normal conditions (9%) compared to type IIa (24.2%), IIx fibers

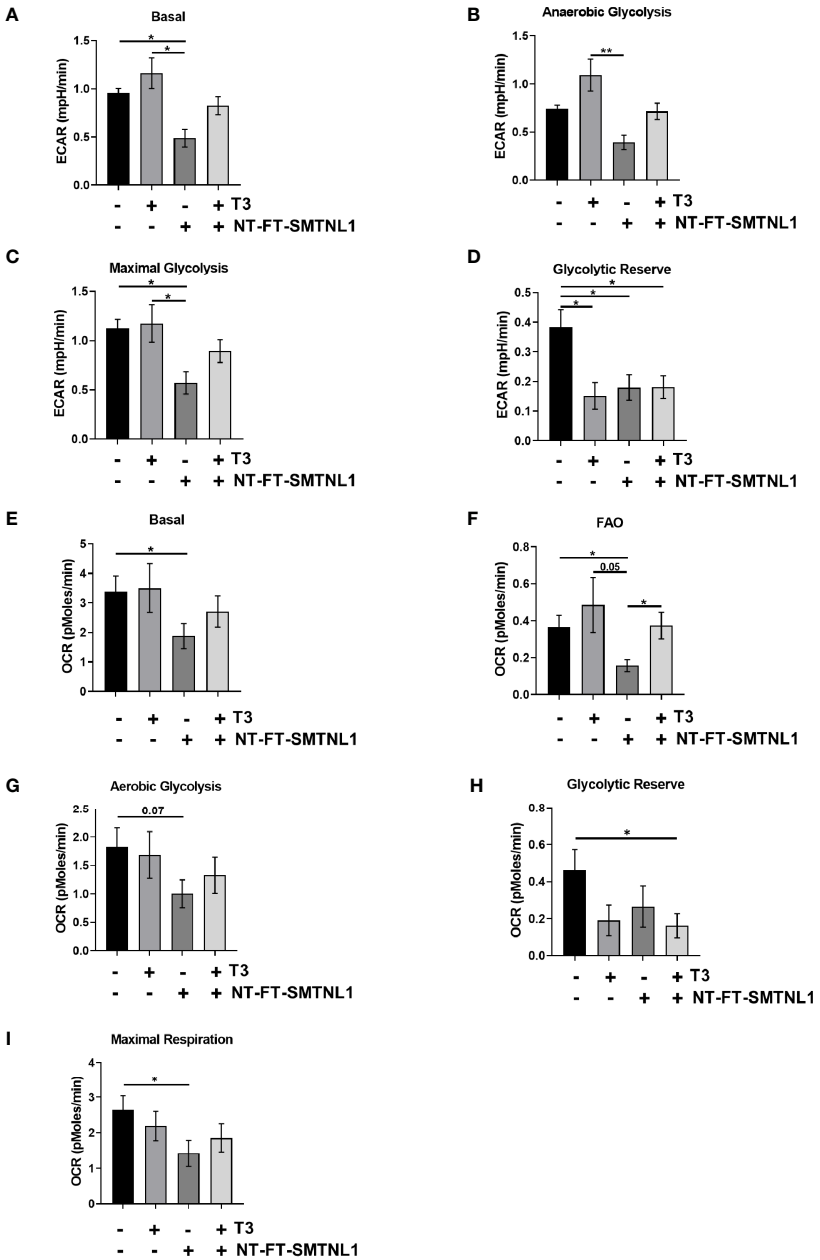


FIGURE 9 | Measurement of Extracellular Acidification Rate (ECAR) and Oxygen Consumption Rate (OCR) by SeaHorse Analysis of C2C12 Myoblasts. **(A–I)** Following a 72-hour T3 treatment of empty vector or NT-FT-SMTNL1-transfected myoblasts, XF assay media supplemented with glucose was added to the cells. Myoblasts and the previously hydrated XF sensor cartridge loaded with inhibitors, etomoxir (50 μM), oligomycin (2 μM), FCCP (4 μM) and antimycin (10 μM) + 2-deoxy-D-glucose (100 mM), were incubated in a non-CO_2 incubator before the assay. The rate of proton concentration increase **(A–D)** and the rate of oxygen concentration decrease **(E–I)** were measured. Values represent 4 groups with 23 technical replicates/group, n=2, mean +/- SEM. Data were normalized to protein content. Groups were compared using One-way ANOVA and Tukey's post hoc test, $p < 0.05$ (*), $p < 0.01$ (**).

(20.8%), and type IIb (44.2%) (43) in sternohyoid muscle. Our data show that during C2C12 differentiation, T3 increased desmin and MyHC expression, indicating a more prominent myotube formation and accelerated muscle cell differentiation. The expression of SMTNL1 increased parallel to SKM markers under physiological conditions (**Figures 4A–C**). These results are in line with previous data showing that type I fibers decrease and type IIa markers gradually increase during C2C12 cell differentiation (40).

Second, SMTNL1 also regulates normal muscle homeostasis and development in SKM by regulating T3 signaling elements. A drastic decrease in TRα expression was observed when SMTNL1

lontay.beata_285_24

was overexpressed under physiological and supraphysiological conditions (**Figure 5C**). These results are in agreement with a microarray analysis of SMTNL1 KO murine SKM that showed a significant elevation of nuclear receptor families, such as TRs; the ratio of TRα/TRβ expression decreased in SKM in response to hyperthyroidism (3). However, SMTNL1 affected neither the local control of T4 and T3 uptake by MCT8 nor T4 and T3 activation by DIO2 in SKM. These results suggest that SMTNL1 plays a regulatory role in TH signaling during SKM differentiation and development through the regulation of gene expression.

The capacity of THs to alter muscle phenotype is obvious for muscle performance and development in hyperthyroidism, but the phenotypic changes also affect whole-body glucose homeostasis. Patients with hyperthyroidism have elevated endogenous glucose production and often have disrupted intermediary metabolism associated with insulin resistance (44, 45). Physiological T3 levels enhance insulin signaling indirectly through insulin-induced activation of IRS1 and PI3K without affecting insulin receptor (IR) protein levels or phosphorylation (46). SMTNL1 regulates the gene expression of insulin signaling elements and promotes glycolysis and insulin sensitivity (24). Herein, we also demonstrated the impact of SMTNL1 on the metabolic properties of SKM. Current evidence suggests that excessive Ser phosphorylation of IR or downstream signaling molecules play a pivotal role in the pathogenesis of insulin resistance in SKM. Phosphorylation of IRS1 at Ser307 and Ser612 prevents interactions between IRS1, IRβ, and PI3K, leading to defective insulin signaling (47). Supraphysiological levels of T3 elevate the phosphorylation of IRS1 at Ser307 and Ser612 residues and SMTNL1 overexpression attenuates Ser phosphorylation of IRS1, suggesting insulin-sensitizing effects of SMTNL1 (**Figures 6B, C**). In hyperthyroid conditions, the downregulation of SMTNL1 resulted in an increase in JNK activity and consequently $IRS1^{S307}$ phosphorylation. As JNK expression was unchanged, changes in IRS1 Ser phosphorylation are likely due to altered expression of Dual Specific Phosphatase-9 (DUSP9). DUSP9 is positively regulated by SMTNL1 (24) and dephosphorylates and inactivates JNK (48). In prolonged T3 exposure, inhibition of SMTNL1 also caused an increase in PKCδ expression, another IRS-kinase (**Figure 7D**). PKCδ is associated with increased $IRS1^{S307}$ (49) and ERK1/2 activation (50). ERK1/2 is also activated by elevated T3 exposure (**Figure 7B**) *via* a non-genomic effect and its activity is responsible for $IRS1^{S612}$ phosphorylation (51).

Hyperthyroidism is a hypermetabolic state characterized by increased demand for glucose, which is provided by increased glucose transport and phosphorylation and lactate formation (19). Thyrotoxic subjects show increased glucose turnover with elevated peripheral glucose transport and utilization (20). SKM of hyperthyroid rats exhibited an increase in the number and translocation of GLUT4 to the sarcolemma in response to insulin (52, 53). In our model, prolonged T3 exposure enhanced the expression of GLUT4 suggesting its genomic action on glucose transport.SMTNL1 overexpression also elevate GLUT4 level. In addition, deletion of *SMTNL1* is known to reduce GLUT4 protein expression in SKM (24). Here, we show that SMTNL1 elicits insulin-sensitizing effects by markedly increasing GLUT4 expression and reducing Ser phosphorylation of IRS1 ameliorating the malfunction of insulin signaling (**Figures 5** and **7**). In this manner, SMTNL1 may be able to restore the normal responsiveness of glucose transport to insulin.

As insulin-stimulated rates of glycogen synthesis are reduced in muscle during hyperthyroidism, glucose residues are utilized by glycolysis and converted to glucose-6-phosphate catalyzed by hexokinases (HKs) (54). Both the expression and activity of HK II, the most abundant isoform in muscle, are increased in hyperthyroid muscle leading to enhanced glucose phosphorylation (55–57). HK II levels were elevated in hyperthyroid conditions and SMTNL1 overexpression attenuated this effect (**Figure 8B**). This result is supported by previous results in SMTNL1 KO mice showing an increase of HK II in SKM (24).

Hyperthyroidism also increases the rates of lactate formation and glucose oxidation in SKM; however, lactate formation is preferentially increased over glucose oxidation (58). The increase in acidification may be due to the enhanced rate of glycogenolysis observed in hyperthyroidism (19). Our data are supported by cellular bioenergetics measurements on DIO2-overexpressing C2C12 cells showing that increased intracellular T3 level caused a shift to glycolysis and increased ECAR (59). Similarly, deletion of *SMTNL1* also leads to elevated glycogenolysis in mice (24). Our data are in line with these findings; T3 overload strongly induced anaerobic glycolysis, which was accompanied by a fall in glycolytic reserve. T3 overload did not affect maximum glycolysis compared to the control. Interestingly, SMTNL1 overexpression not only prevented this increase in anaerobic glycolysis but also caused a massive drop in basal and maximal glycolysis (**Figure 9**).

Another regulator of metabolism through the regulation of mitochondrial biogenesis is AMP-activated protein kinase (AMPK), which is increased in SKM of hyperthyroid rats (28). The activation of AMPK evokes important downstream effects on non-genomic T3 signaling in the experimental hyperthyroid model of SKM (**Figure 7A**), resulting in chronic activation of AMPK and increased energy demand. In addition, PP2A expression is decreased (**Figure 7E**), leading to persistent phosphorylation of AMPK (60). Moreover, basal oxygen consumption and fatty acid oxidation were elevated in response to elevated T3. Of note, SMTNL1 did not affect AMPK activity, nor did SMTNL1 antagonize the T3 effects on AMPK. Based on these data, SMTNL1 appears to have not just a T3-antagonistic effect but also a role in metabolic regulation mainly through the control of glycolysis under hyperthyroid conditions.

SMTNL1 modulation holds great promise for treating hyperthyroidism for the following reasons: 1) SMTNL1 regulates muscle cell differentiation and compensates for the glycolytic shift in SKM triggered by pathological T3 exposure;

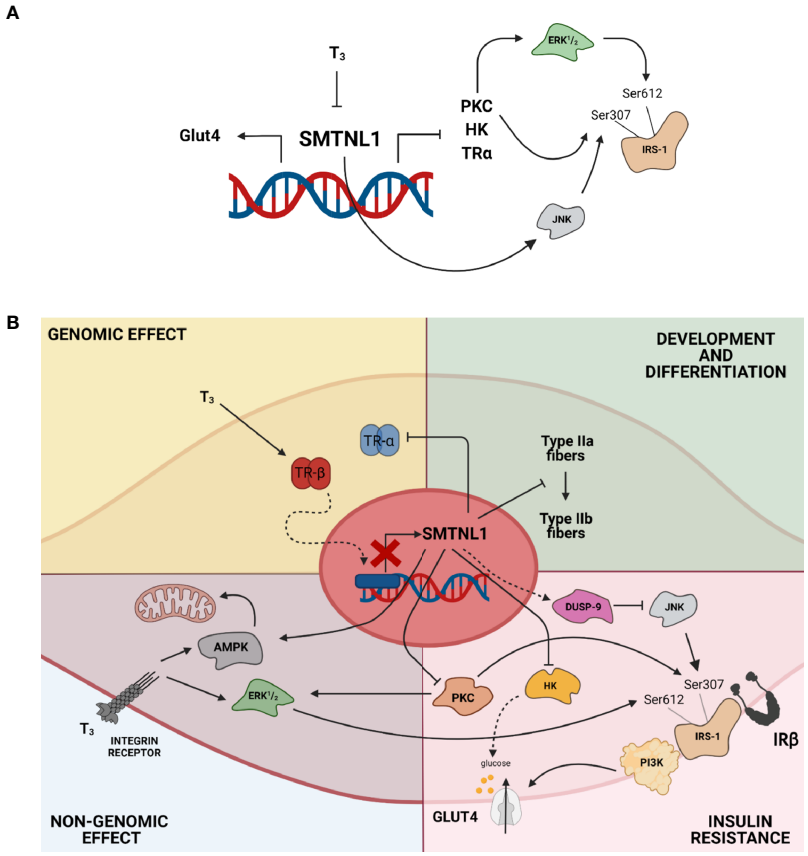


FIGURE 10 | SMTNL1 maintains the homeostasis of SKM in hyperthyroidism. **(A, B)** SMTNL1 potentially prevents hyperthyroidism-induced changes in SKM *via* the following mechanisms: 1) SMTNL1 compensates for the glycolytic phenotype shift of SKM triggered by pathological T3 exposure; 2) SMTNL1 induces insulin sensitivity through an insulin-independent heterologous pathway by inhibiting the activity of JNK; 3) SMTNL1 hampers the non-genomic effect of T3 by decreasing the activity of ERK1/2 through PKCδ; 4) SMTNL1 regulates glucose phosphorylation and balances glycolysis and glycogen synthesis by the regulation of HK II; and 5) SMTNL1 selectively inhibits TRα expression, which is a key target of insulin-dependent signaling governed by T3.

2) SMTNL1 induces insulin sensitivity through an insulin-independent heterologous pathway by inhibiting JNK activity; 3) SMTNL1 hampers the non-genomic effects of T3 by decreasing the activity of ERK1/2 through PKCδ; 4) SMTNL1 regulates glucose phosphorylation and balances glycolysis and glycogen synthesis *via* the regulation of HK II; and 5) SMTNL1 selectively inhibits TRα expression, which is a key target of insulin-dependent signaling governed by T3. The overexpression of SMTNL1 or an SMTNL1-mimicking membrane-permeable peptide might counteract the effects of hyperthyroidism selectively in SKM, promoting insulin-sensitizing effects and maintaining the homeostasis of SKM (**Figure 10**).

DATA AVAILABILITY STATEMENT

The datasets presented in this study can be found in online repositories. The names of the repository/repositories and accession number(s) can be found in the article.

ETHICS STATEMENT

The studies involving human participants were reviewed and approved by Regional and Institutional Ethics Committee of the University of Debrecen and were in accordance with guidelines of the European Union Council and Hungarian regulations under license number DEOEC RKEB/IKEB 3517-2011. The patients/participants provided their written informed consent to participate in this study.

AUTHOR CONTRIBUTIONS

BL and PF: conceptualization. EM and BL: data curation. EM and IK: visualization. EM, DH, FG, and IT: methodology. FG: tissue collection. EM: prepared figures and analyzed data. PF and BL: funding acquisition. EM, PF, KU, and BL wrote and reviewed the manuscript. All authors contributed to the article and approved the submitted version.

lontay.beata_285_24

FUNDING

This work was supported by grants from the National Research, Development and Innovation Office (FK125043), the University of Debrecen, Faculty of Medicine Research Fund (1G3DBKJ0BFTK 247) for BL, from the EU co-financed by the European Regional Development Fund under project EFOP-3.6.2-16-2017-00006 and from the EFOP-3.6.3-VEKOP-16-2017-00009 project co-financed by EU and the European Social Fund. BL and PF MECENATURA from the University of Debrecen.

ACKNOWLEDGMENTS

We would like to thank Dr Szilárd Póliska for Affymetrix Analysis and Andrea Docsa, Ágota Kelemenné Szántó and Adam Ungvari for technical assistance.

SUPPLEMENTARY MATERIAL

The Supplementary Material for this article can be found online at: https://www.frontiersin.org/articles/10.3389/fendo.2021.751488/full#supplementary-material

REFERENCES

1. De Leo S, Lee SY, Braverman LE. Hyperthyroidism. *Lancet* (2016) 388:906–18. doi: 10.1016/S0140-6736(16)00278-6
2. Boelaert K, Franklyn JA. Thyroid Hormone in Health and Disease. *J Endocrinol* (2005) 187:1–15. doi: 10.1677/joe.1.06131
3. Haddad F, Qin AX, McCue SA, Baldwin KM. Thyroid Receptor Plasticity in Striated Muscle Types: Effects of Altered Thyroid State. *Am J Physiol* (1998) 274:E1018–26. doi: 10.1152/ajpendo.1998.274.6.E1018
4. Evans RM. The Steroid and Thyroid Hormone Receptor Superfamily. *Science* (1988) 240:889–95. doi: 10.1126/science.3283939
5. Williams GR. Cloning and Characterization of Two Novel Thyroid Hormone Receptor Beta Isoforms. *Mol Cell Biol* (2000) 20:8329–42. doi: 10.1128/MCB.20.22.8329-8342.2000
6. Salvatore D, Simonides WS, Dentice M, Zavacki AM, Larsen PR. Thyroid Hormones and Skeletal Muscle–New Insights and Potential Implications. *Nat Rev Endocrinol* (2014) 10:206–14. doi: 10.1038/nrendo.2013.238
7. Bloise FF, Oliveira TS, Cordeiro A, Ortiga-Carvalho TM. Thyroid Hormones Play Role in Sarcopenia and Myopathies. *Front Physiol* (2018) 9:560. doi: 10.3389/fphys.2018.00560
8. Di Cosmo C, Liao XH, Ye H, Ferrara AM, Weiss RE, Refetoff S, et al. Mct8-Deficient Mice Have Increased Energy Expenditure and Reduced Fat Mass That is Abrogated by Normalization of Serum T3 Levels. *Endocrinology* (2013) 154:4885–95. doi: 10.1210/en.2013-1150
9. Mebis L, Paletta D, Debaveye Y, Ellger B, Langouche L, D'Hoore A, et al. Expression of Thyroid Hormone Transporters During Critical Illness. *Eur J Endocrinol* (2009) 161:243–50. doi: 10.1530/EJE-09-0290
10. Ambrosio R, De Stefano MA, Di Girolamo D, Salvatore D. Thyroid Hormone Signaling and Deiodinase Actions in Muscle Stem/Progenitor Cells. *Mol Cell Endocrinol* (2017) 459:79–83. doi: 10.1016/j.mce.2017.06.014
11. Ortiga-Carvalho TM, Chiamolera MI, Pazos-Moura CC, Wondisford FE. Hypothalamus-Pituitary-Thyroid Axis. *Compr Physiol* (2016) 6:1387–428. doi: 10.1002/cphy.c150027
12. Huang YH, Tsai MM, Lin KH. Thyroid Hormone Dependent Regulation of Target Genes and Their Physiological Significance. *Chang Gung Med J* (2008) 31:325–34.
13. Cordeiro A, Souza LL, Einicker-Lamas M, Pazos-Moura CC. Non-Classic Thyroid Hormone Signalling Involved in Hepatic Lipid Metabolism. *J Endocrinol* (2013) 216:R47–57. doi: 10.1530/JOE-12-0542
14. Incerpi S, Luly P, De Vito P, Farias RN. Short-Term Effects of Thyroid Hormones on the Na/H Antiport in L-6 Myoblasts: High Molecular Specificity for 3,3',5-Triiodo-L-Thyronine. *Endocrinology* (1999) 140:683–9. doi: 10.1210/endo.140.2.6535
15. Irrcher I, Walkinshaw DR, Sheehan TE, Hood DA. Thyroid Hormone (T3) Rapidly Activates P38 and AMPK in Skeletal Muscle In Vivo. *J Appl Physiol (1985)* (2008) 104:178–85. doi: 10.1152/japplphysiol.00643.2007
16. Bloise FF, Cordeiro A, Ortiga-Carvalho TM. Role of Thyroid Hormone in Skeletal Muscle Physiology. *J Endocrinol* (2018) 236:R57–68. doi: 10.1530/JOE-16-0611
17. Simonides WS, van Hardeveld C. Thyroid Hormone as a Determinant of Metabolic and Contractile Phenotype of Skeletal Muscle. *Thyroid* (2008) 18:205–16. doi: 10.1089/thy.2007.0256
18. Saltiel AR, Kahn CR. Insulin Signalling and the Regulation of Glucose and Lipid Metabolism. *Nature* (2001) 414:799–806. doi: 10.1038/414799a
19. Mitrou P, Raptis SA, Dimitriadis G. Insulin Action in Hyperthyroidism: A Focus on Muscle and Adipose Tissue. *Endocr Rev* (2010) 31:663–79. doi: 10.1210/er.2009-0046
20. Brunetto EL, Teixeira Sda S, Giannocco G, Machado UF, Nunes MT. T3 Rapidly Increases SLC2A4 Gene Expression and GLUT4 Trafficking to the Plasma Membrane in Skeletal Muscle of Rat and Improves Glucose Homeostasis. *Thyroid* (2012) 22:70–9. doi: 10.1089/thy.2010.0409
21. Teixeira SS, Tamrakar AK, Goulart-Silva F, Serrano-Nascimento C, Klip A, Nunes MT. Triiodothyronine Acutely Stimulates Glucose Transport Into L6 Muscle Cells Without Increasing Surface GLUT4, GLUT1, or GLUT3. *Thyroid* (2012) 22:747–54. doi: 10.1089/thy.2011.0422
22. Borman MA, MacDonald JA, Haystead TA. Modulation of Smooth Muscle Contractility by CHASM, a Novel Member of the Smoothelin Family of Proteins. *FEBS Lett* (2004) 573:207–13. doi: 10.1016/j.febslet.2004.08.002
23. Lontay B, Bodoor K, Weitzel DH, Loiselle D, Fortner C, Lengyel S, et al. Smoothelin-Like 1 Protein Regulates Myosin Phosphatase-Targeting Subunit 1 Expression During Sexual Development and Pregnancy. *J Biol Chem* (2010) 285:29357–66. doi: 10.1074/jbc.M110.143966
24. Lontay B, Bodoor K, Sipos A, Weitzel DH, Loiselle D, Safi R, et al. Pregnancy and Smoothelin-Like Protein 1 (SMTNL1) Deletion Promote the Switching of Skeletal Muscle to a Glycolytic Phenotype in Human and Mice. *J Biol Chem* (2015) 290:17985–98. doi: 10.1074/jbc.M115.658120
25. Dedinszki D, Sipos A, Kiss A, Batori R, Konya Z, Virag L, et al. Protein Phosphatase-1 is Involved in the Maintenance of Normal Homeostasis and in UVA Irradiation-Induced Pathological Alterations in Hacat Cells and in Mouse Skin. *Biochim Biophys Acta* (2015) 1852:22–33. doi: 10.1016/j.bbadis.2014.11.005
26. Sipos A, Ivan J, Becsi B, Darula Z, Tamas I, Horvath D, et al. Myosin Phosphatase and Rhoa-Activated Kinase Modulate Arginine Methylation by the Regulation of Protein Arginine Methyltransferase 5 in Hepatocellular Carcinoma Cells. *Sci Rep* (2017) 7:40590. doi: 10.1038/srep40590
27. Wong CY, Al-Salami H, Dass CR. C2C12 Cell Model: Its Role in Understanding of Insulin Resistance at the Molecular Level and Pharmaceutical Development at the Preclinical Stage. *J Pharm Pharmacol* (2020) 72:1667–93. doi: 10.1111/jphp.13359
28. Branvold DJ, Allred DR, Beckstead DJ, Kim HJ, Fillmore N, Condon BM, et al. Thyroid Hormone Effects on LKB1, MO25, Phospho-AMPK, Phospho-CREB, and PGC-1alpha in Rat Muscle. *J Appl Physiol* (2008) 105:1218–27. (1985). doi: 10.1152/japplphysiol.00997.2007
29. Thorson L. Thyroid Diseases in Rodent Species. *Vet Clin North Am Exot Anim Pract* (2014) 17:51–67. doi: 10.1016/j.cvex.2013.09.002
30. Kenessey A, Ojamaa K. Ligand-Mediated Decrease of Thyroid Hormone Receptor-Alpha1 in Cardiomyocytes by Proteosome-Dependent Degradation and Altered mRNA Stability. *Am J Physiol Heart Circ Physiol* (2005) 288:H813–21. doi: 10.1152/ajpheart.00804.2004
31. Muscat GE, Mynett-Johnson L, Dowhan D, Downes M, Griggs R. Activation of Myod Gene Transcription by 3,5,3'-Triiodo-L-Thyronine: A Direct Role for the Thyroid Hormone and Retinoid X Receptors. *Nucleic Acids Res* (1994) 22:583–91. doi: 10.1093/nar/22.4.583
32. Lee JW, Kim NH, Milanesi A. Thyroid Hormone Signaling in Muscle Development, Repair and Metabolism. *J Endocrinol Diabetes Obes* (2014) 2:1046.
33. Brenta G. Why can Insulin Resistance be a Natural Consequence of Thyroid Dysfunction? *J Thyroid Res* (2011) 2011:152850. doi: 10.4061/2011/152850

lontay.beata_285_24

34. Clement K, Viguerie N, Diehn M, Alizadeh A, Barbe P, Thalamas C, et al. In Vivo Regulation of Human Skeletal Muscle Gene Expression by Thyroid Hormone. *Genome Res* (2002) 12:281–91. doi: 10.1101/gr.207702
35. Bodoor K, Lontay B, Safi R, Weitzel DH, Loiselle D, Wei Z, et al. Smoothelin-Like 1 Protein is a Bifunctional Regulator of the Progesterone Receptor During Pregnancy. *J Biol Chem* (2011) 286:31839–51. doi: 10.1074/jbc.M111.270397
36. Ulke-Lemee A, Turner SR, Mughal SH, Borman MA, Winkfein RJ, MacDonald JA. Mapping and Functional Characterization of the Murine Smoothelin-Like 1 Promoter. *BMC Mol Biol* (2011) 12:10. doi: 10.1186/1471-2199-12-10
37. Desbois C, Aubert D, Legrand C, Pain B, Samarut J. A Novel Mechanism of Action for V-Erba: Abrogation of the Inactivation of Transcription Factor AP-1 by Retinoic Acid and Thyroid Hormone Receptors. *Cell* (1991) 67:731–40. doi: 10.1016/0092-8674(91)90068-A
38. Miner JN, Diamond MI, Yamamoto KR. Joints in the Regulatory Lattice: Composite Regulation by Steroid Receptor-AP1 Complexes. *Cell Growth Differ* (1991) 2:525–30.
39. Lee SH, Kim BJ, Park DR, Kim UH. Exercise Induces Muscle Fiber Type Switching *via* Transient Receptor Potential Melastatin 2-Dependent Ca(2+) Signaling. *J Appl Physiol* (2018) 124:364–73. doi: 10.1152/japplphysiol.00687.2017
40. Brown DM, Parr T, Brameld JM. Myosin Heavy Chain Mrna Isoforms are Expressed in Two Distinct Cohorts During C2C12 Myogenesis. *J Muscle Res Cell Motil* (2012) 32:383–90. doi: 10.1007/s10974-011-9267-4
41. Izumo S, Nadal-Ginard B, Mahdavi V. All Members of the MHC Multigene Family Respond to Thyroid Hormone in a Highly Tissue-Specific Manner. *Science* (1986) 231:597–600. doi: 10.1126/science.3945800
42. Smerdu V, Soukup T. Demonstration of Myosin Heavy Chain Isoforms in Rat and Humans: The Specificity of Seven Available Monoclonal Antibodies Used in Immunohistochemical and Immunoblotting Methods. *Eur J Histochem* (2008) 52:179–90. doi: 10.4081/1210
43. Rhee HS, Hoh JF. Immunohistochemical Analysis of the Effects of Cross-Innervation of Murine Thyroarytenoid and Sternohyoid Muscles. *J Histochem Cytochem* (2010) 58:1057–65. doi: 10.1369/jhc.2010.956706
44. Chu CH, Lam HC, Lee JK, Lu CC, Sun CC, Wang MC, et al. Hyperthyroidism-Associated Insulin Resistance is Not Mediated by Adiponectin Levels. *J Thyroid Res* (2011) 2011:194721. doi: 10.4061/2011/194721
45. Dimitriadis G, Baker B, Marsh H, Mandarino L, Rizza R, Bergman R, et al. Effect of Thyroid Hormone Excess on Action, Secretion, and Metabolism of Insulin in Humans. *Am J Physiol* (1985) 248:E593–601. doi: 10.1152/ajpendo.1985.248.5.E593
46. Lin Y, Sun Z. Thyroid Hormone Potentiates Insulin Signaling and Attenuates Hyperglycemia and Insulin Resistance in a Mouse Model of Type 2 Diabetes. *Br J Pharmacol* (2011) 162:597–610. doi: 10.1111/j.1476-5381.2010.01056.x
47. Tanti JF, Jager J. Cellular Mechanisms of Insulin Resistance: Role of Stress-Regulated Serine Kinases and Insulin Receptor Substrates (IRS) Serine Phosphorylation. *Curr Opin Pharmacol* (2009) 9:753–62. doi: 10.1016/j.coph.2009.07.004
48. Sabio G, Davis RJ. Cjun NH2-Terminal Kinase 1 (JNK1): Roles in Metabolic Regulation of Insulin Resistance. *Trends Biochem Sci* (2010) 35:490–6. doi: 10.1016/j.tibs.2010.04.004
49. Greene MW, Morrice N, Garofalo RS, Roth RA. Modulation of Human Insulin Receptor Substrate-1 Tyrosine Phosphorylation by Protein Kinase Cdelta. *Biochem J* (2004) 378:105–16. doi: 10.1042/bj20031493
50. Ueda Y, Hirai S, Osada S, Suzuki A, Mizuno K, Ohno S. Protein Kinase C Activates the MEK-ERK Pathway in a Manner Independent of Ras and Dependent on Raf. *J Biol Chem* (1996) 271:23512–9. doi: 10.1074/jbc.271.38.23512
51. Gual P, Le Marchand-Brustel Y, Tanti JF. Positive and Negative Regulation of Insulin Signaling Through IRS-1 Phosphorylation. *Biochimie* (2005) 87:99–109. doi: 10.1016/j.biochi.2004.10.019
52. Weinstein SP, O'Boyle E, Haber RS. Thyroid Hormone Increases Basal and Insulin-Stimulated Glucose Transport in Skeletal Muscle. The Role of GLUT4 Glucose Transporter Expression. *Diabetes* (1994) 43:1185–9. doi: 10.2337/diab.43.10.1185
53. Weinstein SP, Watts J, Haber RS. Thyroid Hormone Increases Muscle/Fat Glucose Transporter Gene Expression in Rat Skeletal Muscle. *Endocrinology* (1991) 129:455–64. doi: 10.1210/endo-129-1-455
54. Dimitriadis GD, Leighton B, Vlachonikolis IG, Parry-Billings M, Challiss RA, West D, et al. Effects of Hyperthyroidism on the Sensitivity of Glycolysis and Glycogen Synthesis to Insulin in the Soleus Muscle of the Rat. *Biochem J* (1988) 253:87–92. doi: 10.1042/bj2530087
55. Mandarino LJ, Printz RL, Cusi KA, Kinchington P, O'Doherty RM, Osawa H, et al. Regulation of Hexokinase II and Glycogen Synthase Mrna, Protein, and Activity in Human Muscle. *Am J Physiol* (1995) 269:E701–8. doi: 10.1152/ajpendo.1995.269.4.E701
56. Martins Pecanha FL, Dos Santos RS, da-Silva WS. Thyroid States Regulate Subcellular Glucose Phosphorylation Activity in Male Mice. *Endocr Connect* (2017) 6:311–22. doi: 10.1530/EC-17-0059
57. Dimitriadis G, Parry-Billings M, Bevan S, Leighton B, Krause U, Piva T, et al. The Effects of Insulin on Transport and Metabolism of Glucose in Skeletal Muscle From Hyperthyroid and Hypothyroid Rats. *Eur J Clin Invest* (1997) 27:475–83. doi: 10.1046/j.1365-2362.1997.1380688.x
58. Dimitriadis GD, Richards SJ, Parry-Billings M, Leighton B, Newsholme EA, Challiss RA. Beta-Adrenoceptor-Agonist and Insulin Actions on Glucose Metabolism in Rat Skeletal Muscle in Different Thyroid States. *Biochem J* (1991) 278(Pt 2):587–93. doi: 10.1042/bj2780587
59. Sagliocchi S, Cicatiello AG, Di Cicco E, Ambrosio R, Miro C, Di Girolamo D, et al. The Thyroid Hormone Activating Enzyme, Type 2 Deiodinase, Induces Myogenic Differentiation by Regulating Mitochondrial Metabolism and Reducing Oxidative Stress. *Redox Biol* (2019) 24:101228. doi: 10.1016/j.redox.2019.101228
60. Joseph BK, Liu HY, Francisco J, Pandya D, Donigan M, Gallo-Ebert C, et al. Inhibition of AMP Kinase by the Protein Phosphatase 2A Heterotrimer, PP2APpp2r2d. *J Biol Chem* (2015) 290:10588–98. doi: 10.1074/jbc.M114.626259

Conflict of Interest: The authors declare that the research was conducted in the absence of any commercial or financial relationships that could be construed as a potential conflict of interest.

Publisher's Note: All claims expressed in this article are solely those of the authors and do not necessarily represent those of their affiliated organizations, or those of the publisher, the editors and the reviewers. Any product that may be evaluated in this article, or claim that may be made by its manufacturer, is not guaranteed or endorsed by the publisher.

Copyright © 2021 Major, Győry, Horváth, Keller, Tamás, Uray, Fülöp and Lontay. This is an open-access article distributed under the terms of the Creative Commons Attribution License (CC BY). The use, distribution or reproduction in other forums is permitted, provided the original author(s) and the copyright owner(s) are credited and that the original publication in this journal is cited, in accordance with accepted academic practice. No use, distribution or reproduction is permitted which does not comply with these terms.

GLOSSARY

2-DG	2-deoxy-D-glucose
8BrcAMP	8-Bromoadenosine 3',5'-cyclic monophosphate
AMPK	AMP-activated protein kinase
DIO2	iodothyronine deiodinase type 2
DMEM	Dulbecco's Modified Eagle's Medium
DUSP	dual specific phosphatase-9
ECAR	extracellular acidification rate
ECL	enhanced chemilumineswfi 2cence
ERK1/2	extracellular signal-regulated kinase
FAO	fatty acid oxidation
FBS	fetal bovine serum
FCCP	carbonyl cyanide-p-trifluoromethoxyphenylhydrazone
GLUT4	glucose transport molecule 4
GR	glucocortiocoid receptor
HK II	hexokinase II
HRP	horseradish peroxidase
HS	horse serum
IR	insulin receptor
IRS1	insulin receptor substrate 1
MCT8	monocarboxylate transporter 8
mTOR	mammalian target of rapamycin
MyHC	myosin heavy chain
MyoD1	myogenic differentiation 1
OCR	oxygen consumption rate
PI3K	phosphatidylinositol 3-kinase
PKA	protein kinase A
PKCδ	protein kinase C delta
PP2Aα	protein phosphatase 2A alpha
RIPA	radioimmunoprecipitation assay buffer
RXR	retinoid X receptor
SAPK/JNK	stress-activated protein kinase/Jun N-terminal kinase
SKM	skeletal muscle
SMTNL1	smoothelin-like protein 1
T3	3,3′,5-Triiodo-L-thyronine
T4	thyroxine
TH	thyroid hormone
TR	thyroid receptor
TRE	thyroid-responsive element

lontay.beata_285_24

International Journal of *Molecular Sciences*

MDPI

Article

Smoothelin-like Protein 1 Regulates the Thyroid Hor-Mone-Induced Homeostasis and Remodeling of C2C12 Cells via the Modulation of Myosin Phosphatase

Evelin Major, Ilka Keller, Dániel Horváth, István Tamás, Ferenc Erdődi and Beáta Lontay *

Department of Medical Chemistry, Faculty of Medicine, University of Debrecen, H-4032 Debrecen, Hungary; evelinmajor@med.unideb.hu (E.M.); ilka.keller@med.unideb.hu (I.K.); horvath.daniel@med.unideb.hu (D.H.); tamas.istvan@med.unideb.hu (I.T.); erdodi@med.unideb.hu (F.E.)

* Correspondence: lontay@med.unideb.hu; Tel.: +36-52-412-345

Abstract: The pathological elevation of the active thyroid hormone (T_3) level results in the manifestation of hyperthyroidism, which is associated with alterations in the differentiation and contractile function of skeletal muscle (SKM). Myosin phosphatase (MP) is a major cellular regulator that hydrolyzes the phosphoserine of phosphorylated myosin II light chain. MP consists of an MYPT1/2 regulatory and a protein phosphatase 1 catalytic subunit. Smoothelin-like protein 1 (SMTNL1) is known to inhibit MP by directly binding to MP as well as by suppressing the expression of MYPT1 at the transcriptional level. Supraphysiological vs. physiological concentration of T_3 were applied on C2C12 myoblasts and differentiated myotubes in combination with the overexpression of SMTNL1 to assess the role and regulation of MP under these conditions. In non-differentiated myoblasts, MP included MYPT1 in the holoenzyme complex and its expression and activity was regulated by SMTNL1, affecting the phosphorylation level of MLC20 assessed using semi-quantitative Western blot analysis. SMTNL1 negatively influenced the migration and cytoskeletal remodeling of myoblasts measured by high content screening. In contrast, in myotubes, the expression of MYPT2 but not MYPT1 increased in a T_3-dependent and SMTNL1-independent manner. T_3 treatment combined with SMTNL1 overexpression impeded the activity of MP. In addition, MP interacted with Na^+/K^+-ATPase and dephosphorylated its inhibitory phosphorylation sites, identifying this protein as a novel MP substrate. These findings may help us gain a better understanding of myopathy, muscle weakness and the disorder of muscle regeneration in hyperthyroid patients.

Keywords: SMTNL1; thyroid hormone; C2C12 cell migration; myogenesis; myosin phosphatase; Na^+/K^+-ATPase

Citation: Major, E.; Keller, I.; Horváth, D.; Tamás, I.; Erdődi, F.; Lontay, B. Smoothelin-Like Protein 1 Regulates the Thyroid Hor-Mone-Induced Homeostasis and Remodeling of C2C12 Cells via the Modulation of Myosin Phosphatase. *Int. J. Mol. Sci.* **2021**, *22*, 10293. https://doi.org/10.3390/ijms221910293

Academic Editor: Maria Ruzzene

Received: 14 August 2021
Accepted: 21 September 2021
Published: 24 September 2021

Publisher's Note: MDPI stays neutral with regard to jurisdictional claims in published maps and institutional affiliations.

Copyright: © 2021 by the authors. Licensee MDPI, Basel, Switzerland. This article is an open access article distributed under the terms and conditions of the Creative Commons Attribution (CC BY) license (http://creativecommons.org/licenses/by/4.0/).

1. Introduction

Thyroid hormones (THs) have important regulatory actions in skeletal muscle (SKM) [1–3]. The main forms of thyroid hormone produced and secreted by the thyroid gland are tetraiodothyronine (T_4) and 3,3′,5-triiodothyronine (T_3). Although it has been assumed that THs enter cells by passive diffusion due to their lipophilic properties, THs are primarily transported through the cell membrane by the monocarboxylate transporter 8 (MCT8) in SKM [4]. T_4 is considered to be a prohormone and most of the peripheral effects of THs are ascribed to the action of T_3. Intracellular monodeiodination of T_4 by deiodinase type II (DIO2) produces T_3, the active form of thyroid hormone in SKM [5]. The final level of thyroid hormone signaling control is given by the expression of nuclear thyroid hormone receptors (TRs), which positively or negatively regulate the transcription of TH responsive genes [3]. Functional TRs mediate the vast majority of TH actions on the level of gene transcription; however, so-called non-genomic effects using other target molecules have been reported as well [6].

Pathological elevation in serum or tissue TH levels results in the manifestation of hyperthyroidism, which is associated with significant alterations in differentiation, contractile function and the metabolism of SKM [3]. Above all, hyperthyroidism is often accompanied by muscle weakness in the face, throat and respiratory muscle, and wasting of muscles around the shoulders and hips leading to hyperthyroid myopathy [7,8]. Even though several cellular mechanisms have been identified in muscle tissues [9], which can explain the observed effects on the molecular level, the detailed molecular mechanism is not fully characterized yet.

Filamentous contractile motor protein myosin II consists of two 200 kDa heavy chains and two pairs of light chains of 17 and 20 kDa. Regulation of myosin II by phosphorylation is essential in muscle contraction or in the motile and other functions of non-muscle cells, e.g., shape changes, cell division, cell adhesion, cell migration or regulation of ion channels. After the phosphorylation of the 20 kDa myosin light chain (MLC20), myosin II reversibly binds to actin filaments via cross-bridges initiating contractile or motile events [10]. MLC20 phosphorylation depends on the balance between Ca^{2+}/calmodulin-dependent myosin light chain kinase (MLCK) and myosin phosphatase (MP) [11].

Myosin phosphatase (MP) is a heterotrimer enzyme that hydrolyses phosphorylated myosin II light chains, as well as other cytoskeletal and cellular proteins such as adducin, tau, SNAP25 and PRMT5, etc. [12]. MP consists of a type 1 protein phosphatase catalytic subunit δ isoform (PP1cδ), a myosin phosphatase target subunit (MYPT) and a ~20 kDa small subunit of a yet unknown function (M20). The MYPT protein family includes MYPT1 (PPP1R12A) [13], MYPT2 (PPP1R12B) [14], MYPT3 [15], protein phosphatase 1 myosin binding 85 kDa subunit (MBS85) [16] and TGF-β1-inhibited membrane-associated protein (TIMAP) [17], which are responsible for targeting PP1cδ to its substrates [18]. MYPT1, first identified in smooth muscle, is ubiquitously expressed in most eukaryotic cells. MYPT2 was found mainly in cardiac and skeletal muscles [14,19].

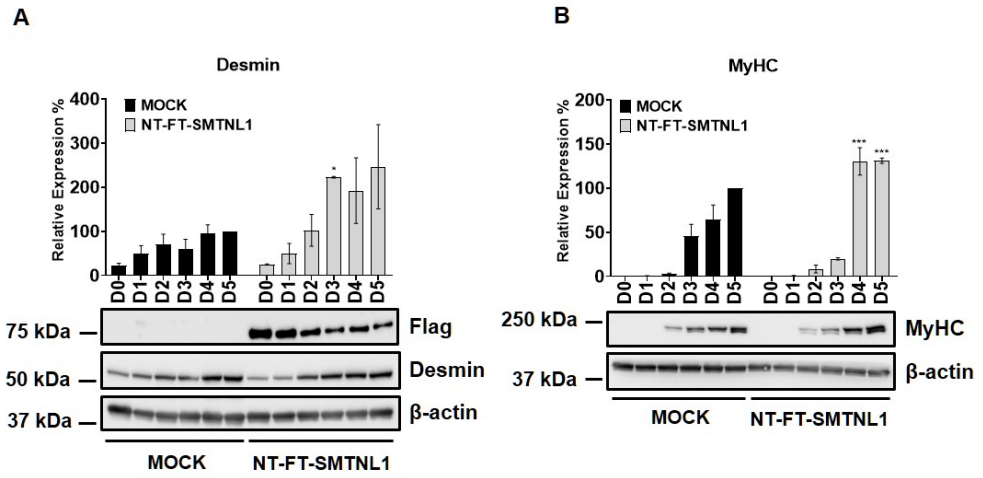
The activity of MP holoenzyme is regulated through several mechanisms. The phosphorylation of MYPT by a variety of Ser/Thr kinases is one of the principal regulatory mechanisms leading to the activation or inhibition of MP. The phosphorylation of MYPT1 on Thr^{696} and/or on Thr^{853} results in the inhibition of MP activity [20,21]. In addition, the phosphorylation of Thr^{853} in MYPT1 by RhoA- associated kinase (ROCK) triggers the dissociation of MYPT1 from its substrate, myosin [22]. On the other hand, MP can be regulated via the formation of protein–protein interactions: an example is association with the smoothelin-like protein 1 (SMTNL1). SMTNL1 was identified in gastrointestinal smooth muscle as an early target of protein kinase A and G (PKA/PKG) [23,24]; however, it is also expressed in SKM and steroid hormone sensitive tissues. SMTNL1 inhibits the activity of MP, thereby regulating muscle contraction and cytoskeletal elements in various cells [25,26]. Through the inhibition of MP, SMTNL1 could enhance the phosphorylation of MLC20. Besides that, SMTNL1 is a transcriptional regulator of the progesterone receptor-B (PR-B), thereby regulating the gene expression of numerous metabolic enzymes, cytoskeletal proteins, steroid receptors and cytokines [26]. SMTNL1 is downregulated in hyperthyroid SKM and it selectively inhibits TRα expression, which is a key target of insulin-dependent signaling governed by T_3. In addition, SMTNL1 overexpression reduced IRS1 Ser phosphorylation in a hyperthyroid model to restore the normal responsiveness of glucose transport to insulin [27].

Given the major role of thyroid hormones in the skeletal muscle system, it is important to study their actions as pathophysiological agents in myopathy. The objective of our work was to investigate the effect of supraphysiological vs. the physiological T_3 level on the expression and regulation of MP via the modulation of SMTNL1 in myoblast differentiation and the homeostasis of C2C12 myoblasts and myotubes.

2. Results

2.1. Overexpression of SMTNL1 Promotes C2C12 Mouse Myoblast Differentiation

Myogenic differentiation is a highly coordinated process, which is essential for the development and regeneration of skeletal muscle. The mouse myoblast cell line C2C12 is a widely used model to study skeletal muscle myogenesis in vivo [28–30]. SMTNL1, a transcriptional cofactor, has been shown to regulate the adaptation of skeletal muscle to sexual development [26] and pregnancy [28] through altering the expression of contractile and metabolic proteins. In order to investigate the possible physiological relevance of SMTNL1 in skeletal muscle differentiation, SMTNL1 was transiently overexpressed in C2C12 cells. Following transfection, myoblasts were differentiated and Western blot analysis (Figure 1A,B) or immunofluorescence staining (Figure 1C) was performed. Desmin, a major intermediate filament protein, is present at low levels at early stages of myogenesis, and its expression increases as normal differentiation proceeds [29]. Our results demonstrate that desmin levels were significantly elevated in the NT-FT-SMTNL1-transfected cells compared to the empty vector-transfected control on Day three (Figure 1A). However, by the end of differentiation, the empty vector-transfected cells showed the same expression level of desmin as the NT-FT-SMTNL1-overexpressed cells. We also examined the expression of a late myogenic marker, myosin heavy chain (MyHC), the expression of which increases sharply during regular differentiation [30]. Here, we show that MyHC expression significantly rose on Day four and Day five due to SMTNL1 overexpression compared to the control (Figure 1B). To further confirm the upregulation of desmin expression caused by SMTNL1 overexpression, we performed immunofluorescence staining on empty vector-transfected or NT-FT-SMTNL1-transfected cells. As shown in Figure 1C, NT-FT-SMTNL1 overexpressing cells showed stronger fluorescent signals even at Day zero of differentiation, which was more pronounced on Day five compared to the control. These results demonstrate that SMTNL1 overexpression leads to the upregulation of early and late myogenic markers, suggesting that SMTNL1 promotes myoblast differentiation. To assess morphological changes throughout the differentiation of empty vector-transfected and NT-FT-SMTNL1-transfected cells, light microscopy images with the same parameter settings were taken and used to calculate the average area, average perimeter and myotube number using ImageJ software (Figure S1A). We observed that SMTNL1 expression significantly decreases the average area and perimeter of myotubes on Day three and Day five of differentiation, respectively. However, SMTNL1 overexpression markedly increased the number of myotubes on Day three and Day five of differentiation. Taken together, these data indicate that SMTNL1 overexpression leads to accelerated myogenesis with myotubes that are significantly smaller in size but bigger in number.



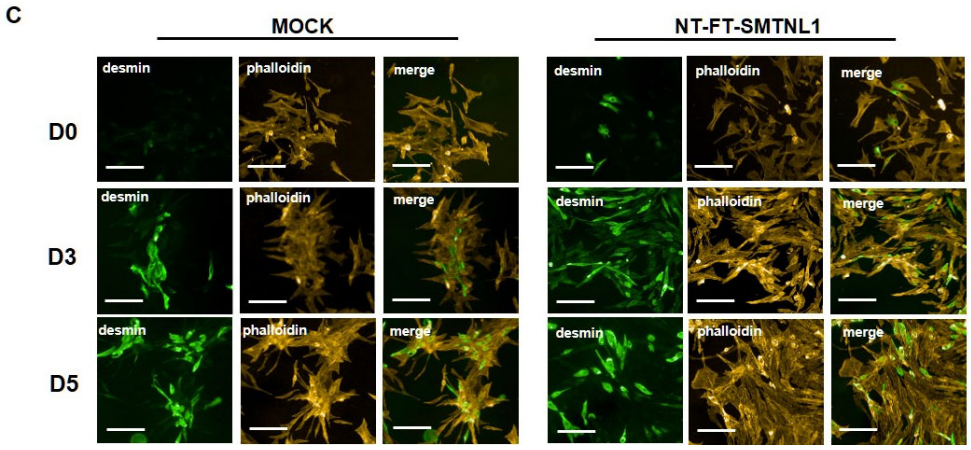


Figure 1. Effect of SMTNL1 overexpression on desmin and MyHC expression during myogenesis. Lysates from NT-FT-SMTNL1 or empty vector-transfected differentiated C2C12 cells were analyzed using Western blot with antibodies specific for early and late differentiation markers desmin (**A**) and MyHC (**B**), respectively. Transfection efficiency was determined using immunoblotting with anti-Flag antibody. Values represent $n = 3$, mean ± SEM. Differences between group means were determined using Two-way ANOVA followed by Sidak multiple comparisons post hoc test, $p < 0.05$ (*), $p < 0.001$ (***). (**C**) Immunofluorescent staining of cells at Day 0, Day 3 and Day 5 of differentiation after transfection with empty vector or NT-FT-SMTNL1. For staining, anti-desmin antibody (green) and Texas-Red Phalloidin (red) were used. Fluorescent signals were detected using an automated high-content screening instrument. Scale bars: 500 μm.

2.2. Myosin Phosphatase Expression during C2C12 Myogenesis in the Presence of Excess T_3

Intracellular T_3 hormone availability depends on the presence of TH transporters in the plasma membrane, the activity of iodothyronine deiodinases and the expression of TRs, from which DIO2 and TRα were proved to play crucial roles in myogenesis, too [31,32]. Moreover, Wu et al. described the importance of myosin phosphorylation throughout the course of C2C12 differentiation, which is known to be partially dependent on the activity of MP [33]. Thus, we investigated the effect of excess T_3 on these regulatory proteins during myoblast differentiation. MCT8 expression demonstrated a small increase during normal differentiation. In the presence of excess T_3, MCT8 expression decreased slightly by Day six, which was 24% smaller compared to the vehicle control (Figure 2A). The expression of DIO2 demonstrated a sharp increase from Day three to Day four and continued to rise until the end of regular differentiation. In response to T_3 treatment, DIO2 expression was induced consecutively until Day three and started to decline from Day four. By the end of differentiation, it was significantly diminished by 65% compared to the vehicle control (Figure 2B). In terms of TRα expression, it started to increase from Day four under regular differentiation. Upon T_3 treatment, the TRα levels were significantly reduced from Day four until the end of differentiation compared to the vehicle control (Figure 2C). MYPT1/2 and MYPT2 expression was gradually increased during normal differentiation, while it showed an opposite tendency in the presence of excess T_3 (Figure 3A,C). Despite the increase in MYPT1 expression on the first days of differentiation, it was reduced by Day six compared to the vehicle control (Figure 3B). Similarly, PP1cδ expression was moderately risen throughout normal differentiation; however, T_3 overload caused an increase at first, and a modest decrease in its expression by the end of differentiation (Figure 3D).

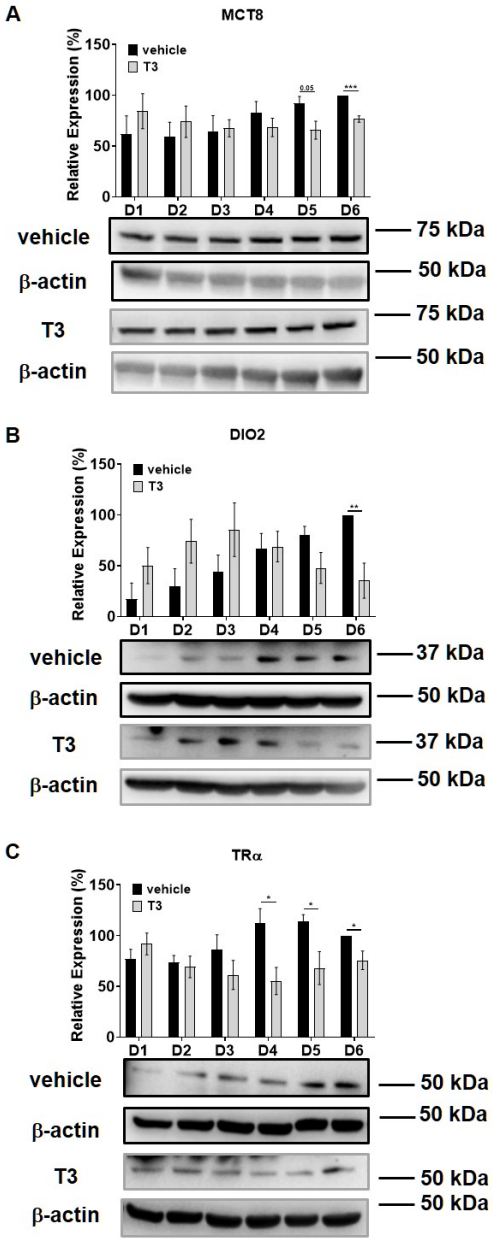


Figure 2. MCT8, DIO2 and TRα expression throughout the differentiation of C2C12 myoblasts in the presence of T_3. (**A–C**) Myoblasts were differentiated for 6 days receiving either 10 nM T_3 or equal amounts of HCl:EtOH solution. Proteins from whole-cell lysates were analyzed using Western blot with anti-MCT8 (**A**), anti-DIO2 (**B**) and anti-TRα (**C**) antibodies. Values represent n = 4–5, mean ± SEM. Data were normalized to the Day 6 vehicle control. Differences between group means were determined using Two-way ANOVA followed by Sidak post hoc test and by multiple unpaired two-tailed t-tests, $p < 0.05$ (*), $p < 0.01$ (**), $p < 0.001$ (***).

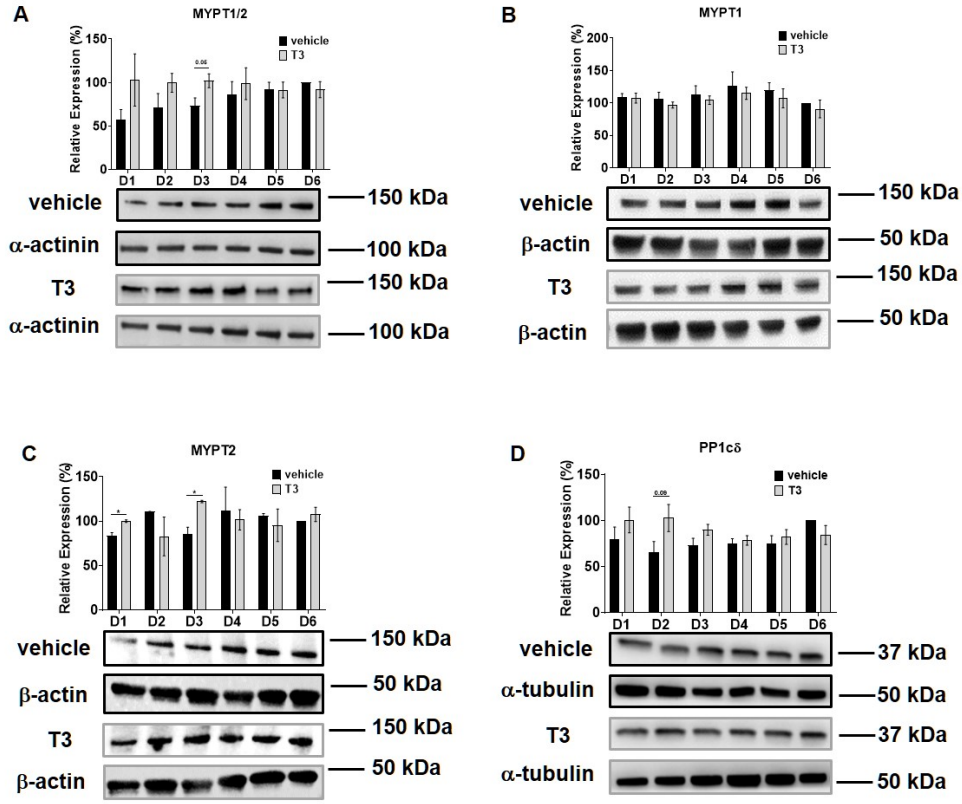


Figure 3. MYPT1/2 and PP1cδ expression during C2C12 myogenesis in the presence of T_3. Myoblasts were differentiated for 6 days in the presence of 10 nM T_3 or equal amounts of HCl:EtOH solution. Proteins from whole-cell lysates were analyzed using Western blot with anti-MYPT$^{1–296}$ (**A**), anti-MYPT$^{1–38}$ (**B**), anti-MYPT2 (**C**) and anti-PP1cδ (**D**) antibodies. Values represent $n = 4$, mean ± SEM. Data were normalized to the Day 6 vehicle control. Differences between group means were determined using Two-way ANOVA followed by Sidak post hoc test and by multiple unpaired two-tailed *t*-tests, $p < 0.05$ (*).

2.3. SMTNL1 Overexpression Induces the Phosphorylation of MYPT1 and MLC20 in Myoblasts

SMTNL1 is known to inhibit the MP holoenzyme by directly binding to MP in the cytoplasm and by suppressing the expression of its regulatory subunit (MYPT1) at the transcriptional level *[28]*. Since MYPT1 is the main isoform in the MP present in non-differentiated C2C12 cells (Figure 3A,B) we examined the effect of SMTNL1 overexpression on the expression and phosphorylation of MP and its substrate, MLC20, under supraphysiological T_3 exposure in myoblasts. Our data demonstrate that SMTNL1 expression was induced by 85% as a result of transfection in myoblasts (Figures S2A and S1C). T_3 treatment resulted in a slight decrease in the inhibitory phosphorylation of MYPT1, while the expression of MYPT1 showed no changes (Figure 4A,B). In contrast, SMTNL1 overexpression alone and in combination with T_3 significantly reduced the expression of MYPT1, and enhanced the Thr696 phosphorylation of MYPT1 by 22 and 24%, respectively (Figure 4A,B). Remarkably, the SMTNL1-induced elevation in MYPT1 inhibitory phosphorylation was accompanied by an increase in the phosphorylation of MLC20 on Ser19 residue (Figure 4D). T_3 treatment caused a small but not significant decrease in MLC20 phosphorylation (Figure 4D). The PP1cδ and MLC20 levels remained unchanged in response to any treatment (Figure 4C,E). Notably, SMTNL1 overexpression did not change the expression of MYPT2, while T_3 treatment alone or in combination with SMTNL1 overexpression elevated MYPT2 expression (Figure S3). These results indicate that SMTNL1 has a major impact on MYPT1 in myoblasts.

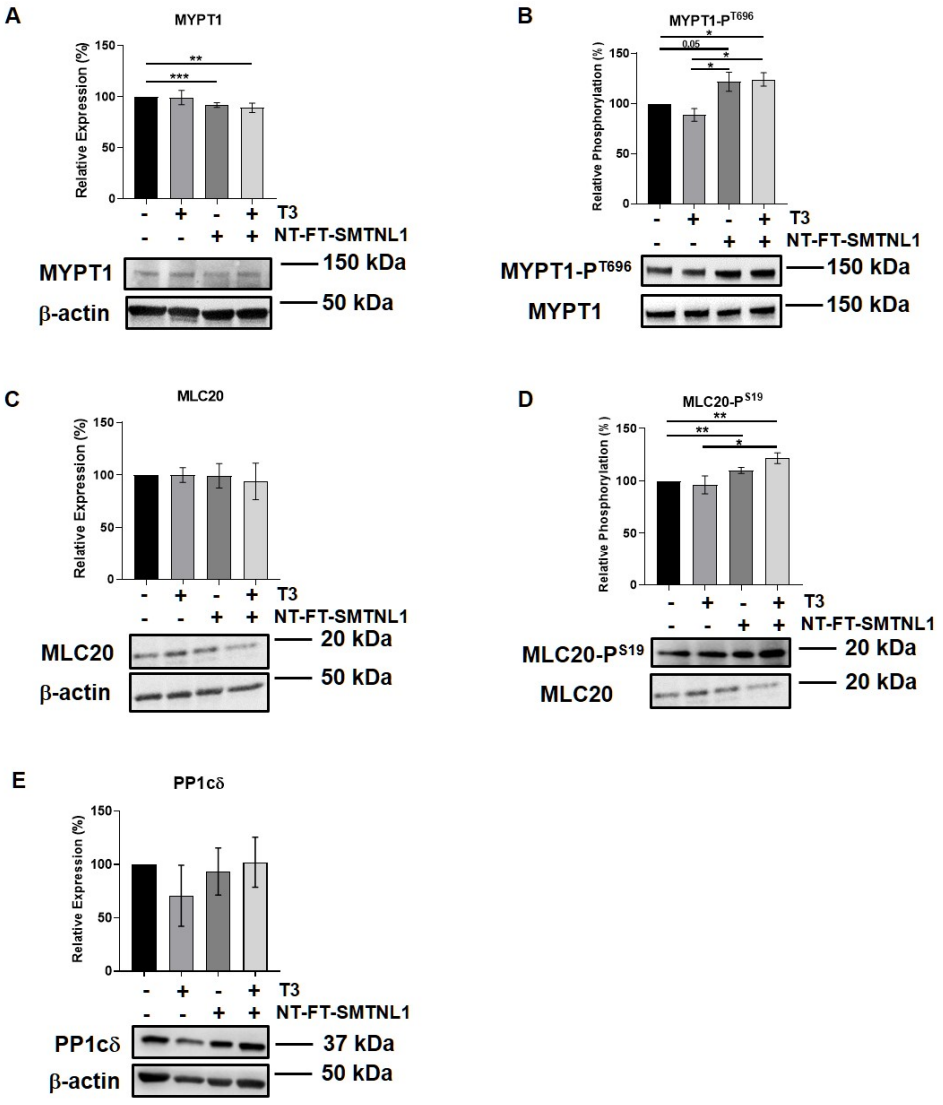


Figure 4. SMTNL1 overexpression controls the phosphorylation of myosin phosphatase and its substrate in myoblasts. Myoblasts were transfected with empty vector or NT-FT-SMTNL1 and were treated with 10 nM T_3 for 24 h. Whole-cell lysates were analyzed using Western blot with anti-MYPT1 (**A**), anti-MYPT1-P^{T696} (**B**), anti-MLC20 (**C**), anti-MLC20-P^{S19} (**D**) and anti-PP1cδ (**E**) antibodies. Values represent $n = 3$, mean ± SEM. Data were normalized to the empty vector-transfected control. Differences between group means were determined using One-way ANOVA and Tukey's post hoc test, $p < 0.05$ (*), $p < 0.01$ (**), $p < 0.001$ (***).

2.4. SMTNL1 Overexpression Inhibits the Migration of Myoblasts

It has previously been shown that the silencing of MP results in the inhibition of migration *[34]*. Considering the significant impact that SMTNL1 has on the expression and phosphorylation level of MYPT1 and MLC20, we investigated the effect of SMTNL1 overexpression and T_3 overload on the migratory capacity of C2C12 myoblasts since this ability is important in skeletal muscle differentiation and regeneration *[35]*. For this purpose, NT-FT-SMTNL1-transfected C2C12 cells labelled with fluorescent dye were uniformly scratched and cultured in the presence of supraphysiological T_3 and changes were monitored for 24 h in real-time. Our results demonstrate that SMTNL1 overexpression alone or in combination with T_3 markedly slowed down the closure of the scratch, while T_3 treatment had negligible effects (Figure 5A). By monitoring the kinetics of cell migration, we detected a lower migration rate in the NT-FT-SMTNL1-transfected cells compared to the

empty vector-transfected and to the T_3-treated cells. Remarkably, this effect was more pronounced in response to the combined treatment with T_3 and SMTNL1 overexpression (Figure 5B). As shown in Figure 5C, migratory capacity was slightly decreased upon T_3 treatment, while SMTNL1 overexpression alone or in combination with T_3 caused a 27 and a 34% decrease, respectively, compared to the empty vector-transfected control. Collectively, these data suggest that SMTNL1 negatively influences the migration of myoblasts, possibly through the inhibition of MP.

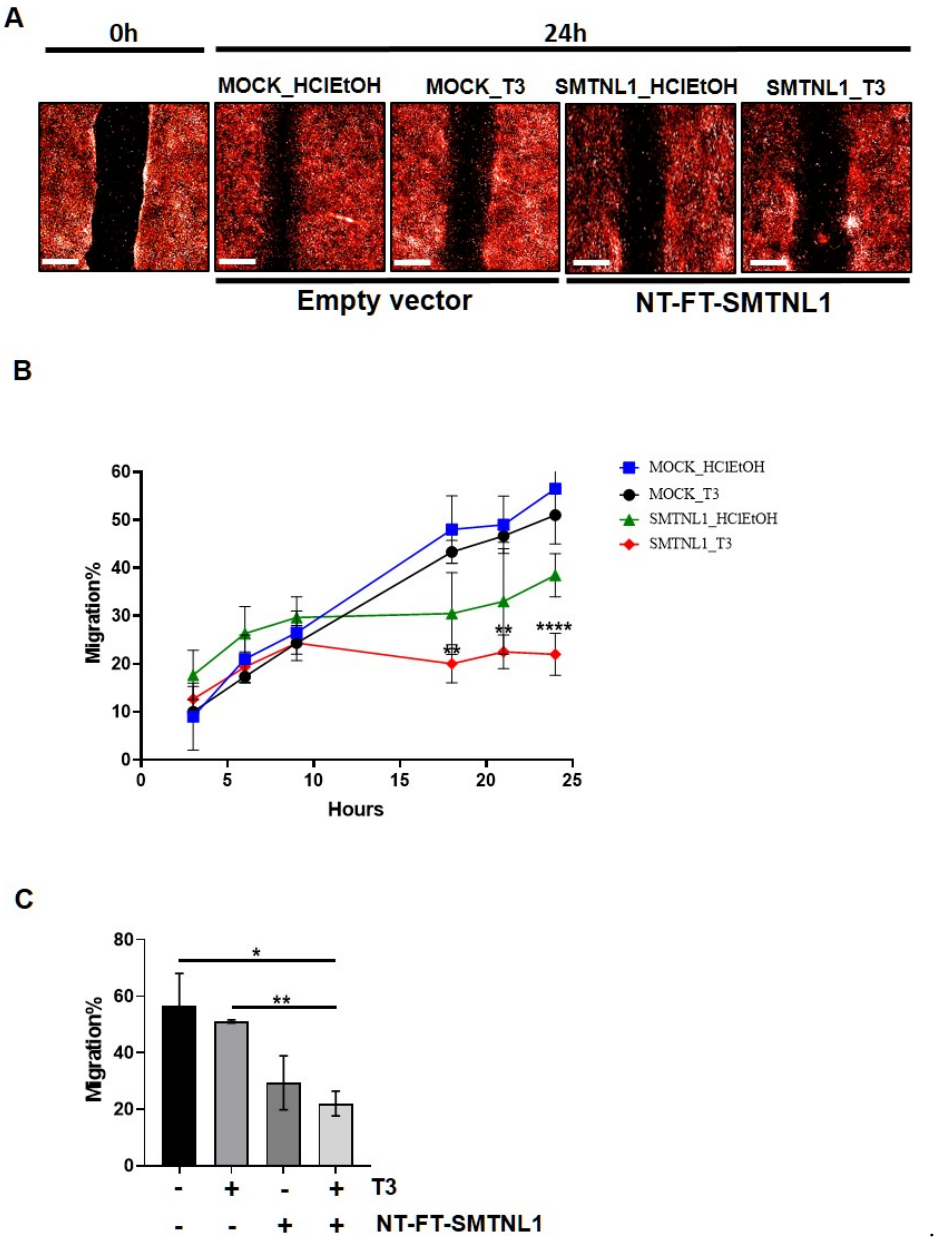


Figure 5. Scratch assay of T_3-treated and SMTNL1 overexpressing myoblasts. Myoblasts were stained and transfected with empty vector or NT-FT-SMTNL1. After 48 h of culturing and a 5-h serum starvation, cells were scratched and were grown for additional 24 h in the presence of 10 nM T_3. (**A**) Photos of scratch areas were taken with a 10× air objective at the indicated times. Scale bars: 500 μm. (**B**) 24-h kinetic curve of migrating C2C12 myoblasts. (**C**) Bar charts show covered scratch areas after 24 h. Values represent $n = 3$, mean ± SEM. Data were normalized to the empty vector-transfected control (MOCK). Differences between group means were determined using Two-way ANOVA (**B**) or One-way ANOVA (**C**) followed by Tukey's post hoc test, $p < 0.05$ (*), $p < 0.01$ (**), $p < 0.0001$ (****).

2.5. Differential Regulation of Myosin Phosphatase Target Subunit Isoforms by T_3 Treatment and SMTNL1 Overexpression in Myotubes

Previous studies reported that there is a slight shift during myoblast differentiation from MYPT1 to MYPT2 *[33]*. Therefore, we examined these regulatory subunit isoforms of MP in differentiated C2C12 cells, too. Additionally, Lontay et al. reported that the expression levels of the MYPT2 isoform are unaffected by SMTNL1 deletion in developing muscle *[26]*. Thus, we investigated whether SMTNL1 overexpression affects MYPT2 expression or not. First, the overexpression of SMTNL1 was successfully confirmed using Western blot analysis showing a 43% increase in total SMTNL1 expression (Figures S2B and S1C). Similarly to the results obtained on C2C12 myoblasts, the expression of MYPT1 did not change in response to excess T_3 but it was significantly reduced by 23 and 38%, respectively, owing to SMTNL1 overexpression alone and in combination with T_3 in myotubes (Figure 6A). MYPT2 expression was significantly increased by 56 and 64%, respectively, in response to excess T_3 and to combined treatment with T_3 and SMTNL1 overexpression, while it did not change upon SMTNL1 overexpression (Figure 6B). The phosphorylation of MYPT1/2 on Thr696 residue was significantly elevated upon T_3 treatment by 29% and upon combined treatment with T_3 and SMTNL1 overexpression by 53%, and it demonstrated a marginally significant increase due to the overexpression of SMTNL1 (Figure 6C). The phosphorylation of Thr853, another inhibitory phosphorylation site of MYPT1, was markedly enhanced under each condition compared to the empty vector-transfected control (Figure S4). Regarding PP1cδ, its levels were slightly increased following T_3 treatment and/or SMTNL1 overexpression (Figure 6D). These results suggest that T_3 and SMTNL1 are selective to the different MYPT isoforms.

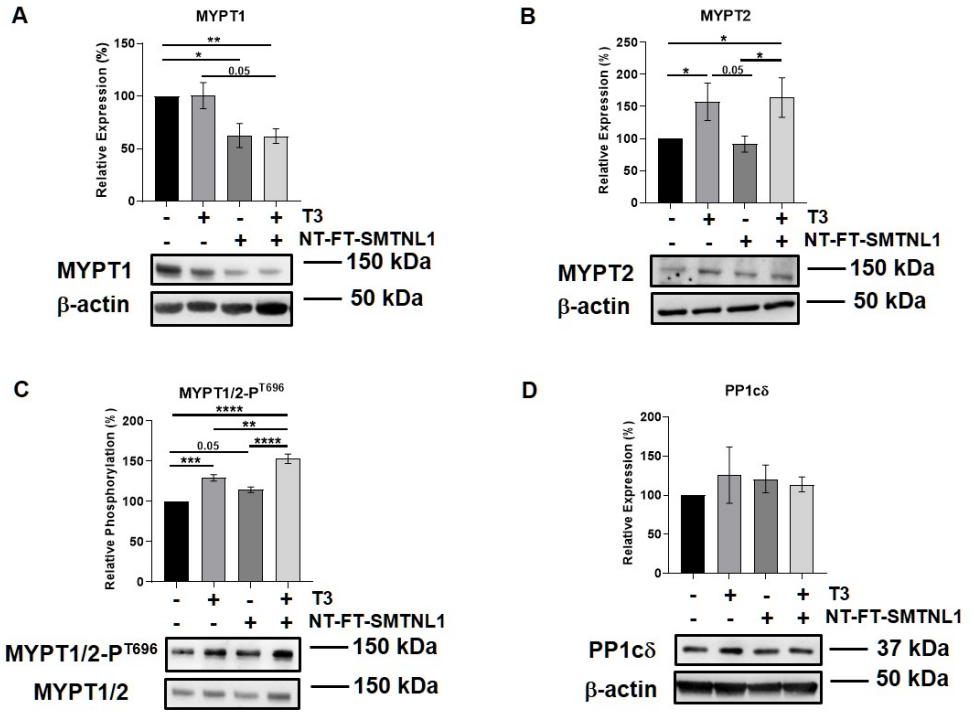


Figure 6. T_3 Treatment and SMTNL1 overexpression influence the expression and phosphorylation of myosin phosphatase target subunits in myotubes. Myoblasts were transfected with empty vector or NT-FT-SMTNL1 and were differentiated with a simultaneous 72-h T_3 treatment started from Day 4. Whole-cell lysates were analyzed using Western blot with anti-MYPT1 (**A**), anti-MYPT2 (**B**), anti-MYPT1/2-P^{T696} (**C**) and anti-PP1cδ (**D**). Values represent $n = 3$, mean ± SEM. Data were normalized to the empty vector-transfected control. Differences between group means were determined using One-way ANOVA and Tukey's post hoc test, $p < 0.05$ (*), $p < 0.01$ (**), $p < 0.001$ (***), $p < 0.0001$ (****).

2.6. Effect of T_3 Treatment and/or SMTNL1 Overexpression on the Expression and Activity of the Na^+/K^+-ATPase, an Alternative MP Substrate in Myotubes

Since the expression and importance of the major substrate of MP, MLC20, decreases in SKM, we assumed that MP targets alternative substrate(s) in SKM. Moreover, we have identified Na^+/K^+-ATPase as a MYPT1 interacting protein using a pull-down assay followed by mass spectrometry analysis from a mouse synaptosome extract [36]. Thus, we examined the expression and activity of Na^+/K^+-ATPase in our current model system. Na^+/K^+-ATPase is a widely expressed transmembrane protein, which is essential to maintain whole body homeostasis as well as muscle function [37]. Its expression was found to increase in hyperthyroid muscle [38]. First, we studied the interaction between the Na^+/K^+-ATPase and MYPT in the C2C12 mouse myoblast cell line. Na^+/K^+-ATPase and MYPT were reciprocally co-precipitated. These data suggest that the Na^+/K^+-ATPase is capable of binding to MP, possibly through its regulatory subunit (Figure S5). The G-protein-coupled muscarinic receptor mimetic carbachol, as a positive control [39], and the PP1 selective inhibitor tautomycetin were applied on muscle strips, and the phosphorylation of Na^+/K^+-ATPase was assessed. Both the carbachol and TMC increased the phosphorylation of Ser23 in the α1 subunit of Na^+/K^+-ATPase (Figure 7A). We also investigated the effect of T_3 treatment and/or SMTNL1 overexpression on Na^+/K^+-ATPase in C2C12 myotubes. T_3 treatment alone and in combination with SMTNL1 overexpression significantly elevated Na^+/K^+-ATPase expression by 41 and 32%, respectively, while it remained unchanged upon SMTNL1 overexpression (Figure 7B). The phosphorylation of Na^+/K^+-ATPase on Ser16 and Ser23 residues was significantly increased in response to all the conditions (Figure 7C,D). These results indicate that both T_3 and SMTNL1 regulates the activity of Na^+/K^+-ATPase by increasing its phosphorylation through the inhibition of distinct MYPT isoforms.

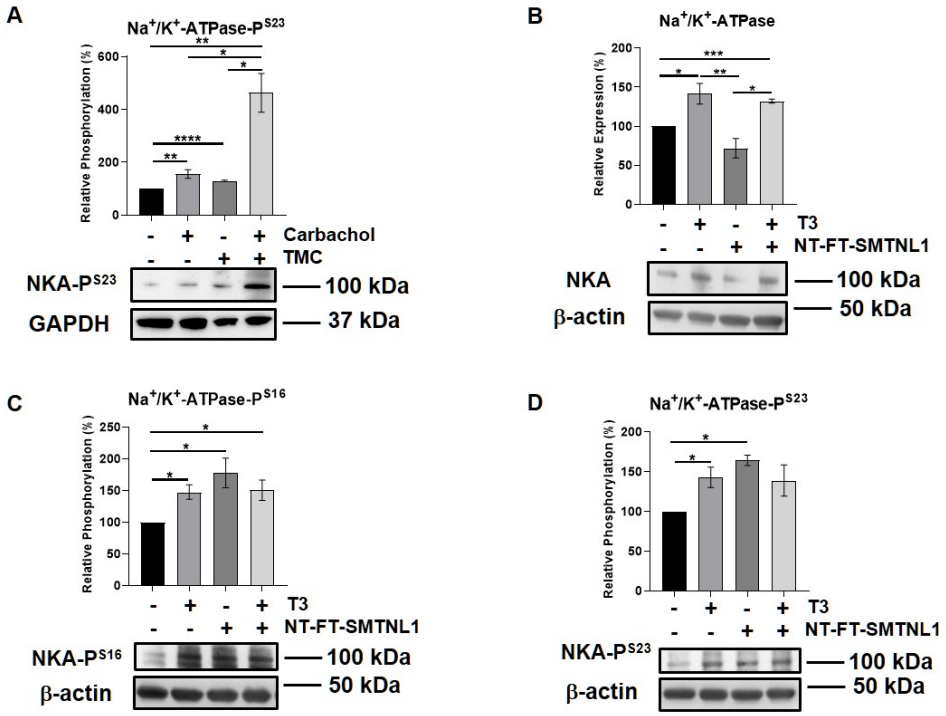


Figure 7. T_3 Treatment and SMTNL1 overexpression influence the expression and phosphorylation of Na^+/K^+-ATPase in myotubes. (**A**) Plantaris muscle strips of mice were treated with 10 μM TMC for 30 min followed by 10 μM carbachol for 10 min. Samples were lysed and subjected to Western blot using anti-Na^+/K^+-ATPase. (**B**–**D**) Myoblasts were transfected with empty vector or NT-FT-SMTNL1 and were differentiated in parallel with a 72-h T_3 treatment started from Day 4. Proteins from whole-cell lysates were separated by size and were analyzed using Western blot with anti-Na^+/K^+-ATPase (**B**), anti-Na^+/K^+-ATPase-P^{S16} (**C**) and anti-Na^+/K^+-ATPase-P^{S23} (**D**). Values represent

n = 3, mean ± SEM. Data were normalized to the empty vector-transfected control. Differences between group means were determined using One-way ANOVA and Tukey's post hoc test, $p < 0.05$ (*), $p < 0.01$ (**), $p < 0.001$ (***), $p < 0.0001$ (****).

3. Discussion

Thyroid hormones are key regulators of the development, regeneration, metabolism and myogenesis of SKM [40]. Myogenic differentiation is a highly coordinated process, which is essential for the development and regeneration of SKM. During differentiation, myoblasts undergo remodeling and fuse to form multinucleated, contractile myotubes in parallel with an increased expression of muscle-specific proteins that coordinate the contractile and metabolic functions of SKM. Moreover, SMTNL1 expression is increased in SKM during development [26]. These data correlate with our findings that SMTNL1 overexpression moderately promoted the differentiation of C2C12 myoblasts to myotubes by increasing the levels of myogenic markers, such as MyHC and desmin (Figure 1). Moreover, SMTNL1 overexpression alters the phenotype of differentiated cells creating smaller myotubes (Figure S1).

In humans, the T_3 level is maintained at low at the beginning of the myogenic process but it is increased parallel with the elevation of DIO2 upregulation [41]. It supports our data on C2C12 cell differentiation showing a significant increase in DIO2 expression upon T_3 treatment; however, it markedly decreases in response to prolonged T_3 treatment, suggesting a negative feedback mechanism (Figure 2B). The effect of MCT8 in myogenesis is debated since MCT8KO mice presented the same motor activity as WT mice [42]. In accord with that, we observed modest changes in MCT8 levels under each experimental setup during differentiation (Figure 2A). TRα was also changed during myoblast differentiation and showed a significant decrease upon prolonged T_3 treatment (Figure 2C). TRα is crucial in the proliferation, migration and differentiation of myoblast cells and TRαKO mice showed impaired muscle regeneration [43]. In addition, SMTNL1, a co-regulator of TRα expression, is downregulated by supraphysiological T_3 concentration and it hampers TRα expression [27]. Collectively, the C2C12 model proved to provide a sufficient hyperthyroid model for myogenesis with similar effects to that shown in human SKM. The effect of SMTNL1 in combination with the supraphysiological T_3 level did not change the cell viability of differentiated C2C12 cells, suggesting that it has an impact not on the proliferation but the differentiation process itself [27].

The expression of MYPT isoforms and the enzyme activity of MP have already been assessed by Wu et al. [33] during C2C12 myoblast differentiation; they reported an increase in the expression level in MYPT2 and a decline in the MYPT1 isoform. These findings are supported by our data showing a slight increase in MYPT2 and a non-significant decline of MYPT1 expression (assessed by an anti-MYPT$^{1-38}$ antibody that recognizes the MYPT1 isoform) [44] with no significant changes in PP1cδ expression (Figure 3). Interestingly, a supraphysiological T_3 level elevated MYPT2 and PP1cδ expression but had no effect on MYPT1 expression, suggesting a selective regulation of MYPT isoforms. Surprisingly, the PP1-MYPT1 complex functioned even in differentiated C2C12 cells [33] and MYPT1 expression but not MYPT2 expression, was regulated by SMTNL1 (Figure 6A,B). Since MYPT1 and MYPT2 coding genes are located on chromosome 12q15–q21.2 and 1q32.1, respectively [14], their differential gene expression regulation is feasible. MYPT1 expression showed a significant decrease upon SMTNL1 overexpression, which was independent of T_3-exposure in myoblasts and myotubes as well. It is in line with previous findings, showing that SMTNL1 downregulates the gene expression of MYPT1 in SKM [28]. MYPT2 expression is independent of SMTNL1 overexpression, which might be explained by the fact that SMTNL1 and MYPT1 are expressed exclusively in type 2A SKM fibers, while MYPT2 showed a homogenous distribution [28]. In the course of C2C12 differentiation, a shift from type 1 to 2A than to 2X and type 2B fiber marker proteins has been observed [45] and supraphysiological T_3 exposure promotes this shift [46], supporting this hypothesis.

Non-muscle myosin (nm-myosin) has a fundamental role in processes that require cellular reshaping and movement, such as cell adhesion, cell migration, morphogenesis, development and cell division through its actin cross-linking and contractile functions in myoblasts [47]. The role of MP is inevitable in these processes [48]. Based on our data and other studies [33], MYPT1 is the major isoform in the MP present in non-differentiated C2C12 cells. Neither MYPT1 expression nor its activity was influenced significantly by T_3 but only by the overexpression of SMTNL1 (Figure 4A,B). It has been reported that T_3-induced ROCK activation resulted in an increased phosphorylation of MYPT1 in hepatic stellate cells [49]. It was also found to be time-dependent in osteoblast-like cells showing that the phosphorylation of MYPT1 was faded away by 6 h of T_3 treatment [50]. It might explain the relatively low decrease in MYPT1 phosphorylation since our treatment lasted for 24 h (Figure 4B). In lung tissues, it was demonstrated that THs are able to modulate MLC20 phosphorylation and a moderate reduction in the level of phospho-MLC20 was detected in hyperthyroid mice compared to their euthyroid counterparts [51]. It supports our data on marginally decreased MLC20 phosphorylation upon T_3-treatment, while it was greatly increased in response to the combined effect of T_3 and SMTNL1 overexpression (Figure 4D). The T_3 and SMTNL1-dependent phosphorylation of MLC20 resembles the migration activity and the ability of cytoskeletal remodeling of C2C12 cells. The combined effect of supraphysiological T_3 and SMTNL1 hampered C2C12 migration; however, we need to note that drastic changes happened after 9 h of treatment (Figure 5B). The inhibition of MP by its phosphorylation at Thr696 could result in a slower turnover rate of nm-myosin phosphorylation causing more stable adhesive structures in the cells preventing migration and cytoskeletal remodeling. It is in accordance with a migration assay on HaCaT cells showing that PP1 enzyme inhibition started to cause a significant effect after 9 h of treatment [52]. In addition, SMTNL1 can also inhibit MP activity [26] by altering its phosphorylation that is clearly visible on MLC20 phosphorylation in SMTNL1-overexpressed myoblasts (Figure 4D). Since the MLC20 phosphorylation and MP activity were not fully in accordance with the migration features of the C2C12 myoblast, we assume that T_3 has additional, most probably non-genomic effects on the cytoskeletal remodeling. These collectively lead to the arrest of myoblast migration and impede the remodeling of the actomyosin complex in non-differentiated C2C12 cells. We can conclude that MP facilitates myoblast migration that is hampered in a hyperthyroid state regulated by SMTNL1.

By the differentiation of C2C12 cells, a shift from the nm-myosin to the skeletal muscle type of myosin (sk-myosin) is observed, and at Day six the nm-myosin was barely detectable in the myotubes, while the concentration of sk-myosin was increased [33]. This is consistent with the slow rate of dephosphorylation of the sk-myosin phospho-light chain in vivo [53]. The MYPT1-PP1cδ smooth muscle-type holoenzyme shows low affinity to the phosphorylated sk-myosin and the sk-myosin phosphorylation was reduced but not eliminated at Day six of differentiation [33], suggesting that alternative substrates of myosin phosphatase exist in SKM.

One of the potential candidates as a substrate of MP is the Na^+/K^+-ATPase (NKA). NKA is a transmembrane pump that is essential for cellular ion and water homeostasis, maintaining membrane potentials and Na^+-coupled transport of various substances. SKM has one of the largest and most dynamic pools of NKA in the body [37]. Therefore, the regulation of NKA either by the concentrations of its substrates or by protein–protein interactions with FXYD proteins or by covalent modification—predominantly by phosphorylation—is crucial [37]. We have already identified NKA as an MYPT1 interacting protein using a pull-down assay followed by mass spectrometry analysis from a mouse synaptosome extract [36]. The co-immunoprecipitation from C2C12 cell lysate also revealed the interaction between NKA and MYPT (Figure S5). In addition, NKA was proven to be a potential substrate of a PPP1 enzyme, possibly MP, due to the elevated phosphorylation at Ser23 residue upon the selective inhibition of PP1c by tautomycetin (Figure 7A). It is in line with previous studies showing that the inhibition of PP1c/PP2Ac by okadaic acid and

calyculin A resulted in a decrease in NKA activity [54]. T_3 stimulates the intrinsic activity of NKA in a transcription-independent manner via the stimulation of its cell surface expression through the PI3K/PKB pathway [55]. We have also detected this increase under the supraphysiological T_3 exposure of C2C12 myotubes (Figure 7) and it is in accordance with findings showing the increased number of ouabain sites, also known as NKA level, in the SKM of hyperthyroid patients compared to healthy controls [56]. In addition, we proved that NKA gene expression occurs in an SMTNL1-independent manner (Figure 7B). Not only the protein level and translocation but the phosphorylation of the α subunit of NKA by Ser/Thr kinases can regulate the activity of NKA [55]. Although, the effects of THs are controversial due to the tight interplay between different signaling pathways; nevertheless, NKA phosphorylation by novel PKCs at Ser16 and Ser23 possessed mostly negative regulatory effect on NKA activity [57–59].

In myotubes, the expression of MYPT2 but not MYPT1 increased in a T_3-dependent but SMTNL1-independent manner along with a marginal increase in the expression of PP1 catalytic subunit. Interestingly, T_3 and its combined treatment with SMTNL1 overexpression impeded the activity of MP assessed by its regulatory Thr696 phosphorylation (Figure 6C). Parallel with these processes, the phosphorylation of NKA at Ser16 and Ser23 also significantly increased upon T_3 treatment and SMTNL1 overexpression as well (Figure 7C,D). We strongly suggest that SMTNL1 took effect on increased NKA phosphorylation and activity via the downregulation of MP. The phosphorylation and inactivation of MP might be evoked by ROCK that was stimulated by T_3 in osteoblasts resulting in the phosphorylation of MYPT1 at Thr696 and hampered osteocalcin synthesis [50]. It is important to note that both the overstimulation of NKA expression by T_3 or hyper- or downregulation of its activity do not necessarily translate into improved muscle performance, and it could cause muscle weakness and myopathy [37].

In conclusion, we suggest a differential regulation and role of MP in myoblasts and myotubes upon supraphysiological T_3 exposure. In non-differentiated myoblasts, MP is in complex with MYPT1 and its expression and activity is regulated by SMTNL1 that modulates the MLC20 phosphorylation, cytoskeletal remodeling and migration. In contrast, in myotubes, where the action of MP is less profound in the regulation of muscle contractility, since sk-myosins are regulated by a separate set of proteins that are bound to the actin filaments, and in the MP holoenzyme, PP1c is predominantly complexed with MYPT2. MYPT2 expression is stimulated by T_3, and MP is regulated by the T_3-induced ROCK phosphorylation. MP acts as a possible regulator of NKA by dephosphorylating its inhibitory phosphorylation sites. These findings should lead to a better understanding of myopathy and muscle weakness and the disorder of muscle regeneration in hyperthyroid patients.

4. Materials and Methods

4.1. Chemicals

All chemicals were obtained from Sigma-Aldrich (St. Louis, MO, USA) unless otherwise indicated.

4.2. Antibodies

Western blot analyses were performed using antibodies specific for desmin 1:1500 (Cell Signaling Technology, Danvers, MA, USA, #5332), MyHC 1:1500 (R&D Systems, Minneapolis, MN, USA, MAB4470), Flag 1:2000 (Sigma-Aldrich, St. Louis, MO, USA, F7405), MYPT$^{1–296}$ 1:1000 [44], MYPT$^{1–38}$ 1:1000 [33], MYPT1 1:1000 (BD Transduction Technologies, Becton, NJ, USA, #612164), PP1cδ 1:1000 (Santa Cruz Biotechnology, Dallas, TX, USA, #sc-365678), MYPT1-P^{T696} 1:1000 (Merck Millipore, Burlington, MA, USA, #ABS45), MYPT1-P^{T853} 1:500 (Merck Millipore, #36-003), MLC20 1:1000 (Cell Signaling Technology, #3672), MLC20-P^{S19} 1:500 (Cell Signaling Technology, #3671), MYPT2 1:1000 [14], Na^+/K^+-

ATPase 1:1000 (Cell Signaling Technology, #3010), Na^+/K^+-ATPase-P^{S16} 1:250 (Cell Signaling Technology, #4020), Na^+/K^+-ATPase-P^{S23} 1:500 (Cell Signaling Technology, #4006), MCT8 1:1500 (Proteintech, Rosemont, IL, USA, #20676-1-AP), DIO2 1:1500 (NovusBio, Littleton, CO, USA, #NBP1-00178), TRα 1:650 (Abcam, Cambridge, UK, ab53729), SMTNL1 (Santa Cruz Biotechnology, #sc-390369), β-actin 1:20,000 (Santa Cruz Biotechnology, #sc-47778), α-actinin 1:8000 (Sigma-Aldrich, A2543) α-tubulin 1:1000 (Santa Cruz Biotechnology, #sc-53646), anti-mouse 1:5000 (Cell Signaling Technology, #7076), anti-rabbit 1:5000 (Sigma-Aldrich, A0545), anti-goat 1:5000 (Sigma-Aldrich, A5420).

4.3. Cell Culture Maintenance

C2C12 mouse myoblast cells (ECACC 91031101) were maintained in Dulbecco's Modified Eagle's Medium (DMEM) containing 1000 mg/L glucose, 2 mM L-glutamine (Lonza; Basel, Switzerland), 10% (*v*/*v*) foetal bovine serum (FBS) and phenol red. Cells were grown in a humidified incubator that provided an atmosphere of 5% CO_2 at 37 °C.

4.4. Thin Coating of Tissue Culture Plates

Rat tail collagen I (Thermo Fisher Scientific; Waltham, MA, USA) was diluted in 20 mM acetic acid at a final amount of 5 μg/cm^2 and was added to each well. After 1 h, the solution was removed, and wells were rinsed twice with 1× phosphate buffered saline (PBS) to remove the acid. Plates (VWR International; West Chester, PA, USA) were used immediately or air dried and stored at 4 °C until use.

4.5. Transient Transfection and Differentiation

GeneJuice transfection reagent was added dropwise to serum-free DMEM and incubated at room temperature (RT) for 5 min. According to the manufacturer's intructions, 2 μg of pM13-NT-FT-SMTNL1 per well was added to the serum-free DMEM/transfection reagent mixture and was incubated at RT for 15 min. Meanwhile, cells were washed with 1× PBS and were detached with 0.25% (*w*/*v*) trypsin/EDTA solution. After the 15-min incubation ended, the entire volume of the transfection mixture was added dropwise to cells in complete growth medium. Finally, cells were seeded in 6-well tissue culture plates and incubated at 37 °C overnight (O/N). Transfection with empty vector (MOCK) acted as the control in all experiments. The day after transfection, cells were washed with 1× PBS and complete growth medium was replaced by phenol red-free DMEM supplemented with 1000 mg/L glucose, 2 mM L-glutamine and 2% (*v*/*v*) horse serum (HS). From then on, differentiation medium was changed daily for 5 days.

4.6. Immunofluorescence Staining

Transfected myoblasts were seeded into collagen-coated OptiPlate-96 Black plates (PerkinElmer; Waltham, MA, USA) and were differentiated for 5 days. On days 0, 3 and 5 of differentiation, cells were fixed with 4% (*w*/*v*) paraformaldehyde for 15 min at RT. Then, cells were washed 3 times with 1× PBS and were permeabilized with 0.2% (*w*/*v*) Triton-X-100 for 4 min at RT. After blocking with 1% HS for 1 h at 4 °C, immunofluorescence staining was carried out using anti-desmin (1:100) antibody (green), anti-Flag (1:100) antibody (green) and F-actin-binding peptide phalloidin (1:500) (red). Fluorescent signals were detected using an automated high-content imaging reader (PerkinElmer; Waltham, MA, USA).

4.7. 3,3',5-Triiodo-L-thyronine (T_3) Hormone Treatment

According to the manufacturer's instructions, 3,3',5-Triiodo-L-thyronine sodium salt was dissolved in 1 M HCl:EtOH with a ratio of 1:4. In Figures 2 and 3, cells received 10 nM of T_3 from Day 1 to Day 6 of differentiation. In Figure 4, 48 h after transfection, myoblasts were treated with 10 nM T_3 for 24 h. In Figures 6 and 7, myoblasts were transfected the day before the beginning of differentiation. From the beginning of Day 4 to the end of

Day 6 of differentiation, differentiation medium was supplemented with 10 nM of T_3. In all cases, equal amounts of HCl:EtOH (1:4) were added to the non-treated control called 'vehicle' in Figures 2 and 3.

4.8. Cell Lysis

Myotubes were washed with 1× PBS and were harvested in ice-cold RIPA buffer complemented with protease and phosphatase inhibitors (25 mM Tris-HCl (pH 7.6), 150 mM NaCl, 1% sodium deoxycholate, 0.1% SDS, 1% Triton-X 100, 1 mM PMSF, 10× protease inhibitor cocktail, 50× phosphatase inhibitor cocktail, 1 μM microcystin-LR). Cell suspensions were sonicated for 30 s with a 10% pulse using a Branson Sonifier 250 sonicator (Thermo Fisher Scientific; Waltham, MA, USA) and were centrifuged at 16,000× *g*, 4 °C for 10 min. Supernatants were transferred to fresh tubes and total protein concentration was measured with a Bicinchoninic acid (BCA) assay kit (Thermo Fisher Scientific; Waltham, MA, USA).

4.9. Western Blot Analysis

Whole-cell lysates were boiled in 4× sodium dodecyl sulphate (SDS) sample buffer (Bio-Rad Laboratories; Hercules, CA, USA) at 100 °C for 5 min. A total of 30 μg of protein was loaded onto 4–20% precast Criterion gels (Bio-Rad Laboratories; Hercules, CA, USA) and was separated by size at a constant voltage of 200 V. Next, proteins were transferred onto nitrocellulose membranes using a Criterion blotter (Bio-Rad Laboratories; Hercules, CA, USA) at 100 V for 75 min. Membranes were blocked in 5% (*w*/*v*) bovine serum albumin (BSA) dissolved in 1× Tris buffered saline (TBS) containing 0.1% (*v*/*v*) Tween 20 at RT for 1.5 h. After that, membranes were incubated with primary antibodies, diluted in 5% BSA/TBST, at 4 °C O/N. On the next day, membranes were incubated with HRP-conjugated secondary antibodies at RT for 1.5 h and immunoreactions were visualized by enhanced chemiluminescence (ECL) using a mixture of WesternBright ECL or WesternBright Sirius and WesternBright Peroxide reagents (Advansta Inc.; San Jose, CA, USA) with a ratio of 1:1 in a ChemiDoc Touch Imaging System (Bio-Rad Laboratories; Hercules, CA, USA). In case of phospho-blots, membranes were stripped as described in Supplementary Methods and were reprobed with non-phospho antibodies.

4.10. Scratch Assay and High Content Screening (HCS) Analysis

Myoblasts were suspended in serum-free medium containing 5 μL/mL of DiI (Thermo Fischer Scientific; Waltham, MA, USA), a highly lipophilic carbocyanine dye, and were incubated for 15 min at 37 °C. After washing 3 times with warm complete medium, myoblasts were transfected with an empty vector or NT-FT-SMTNL1 and were seeded into collagen-coated OptiPlate-96 Black plates (PerkinElmer; Waltham, MA, USA). After 48 h, cells were serum-starved for 5 h and were scratched with a 10-microliter pipette tip. Myoblasts were washed with 1× PBS and were cultured in the presence of 10 nM T_3 for an additional 24 h under real-time screening with an HCS equipment using a 10× air objective. Data were analyzed and evaluated using the Harmony software (PerkinElmer; Waltham, MA, USA).

4.11. Carbachol and Tautomycetin Treatment

Mice were housed as described before [28]. All procedures were approved by the University of Debrecen Faculty of Medicine Ethical Committee and are consistent with the NIH 'Guide for the Care and Use of Laboratory Animals'. Plantaris muscle strips were removed and maintained as described before [24] in an organ bath filled with Krebs solution (118 mM NaCl; 4.75 mM KCl; 1.2 mM $MgSO_4$; 1.2 mM KH_2PO_4; 2.5 mM $CaCl_2$; 25 mM $NaHCO_2$; 11.5 mM glucose) warmed at 37 °C and gassed with 95% O_2 and 5% CO_2. The effects of PP1 inhibitor on muscle tissues were investigated by a 30-min preincubation

with 10 μM tautomycetin (TMC) followed by a 10-min incubation with 10 μM carbachol. Tissues were lysed and subjected to Western blot analysis.

4.12. Statistical Analysis

Immunoblots were analyzed using ImageJ software. Bar charts were created and statistical analyses were performed using GraphPad Prism 8 software. Phosphorylated proteins were normalized to non-phosphorylated protein expression, while non-phosphorylated protein expression was normalized to the loading control. All data are presented as mean ± SEM, where n is the number of independently performed experiments. Differences were considered to be statistically significant at $p < 0.05$.

Supplementary Materials: The following are available online at www.mdpi.com/1422-0067/221/91/293/s1.

Author Contributions: B.L., conceptualization; E.M. and B.L., data curation; E.M. and I.K., visualization; E.M., D.H., I.T. and I.K., methodology; E.M., Figureure preparation and data analysis; B.L. and F.E., funding acquisition; E.M. and B.L., writing—original draft preparation and editing; F.E., writing—review. All authors have read and agreed to the published version of the manuscript.

Funding: This work was supported by grants from the National Research, Development and Innovation Office FK125043 (to B.L.) and K129104 (to F.E.), the University of Debrecen, Faculty of Medicine Research Fund (1G3DBKJ0BFTK 247) for B.L. and from the EU co-financed by the European Regional Development Fund under project EFOP-3.6.2-16-2017-00006 and from the EFOP-3.6.3-VEKOP-16-2017-00009 project co-financed by EU and the European Social Fund. B. L. MECENATURA from the University of Debrecen.

Acknowledgements: Thank for Karen Uray for providing the animals for the study and for Tibor Docsa and for Ádám Ungvári for his technical help with the mouse experiment. We also thank for Andrea Docsa and Ágota Kelemenné Szántó for their technical assistance.

Conflicts of Interest: The authors have declared that no competing interests exist.

References

1. Vale, C.; Neves, J.S.; von Hafe, M.; Borges-Canha, M.; Leite-Moreira, A. The Role of Thyroid Hormones in Heart Failure. *Cardiovasc. Drugs Ther.* **2019**, *33*, 179–188, doi:10.1007/s10557-019-06870-4.
2. Goncalves, A.; Resende, E.S.; Fernandes, M.L.; da Costa, A.M. Effect of thyroid hormones on cardiovascular and muscle systems and on exercise tolerance: A brief review. *Arq. Bras. Cardiol.* **2006**, *87*, e45–e47, doi:10.1590/s0066-782x2006001600033.
3. Bloise, F.F.; Cordeiro, A.; Ortiga-Carvalho, T.M. Role of thyroid hormone in skeletal muscle physiology. *J. Endocrinol.* **2018**, *236*, R57–R68, doi:10.1530/JOE-16-0611.
4. Friesema, E.C.; Jansen, J.; Visser, T.J. Thyroid hormone transporters. *Biochem. Soc. Trans.* **2005**, *33*, 228–232, doi:10.1042/BST0330228.
5. Bianco, A.C.; Kim, B.W. Deiodinases: Implications of the local control of thyroid hormone action. *J. Clin. Investig.* **2006**, *116*, 2571–2579, doi:10.1172/JCI29812.
6. Davis, P.J.; Goglia, F.; Leonard, J.L. Nongenomic actions of thyroid hormone. *Nat. Rev. Endocrinol.* **2016**, *12*, 111–121, doi:10.1038/nrendo.2015.205.
7. Cakir, M.; Samanci, N.; Balci, N.; Balci, M.K. Musculoskeletal manifestations in patients with thyroid disease. *Clin. Endocrinol.* **2003**, *59*, 162–167, doi:10.1046/j.1365-2265.2003.01786.x.
8. Olson, B.R.; Klein, I.; Benner, R.; Burdett, R.; Trzepacz, P.; Levey, G.S. Hyperthyroid myopathy and the response to treatment. *Thyroid* **1991**, *1*, 137–141, doi:10.1089/thy.1991.1.137.
9. Short, K.R.; Nygren, J.; Barazzoni, R.; Levine, J.; Nair, K.S. T_3 increases mitochondrial ATP production in oxidative muscle despite increased expression of UCP2 and -3. *Am. J. Physiol. Endocrinol. Metab.* **2001**, *280*, E761–E769, doi:10.1152/ajpendo.2001.280.5.E761.
10. Chacko, S.; Conti, M.A.; Adelstein, R.S. Effect of phosphorylation of smooth muscle myosin on actin activation and Ca^{2+} regulation. *Proc. Natl. Acad. Sci. USA* **1977**, *74*, 129–133.
11. Ikebe, M.; Hartshorne, D.J. The role of myosin phosphorylation in the contraction-relaxation cycle of smooth muscle. *Experientia* **1985**, *41*, 1006–1010.
12. Kiss, A.; Erdodi, F.; Lontay, B. Myosin phosphatase: Unexpected functions of a long-known enzyme. *Biochim. Biophys. Acta Mol. Cell Res.* **2019**, *1866*, 2–15, doi:10.1016/j.bbamcr.2018.07.023.
13. Shimizu, H.; Ito, M.; Miyahara, M.; Ichikawa, K.; Okubo, S.; Konishi, T.; Naka, M.; Tanaka, T.; Hirano, K.; Hartshorne, D.J.; et al. Characterization of the myosin-binding subunit of smooth muscle myosin phosphatase. *J. Biol. Chem.* **1994**, *269*, 30407–30411.

14. Fujioka, M.; Takahashi, N.; Odai, H.; Araki, S.; Ichikawa, K.; Feng, J.; Nakamura, M.; Kaibuchi, K.; Hartshorne, D.J.; Nakano, T.; et al. A new isoform of human myosin phosphatase targeting/regulatory subunit (MYPT2): cDNA cloning, tissue expression, and chromosomal mapping. *Genomics* **1998**, *49*, 59–68, doi:10.1006/geno.1998.5222.
15. Skinner, J.A.; Saltiel, A.R. Cloning and identification of MYPT3: A prenylatable myosin targetting subunit of protein phosphatase 1. *Biochem. J.* **2001**, *356 Pt 1*, 257–267.
16. Tan, I.; Ng, C.H.; Lim, L.; Leung, T. Phosphorylation of a novel myosin binding subunit of protein phosphatase 1 reveals a conserved mechanism in the regulation of actin cytoskeleton. *J. Biol. Chem.* **2001**, *276*, 21209–21216, doi:10.1074/jbc.M102615200.
17. Cao, W.S.; Mattagajasingh, S.N.; Xu, H.X.; Kim, K.H.; Fierlbeck, W.; Deng, J.; Lowenstein, C.J.; Ballermann, B.J. TIMAP, a novel CAAX box protein regulated by TGF-beta 1 and expressed in endothelial cells. *Am. J. Physiol.-Cell Physiol.* **2002**, *283*, C327–C337, doi:10.1152/ajpcell.00442.2001.
18. Matsumura, F.; Hartshorne, D.J. Myosin phosphatase target subunit: Many roles in cell function. *Biochem. Biophys. Res. Commun.* **2008**, *369*, 149–156, doi:10.1016/j.bbrc.2007.12.090.
19. Arimura, T.; Suematsu, N.; Zhou, Y.B.; Nishimura, J.; Satoh, S.; Takeshita, A.; Kanaide, H.; Kimura, A. Identification, characterization, and functional analysis of heart-specific myosin light chain phosphatase small subunit. *J. Biol. Chem.* **2001**, *276*, 6073–6082, doi:10.1074/jbc.M008566200.
20. Ichikawa, K.; Ito, M.; Hartshorne, D.J. Phosphorylation of the large subunit of myosin phosphatase and inhibition of phosphatase activity. *J. Biol. Chem.* **1996**, *271*, 4733–4740.
21. Muranyi, A.; Derkach, D.; Erdodi, F.; Kiss, A.; Ito, M.; Hartshorne, D.J. Phosphorylation of Thr695 and Thr850 on the myosin phosphatase target subunit: Inhibitory effects and occurrence in A7r5 cells. *FEBS Lett.* **2005**, *579*, 6611–6615, doi:S0014-5793(05)01328-1.
22. Velasco, G.; Armstrong, C.; Morrice, N.; Frame, S.; Cohen, P. Phosphorylation of the regulatory subunit of smooth muscle protein phosphatase 1M at Thr850 induces its dissociation from myosin. *FEBS Lett.* **2002**, *527*, 101–104, doi:S0014579302031757.
23. Borman, M.A.; MacDonald, J.A.; Haystead, T.A. Modulation of smooth muscle contractility by CHASM, a novel member of the smoothelin family of proteins. *FEBS Lett.* **2004**, *573*, 207–213, doi:10.1016/j.febslet.2004.08.002.
24. Wooldridge, A.A.; Fortner, C.N.; Lontay, B.; Akimoto, T.; Neppl, R.L.; Facemire, C.; Datto, M.B.; Kwon, A.; McCook, E.; Li, P.; et al. Deletion of the protein kinase A/protein kinase G target SMTNL1 promotes an exercise-adapted phenotype in vascular smooth muscle. *J. Biol. Chem.* **2008**, *283*, 11850–11859, doi:10.1074/jbc.M708628200.
25. Hartshorne, D.J.; Ito, M.; Erdodi, F. Role of protein phosphatase type 1 in contractile functions: Myosin phosphatase. *J. Biol. Chem.* **2004**, *279*, 37211–37214, doi:10.1074/jbc.R400018200.
26. Lontay, B.; Bodoor, K.; Weitzel, D.H.; Loiselle, D.; Fortner, C.; Lengyel, S.; Zheng, D.; Devente, J.; Hickner, R.; Haystead, T.A. Smoothelin-like 1 protein regulates myosin phosphatase-targeting subunit 1 expression during sexual development and pregnancy. *J. Biol. Chem.* **2010**, *285*, 29357–29366, doi:10.1074/jbc.M110.143966.
27. Major, E.; Győry, F.; Horváth, D.; Keller, I.; Tamás, I.; Uray, K.; Fülöp, P.; Lontay, B. Smoothelin-like protein 1 regulates development and metabolic transformation of skeletal muscle in hyperthyroidism. *Front. Endocrinol.* **2021**, in press.
28. Lontay, B.; Bodoor, K.; Sipos, A.; Weitzel, D.H.; Loiselle, D.; Safi, R.; Zheng, D.; Devente, J.; Hickner, R.C.; McDonnell, D.P.; et al. Pregnancy and Smoothelin-like Protein 1 (SMTNL1) Deletion Promote the Switching of Skeletal Muscle to a Glycolytic Phenotype in Human and Mice. *J. Biol. Chem.* **2015**, *290*, 17985–17998, doi:10.1074/jbc.M115.658120.
29. Li, H.; Choudhary, S.K.; Milner, D.J.; Munir, M.I.; Kuisk, I.R.; Capetanaki, Y. Inhibition of desmin expression blocks myoblast fusion and interferes with the myogenic regulators MyoD and myogenin. *J. Cell Biol.* **1994**, *124*, 827–841, doi:10.1083/jcb.124.5.827.
30. Nie, Y.; Chen, H.; Guo, C.; Yuan, Z.; Zhou, X.; Zhang, Y.; Zhang, X.; Mo, D.; Chen, Y. Palmdelphin promotes myoblast differentiation and muscle regeneration. *Sci. Rep.* **2017**, *7*, 41608, doi:10.1038/srep41608.
31. Dentice, M.; Marsili, A.; Ambrosio, R.; Guardiola, O.; Sibilio, A.; Paik, J.H.; Minchiotti, G.; DePinho, R.A.; Fenzi, G.; Larsen, P.R.; et al. The FoxO3/type 2 deiodinase pathway is required for normal mouse myogenesis and muscle regeneration. *J. Clin. Investig.* **2010**, *120*, 4021–4030, doi:10.1172/JCI43670.
32. Milanesi, A.; Lee, J.W.; Kim, N.H.; Liu, Y.Y.; Yang, A.; Sedrakyan, S.; Kahng, A.; Cervantes, V.; Tripuraneni, N.; Cheng, S.Y.; et al. Thyroid Hormone Receptor alpha Plays an Essential Role in Male Skeletal Muscle Myoblast Proliferation, Differentiation, and Response to Injury. *Endocrinology* **2016**, *157*, 4–15, doi:10.1210/en.2015-1443.
33. Wu, Y.; Erdodi, F.; Muranyi, A.; Nullmeyer, K.D.; Lynch, R.M.; Hartshorne, D.J. Myosin phosphatase and myosin phosphorylation in differentiating C2C12 cells. *J. Muscle Res. Cell Motil.* **2003**, *24*, 499–511, doi:10.1023/b:jure.0000009810.36038.53.
34. Lontay, B.; Kiss, A.; Gergely, P.; Hartshorne, D.J.; Erdodi, F. Okadaic acid induces phosphorylation and translocation of myosin phosphatase target subunit 1 influencing myosin phosphorylation, stress fiber assembly and cell migration in HepG2 cells. *Cell Signal.* **2005**, *17*, 1265–1275, doi:10.1016/j.cellsig.2005.01.008.
35. Lehka, L.; Redowicz, M.J. Mechanisms regulating myoblast fusion: A multilevel interplay. *Semin. Cell Dev. Biol.* **2020**, *104*, 81–92, doi:10.1016/j.semcdb.2020.02.004.
36. Lontay, B.; Pal, B.; Serfozo, Z.; Koszeghy, A.; Szucs, G.; Rusznak, Z.; Erdodi, F. Protein phosphatase-1M and Rho-kinase affect exocytosis from cortical synaptosomes and influence neurotransmission at a glutamatergic giant synapse of the rat auditory system. *J. Neurochem.* **2012**, *123*, 84–99, doi:10.1111/j.1471-4159.2012.07882.x.
37. Pirkmajer, S.; Chibalin, A.V. Na,K-ATPase regulation in skeletal muscle. *Am. J. Physiol. Endocrinol. Metab.* **2016**, *311*, E1–E31, doi:10.1152/ajpendo.00539.2015.

38. Riis, A.L.; Jorgensen, J.O.; Moller, N.; Weeke, J.; Clausen, T. Hyperthyroidism and cation pumps in human skeletal muscle. *Am. J. Physiol. Endocrinol. Metab.* **2005**, *288*, E1265–1269, doi:10.1152/ajpendo.00533.2004.
39. Soltoff, S.P.; Asara, J.M.; Hedden, L. Regulation and identification of Na,K-ATPase alpha1 subunit phosphorylation in rat parotid acinar cells. *J. Biol. Chem.* **2010**, *285*, 36330–36338, doi:10.1074/jbc.M110.136465.
40. Ambrosio, R.; De Stefano, M.A.; Di Girolamo, D.; Salvatore, D. Thyroid hormone signaling and deiodinase actions in muscle stem/progenitor cells. *Mol. Cell Endocrinol.* **2017**, *459*, 79–83, doi:10.1016/j.mce.2017.06.014.
41. Dentice, M.; Ambrosio, R.; Damiano, V.; Sibilio, A.; Luongo, C.; Guardiola, O.; Yennek, S.; Zordan, P.; Minchiotti, G.; Colao, A.; et al. Intracellular inactivation of thyroid hormone is a survival mechanism for muscle stem cell proliferation and lineage progression. *Cell Metab.* **2014**, *20*, 1038–1048, doi:10.1016/j.cmet.2014.10.009.
42. Di Cosmo, C.; Liao, X.H.; Ye, H.; Ferrara, A.M.; Weiss, R.E.; Refetoff, S.; Dumitrescu, A.M. Mct8-deficient mice have increased energy expenditure and reduced fat mass that is abrogated by normalization of serum T3 levels. *Endocrinology* **2013**, *154*, 4885–4895, doi:10.1210/en.2013-1150.
43. Milanesi, A.; Lee, J.W.; Yang, A.; Liu, Y.Y.; Sedrakyan, S.; Cheng, S.Y.; Perin, L.; Brent, G.A. Thyroid Hormone Receptor Alpha is Essential to Maintain the Satellite Cell Niche During Skeletal Muscle Injury and Sarcopenia of Aging. *Thyroid* **2017**, *27*, 1316–1322, doi:10.1089/thy.2017.0021.
44. Lontay, B.; Serfozo, Z.; Gergely, P.; Ito, M.; Hartshorne, D.J.; Erdodi, F. Localization of myosin phosphatase target subunit 1 in rat brain and in primary cultures of neuronal cells. *J. Comp. Neurol.* **2004**, *478*, 72–87, doi:10.1002/cne.20273.
45. Brown, D.M.; Parr, T.; Brameld, J.M. Myosin heavy chain mRNA isoforms are expressed in two distinct cohorts during C2C12 myogenesis. *J. Muscle Res. Cell Motil.* **2012**, *32*, 383–390, doi:10.1007/s10974-011-9267-4.
46. Izumo, S.; Nadal-Ginard, B.; Mahdavi, V. All members of the MHC multigene family respond to thyroid hormone in a highly tissue-specific manner. *Science* **1986**, *231*, 597–600, doi:10.1126/science.3945800.
47. Vicente-Manzanares, M.; Horwitz, A.R. Myosin light chain mono- and di-phosphorylation differentially regulate adhesion and polarity in migrating cells. *Biochem. Biophys. Res. Commun.* **2010**, *402*, 537–542, doi:10.1016/j.bbrc.2010.10.071.
48. Tullio, A.N.; Accili, D.; Ferrans, V.J.; Yu, Z.X.; Takeda, K.; Grinberg, A.; Westphal, H.; Preston, Y.A.; Adelstein, R.S. Nonmuscle myosin II-B is required for normal development of the mouse heart. *Proc. Natl. Acad. Sci. USA* **1997**, *94*, 12407–12412, doi:10.1073/pnas.94.23.12407.
49. Zvibel, I.; Atias, D.; Phillips, A.; Halpern, Z.; Oren, R. Thyroid hormones induce activation of rat hepatic stellate cells through increased expression of p75 neurotrophin receptor and direct activation of Rho. *Lab. Investig.* **2010**, *90*, 674–684, doi:10.1038/labinvest.2010.48.
50. Kondo, A.; Tokuda, H.; Kato, K.; Matsushima-Nishiwaki, R.; Kuroyanagi, G.; Mizutani, J.; Kozawa, O.; Otsuka, T. Rho-kinase negatively regulates thyroid hormone-stimulated osteocalcin synthesis in osteoblasts. *Biochimie* **2013**, *95*, 719–724, doi:10.1016/j.biochi.2012.10.020.
51. Pajouhi, N.; Owji, M.; Naghibalhossaini, F.; Omrani, G.H.; Varedi, M. Modulation by thyroid hormone of myosin light chain phosphorylation and aquaporin 5 protein expression in intact lung. *J. Physiol. Biochem.* **2015**, *71*, 99–106, doi:10.1007/s13105-015-0386-z.
52. Horvath, D.; Sipos, A.; Major, E.; Konya, Z.; Batori, R.; Dedinszki, D.; Szoll Si, A.; Tamas, I.; Ivan, J.; Kiss, A.; et al. Myosin phosphatase accelerates cutaneous wound healing by regulating migration and differentiation of epidermal keratinocytes via Akt signaling pathway in human and murine skin. *Biochim. Biophys. Acta Mol. Basis Dis.* **2018**, *1864*, 3268–3280, doi:10.1016/j.bbadis.2018.07.013.
53. Stull, J.T.; Kamm, K.E.; Taylor, D.A. Calcium control of smooth muscle contractility. *Am. J. Med. Sci.* **1988**, *296*, 241–245, doi:10.1016/s0002-9629(15)40865-1.
54. Ragolia, L.; Cherpalis, B.; Srinivasan, M.; Begum, N. Role of serine/threonine protein phosphatases in insulin regulation of Na+/K+-ATPase activity in cultured rat skeletal muscle cells. *J. Biol. Chem.* **1997**, *272*, 23653–23658, doi:10.1074/jbc.272.38.23653.
55. Lei, J.; Mariash, C.N.; Ingbar, D.H. 3,3',5-Triiodo-L-thyronine up-regulation of Na,K-ATPase activity and cell surface expression in alveolar epithelial cells is Src kinase- and phosphoinositide 3-kinase-dependent. *J. Biol. Chem.* **2004**, *279*, 47589–47600, doi:10.1074/jbc.M405497200.
56. Kjeldsen, K.; Norgaard, A.; Gotzsche, C.O.; Thomassen, A.; Clausen, T. Effect of thyroid function on number of Na-K pumps in human skeletal muscle. *Lancet* **1984**, *2*, 8–10, doi:10.1016/s0140-6736(84)91996-2.
57. Logvinenko, N.S.; Dulubova, I.; Fedosova, N.; Larsson, S.H.; Nairn, A.C.; Esmann, M.; Greengard, P.; Aperia, A. Phosphorylation by protein kinase C of serine-23 of the alpha-1 subunit of rat Na+,K(+)-ATPase affects its conformational equilibrium. *Proc. Natl. Acad. Sci. USA* **1996**, *93*, 9132–9137, doi:10.1073/pnas.93.17.9132.
58. Feraille, E.; Beguin, P.; Carranza, M.L.; Gonin, S.; Rousselot, M.; Martin, P.Y.; Favre, H.; Geering, K. Is phosphorylation of the alpha1 subunit at Ser-16 involved in the control of Na,K-ATPase activity by phorbol ester-activated protein kinase C? *Mol. Biol. Cell* **2000**, *11*, 39–50, doi:10.1091/mbc.11.1.39.
59. Vasilets, L.A.; Postina, R.; Kirichenko, S.N. Mutations of Ser-23 of the alpha1 subunit of the rat Na+/K+-ATPase to negatively charged amino acid residues mimic the functional effect of PKC-mediated phosphorylation. *FEBS Lett.* **1999**, *455*, 8–12, doi:10.1016/s0014-5793(99)00851-0.

lontay.beata_285_24

SCIENTIFIC REPORTS

OPEN

Received: 01 June 2016
Accepted: 08 December 2016
Published: 11 January 2017

Myosin phosphatase and RhoA-activated kinase modulate arginine methylation by the regulation of protein arginine methyltransferase 5 in hepatocellular carcinoma cells

Adrienn Sipos[1], Judit Iván[1,2], Bálint Bécsi[1,2], Zsuzsanna Darula[3], István Tamás[1], Dániel Horváth[1], Katalin F. Medzihradszky[3], Ferenc Erdődi[1,2] & Beáta Lontay[1]

Myosin phosphatase (MP) holoenzyme is a protein phosphatase-1 (PP1) type Ser/Thr specific enzyme that consists of a PP1 catalytic (PP1c) and a myosin phosphatase target subunit-1 (MYPT1). MYPT1 is an ubiquitously expressed isoform and it targets PP1c to its substrates. We identified the protein arginine methyltransferase 5 (PRMT5) enzyme of the methylosome complex as a MYPT1-binding protein uncovering the nuclear MYPT1-interactome of hepatocellular carcinoma cells. It is shown that PRMT5 is regulated by phosphorylation at Thr80 by RhoA-associated protein kinase and MP. Silencing of MYPT1 increased the level of the PRMT5-specific symmetric dimethylation on arginine residues of histone 2A/4, a repressing gene expression mark, and it resulted in a global change in the expression of genes affecting cellular processes like growth, proliferation and cell death, also affecting the expression of the retinoblastoma protein and c-Myc. The phosphorylation of the MP inhibitory MYPT1^{T850} and the regulatory PRMT5^{T80} residues as well as the symmetric dimethylation of H2A/4 were elevated in human hepatocellular carcinoma and in other types of cancers. These changes correlated positively with the grade and state of the tumors. Our results suggest the tumor suppressor role of MP via inhibition of PRMT5 thereby regulating gene expression through histone arginine dimethylation.

Hepatocellular carcinoma (HCC) is one of the most common cancers worldwide and is a leading cause of cancer-related deaths. The molecular mechanism behind the pathogenesis of HCC is poorly understood, although molecular markers and more precise classification would be crucial[1]. One of the potential therapeutic target mechanisms is reversible protein phosphorylation at serine (Ser) and threonine (Thr) residues by the coordinated action of protein kinases and phosphatases. More than 98% of cellular protein phosphorylation occurs at Ser/Thr[2] and it regulates intracellular signal transduction pathways resulting in profound changes in cellular responses. Many protein kinases are identified as oncogenes and protein dephosphorylation by protein phosphatases may also play a critical role in malignant transformation of cells[3]. Protein phosphatase-1 (PP1) is one representative of the major phospho-Ser/Thr (P-Ser/Thr) specific eukaryotic protein phosphatases. Mammalian genomes contain three different genes that encode five distinct PP1 catalytic subunits (PP1c): PP1cα*1*/*a2*, PP1cβ/δ and PP1cγ_1/γ_2[4]. Several lines of evidence suggest that PP1 activity is required for exit from mitosis, yet may also block cell cycle progression and facilitate apoptosis[5]. Moreover, okadaic acid, a potent and specific inhibitor of PP1 and protein phosphatase 2 A (PP2A) enzymes was described as a powerful tumor promoter that triggers tumor formation in various organs such as liver[6]. Previous studies reported that the nuclear PP1cα and PP1cβ/δ activity significantly decreased in human HepG2 and rat AH13 hepatoma cells compared with primary cultured hepatocytes also suggesting that PP1 is a tumor suppressor in its own right[5].

[1]Department of Medical Chemistry, Faculty of Medicine, University of Debrecen, Debrecen, H-4032, Hungary. [2]MTA-DE Cell Biology and Signaling Research Group, Faculty of Medicine, University of Debrecen, Debrecen, H-4032, Hungary. [3]Laboratory of Proteomics Research, Biological Research Centre, Hungarian Academy of Sciences, Szeged, H-6726, Hungary. Correspondence and requests for materials should be addressed to B.L. (email: lontay@med.unideb.hu)

lontay.beata_285_24

It is assumed that free PP1c is not present in the cells, but it performs its diverse biological activities by forming holoenzymes with one of the almost 200 PP1c-binding proteins, termed targeting/inhibitory subunits, in a mutually exclusive manner[7]. The functions of these proteins are to target PP1c to the substrate, to modulate the enzyme activity and to determine the subcellular localization[8]. Myosin phosphatase target subunit 1 (MYPT1) is one of the regulatory proteins that binds to PP1c to form a highly stable holoenzyme referred to as myosin phosphatase (MP). MP is a heterotrimer composed of the β/δ isoform (termed both ways) of PP1c and two non-catalyic subunits, MYPT1 and a 20 kDa subunit with essentially unknown function[9]. It is the dominant form in smooth muscle but is expressed ubiquitously in mammalian tissues[10]. Much of the earlier works have focused on smooth muscle MP, which regulates the phosphorylation level of the 20 kDa regulatory light chains of myosin II, thereby mediating contractile and motile events in these cells[11]. Although numerous cytoskeletal MP substrates have been identified so far[12] suggesting its role in cell migration and metastasis formation, MYPT1 was also found in the nuclear and microsomal fraction of HepG2 cells[13], and in the nucleus of neuronal cells[14]. MP plays important roles in nucleus related cellular processes, including mitosis by antagonizing polo-like kinase-1[15], apoptosis by dephosphorylating and facilitating the nuclear localization of the histone deacetylase protein and repression of *Nur77*, a proapoptotic gene[16]. MP also inhibits oncogenic signaling cascades by modulating the dephosphorylation of merlin tumor suppressor protein, which regulates the Ras-signaling extracellular signal-regulated kinase (ERK) pathway driving tumorigenic transformation[17]. MP also modulates the dephosphorylation of the retinoblastoma protein, which plays a role in G1/S transition of cell cycle[18]. Moreover, MYPT1 KO mice develops a lethal phenotype indicating the crucial role of MP in cell proliferation and gene expression[19]. Thus, the above data suggest that dysregulation of phosphorylation signaling pathways related to MP is directly correlated with a plethora of diseases such as cancer and diabetes.

One of the potential regulatory pathways related to MP function is driven by the RhoA GTPase and its downstream Ser/Thr kinase termed RhoA-activated kinase (ROK) which was shown to phosphorylate MYPT1 at Thr696 and Thr850, thereby causing inhibition of MP activity[20]. Although Thr696 of MYPT1 can be phosphorylated by other kinases, the Thr850 (by human sequence) inhibitory phosphorylation site is dominantly regulated by ROK[21]. Additionally, numerous other downstream targets of ROK have been identified including intermediate filaments, adducin and the dephosphorylation of these substrates at the ROK-specific phosphorylation site are catalyzed by MP[22]. It was shown that initiation of HCC formation[23] is mediated by ROK and hyperactivation of RhoA/ROK is associated with aggresive tumors with enhanced metastatic features in numerous organs[24]. Moreover, Y27632, the selective inhibitor of ROK suppresses invasiveness of several animal cancers such as HCC[25]. A plethora of studies have suggested that ROK inhibitors might be drug candidates in the treatment of cancer by targetting stromal cells rather than tumor cells[26].

To elucidate the contribution of the ROK/MP axis in tumorigenesis beyond their already described role in angiogenesis and metastasis our goal was to describe the nuclear function of MP. Our present data indicate a potential tumorsuppressor role for MP in human hepatocarcinoma cells via antagonizing the tumorigenic effect of ROK. Our results shed light on the involvement of ROK/MP enzyme pair in the phosphorylation/dephosphorylation of the protein arginine methyltransferase 5 (PRMT5) via regulating arginine methylation of histones thereby affecting signaling for cancer formation.

Results

MYPT1 nuclear interactome: interaction with PRMT5 of the methylosome complex. Initial reports have already described the presence of MYPT1 in the nucleus but its exact subnuclear localization and function remained unknown[13]. MYPT1, PP1cα/γ1 and PP1cδ were distributed in the cytoplasmic and nuclear subcellular fractions (Fig. S1A). Specific activity measured in the presence of 2 μM inhibitor-2 (I2) which is a highly selective inhibitor of PP1, but does not influence PP2A activity[27] suggested that ~60% of total phosphatase activity of nuclear fraction was due to PP1 (Fig. S1B). Myosin phosphatase was found to be localized to the chromatin and the spliceosomes in the nucleus of HepG2 cells (Fig. S1C). To gain more data for the role of MP, we determined the nuclear interactome of Flag (FT)-MYPT1 by mass spectrometry. Pull-down assays were carried out using FT-MYPT1 protein bound to anti-Flag M2 affinity gel which was incubated with the nuclear extract of HepG2 cells. The FT-MYPT1 binding proteins were eluted from the beads, separated by SDS-PAGE then the protein bands were silver-stained, excised and subjected to LC-MS/MS analysis. Twenty-two potential MYPT1-interacting proteins were identified (Table 1). The peptide sequences identified are presented in Table S1 together with the percentage distribution for cellular roles of their parent proteins (Table S2). Nuclear MYPT1-binding proteins may play roles in RNA processing and splicing and in gene expression (Table 1). Mitogen-activated protein kinase and magnesium-dependent protein phosphatase 1B (PP1B/PP2C) were also among the potential interacting partners of MYPT1. Strikingly, the protein arginine methyltransferase 5 (PRMT5/JBP1), the member of the methylosome complex was also identified. PRMT5 is one of the nine PRMTs in mammalian cells and plays an unique and specific role in the generation of the ω-N^G, N^G-symmetric dimethylarginine (SDMA) as a type II PRMT. It has multiple cytosolic and nuclear binding partners and is implicated in the regulation of transcription, RNA transport and cellular signaling[28].

PRTM5 of the methylosome complex interacts with MP through the N-terminal region in MYPT1. Since PRMT5 was identified as a nonspecific interacting protein in affinity purified Flag-tagged complexes from HeLa and tsa cell lysates[29], we verified the interaction between the nuclear PRMT5 and MYPT1 with additional methods. Anti-$MYPT1^{1\text{-}296}$ and anti-PRMT5 antibodies were used to immunoprecipitate target proteins and a possible association between MYPT1 and PRMT5 was assayed in HepG2 cells (Fig. 1A). PRMT5 and MYPT1 were identified in each precipitates as judged by Western blots implying that these two proteins were co-precipitated. No cross reactions were detected in the non-immune serum control (Fig. 1A). Surface plasmon resonance (SPR)-based binding assays were carried out to investigate the molecular background of

lontay.beata 285 24

NCBI gi#	Protein	MW, Da	Peptide number	Function
4505317	Protein phosphatase 1 regulatory subunit 12 A isoform a (MYPT1)	115610	20	Signal transduction
13699824	Kinesin family member 11	120111	7	Motor protein, mitosis
338443	Beta-spectrin	275259	3	Protein targeting
20070220	Protein arginine methyltransferase 5 isoform a	73322	8	Transcription regulation
4507361	Mitogen-activated protein kinase kinase kinase 7 isoform A	64930	3	Signal transduction, transcription regulation
4506583	Replication protein A1	68723	2	DNA replication, DNA damage
4505995	Protein phosphatase 1B isoform 1	53180	6	Signaling pathways, cell stress response pathways
307383	RNA helicase A	143405	3	Translation initiation, splicing, spliceosome assembly
29881667	Splicing factor proline/glutamine-rich	76255	8	Splicing
11067747	CDC5-like protein	92422	2	Cell cycle control, transcription regulation
288100	Initation factor 4B	69240	2	Translation initiation
4885225	Ewing sarcoma breakpoint region 1 isoform 2	68721	2	Gene expression, cell signaling, RNA processing
693937	Polyadenylate binding protein II	58709	12	Gene expression, RNA processing
56237027	Insulin-like growth factor 2 mRNA binding protein 1 isoform 1	63783	2	Translation regulation, mRNA transport
4504447	Heterogeneous nuclear ribonucleoprotein A2/B1 isoform A2	36041	3	Gene expression, mRNA processing
4504445	Heterogeneous nuclear ribonucleoprotein A1 isoform a	34289	2	mRNS processing and transport, RNA splicing
356168	Histone H1b	21721	2	DNA-binding, nucleosome assembly

Table 1. FT-MYPT1 binding proteins of HepG2 nuclear fraction.

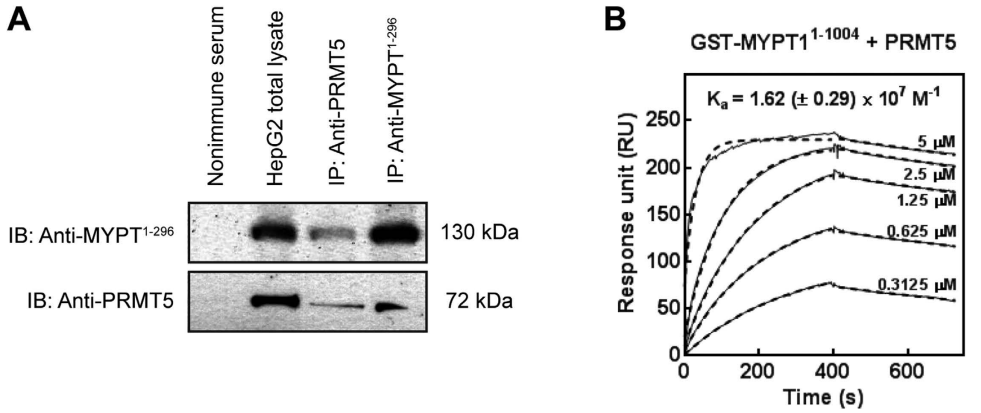


Figure 1. Interaction of MYPT1 with PRMT5. (**A**) Immunoprecipitations were carried out using anti-MYPT1$^{1\text{-}296}$ and anti-PRMT5 antibodies as well as nonimmune rabbit serum as negative control. Immunoprecipitates and HepG2 total lysate were analysed by Western blots using antibodies specific for MYPT1 and PRMT5. (**B**) SPR analysis of the interaction of MYPT1 with PRMT5. Full-length GST-MYPT1$^{1\text{-}1004}$ was immobilized on anti-GST coupled CM5 sensor chip. FT-PRMT5 was injected over the surfaces in the indicated concentrations. The interaction was monitored using Biacore 3000. The association constant (K_a) value was indicated in the figure.

MYPT1-PRMT5 interaction using full-length GST-MYPT1 as well as a GST-fusion C-terminal fragment of residues 667 to 1004 (GST-MYPT1$^{667\text{-}1004}$). These MYPT1 species were bound on SPR sensorchips to immobilized anti-GST and purified FT-PRMT5 was flown through the flow cells as an analyte. PRMT5 formed a stable complex with the full-length GST-MYPT1$^{1\text{-}1004}$ in a concentration range of 0.3125–5 μM and the association constant for binding was $K_a = (1.62 \pm 0.29) \times 10^7 M^{-1}$ (Fig. 1B), while no signal for binding was obtained with GST-MYPT1$^{667\text{-}1004}$ (data not shown). Fitting the sensograms with a 1:1 binding model resulted in overlaps with the experimental curves suggesting a 1. 1 molar ratio in the GST-MYPT1$^{1\text{-}1004}$- PRMT5 complex formed. These data demonstrate also that PRMT5 forms a stable interaction with the N-terminal region of MYPT1.

PRMT5 is a substrate of ROK and MP and its methyltransferase activity is regulated via phosphorylation/dephosphorylation of its Thr80 residue. The putative phosphorylation sites of PRMT5 were screened and the identities of protein kinases that may target these sites were predicted by a P-Si

lontay.beata_285_24

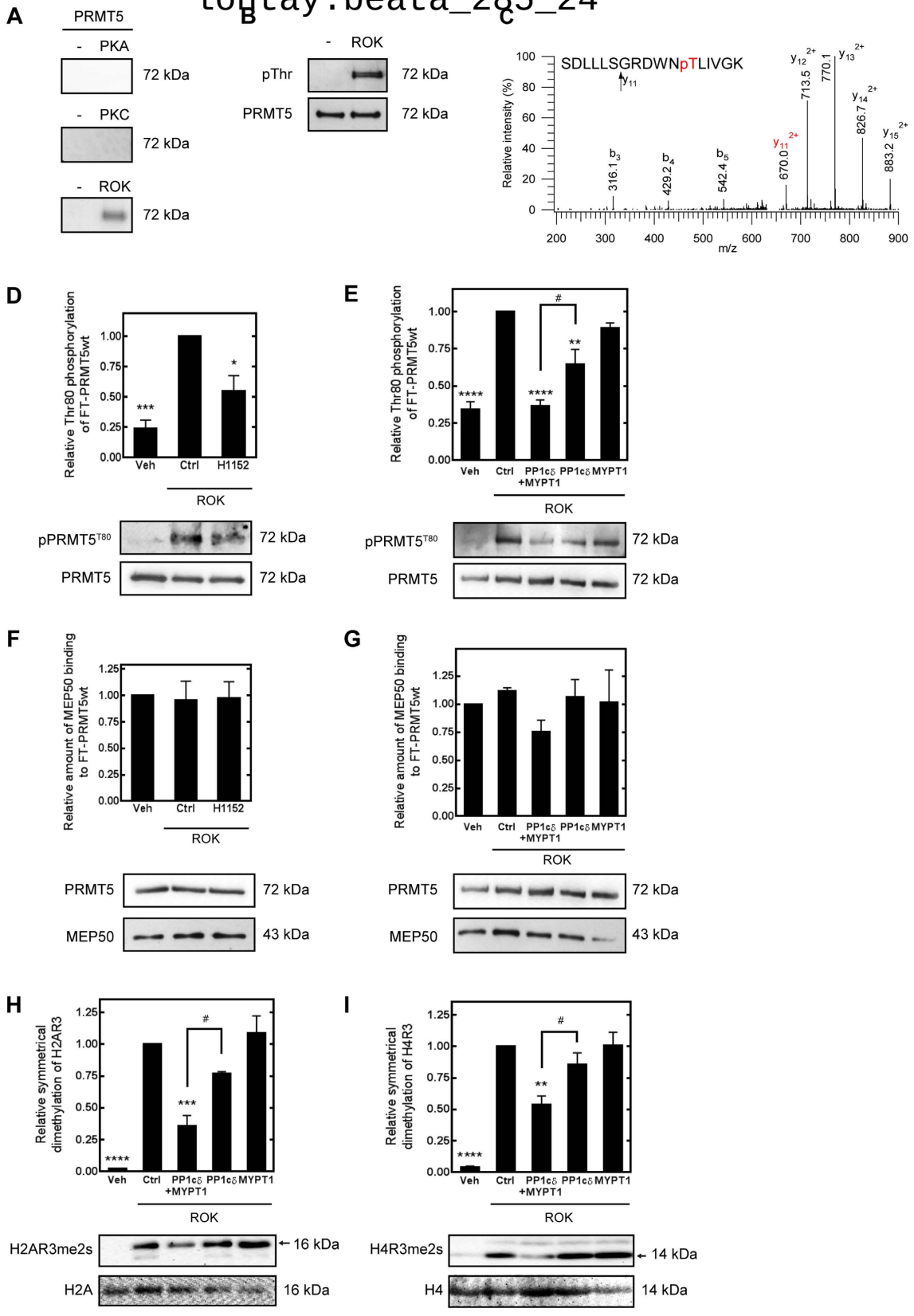


Figure 2. ROK and MP regulate the methyltransferase activity of PRMT5 through phosphorylation/dephosphorylation at Thr80. (**A**) Autoradiograms of PRMT5 phosphorylated in the absence or in the presence of 0.1 μg/ml protein kinase A (PKA, left panel), 0.1 μg/ml protein kinase C (PKC, middle panel) or 0.4 U/ml Rho-associated kinase (ROK, right panel) with ^{32}P-ATP. (**B**) Western blot analysis of ROK-phosphorylated PRMT5 using antibody specific for phospho-Thr. After stripping the membrane anti-PRMT5 antibody was applied to detect PRMT5 as an input control. (**C**) Ion trap collision-induced dissociation (CID)

lontay.beata 285 24

spectra of PRMT5 phosphopeptides. CID of m/z: 656.338 (3+) identified as SDLLLSGRDWNpTLIVGK representing [69–85] of the wild type protein. Thr80 was identified as the modification site (see fragment ion y_{11} (phosphorylated)). Peptide fragments are labeled according to the nomenclature by Biemann[56]. (**D**) Effect of ROK inhibitor (10 μM H1152) on the phosphorylation level of PRMT5 during *in vitro* ROK assay. Control samples were prepared in the absence of ROK, positive control samples were prepared in the presence of ROK without ROK inhibitor. Relative phosphorylation level of Thr80 was judged by Western blot using anti-pPRMT5^{T80} antibody and blots for PRMT5 served as loading control. (**E**) Effect of 25 nM FT-MYPT1 and 5 nM rPP1cδ or their combination on the phosphorylation level of PRMT5 at Thr80[80] as judged by Western blot. Data were compared to ROK-phosphorylated PRMT5. (**F**,**G**) Amount of MEP50 bound to FT-PRMT5 during ROK-phosphorylation (**F**) and dephosphorylation by MP (**G**) compared to unphosphorylated control samples. MEP50 was detected by anti-MEP50 antibody during Western blot and relative amount was normalized to the level of PRMT5. (**H**,**I**) *In vitro* arginine methyltransferase assay of unphosphorylated and ROK-phosphorylated PRMT5 measured by the symmetric dimethylation level of histone H2A Arg3 (H2AR3me2s, F) or histone H4 Arg3 (H4R3me2s, G) in the presence of 25 nM FT-MYPT1, 5 nM rPP1cδ or their combinations. Gels have been processed under the same experimental conditions. Values represents mean ± SEM; $^{**}p < 0.01$, $^{***}p < 0.001$, $^{****}p < 0.0001$, $^{\#}p < 0.05$, one-way ANOVA followed by Tukey's multiple comparison test, n = 3.

Predictor alogrithm developed by Kinexus (http://www.phosphonet.ca/). Protein kinase A (PKA), protein kinase C (PKC) and ROK were suggested as potential phosphorylating enzymes therefore they were probed in *in vitro* phosphorylation assays. The autoradiogram in Fig. 2A shows that PRMT5 was phosphorylated by ROK but not by PKA or PKC in kinase assays when radioactive ATP (γ- ^{32}P-ATP) was used as phosphoryl donor substrate. Western blot analysis of ROK-phosphorylated PRMT5 by antibody specific for phosphorylated Thr (Fig. 2B) indicated that ROK phosphorylates PRMT5 definitely on Thr residue. Thr80 residue was identified as a ROK phosphorylation site in PRMT5 by mass spectometry analysis of ROK-phosphorylated FT-PRMT5 samples compared to non-phosphorylated ones (Fig. 2C). Ser15/16, Thr67 were Ser69 were also identified as potential phosphorylation sites of PRMT5 from LC-MS/MS data. However, only Thr80 phosphorylation was unambiguously linked to the ROK-treatment since the phosphorylation of Ser15/16 was also identified in control samples which were incubated without ROK and the Thr67 and Ser69 phosphorylation sites were infirm even after the enrichment using titanium-oxide chromatography (Fig. S6.).

ROK-specific phosphorylation of PRMT5^{T80} was confirmed by ROK-assay (Fig. 2D, Fig. S3A) in which the relative Thr80 phosphorylation level of wild type PRMT5 determined by anti-phospho-PRMT5^{T80} antibody (anti-pPRMT5^{T80}) was significantly decreased in the presence of H1152, a selective Rho-kinase inhibitor. Alanine mutant of PRMT5^{T80} (PRMT5^{T80A}) was generated by site-directed mutagenesis and phosphorylation of this mutant was probed in ROK assay in the presence and absence of H1150. As judged with anti- anti-PPRMT5^{T80} antibody on Western blot no signal was detected confirming the Thr80 specificity of ROK in PRMT5 phosphorylation (Fig. S3B).

To prove the regulatory role of MP on PRMT5, FT-PRMT5 was phosphorylated by ROK and *in vitro* phosphatase assays were carried out using recombinant PP1cδ and purified FT-MYPT1 proteins or their combination representing MP holoenzyme (Fig. 2E). Western blot data using anti-pPRMT5^{T80} showed that the FT-MYPT1 had no effect on the phosphorylation level of PRMT5 at Thr80, whereas recombinant PP1cδ or the mixture of PP1cδ and FT-MYPT1 caused ~14% and ~40% decrease in phospho-PRMT5^{T80}, respectively comparing to the ROK-phosphorylated samples. The increased dephosphorylation of PRMT5 at Thr80 by PP1cδ in presence of FT-MYPT1 indicates that the phosphorylated PRMT5 is a substrate of MP holoenzyme and MYPT1 has a targeting role in this dephosphorylation process.

To determine the effect of the phosphorylation of PRMT5 at Thr80 on its methyltransferase activity we assayed PRMT5 activity by determining symmetric dimethylation of histone 2A and 4 (H2A and H4) on their common arginine 3, the so called "R3 motif"[30]. No significant changes in symmetrical dimethylation of H2AR3 or H4R3 were detected when FT-MYPT1 without PP1cδ was used (Fig. 2H and I). Nevertheless, in accordance with the rate of PRMT5-dephosphorylation represented in Fig. 3G symmetrical dimethylation of H4R3 was decreased by 15% and 46% when PP1cδ and the mixture of FT-MYPT1 and PP1cδ was applied during methyltransferase assay. Changes in the symmetrical dimethylation level of H2AR3 (Fig. 2F) were even more profound, 23% adding PP1cδ and 67% adding the mixture of PP1cδ and FT-MYPT1. Since MEP50 is an essential component of the methyltransferase activity of PRMT5, we tested if the phosphorylation at Thr80 increases the affinity of MEP50 to PRMT5 resulting the enhanced activity upon ROK phosphorylation. The phosphorylation by ROK with or without the inhibition of ROK by H1152 had no effect on the amount of the MEP50 bound to the wt PRMT5 (Fig. 2F.). The relative amount of MEP50 binding to wt PRMT5 showed no significant differences either upon ROK phosphorylation or the dephosphorylation by MP (Fig. 2G.) suggesting that the phosphorylation of PRMT5 at Thr80 has no effect on MEP50 binding. These data indicate that Thr80 residue is a regulatory phosphorylation site of PRMT5 and the phosphorylation increases, while the dephosphorylation decreases its methytransferase activity.

Silencing of MYPT1 increased H2A and H4 Arg3 dimethylation and PRMT5 phosphorylation at Thr80 in HepG2 cells. Histone 2AR3 and −4R3 are symmetrically dimethylated by PRMT5 which shifts the balance from an activating asymmetric (ADMA) to a suppressive symmetric dimethylarginine (SDMA) mark at these motifs with respect to gene expression[31]. The fact that MP dephosphorylated PRMT5 at the ROK-specific phosphorylation site *in vitro* led us to examine whether MP plays a role in the regulation of gene expression through the arginine methylation of H2A and 4 at the gene repression sites *in vivo*. We first transfected HepG2 cells with MYPT1-specific siRNAs (siMYPT1) or non-targeting siRNA as a control. SiMYPT1 was able to lower

lontay.beata_285_24

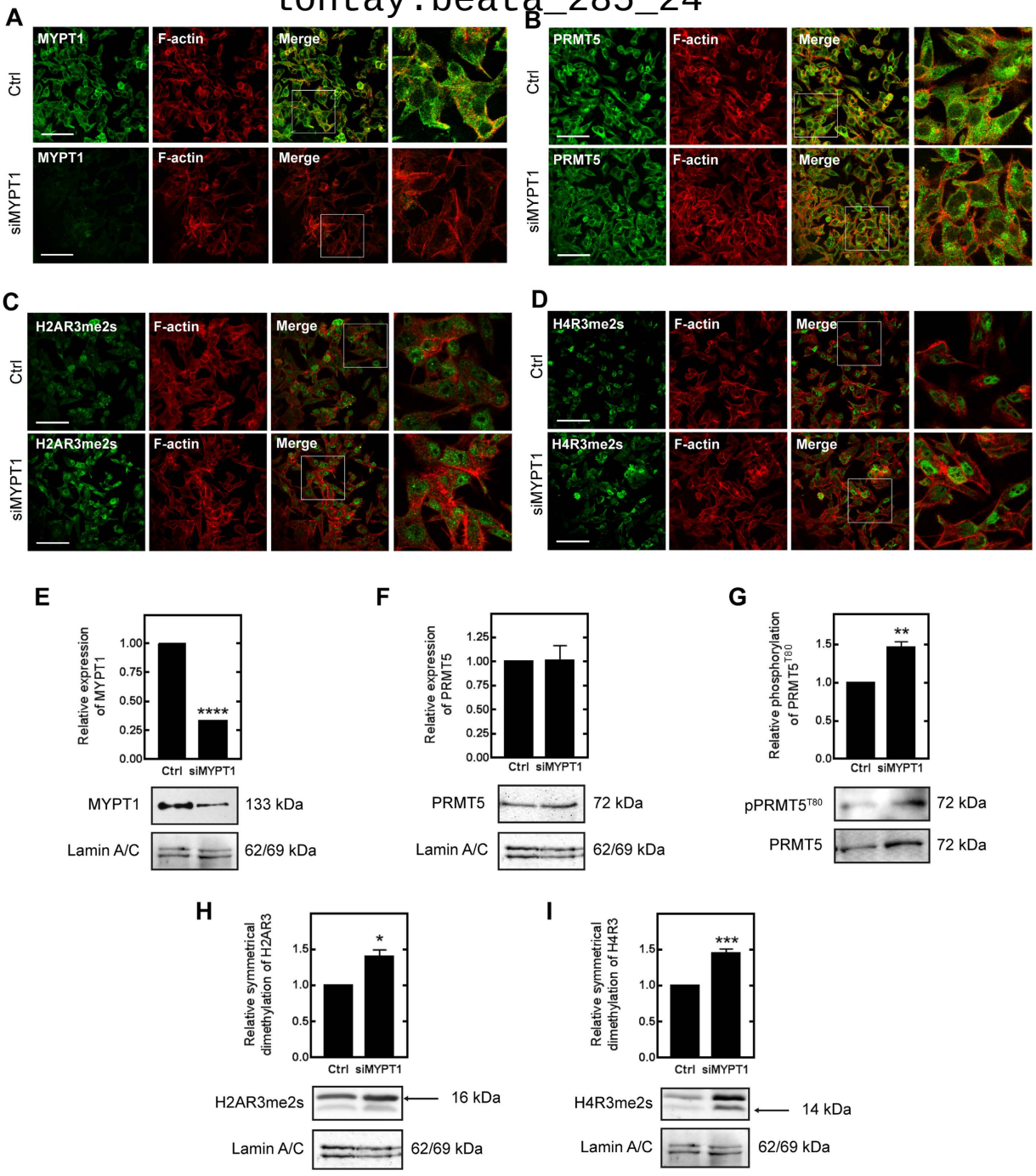


Figure 3. Effect of MYPT1 silencing on the methyltransferase activity of PRMT5 in HepG2 cells. Immunofluorescent staining of non-target control (Ctrl) and MYPT1-silenced (siMYPT1) cells using antibodies specific for MYPT1$^{1\text{-}296}$ (**A**), PRMT5 (**B**), histone H2A symmetric dimethyl Arg3 (H2AR3me2s (**C**) and histone H4 symmetric dimethyl Arg3 (H4R3me2s (**D**) and actin as inducated in the figures. Scale bars: 50 μM. Enlargement of framed regions in merged images are shown on the right on A, B, C and D panels. Nuclear fractions of non-target control (Ctrl) and MYPT1-silenced (siMYPT1) HepG2 cells were prepared and analysed by Western blot using anti-MYPT1$^{1\text{-}296}$ (**E**), anti-PRMT5 (**F**), anti-pPRMT5^{T80} (**G**), anti-histone H2A symmetric dimethyl Arg3 (**H**) and anti-histone H4 symmetric dimethyl Arg3 (**I**) specific antibodies. The relative expression of MYPT1 or PRMT5 and the relative symmetric dimethylation level of H2AR3 or H4R3 were normalized to lamin A/C as internal control. Samples derived from the same experiment and the blots were processed in parallel or assayed after stripping. The relative phosphorylation level of PRMT5^{T80} was normalized to the expression level of PRMT5 and then to lamin A/C as internal control by densitometry. Mean ± SEM; n = 3; *$p < 0.05$, **$p < 0.01$, ***$p < 0.001$, ****$p < 0.0001$ by student *t*-test.

lontay.beata_285_24

the protein expression of MYPT1 by >70% (Fig. 3E) without causing any significant decrease either in the survival (Fig. S4A) or the caspase-3 activity (Fig. S4B) as signs for apotosis of HepG2 cells. Upon MYPT1-silencing drastic changes in cell morphology and in formation of stress fibers were detected by immunofluorescent staining (Fig. 3A). PRMT5 was localized to the cytosolic as well as to the nuclear fraction (Fig. 3B). MYPT1-silencing had no effect on either the protein expression (Fig. 3F) or on the subcellular localization of PRMT5, however, the phosphorylation of PRMT5 at Thr80 was increased by 46% (Fig. 3G). Moreover, we examined the effect of siMYPT1 on the level of dimethylation of H2AR3 (Fig. 3H) and H4R3 (Fig. 3I) and it was elevated by 40% and 45%, respectively, whereas the expression of both histone proteins remained constant. The fluorescence intensity of the dimethylation of H2AR3 (Fig. 3C) and H4R3 (Fig. 3D) increased followed by MYPT1-silencing. Fluorescent mean intensity of H2AR3 symmetrical dimethylation increased from 12.8 to 21.79 (arbitrary unit) due to MYPT1-silencing. Difference in symmetrical dimethylation was more considerable in case of H4R3 (from 8.19 to 22.58) compared to non-significant intensity changes of H2A or H4 expression (Table S6). To verify our data we applied the nuclear extract of non-target and MYPT1-silenced HepG2 and MCF7 cells on quantitative methyltransferase assay (Fig. S5A and B). Knocking down MYPT1 increased the specific activity of PRMT5 by ~65% comparing to the control samples. Taken together, our results reflect the physiological regulatory role of MP in the methyltransferase activity of PRMT5 and thus influence the dimethylation of histone respression marks.

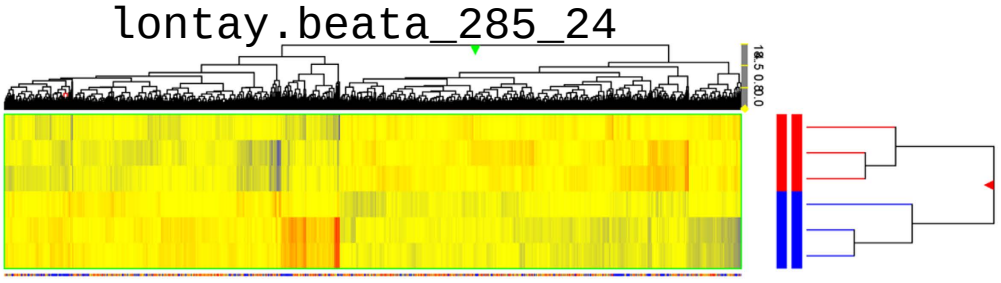
Silencing of MYPT1 results in altered gene expression pattern and downregulates the expression of tumor suppressors in HepG2 cells. To more precisely define the role of MP in functions related to the regulation of dimethylation of histone proteins, we performed microarray studies using the Affymetrix Human Gene 1.0 ST Array for the analysis of gene expression. Over 39,000 transcripts/single array were examined encompassing the entire expressed human genome. Total RNA was isolated from control and MYPT1-silenced (siMYPT1) HepG2 cells (Fig. 4). The comparison of control and siMYPT1 samples identified 2728 genes differentially regulated between the two groups. Complete lists of genes are available at www.figshare.com website. Table S7 shows a list of genes that were up- or downregulated by more than 1.5-fold ($n = 3$) in the siMYPT1 samples when compared to gene expression pattern. Hierarchical cluster analysis was performed on all differentially expressed genes using average linkage with Pearson's dissimilarity and the number of induced and repressed genes were presented in a heat map (Fig. 4A). Bioinformatic analysis was assigned to different canonical pathways such as LPS/IL-1 mediated inhibition of RXR function (PPAR α, γ, IL1R, JUN), antioxidant action of vitamin C (STAT5, MAPK3 and 9), cell cycle regulation (Not7, PPP2C, CDK2, E2F3, Rb protein) as well as IL-4 and IL-8 signaling. Knocking down of MYPT1 also influenced molecular and cellular functions such as lipid metabolism, molecular transport, cell growth and differentiation and cell death. Additionally, the siMYPT1-related genes were analyzed for identifying diseases and disorders relevant to the list. Strikingly, 36% of all related genes (960) were linked to cancer disease such as lymphohematopoietic, liver and breast cancer and renal-cell carcinoma formation. Genes related to infectious diseases and developmental disorders were also identified in 10% and 6%, respectively. Taken together, microarray analysis identified a number of signaling pathways strongly point to a role of MP in the regulation of gene expression.

The evaluation of genes related to MYPT1-silencing revealed the significant downregulation of several tumor suppressors and transcription factors. One of them is the retinoblastoma protein (pRb) that plays a pivotal role in the negative control of the cell cycle and in tumor progression as a major regulator of G1 checkpoint[32]. The other is c-Myc that regulates the cell cycle progression and cellular transformation as a multifunctional transcription factor[33]. The protein expressions of pRb and c-Myc were significantly decreased upon MYPT1 silencing and these were also confirmed by Western blot analysis (Fig. 4C and D). To clarify fully the connection between the MP activity and the PRMT5-regulated gene expression we screened for genes related to both PRMT5 and MP in the database of the siPRMT5[34] and siMYPT1 microarray analysis, respectively. Rap1 gene expression was 2.3 fold reduced upon PRMT5 silencing in human embryonic stem cells and the expression of this gene was found to be significantly increased in siMYPT1 cells (Fig. 4E).

Myosin phosphatase is involved in the regulation of gene expression through the suppression mark of PRMT5 on histone 2A and 4 in human cancer. The microarray analysis indicated that in case of decreased level of MP cancer-related processes dominate. Reverse phase protein microarray analysis was conducted in multiple tissue lysates of patients for the validation of changes in the protein levels and their posttranslational modifications in cancer. Tumor tissue lysates obtained from a large group of human patients with grade 2 and 3 and state II and III (Fig. 5 dark grey columns) hepatocellular carcinoma (n = 20), four different types of metastatic liver cancers (Fig. 5 light grey columns) as well as 15 other types of cancer cell lines with their adequate normal cell type controls (Fig. 5 black columns) were analysed using high throughput screening for multiple protein targets such as PRMT5 (Fig. 5A), $pPRMT5^{T80}$ (Fig. 5B), MYPT1 (Fig. 5C), $pMYPT1^{T850}$ (Fig. 5D), histone 2A (Fig. 5E) and histone 2A symmetric arginine methylation (Fig. 5F).

The protein expression of PRMT5 showed an increase in ~75% of the investigated cancer tissues comparing to the healthy controls. THP-1 monocytic leukemia and Raji Burkitt lyphomoma cells presented the largest increase (Fig. 5A). The relative phosphorylation of PRMT5 at Thr80 in cancer tissues were significantly elevated in all cases escpecially in the leukemia, lung, colon and breast cancer carcinoma as well as in HCC tissues (Fig. 5B). The relative MYPT1 expression exhibited a diverse expression pattern since it was significantly downregulated in few cases (HeLa cervix and A549 lung carcinoma) but in uterine carcinoma it showed a twofold increase. However, MYPT1 expression did not change in the majority of cancer types (65%). Since MP holoenzyme activity is regulated through the phosphorylation of MYPT1 at the Thr850 inhibitory site, we were able to draw conclusions about the activity of PP1M in tumor cells based on the phosphorylation state of MP. Increased phosphorylation level of $MYPT1^{Thr850}$ was found in almost all cases up to a 10–12-fold elevation in breast and lung carcinomas

A



B

	Name	p-value	# molecules
Diseases and Disorders	Cancer	4.37E-06 - 7.75E-03	960
	Infectious Disease	4.44E-06 - 6.46E-03	263
	Neurological Disease	9.35E-06 - 6.93E-03	350
	Skeletal and Muscular Disorders	9.35E-06 - 7.48E-03	278
	Developmental Disorder	3.02E-05 - 6.93E-03	170
Molecular and Cellular Functions	Lipid Metabolism	1.75E-07 - 7.60E-03	231
	Molecular Transport	1.75E-07 - 7.60E-03	339
	Small Molecule Biochemistry	1.75E-07 - 7.60E-03	266
	Cellular Growth and Proliferation	1.26E-06 - 7.75E-03	509
	Cell Death and Survival	1.93E-06 - 7.53E-03	474
Physiological System Development and Function	Hair and Skin Development and Function	2.38E-05 - 7.52E-03	41
	Organismal Survival	2.50E-05 - 5.29E-04	368
	Immune Cell Trafficking	4.01E-05 - 7.68E-03	185
	Tumor Morphology	4.92E-05 - 6.82E-03	68
	Digestive System Development and Function	6.69E-05 - 7.52E-03	133

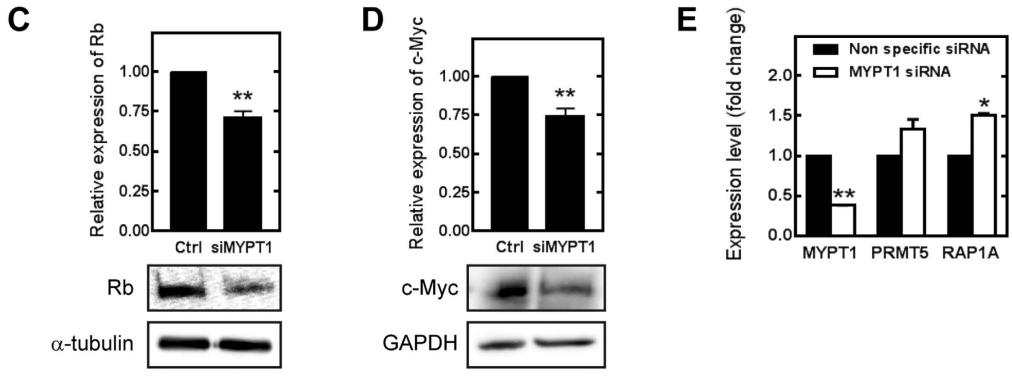


Figure 4. Microarray analysis of MYPT1-silenced HepG2 cells. (**A**) Heat map of genes related to MYPT1 silencing in HepG2 cells by microarray analysis. The color code for the signal strength is shown in the box at the bottom in which induced genes are indicated by red and repressed genes are indicated by blue. (**B**) The onthology of the related genes and their classification by GO terms. Detection of retinoblastoma protein (**C**) and c-Myc (**D**) protein expression changes due to MYPT1 silencing from HepG2 whole cell lysates by Western blot. Protein levels were quantified by densitometry normalized to α-tubulin or GAPDH expression level. Samples derived from the same experiment and processed in parallel. RT-PCR analysis of MYPT1, PRMT5 and RAP1A mRNA levels in non-specific siRNA treated and MYPT1 silenced HepG2 cells (**E**). GAPDH was used as an invariant gene. Values are mean ± SEM from three independent experiments; $^{*}p < 0.05$, $^{**}p < 0.01$ by student *t*-test.

(Fig. 5D). The overexpression of histone proteins in cancer cells and the elevated symmetric dimethylation of them have been already described in colorectal, glioblastoma and numerous other cancer types[35,36]. We also verified either no changes (Burkitt lymphoma, hepatocellular adenomatoid and trabecular adenocarcinoma) or significant elevation in histone protein expression (Fig. 5E) and 85% of all examined cancer types showed an increase in the repressive Arg3 symmetrical dimethylation mark. Our results imply that the decreased activity of MP bears an obvious relation to the increased activity of PRMT5 and the increased gene repression mark on histones in almost every investigated cancer types particularly in bladder and colon carcinoma, MCF7 breast cancer, THP1 monocytic leukemia, kidney adenocarcinoma and in hepatocellular carcinoma. Except for the expression

lontay.beata_285_24

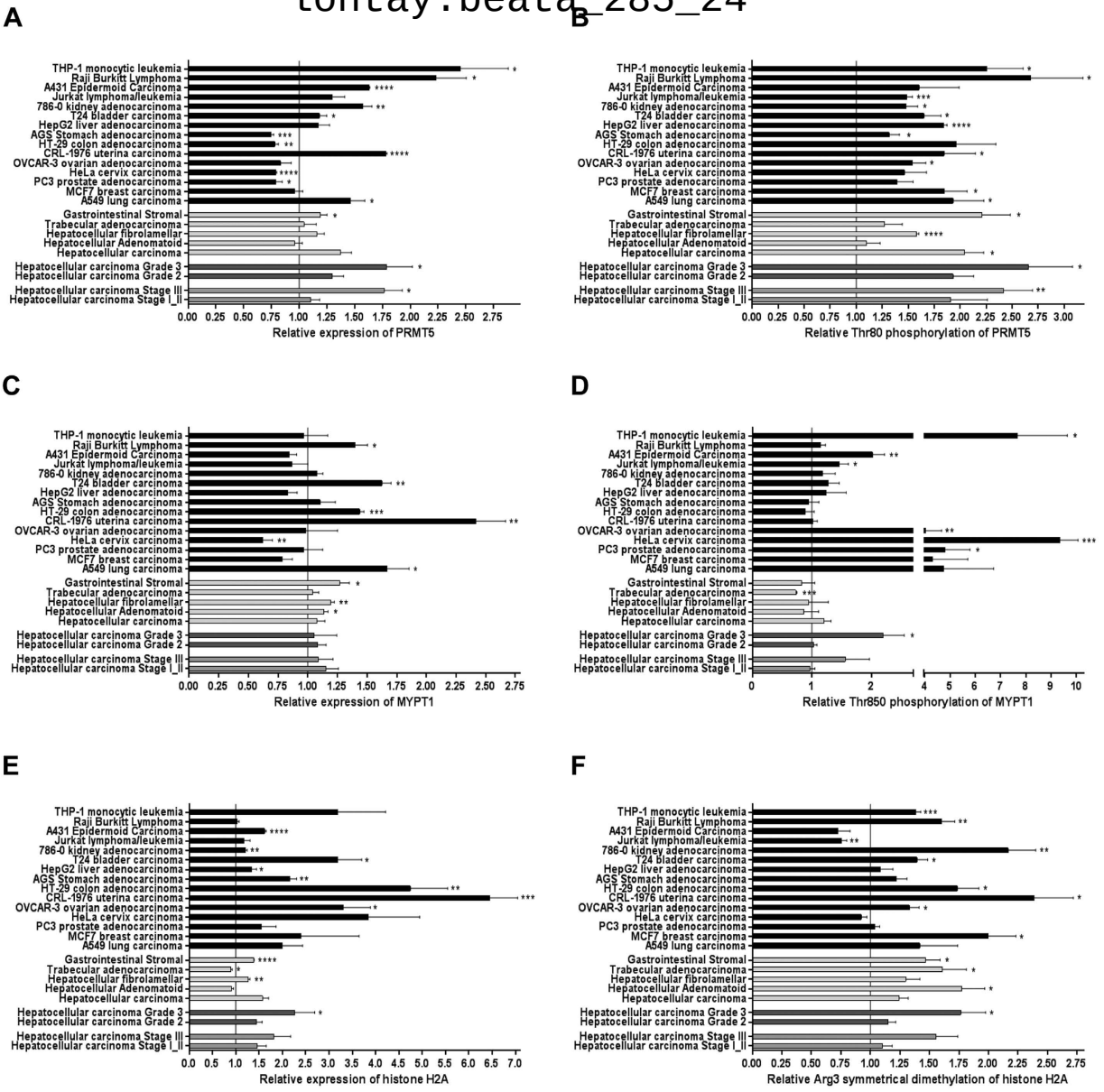


Figure 5. Protein expression profile of HCC and other cancer cell lines. Reverse phase protein microarray analysis was conducted to study the changes in protein expression and posttranslational modification of PRMT5 (**A**,**B**), MYPT1 (**C**,**D**) and histone H2A (**E**,**F**) proteins in normal and tumor human cell lysates. Human HCC samples (n = 20) were grouped based on their clinically verified stage (middle grey columns) or grade (dark grey columns) classification of tumor. Average of HCC samples irrespectively of grouping and other types of metastatic liver cancer tissues are shown next to each other (light grey columns). Protein microarray contains 15 cancer cell lines and normal tissue lysate of controls of corresponding organs in triplicates (black columns). Value of 1 means average of relative expression, phosphorylation or symmetrical dimethylation of the given protein or residue to the corresponding non-tumor samples. Blots were processed under the same experimental procedure. Datas are mean ± SEM; *$p < 0.05$, **$p < 0.01$, ***$p < 0.001$, ****$p < 0.0001$ by student *t*-test.

of MYPT1 in all other cases, the protein expression as well as the phosphorylation of PRMT5 at Thr80, and the arginine methylation of histone 2A and 4 increased in the higher grade and stage in hepatocellular carcinoma tissues (n = 11–13) exhibiting a strong correlation to the grade and state of the tumor. These data suggest the involvement of the ROK/MP/PRMT5/histone dimethylation pathway in tumorigenesis.

Discussion

In the present study we have characterized a novel mechanism of tumorigenesis governed by ROK and MP in hepatocarcinoma cells (HCC). We have identified Thr80 in PRMT5 as the target of ROK/MP and the phosphorylation/dephosphorylation of this site is shown to modulate the activity of PRMT5. At high phosphorylation of PRMT5 at Thr80 symmetric dimethylation of the histone R3-motif is preferred which accompanied

lontay.beata_285_24

by tumorogenesis, while dephosphorylation by MP has an opposite effect. Therefore, MP could be assumed as a tumorsuppressor in HCC. The interplay between MP and PRMT5 is also supported by interaction analysis. First, the presence of PRMT5 in the MYPT1 nuclear interactome is appealing for an interacting protein complex. Second, SPR-based *in vitro* binding assay identified a stable interaction between MYPT1 (the large targeting subunit of MP) and PRMT5 and it was verified that PRMT5 binds to the N-terminal region of MYPT1.

Our findings show that ROK/MP counteract on the Thr80 phosphorylation site of PRMT5 regulating its methyltransferase activity both *in vitro* (Fig. 2) and *in vivo* (Fig. 3). The PRMT5 protein includes multiple tyrosyl and seryl/threonyl residues that could be potentially targeted by phosphorylation. PRMT5 can be phosphorylated by a constitutively active janus kinase 2 mutant at the tyrosyl 304 and 307 residue resulting in the disruption of the interaction between MEP50 and PRMT5 and the inhibition of the activity of PRMT5 in patients with myoproliferative neuroplasm[37]. The ROK/MP regulated Thr80 residue and its surrounding peptide sequences are not part of the methyltransferase domain of PRMT5 and play no role in the formation of the heterooctameric structure of $PRMT5_4$:$MEP50_4$ based on the crystal structure of human PRMT5[38]. $PRMT5^{T80}$ is located in a peptide sequence (GRDWNTLI/VV) well conserved among vertebrates but not in invertebrate orthologs. Furthermore, PRMT5 exhibits no sequence homology with PRMT1-4 enzymes[39] suggesting a selective regulatory function of its phosphorylation at Thr80. The fact that PRMT5-Thr80 phosphorylation increases the activity of the enzyme without the recruitment of more MEP50 into the complex supports the hypothesis that this modification triggers changes either in the substrate- or in the S-adenosylmethionine methyl donor binding sites. Our findings provide a yet unrecognized signaling mechanism which regulates PRMT5 activity directly with posttranslational modification.

Histone tail modifications are major components of the epigenetic regulation of gene transcription. It is well established that PRMT5 has preference for the symmetrical dimethylation of H4R3, H2AR3 and H3R8 shifting the balance to a suppressive mark[40,31]. The symmetrically dimethylated R3-motif recruites the DNA methyltransferase DNMT3A to chromatin domains via its ADD domain to suppress gene expression thus representing epigenetic silencing of gene expression[41]. We provided several lines of evidence that silencing of MYPT1 results in a global change in gene expression through the activation of PRMT5 and by the indirect modulation of the "R3-motifs" of H2A and H4. Moreover, the general assumption that PRMT5 functions as a transcriptional corepressor is not definite since symmetric-dimethyl-arginine-containing protein(s) can specifically associate with the IL-2 promoter after T-cell activation and increase gene expression[42]. Our observation that cancer-related pathways are upregulated in HCC upon MYPT1 silencing is the results of the higher expression and hyperactivation of PRMT5, which suppresses gene and protein expression of several tumor suppressors or increasing that of potential oncogenes. First, the tumor suppressor pRb expression was significantly decreased in siMYPT1 HepG2 cells suggesting the anti-tumor role of MYPT1 in HCC. This is well in line with the findings that PRMT5 overexpression triggered the suppression of the transcription of the pRb in leukemia and in lymphoma cell[43]. Second, c-Myc as a global transcriptional regulator can activate genes involved in cell proliferation and growth but it is also able to repress genes involved in cell cycle and adhesion[44] raising the possibility of a yet-unexplored mechanism used by tumors to suppress differentiation and potentiate agressiveness. C-Myc expression is significantly lower in HCC than in nontumor tissues and is inversely proportional to the grade of differentiation[45]. We found that MYPT1 silencing resulted in a decrease in c-Myc gene and protein expression suggesting again the tumorsuppressor effect of this MP subunit, and presumably MP itself, in HCC. Finally, we also found that Rap1, one of the target genes induced by PRMT5[34] was upregulated in siMYPT1 HepG2 cells (Fig. 5E). Rap1 functions as a genomwide transcriptional regulator and a critical player in tumor malignancy. The fact that inhibition of Rap1 interfered with tumor development and induced higher apoptosis rates[46] also suggest that silencing of MYPT1 mimicks the protein expression pattern of cancer cells and the tumor suppressor activity of MYPT1 and therefore MP.

Previous studies speculated that constant and unbalanced phosphorylation of MYPT1 at Thr850 might be related to cancer formation[47]. Based on the phosphorylation of $MYPT1^{T850}$ we confirmed that the activity of the nuclear MP decreased, the activity of PRMT5 phophorylated at Thr80 increased and PRMT5-specific repressive R3-dimethylation increased in HCC and in other cancer cell lines suggesting the fundamental role of this pathway in tumorigenesis. Since both the stage and the grade of the tumors were directly related to the activity of this pathway, we hypothesized that this is an action governed by ROK. The downregulation of RhoA, an upstream activator of ROK[48] and the direct inhibition of ROK by Incarvine C and Y27632 decreased the phosphorylation of MYPT1 at Thr850 in lung cancer and HCC[49], respectively, and the ROK-phosphorylated MYPT1 was localized not only in the cytoplasm but in the nucleus as well[50].

PRMT5 was overexpressed in multiple tumor types including leukemia, lymphoma, lung[27], colorectal and breast cancer as well as in HCC and it resulted in increased symmetrical dimethylation on H2A and H4 R3-motifs[35]. The prognosis of patients with HCC is associated with the expression level of PRMT5. The overexpression of PRMT5 increased the symmetric dimethylation of histone R3 motifs and we provided evidence that it is related to the enhanced phosphorylation level of PRMT5 at Thr80 (Fig. 6).

In this study we have provided new insights into the regulation of tumor suppressor pathways demonstrating that MP is a negative regulator of the PRMT5 oncoprotein. MP possesses a dual function in cancer-related pathways as it is not only a cytoskeletal regulator governing cell migration and metastasis but it also functions as a key regulator of gene expression and has anti-tumor features. Taken together, the "MP/PRMT5/histone R3" pathway plays a critical role in tumorigenesis and cancer development, therefore the pharmacological interventions of this pathway by targeting MP may have important and promising clinical implications in therapeutics.

Material and Methods

Chemicals and antibodies. All chemicals were obtained from Sigma Aldrich unless otherwise indicated. Antibodies used are listed in the Supplementary Information Materials and Methods section. Buffer compositions are described in Supplementary Materials.

lontay.beata_285_24

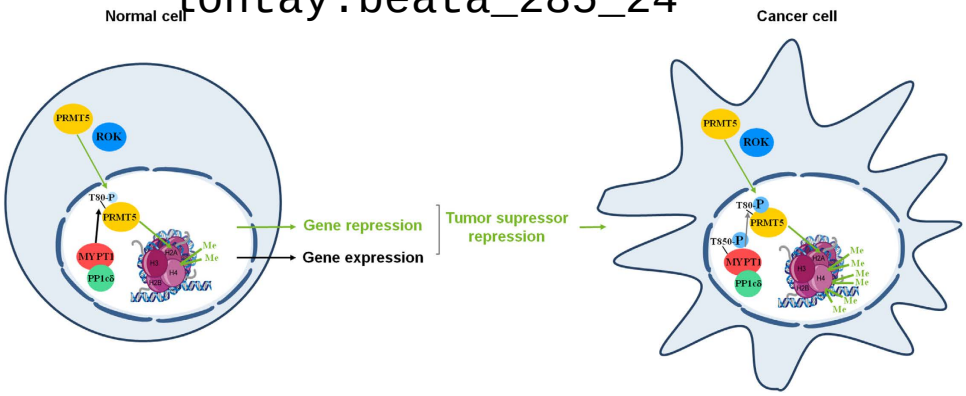


Figure 6. MP plays a tumorsuppressor role and antagonizes ROK in HCC. We hypothesize that MP and ROK are involved in gene expression. Under normal conditions MP modulates symmetrical dimethylation of histone core proteins in cell nucleus via dephosphorylation of PRMT5 at its activatory phosphorylation site (Thr80) causing changes in gene expression. In tumor cells inhibitory phosphorylation of MP on Thr850 is increased leading to higher phosphorylation level of PRMT5 at Thr80 by ROK. Activated PRMT5 provokes gene repression by raising symmetrical dimethylation of histone H4 Arg3 that triggers proto-oncogene activation and tumor formation.

Recombinant proteins. PP1cδ, GST-MYPT1$^{1\text{-}1004}$ and GST-MYPT1$^{667\text{-}1004}$ were expressed in *E. coli* and purified as described before[51,52]. FT-PRMT5 (Sino Biological) for SPR and phosphorylation assays for MS analysis was free from MEP50 (Fig. S2C). FT-PRMT5wt (FT-PRMT5wt), -PRMT5^{T80A} and FT-MYPT1 was purified from transfected tsA201 lysates using anti-Flag M2 affinity gel (Sigma Aldrich) applying the manufacturer's protocol. FT-PRMT5wt and -PRMT5^{T80A} proteins were bound to anti-Flag M2 affinity gel during kinase and phosphatase assays and *in vitro* protein arginine methyltransferase assays. FT-PRMT5 was in complex with MEP50 (Fig. S2C). PP1c-free FT-MYPT1 was produced for the execution of phosphatase assays and *in vitro* protein arginine methyltransferase assays. The FT-MYPT1 bound to the anti-Flag M2 affinity gel was incubated with MYPT1$^{1\text{-}296}$ peptide[13] several times to dissociate the PP1c subunit then FT-MYPT1 was eluted from the beads with 300 μg/ml Flag-peptide (Sigma Aldrich). The lack of PP1c in the FT-MYPT1 preparation was validated by Western blot with anti-PP1c antibody and phosphatase assay with 32P-MLC20 substrate, The purity of all the PP1cδ (Fig. S2D), GST-MYPT1$^{1\text{-}1004}$ and GST-MYPT1$^{667\text{-}1004}$ (Fig. S2A) were jugjed by sodium dodecyl sulfate-polyacrylamide gel electrophoresis (SDS-PASGE).

Cell cultures, transient transfections and silencing of MYPT1. HepG2 cells and human embryonal kidney (tsA201) cells from The European Collection of Cell Cultures were grown as described[13]. All materials used for cell culture were purchased from PAA Laboratories, AustriaThe endogenous MYPT1 protein level was knocked down using double-stranded siRNAs (Table S5, Thermo Scientific Inc.) and a non-target sequence (ON-TARGETplus Non-targeting siRNA #1 from Thermo Scientific Inc.) with the G–C content of siMYPT1 sequences was used as a control. TsA201 cells were transfected with pReceiver-M11 plasmids for overexpression. Protocols are detailed in the Supplementary Methods. The cell lysis and protein measurement were performed as described before[14].

HepG2 fractionation method. HepG2 cells were grown to 80% confluency, washed with ice-cold PBS, collected and centrifuged at 4 °C at 1,500 × g for 3 min. After the removal of PBS cells were homogenized in 400 μl buffer A by suspending with a 26 gauge needle 10 times using a 1 ml syringe. The lysate was vortexed for 15 sec. The efficiency of lysis was judged by trypan blue staining monitoring intact nuclei. The lysate was centrifuged at 4 °C at 16,000 × g for 1 min and the supernatant was used as cytosolic fraction. The pellet was resuspended in 200 μl buffer A and passed through the 26G needle 10 times as a washing step. After centrifugation at 4 °C at 16,000 × g for 1 min 100 μl buffer B was added to the pellet and sonicated and used as nuclear fraction.

Cell viability and caspase assays. HepG2 cells were grown in 96-well plates to determine viability by MTT assay and caspase-3 activity and were carried out as detailed before[53].

Immunoblotting. SDS-PAGE and immunoblotting were carried out as describe previously[13]. For quantitative comparisons samples derived from the same experiments. For quantification of PRMT5-Thr80 phosphorylation membranes were stripped and assayed for PRMT5 content as it is described on the Supplementary Methods. Internal controls were either assayed on the same gel or were processed in parallel. Densitometry of the proteins of interest were performed by Image J. 1.46 and normalized to an internal control protein and plotted as relative numbers as detailed in figure legends.

Immunofluorescence microscopy. HepG2 cells were grown on rat tail collagen-coated coverslips (BD Biosciences) and fixed using 4% paraformaldehyde and treated as described[53]. Primary and secondary antibodies

lontay.beata_285_24

were applied in 1:100 and 1:200 dilutions, respectively. DAPI (1:2000) were added as a nuclear marker as indicated in figure legends. Images were taken by Leica X8 confocal microscope and were processed using Leica X8 software program and PhotoShop Imaging software.

Surface Plasmon resonance (SPR). SPR-based binding studies were carried out using a Biacore 3000 instrument to monitor the interaction of MYPT1 with PRMT5. GST-MYPT1$^{1\text{-}1004}$ and GST-MYPT1$^{667\text{-}1004}$ were immobilized on anti-GST coupled CM5 sensorchip[54]. FT-PRMT5 was injected over the surfaces in various concentrations and the responses recorded. Binding of FT-PRMT5 was characterized by kinetic parameters and association constant (K_a) values determined by BIAevaluation 3.1 software.

Site-directed mutagenesis. Expression vector pReceiver-M11 encoding wild-type human full-length PRMT5 (NM_006109.3) transcript variant 1 was purchased from GeneCopoeia Inc., USA. Point mutations of PRMT5^{T80A} in pReceiver-M11 were performed using QuickChange II XL Site-Directed Mutagenesis Kit according to the manufacturer's instructions (Agilent Technologies). Primer pairs are listed in Table S3. The sequence of mutants were verified by DNA sequencing, primers are listed in Table S4.

Immunoprecipitation and pull-down assays. For LC-MS/MS analysis of FT-MYPT1 interacting proteins FT-MYPT1 and Flag-peptide as control were bound to anti-Flag M2 affinity gel. The samples were precleared on the anti-Flag M2 affinity gel prior to affinity isolation. After washing with Tris-buffered saline solution (TBS) three times, beads were incubated with HepG2 nuclear extract for 2 hr on 4 °C. The FT-MYPT1 was eluted with 300 μg/ml Flag-peptide from the beads with the anchored proteins. Eluted samples were subjected to SDS-PAGE. Bands of interest were visualized by MS compatible silver staining and the proteins were subjected to in-gel digestion using trypsin. No proteins other than human keratin contamination were identified from the control samples.

For immunoprecipitation (IP) anti-MYPT$^{1\text{-}296}$ and -PRMT5 antibodies were incubated with Protein-A Sepharose (GE Healthcare) as described before[14]. The blots were developed with anti-MYPT$^{1\text{-}296}$and anti-PRMT5 antibodies followed by Clean-blot IP detection reagent (HRP).

***In vitro* protein arginine methyltransferase assay.** FT-PRMT5wt was bound to anti-Flag M2 affinity gel following phosphorylation by protein kinases and was applied for the methylation assay. 2 μM S-adenosyl-L-methionine and 0.02 mg/ml of histone mixture from calf thymus (Roche) were added to the reaction in a total volume of 50 μl. Methylation reaction was allowed to proceed for 2 hours at 30 °C in the presence or in the absence of 5 nM recombinant PP1cδ[51], 25 nM FT-MYPT1 or the combination of PP1cδ and FT-MYPT1 (assumed as MP holoenzyme). Products of the methylation reactions were analysed by Western blots using antibodies specific for symmetrical dimethylation of H2A Arg3 and H4 Arg3. Membranes were stripped on 50 °C for 30 min in stripping buffer in every case and were assayed with anti-H2A and anti-H4 antibodies as input controls. Changes of symmetrical dimethylation levels were calculated by densitometry normalized to histone H2A and histone H4 internal controls. Methyltransferase assay was also carried out with colorimetric Epigenase PRMT methyltransferase type II-specific assay kit (Epigentech) following the instructions of the manufacturer.

Protein kinase and protein phosphatase assays. Phosphorylation of recombinant human PRMT5 (Sino Biological Inc.) was initiated by 0.2 mM ^{32}P-ATP or for LC-MS/MS analysis by 0.5 mM ATP in the absence (control) or in the presence of 0.4 U/ml ROK (Upstate, Millipore), 0.1 μg/ml PKA or 0.1 μg/ml PKC at 30 °C for 120 min. ROK was applied in buffer C and all kinase assay buffers contained 1 μM mycrocystin-LR (MC-LR). PKA and PKC assay buffer are described in Supplementary Methods. The reaction mixtures were subjected to SDS-PAGE and bands were detected by autoradiography or visualized by MS/MS compatible silver staining and were cut out and subjected to LC-MS/MS analysis.

Phosphorylation reaction by ROK (0.4 U/ml) was also carried out in the absence or in the presence of 10 μM H1152 with 0.5 mM ATP, 5mM $MgCl_2$ and 1 μM MC-LR at 30 °C using FT-PRMT5wt bound to anti-Flag M2 affinity gel. After 15 min incubation kinase assay medium was removed and beads were washed by TBS. Dephosphorylation of ROK-phosphorylated FT-PRMT5wt bound to the beads (the product of the kinase assay) was initiated by adding 25 nM FT-MYPT1, 5 nM rPP1cδ or the combination of these two proteins at 30 °C for 15 min, then the beads were washed by TBS and the bound (eluted??) proteins were subjected to SDS-PAGE. Bands were detected by autoradiography or visualized by MS/MS compatible silver staining. Bands of PRMT5 were cut out and subjected to in-gel digestion using trypsin. Approximately 80% of the peptide mixtures were subjected to phosphopeptide enrichment using TiO_2[55], then the phosphopeptide fractions as well as the remaining 20% of the original samples were analyzed by data-dependent LC-MS/MS using an Orbitrap Elite mass spectrometer (MS spectra acquired in the Orbitrap, MS/MS spectra in the linear ion trap). Phosphorylation level of Thr80 of PRMT5 was detected by phospho-PRMT5^{T80} specific antibody on Western blots and analysed by densitometry normalized to the PRMT5 input using Image J. (NIH) software.

Gene expression analysis. Total RNA was extracted from non-target control and MYPT1 silenced HepG2 cells using TRIzol reagent (Invitrogen) as described in the manufacturer's protocol. NanoDrop ND-1000 spectrophotometer (Thermo Scientific) was used to determine the RNA concentration. RNA was treated with RNase free DNase I (Thermo Scientific) and reverse transcription was performed with qPCRBIO cDNA synthesis kit (PCR Biosystems). PCR amplification was carried out with Maxima Hot Start PCR Master Mix (Thermo Scientific) based on manufacturer's protocol. RT-PCR products were analyzed by agarose gel electrophoresis. The expression level of the genes of interest were performed by Image J. 1.46, normalized to GAPDH and represented as relative numbers. The primer pairs used in the RT-PCR experiments are summarized in Table S8.

lontay.beata_285_24

Microarray processing and data analysis. Expression pattern of non-target and MYPT1 silenced HepG2 cells was examined and analysed as detailed before[53] using total RNA extracted as described in the previous section. Statistically significant difference was considered at $p < 0.05$ and fold change cut off value was 1.5.

LC-MS/MS analysis. Bands of interest were subjected to in-gel digestion using side-chain protected porcine trypsin (37 °C, 4 h) [http://msf.ucsf.edu/ingel.html]. For the identification of MYPT1 interacting proteins, the resulting peptide mixtures were analyzed directly by data-dependent „triple play" LC-MS/MS using a 3D-ion trap mass spectrometer (LCQ-Fleet, Thermo). Identification of MYPT1 interacting proteins and the PRMT5 phosphorylation sites from LC-MS/MS data were detailed in the Supplementary Methods section.

Tissue array analysis. SomaPlex reverse phase protein microarray slides containing human liver and normal tissue samples from 25 clinical cases and 15 common cancer cell line lysates in triplicates were purchased from Protein Biotechnologies. Microarray slides were handled following the manufacturer's instructions as detailed in Supplementary Methods. Dots of interest were analysed by densitometry and were all normalized to their adequate tubulin internal control. Values of the phosphorylation of PRMT5 at Thr80, -MYPT at Thr850 and H2AR3me2s were normalized to PRMT5, MYPT and H2A, respectively. Values of cancer tissues were related to normal tissue data and plotted as relative numbers.

Statistical analysis. Normalized data were analyzed using either Student's t-test (for two groups) or analysis of variance (one-way ANOVA, for >2 groups). Post hoc testing for one-way ANOVA was determined by Tukey's test. Parametric statistical tests were used if the assumptions of such tests were met. All normalized variables used in statistical analyses were found to be normally distributed. Tests were conducted using GraphPad for Windows. All data presented in this work represent mean ± SEM, *n* means the number of independently performed experiments.

References

1. Hou, J. *et al.* Hepatic RIG-I predicts survival and interferon-alpha therapeutic response in hepatocellular carcinoma. *Cancer cell* **25,** 49–63, doi: 10.1016/j.ccr.2013.11.011 (2014).
2. Peti, W., Nairn, A. C. & Page, R. Structural basis for protein phosphatase 1 regulation and specificity. *The FEBS journal* **280,** 596–611, doi: 10.1111/j.1742-4658.2012.08509.x (2013).
3. Nagao, M. *et al.* Role of protein phosphatases in malignant transformation. *Princess Takamatsu symposia* **20,** 177–184 (1989).
4. Dombradi, V., Axton, J. M., Barker, H. M. & Cohen, P. T. Protein phosphatase 1 activity in Drosophila mutants with abnormalities in mitosis and chromosome condensation. *FEBS Lett* **275,** 39–43 (1990).
5. Berndt, N. Protein dephosphorylation and the intracellular control of the cell number. *Frontiers in bioscience: a journal and virtual library* **4,** D22–42 (1999).
6. Suganuma, M. *et al.* Okadaic acid: an additional non-phorbol-12-tetradecanoate-13-acetate-type tumor promoter. *Proceedings of the National Academy of Sciences of the United States of America* **85,** 1768–1771 (1988).
7. Cohen, P. T. Protein phosphatase 1–targeted in many directions. *Journal of cell science* **115,** 241–256 (2002).
8. Heroes, E. *et al.* The PP1 binding code: a molecular-lego strategy that governs specificity. *The FEBS journal* **280,** 584–595, doi: 10.1111/j.1742-4658.2012.08547.x (2013).
9. Hartshorne, D. J., Ito, M. & Erdodi, F. Myosin light chain phosphatase: subunit composition, interactions and regulation. *J Muscle Res Cell Motil* **19,** 325–341 (1998).
10. Boudrez, A. *et al.* Identification of MYPT1 and NIPP1 as subunits of protein phosphatase 1 in rat liver cytosol. *FEBS Lett* **455,** 175–178 (1999).
11. Somlyo, A. P. & Somlyo, A. V. Ca2+ sensitivity of smooth muscle and nonmuscle myosin II: modulated by G proteins, kinases, and myosin phosphatase. *Physiological reviews* **83,** 1325–1358, doi: 10.1152/physrev.00023.2003 (2003).
12. Matsumura, F. & Hartshorne, D. J. Myosin phosphatase target subunit: Many roles in cell function. *Biochemical and biophysical research communications* **369,** 149–156, doi: 10.1016/j.bbrc.2007.12.090 (2008).
13. Lontay, B., Kiss, A., Gergely, P., Hartshorne, D. J. & Erdodi, F. Okadaic acid induces phosphorylation and translocation of myosin phosphatase target subunit 1 influencing myosin phosphorylation, stress fiber assembly and cell migration in HepG2 cells. *Cell Signal* **17,** 1265–1275, doi: 10.1016/j.cellsig.2005.01.008 (2005).
14. Lontay, B. *et al.* Localization of myosin phosphatase target subunit 1 in rat brain and in primary cultures of neuronal cells. *J Comp Neurol* **478,** 72–87, doi: 10.1002/cne.20273 (2004).
15. Yamashiro, S. *et al.* Myosin phosphatase-targeting subunit 1 regulates mitosis by antagonizing polo-like kinase 1. *Developmental cell* **14,** 787–797, doi: 10.1016/j.devcel.2008.02.013 (2008).
16. Parra, M., Mahmoudi, T. & Verdin, E. Myosin phosphatase dephosphorylates HDAC7, controls its nucleocytoplasmic shuttling, and inhibits apoptosis in thymocytes. *Genes & development* **21,** 638–643, doi: 10.1101/gad.1513107 (2007).
17. Jin, H., Sperka, T., Herrlich, P. & Morrison, H. Tumorigenic transformation by CPI-17 through inhibition of a merlin phosphatase. *Nature* **442,** 576–579, doi: 10.1038/nature04856 (2006).
18. Kiss, A. *et al.* Myosin phosphatase interacts with and dephosphorylates the retinoblastoma protein in THP-1 leukemic cells: its inhibition is involved in the attenuation of daunorubicin-induced cell death by calyculin-A. *Cell Signal* **20,** 2059–2070, doi: 10.1016/j.cellsig.2008.07.018 (2008).
19. Okamoto, R. *et al.* The targeted disruption of the MYPT1 gene results in embryonic lethality. *Transgenic research* **14,** 337–340 (2005).
20. Muranyi, A. *et al.* Phosphorylation of Thr695 and Thr850 on the myosin phosphatase target subunit: inhibitory effects and occurrence in A7r5 cells. *FEBS Lett* **579,** 6611–6615, doi: 10.1016/j.febslet.2005.10.055 (2005).
21. Muranyi, A. *et al.* Phosphorylation of the myosin phosphatase target subunit by integrin-linked kinase. *Biochem J* **366,** 211–216, doi: 10.1042/BJ20020401 (2002).
22. Loirand, G., Guerin, P. & Pacaud, P. Rho kinases in cardiovascular physiology and pathophysiology. *Circulation research* **98,** 322–334, doi: 10.1161/01.RES.0000201960.04223.3c (2006).
23. Takeba, Y. *et al.* The Rho kinase inhibitor fasudil is involved in p53-mediated apoptosis in human hepatocellular carcinoma cells. *Cancer chemotherapy and pharmacology* **69,** 1545–1555, doi: 10.1007/s00280-012-1862-6 (2012).
24. Takamura, M. *et al.* Inhibition of intrahepatic metastasis of human hepatocellular carcinoma by Rho-associated protein kinase inhibitor Y-27632. *Hepatology* **33,** 577–581, doi: 10.1053/jhep.2001.22652 (2001).
25. Itoh, K. *et al.* An essential part for Rho-associated kinase in the transcellular invasion of tumor cells. *Nature medicine* **5,** 221–225, doi: 10.1038/5587 (1999).

lontay.beata_285_24

26. Rath, N. & Olson, M. F. Rho-associated kinases in tumorigenesis: re-considering ROCK inhibition for cancer therapy. *EMBO reports* **13,** 900–908, doi: 10.1038/embor.2012.127 (2012).
27. Sheng, X. & Wang, Z. Protein arginine methyltransferase 5 regulates multiple signaling pathways to promote lung cancer cell proliferation. *BMC Cancer* **16,** 567, doi: 10.1186/s12885-016-2632-3 (2016).
28. McBride, A. E., Weiss, V. H., Kim, H. K., Hogle, J. M. & Silver, P. A. Analysis of the yeast arginine methyltransferase Hmt1p/Rmt1p and its *in vivo* function. Cofactor binding and substrate interactions. *The Journal of biological chemistry* **275,** 3128–3136 (2000).
29. Mellacheruvu, D. *et al.* The CRAPome: a contaminant repository for affinity purification-mass spectrometry data. *Nature methods* **10,** 730–736, doi: 10.1038/nmeth.2557 (2013).
30. Di Lorenzo, A. & Bedford, M. T.Histone arginine methylation. *FEBS Lett* **585,** 2024–2031, doi: 10.1016/j.febslet.2010.11.010 (2011).
31. Feng, Y. *et al.* Histone H4 acetylation differentially modulates arginine methylation by an in Cis mechanism. *J Biol Chem* **286,** 20323–20334, doi: 10.1074/jbc.M110.207258 (2011).
32. Witkiewicz, A. K. & Knudsen, E. S. Retinoblastoma tumor suppressor pathway in breast cancer: prognosis, precision medicine, and therapeutic interventions. *Breast cancer research: BCR* **16,** 207, doi: 10.1186/bcr3652 (2014).
33. Shalaby, T. & Grotzer, M. A. MYC as Therapeutic Target for Embryonal Tumors: Potential and Challenges. *Current cancer drug targets* **16,** 2–21 (2015).
34. Gkountela, S., Li, Z., Chin, C. J., Lee, S. A. & Clark, A. T. PRMT5 is required for human embryonic stem cell proliferation but not pluripotency. *Stem cell reviews* **10,** 230–239, doi: 10.1007/s12015-013-9490-z (2014).
35. Zhang, B. *et al.* Targeting protein arginine methyltransferase 5 inhibits human hepatocellular carcinoma growth via the downregulation of beta-catenin. *Journal of translational medicine* **13,** 349, doi: 10.1186/s12967-015-0721-8 (2015).
36. Sheng, X., Bowen, N. & Wang, Z. GLI pathogenesis-related 1 functions as a tumor-suppressor in lung cancer. *Molecular cancer* **15,** 25, doi: 10.1186/s12943-016-0508-4 (2016).
37. Liu, F. *et al.* JAK2V617F-mediated phosphorylation of PRMT5 downregulates its methyltransferase activity and promotes myeloproliferation. *Cancer cell* **19,** 283–294, doi: 10.1016/j.ccr.2010.12.020 (2011).
38. Antonysamy, S. *et al.* Crystal structure of the human PRMT5:MEP50 complex. *Proceedings of the National Academy of Sciences of the United States of America* **109,** 17960–17965, doi: 10.1073/pnas.1209814109 (2012).
39. Krause, C. D. *et al.* Protein arginine methyltransferases: evolution and assessment of their pharmacological and therapeutic potential. *Pharmacology & therapeutics* **113,** 50–87, doi: 10.1016/j.pharmthera.2006.06.007 (2007).
40. Saha, K., Adhikary, G. & Eckert, R. L. MEP50/PRMT5 Reduces Gene Expression by Histone Arginine Methylation and this Is Reversed by PKCdelta/p38delta Signaling. *The Journal of investigative dermatology* **136,** 214–224, doi: 10.1038/JID.2015.400 (2016).
41. Pal, S. *et al.* Low levels of miR-92b/96 induce PRMT5 translation and H3R8/H4R3 methylation in mantle cell lymphoma. *The EMBO journal* **26,** 3558–3569, doi: 10.1038/sj.emboj.7601794 (2007).
42. Richard, S., Morel, M. & Cleroux, P. Arginine methylation regulates IL-2 gene expression: a role for protein arginine methyltransferase 5 (PRMT5). *Biochem J* **388,** 379–386, doi: 10.1042/BJ20040373 (2005).
43. Wang, L., Pal, S. & Sif, S. Protein arginine methyltransferase 5 suppresses the transcription of the RB family of tumor suppressors in leukemia and lymphoma cells. *Molecular and cellular biology* **28,** 6262–6277, doi: 10.1128/MCB.00923-08 (2008).
44. Uribesalgo, I., Benitah, S. A. & Di Croce, L. From oncogene to tumor suppressor: the dual role of Myc in leukemia. *Cell cycle* **11,** 1757–1764, doi: 10.4161/cc.19883 (2012).
45. Yuen, M. F., Wu, P. C., Lai, V. C., Lau, J. Y. & Lai, C. L. Expression of c-Myc, c-Fos, and c-jun in hepatocellular carcinoma. *Cancer* **91,** 106–112 (2001).
46. Zha, Y., Gan, P., Yao, Q., Ran, F. M. & Tan, J. Downregulation of Rap1 promotes 5-fluorouracil-induced apoptosis in hepatocellular carcinoma cell line HepG2. *Oncology reports* **31,** 1691–1698, doi: 10.3892/or.2014.3033 (2014).
47. Wong, C. C. *et al.* Deleted in liver cancer 1 (DLC1) negatively regulates Rho/ROCK/MLC pathway in hepatocellular carcinoma. *PLoS One* **3,** e2779, doi: 10.1371/journal.pone.0002779 (2008).
48. Yang, X., Zheng, F., Zhang, S. & Lu, J. Loss of RhoA expression prevents proliferation and metastasis of SPCA1 lung cancer cells *in vitro*. *Biomedicine & pharmacotherapy = Biomedecine & pharmacotherapie* **69,** 361–366, doi: 10.1016/j.biopha.2014.12.004 (2015).
49. Zhang, J. G. *et al.* Incarvine C suppresses proliferation and vasculogenic mimicry of hepatocellular carcinoma cells via targeting ROCK inhibition. *BMC Cancer* **15,** 814, doi: 10.1186/s12885-015-1809-5 (2015).
50. Genda, T. *et al.* Cell motility mediated by rho and Rho-associated protein kinase plays a critical role in intrahepatic metastasis of human hepatocellular carcinoma. *Hepatology* **30,** 1027–1036, doi: 10.1002/hep.510300420 (1999).
51. Kiss, E. *et al.* Integrin-linked kinase phosphorylates the myosin phosphatase target subunit at the inhibitory site in platelet cytoskeleton. *Biochem J* **365,** 79–87, doi: 10.1042/BJ20011295 (2002).
52. Toth, A. *et al.* Study of the subunit interactions in myosin phosphatase by surface plasmon resonance. *European journal of biochemistry/FEBS* **267,** 1687–1697 (2000).
53. Dedinszki, D. *et al.* Protein phosphatase-1 is involved in the maintenance of normal homeostasis and in UVA irradiation-induced pathological alterations in HaCaT cells and in mouse skin. *Biochimica et biophysica acta* **1852,** 22–33, doi: 10.1016/j.bbadis.2014.11.005 (2015).
54. Kolozsvari, B. *et al.* Calcineurin regulates endothelial barrier function by interaction with and dephosphorylation of myosin phosphatase. *Cardiovascular research* **96,** 494–503, doi: 10.1093/cvr/cvs255 (2012).
55. Larsen, M. R., Thingholm, T. E., Jensen, O. N., Roepstorff, P. & Jorgensen, T. J. Highly selective enrichment of phosphorylated peptides from peptide mixtures using titanium dioxide microcolumns. *Molecular & cellular proteomics: MCP* **4,** 873–886, doi: 10.1074/mcp.T500007-MCP200 (2005).
56. Biemann, K. Appendix 5. Nomenclature for peptide fragment ions (positive ions). *Methods in enzymology* **193,** 886–887 (1990).

Acknowledgements

This work was supported by grants from the Hungarian Scientific Research Fund OTKA PD104878 and K109249, the Hungarian Academy of Sciences and from the University of Debrecen (RH/751/2015). We acknowledge the help of Szilárd Póliska (UD Genomed, Debrecen, Hungary) in microarray analysis, Beatrix Dienes for her help in confocal microscopy and Zoltan Kónya for the preparation of rPP1cδ. The authors are indebted to Ágnes Németh, Andrea Docsa and Ágota Kelemen for their technical assistance.

Author Contributions

B.L. and A.S., designed the study; K.M. and Zs.D. conducted proteomic analysis, B.B. performed the SPR studies, I.T., D.H. and J.I. completed experiments for Figs 4, S2 and S6. A.S. performed experiments and analysed data for Figs 1–3, 5–6., Table 1. and Supplementary figures and tables. B.L., A.S., Zs.D., F.E. wrote the paper. All author reviewed the manuscript.

lontay.beata_285_24

Additional Information

Supplementary information accompanies this paper at http://www.nature.com/srep

Competing financial interests: The authors declare no competing financial interests.

How to cite this article: Sipos, A. *et al.* Myosin phosphatase and RhoA-activated kinase modulate arginine methylation by the regulation of protein arginine methyltransferase 5 in hepatocellular carcinoma cells. *Sci. Rep.* **7**, 40590; doi: 10.1038/srep40590 (2017).

Publisher's note: Springer Nature remains neutral with regard to jurisdictional claims in published maps and institutional affiliations.

This work is licensed under a Creative Commons Attribution 4.0 International License. The images or other third party material in this article are included in the article's Creative Commons license, unless indicated otherwise in the credit line; if the material is not included under the Creative Commons license, users will need to obtain permission from the license holder to reproduce the material. To view a copy of this license, visit http://creativecommons.org/licenses/by/4.0/

© The Author(s) 2017

lontay.beata_285_24

Molecular and Cellular Endocrinology 551 (2022) 111663

Contents lists available at ScienceDirect

Molecular and Cellular Endocrinology

journal homepage: www.elsevier.com/locate/mce

Mechanisms by which smoothelin-like protein 1 reverses insulin resistance in myotubules and mice

Istvan Tamas [a], Evelin Major [a], Daniel Horvath [a], Ilka Keller [a], Adam Ungvari [a], Timothy A. Haystead [b], Justin A. MacDonald [c], Beata Lontay [a,*]

[a] Department of Medical Chemistry, Faculty of Medicine, University of Debrecen, Debrecen, Hungary
[b] Duke University School of Medicine, Department of Pharmacology and Cancer Biology, Durham, NC, USA
[c] Department of Biochemistry and Molecular Biology, Cumming School of Medicine, University of Calgary, Calgary, AB, Canada

ARTICLE INFO

Keywords:
Insulin resistance
Skeletal muscle metabolism
Pregnancy
Insulin signaling
Insulin receptor substrate-1
Phosphorylation

ABSTRACT

Insulin resistance (InR) is manifested in skeletal muscle by decreased insulin-stimulated glucose uptake due to impaired insulin signaling and multiple post-receptor intracellular defects. Chronic glucose-induced insulin resistance leads to the activation of Ser/Thr kinases and elevated phosphorylation of insulin receptor substrate 1 (IRS1) on Ser residues. Phosphorylation of IRS1 triggers the dissociation of IRS1 and its downstream effector, phosphatidylinositol 3-kinase. In the present study, we provide evidence for the insulin-sensitizing role of smoothelin-like protein 1 (SMTNL1) that is a ligand-dependent co-regulator of steroid receptors, predominantly the progesterone receptor. SMTNL1 was transiently overexpressed in insulin-resistant C2C12 myotubes. A proteome profiler array revealed that mTOR and Ser/Thr kinases were SMTNL1-dependent signaling pathways. In the presence of progesterone, overexpression was coupled to decreased Ser phosphorylation of IRS1 at Ser307, Ser318, and Ser612 residues. SMTNL1 also induced the expression and activity of the p85 subunit of PI3K. SMTNL1 regulated the expression of PKCε, which phosphorylates IRS1 at Ser318 residue. SMTNL1 also regulated ERK1/2 and JNK, which phosphorylate IRS1 at Ser612 and Ser307, respectively. Real-time metabolic measurements of oxygen consumption rate and extracellular acidification rate revealed that SMTNL1 improved glycolysis and promoted the utilization of alternative carbon fuels. SMTNL1 also rescued the mitochondrial respiration defect induced by chronic insulin exposure. Collectively, SMTNL1 plays a crucial role in maintaining the physiological ratio of Tyr/Ser IRS1 phosphorylation and attenuates the insulin-signaling cascade that contributes to impaired glucose disposal, which makes it a potential therapeutic target for improving InR.

Highlights.

- SMTNL1 promotes insulin sensitivity in insulin-resistant skeletal muscle
- SMTNL1 regulates the expression of novel PKCε that contributes to the phosphorylation of IRS1 at Ser318 residue
- SMTNL1 regulates ERK1/2 activity therefore IRS1 Ser612 phosphorylation
- SMTNL1 hampers JNK1 activity to regulate IRS1 Ser307 phosphorylation
- SMTNL1 promotes glucose uptake via activation of Akt activity and by inducing GLUT4 expression

1. Introduction

Insulin resistance syndrome affects about 24% of adults older than 20 years and is manifested as a variety of disorders, including glucose tolerance impairment, type 2 diabetes, obesity, and reproductive disorders (Meigs, 2003). Insulin resistance (InR) is characterized by decreased cellular responsiveness to insulin signaling in insulin-dependent tissues, such as skeletal muscle, liver, and adipose tissue. When muscle, fat, and liver cells become resistant to the action of insulin, pancreatic β-cells respond by pumping increased amounts of insulin into the circulation to maintain homeostatic control of glucose level (Boucher et al., 2014).

Skeletal muscle (SKM) is the major site of ingested glucose disposal in normal glucose tolerant individuals (Abdul-Ghani and DeFronzo, 2009). While the liver takes up approximately one-third of post-prandial

* Corresponding author. Department of Medical Chemistry, Faculty of Medicine University of Debrecen, H-4032, Debrecen, Egyetem tér 1, Hungary.
E-mail address: lontay@med.unideb.hu (B. Lontay).

https://doi.org/10.1016/j.mce.2022.111663
Received 29 September 2021; Received in revised form 27 April 2022; Accepted 27 April 2022
Available online 1 May 2022
0303-7207/Crown Copyright © 2022 Published by Elsevier B.V. This is an open access article under the CC BY license (http://creativecommons.org/licenses/by/4.0/).

Abbreviations

2-DG	2-deoxy-D-glucose
ANOVA	analysis of variance
DMEM	Dulbecco's modified Eagle's medium
ECAR	extracellular acidification rate
ERK1/2	extracellular signal-regulated kinase
FT-SMTNL1	N-terminal FLAG tag SMTNL1
GDM	gestational diabetes mellitus
Glut4	glucose transporter 4
InR	insulin resistance
IR	insulin receptor
IRS1	insulin receptor substrate
JNK	c-Jun N-terminal kinase
MPA	medroxyprogesterone-17-acetate
OCR	oxygen consumption rate
PI3K	phosphatidylinositol 3-kinase
PKA	protein kinase A
PKCε	protein kinase epsilon
PKCζ	protein kinase C zeta
PKG	protein kinase A
PR	progesterone receptor
RIPA	radioimmunoprecipitation assay buffer
SKM	skeletal muscle
SMTNL1	smoothelin-like protein 1

glucose in the bloodstream, the remainder is taken up by peripheral tissues, primarily by SKM via an insulin-dependent mechanism. The binding of insulin to the insulin receptor (IR) initiates a signaling cascade that results in the translocation of the insulin-sensitive glucose transporter protein 4 (GLUT4) to the plasma membrane to facilitate the transport of glucose into the cell. IR activation upon insulin binding results in phosphorylation of the insulin receptor substrate 1 (IRS1) protein, that in turn docks and activates phosphatidylinositol 3-kinase (PI3K) that goes under conformational changes in its catalytic domain, which in turn results in kinase activation. This is followed by the PI3K-mediated phosphorylation of membrane bound PIP2 to generate PIP3. PIP3 then binds to the PH domain of Akt, thereby anchoring it to the plasma membrane to transduce the insulin signal to a serine/threonine (Ser/Thr) protein kinase, Akt/protein kinase B (Boucher et al., 2014). Upon membrane recruitment of Akt, it is phosphorylated and activated in its kinase domain at Thr308 and for substrate selectivity and activity enhancement at Ser473 by phosphoinositide-dependent protein kinase 1 and mTORC2, respectively (Beg et al., 2017). Akt phosphorylates and inhibits AS160, removing its inhibition of Rab proteins. Ultimately, Akt can promotes the translocation of GLUT4-containing vesicles to the plasma membrane to mediate insulin-stimulated glucose transport in SKM (Kupriyanova and Kandror, 1999) (Kohn et al., 1996).

InR is manifested in SKM by decreased insulin-stimulated glucose uptake resulting from impaired insulin signaling and multiple intracellular post-receptor defects, including impaired glucose transport and conversion to glucose-6-phosphate, reduced glucose oxidation, and attenuated glycogenesis. Insulin action is inhibited by enhanced Ser/Thr phosphorylation of either the receptor or its downstream effectors; this increased phosphorylation affects their mutual interactions and reduces the relative contribution of each of the elements in this signaling cascade, resulting in decreased IRS activity or its ability to recruit substrate proteins and thus to propagate insulin signaling (Mlinar et al., 2007). Cytokines, and hyperinsulinemia initiate phosphorylation by enhancing Ser phosphorylation and reducing Tyr phosphorylation of IRS1, which leads to decreased glucose uptake and insulin resistance (Boucher et al., 2014).

One potential regulator of insulin resistance in SKM is the smoothelin-like 1 protein (SMTNL1). SMTNL1 is a target of protein kinase A and G (PKA/PKG) and is expressed in smooth and skeletal muscles (Borman et al., 2004) as well as steroid hormone-sensitive tissues (Bodoor et al., 2011; Wooldridge et al., 2008). It has a dual function: on one hand, it regulates muscle contraction and the cytoskeletal elements of various cells through the inhibition of the activity of myosin phosphatase holoenzyme. Through this regulation, it enhances the phosphorylation of the regulatory 20 kDa light chain of myosin (Bodoor et al., 2011; Lontay et al., 2010). On the other hand, upon phosphorylation at Ser301 by PKG/PKA, SMTNL1 translocates to the nucleus where it functions as a transcriptional regulator of steroid receptors, predominantly the progesterone receptor (PR). (Bodoor et al., 2011; Lontay et al., 2010). In a progesterone-dependent manner, SMTNL1 can regulate the gene expression of dozens of metabolic enzymes, cytoskeletal elements, steroid receptors, and cytokines (Bodoor et al., 2011). In addition, SMTNL1 promotes adaptive responses to pregnancy in mice by reprogramming the metabolic and contractile character of SKM to increase power/strength and the glycogen content required for managing weight gain during fetal development (Lontay et al., 2015). Pregnancy promotes muscle fiber-type changes from an oxidative to a glycolytic isoform in SKM. This phenomenon is regulated through the interaction between SMTNL1 and PR, which alters the expression of contractile and metabolic proteins (Lontay et al., 2015).

The current study aimed to explore the detailed molecular impact of SMTNL1 on InR development in SKM during pregnancy using *Smtnl1* knockout (KO) mice and insulin-resistant differentiated C2C12 myotubes. We hypothesized that SMTNL1 modulates insulin signaling pathways by regulating the expression of upstream modulators of Ser/Thr kinases responsible for the phosphorylation of IRS-1 and resulting in the dissociation of PI3K and the inactivation of the IRS-1/PI3K/Akt/mTOR pathway.

2. Material and methods

2.1. Materials

All chemicals were obtained from Sigma-Aldrich (St. Louis, MO, USA) unless indicated otherwise. Microcystin-LR was produced and purified as described previously (Mathe et al., 2009).

2.2. Antibodies

All antibodies are listed in Table S1.

2.3. Cell maintenance, differentiation, and insulin resistance model

The C2C12 mouse myoblast cell line (Sigma-Aldrich) was cultured in low-glucose (5.5 mM) DMEM supplemented with 2 mM L-glutamine and 10% (v/v) FBS in a 5% CO_2-humidified atmosphere at 37 °C. Cells were grown in collagen-coated petri dishes for differentiation (VWR West Chester, PA, USA) and maintained in differentiation medium (5.5 mM DMEM without phenol red, supplemented with 2 mM L-glutamine and 2% (v/v) horse serum) for 5 days (Fig. S1). Cells were lysed in radioimmunoprecipitation assay (RIPA) buffer (25 mM Tris-HCl pH 7.6, 150 mM NaCl, 0.25% (m/v) sodium deoxycholate, 1% (v/v) NP-40, 0.1% (m/v) sodium dodecyl sulphate) containing protease and phosphatase inhibitors (1 mM NaF, 1 mM $Na_4P_2O_7$, 1 mM β-glycerol-phosphate, 1 mM Na_3VO_4) and 1 μM of microcystin-LR.

For the InR treatment, high glucose (HG, 25 mM glucose) DMEM without phenol red was supplemented with 2 mM L-glutamine, 2% horse

lontay.beata_285_24

serum, and 100 nM of insulin (chronic insulin). The low glucose (LG, 5.5 mM glucose) DMEM without phenol red was supplemented with 2 mM L-glutamine, 2% (v/v) horse serum, and 50 pM of insulin and 10 nM of medroxyprogesterone-17-acetate (MPA) was added as described in Fig. S1. For Western-blotting, Proteome Profiler, and PI3K activity experiments the media was changed to serum and hormone-free DMEM medium for 5 h and cells were treated again for 30 min with 100 nM of insulin (acute insulin) before harvesting. Samples were prepared for the PI3K assay according to the supplementary protocol section for PI3K activity measurement. Proteins were solubilized as described before (Lontay et al., 2010). Protein concentrations were determined as described before (Sipos et al., 2017) (Fig. S1.).

2.4. Transient transfections

The full-length mouse SMTNL1 construct (pcDNA-3.1 expression vector) with N-terminal FLAG tag, referred to as FT-SMTNL1, and the empty pcDNA-3.1 plasmid as a transfection control, referred to as empty vector/control, were overexpressed in C2C12 cells on day 0 of the full-length protocol using GeneJuice Transfection Reagent (Novagen, Merck Millipore, Darmstadt, Germany).

2.5. Western blotting

Western blot analysis was conducted as described before (Sipos et al., 2017). Briefly, proteins were separated on Bio-Rad 4–20% Criterion TGX Precast Midi protein gels. Antibody binding was detected using enhanced chemiluminescence (Advansta WesternBright ECL, San Jose, CA, USA) and visualized using the Bio-Rad ChemiDoc Touch imaging system. Densitometric analysis was performed with Bio-Rad ImageLab 6.0 software. Membrane stripping was also applied with heat and detergent. Shortly, membranes were incubated in Stripping buffer [0.5 M Tris-HCl pH 6.8; 10% SDS, β-mercaptoethanol] at 50 °C for 30 min in a Thermo-Shaker (Biosan) and were washed 6 times for 5 min with 1x TBST and reblocked with 5% BSA/TBST at RT for 1 h and reprobed as described above.

2.6. Proteome profiler analysis

Phosphorylation levels of various proteins were analyzed with a R&D Systems Proteome Profiler Human Phospho-Kinase Array kit (Minneapolis, MN, USA). After the previously described treatments, cells were harvested and 200 μg of protein was used for each experiment, according to the manufacturer's instructions. Dot intensities were analyzed with ImageJ software (NIH, Bethesda, MD, USA) and normalized to control dots on each membrane.

2.7. PI3K activity measurement

PI3K activity was measured with an ELISA kit (PI3-Kinase Activity ELISA, Pico, Echelon Biosciences Inc., Salt Lake City, UT, USA) following the manufacturer's protocol. Absorbance was measured at 450 nm (Multiskan GO, Thermo Scientific). Immunoprecipitation was conducted with the p85 subunit antibody (Merck Millipore) to validate the input. Liberated phosphatidylinositol (3,4,5)-trisphosphate (PIP_3) values were normalized to the PI3K expression levels.

2.8. Seahorse XF96 measurements

For the metabolic measurements we altered the original differentiation/treatment protocol (Fig. S1.). After transfection, cells were plated, and 24 h after transfection, were treated for 72 h as described in 2.3. Cells were seeded in small petri dishes, to confirm the effectivity of transfection. After the 72 h, myoblast cells were washed, and metabolic measurements were made on Agilent Seahorse XF (ASX) 96 plates using ASX assay-medium with 5.5 mM glucose. Etomoxir (50 μM), which is an inhibitor of fatty acid oxidation (FAO) was added. Oligomycin (2 μM) was applied to inhibit ATP synthesis and distinguish between the O_2 consumption devoted to ATP synthesis. FCCP (4 μM, carbonyl cyanide p-trifluormethoxyphenylhydrazone) was used as a mobile ion carrier to calculate the respiratory capacity of cells. Antimycin A (10 μM) was applied as the inhibitor of complex III to shut down electron transport chain function, revealing the non-mitochondrial respiration. Finally, 100 mM 2-deoxy-D-glucose (2-DG) was added; 2-DG is a glucose analog that inhibits glycolysis through competitive binding to glucose hexokinase to confirm ECAR due to glycolysis. Five measurement points were taken at baseline and after each injection event. After the measurements, cells were solubilized in 1N NaOH and protein content was determined by BCA assay.

2.9. Glucose uptake assay

2-NBDG (2-(*N*-(7-Nitrobenz-2-oxa-1,3-diazol-4-yl)Amino)-2-Deoxyglucose) uptake measurements were carried out as described previously, shortly. C2C12 cells were cultured, differentiated and treated as described before (Section 2.3-4.). The myotubes were washed with PBS buffer and incubated in glucose free DMEM supplemented with 2% horse serum. 100 nM insulin was applied for 30 min and cells were incubated with glucose-free medium containing 100 μM 2-NBDG (SIGMA) for 120 min at 37 °C. Fluorescence was measured at an extinction of 485 nm and emission of 535 nm using a Tecan Spark Multimode microplate reader (Tecan Treading AG, Mannedorf, Germany), and negative and blank controls as well as standard curve were also sat up to quantify glucose uptake. Cells were washed three-times and were solubilized in 0.1 M KH_2PO_4 pH 11.0 to determine protein concentration. Fluorescent data in pmol were related to 1 mg of proteins in each case and presented as fold induction.

2.10. Statistical analysis

Post hoc testing for two-way ANOVA was determined by Tukey's test and Sidak's test. The mouse tissue sample data were analyzed with one-way ANOVA and Dunnett's *post hoc* test. Parametric tests were used when normalized values were normally distributed. GraphPad software was used for all analyses. The data are presented as mean ± SEM; n is the number of independently performed experiments or animals. $P < 0.05$ was considered statistically significant.

3. Results

3.1. SMTNL1 influences insulin signaling, cell cycle, and apoptosis in insulin resistant C2C12 cells

The mouse myoblast cell line, C2C12, is a widely-used model for the *in vitro* examination of metabolic diseases, such as insulin resistance (Wong et al., 2020). InR was induced with chronic insulin treatment and 10 nM MPA (synthetic progesterone) with or without the overexpression of Flag-tag-SMTNL1 (FT-SMTNL1) in C2C12 myotubes (Fig. S1.). The overexpression of FT-SMTNL1 and differentiation was verified by high content screening analysis (Fig. S2). Protein arrays were used to monitor the phosphorylation and activity status of Tyr and Ser/Thr kinases and receptors, transcription factors, and other elements of insulin signaling (Fig. 1). Data were compared to control samples under conditions of low glucose (Figs. 1 and S3). Two-fold increases in phosphorylation levels of transcription factors, including STAT5a and b, were observed in cells overexpressing SMTNL1; however, the phosphorylation levels of STAT2 and 6, CREB, and c-Jun were unaffected (Fig. S3B). Regarding cell cycle regulation, only p53 Ser46 phosphorylation was increased in the InR cells overexpressing FT-SMTNL1 (Fig. S3A). Pyk2 non-receptor tyrosine kinase and PDGF receptor tyrosine kinase phosphorylation increased after MPA treatment and in combination with SMTNL1 overexpression in InR cells (Figs. S3C and S3F). Several important Ser/Thr kinases were

lontay.beata_285_24

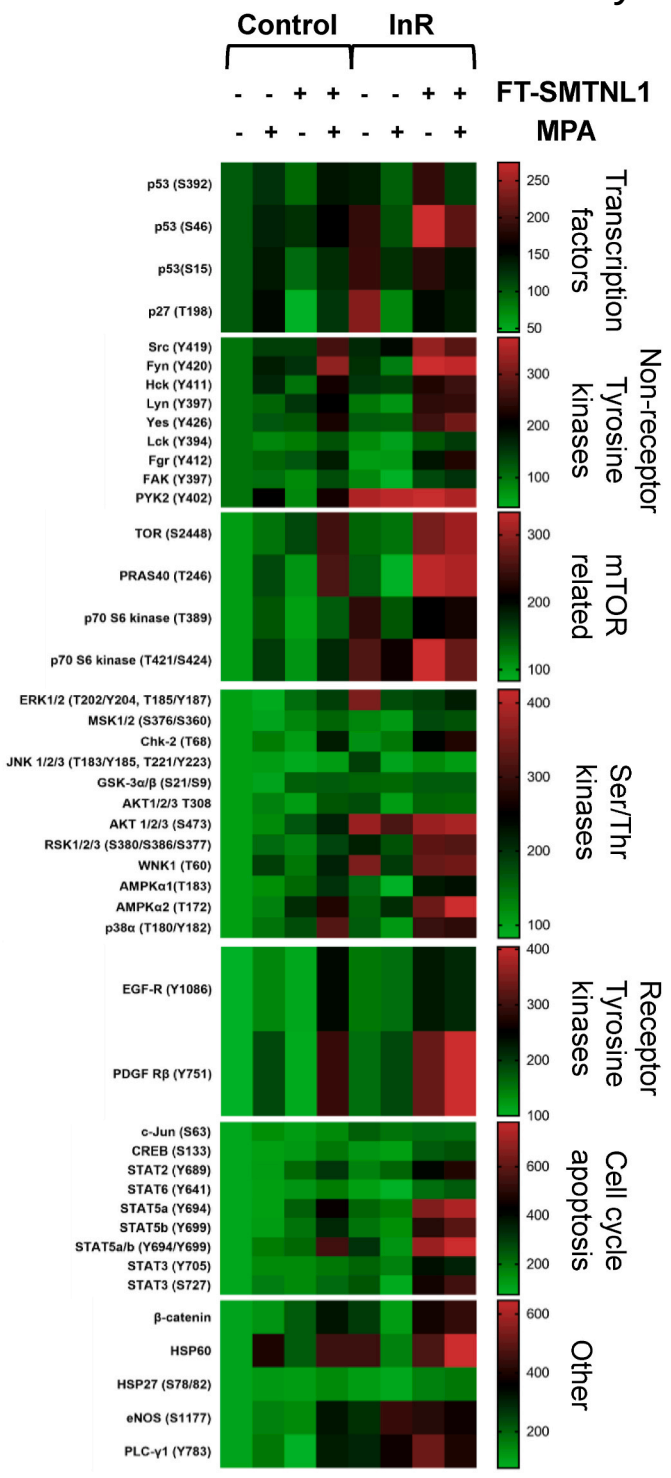


Fig. 1. Proteome profiler analysis of transfected and treated C2C12 cell lysates. A heatmap of various protein phosphorylation levels is shown. Color coding for the heatmap: red indicates more phosphorylated, while green indicates less phosphorylated protein levels. 200 μg of protein was used for the A and B part of membrane. The spot intensities were analyzed using ImageJ software and normalized to the control spots on each membrane.

elevated in response to induction of InR and were further increased by SMTNL1 overexpression (Fig. S3D). Phosphorylation of Thr172 in APMKα2 and Ser473 in Akt1/2/3 were increased by SMTNL1 overexpression in InR cells. In addition, phosphorylation of mTOR Ser2448 (Fig. S3E), c-Jun N-terminal kinase (JNK1/2/3) Thr183, and extracellular signal-regulated kinase (ERK1/2) Thr202 was increased (Fig. S3D); however, phosphorylation of p38, Chk2, and MSK1/2 did not change (Fig. S3D). These results indicate that SMTNL1 modulates critical signal transduction elements involved in insulin signaling and its downstream regulatory effects.

3.2. SMTNL1 overexpression decreases phosphorylation of ser residues of IRS1 in differentiated C2C12 insulin-resistant cells

To verify the protein phosphorylation results from the Proteome Profiler analysis and to elucidate the molecular mechanism underlying the effect of SMTNL1, we analyzed site-specific phosphorylations of IRS1 in InR C2C12 cells by Western blotting (Fig. 2). Moreover, to gain an understanding of the transcriptional changes induced by FT-SMTNL1 overexpression, we also looked at the levels of IRS1 and other signaling proteins (Figs. S5 and S6). Chronic insulin treatment significantly decreased IRS1 expression (Fig. 2E). However, IRS1 Ser307 (Fig. 2A), Ser318 (Fig. 2B), and Ser612 (Fig. 2C) phosphorylations were significantly elevated in InR cells and treatment with MPA had no effects. Ser phosphorylation levels were significantly lower in cells overexpressing FT-SMTNL1 in the presence of MPA in all cases (Fig. 2A–C). In contrast, IRS1 Ser1101 phosphorylation decreased in InR with or without progesterone (Fig. 2D), and the overexpression of SMTNL1 significantly decreased the Ser1101 phosphorylation of IRS1 in the presence of high concentrations of insulin and progesterone (Fig. 2D). We confirmed these findings in WT and KO *Smtnl1* non-pregnant and pregnant mice where the IRS1 phosphorylation at Ser612 (Fig. S4B.) and Ser1101 (Fig. S4A.) was significantly increased in SKM of pregnant *Smtnl1*−/− mice. Since SMTNL1 acts to attenuate the phosphorylation of IRS1 on Ser307, Ser318, and Ser612 in the presence of its natural ligand, it suggest that SMTNL1 modulate the activity or gene expression of IRS-1-Ser/Thr kinases or phosphatase, while IRS1 Ser1101 regulation is a ligand-independent process.

3.3. SMTNL1 promotes the activity of PI3K in insulin resistant C2C12 cells

To elucidate the effect of SMTNL1 on PI3K activity in insulin treatment, we determined the protein level of the p85 subunit of PI3K (Fig. 3A). Chronic insulin exposure significantly decreased p85 levels; however, FT-SMTNL1 overexpression increased p85 expression when compared to the empty vector transfection control. The PI3K enzyme activity, as determined by measuring the liberated PIP_3 product (Fig. 3B.), was not affected by either MPA exposure or FT-SMTNL1; however, PI3K activity was significantly increased in InR cells. Moreover, chronic insulin treatment in the presence of MPA induced higher PI3K activity compared to InR alone, and FT-SMTNL1 overexpression increased PI3K activity under conditions of InR. Collectively, these results demonstrate that SMTNL1 promotes PI3K activity in C2C12 myotubes by counteracting the decrease in PI3K protein levels triggered in response to chronic insulin exposure and by decreasing Ser phosphorylation of IRS1, which initiates the IRS1/PI3K complex.

3.4. Regulation of downstream effectors of insulin signaling by SMTNL1 in insulin resistance

The phosphorylation and activation of Akt/PKB in C2C12 myotubes was upregulated in the insulin-resistant state (Fig. 4A and B) and resulted in the propagation of downstream insulin signaling. Both Thr308 and Ser473 phosphorylation of Akt1 were stimulated by acute, 30 min insulin treatment, while MPA had no effect. Furthermore, the activity of Akt1 was increased in the InR model. FT-SMTNL1 overexpression did not influence the expression of Akt1 (Fig. S6B), but it drastically influenced the phosphorylation of Akt1 Ser473, but not Thr308, in InR myotubes, suggesting an insulin-sensitizing effect. These results are supported by interrogations of *Smtnl1* KO mice where Akt1 expression was unaffected in any experimental group (Fig. S4C.) but the

lontay.beata_285_24

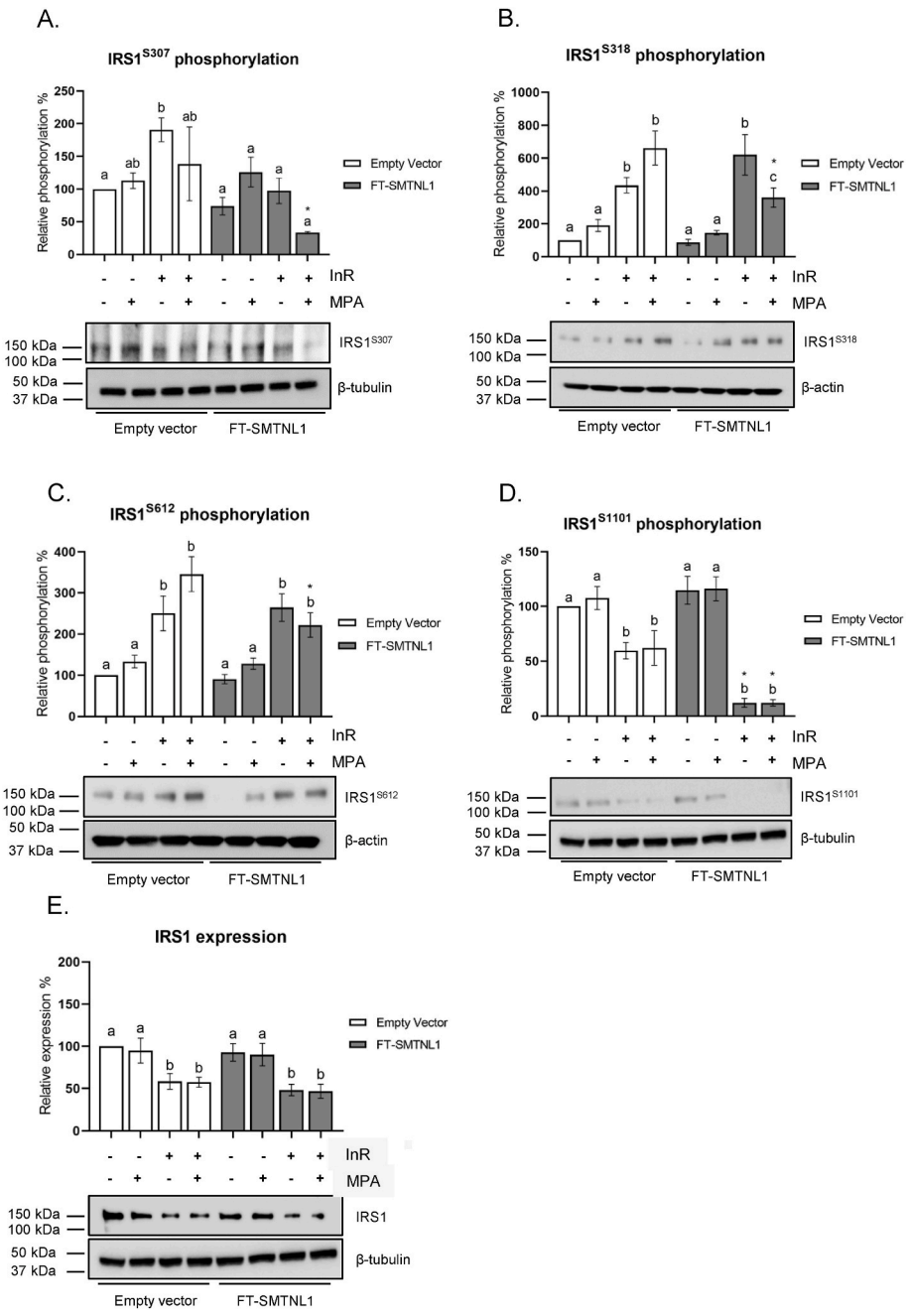


Fig. 2. Western-blot analysis of IRS1 expression and phosphorylation in insulin-resistant C2C12 myotubes. After differentiation and induction of insulin resistance, cells were harvested and prepared for Western blot analysis of $IRS1^{S307}$ **(A)**, $IRS1^{S318}$ **(B)**, $IRS1^{S612}$ **(C),** and $IRS1^{S1101}$ **(D)** phosphorylation and (E) IRS expression. The phosphorylation levels were normalized to non-phosphorylated protein which in turn was normalized to β-tubulin as an internal loading control. The effects of SMTNL1 vs. the empty vector-transfected cells were compared (Two-way ANOVA and Sidak's *post hoc* test, Mean ± SEM; n = 3; *, $p < 0.05$). The effects of various treatments were also compared (Two-way ANOVA and Tukey's *post hoc* test, Mean ± SEM; n = 3; $p < 0.05$; Different letters indicate significant differences between the groups compared).

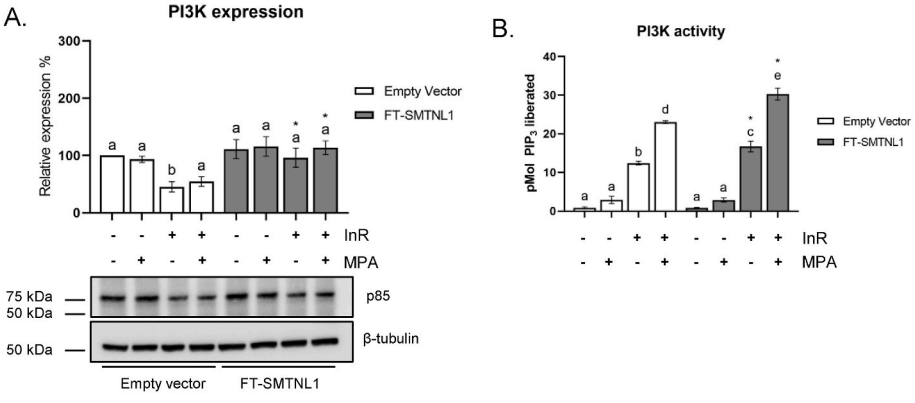


Fig. 3. SMTNL1 Promotes the activity of PI3K in insulin resistant C2C12 cells (A) Western blot analysis was conducted to determine the PI3K p85 subunit levels. Protein expression was normalized to the loading control. **(B)** PI3K activity was measured using a PI3K pico-ELISA kit. InR: insulin resistant; MPA: medroxyprogesterone-17-acetate. The effects of SMTNL1 vs. the empty vector-transfected cells were compared (Two-way ANOVA and Sidak's *post hoc* test, Mean ± SEM; n = 3; *, $p < 0.05$), and the effects of various treatments were compared (Two-way ANOVA and Tukey's *post hoc* test, Mean ± SEM; n = 3; $p < 0.05$; Different letters indicate significant differences between the groups compared).

lontay.beata_285_24

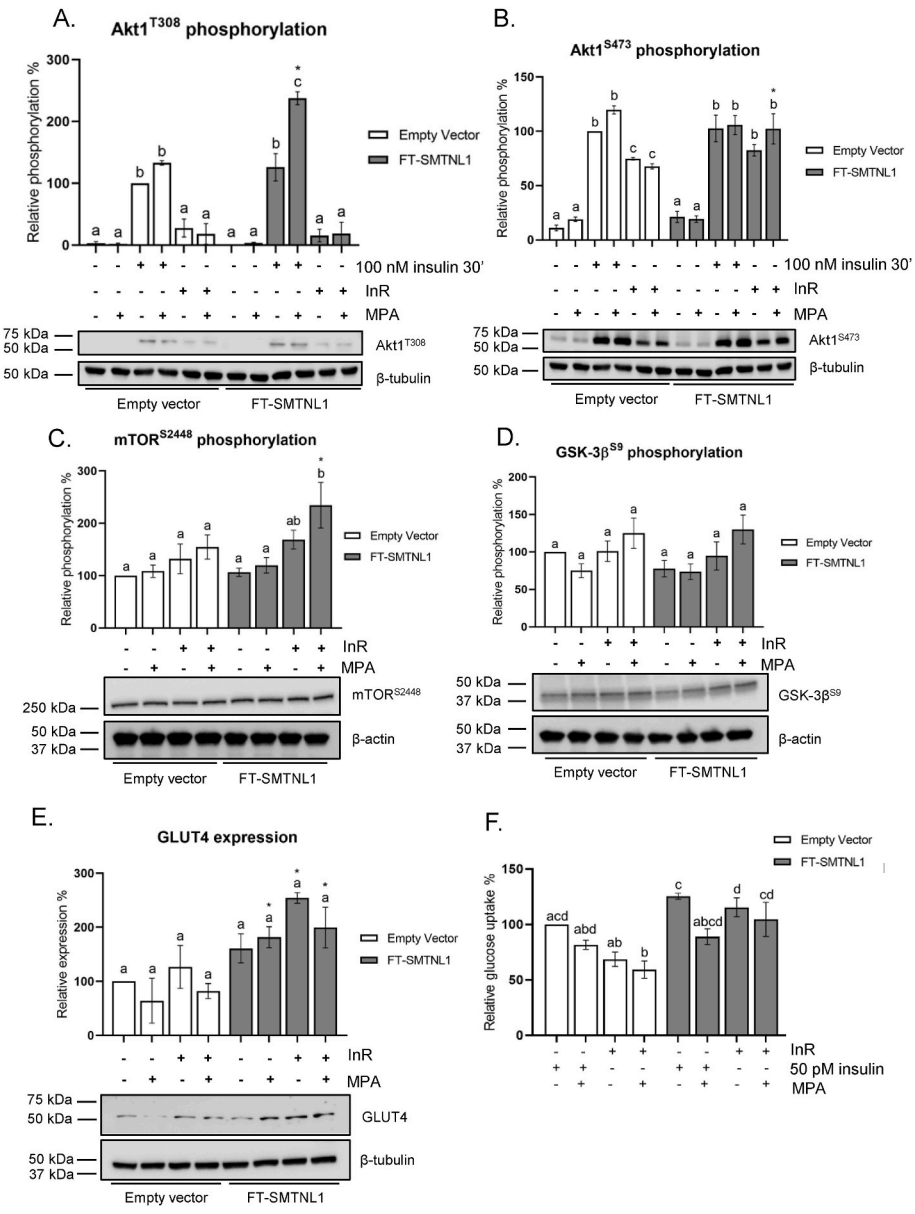


Fig. 4. Effects of SMTNL1 overexpression and insulin resistance on the insulin signaling pathway. For Akt1 phosphorylation **(A–B)** the same treatment method was used, except two more samples were introduced for each transfection. After the 72h of differentiation in physiological conditions, 100 nM of insulin were added to the cells for the final 30 min of treatment to assess if insulin resistance was present in the long-term treated cells. Samples were also collected to analyze other parts of the insulin signaling pathway, including **(C)** mTOR^{S2448}, **(D)** GSK-3β^{S9}, and **(E)** Expression of GLUT4 was assessed in the *in vitro* model. The phosphorylated proteins are normalized to the non-phosphorylated protein levels, which in turn was normalized to β-tubulin or β-actin as internal loading controls. The effects of SMTNL1 vs. the empty vector-transfected cells were compared. **(F)** Relative glucose uptake was measured using 2-NBDG and the fluorescence values normalized to the protein concentration. Normalized values were compared to the empty vector-transfected cells treated with physiological levels of insulin InR: insulin resistant; MPA: medroxyprogesterone-17-acetate. (Two-way ANOVA and Sidak's *post hoc* test Mean ± SEM; n = 3; *, $p < 0.05$), and the effects of various treatments were also compared (Two-way ANOVA and Tukey's *post hoc* test Mean ± SEM; n = 3; $p < 0.05$; Different letters indicate significant differences between the groups compared). Fig. 4A and B were analyzed on the membrane after stripping.

Akt1 phosphorylation was significantly decreased in pregnant *Smtnl1* KO animals (Fig. S4D.).

To examine a wider range of Akt function in insulin signaling, the phosphorylation of two downstream Akt substrates was examined. Neither the expression level (Fig. S6A) nor the phosphorylation of mTOR at Ser2448 (Fig. 4C) was altered in the presence of chronic insulin administration or MPA exposure. However, when cells were co-treated with insulin and MPA, overexpression of FT-SMTNL1 activated mTOR. In addition, GSK-3β expression (Fig. S6C) and Ser9 phosphorylation levels (Fig. 4D) and p70S6 kinase phosphorylation at Thr389 (Fig. S5A) did not change, although p70S6 kinase protein expression showed InR-dependent elevation (Fig. S5B).

Finally, GLUT4 expression significantly increased in response to FT-SMTNL1 overexpression in InR cells compared to the transfection control (Fig. 4E). Moreover, glucose uptake was significantly elevated in SMTNL1-overexpressed myotubes compared to each of the vehicle control in insulin resistant samples, while it was decreased upon combined treatment of high glucose/high insulin and progesterone (Fig. 4F.). Collectively, these data demonstrate that FT-SMTNL1 overexpression promotes insulin signaling in myotubes by regulating the phosphorylation of several insulin-related downstream elements and leads elevated glucose uptake.

3.5. *SMTNL1 regulates JNK and ERK1/2 and IRS1 phosphorylation through expression of a novel PKC gene*

Next, we examined the potential upstream regulators of insulin signaling. Since both ERK1/2 and JNK were significantly altered in InR cells by Proteome Profiler analysis (Fig. 2.), we measured the expression and phosphorylation of these MAP kinases. JNK and ERK1/2 expressions were not modulated by any experimental condition (Fig. 5A and C). However, interestingly, the activating phosphorylation of JNK at Y185 and ERK1/2 at Thr202/Tyr204 increased significantly in response to 100 nM insulin treatment but was attenuated with FT-SMTNL1 overexpression in InR and MPA-treated C2C12 cells (Fig. 5B and D). We evaluated the target of SMTNL1 action on ERK1/2 and the upstream regulators of ERK1/2 activity. Protein phosphatase 2A expression did not change (Fig. 5E) but the levels of a novel protein kinase C, PKCε, were reduced by 50%

In response to FT-SMTNL1 overexpression compared to control

lontay.beata_285_24

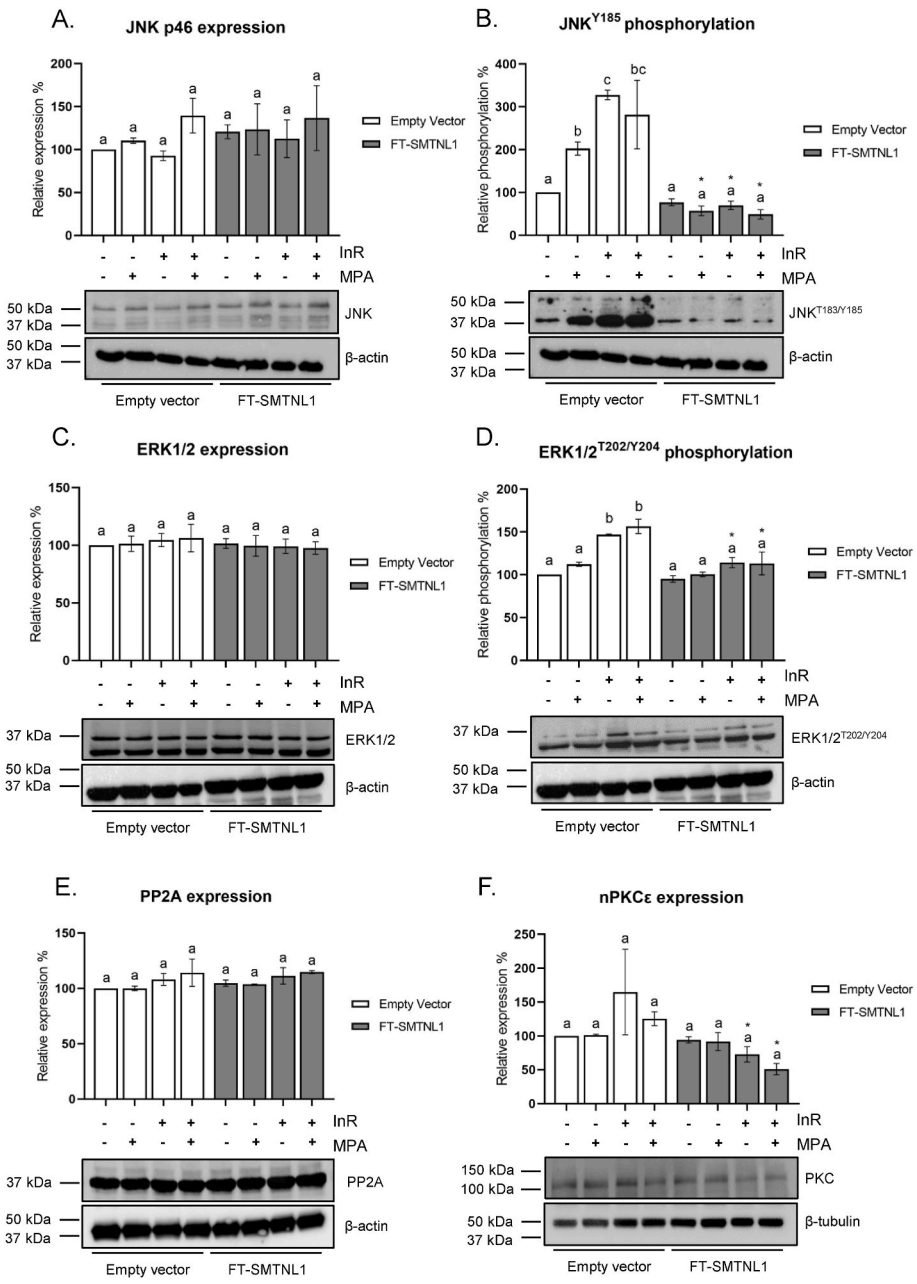


Fig. 5. Western blot analysis of JNK expression and phosphorylation, ERK1/2 expression and phosphorylation, and PP2A and PKC expression cells after induction of insulin resistance. Harvested samples were subjected to western blotting with **(A)** SAPK/JNK, **(B)** SAPK/JNK^{Y185}, **(C)** ERK1/2, **(D)** ERK1/2$^{T202/Y204}$, **(E)** PP2A, and **(F)** nPKCε antibodies. The phosphorylated proteins were normalized to the non-phosphorylated protein levels which in turn was normalized to β-actin as an internal loading control. InR: insulin resistant; MPA: medroxyprogesterone-17-acetate. The effect of SMTNL1 vs. the empty vector-transfected cells were compared (Two-way ANOVA and Sidak's *post hoc* test, Mean ± SEM; n = 3; *, $p < 0.05$), and the effects of various treatments were also compared (Two-way ANOVA and Tukey's *post hoc* test Mean ± SEM; n = 3; $p < 0.05$; Different letters indicate significant differences between the groups). Fig. 5A and B and 55C and D were analyzed on the membrane after stripping.

transfection in InR cells (Fig. 5F). Another potential regulator of IRS1 is atypical protein kinase C zeta (PKCζ), but no significant expression differences were detected for this kinase (Fig. S6D). These data indicate that SMTNL1 regulates ERK1/2 activity by reducing its upstream activator, PKCε.

3.6. *SMTNL1 improves glycolysis and mitochondrial respiration in insulin resistant myoblasts*

Changes in energy-producing pathways were determined using real-time, simultaneous measurements of oxygen consumption rate (OCR) and extracellular acidification rate (ECAR), as indicators of oxidative phosphorylation and glycolysis. We compared the effects of FT-SMTNL1 overexpression to empty vector controls in C2C12 cells after InR and MPA treatments. The conversion of glucose to lactate independent of oxygen releases protons into the extracellular medium and causes acidification that was measured as ECAR (Fig. 6A). Sequential injections of oligomycin and 2-DG combined with antimycin A measured glycolysis, glycolytic capacity, and allowed calculation of glycolytic reserve and non-glycolytic acidification. Baseline ECAR increased significantly in response to MPA treatment but drastically decreased in response to chronic insulin treatment. This reduction was ameliorated by FT-SMTNL1 overexpression in the presence of MPA (Fig. 6C). Similar tendencies were observed for anaerobic glycolytic values;

FT-SMTNL1 overexpression was associated with significant increase in ECAR only after treatment with MPA in InR when compared to cells transfected with the empty vector (Fig. 6E). Maximal glycolysis was increased by MPA and decreased in response to chronic insulin treatment but FT-SMTNL1 overexpression did not influence maximal glycolysis (Fig. 6G) nor the glycolytic reserve (Fig. S7A.).

Mitochondrial respiration was measured as OCR through chronological injection of etomoxir, oligomycin, FCCP, and antimycin A (Fig. 6B) to assess basal respiration, ATP production, proton leak, maximal respiration, and non-mitochondrial respiration. MPA increased

lontay.beata_285_24

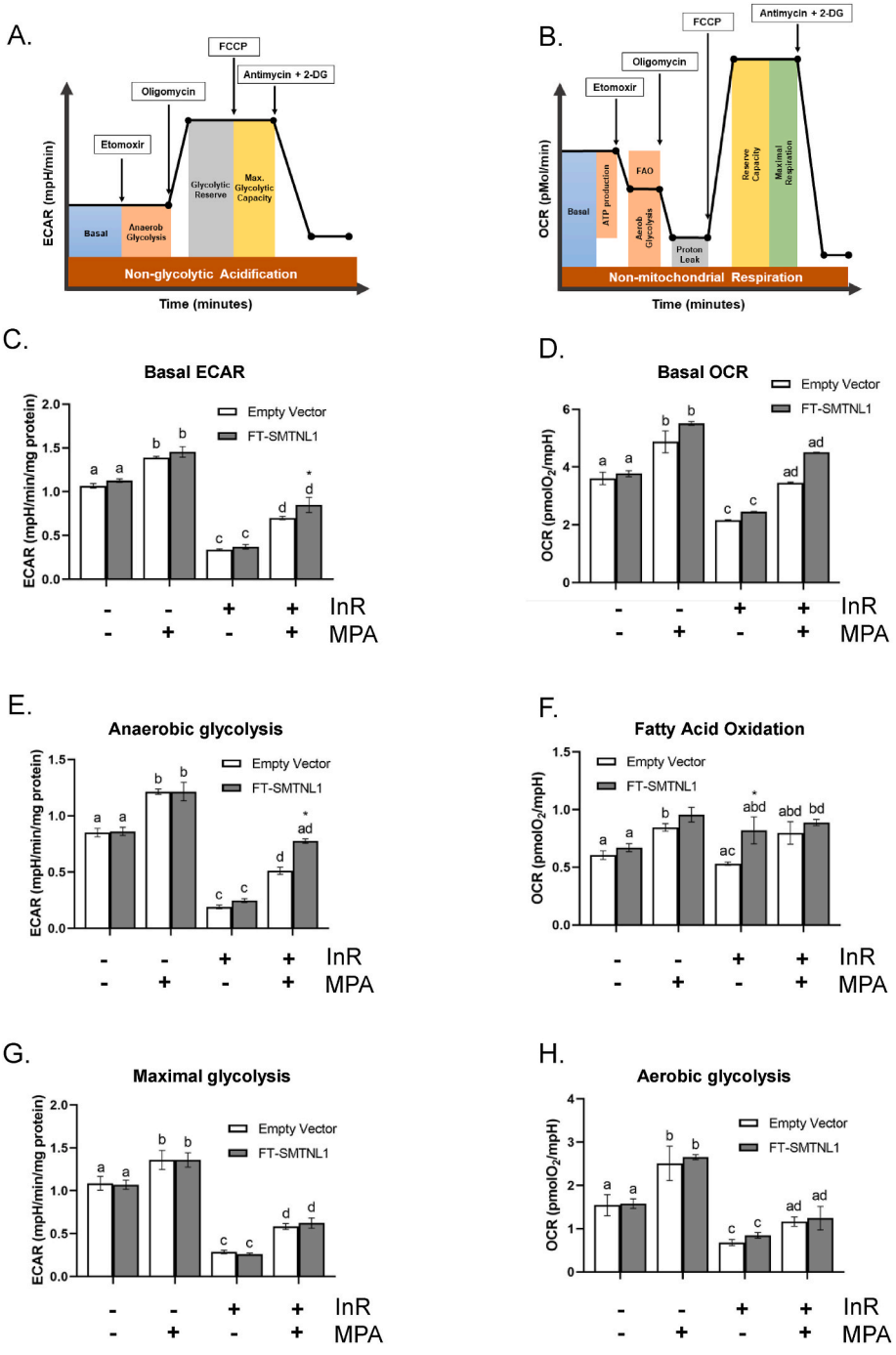


Fig. 6. Energetic parameters after transfection with SMTNL1 or empty vector in the C2C12 cell insulin resistance in vitro model. C2C12 cells were seeded on Seahorse XF 96, and cellular parameters were measured. Both glycolytic (ECAR – Extracellular Acidification Rate) and oxidative (OCR – Oxygen Consumption Rate) variables were measured. **(A–B)** Injection strategy used during the seahorse measurements. Before injecting the inhibitors, the baseline ECAR **(C)** and OCR **(D)** levels of the cells were measured. **(E)** Anaerobic glycolysis parameters independent of mitochondrial activity were calculated by subtracting the Antimycin A + 2-DG values from the baseline values. Fatty acid oxidation **(F)** was calculated by subtracting the OCR values measured after etomoxir injection from the baseline. **(G)** Maximal glycolysis was calculated by subtracting Antimycin A + 2-DG from values determined with oligomycin injection. **(H)** Aerobic glycolysis was calculated by subtracting the oligomycin injection values from the etomoxir injection; the difference is the glycolysis connected to mitochondrial activity. InR: insulin resistant; MPA: medroxyprogesterone-17-acetate. The effects of SMTNL1 vs. the empty vector-transfected cells were compared (Two-way ANOVA and Sidak's *post hoc* test, Mean ± SEM; n = 3; *, $p < 0.05$), and the effects of various treatments were compared (Two-way ANOVA and Tukey's *post hoc* test, Mean ± SEM; n = 3; $p < 0.05$; Different letters indicate that significant differences between the groups). The technical replicates were n = 23 per plate per treatment by dividing the 96 well plates into four regions (24–1) for the treatments and leaving one well for a blank in each region. After the measurements, values were normalized to protein content.

OCR in both control and InR cells. Chronic insulin exposure decreased basal OCR and MPA treatment prevented this reduction(Fig. 6D). The utilization of alternative carbon fuels, such as fatty acids was assessed as the difference between OCR values upon etomoxir and oligomycin treatments. MPA increased, InR decreased, and FT-SMTNL1 overexpression resulted in a slight elevation in fatty acid oxidation potential (Fig. 6F). Aerobic glycolysis (Fig. 6H), OCR reserve (Fig. S7B) and maximal respiration (Fig. S7C) were unaffected by the overexpression of SMTNL1. Collectively, these data imply that SMTNL1 predominantly acts on the glycolytic pathway where it significantly increased basal ECAR when compared to control cells. Taken together, the results confirm the insulin-sensitizing effects of SMTNL1 on the metabolism of InR cells.

4. Discussion

In the present study, we provide evidence for the metabolic role of SMTNL1 in differentiated C2C12 cells and a *Smtnl1* KO mouse model. In the presence of its natural ligand, progesterone, SMTNL1 overexpression was coupled to decreased Ser phosphorylation of IRS1, which induces the PI3K/Akt signaling pathway in C2C12 hyperinsulinemic/hypoglycemic insulin-resistant myotubes. Our data indicate that SMTNL1 exerts its effects by regulating the expression of a novel PKC that contributes to the phosphorylation of IRS1 directly at Ser318 residue and indirectly at Ser612 through the regulation of ERK1/2.

Insulin signaling and the related signal transduction cascades involved in insulin resistance in SKM pathology were previously investigated by comprehensive mass spectrometry-based proteomic analysis

lontay.beata_285_24

(Mullen and Ohlendieck, 2010). In addition, numerous studies have revealed the phosphorylation-level changes of players in insulin signaling showing the importance of this field. We prescreened the possible signaling pathways altered by SMTNL1 with InR of C2C12 myotubes using a series of proteome profiler assays. To differentiate between the cytoskeletal and transcriptional effects of SMTNL1, experiments were completed with progesterone as the natural ligand of SMTNL1. We narrowed down the SMTNL1-related pathways primarily to mTOR and Ser/Thr kinase signaling (Fig. 1). These results are broadly in line with an earlier report of *Smtnl1* KO mice using proteomic and microarray analyses (Lontay et al., 2015).

Our results indicate that IRS1 phosphorylation at Ser307, Ser318, and Ser612 was upregulated in the InR model and SMTNL1 overexpression decreased phosphorylation at these residues but only in the presence of progesterone. Under InR conditions, the shift from Tyr to Ser phosphorylation of IRS1 leads to the dissociation of IRS1 from PI3K, which accounts for insulin signaling defects (Morino et al., 2006). IRS1 Ser307 and Ser318 phosphorylation disrupts the IR/IRS1 complex and enables desensitization to insulin (Copps and White, 2012). Ser307 is the major site on IRS1 for JNK phosphorylation (Mussig et al., 2005) our results were in accordance with other *in vivo* diabetic animal and *in vitro* studies (Manning and Davis, 2003) showing that JNK activity was upregulated in InR cells. Over-expression of SMTNL1 did not change the expression of JNK, but their activation were significantly suppressed in response to SMTNL1 overexpression in InR model. We also characterized IRS1 Ser318 phosphorylation, which is the target of insulin-induced PKCζ (Moeschel et al., 2004); however, the activity and expression of this PKC isoform were not SMTNL1-dependent. Deletion of any member of the novel PKC family prevents InR by decreasing IRS1 phosphorylation on Ser308 and Ser318 (Boucher et al., 2014); we showed that Ser318 phosphorylation was attenuated by SMTNL1 overexpression with coincident downregulation of novel PKCε levels.

The phosphorylation of the Ser612 residue of IRS1, located proximal to the regulatory Tyr residues, provides negative regulation of the insulin signaling pathway involving predominantly ERK1/2 and the mTOR pathways in its regulation. ERK1/2 activation plays a major role in maintaining insulin-induced PI3K-dependent InR (Gual et al., 2003) and specific inhibition of ERK1/2 by PD98059 restored insulin sensitivity (Fujishiro et al., 2003). In our model, ERK1/2 was phosphorylated after chronic insulin treatment and overexpression of SMTNL1 suppressed ERK1/2 activity, especially in the presence of MPA. In addition, IRS1 Ser612 phosphorylation was reduced, likely resultant of the SMTNL1-dependent reduction of ERK1/2 activity. We suggest that ERK1/2 exerts insulin-desensitizing effect in C2C12 myotubes not only through the phosphorylation of Ser612 but also through the regulation of GLUT4 since chronic activation of ERK1/2 leads to the downregulation of GLUT4 expression and decreased insulin-induced glucose transport (Krook et al., 2000).

JNK and ERK1/2 protein expression did not change but their phosphorylation and, presumably, activity decreased in response to SMTNL1 overexpression with progesterone, suggesting that SMTNL1 regulates upstream Ser/Thr kinases or phosphatases at the gene expression level. None of the MAP kinase kinases were altered in the microarray analysis of pregnant *Smtnl1* KO mice compared to WT (Lontay et al., 2015). Therefore, we investigated protein phosphatase 2A (PP2A), the negative regulator of ERK1/2 (Yu et al., 2004) but its gene expression was unaffected in this study (Fig. 5E). Another potential regulator is the novel PKCε that phosphorylates and activates ERK1/2 in SKM. In our study, PKCε expression was downregulated by SMTNL1 in the InR C2C12 cells, promoting insulin sensitivity through several mechanisms. In diabetic rats, PKCε was prominently overexpressed in the SKM and hyperinsulinemia leading to insulin resistance in SKM was associated with chronic activation of PKCε but not other novel PKC isoforms (Ikeda et al., 2001). It is in line with previous findings showing an alteration in PKC isoforms in SMTNL1 KO animals by microarray analysis (Lontay et al., 2015). We suggest that JNK activity is regulated by its upstream regulator, dual specific phosphatase 9 (Major et al., 2021) that was identified as an SMTNL1-dependent gene in SKM in mice (Lontay et al., 2015).

The mTORC1/S6K1 pathway provides a negative feedback loop to attenuate PI3K/Akt signaling downstream of IRS1 via the phosphorylation of Ser1101 in SKM (Kido et al., 2020). Strikingly, our results showed a significant decrease in IRS1 Ser1101 phosphorylation with InR, which was further suppressed with overexpression of SMTNL1. Consistent with this finding, phosphorylation of IRS1 Ser1101 was elevated in pregnant *Smtnl1* KO animals but not pregnant WT animals. No other studies have monitored the effects of long-term hyperinsulinemia on Ser1101 phosphorylation in differentiated C2C12 cells. We presume that these results are due to the long-term InR state of myotubes and the activation of inhibitory regulatory feedback signals for the phosphorylation of the Ser1101 residue. IRS1 degradation also contributes to the downregulation of insulin-induced signaling, as revealed in our InR model in a SMTNL1-independent manner and in the literature (Pederson et al., 2001).

PI3K activity, measured by the concentration of liberated PIP_3 (Fig. 3), was increased upon insulin stimulation of C2C12 myotubes but this level was significantly lower in cells with InR. The expression of p85 expression decreased in InR cells, but SMTNL1 overexpression restored p85 expression and PI3K activity in the presence of MPA. Alteration in PI3K also affects the activity of its downstream effector, Akt. Interestingly, the protein levels of Akt1 did not change in response to any treatments in differentiated C2C12 cells similarly to the findings in human diabetic SKM samples (Czech and Corvera, 1999). Based on our results, SMTNL1 differentially regulated Ser473 and Thr308 phosphorylation of Akt (Fig. 4A and B). Insulin-induced Akt phosphorylation at both Thr308 and Ser473 was significantly decreased in InR non-transfected cells. However, SMTNL1 overexpression elevated Thr308 phosphorylation in insulin-induced control cells but only slightly induced Ser473 phosphorylation in InR cells compared to the control. For insulin-induced activation, Akt requires the hierarchical phosphorylation of both Thr308 and Ser473 phosphorylated by phosphoinositide-dependent kinase-1 (PDK1) and mTORC2, respectively (Copps and White, 2012). Chronic insulin exposure inhibits Akt activation via inhibition of Akt Thr308 phosphorylation, even without changes in Akt Ser473 phosphorylation (Kondapaka et al., 2004). These results indicate that Akt Ser473 does not fully reflect upstream IRS1/PI3K signaling.

Akt also phosphorylates and inactivates its downstream substrate, GSK-3β, resulting in glycogen synthase activation and glycogen accumulation (Kim et al., 2004). Surprisingly, the phosphorylation of GSK-3β was unaffected under every experimental condition. Similarly, *Shao* et al. showed no change in GSK3β phosphorylation in the muscle after insulin treatment in *db/db* mice even with a twofold increase in Akt Ser473 phosphorylation (Shao et al., 2000) and the phosphorylation of downstream Akt substrates Akt substrate of 160 kDa was also unaffected (Karlsson et al., 2006). Based on our proteome profiler analysis, eNOS, PRAS40, and WNK1, which are classic substrates of PI3K/Akt, were phosphorylated by Akt activation. These combined results suggest that SMTNL1 selectively regulates impaired Akt activity related to insulin resistance and may be responsible for the heterogeneous downstream effects of Akt (Gonzalez et al., 2011; Li et al., 2010).

The PI3K/Akt pathway regulates downstream signaling in the mTOR pathway to coordinate cell growth and modulate the nutrient response. Akt phosphorylates mTOR at Thr2446/Ser2448 (Sekulic et al., 2000); this residue can also be phosphorylated by p70S6 kinase (p70S6K) (Chiang and Abraham, 2005). Our results are in line with these findings. Changes in Akt1 Ser473 mirrored that of mTOR and increased in InR and insulin-induced cells in response to SMTNL1. These data demonstrate that the PI3K-Akt-mTOR pathway is regulated by SMTNL1, without modulating the expression and activity of p70S6K. Another downstream target of insulin/PI3K signaling is Glut4, which is translocated to the plasma membrane, leading to increased glucose transport *in vitro* (Czech

lontay.beata_285_24

and Corvera, 1999; Shepherd et al., 1998). Overexpression of SMTNL1 in C2C12 myotubes was associated with enhanced GLUT4 expression in InR (Fig. 4F). Enhanced GLUT4 expression in muscle tissue reduces blood glucose. In agreement with these findings, skeletal muscle GLUT4 expression was significantly lower in *Smtnl1*−/− mice (Lontay et al., 2015).

Glycolytic function and mitochondrial respiration also demonstrated the insulin-sensitizing effects of SMTNL1 on InR C2C12 cells. Base ECAR and anaerobic glycolysis were decreased in InR cells. However, SMTNL1 overexpression in the presence of progesterone attenuated the decreased ECAR and glycolysis without affecting either maximal glycolysis or glycolytic reserve capacity. Progesterone increased glycolytic activity and ATP production in skeletal muscle cells but the activities were still below control levels in InR cells; only SMTNL1 overexpression in the presence of progesterone could rescue glycolytic activity and ATP production. In agreement with these results, *smtnl1* KO mice were metabolically less efficient and showed glucose intolerance; pregnancy increased glucose tolerance to the level of WT animals (Lontay et al., 2015), confirming the regulatory effects of SMTNL1 on gene expression in the insulin signaling pathway. The rate of fatty acid uptake was higher and the rate of fatty acid oxidation was lower in insulin-resistant muscle cells compared to healthy cells (Turcotte and Fisher, 2008), which was confirmed in our cell culture model. Interestingly, SMTNL1 induced fatty acid oxidation in InR cells. This is in line with data in *smtnl1* KO pregnant animals, in which skeletal muscle glycolysis and fatty acid oxidation were decreased (Lontay et al., 2015).

Our data might have implications in gestational diabetes mellitus (GDM). GDM is characterized by severe insulin resistance and an increased risk of developing subsequent type 2 diabetes. MPA is a co-regulator in this study, but also serves as a model for GDM, where glucose, insulin, and progesterone levels are elevated. In patients with GDM, the maximal insulin-stimulated IRS1 Tyr phosphorylation was significantly lower compared with non-pregnant control subjects and glucose transport activity was reduced (Friedman et al., 1999). Furthermore, redistribution of PI3K to the IR was impaired due to increased insulin-stimulated IRS1 Ser-phosphorylation and PI3K activity was reduced with hampered GLUT4 translocation in GDM patients (Shao et al., 2002). *Smtnl1* KO animals developed insulin resistance, which was significantly worsened in pregnancy (Lontay et al., 2015). The promotion of Ser phosphorylation on residues Ser307, Ser612 and Ser318 of IRS1 with SMTNL1 overexpression was dependent on progesterone and correlated with PI3K activity. These results indicate that SMTNL1 regulation of gene expression can prevent GDM.

5. Conclusions

These data collectively suggest that SMTNL1 induces insulin-sensitization of C2C12 myotubes through several mechanisms. 1) SMTNL1 negatively regulates the expression of the upstream regulators of insulin-dependent Ser/Thr kinases that are activated by prolonged insulin and glucose exposure. By decreasing PKCε expression, SMTNL1 hampers the activity of ERK1/2 with subsequent decrease in IRS1 Ser612 phosphorylation and initiation of PI3K association to activate the PI3K-Akt-mTOR pathway. 2) SMTNL1 also acts on heterologous IRS1 kinases to inhibit insulin action during the development of insulin resistance by regulating IRS1 Ser307 phosphorylation that in turn would affect IR/IRS1 interactions. 3) SMTNL1 promotes glucose uptake via activation of Akt pathways and by inducing GLUT4 expression to overcome insulin resistance (Fig. 7). Taken together, these findings indicate that SMTNL1 serves as an important regulator of insulin

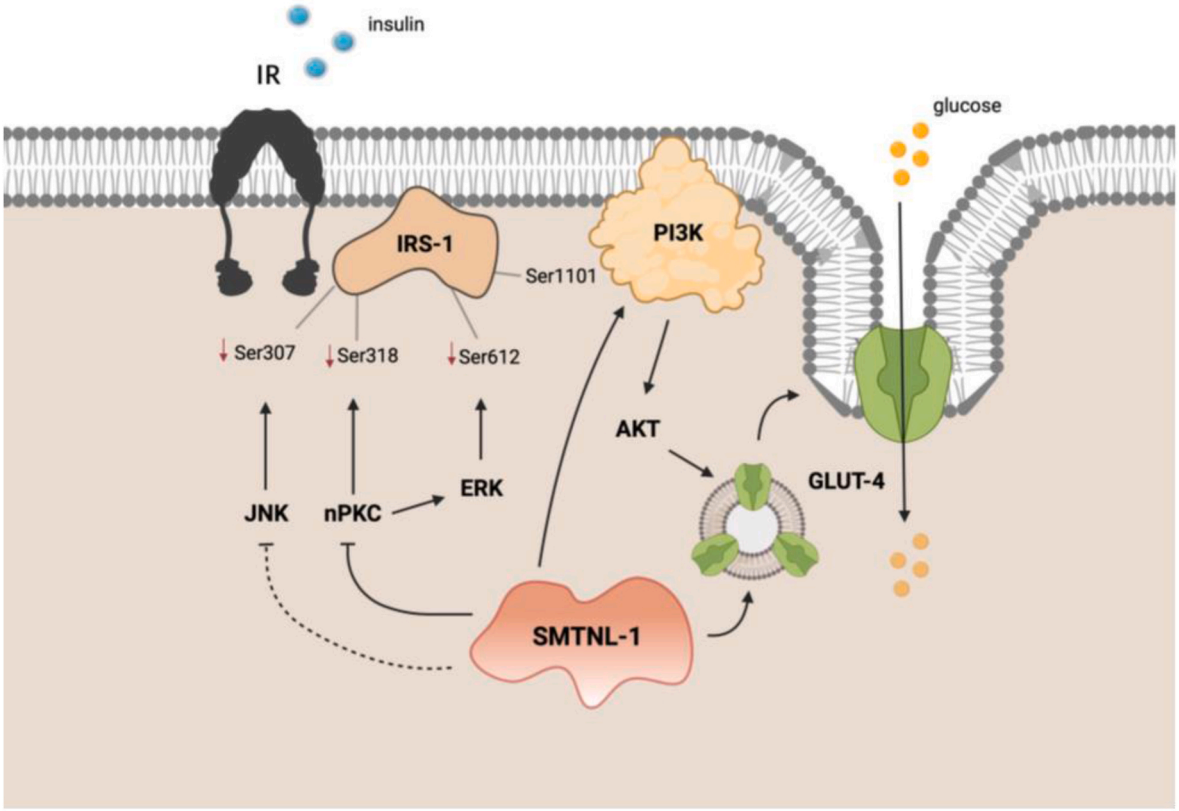


Fig. 7. Insulin sensitizing effects of SMTNL1 in InR C2C12 myotubes. SMTNL1 decreased PKCε gene expression, which hampered the activity of ERK1/2 leading to a decrease in IRS1 Ser612 phosphorylation. Ser612 phosphorylation initiates the PI3K association, activates the PI3K-Akt-mTOR pathway, and downregulates JNK activation, leading to a decreased IRS1 Ser307 phosphorylation. SMTNL1 promotes glucose uptake via activation of Akt and AMPK pathways and by inducing GLUT4 expression.

lontay.beata_285_24

signaling in SKM. Thus, SMTNL1 is a potential therapeutic target for improving insulin resistance.

6. Funding information

This work was supported by grants from the National Research, Development and Innovation Office (FK125043), the University of Debrecen, Faculty of Medicine Research Fund (1G3DBKJ0BFTK 247) for B. L, and from the EU co-financed by the European Regional Development Fund under project EFOP-3.6.2-16-2017-00006 and EFOP-3.6.3-VEKOP-16-2017-00009.

8. Conflicts of interest

The authors have declared no competing interests.

CRediT authorship contribution statement

Istvan Tamas: Writing – review & editing, completed Fig. 1, 2 and 3Fig. 1fig2fig3, wrote the paper. All authors reviewed the manuscript. **Evelin Major:** performed Fig S2 and assisted in Fig. 6. **Daniel Horvath:** completed Fig. 5A-Bfig5, 4E-F. **Ilka Keller:** created Fig. 7. **Adam Ungvari:** completed Fig. 5A–B, 4E-F. **Timothy A. Haystead:** Writing – review & editing, wrote the paper. All authors reviewed the manuscript. **Justin A. MacDonald:** supported animal experiments. **Beata Lontay:** Writing – review & editing, designed the study, wrote the paper. All authors reviewed the manuscript.

9. Acknowledgements

We thank Dr Karen Uray for providing language help and Andrea Docsa and Ágota Kelemenné Szántó for technical assistance.

Appendix A. Supplementary data

Supplementary data to this article can be found online at https://doi.org/10.1016/j.mce.2022.111663.

References

Abdul-Ghani, M.A., DeFronzo, R.A., 2009. Plasma glucose concentration and prediction of future risk of type 2 diabetes. Diabetes Care 32 (Suppl. 2), S194–S198.
Beg, M., Abdullah, N., Thowfeik, F.S., Altorki, N.K., McGraw, T.E., 2017. Distinct Akt phosphorylation states are required for insulin regulated Glut4 and Glut1-mediated glucose uptake. Elife 6.
Bodoor, K., Lontay, B., Safi, R., Weitzel, D.H., Loiselle, D., Wei, Z., Lengyel, S., McDonnell, D.P., Haystead, T.A., 2011. Smoothelin-like 1 protein is a bifunctional regulator of the progesterone receptor during pregnancy. J. Biol. Chem. 286, 31839–31851.
Borman, M.A., MacDonald, J.A., Haystead, T.A., 2004. Modulation of smooth muscle contractility by CHASM, a novel member of the smoothelin family of proteins. FEBS Lett. 573, 207–213.
Boucher, J., Kleinridders, A., Kahn, C.R., 2014. Insulin receptor signaling in normal and insulin-resistant states. Cold Spring Harbor Perspect. Biol. 6.
Chiang, G.G., Abraham, R.T., 2005. Phosphorylation of mammalian target of rapamycin (mTOR) at Ser-2448 is mediated by p70S6 kinase. J. Biol. Chem. 280, 25485–25490.
Copps, K.D., White, M.F., 2012. Regulation of insulin sensitivity by serine/threonine phosphorylation of insulin receptor substrate proteins IRS1 and IRS2. Diabetologia 55, 2565–2582.
Czech, M.P., Corvera, S., 1999. Signaling mechanisms that regulate glucose transport. J. Biol. Chem. 274, 1865–1868.
Friedman, J.E., Ishizuka, T., Shao, J., Huston, L., Highman, T., Catalano, P., 1999. Impaired glucose transport and insulin receptor tyrosine phosphorylation in skeletal muscle from obese women with gestational diabetes. Diabetes 48, 1807–1814.
Fujishiro, M., Gotoh, Y., Katagiri, H., Sakoda, H., Ogihara, T., Anai, M., Onishi, Y., Ono, H., Abe, M., Shojima, N., et al., 2003. Three mitogen-activated protein kinases inhibit insulin signaling by different mechanisms in 3T3-L1 adipocytes. Mol. Endocrinol. 17, 487–497.
Gonzalez, E., Flier, E., Molle, D., Accili, D., McGraw, T.E., 2011. Hyperinsulinemia leads to uncoupled insulin regulation of the GLUT4 glucose transporter and the FoxO1 transcription factor. Proc. Natl. Acad. Sci. U. S. A. 108, 10162–10167.
Gual, P., Gremeaux, T., Gonzalez, T., Le Marchand-Brustel, Y., Tanti, J.F., 2003. MAP kinases and mTOR mediate insulin-induced phosphorylation of insulin receptor substrate-1 on serine residues 307, 612 and 632. Diabetologia 46, 1532–1542.
Ikeda, Y., Olsen, G.S., Ziv, E., Hansen, L.L., Busch, A.K., Hansen, B.F., Shafrir, E., Mosthaf-Seedorf, L., 2001. Cellular mechanism of nutritionally induced insulin resistance in Psammomys obesus: overexpression of protein kinase Cepsilon in skeletal muscle precedes the onset of hyperinsulinemia and hyperglycemia. Diabetes 50, 584–592.
Karlsson, H.K., Ahlsen, M., Zierath, J.R., Wallberg-Henriksson, H., Koistinen, H.A., 2006. Insulin signaling and glucose transport in skeletal muscle from first-degree relatives of type 2 diabetic patients. Diabetes 55, 1283–1288.
Kido, K., Sase, K., Yokokawa, T., Fujita, S., 2020. Enhanced skeletal muscle insulin sensitivity after acute resistance-type exercise is upregulated by rapamycin-sensitive mTOR complex 1 inhibition. Sci. Rep. 10, 8509.
Kim, K.H., Song, M.J., Yoo, E.J., Choe, S.S., Park, S.D., Kim, J.B., 2004. Regulatory role of glycogen synthase kinase 3 for transcriptional activity of ADD1/SREBP1c. J. Biol. Chem. 279, 51999–52006.
Kohn, A.D., Summers, S.A., Birnbaum, M.J., Roth, R.A., 1996. Expression of a constitutively active Akt Ser/Thr kinase in 3T3-L1 adipocytes stimulates glucose uptake and glucose transporter 4 translocation. J. Biol. Chem. 271, 31372–31378.
Kondapaka, S.B., Zarnowski, M., Yver, D.R., Sausville, E.A., Cushman, S.W., 2004. 7-hydroxystaurosporine (UCN-01) inhibition of Akt Thr308 but not Ser473 phosphorylation: a basis for decreased insulin-stimulated glucose transport. Clin. Cancer Res. 10, 7192–7198.
Krook, A., Bjornholm, M., Galuska, D., Jiang, X.J., Fahlman, R., Myers Jr., M.G., Wallberg-Henriksson, H., Zierath, J.R., 2000. Characterization of signal transduction and glucose transport in skeletal muscle from type 2 diabetic patients. Diabetes 49, 284–292.
Kupriyanova, T.A., Kandror, K.V., 1999. Akt-2 binds to Glut4-containing vesicles and phosphorylates their component proteins in response to insulin. J. Biol. Chem. 274, 1458–1464.
Li, S., Brown, M.S., Goldstein, J.L., 2010. Bifurcation of insulin signaling pathway in rat liver: mTORC1 required for stimulation of lipogenesis, but not inhibition of gluconeogenesis. Proc. Natl. Acad. Sci. U. S. A. 107, 3441–3446.
Lontay, B., Bodoor, K., Sipos, A., Weitzel, D.H., Loiselle, D., Safi, R., Zheng, D., Devente, J., Hickner, R.C., McDonnell, D.P., et al., 2015. Pregnancy and smoothelin-like protein 1 (SMTNL1) deletion promote the switching of skeletal muscle to a glycolytic phenotype in human and mice. J. Biol. Chem. 290, 17985–17998.
Lontay, B., Bodoor, K., Weitzel, D.H., Loiselle, D., Fortner, C., Lengyel, S., Zheng, D., Devente, J., Hickner, R., Haystead, T.A., 2010. Smoothelin-like 1 protein regulates myosin phosphatase-targeting subunit 1 expression during sexual development and pregnancy. J. Biol. Chem. 285, 29357–29366.
Major, E., Gyory, F., Horvath, D., Keller, I., Tamas, I., Uray, K., Fulop, P., Lontay, B., 2021. Smoothelin-like protein 1 regulates development and metabolic transformation of skeletal muscle in hyperthyroidism. Front. Endocrinol. 12, 751488.
Manning, A.M., Davis, R.J., 2003. Targeting JNK for therapeutic benefit: from junk to gold? Nat. Rev. Drug Discov. 2, 554–565.
Mathe, C., Beyer, D., Erdodi, F., Serfozo, Z., Szekvolgyi, L., Vasas, G.M.M.H., Jambrik, K., Gonda, S., Kiss, A., et al., 2009. Microcystin-LR induces abnormal root development by altering microtubule organization in tissue-cultured common reed (Phragmites australis) plantlets. Aquat. Toxicol. 92, 122–130.
Meigs, J.B., 2003. Epidemiology of the insulin resistance syndrome. Curr. Diabetes Rep. 3, 73–79.
Mlinar, B., Marc, J., Janez, A., Pfeifer, M., 2007. Molecular mechanisms of insulin resistance and associated diseases. Clin. Chim. Acta 375, 20–35.
Moeschel, K., Beck, A., Weigert, C., Lammers, R., Kalbacher, H., Voelter, W., Schleicher, E.D., Haring, H.U., Lehmann, R., 2004. Protein kinase C-zeta-induced phosphorylation of Ser318 in insulin receptor substrate-1 (IRS-1) attenuates the interaction with the insulin receptor and the tyrosine phosphorylation of IRS-1. J. Biol. Chem. 279, 25157–25163.
Morino, K., Petersen, K.F., Shulman, G.I., 2006. Molecular mechanisms of insulin resistance in humans and their potential links with mitochondrial dysfunction. Diabetes 55 (Suppl. 2), S9–S15.
Mullen, E., Ohlendieck, K., 2010. Proteomic profiling of non-obese type 2 diabetic skeletal muscle. Int. J. Mol. Med. 25, 445–458.
Mussig, K., Fiedler, H., Staiger, H., Weigert, C., Lehmann, R., Schleicher, E.D., Haring, H. U., 2005. Insulin-induced stimulation of JNK and the PI 3-kinase/mTOR pathway leads to phosphorylation of serine 318 of IRS-1 in C2C12 myotubes. Biochem. Biophys. Res. Commun. 335, 819–825.
Pederson, T.M., Kramer, D.L., Rondinone, C.M., 2001. Serine/threonine phosphorylation of IRS-1 triggers its degradation: possible regulation by tyrosine phosphorylation. Diabetes 50, 24–31.
Sekulic, A., Hudson, C.C., Homme, J.L., Yin, P., Otterness, D.M., Karnitz, L.M., Abraham, R.T., 2000. A direct linkage between the phosphoinositide 3-kinase-AKT signaling pathway and the mammalian target of rapamycin in mitogen-stimulated and transformed cells. Cancer Res. 60, 3504–3513.
Shao, J., Yamashita, H., Qiao, L., Draznin, B., Friedman, J.E., 2002. Phosphatidylinositol 3-kinase redistribution is associated with skeletal muscle insulin resistance in gestational diabetes mellitus. Diabetes 51, 19–29.
Shao, J., Yamashita, H., Qiao, L., Friedman, J.E., 2000. Decreased Akt kinase activity and insulin resistance in C57BL/KsJ-Leprdb/db mice. J. Endocrinol. 167, 107–115.
Shepherd, P.R., Withers, D.J., Siddle, K., 1998. Phosphoinositide 3-kinase: the key switch mechanism in insulin signalling. Biochem. J. 333 (Pt 3), 471–490.
Sipos, A., Ivan, J., Becsi, B., Darula, Z., Tamas, I., Horvath, D., Medzihradszky, K.F., Erdodi, F., Lontay, B., 2017. Myosin phosphatase and RhoA-activated kinase modulate arginine methylation by the regulation of protein arginine methyltransferase 5 in hepatocellular carcinoma cells. Sci. Rep. 7, 40590.

lontay.beata_285_24

Turcotte, L.P., Fisher, J.S., 2008. Skeletal muscle insulin resistance: roles of fatty acid metabolism and exercise. Phys. Ther. 88, 1279–1296.

Wong, C.Y., Al-Salami, H., Dass, C.R., 2020. C2C12 cell model: its role in understanding of insulin resistance at the molecular level and pharmaceutical development at the preclinical stage. J. Pharm. Pharmacol. 72, 1667–1693.

Wooldridge, A.A., Fortner, C.N., Lontay, B., Akimoto, T., Neppl, R.L., Facemire, C., Datto, M.B., Kwon, A., McCook, E., Li, P., et al., 2008. Deletion of the protein kinase A/protein kinase G target SMTNL1 promotes an exercise-adapted phenotype in vascular smooth muscle. J. Biol. Chem. 283, 11850–11859.

Yu, L.G., Packman, L.C., Weldon, M., Hamlett, J., Rhodes, J.M., 2004. Protein phosphatase 2A, a negative regulator of the ERK signaling pathway, is activated by tyrosine phosphorylation of putative HLA class II-associated protein I (PHAPI)/pp32 in response to the antiproliferative lectin, jacalin. J. Biol. Chem. 279, 41377–41383.